MECHANICAL PROPERTIES AND STRUCTURE OF BOVINE PERICARDIUM

by

Peter N. ZIOUPOS,

This thesis is submitted for the
Degree of Doctor of Philosophy in the
Bioengineering Unit
of the University of Strathclyde

Glasgow,
April, 1989.

ABSTRACT

Chemically modified bovine pericardium has been used for heart valve substitutes for over 15 years. Nevertheless, a significant proportion of such valves show unsatisfactory performance, which may be related to the mismatch of the mechanical properties of the leaflets. This thesis reports an investigation of the mechanical properties and structure of native bovine pericardium, from which the leaflets are ultimately made.

The thesis consists of 11 chapters, each containing an introduction defining the main theme of the chapter and where appropriate, short literature reviews. There are summaries and discussions at the ends of each section highlightling important conclusions.

The first chapter outlines the reasons for studying the mechanical properties of native bovine pericardium and the methods and rationale of the experimental studies. The next 3 chapters discuss the mechanical properties of the tissue. Chapter 3 reviews currently available test methods and the results obtained using them to study pericardium. Chapter 4 describes the development and validation of a non-destructive biaxial inflation test, and results obtained on native pericardial specimens. These specimens were then subjected to uniaxial tension tests which are described in chapter 5, which also describes the regional heterogeneity of the pericardial sac. Chapter 6 describes the angular variation of the strength, extensibility and stiffness of the tissue under uniaxial tension and presents empirical and structure based descriptions of the results.

Chapter 7 describes the optical properties and histological structure of the tissue, and draws comparisons with the mechanical anisotropy.

Chapter 8 describes the function of natural heart valves and the requirements of bioprosthetic substitutes. The next chapter describes the effect of chemical modification by glutaraldehyde on the mechanical behaviour of pericardium; the modifications in properties produced by fatigue testing and in-vivo implantations are also reported.

Chapter 10 describes the development of a structure-based model of the mechanical properties of the tissue and shows that it can adequately describe the mechanical responce under different loading conditions. The last chapter contains a summary of the conclusions reached.

The thesis is completed by a bibliography and appendices.

ACKNOWLEDGEMENTS

I am grateful to my supervisor Professor J.C.Barbenel for his advice during the preparation of this thesis and guidance during the research project.

I am also grateful to Dr.J.Fisher for posing interesting and stimulating questions and for supplying me with material for the experiments of this project.

My special thanks to Professor J.P.Paul for his encouragement and support during the time I spent in the Bioengineering Unit.

I should like to thank the secretaries of the Unit and especially Miss Alexis Ross for her help.

I would like to acknowledge the financial contribution of the British Council.

Special thanks to Mr.Dave Smith for his help and his family for their friendship. The same is true for all the other friends I made in this land.

Most of all I should like to thank my parents, Nicholas and Maria, for their constant encouragement, support, love and understanding.

1.1 INTRODUCTION

Examination and characterisation of the mechanical behaviour of human and other biological tissues has always been one of the cornerstones of biomechanics. The initial interest of obtaining a better understanding of the human body has in recent years been substituted by an ever increasing interest in the study of biomaterials. Bovine pericardium constitutes a suitable candidate for the construction of leaflets for bioprosthetic valves. Knowledge of the structure and mechanical properties of bovine pericardium can significantly contribute to the production of an improved pericardial bioprosthetic valve by exploiting the use of the pericardial tissue in the most appropriate manner. The tissue is used after suitable chemical modification by the use of glutaraldehyde, but it was decided that the material properties of the native tissue to be studied first. The decision was based on the idea that the fixation process may modify the mechanical behaviour of the tissue and even hide some of the features of the pericardial responce to loading. If the properties of the native tissue are thoroughly studied then during fixation, where a degree of human intervention is always possible, these properties can be improved to provide a material more appropriate to its end use.

The properties of the native pericardia of some species have been studied but this information is only of limited help because interspecies variations render the results on the tissue of one species not generally applicable. A common practice in tissue mechanics studies is to use only one test mode in the examination of the material properties and this has the major drawback that some aspects of the mechanical behaviour may only be revealed if the tissue is subjected to a combination of test modes. In the present study the

Table 1.1:in the present report samples from 4 sites on the pericardial membrane have been examined by a biaxial and uniaxial mechanical test modes and an optical non-invasive method. The tissue was either in the fresh or the fixed form. Valve tissue was always fixed.

	Biaxial	Uniaxial	Optical
fresh	I	I,II,II′,III	*
fixed		I	I
valve tissue			
Glasgow		*	*
Commercial ISU		*	*

ISU :Ionescu Shiley universal
I,II,II′,III :test sites on the pericardial membrane
* :irrespectively of position on the membrane

native bovine pericardial samples were subjected to both biaxial and uniaxial tests which were thought as being complementary and both necessary in investigating the material's mechanical behaviour in full. For the biaxial mode an inflation method was developed and used which has proved to have a potential for qualitative and quantitative characterisation of the material properties.

One of the most interesting aspects of the mechanical behaviour of pericardium would be the presence of mechanical and/or structural anisotropy. Human valve leaflets are both structurally and mechanically anisotropic and thus it would be of great importance if the biomaterial to be used for the construction of the bioprosthetic leaflets could match the natural ones in these respects. Once more it is unfortunate that occasionally tissue mechanicians presume the presence of isotropy and thus by using an inappropriate test program are unable to detect and quantify anisotropy. In the present study the biaxial and uniaxial testing protocols were developed and applied in such a manner that the presence of anisotropy would be clearly apparent, and the results justified this approach.

Table1.1 summarises the present experimental investigation performed on native pericardial samples originating from 4 different areas on the pericardial sac and for material in the fresh or fixed form. A non-invasive optical method utilising transmitted polarised light microscopy is also included and has been found to be extremely helpful in identification of the axes of elastic symmetry for the material. Thus the optical method and the biaxial inflation test constituted two non-destructive methods for the characterisation of the tissue properties. This is of great practical importance since the pericardial sample can be previewed and mechanically characterised and subsequently used in the construction of a leaflet.

A more detailed examination of the tissue structure has helped in understanding some of the features of the pericardial response to either biaxial or uniaxial loading and it was later used to build a structure based model. The model can adequately describe and predict the mechanical behaviour of the pericardial specimens under multiaxial loading conditions. The model provides a constitutive relation which accounts for non-linearity, anisotropy and multiaxial stretching, and which can be used by bioengineers of the future who will attempt the solution of boundary value problems.

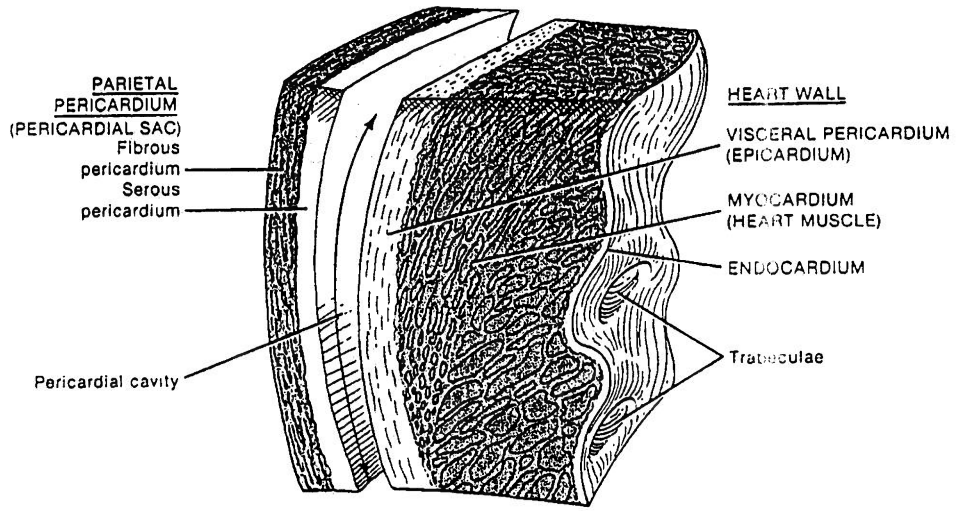

Figure 2.1:The parietal pericardium, pericardial cavity, visceral pericardium and the heart wall.

2.1 INTRODUCTION.

This chapter describes the tissue under examination. The information presented refers to the origin, shape, retrieval and the various functions that the pericardium performs. Material found in the literature has been combined with the experimental establishment of the tissue topography and its morphological characteristics.

2.2 THE TISSUE.

2.2.1 Definitions.

The vertebrate heart is enclosed in a loose-fitting fibrous sac. It is usually called a **serous membrane**. As a membrane it comprises an underlying connective tissue layer and an epithelial layer of cells and it is a serous one because it does not open to the exterior but faces inside covering the organs of a cavity. This membrane together with a thin transparent layer intimately attached and covering the myocardium of the heart constitutes the **pericardium**. The outer sac is called the parietal part of the pericardium while the one attached to the heart is the visceral pericardium or epicardium. Between the two there is a small space, the **pericardial cavity** containing a watery fluid known as the **pericardial fluid**(fig.2.1). The work reported herein is exclusively focussed on the parietal pericardium of **beef-cattle**.

2.2.2 Anatomy.

The mammalian pericardia of different species are more or less similar to each other and thus their descriptions are usually generally applicable. In the literature human pericardium has attracted attention but animal pericardia which are easier to obtain are much better studied. The results from clinical studies and laboratory tests of animal pericardia have been assumed to apply equally well to the human tissue because of their general

similarities.

In humans the heart seems invaginated into the pericardial cavity, which resembles an asymmetric inverted and truncated cone whose apex is the diaphragm and whose base extends to the aortic arch. The parietal pericardium is continuous with the visceral pericardium and extends upwards to enclose the origin of the aorta and the pulmonary artery where it is known as the arterial mesocardium (Shabetai 1981). The pulmonary veins and venae cavae are likewise invested by the venous mesocardium, not present in some species, e.g. dogs. The arterial orifice of the tissue dorsally covers the veins which empty into the atria and if the animal posesses an azygos vein or superior vena cava these vessels are covered as well (Elias and Boyd,1960).

Apart from the great vessels the pericardial sac is attached to the sternum, the vertebral column and the diaphragm. Elias and Boyd(1960) distinguish a pars sternocostalis, pars diaphragmatica, pars parietalis and pars mediastinalis on the tissue. In humans the pars-sternocostalis consists of a narrow strip between the lines of the pleural reflection. In cattle the heart is placed in a more vertical position and thus the pericardial area facing the sternum is limited and lies towards the apex. Pars diaphragmatica in the human tissue is the triangular area of the attachment of the diaphragm and pericardium. It lies from right posteriorly to the left anteriorly. Pericardium and diaphragmatic fascia are interlaced and united in the pars tendinea of the diaphragm (Elias and Boyd,1960). In beef cattle again this area lies posteriorly where pericardial condensations and tendinous attachments join the tissue to the diaphragm. Pericardial pars parietalis extends upwards around the great vessels and unites with the adventitia of the aorta and pulmonary artery, which originate from within the pericardial cavity. The venae cavae are covered up to

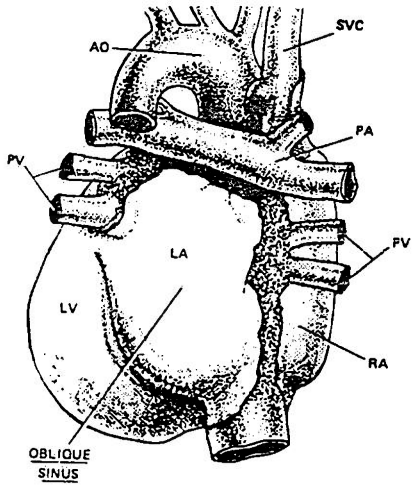

A

SVC: superior vena cava
PV : pulmonary veins
AO : aorta
LV : left ventricle
PA : pulmonary artery
RA : right atrium
LA : left atrium

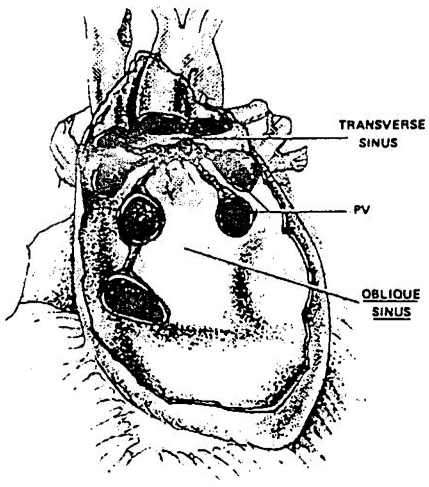

B

Figure 2.2:The oblique sinus viewed from behind (A), relation of the transverse sinus to the oblique sinus(reproduced from Shabetai,1981).

a point which can be either proximal or distal to the venous bifurcation into a superior and inferior branch depending on the animal species. The inferior vena cava, in cattle, passes through a distinct pericardial ring, the "foramen quadrilaterum". In Pars mediastinalis pericardii the tissue is usually in contact with the aorta thoracica, vena azygos and the esophagus (Elias and Boyd,1960). Vertebropericardial ligaments exist dorsally in humans and cephalically in calves and they are a fusion of the tissue with the prevertebral fascia.

Pericardial recesses and sinuses occur between the visceral and parietal pericardium as complementary spaces, which are useful in identification and of some mechanical importance. When pericardial effusion is present the tissue there yields outwards although usually the voids on the pericardial-mediastinal interface are filled with fat. Sinuses are formed early in the development of the tissue and can accomodate substantial quantities of pericardial fluid. The sinus obliquus lies between the right and left pulmonary veins and results in the separation of the posterior wall of the left atrium from the pericardial space. The sinus transversus is formed between the arterial and venous pericardial sheaths. The venous sheath forms rings around the pulmonary veins and the vevae cavae and the arterial sheath surrounds the aorta and pulmonary arteries. Sinuses, atria, ventricles and the position of the major vessels (as in the human heart) are shown in fig.2.2.

The development and relative position of the sac in the thorax differs in different species,and has interesting physiological and mechanical implications. The differences should be kept in mind when results of studies on canine pericardia or of other species are applied to humans. The fibrous pericardium is well developed in

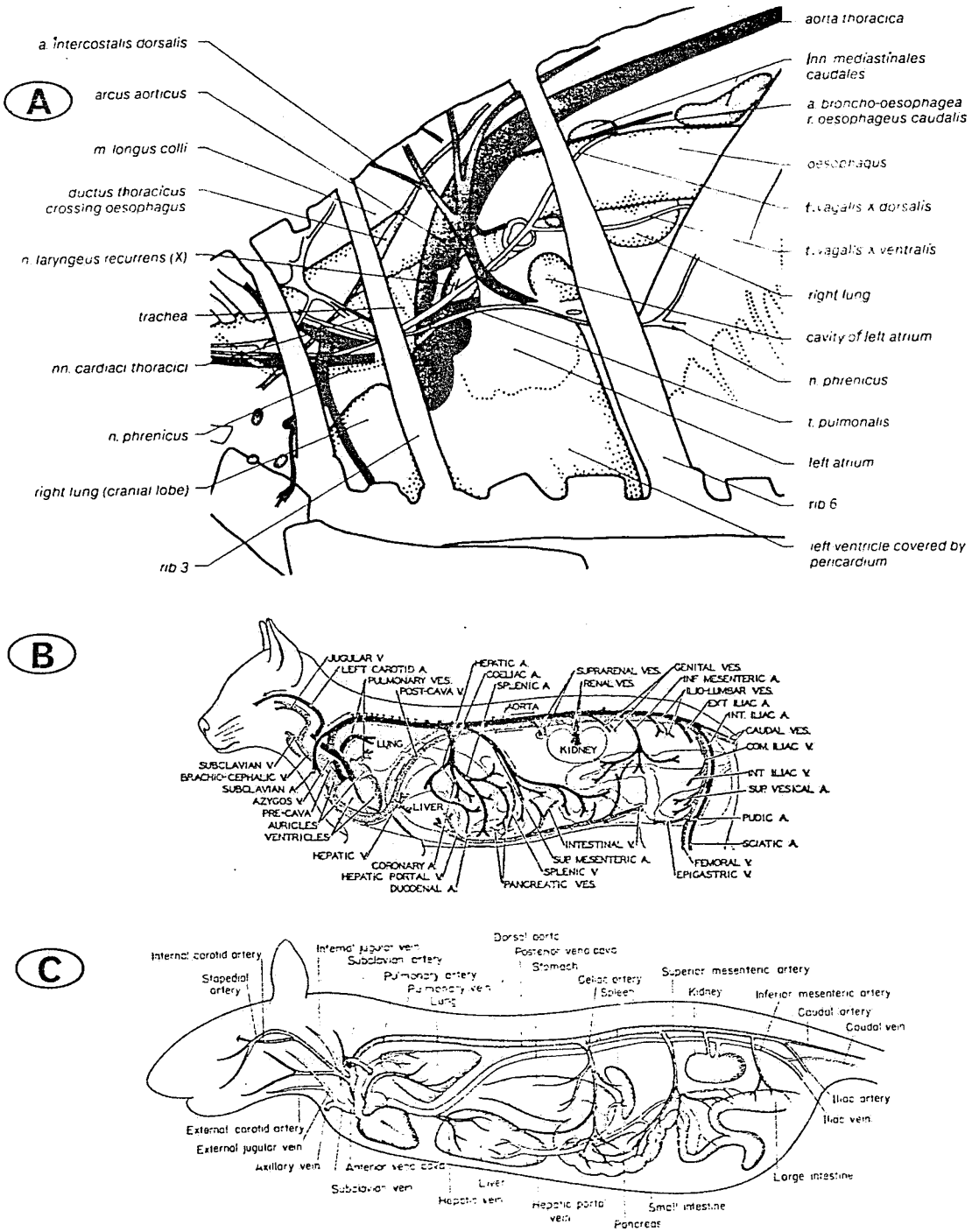

Figure 2.3:Thoracic anatomy of cattle(A), (from Ashdown and Done); cat(B), (from Neal and Rand,1936); and a rat(C),(from Romer and Parsons,1977). All presented in the different scales as in original diagrams.

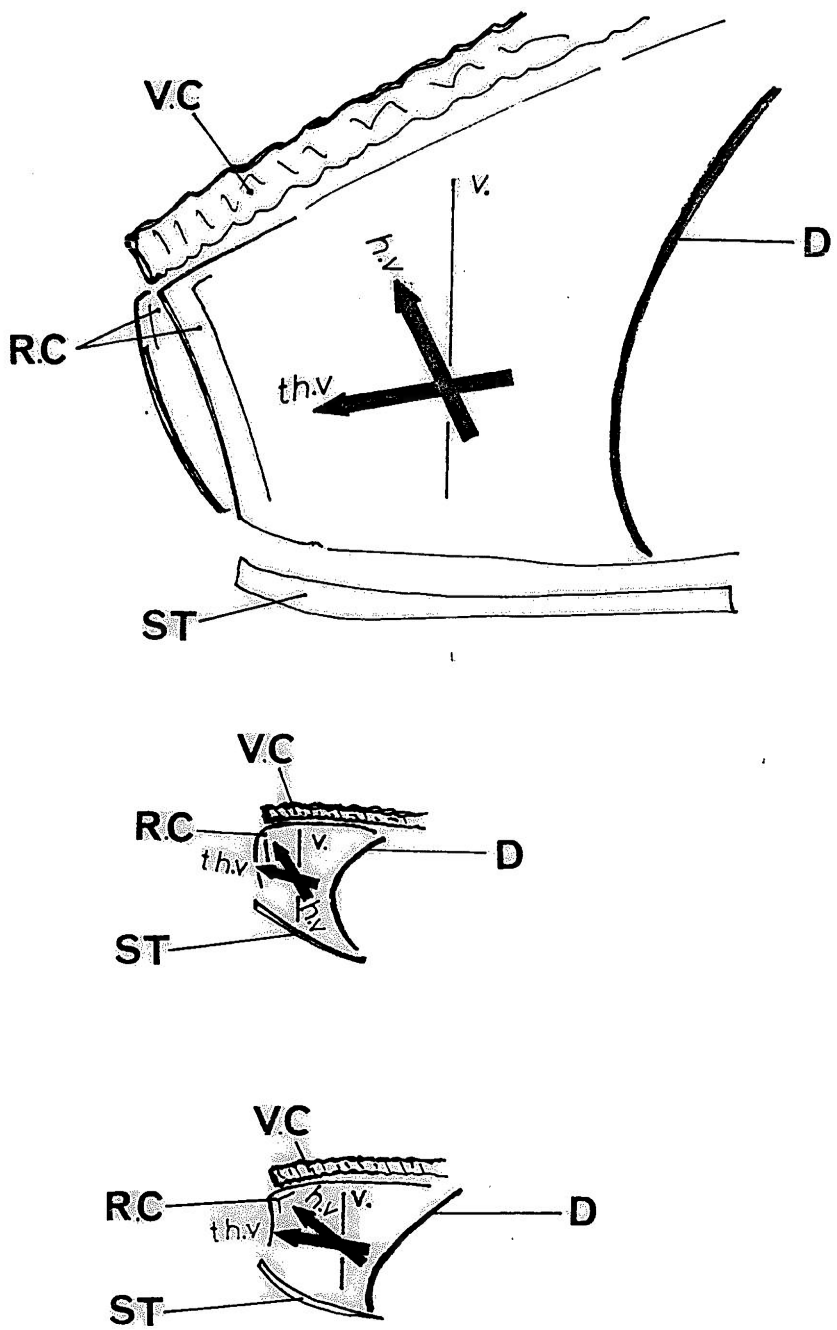

Figure 2.4:By using a vector for the thorax and one for the heart the differently inclined heart of the mammals is easier to appreciate. R.C.:rib cage, V.C.:vertical column, D:diaphragm, ST:sternum, h.v.:heart vector, th.v.:thorax vector, v:vertical.

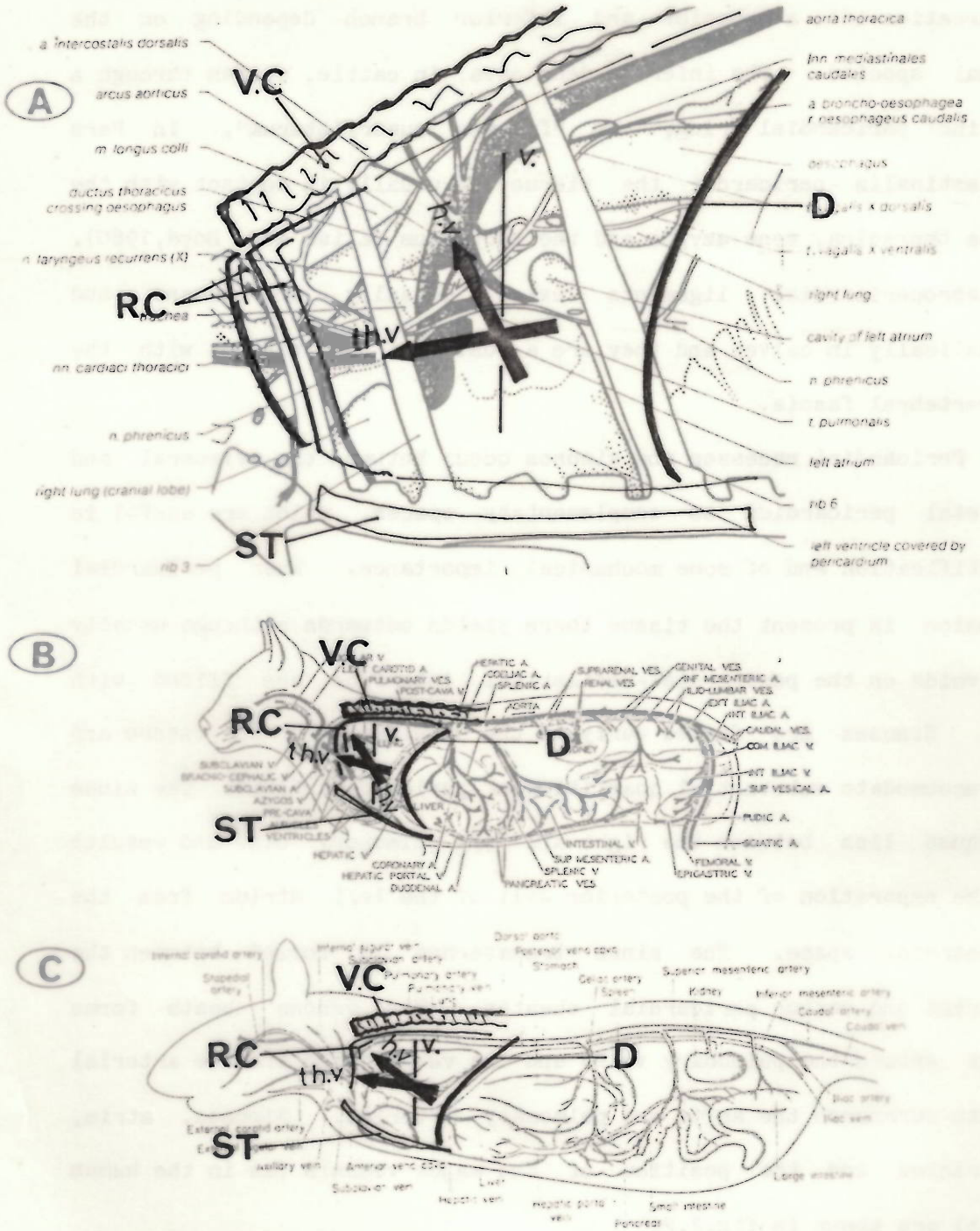

Figure 2.3:Thoracic anatomy of cattle(A), (from Ashdown and Done); cat(B), (from Neal and Rand,1936); and a rat(C), (from Romer and Parsons,1977). All represented with the original scales as in original diagrams.

Figure 2.4:By using a vector for the thorax and one for the heart the differently inclined heart of the mammals is easier to appreciate. R.C.:rib cage, V.C.:vertical column, D:diaphragm, ST:sternum, h.v.:heart vector, th.v.:thorax vector, v:vertical.

humans, being relatively thicker than in all other species. From the rest of the species the pericardia of herbivora is generally thicker. In humans there is an extensive attachment to the diaphragm, while in horses there is an extensive attachment to the sternum (Shabetai,1981). Differences appear early in embryonic life and probably reflect the different functional requirements imposed on the tissue. Heart and pericardium develop in a primitive pericardial coelomic cavity. The heart is surrounded by the pericardial coelom which lies in a coronal plane, which starts in a vertical position and bends into a ventral-dorsal plane. The pleuropericardial membrane develops in two halves which fuse together and eventually separate the heart (developed from an early cardiogenic plate) from the lungs and pleurae. The long axis of the heart and pericardium is, in humans, ventral and diverted to the left. In horse and cattle it lies almost vertical while in swine the position is more oblique in a caudo-ventral plane, in the dog the apex is turned caudad so markedly that the heart is almost horizontal (Kingsley,1926; Delahunta,1986).

In fig.2.3 the anatomy of the thorax of a series of animals is presented. It is obvious that the heart is horizontal in the rat and turns more upright as the size of the animal increases. In the following fig.2.4 there is a diagramatic representation of the thoracic cavity as comprised by the rib cage(R.C), the diaphragm(D), the vertebral column(V.C) and the sternum(ST). Two vectors have been used to represent the heart and the rib-cage. The heart-vector is aligned to the long axis of the heart, while the thorax-vector bisects the angle between the vertebral column and the sternum. The vector of the thorax is placed according to a Cartesian system of coordinates in a manner that expresses the posture of the animal in life. The relative position of the heart-vector to the thorax-vector shows that

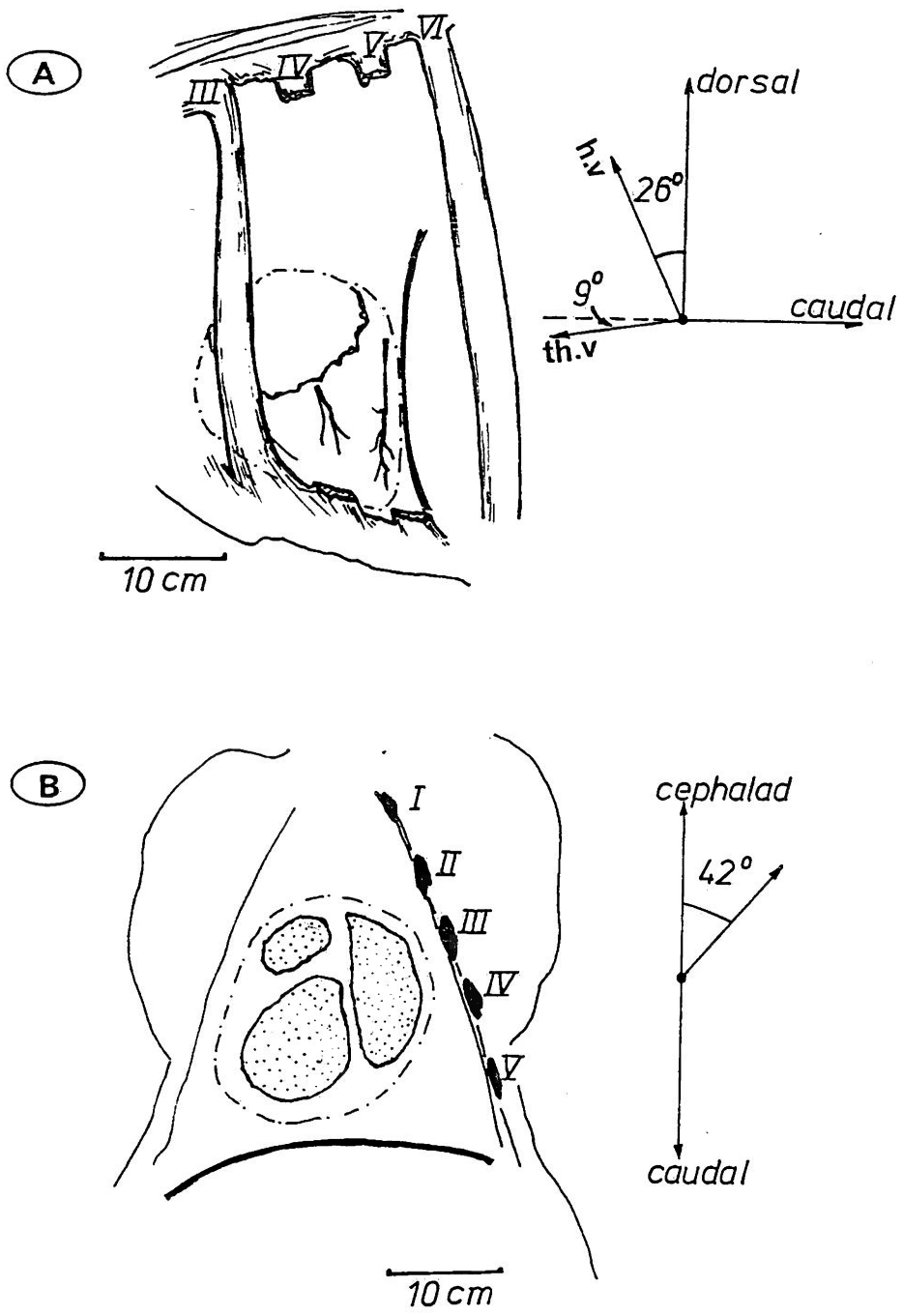

Figure 2.5:A left lateral aspect of the cattle thoracic cavity (A) (dashed line:heart boundary); a horizontal section of the cattle thorax (B), both were traced from the original photos by Paraux(1982).

the heart's place in the mediastinum is important for any considerations on the suspension provided by the pericardial membrane.

Observations into the thoracic cavity of cows revealed that the heart of cattle is tilted slightly forwards and to the left, the apex points ventral and lies in a median plane (Ghoshal,1975) about 2.5cm from the diaphragm. Measurements of the tilt and rotation of the heart were made after tracing on paper sagittal and frontal sections of the thorax of cattle of similar age, as presented in literature (Paraux,1982). On a lateral view the heart is inclined forward between 24° and 26° if projected in a mid-sagittal plane. The thoracic cavity is pointing downwards about 9°. The heart itself, if considered to posses a plane of symmetry across the two ventricles (or atria) and containing the long axis, is rotated anticlockwise between 45° and 48°. Thus the right ventricle-atrium is on the front while the left half is positioned on the rear.

Fig.2.5a represents a left lateral aspect of the cattle thoracic cavity with the heart demarcated with the dashed line. On the left side the greater part of the pericardium is in contact with the lateral thoracic wall as far caudally as the fourth intercostal space. On the right side the pericardium may be covered by the lung and have no contact with the lateral thoracic wall. In most cases there is a triangular cardiac notch on the right lung opposite the ventral part of the fourth rib and adjacent intercostal spaces. The heart is off-centered to the left and this is the reason why the pericardium touches the ribs on the left and not on the right side. I have measured the distance of the centre of gravity of the area of the heart in fig.2.5b and found it to be 2 to 3 cm left of a mid-sagittal plane. In the figures Latin numbers indicate the order of the ribs and the dashed line the shape of the heart. The topography of the

thorax and this particular arrangement of the heart will be proved to be of some significance later. An early observation is that the lowermost part of the heart and the pericardium is not only the apex area but due to its inclination some of the area covering the right ventricle.

Gravitational forces as well as forces arising from physiological activity both combine to stress the tissue in vivo and the effect might be exaggerated on the lower parts. It seems that the heart is not comfortably sitting on the surrounding tissues but that it is suspended through various ligaments and ligamentous attachments. There are thicker bands in the pericardium which probably act as suspending ligaments and can serve as reference points on the excised membrane.

Ligaments-Ligamentous attachments. The pericardial sac blends with the surrounding tissues over some areas but it is strongly anchored to firm structures by the use of ligaments. The Lig. sternoperdiaca or ligaments of Luschka (Elias and Boyd,1960) pass from the tissue to the sternum or vice versa, one towards the manubrium and the other to the Xiphoid process. In both humans and cattle the Xipho-pericardiacum lig. ascends from the xiphoid to the anterior pericardial surface. In humans the ligament stabilises the heart during ventral-dorsal movements of the trunk, while in cattle the almost vertical position of the heart suggests that the ligament stabilises the heart during cephalad-caudal movements of the animal. A number of upper ligaments, the Lig. sterno-costo-perdiaca superius emerge from the superior posterior aspect of the sternum to the anterior superior surface of the tissue below the origin of the major vessels. Those ligaments suspend the sac in the horizontal and vertical position and are especially important in the case where the

heart has a more vertical position as in cattle. The various ligamentous attachments not only keep the heart fixed in place but in thoracic respiration dynamically enlarge the space available to the dilating heart and create a negative pressure inside the pericardial cavity (Holt,1970; Morgan et al,1965). Superiorly 3 ligaments appear to exist in cattle and humans, one anterior and two lateral. The ligaments diverge inside the tissue and can be traced as high as the adventitia of the aorta and the pulmonary artery; they are usually called ligaments Teutleben. Various other tendinous bands merge with the diaphragmatic fascia and muscles of thorax but it is difficult to identify them individually. On the posterior surface cattle have an extended double row of fibrous flaps which seem to meet and reflect oppositely. They attach the tissue to the diaphragm all along the caudad area of the heart where in humans the Vertebroperdiaca ligaments are.

The blood, nerve and lymph supply of the fibrous pericardium are not of any mechanical importance in the isolated pericardial sac in-vitro but in the intact pericardium in-vivo nervous reflexes in other organs by stimulation of the pericardium have been described (Holt et al,1960). Stimulation of the pericardium in the anaesthetized dog causes a decrease in arterial pressure as reported by Kricheyskaya(1962).

Blood is supplied to the tissue by the internal mammary arteries, the musculophrenic arteries and the aorta. The vessels pass to the tissue from the mediastinum although the attachment points and the return is through the venous circulation. Veins closely follow the arteries inside the tissue and the blood returns through the azygos system to the systemic circulation. The lymphatic system is ordered in 5 subsystems (Elias and Boyd,1960) supplying the heart, the epicardium

and the pericardium. Its mechanical role is again negligible but it has an immunological contribution protecting the heart against infections during life (Holt,1970). The permeability of the membrane has been assessed by the hydraulic conductance (flow volume per unit of hydrostatic pressure), the reflection coefficient and a permeability coefficient by Pegram and Bishop(1975). They found that bulk transfer of fluid across the membrane is possible and thus relief of excessive pressure caused by the accumulation of a substantial amount of fluid. The actual volume of pericardial fluid under normal conditions is under dispute. Volumes of fluid ranging between 38 to 1000ml have been drained from otherwise normal or at least asymptomatic horses (Holt 1970).

2.2.3 Pericardial Cavity.

The actual size of the cavity is the sum of the pericardial fluid and the heart's volume which of course fluctuates during the cardiac cycle. Human pericardium usually occupies 320-460ml, as measured in human cadavers, and if air is pumped into the cavity until the tissue is unfolded, but not stretched, the space has been reported to become 510-800ml (Elias and Boyd,1960). The pericardial fluid in humans has a normal volume of 20-25ml as obtained from the pericardial cavity post-mortem and in extreme cases reached 60ml. The space of the cavity can increase to 150-220ml by unfolding the complementary spaces and 626-650ml by stretching the membrane itself. The last value seems erroneous and does not certainly represent any physiological cases.

A few preliminary strain measures may result from the previous numbers. The pericardial cavity enlarges from a mean value of 400ml to a mean value of 655ml when simply unfolded. If that space is thought to be occupied by a sphere, the radius would vary between 4.57 and 5.38cm. A mean strain value calculated from the two radii would

give an estimate of 17% strain. This could be the range for strains for a membrane moderately stretched. The same could be applied for the second sequence of numbers. The residual normal pericardial fluid volume was 20-25ml and the heart's mean volume is again considered to be 400-20=380ml. If pericardial fluid volume rises to 185ml this would give a mean strain measure of 11% which represents a membrane just unfolded. An excessive pericardial fluid volume of 620ml would add 24% on the previous strain measure. It seems reasonable to suggest that the maximum strain value for the tissue in-situ is 35% and that examination of the membrane properties should in any case be compatible within this limit. If the same volume differences were to be created by the fluctuation of blood volume it would account for most of blood present in the heart at normal conditions. It is reasonable to suggest that the 17% strain of the spherical model mentioned earlier is the maximum strain experienced by the tissue in-vivo. It should also be expected that local areas would have to perform overwhelmingly well to accomodate additional volumes and stresses or be significantly restrictive in the absense of an overall membrane dilatation. Regional variations of the mechanical properties are more likely to exist than uniformity of properties all over the membrane's surface.

Stresses and strains are sustained by the fibrous pericardium whose native properties or those of the chemically modified tissue are in the main interest of our work.

2.2.4 The Tissue Structure.

It consists of 3 layers(Ishihara et al,1981): the Tunica serosa, the epipericardial connective tissue which is a continuation of the adjacent tissues and the Tunica fibrosa.

The Tunica Serosa consists of a layer of cells whose classification is

disputed. They are considered to be mesothelial cells that is epithelial cells of a serous membrane. Their response to physiologic stimuli resembles that of epithelial cells. They possess cilia, form glandular structures, goblet cells and thus feature epithelial-like. Others consider them to be mesenchymal cells and thus developed from embryonic connective tissue cells, possessing though some ability to respond to external stimuli.

The Epipericardial Contents are not distinguished as different by all workers but they are mentioned separately by Elias and Boyd. The interface between the membrane and the mediastinum is made up of scattered unorganised elastin and collagen fibres.

The Tunica Fibrosa is the connective tissue layer, in particular adult connective tissue of the dense form. The fibrosa is responsible for the form and the strength of the pericardium. It is built by collagen fibres with intermingled elastic fibres whose arrangement has not been studied thoroughly, despite their importance in understanding the mechanics of the tissue, and for any- of its other uses like the construction of the bioprosthetic valves leaflets.

Evans(1973) has classified the connective tissues in respect to the simplicity of their function and structure in: simple(i.e.tendons) and complex(i.e.cartilages, skin) and regarding the level at which the various structural elements interact to produce the exhibited mechanical behaviour in: dominant(i.e.collagen's dominance in ligaments) and interactive (i.e.skin). In these respects the fibrous pericardium is both collagen dominated, complex due to the presence of various elements and interactive. We also suspect that if there is a relative orientation in the densely packed collagen fibres in pericardial fibrosa this will have a pronounced effect on the mechanical beheviour of the tissue(anisotropy).

Up to date the tissue has been treated as a whole sac enclosing the heart and of uniform properties which have been considered to vary from site to site only as a consequence of thickness variations(Reece et al,1981) or composition (usually where the sac meets the major vessels, Elias and Boyd,1960). The pericardium has been considered in general to be of a continuum material which is subjected to mechanical loads and deformations due to changes in cardiac form, size and volume in systole and diastole, the phases of respiration, fluctuating blood volume, position of the diaphragm and so forth. Every one seems to have a clear opinion about the forces exerted as a result of suspension or distension and therefore it could be said that there is a pattern for the stresses imposed on the tissue i.e.suspensive forces are directed to the ligaments. A concomitant structural pattern should then follow but instead it is strange that when considering the tissue structure any directional or regional variabilities are generally disregarded probably only because of reasons of convenience.

2.3 PERICARDIAL FUNCTIONS.

2.3.1 Introduction. A number of functions have been attributed to the pericardium and examination of the general role of the tissue should be included in a study of pericardial mechanics. Besides the functions that pericardium performs may be related to the structure and mechanical properties of this tissue. A review of the main topics is presented with an emphasis on the mechanical side of them.

Pericardium is an integrated element in the cardiac part of the circulatory system and the effect it may exert on the heart is not easy to assess in a straightforward manner. The complexities in cardiac mechanics led workers to an "if not there" approach for most of the reports. This means that the results that either the absence of the tissue or an open pericardium have in some measured parameters,

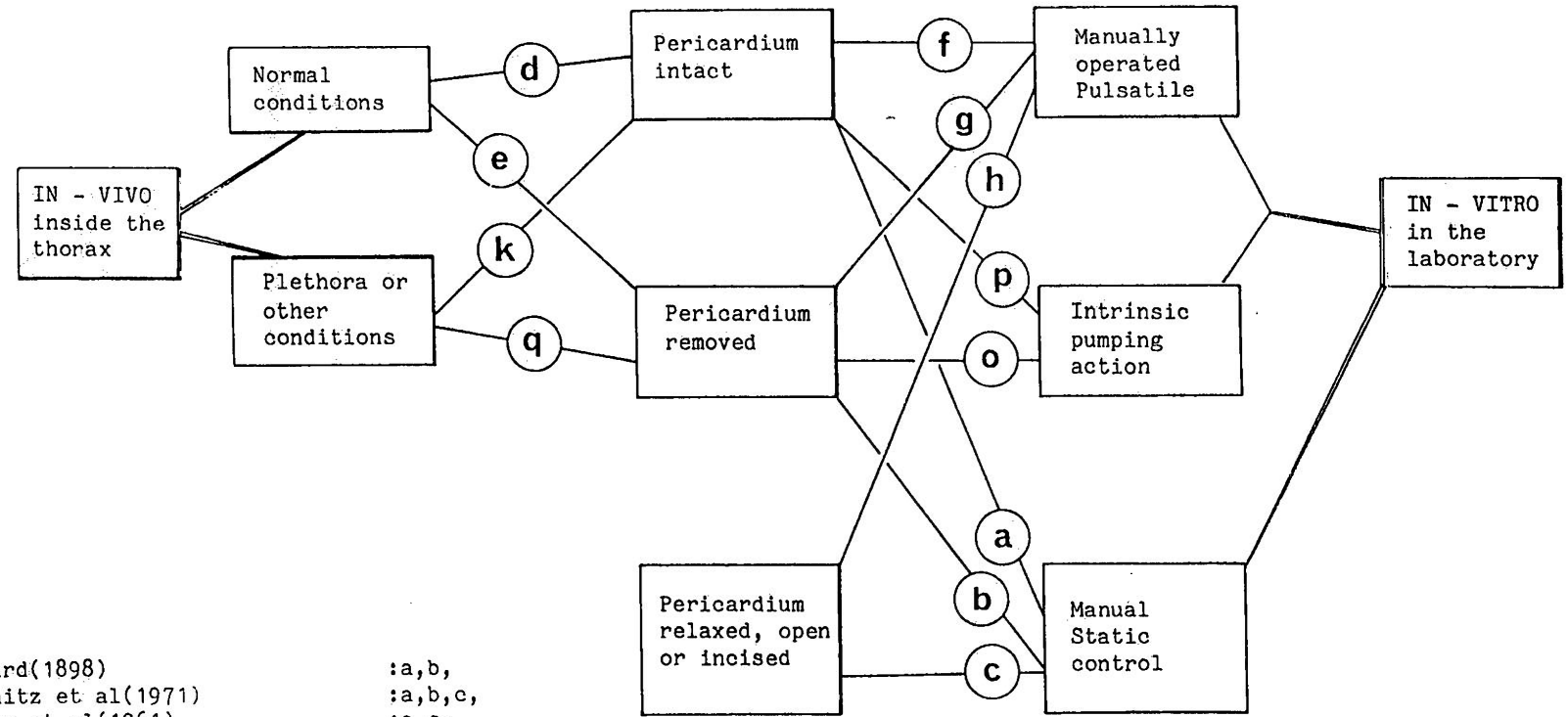

Barnard(1898)	:a,b,
Spotnitz et al(1971)	:a,b,c,
Hefner et al(1961)	:a,c,
Janicki and Weber(1980)	:f,g,
Hess et al(1982)	:f,
Glantz et al(1978)	:f,h,
Berglund et al(1955)	:k,
Carleton(1929)-Bartle et al(1978)	:d,e,
Kuno(1926)	:o,p,
Barnard(1898)-Holt(1960)	:k,q,

Figure 2.6:Strategy for examination of the pericardial contribution to cardiac mechanics.

provided that all other parameters are kept invariable, indicated that the tissue operates in the adverse way when present.

Fig.2.6 shows the various choices that are available as a combination of different approaches. The arrows between tables have been assigned a letter and thus a combination of letters is a comparison between two, in general artificially produced, cardiac conditions.

The two main divisions are: in-vivo or with the chest closed, and in-vitro where the heart and the tissue is examined in the laboratory environment. The in-vivo can be subdivided for animals under normal systemic conditions and those with plethora (excess of blood volume). The in-vitro is subdivided into two categories, the one where static pressures and volumes are employed and the one where the heart is auxotonically beating. The latter dynamic-pulsatile method can be achieved either manually or by exploiting the intrinsic pumping action of the heart.

2.3.2 Pressure-Volume Relationships.

Holt(1970) related the intrapericardial pressure and the associated total volume enclosed by the pericardium. He produced the "exponentially" rising curve of fig.2.7. A volume of almost 225ml was available to the heart and the blood in it, with the pressure at zero level. In between 225 and 300ml, the steep portion of the curve, suggested that the pericardium was restricting the heart and this is probably the case in cardiac tamponade or other pathophysiological conditions. Holt essentially produced an exponential relationship between a stress parameter and deformation which is very similar to all stress/strain relationships of collagenous materials.

The pericardium not only allows a limited volume increase to the heart but reinforces the cardiac wall as shown by Barnard(1898). He found that in absence of pericardium the cat's heart can rupture at a

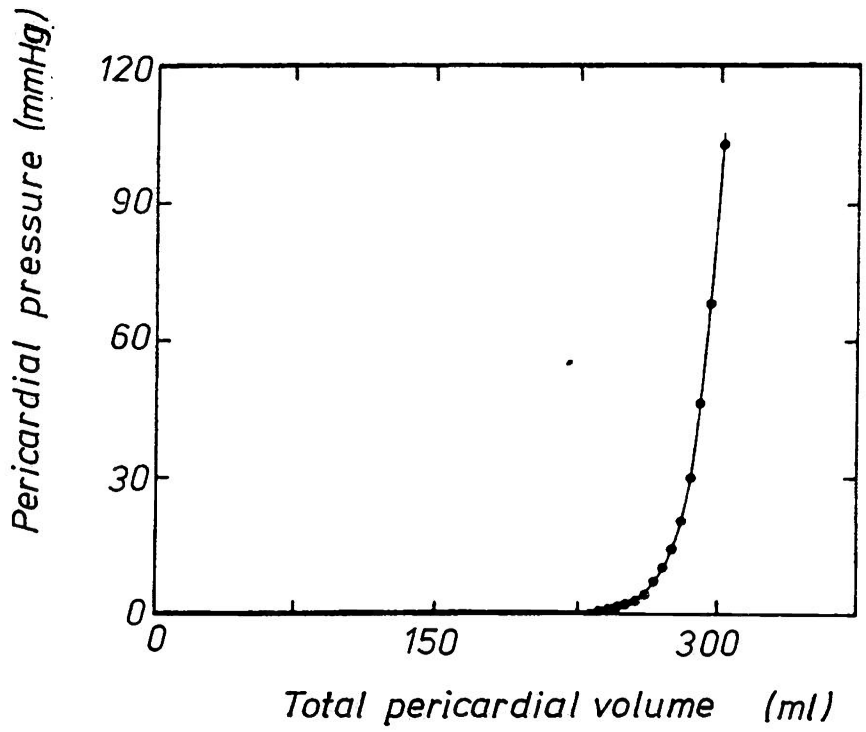

Figure 2.7:Total pericardial pressure-volume curve from a dead dog. The heart was first drained of blood and the great vessels were ligated. The pericardial space was cannulated and fluid was slowly injected. The heart was then removed and its volume determined. The volume of the heart was added to the volume of the fluid injected to obtain the pressure-total volume curve (reproduced from Holt,1970).

pressure of 0.75 to 1.0 atmosphere while with the pericardium intact the limit of pressure is 1.25 to 1.75 atmospheres.

The rest of the workers listed in fig.2.6 established other physiological and/or mechanical functions. Barnard(1898) found that in absence of the tissue additional volume of fluid was required to produce the same intracardiac pressure. Spotnitz et al(1971) claimed that pericardium contributes by a significant amount in diastolic ventricular pressure, thus relieving the myocardium. Hefner et al(1961) discovered that the tissue restricted the left ventricular dimensions. Removal of the tissue resulted in enlargement of the left ventricle according to Bartle et al(1978) and of the whole heart in-vivo according to Carleton(1929). Kuno(1926) said that the tissue had an effect on the systemic pressures where: when removed the venous pressures decreased and cardiac output increased; the increased venous inflow with increased venous pressure resulted in maximum cardiac output with the pericardium present and also that an increased aortic outflow resistance led to an increased arterial pressure in the presence of the pericardium. Both Barnard(1898) and Holt(1960) established that in an anesthetized animal in pericardial absence the arterial pressures slightly increased, that venous pressures fell and that in plethora both effects were exaggerated. All the pressure volume relationships indicated that the tissue is effective in the passive diastolic phase and this is reasonable to suggest for a distension resisting structure.

2.3.3 Pericardium-Ventricular Interaction.

The previous functions result in the pericardium acting as a control systems in cardiac mechanics by coupling the action of the two ventricles. The stroke volume outputs of the ventricles are balanced due to the restrictive action of the surrounding pericardium as

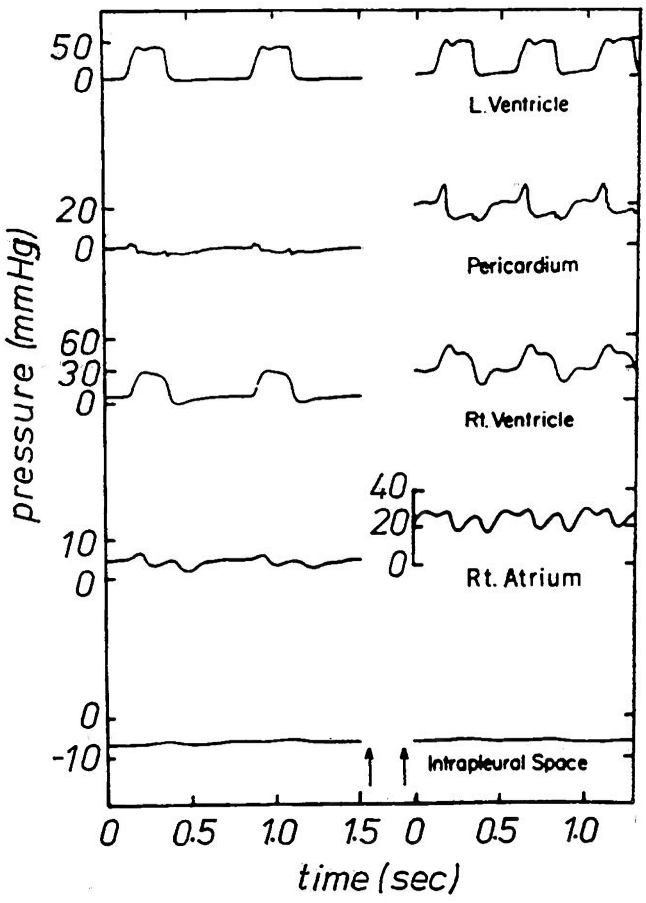

Figure 2.8:Demonstration of the effect that transfusion of blood substitute has on the pressure in the pericardial space, right ventricle, right atrium, left ventricle, and intrapericardial space in a closed-chest dog. Original pressures recorded at the left, after injection of 1000ml of 5% dextran in 0.9%NaCl solution all traces rise during systole and diastole except the pleural space pressure (reproduced from Holt et al,1960).

suggested by Berglund et al(1955). Interaction of the ventricles with the tissue intact has been examined by Janicki and Weber(1980) and the influence of pressures in the one half of the heart to the contralateral one by Hess et al(1982). The conclusions drawn by Hess et al(1982) were the only ones where a comparison has been attempted with the tissue intact in both cases. Instead they subtracted pericardial pressures from the cardiac ones to prove their argument, that pericardium results in interaction of the cardiac chambers while relieving the myocardium by keeping the transmural myocardial pressures constant.

2.3.4 Transmural Pericardial Pressure.

In order to find the level that the native pericardium is stretched in-vivo various workers assumed a certain level of pericardial pressure and used Laplace law to yield the stress values. The concept of pericardial pressure should be handled with care because in-vivo the tissue is subjected to a pressure gradient by having on one side the pressure of the pleural cavity and on the other the pressure of the pericardial cavity. Similarly the transmural pressure across the heart's wall equals the intracardiac pressure minus the pericardial pressure. The distinction between absolute pressures and transmural pressures is essential in understanding cardiac mechanics. Clinicians find the resting absolute pericardial pressure to be subatmospheric, therefore has to be added as a value to the in-chamber absolute pressure value to yield the transmural pressure. Shabetai(1981) gave an example, if left atrial pressure equals 7 (no units) and pericardial pressure equals -4, then transmural left atrial pressure equals 11. Fig.2.8 reveals that the tissue is for most of the cardiac cycle under a positive pressure difference. The pleural pressure is always subatmospheric in either

normal or plethoric conditions. The pericardial pressure varies around zero, being positive for most of the diastolic phase (and thus relieving the cardiac wall), presents a peak at the onset of systole and is relatively reduced for the rest of systole as the cardiac muscle contracts inwards. Holt et al(1960) conducted systematic studies of pericardial pressure by using a liquid or gas-filled balloon passed through a small slit into the pericardial space and found that pericardial pressure was directly influenced by the pleural pressure in the vicinity of the balloon. The pericardial pressure could also be affected by the intracardiac pressure (especially when it was accompanied by a change in volume) and the respiratory cycles (inspiration/expiration, Morgan et al(1965)). Holt et al(1960) found that pressures measured in the mid-distance between base and apex increased at the onset of systole and fell during late systole. When pressures are measured with an open-tip catheter in the region of the atria or apex, there was little or no increase in pressure during early systole. They even suggested that the sudden decrease in pericardial pressure at early ventricular systole lowers the pressure around the atria. Thus the pressure difference between atria and thoracic veins increases and an equally sudden flow of blood fills the atria. The same well known fact has been attributed to the sudden piston-like downward motion of the atrioventricular floor in early systole but the role of the pericardium in the same event should also be significant showing at the same time that it does not always exert a restrictive force on the heart.

Local Variations in pericardial pressures have been shown to exist due to the variations of the intrapleural pressure itself. Brookhart and Boyd(1947) have shown that intrapleural pressure varies and increases in the vicinity of the heart.

Hydrostatic gradients of pressure within the pleural and pericardial spaces have been found to be approximately 1cm of H20 of pressure for 1cm of vertical height by Banchero et al(1967) They measured atrial, pericardial and pleural pressures in dogs subjected to accelerations up to 7g by centrifugation in the supine, prone and both decubitus positions and confirmed that at 1g, mean end-expiratory pericardial pressure varied directly with the vertical height of the recording site in the thorax. Measurements of pleural and pericardial pressures simultaneously, proved that transmural pericardial pressure was 0 at all levels of acceleration between 1 and 7g. Transmural left and right atrial pressures were independent of the height of the recording site in the chest and were unchanged during transverse acceleration, but slightly changed by vertical acceleration because of change in the weight of the heart. The conclusions that they reached were that the pericardial fluid is present as a thin film in all regions of the pericardial space and hence that pericardial pressure is transmitted throughout the space. In that respect the heart is inside a perfectly balanced and well suspended hydrostatic system.

2.3.5 Summary.

The present section attempted to highlight some aspects of the pericardial mechanics. Pericardium in general restricts excessive dilatation of the heart. Related to this topic is the ventricular interaction induced by the tissue through a regulation of right-left stroke volume outputs leading to a balanced cardiac action. Increased cardiac efficiency may also be achieved by an even spread of the gravitational forces around the heart where despite the hydrostatic differences equal transmural pressures at all hydrostatic levels of the cardiac chambers assist maximal cardiac efficiency. It is a significant point to note that absolute intracardiac pressures are not

that important and they should be substituted by transmural pressures in examinations of the myocardial wall or the pericardial membrane. It was also significant that the transpericardial pressure varies considerably from site to site. This means that the requirements imposed on the mechanics of the tissue vary at sites and this may reflect on a regional heterogeneity of the mechanical properties of the tissue.

When examining the position and inclination of the heart in the thorax it was stressed that different body postures should make difficult for results of mechanical tests of the tissue of one species to be in general valid to the rest of the species. This was due the different suspensive needs imposed on each of these tissues. The physiological and hydrostatic considerations of the last section showed that it is likely for regional variations in thickness, composition and mechanical properties to exist even in the pericardial membrane of one animal. An early conclusion which provided a guideline for the present study was that examination of the properties of the isolated native bovine pericardial tissue should only proceed after a detailed mapping and examination of the tissue morphology.

2.4 SHAPE OF HEART AND PERICARDIUM

2.4.1 Introduction.

In an examination of the pericardial shape and morphology it is necessary to find not only the pericardial attachments and reference points on the tissue but the relative position of all references to the enclosed heart. This may enable the specific properties of different sites on the tissue to be related to the activities of the underlying myocardium. Although the heart moves freely inside the sac it is feasible to identify an area in the pericardium and the equivalent one on heart.

The pericardium is a curved sac and when excised and laid flat it wrinkles as a result of its initial shape. If the whole sac is inflated, it assumes more or less a spherical shape and this is known from the very first references(Barnard,1898). It is reasonable though to assume that the natural shape of the tissue more closely resembles that of the heart than of any geometric object. That is true over those areas, atria-ventricles, where the tissue is in continuous contact to the myocardium and follows its motion, while where the recesses and sinuses exist no accurate prediction on the pericardial shape can be made.

2.4.2 Methods.

There are numerous ways in which the cardiac shape has been examined to provide a dimensional analysis of the heart. Sandler(1970) presented an extensive review of all methods employed to examine heart's geometry but they primarily measure the inside atrial-ventricular dimensions in either animals or man. Even in those studies simplified geometrical shapes are adopted, i.e a sphere, a cylinder or an ellipsoid.

Plastic or silastic models of the chambers have been used along with other methods to calculate the volume enclosed by the myocardium. The image contrast and the definition of chamber margins are absolute in casts or models and thus possess advantages over other techniques like biplane radio-opaque images. Radio-opaque images have the advantage of giving in-vivo information but they are inaccurate in defining the borders of various structures.

Techniques for rapid fixation of the heart of dogs have been employed to permit analysis of heart dimensions in systole or diastole by Ross et al(1967). With rapid fixation the heart is arrested in the various configurations but two factors should be considered: a)the

alterations on the myocardial dimensions that are introduced by the fixation itself and b)the rigidity of the final fixed heart tissue which must be of some value to sustain any further treatment or measurements of dimensions. The fact that someone ends-up with a solid structure in either the shape of the fixed heart or any other casts that can be subsequently made of it, has the benefit that any sort of data can be produced by measuring an object which does not alter in time, can be rotated, handled with ease and kept (stored) somewhere for any later measurements. Indeed, if the circumference or the cardiac diameter are under examination today, then the curvatures or the shape can be the interest of tomorrow and the cast is always there to meet the new requirements.

The surface of a cast is accurately described only by an infinite number of points and inevitably some information is lost when the surface is digitised. Janicki et al(1981), cast the inside and outside of hearts by using plastic or gelatin media. The former a polymeric compound hardens with time, while the latter is refrigerated to become solid. The same medium was applied on both surfaces and thus a gradient of hydrostatic forces on the wall was avoided but still the lower parts are expected to be compressed slightly due to forces exerted on both sides. Transverse sections normal to the long axis of the final cast were made and of course the thickness of the slices determines the amount of data lost in at least one of the dimensions. The thickness of the slices is limited by the medium which was used for the cast since it may be brittle below a certain limit. As in histological sections there is a small geometric distortion which is less the better the mounting medium is. The distortion is a slight compression in the direction that the knife of the milling machine travels and this distortion can significantly

impair the 3-Dimensional data. A detailed 3-D analysis of the heart is easier nowadays with the recent advances in computer techniques and their powerful graphics capabilities. The advantages that the 3-D data stored in a computer offers in studying cardiac morphology can be obliterated by inadequate histologic or preparation techniques while making the actual cast of the heart.

2.4.3 Preparation Of A Cast.

Our main interest was focussed on the outside of the myocardial surface. The pericardial membrane used in valves originates from cattle 18 to 30 months in age. Both heart and pericardial tissue vary in size and thus instead of a series of casts a single heart of a mean size was chosen. The size was close to the one most usually encountered and it was thought to be a good representative of the whole population. The upper and lower limits have been considered so that the deviation of any parameters measured can be predicted from this single sample. The heart was supplied by the local abattoir which supplied the pericardial membranes as well. It was put in saline solution after excision and it was cleaned from the quantities of blood contained in its chambers. The blood contained in the coronary circulation and the myocardium itself has not been exsanguinated by exerting any mechanical means but it was let to drain by naturally dissolving in the storing solution. The saline solution filled the chambers and surrounded the heart itself. The heart was removed from the animal after death and it was flaccid enough to allow the shape of the surface to alter due to external forces. Therefore the heart was carefully handled and not subjected to any kind of mechanical violence.

The conditions of death should also be considered because nervous stimulation of the myocardium could arrest the heart in a contracted

form. The administration of drugs or other chemicals in blood can affect the shape. The absence of the surrounding structures supporting the heart in life can also result in post mortem distortions. In a personal communication Dr.J.McGregor stated that his own belief is that a heart removed from the thorax is most unlikely to depict any real in-vivo situation. From the very moment that one opens the chest the position of various organs changes immediately. It is quite different if the animal is exsanguinated or killed instantly by a shot. The thorax appears different if during dissection the intestines are removed before or after the contents of the thorax. In fact the ideal would be an instant fixation of the heart in-situ followed by removal from the thorax.

In absence of any satisfactory technique we took some minimal precautions to preserve natural shape and conditions. The pericardium was kept intact until the heart was brought to the rigor mortis condition. It was thought that the membrane which helps to restrain the heart in-vivo would also protect it from minor injuries during the preparation. The heart was immersed inside a saline bath and as soon as it stiffened, due to rigor mortis, it was taken from the bath and the pericardium was excised at a level around the atria. The heart was suspended from the major vessels. The great vessels had been cannulated and gripped around their circumference, while a number of skewers had been passed through numerous points of the vessels and the piece of pericardium still present in order to distribute the load in a greater area. The heart was rigid enough to sustain the gravitational forces applied to the myocardium at the time. It was then put in deep freeze for 24 hours to further reinforce the stiffness of the tissue. It was thought that the frozen heart could easily sustain any hydrostatic forces arising from a medium used on

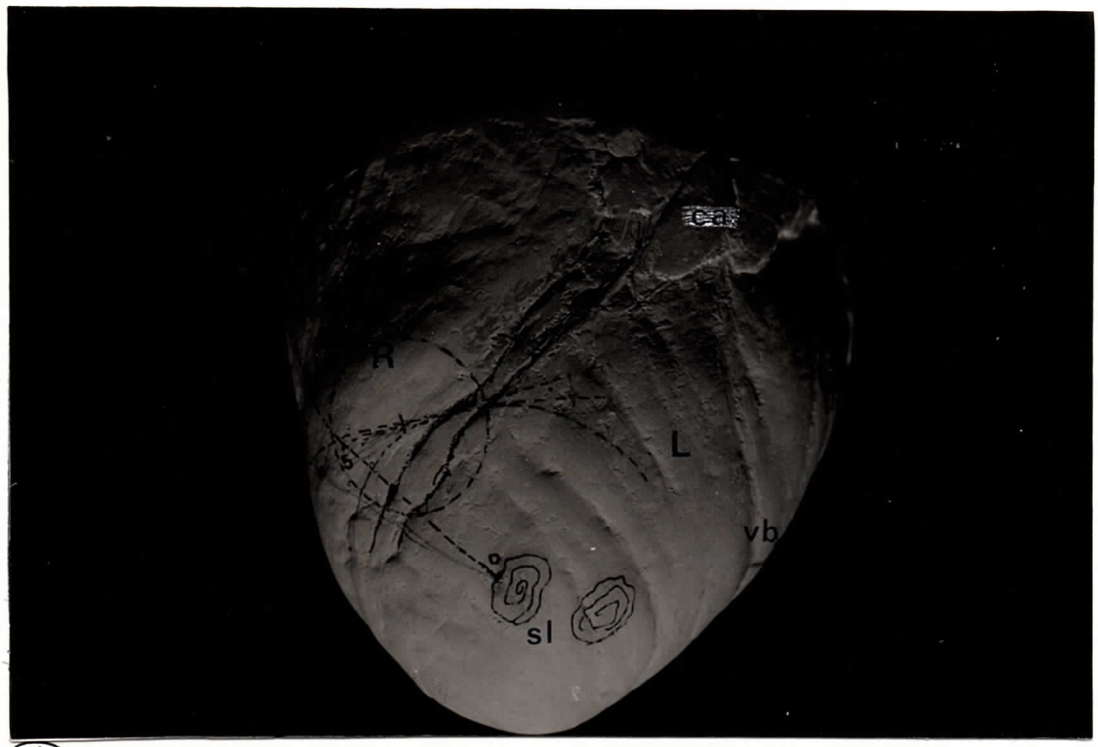

A

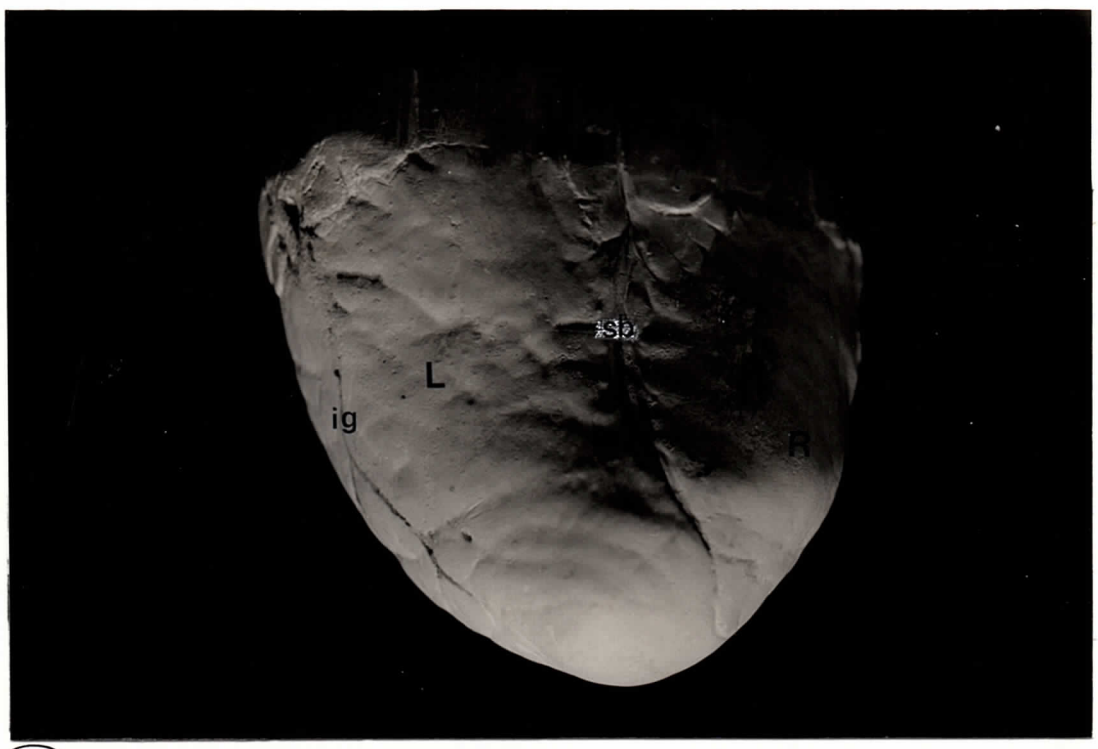

B

Figure 2.9:Two aspects of the cast, A)anterior view, B)posterior view, R:right ventricle, L:left ventricle, v.b:left ventricular border, c.a:conus arteriosus, i.g:intermediate caudal groove, s.l:sternopericardial ligaments, s.b:subsinusoidal intermediate branch.

the outside to produce the female cast. The medium was a diluted plaster solution of which the temperature had been lowered to less than 10°C to bring it closer to the temperature of the frozen heart. The heart was placed upright in a container large enough to accommodate it without any contact of the heart to the container's walls. The heart was again suspended from the major vessels. The container was filled with the plaster solution which took 60min to solidify. The frozen heart was covered with a thin icy layer which upon thawing was incorporated to the watery plaster solution and thus a precise mould of the myocardial surface was produced. Until the time that the plaster had set the container with the heart and the solution was kept at a low temperature to avoid a premature thawing of the frozen heart. When the plaster had set, the heart was pulled from the container and subsequently disposed of. The female cast produced was used to produce a male one which corresponded to the actual shape of the heart itself. It was sent to the Dental Hospital in Glasgow where it was filled with dental stone. The stiffness of the stone is much higher than that of the plaster that surrounded it. With a small hammer we carefully cracked the plaster cast which is relatively brittle if compared to the dental stone.

In fig.2.9 two aspects of the cast are shown. The various regions are identified in the captions and they should be compared to the two figures coming from an atlas of animal anatomy as given by Ghoshal(1975) in fig.2.10. He mentioned that if compared to the equine heart which is very popular with the veterinarian anatomists, bovine heart is a little longer, covered with more fat and somewhat more rounded. The left ventricular border, as in fig.2.9a, lies opposite the fifth intercostal space, in-vivo, it is almost vertical and slightly concave.

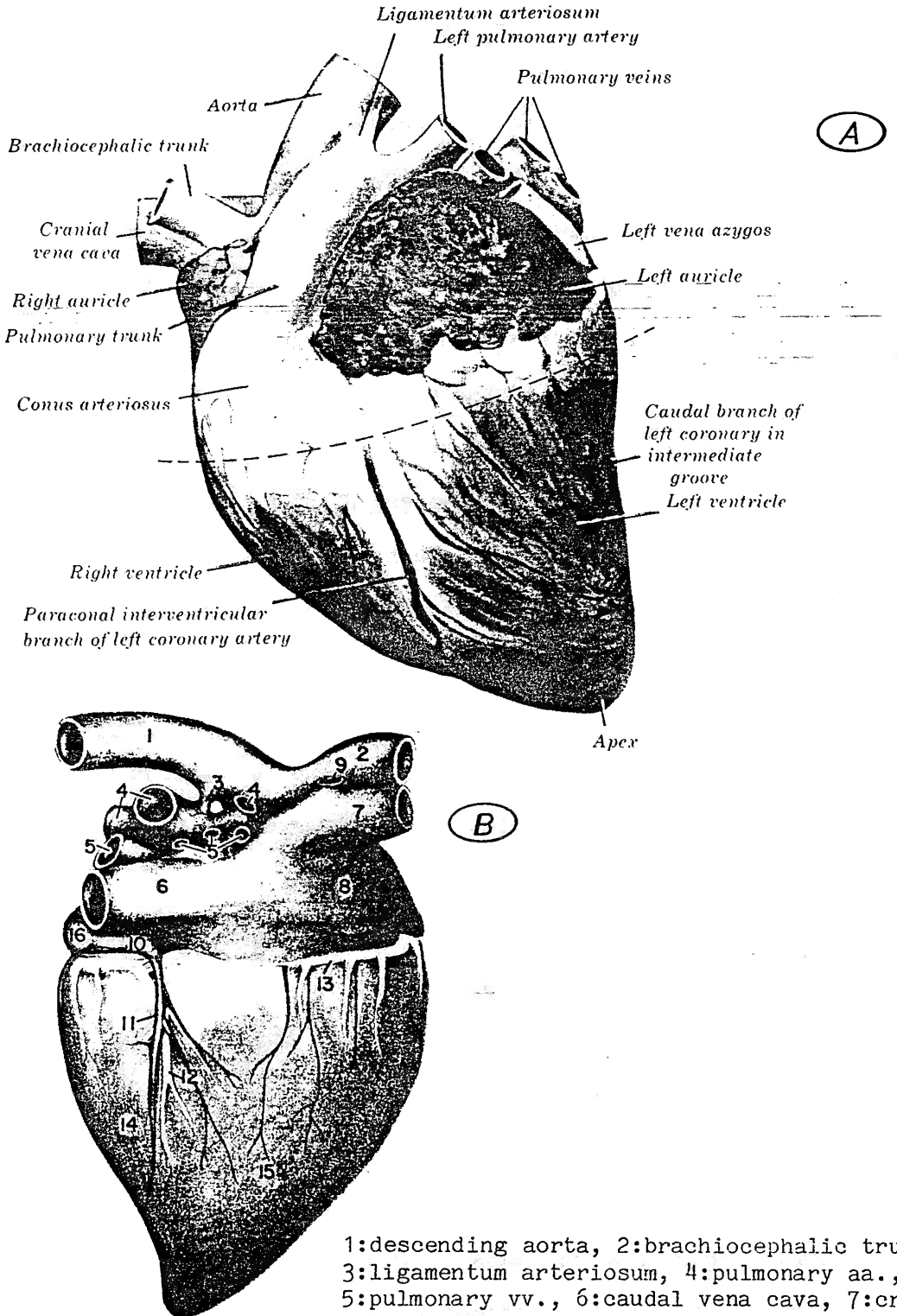

1:descending aorta, 2:brachiocephalic trunk, 3:ligamentum arteriosum, 4:pulmonary aa., 5:pulmonary vv., 6:caudal vena cava, 7:cranial vena cava, 8:right atrium, 9:right vena azygos, 10:coronary sinus, 11:middle cardiac v., 12:subsinuosal interventricular branch, 13:right coronary a., 14:left ventricle, 15:right ventricle, 16:great cardiac v.

Figure 2.10:A)the bovine heart in a cephalad view, B)the bovine heart in a right caudal view (reproduced from Sisson and Grossman,1975).

The cast has been made to a level below the auricles which are mostly covered with fat. The lower part of the conus arteriosus can be seen in the anterior views of both the cast and the figure of the bovine heart. The dashed line in fig.2.10a shows up to what level the cast has been made. The left auricle is larger than the right and the left ventricle was more cylindrical than the right ventricle. The ventricular part is more regularly conical and more pointed while the top is rounded as it looks in fig.2.10a. The pericardial area below the auricles is the one that is relatively conical and of more uniform thickness and thus useful for valve-production. At the top of the heart where the tissue wraps around the vessels it is much thicker and thus of no further use.

There was great similarity between the cast and fig.2.10a suggesting that the cast had succeeded in reproducing the shape of the heart without obvious distortions. Fig.2.10b presents a drawing of a view of a bovine heart and appears more pointed at the apex. I believe that this is a result of a not very succesful drawing since we could not reproduce such a figure by looking at the cast from any view.

The area of the sternopericardial ligaments is drawn on the anterior surface of the cast. As the heart is free to move inside the pericardial sac they can be placed right-left or up-down respectively to this place on the cast. They have been drawn next to each other but this is not always the case. In other species they are placed one below the other and thus connecting the membrane with upper and lower parts of the sternum.

In the left ventricular area and to the posterior there is a shallow so-called intermediate or caudal groove which descends from the coronary groove ventrally to the left side of the left ventricular

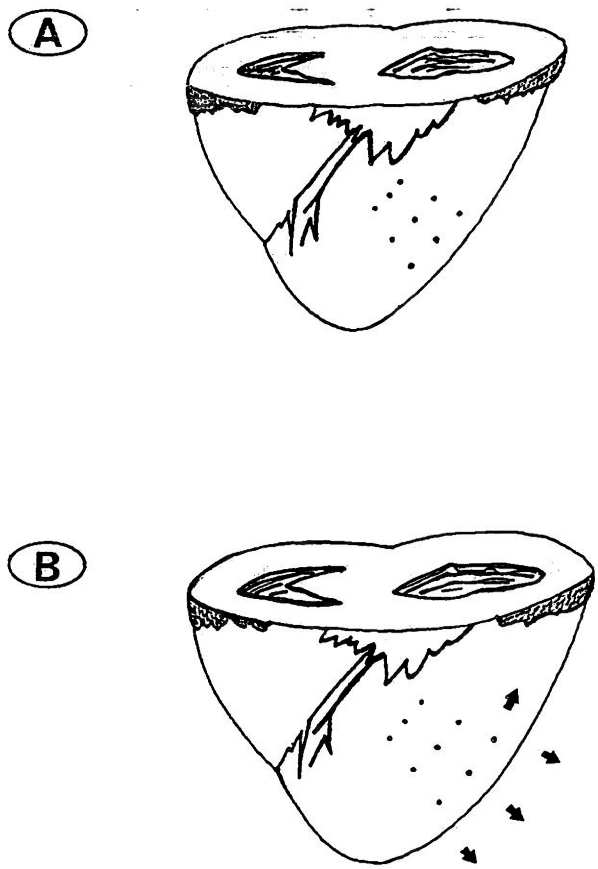

Figure 2.11:A drawing of the heart in systole (A) and diastole (B) based on the findings of Ingels et al,1971, to depict motion of epicardial markers. It is an anterior view of a heart 20% increased in diastole drawn in a manner comparable to the views of our cast. The maximum shortening hapeens along the lines of the markers normally to the left descending coronary artery originating from the conus arteriosus.

border but not reaching the apex. In fig.2.9b which is a caudal view of the heart the intermediate groove is marked on the left side. The subsinusoidal intermediate branch is present in either fig.2.9b or fig.2.10b. It lies almost in the middle of the posterior surface of the heart and descends to the right border and 2-3cm above the apex. This probably reflects the internal geometry and shape of the ventricles. As Janicki et al(1981) found in sectioning their casts of human hearts the ventricles originate at different heights from the apex, the left ventricle only 0.9cm from the apex and the right ventricle 2.6cm from the apex.

But there is more information in what meets the eye, like those foldings or wrinkles on the left ventricle. They look like originating from the paraconal interventricular branch of the left coronary artery and running circumferentially to the left ventricle. They are apparently related to the myocardium since they were aligned to shades of the smooth cardiac muscle, possibly related to the variably orientated myocardial fibres (Fenton et al(1978)). Ingels et al(1971) carried out stereo-photogrammetric studies on the dynamic geometry of the left ventricular epicardium and showed that at least the upper layers of the myocardium shorten maximally at right angles to the descending left coronary artery. The maximum shortening happens in the mid base-apex region and towards the left ventricular border. With those findings an anisotropic asymmetric model was supported for normal ventricular systole in which all points on the lateral free wall move towards to each other while simultaneously pivoting about a point near the apex moving towards a relatively fixed septum as in fig.2.11. What is also apparent from fig.2.11 is that because of the particular geometry of the ventricles, where the left one is shaped in an ellipsoidal form while the right one wraps around

the left, the epicardial area overlying the right ventricle is larger than the area over the left ventricle. This reflects on the pericardium of which more of the surface covers right ventricular area than left ventricular area and despite the fact that the apex is included in the left ventricle.

The rest of the lines drawn on the cast and shown in the anterior view are related to testing sites on the pericardial membrane and they will be clarified when the preparation of the pericardial sac is described. The dashed line starting from the left of the sternopericardial ligaments is ascending towards the inferior vena cava where the pericardium forms what previously has been called "foramen quadrilaterum pericardii" and consists the first of the reference lines we have established on the tissue and the cast.

2.5 ISOLATED PERICARDIAL MEMBRANE.

2.5.1 Introduction.

The main interest of the present study was on the mechanical properties of the isolated native bovine pericardial tissue. The pericardial membranes for the research reported in this thesis have been kindly supplied by Dr.J.Fisher of the Dept. of Cardiac Surgery-Glasgow Royal Infirmary who was simultaneously working on the design and development of an improved pericardial valve bioprosthesis. Fisher(1986) followed a standard procedure of excising the tissue and preparing the pericardial membrane in respect to some reference points. This standardised preparation is being followed by the company (Biomedical Systems,Ltd) which currently manufactures 200-300 BIO-FLO valves a year. Fisher(1986) used pericardial patches coming from suitable sites on the membrane to prepare the leaflets of the bioprosthetic valves. Although the design of a new supporting frame and the leaflet geometry were his main concern, the properties of the

leaflet material in use could make all the difference between a successful and an unsuccessful bioprosthetic valve.

Some of these membranes, randomly selected, were supplying on a regular weekly basis our research work for a 2 years period and thus our knowledge on the properties of the fresh tissue was going alongside the development of the valve. The need soon became clear for establishing particular standardised measures for identifying our testing sites and exchange information. Only if the same consistency that existed along the research and development in the laboratory is kept on an industrial basis, is it possible that a)the design performs as well in practice and b)our results on the fresh tissue be applicable in life.

Because of the valve-construction related interest we concentrated our efforts on those sites of the pericardial membrane most likely to be used for making valves. It was the ambition of this research work that the results on the isolated pericardium can produce a better understanding of the mechanics of collagenous tissues, be usefully incorporated in the construction of a better bioprosthetic valve and enlighten the contribution of the tissue in cardiac mechanics in general.

2.5.2 Preparation Of A Pericardial Membrane.

2.5.2.1 Origin. Pericardial sacs are obtained from beef cattle aged between 12 to 36 months old.

2.5.2.2 Excision. The cattle heart was removed from the thorax with the lungs. In doing so the pericardial ligaments, the various rather weak and irregular attachments to the pleura and the collagenous condensations joining the pericardium to the diaphragm had to be cut. The heart with the pericardium was separated from the other tissues by cutting the major vessels and was stored in

Figure 2.12

physiological saline solution until it reached the laboratory. The tissue was then dissected around the top of the heart circumferentially and adjacent to the major vessels. The pericardial membrane in the form of a conical sac was freed from the heart. It was cut down the posterior surface (as in relation to the heart) along the middle cardiac vein and interventricular branch and between the two flaps or rows of collagenous condensations which joined the tissue to the diaphragm. The dissection continued around the apex and infront, up to the two sternopericardial ligaments existing low in the anterior surface of the heart.

This procedure allowed the otherwise conical membrane to be laid out flat on an illuminating box. Larger or smaller amounts of fat were carefully removed and the tissue was left with its epipericardial surface looking upwards and the thin layer of mesothelial cells facing the illuminating box. The tissue is white and translucent and thus transillumination helps during this cleaning procedure. The tissue was kept moist with physiological saline, and thus the illuminating box had to be adequately waterproof.

The membrane then looked as in fig.2.12 with wrinkles at various sites because its natural shape is not flat. Areas of greater curvature wrinkled more than others and the curvature was supposed to vary not only with the site but with direction as well.

Variations in thickness create shades in various sites and thus thicker and therefore darker areas are easily identified. Two bands of thicker tissue extend over the anterior surface from the two sternopericardial ligaments to the perimetry.

2.5.2.3 Mapping. Although biological variability is accepted for all tissues, some kind of standardisation to a flat configuration as in fig.2.12 is always feasible to the extent that certain sites can be

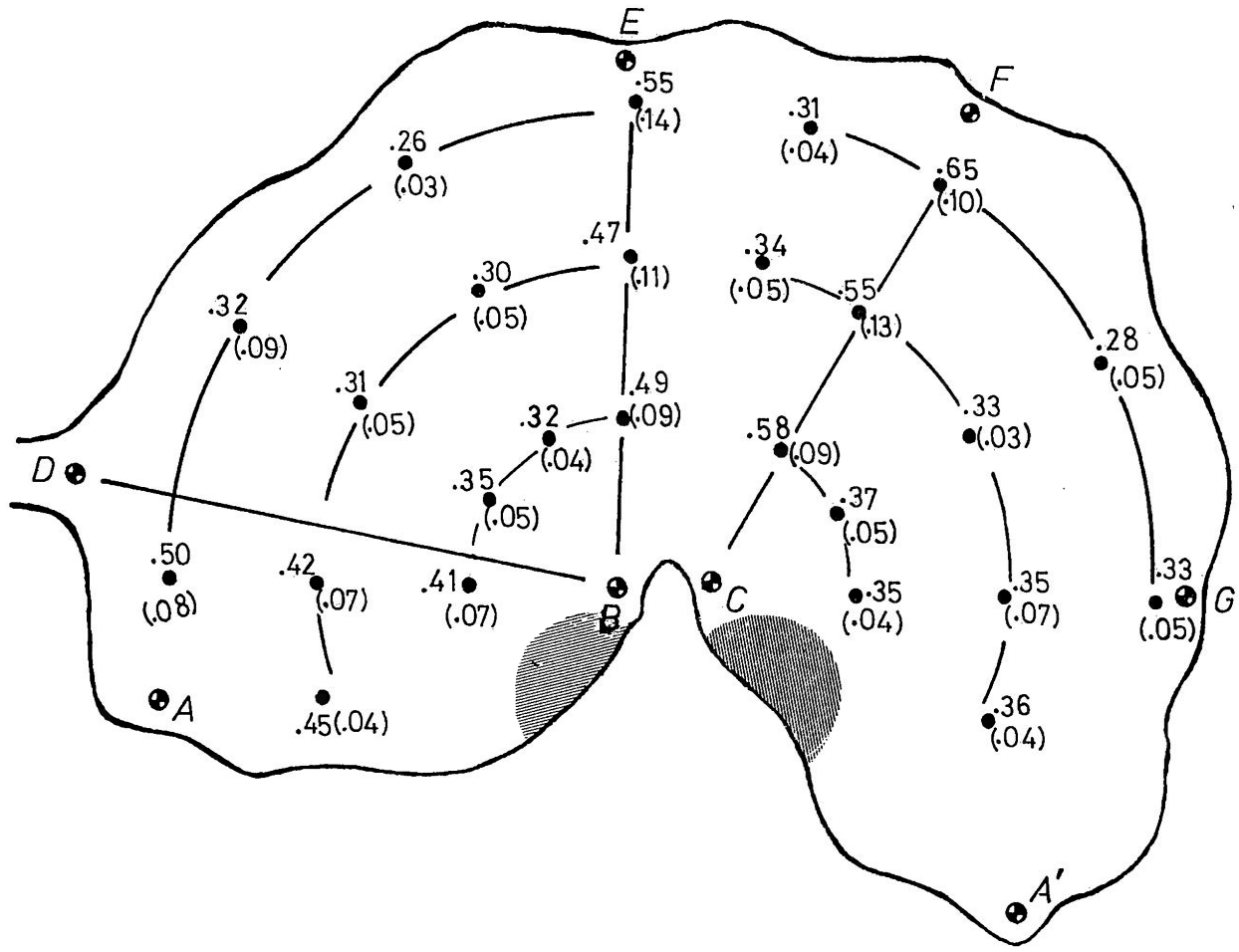

Figure 2.13:Thickness values at 25 points of 10 pericardial membranes excised according to the description in the text. Mean values are given and their standard devations in brackets(reproduced from Fisher,1986).

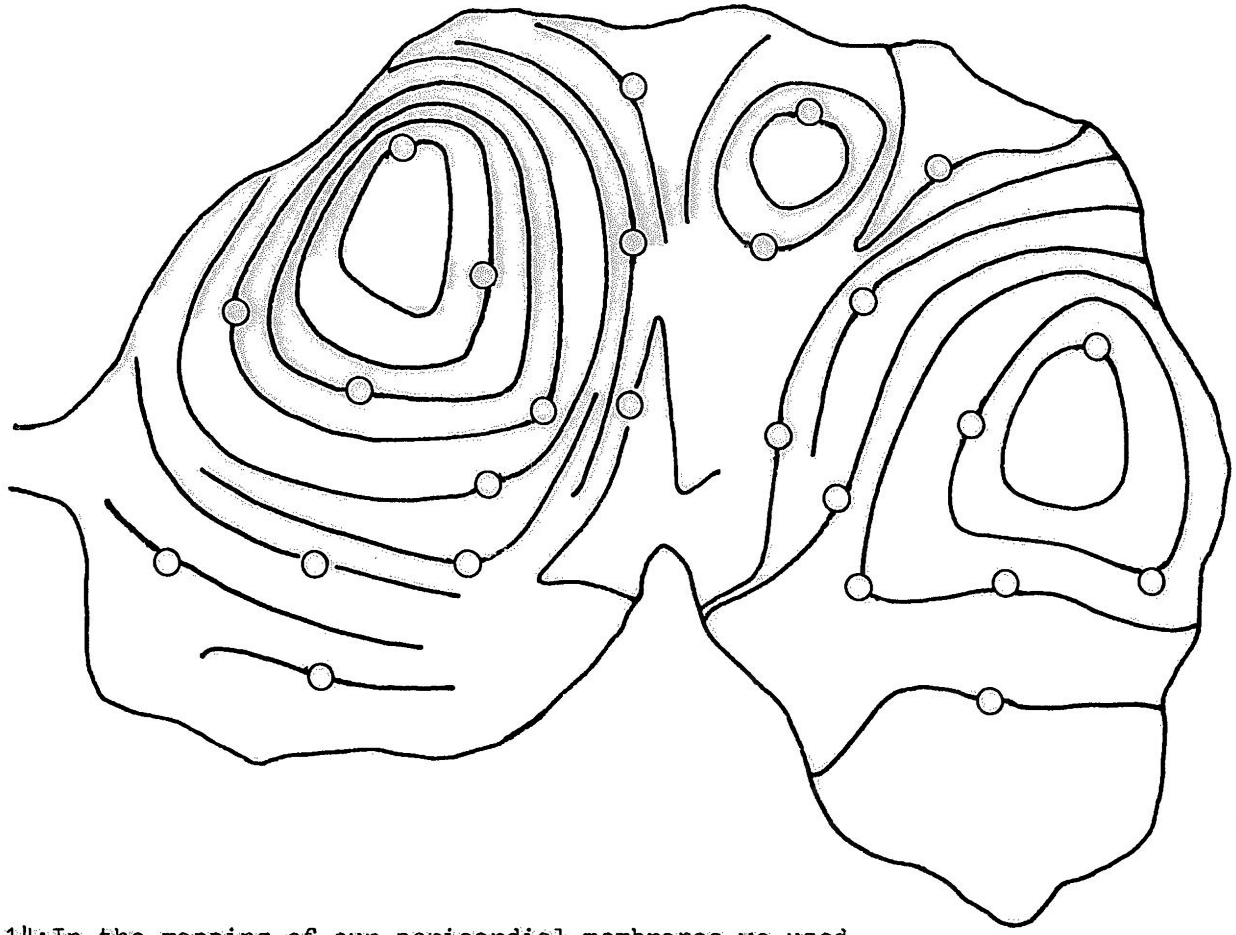

Figure 2.14:In the mapping of our pericardial membranes we used isothickness lines to demonstrate thickness variations. They consist a more comprehensive means of mapping the thickness of the membrane.

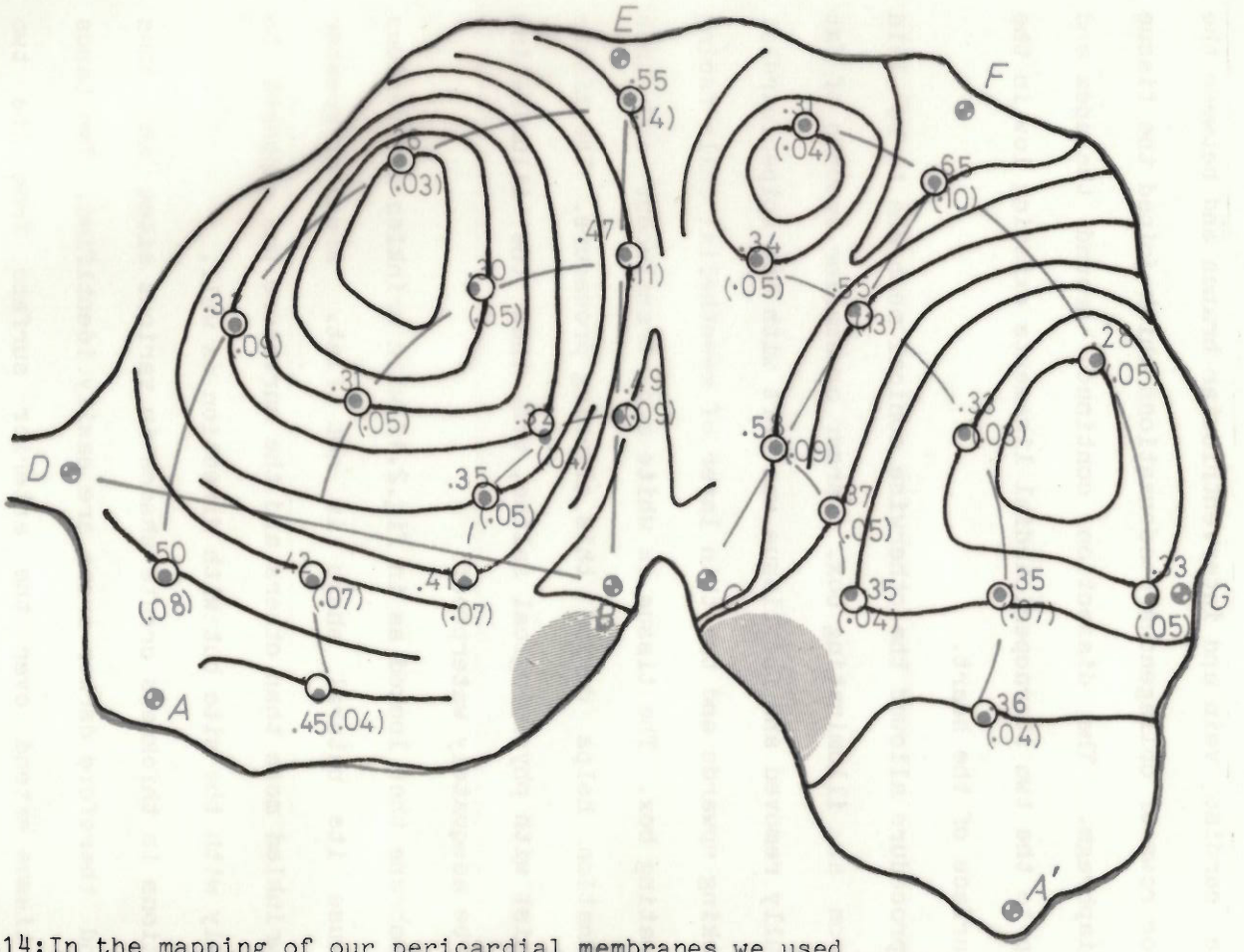

Figure 2.14:In the mapping of our pericardial membranes we used isothickness lines to demonstrate thickness variations. They consist a more comprehensive means of mapping the thickness of the membrane.

positively and accurately identified each time.

In fig.2.13 the two sternopericardial ligaments are in the middle at points B,C. A and A´ are points originally close to each other, before the excision in the posterior surface is done. This excision starts at AA´ and goes along lines AB and A´C which if they are brought together reconstruct the conical membrane with an apex in the dotted area near B, C.

Point D is at the ring formed around the inferior vena cava and the line BD is our first reference line on the tissue. The length of the line varies with the size of the animal, with the point D placed on the ring, even with the configuration of the membrane and the way it is let to lay flat on the illuminating box. The line BD was usually between 15 and 17cm in length very close to the 17cm value of the distance between the coronary groove and the apex for an adult ox as given by Ghoshal(1975). Points E, F, G, are placed at thicker areas associated with major vessels on the top of the heart and can be easily found by anyone following the same procedure. The other two reference lines are along the thick bands in the anterior surface BE and CF. They are believed to lie left and right of the conus arteriosus respectively. In respect to the thorax, the right anterior band (CF) runs parallel to the left 3rd rib, while the 3rd right rib passes obliquely to the left of the left anterior band (BE).

As mentioned before the area of the pericardium over the left ventricle is smaller than the right pericardial ventricular area. Right ventricular pericardium is between lines AB and CF while the rest between CF and AC is over the left ventricle. The dotted area of the apex should be included to the left ventricle.

Thickness varies significantly from site to site. By measuring thickness values at 25 points in 10 membranes Fisher(1986) produced a

mean value of thickness with a standard deviation for each of those 25 points. He chose to measure thickness at points radially emanating from the ligaments and at a particular radial distances along these directions. We made similar measurements which are in close agreement to these values since the pericardial sacs were of the same origin (same population). We both used Mitutoyo thickness gauges with 1cm in diameter pads. The reading on the gauge varies with time as the tissue is slightly compressed by the small spring pressure of the gauge. For this reason we kept the reading that occured after an initial 5s relaxation period. If this rule is not kept different experimenters obtain different results despite the fact that everything else is identical. Instead of presenting our measurements at points we prefer to draw isothickness lines on the map of the sac. They appear to form a more comprehensive manner of expressing the thickness variations and we are helped in drawing them by the amount of light passing through the tissue on the illuminating box. In fig.2.14 on a tracing paper we have drawn what the case would be like for fig.2.13 if the isothickness lines had been used. Points on fig.2.13 underneath label the thickness for each of the lines.
It is obvious that the reference lines BD, BE, CF lie on thicker tissue. The relatively thin area between BD and BE is on the right ventricle. The area between CF and CA′ is on the right ventricle.

There is a strange connection of the isothickness lines and the curvature of the tissue. It is easy to appreciate in fig.2.14 that the shape of the heart especially of the ventricles is somehow depicted by the lines. I have no clear opinion why that is so but it could be suggested that variations on thickness have something to do with the thickness and strength of the underlying myocardium. As Shabetai(1981) mentioned pericardial thickness was inversely

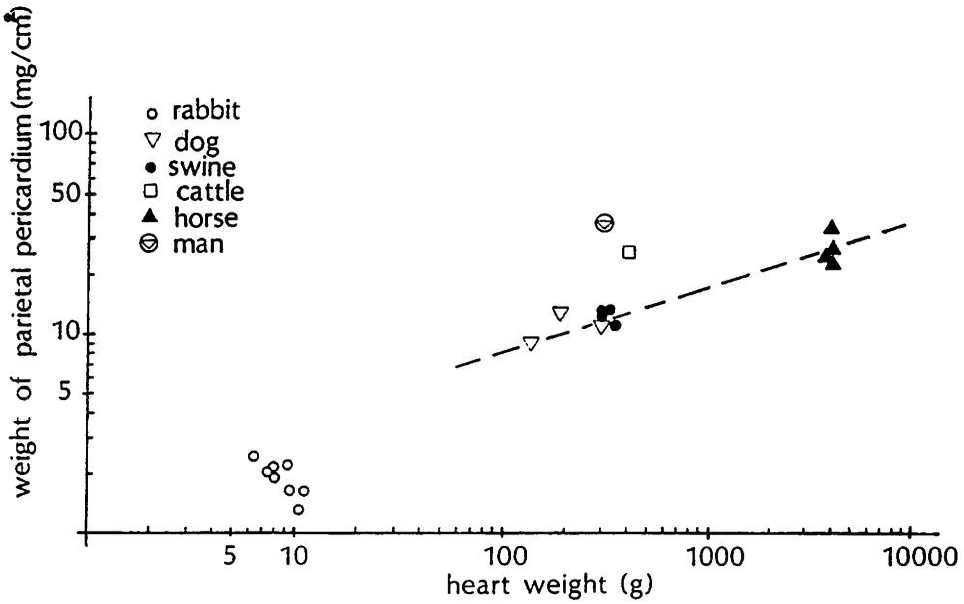

Figure 2.15:The relation of the weight of the parietal pericardium to the heart weight for various mammals has been described by a linear relationship by Hort and Braun(1962).

proportional to the underlying cardiac wall thickness in order to assist thinner areas which are under stress.

When examining the mean thicknesses of pericardia of various species there is a general relation between pericardial thickness and the size of the heart for the various mammals found in the studies by Hort and Braun(1962). The pericardial surface, as calculated by planimetry, has a relation to heart weight approximately: Pericardial Surface=kHeart Weight$^{2/3}$, (k=constant). The heart weight is a function of body weight for mammals: Heart Weight=4.4Body Weight, heart weight in grams and body weight in kilograms. The pericardial surface is proportional to overall body weight but the same happens with the pericardial thickness. Laplace law is: T=P(R/2), for a sphere of radius R and where T:wall tension, P:pressure. The smaller the animal, the smaller the radius of curvature, while the pressure is approximately the same for different species and thus larger animals are expected to have thicker pericardia. This is shown in fig.2.15 where the cattle pericardium is on the open circle and the human appears to be advantageous to other species being stronger to the rest of mammalian pericardia.

2.5.2.4 Testing sites. Our mechanical tests on the fresh tissue described in subsequent chapters were undertaken on tissue specimens from 3 sites on the pericardial sac. The choice of the sites was made on thickness considerations and those are related to the manufacture of valve leaflets. For the manufacture of a leaflet a piece of tissue of 7-8cm and of nearly uniform thickness is needed. Several sites on the tissue could comply with these requirements but the leaflets should also have a thickness in the range of 0.30-0.50mm. Thinner or thicker leaflets are not suitable for making a valve. With those conditions only 3-4 sites on the sac are available and they are shown

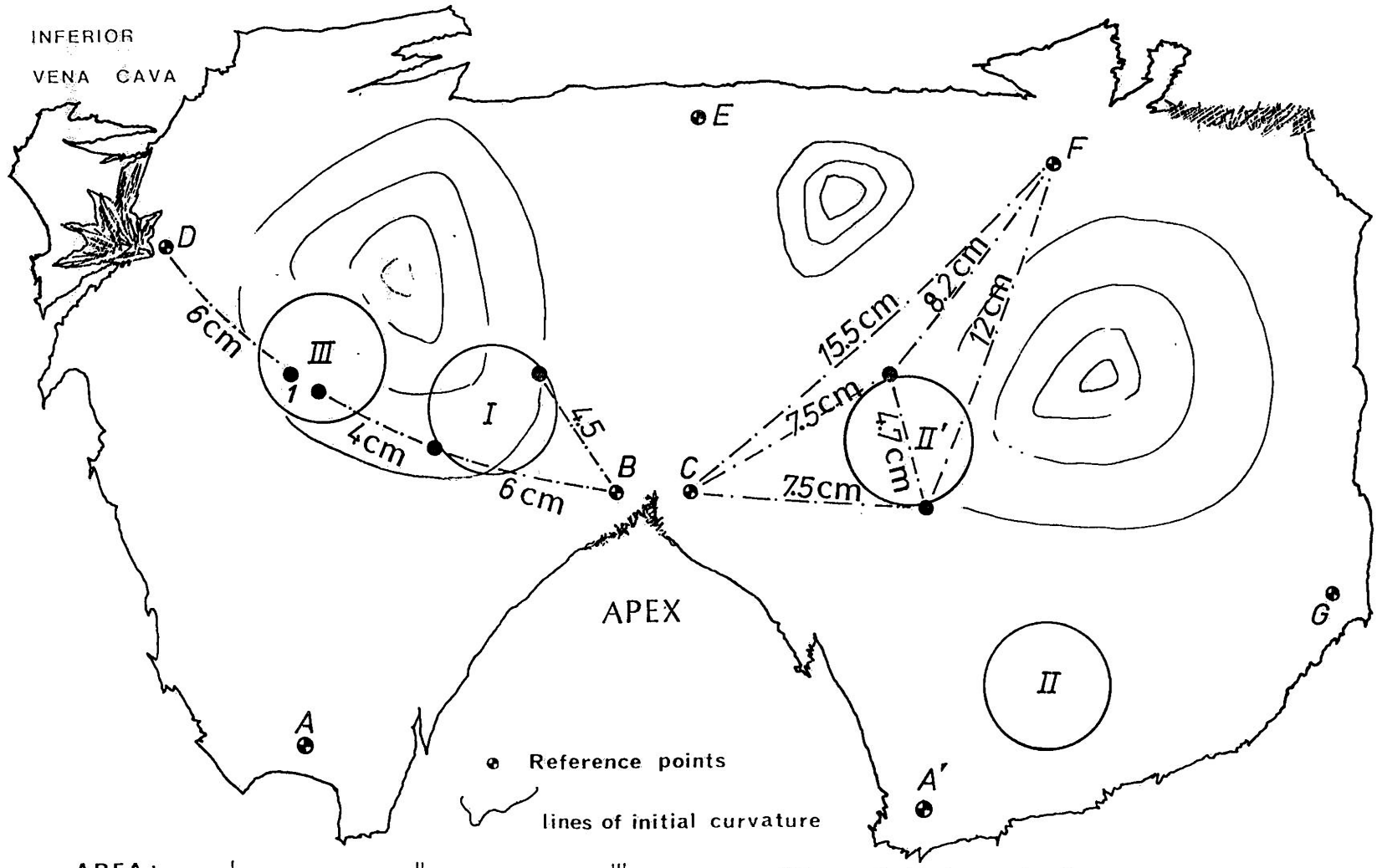

Figure 2.16:An excised pericardial membrane with its reference points A-G and the testing sites I-III.

in fig.2.16 as I,II,II′,III. The distances to various reference points are noted as well. Those distances have to be normalised by using the fraction of the BD distance of any other membrane to the BD distance of this particular sac in fig.2.16

For every membrane a map in the actual size of the sac has been drawn including the isothickness lines. Preparation of the testing samples themselves for each of the mechanical test will be described before the mechanical test in particular, in the following chapters.

2.5.3 Summary.

Biological tissues are not provided in bulk form. They originate from animal species, they have a shape and form, they perform some functions and they usually have a complex structure equivalent only to the most sophisticated of the human designs.

I felt that it was appropriate those relevant topics regarding pericardial anatomy, structure and functions to precede the work that I did on the same topics. The requirements for new information have been brought by the new needs regarding the use of the tissue for the construction of bioprosthetic valves. Some of the information is sought because of the examining procedure itself, i.e.geometry directly affects the results of the mechanical tests.

Pericardial morphology was the first to suggest that the tissue was suitable for manufacture of valve leaflets. It is collagenous like the natural valve tissue and of comparable thickness.

The mechanical properties of the tissue determine the behaviour of the tissue under stress and are examined in the following chapters. Uniformity in the mechanical properties, if present, means that those sites where thickness matches can be expected to behave similarly. If the tissue is anisotropic then mechanical behaviour should also vary with the direction at a particular site.

2.6 DISCUSSION.

This introductory chapter contains information on the shape of the tissue, the differences between pericardia of different species and their structure.

Most of the information included in the envelope of the pericardial functions is widely accepted but some is still under dispute especially where values are extrapolated on the basis of primary investigations not always performed within the same set of experiments by a group of workers. Some points will be brought up in the following chapters where it is relevant and useful to the research work presented in this thesis.

Subsequently and for the needs of our research we presented our own establishment of a set of reference points and a map of the pericardial membrane.

We should be already familiar with the i)the subject of this investigation, ii)aware of the possible variations between species, iii)a gross examination of the structure, iv)the general nature, why and how forces are transmitted by the tissue in-vivo, v)where the testing samples originate and the reason of such a selection.

CHAPTER 3

3.1 INTRODUCTION.

Structures, such as the pericardium discussed in the previous chapter, have a specific load-deformation behaviour. This depends both on the geometry of the structure and on the mechanical properties of the material of which it is made. In order to describe the mechanical properties of the material isolated from the structural effects, the intensive variables of stress and strain are used in place of load-deformation.

The mechanical behaviour of the parietal pericardium as a whole sac presented in the previous chapter was an investigation of the influence of the pericardium on heart function. These results are not amenable to rigorous analysis in order to determine (or characterize) the mechanical properties of the tissue.

The generalized Hooke's law relates the six independent components of the stress tensor to the six indepedent components of the strain tensor by a matrix of 36 stiffness constants. Certain symmetries reduce drastically the number of unknown constants. The determination of the remaining constants even for the simplest structures of the most conveniently elastic material requires a number of tests, each one dedicated to the determination of some of the constants and being complementary to the other tests, so that a combination of them can be adequate to fully examine the material.

Soft connective tissues may be examined, in principle, with the same techniques used for engineering materials but present additional difficulties. They have time-dependent properties (short term = viscoelasticity, long term = degradation, decay). They are very sensitive to the ambient conditions (temperature, presence or absence of water or electrolytes). The tissue mechanical behaviour presents

the same variability that appears between individuals in the animal kingdom. They also present regional heterogeneity or else spatial variability. The cases where one can have large samples of biological materials are rare. Tissues consist of various elements arranged to make a structure and the size and shape of the tested sample can interfere with the results. Most biological materials are fibrous or grain composites and thus the sample dimensions must be large enough to yield the macroscopic behaviour of a material which then can be seen as a continuum (the smaller the sample the more the constituent elements are distinguished from each other).

3.2 THE TESTING METHOD AND THE TESTED MATERIAL.

The internal structure and the interactions of the components in tissues are more complicated than any engineering man-made structure and thus their behaviour can be unpredictable and occasionally inexplicable. The tissues are usually of a composite nature but the simplified view of a "reinforcing" material and a "reinforced" structure is not easy to apply by assigning such roles to various components.

Tests for soft connective tissues because of the peculiarities arising from the nature of the materials, should be as simple as possible (sophisticated techniques complicate the problem itself). They must be easy to repeat and thus self consistent(the test itself should not change at all especially because the material shows such variability on its own). The appropriate test should be applied to a suitable material and thus the combination (test-material) should appear reliable and convincingly applicable. The test should yield those useful parameters sought and not be sensitive to uncontrollable factors. If the limits of either the method or the tissue are violated one may not be certain, when performing a test, if one tests

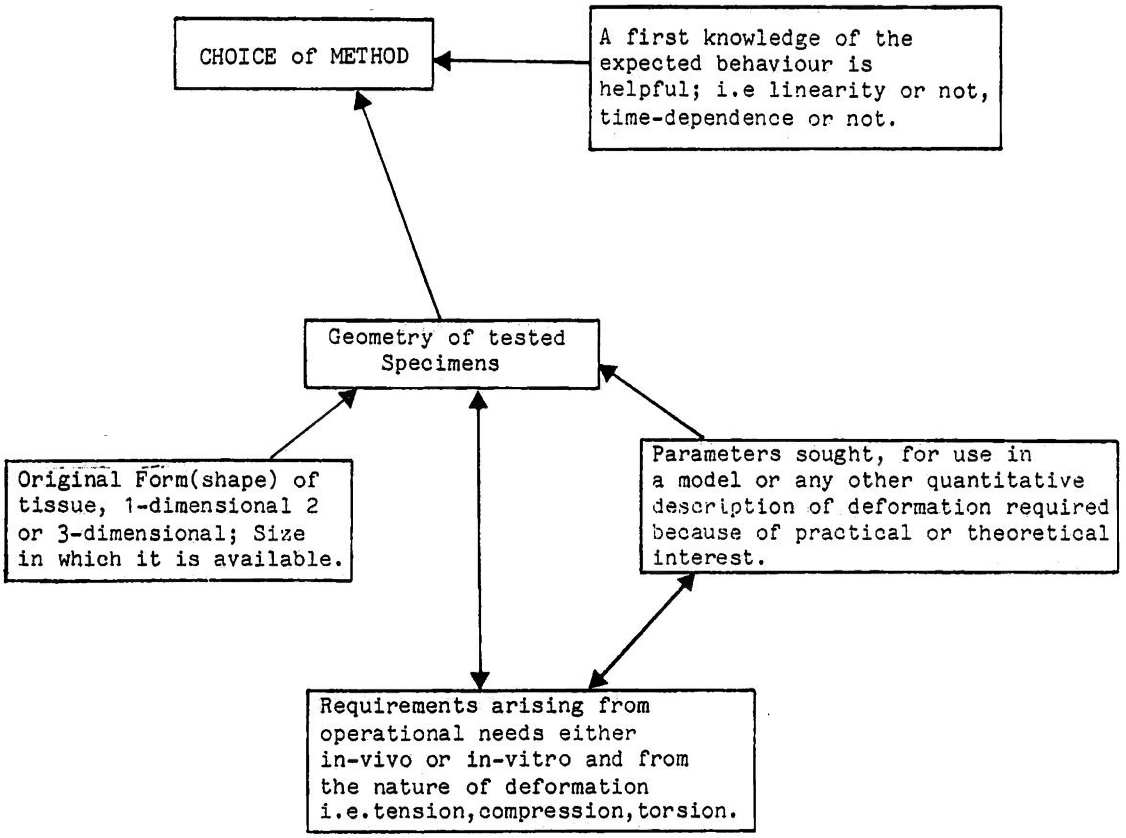

Figure 3.1:Suitability of a testing method. The arrows indicate the course of a decision making based on the considerations included in the blocks.

the specimen or the method and then one has just replaced a problem with another.

3.2.1 Choosing A Testing Method.

In tissue mechanics usually the questions "what are we looking for?" and "how are we going to achieve this?" are inevitably linked to each other. The network of figure3.1 presents various aspects to be considered when deciding about the suitability of a technique. What may seem strange is that the geometry of the specimen is placed as a main parameter in determining the testing mode. This is because tissues originally exist in one(tendons) or two(fasciae) dimensional forms and not in the bulk form of the engineering materials. The dimensions of the specimen as a number are usually equal or less than those of the tissue(string-like specimens or sheets can be prepared only from a 3-dimensional structure). Two dimensional tests can only be made on essentially one dimensional structures with the greatest difficulty. Options for testing methods are similarly affected. There is no point examining the properties of a tissue in compression when the tissue operates in a purely tensile mode in-vivo or in-vitro. Thus tests should yield data appropriate or applicable to the end use of the material. This is possible if the stress/strain (or load/deformation) environment in which the tissue will act can be defined. Those fine details like stress/strain levels, time scales are called the testing protocol. Specific interest in some parameter may exist for the use in further computational studies or in the quantification, which usually follows the tests, of the behaviour exhibited using various formulas. Similarly if behaviour in failure is to be studied a test appropriate for yielding those parameters has to be used.

3.2.2 The Ensemble Of Testing Modes.

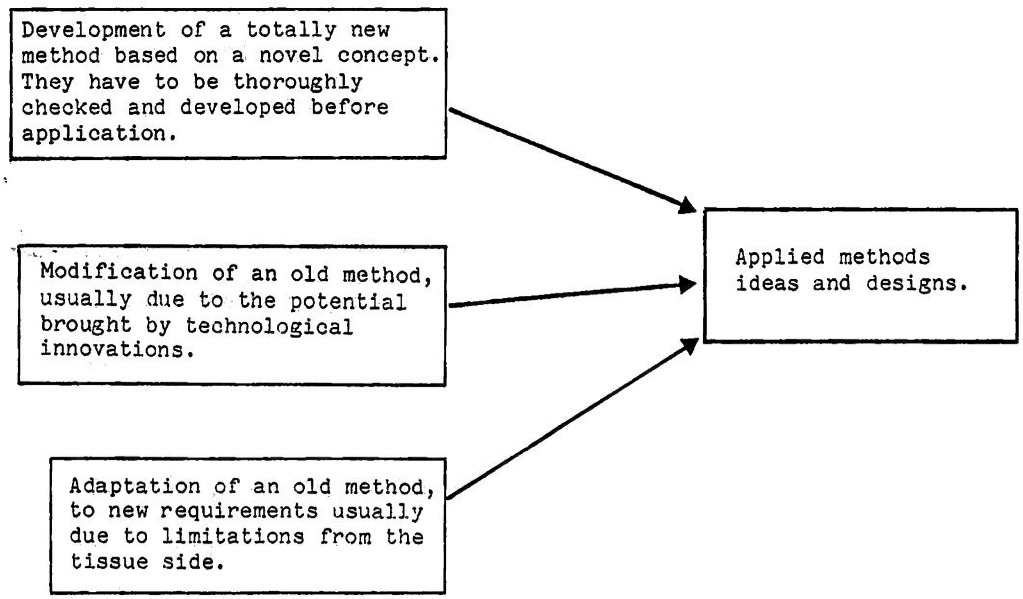

Figure 3.2:The Ensemble of testing modes needs to be constantly modernised in the study of biological materials.

In figure3.2 a network on the modes of mechanical tests is presented. All existing testing modes which have been proved useful in testing biological tissues constitute an envelope which can be expanded by novel ideas and be enriched by developments, modifications and adaptations of the existing modes. It is equally important for the science of biomechanics that those two fields (testing methods and tested materials) keep on moving ahead with fruitful ideas.

3.2.3 Testing Principles And Most Common Methods.

For solid-like materials, the specimen is clamped and in some appropriate way distorted at a controllable fashion while the load and displacement are both recorded. For measuring strains the relative position of the clamps is recorded or non-contacting methods in the form of optical extensometers are employed. The use of optical extensometers may be required when the deformation of either the whole field of strains or strain at a specific site on the sample is to be studied. They can be useful when the effect that the clamps themselves have on the deformation is to be avoided, then the strain of only the central area can be examined. For the stresses, forces may be recorded directly as they are transmitted to the clamps in contact with the tissue or indirectly by a stress parameter and geometrical information i.e.the pressure inside an inflated blood vessel and the dimensions of the vessel's walls yield the stress value.

Common testing methods vary from uniaxial to multiaxial approaches and from replications of in-vivo conditions to idealised and generalised tests.

The Uniaxial test is a standard method and it has improved from the early weight hanging on the strips to the modern tensile testing machines. Suitable candidates for this test have been found in

tendons, ligaments, strips of various membranes. Details such as the specimen's own weight, the weight of the clamps, the test-environment distinguish the various applications of the test which has been proved to be the most useful tool in tissue mechanics and reached significant standards of reproducibility and consistency. Uniaxial tests are important, but give limited information on the mechanical properties of the tissue as deformation in more than one dimension is required to fully examine the tissue behaviour. The analytical treatment of the results of such tests may be relatively easy and it is always qualitatively significant if a distinctive trend exists in the uniaxial load-deformation curves.

Multiaxial tests are more difficult to set-up, perform and analyse but a number of investigators have made attempts to apply such tests. The biaxial with membranous samples stretched along orthogonal directions is one of those tests(Chew et al,1986). This particular mode enables a great number of strain rate combinations on the two extending directions to be performed and this make that mode of test very fertile in producing sets of parameters. Inflation of blood vessels belongs to this group (Young et al,1977). Suction as applied in skin(Grahame,1968) is a multiaxial deformation bearing though some inherent problems in the assumptions that have to be made. Indentation as applied in cartilage(Evans,1973) or torsion as in skin(Barbenel,1979) are tests created to reproduce a physiological loading regime and of straightforward qualitative merit. Indentation is a test that is easy to apply but extremely difficult to analyse while torsion is easier to analyse than apply. A torsion/shear test has also been suggested to have a diagnostic/recording capability but this is still doubtful(Finlay,1970). Patients with Ehlers-Danlos syndrome have different torsional skin characteristics from normal

subjects but the scatter of data due to biological variability was such that the technique was practically never used.

3.3 MECHANICAL PROPERTIES OF ISOLATED PERICARDIUM.

The mechanical properties of isolated pericardium have been thought to be the cause for the behaviour of the whole membrane and particularly its demonstrated limited extensibility. The specific tissue has been subjected both to dedicated experiments or it has been examined as part of a general test program involving a variety of tissues. Uniaxial and biaxial studies have been the most commonly used in order to investigate the mechanical behaviour of the tissue.

3.3.1 Uniaxial Tension.

The uniaxial mode of testing was the first to be applied. Barnard in 1898 reported the strips themselves to be practically inextensible. Later Neelemans (1940) applied the uniaxial test on strips of cat pericardium. He demonstrated the limited extensibility and in addition ascribed some plasticity to the tissue and calculated the value of the elastic modulus to be 10MPa.

Rabkin et al(1974) carried out tests on canine samples and established the basic features of the tissue mechanical behaviour. The complete stress/strain curve was examined, starting from a resting length, defined by the specimen's own weight, to complete failure. During extension a very compliant region was followed by a sharp rise in tension, then a linear region and eventually a failure in a gradual and inconsistent manner. When the tissue was subjected to repeated load cycling, the elastic modulus in the linear region was found to increase with increasing cycle number and stabilised after 3 cycles. Apparently the behaviour was strain rate independent and there was no correlation between elastic modulus and ultimate tensile strength(U.T.S).

The total amount of stress relaxation was proportional to the initial stress value(σ_o). Moduli of elasticity were found to increase for those cycles after a stress relaxation test, in a way which was similar to the effect that a prolonged cyclic preconditioning period had on the tissue. A permanent set in the resting length of the strips was observed after the first cycle for all the strips. By selectively digesting elastin, they observed a drop in the elastic modulus and the U.T.S with a greater amount of relaxation.
In general terms their results are qualitatively valid but the actual value quoted for the parameters should be questioned. The authors did not pay the appropriate attention when preparing their samples especially because species, site and directional variations are a strong possibility. A higher load resolution apparatus could prove wrong their statement that the hysteresis cycles always closed at a larger than zero strain value.

In a subsequent report Rabkin and Hsu(1975) presented a mathematical model which was designed to empirically describe the exponential-like loading phase of the tissue behaviour. A mechanical model of springs and dashpots, with the springs obeying the non-linear mathematical relation and the dashpot contributing by its viscous character, was also proposed. Although easy to conceptualise there is not any real equivalence between model and mathematical formulation, such as exists in linear-viscoelasticity.

In 1981 three reports appeared, reflecting an increased interest for the tissue which was abundant and a convenient choice for studies on collagenous tissues.

Lee and Boughner (1981) investigated, and presented data on, the tissue interaction with the testing environment. In a short introduction they pointed out that the relatively stiffer collagen and

elastin fibres are embedded in a soft matrix resulting in a composite structure. Some of the special problems that the examination of this tissue poses were considered by those workers. During specimen preparation they chose to cut their pericardial strips along the direction of the phrenic nerve (base-to-apex) and horizontally (circumferential), but this selection was according to the geometry of the heart and not related to the tissue properties themselves. The other drawback was that all vertical strips originated from the lower 3/5 of the specimen and the horizontal from the upper 2/5 and thus they did not randomise the site within the specimen.

The samples were tested in 3 different testing environments and preconditioned until a convincingly stabilised curve was achieved. This required a different number of cycles for the two directions. They observed that the stabilised curve was achieved only when the sample had a sufficient width and thus the tissue really behaved as a composite and not like a continuum. They used a width to length aspect ratio of 0.7 and this must have resulted in significant shear interfering with their uniaxial data.

They principally compared the effect of the 3 specific test environments on a constant set of parameters. These were the modulus of elasticity at the linear region of the curve, the ultimate tensile strength calculated over the initial cross sectional area, the resilience as the work done on the tissue strips to fracture and the strain value at rupture. Both the composition and the temperature of the solution could affect the values of the parameters.

The stabilised curve had an exponential-like shape and an exponential formula similar to that of Rabkin and Hsu(1975) was fitted to the unconditioned and preconditioned curves, not equally well though. The preconditioned curve could be achieved by either load cycling or

stress relaxation, and was affected by the maximum load during cycling. All these are features of non-linear viscoelastic behaviour. The strain rate independence was at first restated and disputed afterwards by saying that the elastic modulus of the linear region was strain rate dependent. A thixotropy-based explanation was introduced for this finding. Thixotropic materials do present variable viscosity to variable shear rates but always by shear thinning and showing reduced viscocity with prolonged shearing. The strain rate insensitivity of this tissue could be due to the biological complexity and the great number of constituent materials, each one contributing by different relaxation constants or even the fact that homogeneous strains(or shear rates) at a macroscale does not mean homogeneous strains at a microscale.

Contrary to Rabkin(1974) they found that there was a relation between the modulus of elasticity and the ultimate tensile strength. Contrary to both Neelemans(1940) and Rabkin(1974) they did not observed any plasticity in the tissue strips and attributed this to their accurate control on the environment. Their method, however, is open to some doubt, because in order to set the strain origin they applied a single 10g load stretch/release cycle and then defined the strain origin at the first detectable load point. Thus if any permanent set had occurred in the first cycle (as in the data by Rabkin et al (1974)) it must have been incorporated and resulted in a wrong setting of the zero gauge length. Based on earlier histological findings by Wallraff(1937) and Elias and Boyd(1960) that pericardium is a multilayer collagenous material they suggested that the tissue could be nearly isotropic. Their methods were inadequate for examination of anisotropy and thus their finding that only the U.T.S. value differed with direction while the rest of the parameters were insensitive to

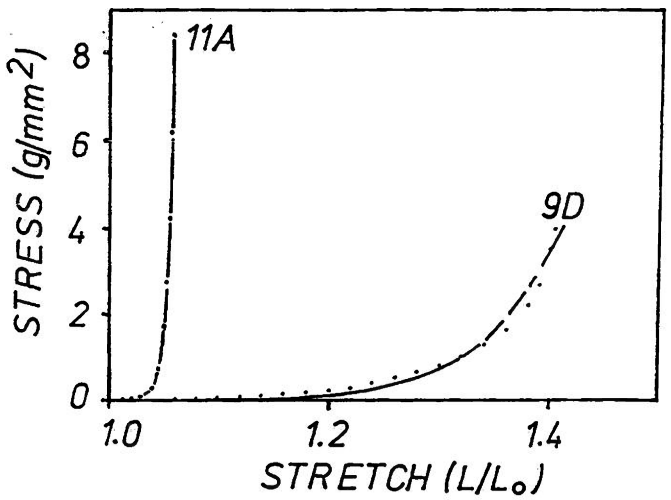

$$\sigma = B(e^{A\varepsilon} - 1), \qquad \varepsilon = \ln(L/L_o)$$

Figure 3.3:Stress/stretch data from strips 9D,11A and their best fit descriptions by using the exponential formula and the sets of parameters: 9D; B=0.037, A=20.3 and for 11A; B=0.00023, A=184 (reproduced from Wiegner and Bing,1981).

direction, could be artifactual.

Wiegner and Bing(1981) attempted to explain the observed mechanical behaviour by examining some of the structural features of the tissue. They reached the reasonable conclusion that some stiffer strips had a collagen fibre prepoderance along the long axis of the strip, but their strips were under tension while fixed which itself could have modified both the resting and strained structures. No systematic method for examining the anisotropic features of the tissue was used. They orientated their strips according to gross geometrical directions and they lacked a technique to identify the axes of elasticity. They considered time dependent properties and implied that structure was responcible for both viscous and elastic behaviour. They realised the importance of accurately defining the stress/strain origin. Due to the very compliant initial region of the curve, the origin of the stress and strain is difficult to define precisely. A minimal force due to the weight of the grips (20mg) was permanently applied and this must have reset the strain origin if any non-elastic behaviour was present; at the same time the stress origin was varying between cycles due to different initial thicknesses and thus different initial cross sectional areas for the strips. A constant number of 10 cycles was used to precondition the strips, irrespectively of whether the load-extension responce had stabilised or not.

By examining the stiffness-stress curve they noticed that the simplified Fung(1981) approach used by the previous workers, where a linear relation between modulus and stress allows the curve to be described by the Fung's modulus, was not applicable. Their stiffness-stress curve was concave with several linear regions.

Three formulae were considered and fitted to the data. As shown in figure3.3 significant differences in response existed between strips

originating from the same area. The strips in figure3.3 had only a 45^{o} angle difference between them but an impressive difference in their stress/strain response in all respects, with the parameter A=20.3 for strip 9D and A=185 for strip 11A. Although the strip numbers indicate that they belong to different samples the shape of the curve is distinctively different within this 45^{o} angle.

What should be pointed out is that the workers recognised that none of their models could adequately describe a group of very compliant strips which were building-up stress over an initial portion of the curve and, following an "elbow", had a rapid transition to high stress values. They could give no qualitative explanation of such a diversity of patterns and values, except the obvious one that the tissue could not have uniform and isotropic properties.

Some preliminary data of histological studies led the authors to suggest that under small stress only those fibers aligned with the stress carried the load. This was integrated in a discussion about the low stress portion of the curve where for a stress of 0.05MPa, Wiegner and Bing gave 18% strain value contrary to the 33% by Hildebrandt (1969), the 41% of Rabkin (1974) and 2% by Vito (1979).

The 3rd report in the same year by Reece et al(1981) examined the effects that chemical treatment with glutaraldehyde had on the mechanical properties of the tissue. The incentive was the growing interest in bovine pericardium as a potentially useful biomaterial for the construction of bioprosthetic valve leaflets. Strips fixed under various loads showed a reduced extensibility. Non-linear viscoelastic features were retained in the treated pericardial tissue. The effect that chemically induced crosslinking had on the tissue properties will be examined more specifically in a subsequent chapter.

Radjeman et al (1984) similarly motivated by the construction of

bioprosthetic valves focussed on the anisotropic elastic behaviour of bovine pericardium strips. They examined strips at 0°, 45° and 90° to the long axis of the heart, but these were not cut from the same specimen. Each orientation was cut from a specific site, but from a different sac. Groups of parallel strips were made from specimens from the anterior and the posterior pericardial surface. Results of 4 specimens from 4 sacs at one direction and from one site, were compared with those of 4 other sacs at a different direction and a similar site. In general it is very optimistic to expect to obtain statistically significant data for 3 directions, 2 sites and 4 different strain rates from only 12 pericardial sacs from not paired data (originating at least from the same sac and thus excluding sac to sac variations). They obtained a sigmoidal-like form of a stress/strain curve from which a secant initial modulus and a final modulus were obtained similarly to Lim and Boughner (1975, on heart valve tissue). Comparison between the 2 different sites on the heart with the other parameters remaining constant showed that there was no statistically significant difference in the elastic response. There was a statistically higher modulus on the circumferential strips than those of the vertical strips with an intermediate value for the strips at 45° angle. Stress values at rupture followed a similar pattern according to directions. The rest of their results and conclusions are more doubtful. The secant modulus, the strain value at transition from the low stress region to the linear region and the strain value at rupture are subjected to the uncertainty caused by the difficulty in defining the resting tissue length described earlier. Inaccurate definition of the origin, something that they did not consider at all, can significantly affect those values.

They pointed out that the geometry of the fibers could be responsible

for some of the differences observed. Contrary to most other workers viscoelastic behaviour was not examined. In a short discussion they admitted that there was no clear suggestion that they could make to explain why the tissue was anisotropic (if it was) and how this attributes towards a proper functioning of the heart.

They remarked that for the construction of valve leaflets an anisotropic material should be orientated with its strong axis to the direction of higher stresses, but did not identify these directions on a valve leaflet, they could not suggest the direction of these axes in the tissue, nor a method to identify them on the tissue or quantify the degree of anisotropy. They seem to overemphasize the suggestion that mismatch between leaflets could be due to anisotropy; while even with a perfectly isotropic material the site on a sac, the structural differences (sac to sac variation) and the thickness may lead to mismatch as well. Mismatch between the mechanical properties and the stress field of the valve leaflet make some of them perform well while others not, and has further mechanical consequences on the leaflet tissue such as fatigue and eventual failure.

Lee and Boughner (1985) are unique in reporting on the mechanical properties of human pericardium. Most other work is performed on animal tissue which is abundant and easily obtained. The results obtained from the pericardia of various species were used to predict and explain the human pericardial functions, and this was the objective for most of reports. Lee and Boughner obtained 10 human pericardial samples with the patients'own consent and from cases which were not related to any pericardial malfunction or disease. The samples were used to make strips in their usual way described earlier in their canine tissue report. No new or improved techniques were employed but the intention was to allow a better comparison between

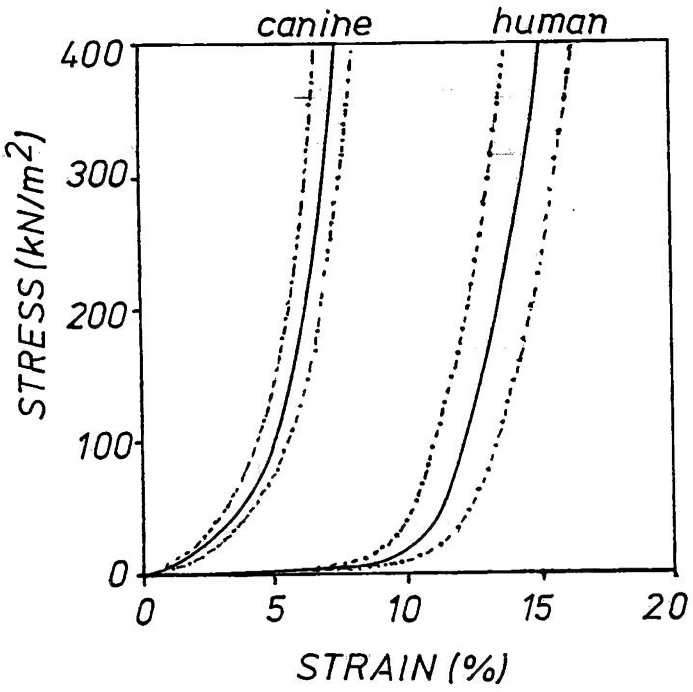

Figure 3.4:Preconditioned stress/strain curves from 9 human and 10 canine pericardial strips. Mean strain ± standard error of the mean (reproduced from Lee and Boughner,1985).

canine and human tissue.

Human tissue "displayed a significantly greater viscous character" than the canine one, showing twice as much hysteretic loss and greater stress relaxation and creep. Human tissue was thicker than the canine tissue in absolute value. Its relative thickness, if one considers the size to thickness relationship of chapter2, showed a tissue significantly stronger than the animal pericardium. They suggested that thickness could compensate for its lower elastic stiffness. They restated that no plasticity was present and that as shown in figure3.4 human strips were in general more extensible. Comparison between strips at various directions did not reveal any differences, but this may reflect the limitations imposed by their restricted samples. In addition to their usual analysis they presented the correlation lines relating ultimate tensile strength and tissue modulus, and found that neither the slopes nor the intercepts were significantly different between the 2 tissues. Human tissue data had a closer correlation between U.T.S and modulus, this possibly indicates that human tissue was superior to animal tissue, having more consistent structural characteristics.

They implicated a lower fibre fraction volume for their failure data, the thickness and the increased viscous character of the human tissue. At the same time a higher fraction volume of matrix for the human tissue could allow a greater fibre rearrangement in this tissue and would allow a greater volume of fluid to be accomodated in the pericardial cavity. Lower fibre fraction volume could also be related to the higher maximum operating strains observed in human pericardial strips compared to the canine ones. Greater collapse of fibre weave in the stress direction allows higher strains. Their interesting suggestion was that a biaxial test is required to quantify the actual

maximum strains during function.

On the isotropy question they pointed out that tests with strips at only two directions are not adequate to totally confirm or reject planar isotropy. The degree of alignment between the elastic axes and the strip directions controls the usefulness of the uniaxial test in examining the directional properties of a tissue.

In addition to these detailed studies of the response of pericardial strips to uniaxial tension, Vito(1979) presented a review of previous work and his own data which he had collected on uniaxial tests made on canine tissue. Instead of a constitutive relation explicitly relating stresses to strains, he adopted a strain energy function(S.E.F) approach and proposed a Mooney form for such a S.E.F. The paper was not dedicated to the mechanical properties of the tissue but incorporated the Mooney form of S.E.F into a larger model of the heart and thus tried to predict and describe the effect of pericardium on the cardiac conditions and on heart's operation. In essence he followed the reverse pathway of the methods that have been presented in chapter2 on the pericardial functions. Vito started from a clear biomechanical study of the tissue to demonstrate that pericardium significantly affects intracardiac pressures. His work still is more important for his approach than his results.

3.3.2 Biaxial Extension.

Biaxial tests were subsequently used to assess the tissue behaviour. The biaxial mode reproduces more closely the natural stress environment of the tissue and could prove that significant differences in the parameters used to quantify the viscoelastic and elastic behaviour of the tissue exist between the uniaxial and biaxial stretching modes. This is due not only to the differences in stretch but to the geometry of the samples themselves. The existence of

lateral loads offers a great number of possible configurations to investigate stress relaxation, creep, load cycling. In terms of such factors as tissue component rearrangement they are of a completely different nature to uniaxial tests.

Lee et al(1985) subjected 3X3cm square samples to biaxial loading. The samples were aligned along the circumferential and meridional directions on the heart from sites on the left and right ventricle and for both normal and volume-overload dogs. They tried to obtain samples as flat as possible from a tissue which was naturally curved. After a first load(0.2N) had been applied in both directions the sample was left to relax to allow definition of the resting length to take place. The cycle-loading protocol involved sinusoidally oscillating load in one direction while in the transverse direction the sample was held at a constant lateral load. By varying the frequency of oscillation of load they observed strain-rate insensitivity over 2,3 orders of magnitude on the Hz scale.

Stress relaxation and creep involved loading by stretching by equal amounts (in both directions) and identical loads (in both directions) respectively. No difference there was observed between normal and volume-overload dogs regarding viscoelastic behaviour and thickness. Creep was absent in their tests contrary to all other uniaxial studies and they attributed this to a lack of shortening in the transverse directions. Lateral loads are absent in the uniaxial test which we think is in essence artificial and destructive while the biaxial is not destructive, at least within the square specimens' area. Biaxial test of this kind also do not interfere with the tissue's integrity by weakening their structure. The composite fibrous structure of tissues can be really affected in the strip preparation especially for those tissues where interaction between fibres is poor or not intense

enough. The degree in which fibres can rearrange in a whole square piece of tissue in a biaxial mode with the laterally existing loads is smaller than in the strips. In addition to this there is only a portion of fibres running from grip to grip and the remnants of the ones left are effectively riveted here and there by crosslinks.
In tissues from animals with chronic dilation the stabilised stress/stretch curves (elastic response) were shifted to the right showing that chronic dilation resulted in a more "compliant" tissue. Thus they found a different response of the tissue in short and long term loading. For those samples with anisotropic behaviour equal stresses in the two directions could distort a central reference circle drawn on the tissue into an ellipse like shape the maximum axis of which, they suggested, coincides with the direction of maximum compliance. There was not any consistency in the direction of maximum compliance and this is probably due to the preparation of their specimens and the alignment of the specimens to the elasticity axes. For comparison between different samples the arithmetic mean of the maximum strains in the two directions was used.

Working on a very similar apparatus with servo controlled linear motors, driving orthogonally arranged wormgears Yin et al(1986b,c) examined the variability of the coefficients used to quantify the mechanical behaviour by testing pericardium and myocardium. Coefficients or exponents of S.E.F., which S.E.F. yield the proper stress/strain relationships through differentiation, have been found to vary widely sometimes over an order of magnitude under replications of similar test conditions because of experimental noise, numerical instabilities in fitting algorithms or the strain history dependence of the tissue. Searching for a method which could evaluate the sources of variability or take it in account when interpreting the

data, they tested pericardium and used (Chew et al,1986) Fung's(1973) assumption that a pseudo S.E.F of the Green's strains(E) can be applicable. They considered the reduced 7-coefficient S.E.F. for skin as in Tong and Fung(1976):

$$W = axE_x^2 + ayE_y^2 + 2axyExEy + 0.5Cexp[AxE_x^2 + AyE_y^2 + 2AxyExEy] \qquad (3.1)$$

and found it to be overparameterized. Consequently a simpler form of S.E.F was used:

$$W = B(E_x^2+E_y^2) + CExEy + D[exp(AxE_x^2 + AyE_y^2)-1] \qquad (3.2)$$

A,B,C,D are coefficients; x,y are directional indices.

A_x was found to differ from Ay and this indicated anisotropy but the relative magnitude of Ax to Ay depended upon the protocol. They claimed that their technique could exclude experimental noise and numerical instability and thus the differences in coefficients reflect real specimen's properties. The coefficients dependent on the testing protocol and the presence anisotropy could only be decided on the restriction that the coefficients had been correctly calculated.
They seemed to be interested more on the evaluation of the Fung S.E.F and their analytical approach in fitting such a S.E.F than on the material properties themselves. For pericardium they said (Yin et al,1986c) that "one major difficulty is unresolved; the direction of anisotropy is ambiguous". We must be cautious in evaluating their technique and their conclusions for the tissue because they neglected a prerequisite in Fung's S.E.F. Elimination of all shearing in the Fung's S.E.F is possible only when the elasticity axes coincide with the testing axes. Thus for this approach to be valid it is necessary that the identification of these axes first takes place and then test and mathematical treatment should follow.

The tissue had been examined in a system of similar philosophy earlier by Vito(1980). He set-up a test mode for biaxial tests of planar specimens and suggested that those could be arterial segments, skin or pericardium. The report is devoted to the capabilities of the system, its software and hardware and in the margin of all these a piece of pericardium was stretched to demonstrate possible applications of the apparatus. This responce of the tissue in the orthogonal directions was then described as being "orthotropic".

3.3.3 Inflation.

We have seen that most of the investigators in biorheological studies of pericardium adopted straightforward test methods in their reports. Hildebrandt, Fukaya and Martin (1969a) called those means of tissue characterisation "traditional". Descriptions are restricted to positive strains, purely empirical models and are not of general applicability. Recognising the inadequacies of previous reports they used a set of a uniaxial and an inflation technique. Inflation is a two-dimensional testing method where the experimenter has very little or no control on the stretch in the two axes. Biaxial testing modes provide such control and choice of stretching modes but as we have seen are accompanied by other inherent problems.

Hildebrandt et al(1969a,b) examined the properties of a variety of soft tissues including dog pericardium, which were subjected in uniaxial tension and inflation. The workers assumed the tissues to be nearly isotropic and incompressible. This allowed them to assume that inflation produced equibiaxial extension which, for isotropic incompressible membranes, is equivalent to simple compression. Thus it is possible to "complete the length-tension curve of the tissue" for simple tension and compression. Simple extension data is provided by the uniaxial tensile test and data in compression by the uniform

in-plane biaxial stretch at the membrane's crown in inflation.

They used large deformational elastomer theory to describe the non-linear elastic behaviour of the tissue. If isotropic biological tissues are subjected to uniform deformation then theoretical formulae of rubber elasticity could very well be applicable. Based in assumptions of isotropy, incompressibility, uniformity of strain, similarity to elastomers and possibility of similar behaviour between tissues they decided that it should be possible to find a function $f(\lambda)$ such that:

$$\sigma = (\lambda^3 - 1/\lambda)f(\lambda) \qquad (3.3)$$

$f(\lambda)$ for rubber is a function of the derivatives of the S.E.F with respect to the stretch invariants and the deformation in particular. With these assumptions they could give a theoretical basis to justify the application of such description to tissues. The assumptions simplify considerably the analysis because of the particular relations of the stretch ratios $\lambda 1$, $\lambda 2$, $\lambda 3$. Even in the case where a tissue is not isotropic in $\lambda 3$, formula(3.3) can be an arbitrary descriptive equation but it loses its theoretical claim. The most probable form for $1/f(\lambda)$ has been found to be that of a 3-parameter parabola:

$$1/f(\lambda) = (\lambda-\lambda m)(\lambda-\lambda M)/K(\lambda m-\lambda M) \qquad (3.4)$$

the stress/strain curve of all 4 tissues appears to rapidly stiffen as a stretch ratio value, different for each tissue is approached asymptotically. Then λm is the minimum asymptote for the greatest thinning during biaxial stretch and λM is the maximum stretch asymptote as obtained by simple extension. It has been found that with appropriate choice of the parameters all 4 tissues can be adequately described by formula3.4 and this was impressive because

dura's asymptote was at 10% while mesentery's asymptote at 130%.

The authors (1969a) thought that their analytical treatment had certain advantages over other approaches. They found that a linearity existed between the maximum biaxial extension of the sheet λM (as calculated by greatest thinning λm) and the uniaxial extension asymptote λM. Thus by knowing the dependence of one variable on another the number of arbitrary constants can be reduced by one. They further noticed that there was an approximate left-right symmetry of the data points about the vertical midline between the asymptotic intercepts. This symmetry can enable one to estimate the left half of the function $f(\lambda)$ by knowing only the right half which results from the uniaxial test which is technically easier to perform. There is no theoretical basis to justify those claims as they were only a result of the symmetry and properties of the parabola used to empirically describe the data.

The authors systematically neglected anisotropy by disregarding biaxial strain diferences which they said could be as much as 20%. This could very well render their analytical treatment non-valid.

3.4 DISCUSSION.

In this chapter we have seen which methods have been employed to examine the mechanical properties of isolated pericardium of various species and the results that have been accumulated on this subject.

It has been shown that the questions raised from time to time still remain, more problems have been posed than solved and occasionally have been overcome by various simplifying assumptions. It is obvious that examination of this particular tissue requires a better definition of the stress/strain origin. Particular attention should be paid in the low load portion of the curve which seems to greatly influence the deformation pattern (shape of the complete

stress/strain curve). There is a dispute over the relation existing between elastic modulus and U.T.S. Absense of any relation would mean that the ultimate tensile strength is not suitable measure for judgement about the tissue structure and the relation of those two parameters (modulus and strength) is an absolutely random event not influenced by the tissue structural built-up. Strain rate independence is still questionable. Most workers have not really paid the proper attention to the site from which the samples originate and the relative direction in respect to references either on the heart or on the tissue itself. The work we reported in chapter2 in mapping the tissue and examining its topography has already been proved how vital it is.

The techniques themselves and the criteria for their selection have been discussed already and are a matter of continuous controversy. The route of research up to now can only prove that usually a combination of methods can better expose the mechanical behavioural characteristics of the tissue. It should be generally agreed that none of the methods used can identify, qualitatively describe and quantify the degree of anisotropy which is inherent in most of the tissues. The Uniaxial test is not capable of detecting anisotropy on its own and requires additional preparatory work. Multiaxial tests also are difficult to operate and interpret. Both indentation and torsion are incapable of examining anisotropy. Thus one of the most salient and useful (as it will be shown later) features stays obscure due to testing limitations. Constitutive equations have the potential of mechanical, structural and physiological description but can be founded on the wrong assumptions (such as the one regarding isotropy). There is a clear need for a method which can be used to determine whether the pericardium is

anisotropic or not, and to detect the directions of the axes of elastic symmetry if the tissue is anisotropic.

A non-destructive technique for the examination of the mechanical properties of membranes has not yet been presented in the literature. Such a technique would be particularly useful as it would allow further use of the already tested samples.

Towards this aim we think that the work by Hildebrandt et al(1969a,b) was a breakthrough and for us the most stimulating. The detailed assumptions made by these workers and some of their conclusions are questionable or simply wrong. However, their analytical approach and the connection they attempted to the elastomeric theory was simple and clear and the inflation method has merits and a far greater potential which has not been fully exploited. Therefore, we will focus on inflation in the next chapter.

4.1 INTRODUCTION.

Inflation is produced by application of a transmembranous pressure difference which yields tensile forces in the plane of the curved membrane. The membrane is firmly clamped on the perimeter(along a boundary) and the force normal to its surface is also normal to the tensile forces at each particular site. Geometrically speaking, the pressure vector lies along the local normal vector at every elemental area of the surface and thus normal to the vectors of the in-plane deformation. In chapter3 it was shown that one of the disadvantages of conventional biaxial testing methods is that the exhibited behaviour is dependent on the applied protocol and the principal testing directions. In inflation the only principal testing direction is normal to the surface and the in-plane stresses are created indirectly through geometry and thus it may constitute in this respect an unbiased testing method since the deformed shape of the membrane will be dependent on the membrane properties themselves. It may also provide a method of identifying the principal mechanical directions of the material.

This chapter begins with a review of the previous applications, mostly involving isotropic materials, in order to clarify the mathematical problems, and the benefit to be gained from the principle and the major features of inflation. We shall seek a suitable anisotropic equivalent material and develop a test method based on inflation.

4.2 A REVIEW ON INFLATION.

The literature abounds with reports on inflation tests applied to engineering materials. Table4.1 and table4.2 tabulate the most interesting of those reports, demonstrating different approaches to the problem.

The early attempts by Flint and Naunton(1937), Treloar(1944) and Rivlin and Saunders(1951) have not been included in the tables since they are represented adequately by the most sophisticated work on this approach by Hart-Crisp and Smith(1967).

The second column contains the purpose of the investigations. They were mostly related to practical applications such as high-altitude balloons, tyres, membranes as moving diaphragms in measuring devices or for the creation of parabolic mirrors (when appropriately coated) of variable focal distance, or to theoretical treatments of the problem in order to predict the behaviour.

The mathematical treatment of the problem (in 4th column) has followed a route from an analytical to a semi-analytical to a completely numerical treatment. The modern methods are completely numerical due to the great progress in computer hardware and software and the introduction of improved numerical approaches.

The solution to the equations which are used in the analyses are never of a closed form or of the analytical type and even in the simplest of cases a power series form is the best one can get. In the non-simplified cases, where fewer assumptions have been made, more than one method has been followed. One can either combine the set of the non-linear differential equations and produce a single equation, or produce another set of linear equations which can be solved numerically to yield a convergent solution, or employ a variation principle where a specific quantity such as the potential energy can be minimised to yield the stable state and thus approximate the solution. Variational principles and minimization of quantities are particularly fashionable lately and between some of the workers as it appears in the 4th column of tables4.1,4.2.

It is fortunate that the primary interest has been on natural

Table 4.1

WORKERS, DATE	INTERESTED IN:	NOVELTIES	METHOD OR SOLUTION	MATERIAL OR TISSUE	LINEAR	NON-LINEAR	ISOTROPIC	IN-PLANE ISOTROPIC	ANISOTROPIC(3-D)	INCOMPRESSIBLE	COMPRESSIBLE	TIME-DEPENDENCE	TIME-INDEPENDENCE	ELASTIC	PLASTIC	INITIAL CONFIGURATION OF THE SAMPLE: BOUNDARY, SHAPE OF ORIFICE	INITIAL CONFIGURATION OF THE SAMPLE	ADDITIONAL ASSUMPTIONS
HART-SMITH, CRISP 1967	inflation of rubber balloons	Partially analytical, regarding thickness distribution	Semi-analytical and numerical	Rubber		√	√			√			√	√		circular	flat	
FOSTER, 1967	theoretical interest	reduction to simpler non-linear ordinary equations, not necessarily inflated but axially loaded	Semi-inverse un-deformed, deformed geometries are set	neo-Hookean		√	√			√			√	√		various configurations	knowledge not always required	meridional stretch ratios $\lambda_\varphi > 2$ symmetrically loaded
ALEXANDER, 1968	high-altitude balloons, determination of properties	new S.E.F(W) form proposed	Laplace's law at the crown to obtain stress/strain data	materials of the new(W) form		√	√			√			√	√		circular	flat	
HILDEBRANDT, FUKAYA, MARTIN, 1969	theoretical and applied interest	elastomer theory	uniaxial and biaxial on tissues	soft tissues		√	√			√			√	√		circular	naturally curved?	elastomer theory applicable
YANG, FENG, 1970	theoretical interest	new modes of deformation not always inflation	reduced equations solved numerically	Mooney materials		√	√			√			√	√		mostly circular	various forms	
JOYE, POEHLEIN, 1972	examination of biaxial flow properties	creep deformation non-uniformity checked, viscocity measured	various forms of Laplace's law	polyiso-butylene, L-80	√	√	√			√		√		√		circular	flat	ideal gas law is used, uniform biaxial deformation over whole bubble
JOYE, POEHLEIN, 1973	examination of biaxial flow	constant pressure	linear elements combined in a non-linear way to yield biaxial viscocity measures	polyiso-butylene, L-80	√	√	√			√		√		√		circular	flat	
YANG, LU, 1973	theoretical interest on non-linear elasticity problems	advanced algorithms for num.solution; Cartesian coordinates in use	num.solution 3non-linear part. diff. equations	neo-Hookean membranes		√	√			√			√	√		rectangular	flat	finite stretch ratios, moderate rates of stretch
DICKEY, 1974	transformation of Foeppl equations	reduction to ordinary diff. equations	conditions for existence of solution		√		√						√	√		circular	flat	small deflections
DONG, 1974	generality of application of this approach	failure data, temperature dependence of functions		LX-04-1		√				√		√		√			hollow cylindrical specimens	
JONES, 1974	theoretical	flat plate equations reduced for elastic membranes	simplified elastic equations; series solution	elastic membranes	√		√						√	√		rectangular elliptic, equi-lateral triangular		minimal flexular rigidity
UENG, SUN, 1974	membranes of revolution from transversely isotropic material	minimisation of total energy	general equations num.solved in simplified form	Mooney membranes		√	√			√			√	√			membranes of revolution	

Table 4.2

WORKERS, DATE	INTERESTED IN:	NOVELTIES	METHOD OR SOLUTION	MATERIAL OR TISSUE	LINEAR	NON-LINEAR	ISOTROPIC	IN-PLANE ISOTROPIC	ANISOTROPIC(3-D)	INCOMPRESSIBLE	COMPRESSIBLE	TIME-DEPENDENCE	TIME-INDEPENDENCE	ELASTIC	PLASTIC	INITIAL CONFIGURATION OF THE SAMPLE: BOUNDARY, SHAPE OF ORIFICE	INITIAL CONFIGURATION OF THE SAMPLE:	ADDITIONAL ASSUMPTIONS
FENG, HUANG, 1974	theoretical	minimum potential energy principle	numerical; minimisation of a multivariable function	Mooney materials		✓	✓			✓			✓	✓		rectangular	flat	
FENG, TIELKING, HUANG, 1974	engineering applications	constant constraint at certain height	minimum energy solution	Mooney materials		✓	✓			✓			✓	✓		rectangular	flat	frictionless constraint
FENG, 1975	viscoelastic non-linear membranes	viscoelastic behavior creep, relaxation	reduction of 3-partial diff. equations	neo-Hookean membranes		✓	✓			✓		✓					ellipsoidal membrane	time dependent strain invariants
SCHMIDT, CARLEY, 1975	thermoplastic polymeric materials	known thickness given at deformed shape	like HART-CRISP and SMITH's solution	Mooney-Rivlin materials		✓	✓			✓			✓			circular		S.E.F applicable to non-isothermal processes
PUJARA, LARDNER, 1978	elastic materials	comparison of Rivlin and STZC S.E.F(W)	reduced equations solved numerically	STZC, RIVLIN materials		✓	✓			✓			✓	✓		circular	various	uniform areal strain
TURVEY, 1980	engineering applications	prestress/prestrain of elastic membranes	dynamic relaxation method	elastic linear	✓			✓						✓		circular	flat	
VAUGHAN, 1980	coated membranes for parabolic mirrors	prediction of levels of prestretch possible	ordinary non-linear diff.equations solved with power series solution	Rubber		✓		✓		✓			✓	✓		circular	flat	deforms into a paraboloid
STORAKERS, 1982	higher accuracy sought	influence of contraction ratio on results	Semi-inverse; analytical, numerical	Hookean materials	✓		✓						✓	✓		circular	flat	uniform pressure small deflections
STORAKERS, 1982	time dependence	viscoelastic correspondence principle		standard linear solid	✓		✓					✓		✓				uniform time dependence for all relaxation moduli
STORAKERS, 1982	variation theory			Hookean materials	✓		✓							✓		circular, elliptic rectangular		small deflections
CHATER, NEALE, 1983	theoretical	transverse isotropy and plasticity	variational principle for equations; finite elements for solution					✓		✓			✓		✓	circular	flat	deformation into a sector of a sphere
CHATER, NEALE, 1983	theoretical	strain-rate sensitivity	variational principle for equations; fin.elements for solution					✓		✓		✓			✓	circular	flat	deformation into a sector of a sphere
MOHAN, MELVIN, 1983	aortic tissue dynamic and static loading	examination of direction of failure	air inflated experimental method	aortic tissue		✓	✓			✓						circular	naturally curved	natural shape neglected in the analysis
WINEMAN, WILSON, MELVIN, 1979	possibility of identification of S.E.F.(W)	use of a non-homogeneous mode for identification of (W)	theoretical identification of (W)	rubbery materials and potential for soft tissues		✓	✓			✓			✓	✓		circular	flat	

rubber and other elastomers. Like the soft tissues, they usually exhibit large deformations for which a specific deformational theory has already been developed. Thus the size of the bubble produced by inflating a soft tissue and an elastomer is of a similar magnitude. This makes the geometrical formulation of the two problems very similar but similarities end there because the load-deformation response is quite different between tissues and elastomers.

In those cases where the response of natural rubber in inflation has been examined the discrepancies between predicted and observed behaviour can be due to inadequate mathematical formulation of the problem or to oversimplifying assumptions, or even to lack of an ideal model to describe the deformational behaviour of rubber.

The rest of the cases are theoretical treatments of mathematically simple but non existent materials such as the neo-Hookean or Mooney-Rivlin material.

In chapter3 we have seen what the general features of the mechanical behaviour of bovine pericardium are likely to be. We are in fact considering the inflation of a material which is non-linear, possibly 3-D anisotropic, may be compressible, certainly time-dependent in response to load and likely to exhibit plasticity. This problem has not even been considered by anyone yet, as it appears from both tables4.1, 4.2.

The orifice through which the material is inflated is in most of the cases circular and the reason for this is that it constrains the membrane's edges to a symmetrical boundary with no preferable orientation to start with. A rectangular boundary has yet to be applied practically (only theoretically) and the reason for this will become apparent as we proceed to the formulation of the problem.

The initial configuration of the material was conveniently flat

in most of the cases and Pujara and Lardner(1978) claimed that this does not seriously affect the final bubble behaviour, but only the point where the onset of loads starts.

The final column includes the main additional assumptions present in some of the papers. They usually exist to simplify the problem and are of the most diverse nature. They may limit the maximum or minimum strains, specify the nature of the inflating medium, the rate of stretch (particularly relevant to tissue mechanics), the nature of the material behaviour (form of S.E.F.), the deformation itself (isothermal or not), or be purely geometrical in nature (deformation to a particular shape). They should all become clearer as we embark in the formulation of the general problem in the next section, because then the additional assumptions can be related to one of the 3 major groups of relations involved.

4.3 FORMULATION OF THE PROBLEM.

4.3.1 A General Problem Of Elasticity.

There are 3 groups of basic equations as presented in a compendium of the theory of Elasticity by Filonenko(1965).

The Static equations which contain: Differential conditions of equilibrium(Navier's equations) for stresses X,Y,Z, in a system of coordinates (x,y,z), for displacements u,v,w and ρ;body density:

$$\frac{\partial X_x}{\partial x} + \frac{\partial X_y}{\partial y} + \frac{\partial X_z}{\partial z} + \rho X = 0 \quad \left(= \rho \frac{\partial^2 u}{\partial t^2}\right)$$

$$\frac{\partial Y_x}{\partial x} + \frac{\partial Y_y}{\partial y} + \frac{\partial Y_z}{\partial z} + \rho Y = 0 \quad \left(= \rho \frac{\partial^2 v}{\partial t^2}\right) \qquad (4.1)$$

$$\frac{\partial Z_x}{\partial x} + \frac{\partial Z_y}{\partial y} + \frac{\partial Z_z}{\partial z} + \rho Z = 0 \quad \left(= \rho \frac{\partial^2 w}{\partial t^2}\right)$$

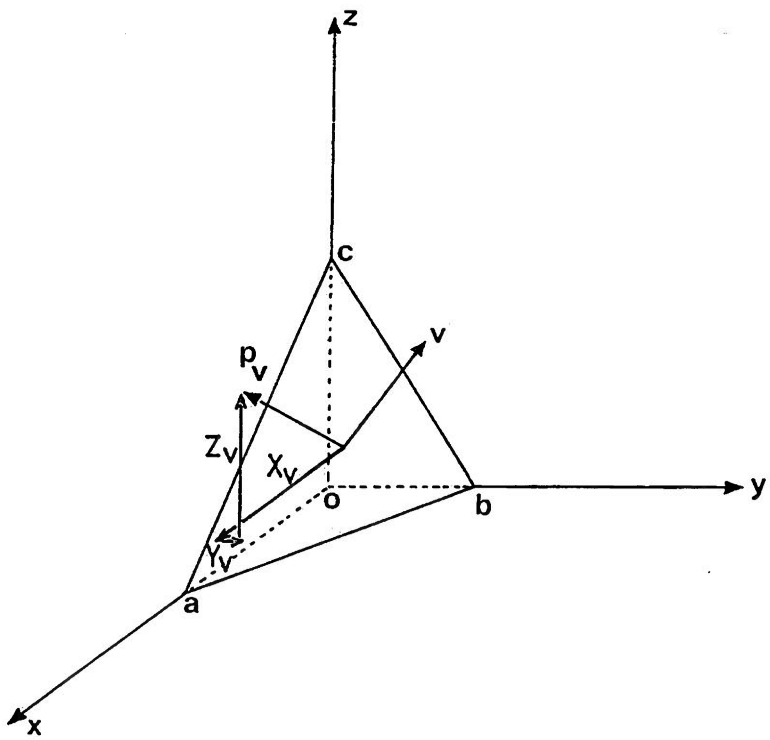

Figure 4.1:conditions of equilibrium between stresses acting on three planes parallel to the coordinate planes and on a fourth plane intersecting the axes at a,b,c.

Surface conditions, yield the projections of the a total stress p_v acting on an area abc (fig.4.1) as a function of the stresses X_i, Y_i, Z_i, i=x,y,z in the system(x,y,z):

$$\begin{aligned} X_v &= X_x\cos(vx)+X_y\cos(vy)+X_z\cos(vz) \\ Y_v &= Y_x\cos(vx)+Y_y\cos(vy)+Y_z\cos(vz) \\ Z_v &= Z_x\cos(vx)+Z_y\cos(vy)+Z_z\cos(vz) \end{aligned} \qquad (4.2)$$

The Geometrical equations which contain: relations of strains(es) and displacements(u,v,w)(Cauchy´s equations),

$$\begin{aligned} e_{xx} &= \frac{\partial u}{\partial x} & e_{yz} &= \frac{\partial w}{\partial y}+\frac{\partial v}{\partial z} \\ e_{yy} &= \frac{\partial v}{\partial y} & e_{zx} &= \frac{\partial u}{\partial z}+\frac{\partial w}{\partial x} \\ e_{zz} &= \frac{\partial w}{\partial z} & e_{xy} &= \frac{\partial v}{\partial x}+\frac{\partial u}{\partial y} \end{aligned} \qquad (4.3)$$

and the compatibility conditions(Saint-Venant´s equations),

$$\begin{aligned} &\frac{\partial^2 e_{xx}}{\partial y^2}+\frac{\partial^2 e_{yy}}{\partial x^2}=\frac{\partial^2 e_{xy}}{\partial x\partial y} \; ; \quad \frac{\partial}{\partial z}\left(\frac{\partial e_{yz}}{\partial x}+\frac{\partial e_{zx}}{\partial y}-\frac{\partial e_{xy}}{\partial z}\right)=2\frac{\partial^2 e_{zz}}{\partial x\partial y} \\ &\frac{\partial^2 e_{yy}}{\partial z^2}+\frac{\partial^2 e_{zz}}{\partial y^2}=\frac{\partial^2 e_{yz}}{\partial y\partial z} \; ; \quad \frac{\partial}{\partial x}\left(\frac{\partial e_{zx}}{\partial y}+\frac{\partial e_{xy}}{\partial z}-\frac{\partial e_{yz}}{\partial x}\right)=2\frac{\partial^2 e_{yy}}{\partial y\partial z} \\ &\frac{\partial^2 e_{zz}}{\partial x^2}+\frac{\partial^2 e_{xx}}{\partial z^2}=\frac{\partial^2 e_{zx}}{\partial z\partial x} \; ; \quad \frac{\partial}{\partial y}\left(\frac{\partial e_{xy}}{\partial z}+\frac{\partial e_{yz}}{\partial x}-\frac{\partial e_{zx}}{\partial y}\right)=2\frac{\partial^2 e_{yy}}{\partial z\partial x} \end{aligned} \qquad (4.4)$$

where E:the modulus of elasticity and G:the modulus of elasticity in shear.

The Physical equations are those of Generalised Hooke's law:

$$e_{xx}=(1/E)\{X_x-\nu(Y_y+Z_z)\} \quad ; \quad e_{yz}=(1/G)Y_z \qquad (4.5)$$
$$e_{yy}=(1/E)\{Y_y-\nu(Z_z+X_x)\} \quad ; \quad e_{zx}=(1/G)Z_x$$
$$e_{zz}=(1/E)\{Z_z-\nu(X_x+Y_y)\} \quad ; \quad e_{xy}=(1/G)X_y$$

where ν:Poisson's ratio.

The unknown stresses, strains and displacements can be determined in one of two ways: a)by regarding the displacements as unknowns u(x,y,z), v(x,y,z), w(x,y,z), when the equations of equilibrium have to be satisfied and the relations of the external forces on the body, or b)by regarding the stresses as unknowns, the 6 variables Xx, Yy, Zz, Yz, Zx, Xy have to satisfy the equilibrium relations together with the compatibility conditions. The first of the methods is simpler and requires less variables to be specified. From the displacements one can subsequently determine strains and then stresses.

4.3.2 Theory For Elastic Membranes.

The theory of thin plates or shells for highly elastic materials differs from that for classical elasticity because, in the former case, the principal extension ratios in the middle surface of the deformed shell are appreciably greater than unity. If variations of stresses throughout the thickness of the shell are small, then shearing stresses and couples may be neglected in comparison with the stress resultants acting on a plane tangent to the deformed midsurface. Under these circumstances the membrane theory is developed.

Green and Zerna(1954) and Green and Adkins(1960) are pioneers in this field and their method of approach has been adopted by Hart-Crisp and Smith(1967), Foster(1967) and Schmidt and Carley(1975) already presented in tables4.1,4.2. The general 3-dimensional theory of

stress systems in plates poses considerable analytical difficulty but it can be reduced to a problem of two-dimensions by introducing the stress resultants and stress couples.

Consider the unstrained body to be sheet(plate) of homogeneous elastic material bounded by the plane surfaces at $x_3=\pm h_0$, where h_0 may be a function of x_1, x_2 (and thus of variable thickness) but with an elastic symmetry about the $x_3=0$ plane. The middle plane becomes the one with $y_3=0$ when the material is deformed. The coordinates of a point of the plate which was originally at x_i become y_i after the deformation, both coordinates being referred to the same Cartesian rectangular axes system. The major surfaces after deformation are now given by $y_3=\pm h$ which is again a function of the y_1, y_2. It is helpful to use the curvilinear coordinate system θ_i which has:

$$y_\alpha = y_\alpha(\theta_1, \theta_2) \qquad y_3 = \theta_3 \tag{4.6}$$

Greek indices take the values 1,2.

$$G_{ij} = \begin{bmatrix} A_{11} & A_{12} & 0 \\ A_{12} & A_{22} & 0 \\ 0 & 0 & 1 \end{bmatrix} \qquad G^{ij} = \begin{bmatrix} A^{11} & A^{12} & 0 \\ A^{12} & A^{22} & 0 \\ 0 & 0 & 1 \end{bmatrix} \qquad G=A \tag{4.7}$$

$$A = |A_{\alpha\beta}| \qquad A^{\alpha\rho}A_{\rho\beta} = \delta^\alpha_\beta$$

$A_{\alpha\beta}$, $A^{\alpha\beta}$ are the covariant and contravariant metric tensors associated to the θ_α coordinates in the middle plane $y_3=0$ of the deformed membrane. A force acting on an elemental area when θ_1=constant is $\bar{T}_1 d\theta^2 d\theta^3$ and the length of the line element on the middle plane $y_3=0$ is:

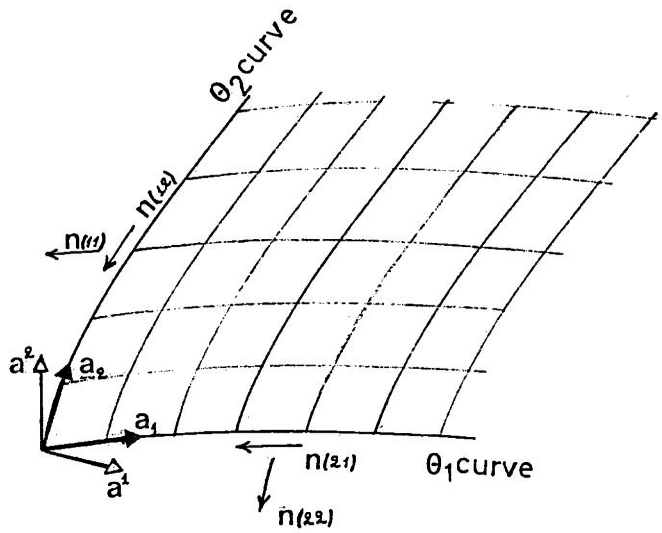

Figure 4.2:an element of the middle surface M which is bounded by the coordinate curves θ_1=ct and θ_2=ct. The stress resultant n_α over the surface θ_α=ct and measured per unit length of the line θ_α=ct has components along the unit base vectors denoted by $n_{(\alpha\beta)}$ which are called physical stress resultants and are not components of a tensor. The physical stress resultants are directed along the covariant base vectors of the middle surface M,(reproduced from Green and Zerna,1969).

$$\sqrt{(A_{22})}d\theta^2=\sqrt{(AA^{11})}d\theta^2 \tag{4.8}$$

This applies similarly to θ_2=constant. Usually for such problems a physical stress resultant $\bar{n}_\alpha$, measured over a unit length of the curve θ_α=constant in the plane y_3=0, is used:

$$\bar{n}_\alpha=\frac{\bar{N}_\alpha}{\sqrt{AA^{\alpha\alpha}}}\ , \qquad \bar{N}_\alpha=\int_{-h}^{h}\bar{T}_\alpha dy_3 \tag{4.9}$$

The stress resultant $\bar{n}$ per unit length of a line in the y_3=0 on the deformed plate whose unit normal in that plane is:

$$\bar{u}=u_\alpha\bar{G}^\alpha\ , \tag{4.10}$$

is given by:
$$\bar{n}=\int_{-h}^{h}\bar{t}dy_3\ , \tag{4.11}$$

then the stress resultant per unit length can also be:

$$\bar{n}=\frac{u_\alpha}{\sqrt{A}}\int_{-h}^{h}\bar{T}_\alpha dy_3=\frac{u_\alpha\bar{N}_\alpha}{\sqrt{A}}=\sum_{\alpha=1}^{2}u_\alpha\bar{n}_\alpha\sqrt{A^{\alpha\alpha}}=u_\alpha(n^{\alpha\rho}\bar{G}_\rho+q^\alpha\bar{G}_3) \tag{4.12}$$

The symmetric contravariant tensor $n^{\alpha\rho}$ and the components of the contravariant tensor q^α are called stress resultants and shearing forces respectively. By the use of the metric tensors $A_{\alpha\beta}$, $A^{\alpha\beta}$ we can form mixed and covariant tensors. The physical components of $\bar{n}_\alpha$ along the coordinate lines are related to the contravariant stress resultant tensor:

$$\bar{n}_\alpha=\frac{n_{(\alpha\beta)}\bar{G}_\beta}{\sqrt{A_{\alpha\alpha}}},\ (\alpha:\text{not summed});\quad n_{(\alpha\beta)}=n^{\alpha\beta}\sqrt{\frac{A_{\beta\beta}}{A^{\alpha\alpha}}}\ \ (\alpha,\beta:\text{not summed}), \tag{4.13}.$$

These physical stress resultants are not components of a proper tensor and this is indicated by the brackets on the indices. Physical stress resultants $n_{(\alpha\beta)}$ are directed along the covariant base vectors of the middle plane of the plate (fig.4.2).

If $a_{\alpha\beta}$, $a^{\alpha\beta}$ are the covariant and contravariant metric tensors associated with the same curvilinear coordinates θ_α in the plane x_3=0 then:

$$\varepsilon_{\alpha\beta}=(1/2)(A_{\alpha\beta}-a_{\alpha\beta}) \tag{4.14}$$

where $\varepsilon_{\alpha\beta}$ is the strain tensor covariant, symmetric and of second order.

Geometrical relations for a surface: if $\bar{R}$ is the position vector of a surface M, so that $\bar{R}=\bar{R}(\theta_1,\theta_2)$ in curvilinear coordinates, we erect the unit normal vector $\bar{A}_3$ at every point on M and then this perpendicular distance on $\bar{A}_3$ can be a function θ_3 where $\theta_3=0$ is the surface M itself. The outer surfaces are at $\theta_3=\pm h(\theta_1,\theta_2)$. Every point on the deformed shell can be represented by $\bar{R}=\bar{R}(\theta_1,\theta_2)+\theta_3\bar{A}_3$.

Such surfaces are examined by differential geometry which uses the covariant and contravariant base vectors $\bar{A}_\alpha$, $\bar{A}^\alpha$ on the surface M and the metric tensor $A_{\alpha\beta}$, $A^{\alpha\beta}$:

$$A_{\alpha\beta}=\bar{A}_\alpha\cdot\bar{A}_\beta, \qquad A^{\alpha\beta}=\bar{A}^\alpha\cdot\bar{A}^\beta, \qquad A^{\alpha\rho}A_{\rho\beta}=\delta^\alpha_\beta \tag{4.15}$$

if $C_{\alpha\beta}$, $C^{\alpha\beta}$ are defined such as:

$$C_{\alpha\beta}=-\bar{A}_\alpha\cdot\bar{A}_{3,\beta}=-\bar{A}_\beta\cdot\bar{A}_{3,\alpha}=\bar{A}_3\cdot\bar{A}_{\alpha,\beta}=\bar{A}_3\cdot\bar{A}_{\alpha,\beta} \tag{4.16a}$$

$$C^\alpha_\beta=A^{\alpha\rho}C_{\rho\beta}, \qquad C^{\alpha\beta}=A^{\alpha\rho}C^\beta_\rho \tag{4.16b}$$

then the Mainardi-Codazzi equations are:

$$C_{\alpha 1}||_2=C_{\alpha 2}||_1 \tag{4.17}$$

where the || line denotes covariant differentiation with respect to the θ_α curves on the middle surface M.

The previously used base vectors $\bar{G}_i$, $\bar{G}^i$ and the corresponding metric tensors G_{ij}, G^{ij} of the deformed shell may now be evaluated using $\bar{R}=\bar{R}(\theta_1,\theta_2)+\theta_3\bar{A}_3$

$$\bar{G}_\alpha=\bar{R}_{,\alpha}=(\delta^\rho_\alpha-\theta_3C^\rho_\alpha)\bar{A}_\rho, \qquad \bar{G}_3=\bar{R}_{,3}=\bar{A}_3, \tag{4.18}$$

The compatibility conditions for the surface are best given as:

$$L_\beta - M_\alpha = L\Gamma^1_{12} + M(\Gamma^2_{12} - \Gamma^1_{11}) - N\Gamma^2_{11} \qquad (4.19a)$$

$$M_\beta - N_\alpha = L\Gamma^1_{22} + M(\Gamma^2_{22} - \Gamma^1_{12}) - N\Gamma^2_{12} \qquad (4.19b)$$

as in Stoker(1969) where L,M,N denote the coefficients of the second fundamental form of the surface and Γ^i_{jj}; i,j,k=1,2=α,β are called the Christoffel symbols of second kind; By the use of the "egregium" theorem of Gauss, the above equations may lead into the (4.17) equations.

Equations (4.17) may also be obtained more easily if it is accepted that $\bar{R}=\bar{R}(\theta_1,\theta_2)$ has to be a function of third order and then the mixed partial derivatives of third order of $\bar{R}$ have to be independent to the order of differentiation, i.e. $(A_\alpha)_{\alpha,\beta}=(A_\alpha)_{\beta,\alpha}$, $(A_\beta)_{\alpha,\beta}=(A_\beta)_{\beta,\alpha}$.

Most workers use the equations in the form (4.17) and not the proper ones(4.19). This is not only because (4.17) are simpler but under some particular assumptions of symmetry for the surface they can be further simplified and related to the principal curvatures of the surface.

For a stress distributed throughout the thickness of a shell similar formulas to (4.9)-(4.13) apply for the stress resultants, stress couples and the physical components of these quantities.

For the external loads and the equations of equilibrium the original shell equations of Green and Zerna(1954) are applied slightly differently in Green and Adkins(1960).

Loads are considered only normal to the surfaces, and for a membrane of thickness(h) small compared to other dimensions of the shell. The unit normal to the surface is:

$$\bar{u} = \frac{\bar{R}_{,1}\times\bar{R}_{,2}}{|\bar{R}_{,1}\times\bar{R}_{,2}|} = \frac{(\bar{G}_1+\bar{A}_3 h_{,1})\times(\bar{G}_2+\bar{A}_3 h_{,2})}{|\bar{R}_{,1}\times\bar{R}_{,2}|}, \qquad \bar{u}=u_i\bar{G}^i \qquad (4.20)$$

if p_2 is the normal pressure on this surface, measured per unit area of the middle surface of the shell,

$$\frac{-p_2 \bar{u}\sqrt{A}}{|\bar{R}_{,1}\times\bar{R}_{,2}|_h}=\left(\frac{u_i\bar{T}_i}{\sqrt{G}}\right)_h \tag{4.21}$$

and then: $$-p_2\bar{u}\sqrt{A}=[\bar{T}_3-h_{,\alpha}\bar{T}_\alpha]_h \tag{4.22}$$

to yield through approximation:

$$(\bar{T}_3)_h\longrightarrow -p_2\bar{A}_3\sqrt{A} \quad ; \quad (h\longrightarrow 0) \tag{4.23}$$

since,

$$\bar{T}_i=(\sigma^{ip}\bar{A}_p+\sigma^{i3}\bar{A}_3)\sqrt{A} \quad \text{then } (t^{33})_h\longrightarrow -p_2 \tag{4.24}$$

similarly $(t^{33})_{-h}\longrightarrow -p_1$

in general $t^{\alpha 3}\longrightarrow 0$, $t^{33}=0(|p_1+p_2|/2)$ for $h\longrightarrow 0$ (4.25)

The equations of equilibrium are:

$$\bar{T}_{i,i}=0 \tag{4.26}$$

integrating through the thickness:

$$\bar{N}_{\alpha,\alpha}+[\bar{T}_3-h_{,\alpha}\bar{T}_\alpha]_h-[\bar{T}_3+h_{,\alpha}\bar{T}_\alpha]_{-h}=0 \tag{4.27}$$

when surface loads can only be normal to each surface:

$$\bar{N}_{\alpha,\alpha}+(p_1-p_2)\bar{A}_3\sqrt{A}=0 \tag{4.28}$$

remembering that $q^\alpha=\int_{-h}^{h}\sigma^{\alpha 3}d\theta_3$, Green and Adkins reached the set of equations;

$$n^{\alpha\beta}\|_\alpha-C^\beta_\alpha q^\alpha=0 \quad ; \; h\to 0 \text{ (small)}$$

$$n^{\alpha\beta}C_{\alpha\beta}+q^\alpha\|_\alpha+(p_1-p_2)=0 \tag{4.29}$$

for $\lim_{h\to 0}(q^\alpha/2h)=0$ (4.29) become:

$$n^{\alpha\beta}\|_\alpha=0,$$

$$n^{\alpha\beta}C_{\alpha\beta}+(p_1-p_2)=0 \tag{4.30}.$$

From this point and further on the stress/strain relations have to be considered and combined to equations (4.29)-(4.30).

4.4 APPLICATIONS.

Particular geometric problems like the radially stretched plane sheet simplify equations(4.30) and reduce them to the case where a power series solution is obtained.

For inflation another route has to be followed. The "magical" word which appears in almost every paper in tables4.1,4.2 is "axisymmetric". What this means is that a symmetry exists around the principal axis of inflation (normal to the membrane's undeformed flat configuration) and this symmetry may apply to loads, deformations or material properties.

Materials with axisymmetrical properties are isotropic at least in the membrane's plane. This could be the case of a fully isotropic material or of the transversely isotropic(2-d) material. The very specialized case of 3-d anisotropy with radially axisymmetric properties around a point as it results from the radial stretch of an isotropic membrane on its plane has been considered by Vaughan(1980) but it is only interesting as an application and has no-real equivalence in natural materials.

Axisymmetrical loading (circumferential stresses independent of the angle) when a non-axisymmetrical deformation occurs has only been considered once(Missirlis and Armeniades,1976). It is an impossible deformational situation since asymmetry in loading is expected to yield asymmetrical deformation and vice-versa.

Deformation into an axisymmetric shape spherical, paraboloidal or elliptical can lead to considerably simplified versions of equations (4.30). A general class of problems has the middle surface of the sheets forming a surface of revolution before and after deformation, around the same axis of symmetry. For an isotropic material these circumstances mean that the system of the deforming forces is also

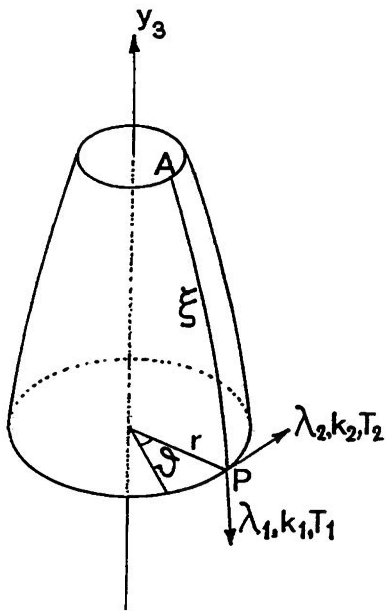

Figure 4.3:creation of the deformed surface of a shell by revolution of the curve C around the axis y_3. Stretch ratios, stress resultants and curvatures are independent of the angle ϑ.

symmetric about the axis. The assumptions of isotropy or incompressibility are not strictly essential for the preservation of the axis of symmetry but for the great majority of materials in tables4.1,4.2 the Mooney form of S.E.F.(W) has been assumed.

For axially symmetrical problems a curve C(fig.4.3) in the undeformed shell creates the middle surface So through revolution around the x_3 axis of the system (ρ,ϑ,x_3). In the deformed shell when the curve C revolves around the axis y_3 creates the surface S in the system of coordinates (r,ϑ,y_3). When C is the plane curve of a plane including the axis x_3, it constitutes a meridian of the surface. For the polar coordinate system (ρ,ϑ,x_3) the arc length AoPo is denoted by n; in the deformed shell this distance along the meridian is denoted by ξ.

Because of the axisymmetrical conditions lines of latitude are normal to the meridians. Principal extension ratios are $\lambda_1,\lambda_2,\lambda_3$ and then:

$$\lambda_1=d\xi/dn,\quad \lambda_2=r/\rho,\quad \lambda_3=1/\lambda_1\lambda_2 \quad \text{(incompressible)} \qquad (4.31)$$

all quantities $\lambda_1,\lambda_2,\lambda_3,r,\xi,n$ are independent of (ϑ) and can become functions of (ρ). Alternatively r,ξ,n may be treated as the independent variables from now on.

For the particular shell of revolution:

$$ds_2^2=d\xi_2^2+r^2d\vartheta^2 \qquad (4.32)$$

$$ds_0^2=dn^2+\rho^2d\vartheta^2=(dn/d\xi)^2d\xi^2+\rho^2d\vartheta^2=1/\lambda_1^2d\xi^2+r^2/\lambda_2^2d\vartheta^2 \qquad (4.33)$$

for curvilinear coordinates θ_α set to coincide to the orthogonal (ξ,ϑ), then $\theta_1=\xi$, $\theta_2=\vartheta$:

$$A_{\alpha\beta}=\begin{bmatrix}1 & 0\\ 0 & r^2\end{bmatrix} \qquad A^{\alpha\beta}=\begin{bmatrix}1 & 0\\ 0 & 1/r^2\end{bmatrix} \qquad A=r^2 \tag{4.34}$$

$$a_{\alpha\beta}=\begin{bmatrix}1/\lambda_1^2 & 0\\ 0 & r^2/\lambda_2^2\end{bmatrix} \qquad a^{\alpha\beta}=\begin{bmatrix}\lambda_1^2 & 0\\ 0 & \lambda_2^2/r^2\end{bmatrix} \qquad a=r^2/\lambda_1^2\lambda_2^2=\lambda_3^2 r^2 \tag{4.35}$$

the relations connecting deformation to stresses are built around an isotropic strain energy function $W(I_1,I_2)$. If curvatures along the parametric lines (meridian-latitude) are k_1,k_2 then:

$$C_1^1=-k_1, \qquad C_2^2=-k_2, \qquad C_2^1=C_1^2=0 \tag{4.36}$$

$$\Gamma_{22}^1=-r\,dr/d\xi, \qquad \Gamma_{12}^2=(1/r)\,dr/d\xi, \tag{4.37}$$

and then equilibrium equations(4.30) reduce to:

$$\frac{d}{d\xi}(T_1 r)=T_2\frac{dr}{d\xi} \tag{4.38a}$$

$$k_1T_1+k_2T_2=P \qquad ; \qquad P=p_1-p_2 \tag{4.38b}$$

the Codazzi equations (4.17) yield:

$$\frac{d}{d\xi}(k_2 r)=k_1\,dr/d\xi \tag{4.39}$$

from elementary differential geometry for the plane curve C:

$$k_1=-\frac{d^2r/d\xi^2}{\left[1-(dr/d\xi)^2\right]^{1/2}} \tag{4.40}$$

putting this into (4.39):

$$k_2 r=\left[1-(dr/d\xi)^2\right]^{1/2} \tag{4.41a}$$

(4.40),(4.41a) can be combined into:

$$k_1 k_2 r = -\frac{d^2 r}{d\xi^2} \tag{4.41b}$$

from (4.38), (4.39):

$$T_1 \frac{d}{d\xi}(k_2 r) + k_2 \frac{d}{d\xi}(T_1 r) = P(dr/d\xi) \tag{4.42}$$

in integrated form: $k_2 T_1 = P/2 + L/r^2$ (4.43)

where L is constant of intergration,

for a shell cutting the axis of revolution at right angles:

$$k_1 = k_2 = k, \qquad \lambda_1 = \lambda_2 = \lambda, \qquad T_1 = T_2 = T, \tag{4.44}$$

at the pole, and we can see then that both (4.43) and the second of (4.38) give the same expression:

$$2kT = P, \qquad L = 0 \tag{4.45}$$

4.5 SIMPLE GEOMETRIES.

4.5.1 Solution Of An Axisymmetrical Case.

It is interesting to examine the way that Hart-Crisp and Smith(1967) handled the problem of inflating a circular membrane of a specific form of S.E.F. What is more interesting is that they also considered the possibility of using the technique as a potential testing method for determining the elastic constants of the material.

The set of equations were non-dimensionalized by dividing the stress resultants T_i by 2hG, all linear dimensions by the radius ρ_o and the pressure by $2hG\rho_o$ to yield the reduced Geometric relations::

$$r' = \lambda_2 \rho' \tag{4.46}$$

$$dr'/d\rho' = \lambda_1 [1 - (k_2' r')^2]^{1/2} \tag{4.47}$$

$$d\lambda_2/d\rho' = (1/\rho')[dr'/d\rho' - \lambda_2] \tag{4.48}$$

$$dk_2'/d\rho' = dr'/d\rho'(k_1' - k_2') \tag{4.49}$$

$$dz'/d\rho' = -\lambda_1 k_2' r' \tag{4.50}$$

z' is measured on the x_3 axis of revolution. Equilibrium equations:

$$k_1'T_1'+k_2'T_2'=P' \tag{4.51}$$

$$2k_2'T_1'=P' \tag{4.52}$$

Elasticity relations:

$$\lambda_3=1/\lambda_1\lambda_2 \tag{4.53}$$

$$E_1=I_1-3=\lambda_1^2+\lambda_2^2+\lambda_3^2-3 \tag{4.54}$$

$$I_2=1/\lambda_1^2+1/\lambda_2^2+1/\lambda_3^2 \tag{4.55}$$

$$T_1'=\lambda_3(\lambda_1^2-\lambda_3^2)[\exp(K_1E_1^2)+\lambda_2^2K_2/I_2] \tag{4.56}$$

$$T_2'=\lambda_3(\lambda_1^2-\lambda_3^2)[\exp(K_1E_1^2)+\lambda_1^2K_2/I_2] \tag{4.57}$$

in those relations the material was assumed to have the exponential elasticity parameters of Hart-Crisp and Smith(1966):

$$\partial W/\partial I_1=G\exp[K_1(I_1-3)^2], \qquad \partial W/\partial I_2=GK_2/I_2 \tag{4.58}$$

with G, K_1, K_2 being material constants.

Note should be taken that equation(4.52) is strictly applied to axisymmetric conditions.

The numerical solution is initiated at the crown and there for a particular stretch ratio $\lambda_1=\lambda_2=\lambda$ the authors derived a calculated value for the curvature $k'=2(\lambda-1)^{1/2}/\lambda$, and determined the non-uniform thickness distribution for the whole shell based on the assumption that acquires the form of a spherical cap.

Determination of $\lambda=\lambda_1=\lambda_2$ and $k'=k_1'=k_2'$ through (4.53)-(4.57) gives $T_c'=T_1'=T_2'$ and the pressure value P'.

P' is kept constant and calculation proceeds for the rest of the points on the bubble at increments ($\Delta p'$) of p',

at a point n from (4.46)-(4.57):

$$(r')_\eta=(\lambda_2\rho')_\eta \tag{4.59}$$

$$(dr'/d\rho')_\eta=(\lambda_1)_\eta[1-(k_2'r')_\eta^2]^{1/2} \tag{4.60}$$

$$(d\lambda_2/d\rho')_\eta=[1/\rho'(dr'/d\rho'-\lambda_2)]_\eta \tag{4.61}$$

$$(dk_2'/d\rho')_\eta=(dr'/d\rho')_\eta[(k_1'-k_2')/r']_\eta \tag{4.62}$$

first approximation of these denoted by the prefix subscript,

are $${}_1(\lambda_2)_{n+1}=(\lambda_2)_n+(d\lambda_2/d\rho')_n\Delta\rho' \tag{4.63}$$

and $${}_1(k_2')_{n+1}=(k_2')_n+(dk_2'/d\rho')_n\Delta\rho' \tag{4.64}$$

used into: $${}_1(T_1')_{n+1}=(P'/2)_1(k_2')_{n+1} \tag{4.65}$$

again although applying only to the polar region they have been used everywhere on the bubble. The first approximations of ${}_1(T_1')_{n+1}$, ${}_1(\lambda_2)_{n+1}$ give through the incompressibility assumption:

$${}_1(\lambda_3)_{n+1}=1/(\lambda_1)_\eta\,{}_1(\lambda_2)_{n+1} \tag{4.66}$$

and by the use of the constitutives:

$${}_1(\lambda_1^2)_{n+1}={}_1(\lambda_3^2)_{n+1}+\frac{{}_1(T_1')_{n+1}}{{}_1[\lambda_3(\exp(K_1E_1^2)+\lambda_2^2K_2/I_2]_{n+1}} \tag{4.67}$$

the successive approximation of ${}_1(\lambda_1)_{n+1}$ is averaged with the previous and substituted into:

$${}_1(\lambda_3)_{n+1}=1/{}_1(\lambda_1)_{n+1}\,{}_1(\lambda_2)_{n+1} \tag{4.68}$$

and back into (4.67) to improve the accuracy on these measures. This safety loop is an innovation introduced by the authors and helps to improve convergence of the iteration procedure for the larger stretch ratios. Knowledge of (λ_1), along with (λ_2) estimates ${}_1(T_2')_{n+1}$ from (4.54), (4.55), (4.57). By combining the general(4.51) and the axisymmetric(4.52) one derives:

$$k_1'=k_2'(2-T_2'/T_1') \tag{4.69}$$

this eliminates P' and then the complete set of $\lambda_2, k_2', T_1', T_2', \lambda_1, k_1'$, is

known and used back into (4.47)-(4.49) to make up second approximations through the same loop for the particular point (n+1).

They claimed also that the specific averaging that is performed, in (4.48):

$$_2(\lambda_2)_{n+1}=(\lambda_2)_n+(\Delta\rho'/2)[(\frac{d\lambda_2}{d\rho'})_n+(\frac{d\lambda_2}{d\rho'})_{n+1}] \qquad (4.70)$$

gives to this system accuracy of a second order integration system much better than using once a second order Taylor series. A final second set of values $_2(\lambda_2)_{n+1}$, $_2(k_2')_{n+1}$, $_2(T_1')_{n+1}$, $_2(\lambda_3)_{n+1}$, $_2(\lambda_1)_{n+1}$, $_2(T_2')_{n+1}$, $_2(k_1')_{n+1}$ is reached and the profile of the bubble is drawn by determination of $(z')_{n+1}$ from (4.50):

$$(z')_{n+1}=(z')_n+(\Delta\rho'/2)[(\frac{dz'}{d\rho'})_n+(\frac{dz'}{d\rho'})_{n+1}] \qquad (4.71)$$

This completed the solution for this particular application. We think that by presenting one of the best numerical solutions we have highlighted the weaknesses inherent in these methods. A numerical solution can handle the system of the 7 non-linear differential equations of the 7 unknowns k_1', k_2', λ_1, λ_2, T_1', T_2', z', but they are depending on basic assumptions and the original membrane equations as much as any analytical solution. Equation (4.51) is essentially the well known Laplace formula applicable to any point of the shell at which the two principal curvatures are k_1',k_2'. Equation (4.52) is applicable only to axisymmetrical deformations and can easily yield (4.51) if $k_1'=k_2'$. Thus the two equations may in principle be only one at the crown, but it is unsatisfactory to use (4.52) anywhere else but at the polar region, even as a minor element in an iteration routine. This could be one of the reasons why discrepancies between observed and predicted profiles were found in this paper. Adoption of an incorrect form for the S.E.F. or the values of its coefficients, or

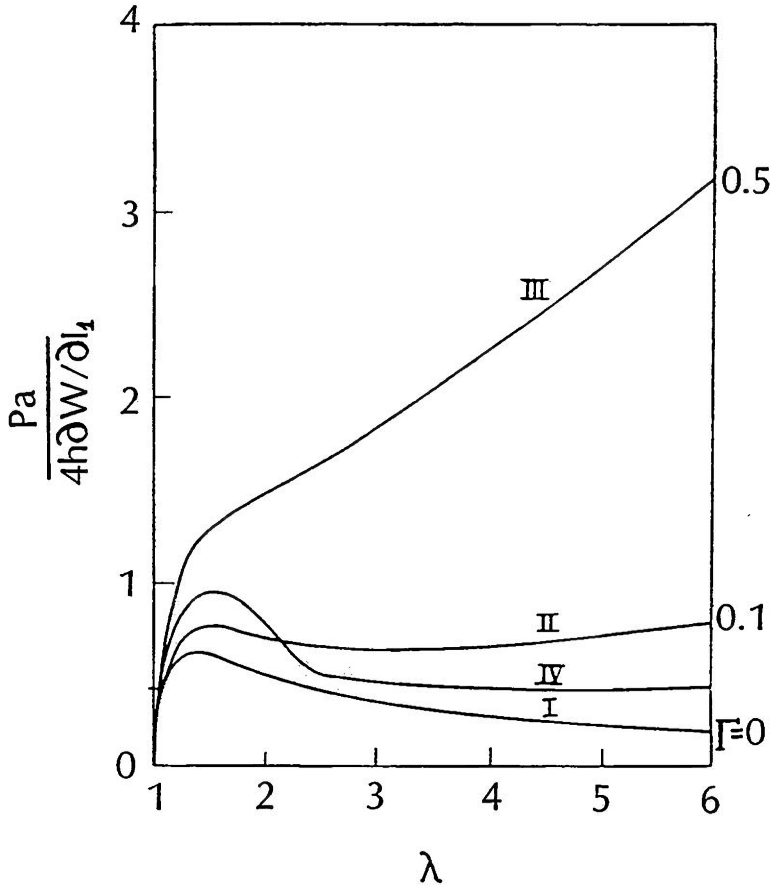

Figure 4.4:variation of the inflating pressure with the stretch ratio at the crown for different rubbers. The softer materials Γ=0,0.1 present bifurcation while for Γ=0.5 a monotically increasing function results; IV:for Γ varying according to the experimental data of Rivlin and Saunders(1951) the bifurcation is inevitable.

errors in the numerical routine itself can have a similar drastic effect on the results.

Comparison between predicted profiles for various parameter values and observed profiles as given by Treloar(1944) or produced by the workers themselves, was attempted. For the best set of coefficients comparison was good only up to a stretch ratio of λ=5, afterwards practical problems like "slipping" of the edges or analytical inadequacies could be responsible for the observed discrepancies.

In general it was shown that the choice of the exponential-hyperbolic function for (W) was better than a Mooney S.E.F. and thus the form of the (W) used was important on its own. Small variations in the coefficients significantly affect the profiles and thus the attempt of predicting the correct values of the parameters through the membrane's behaviour(profiles) is rather insecure.

The basis of the determination of the material parameters involves the relation of a mechanical factor like the inflating pressure to a geometric one like the extension ratio at the crown. In fig.4.4 it is shown that for higher values of Γ where $\Gamma=C_2/C_1$ of a Mooney material in which $W=C_1(I_1-3)+C_2(I_2-3)$, the material has a motonically increasing relation for both normalised pressure and stretch. For lower values of Γ, it reaches a critical point and then depending on the value of Γ itself, it either stabilises in an enlarged configuration or it keeps on flowing till failure. For a Mooney material there is a critical value for Γ under which the material exhibits bifurcation, but for material like pure gum vulcanizate Rivlin and Saunders(1951) have shown that C_2 and thus Γ is a function of the deformation itself and thus these materials

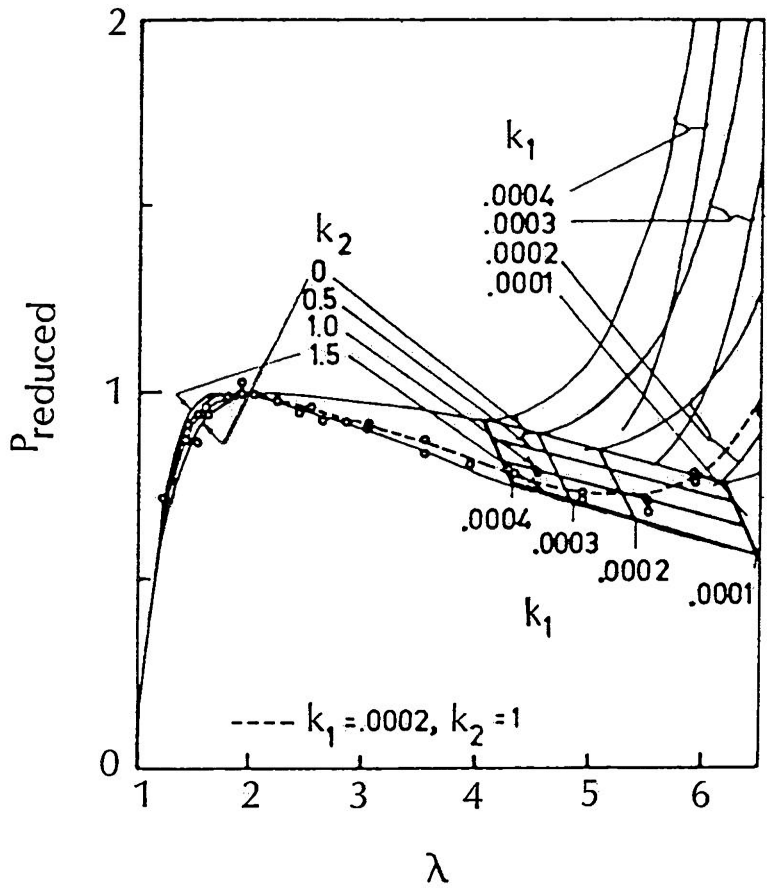

Figure 4.5:by using an overlying chart and the positions of the first peak and the valley Hart-Crisp and Smith(1967) suggested that estimation of the finite elasticity constants for an inflated rubber can result from a plot of the reduced pressure versus the stretch ratio value at the crown.

always demonstrate bifurcation. Hart-Crisp and Smith(1967) considered exactly such a material through their S.E.F. and exploited the shape of the Pressure.v.Stretch curve (first peak followed by a valley) as in fig.4.5. The specific site of the pressure minimum in the valley gives by the use of an overlay chart the value of K_1 and K_2 of equation (4.58).

4.5.2 The Simplified Cylindrical Geometry.

Shells of cylindrical shape have been widely used for practical applications. The analysis introduced previously can be further simplified for a such geometrical shape.

A cylindrical surface is depicted in fig.4.6b, it is the special case of a "line generated surface" of fig.4.6a for the pointing vector $\bar{i}$ having a constant direction along the curve $\bar{K}(\theta_1)$. The position vector is:

$$\bar{r}=\bar{K}(\theta_1)+\theta_2\bar{i}, \quad \theta_1=\theta, \quad \theta_2=\bar{S} \tag{4.72}$$

the unit vector tangent to the surface is:

$$\bar{t}=\partial\bar{K}/\partial\theta=\partial\bar{K}/\partial\theta_1 \tag{4.73}$$

base vectors now are: $\bar{a}_1=\bar{t}$, $\bar{a}_2=\bar{i}$, if R=(1/k)=radius of curvature then:

$$\partial\bar{t}/\partial\theta'=\partial\bar{t}/\partial\theta=-\bar{a}_3/R=-k\bar{a}_3 \tag{4.74}$$

$$\bar{a}_{1,1}=-k\bar{a}_3 \tag{4.75}$$

$$\bar{a}_{1,2}=\bar{a}_{2,1}=\bar{a}_{2,2}=0 \tag{4.75}$$

the contravariant base vectors of the middle surface are:

$$\bar{a}^1=\bar{a}_1=\bar{t}, \qquad \bar{a}^2=\bar{a}_2=\bar{i},$$

then $C_{11}=\bar{a}_3\cdot\bar{a}_{1,1}=-k \quad C_{12}=\bar{a}_3\cdot\bar{a}_{1,2}=0 \quad C_{22}=\bar{a}_3\cdot\bar{a}_{2,2}=0$ (4.76)

Figure 4.6:

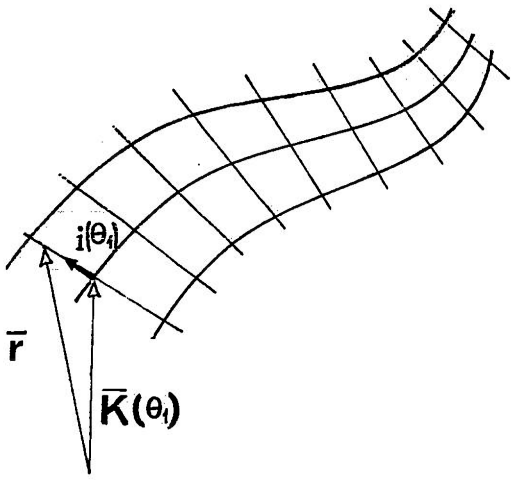

(A)

line generated surface $\bar{r}=\bar{K}(\theta_1)+\theta_2\ \bar{i}(\theta_1)$

for $\theta_1=\theta$, $\theta_2=\bar{s}$, $\bar{r}=\bar{K}(\theta)+\bar{s}\ \bar{i}(\theta)$

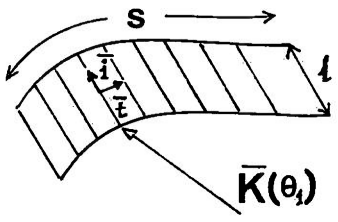

(B)

cylindrical surface $\bar{r}=\bar{K}(\theta)+\bar{s}\ \bar{i}$, $0\leqslant\theta\leqslant\bar{s}$, $0\leqslant\bar{s}\leqslant l$

$$C_1^1=C_{11}=-k \qquad C_2^1=C_1^2=C_2^2=0$$

and the Christoffel symbols: $\Gamma^{\alpha}_{\beta\gamma}=a^{\alpha}.a_{\beta,\gamma}=\Gamma^{\alpha}_{\beta\gamma}=0$ (4.77)

stress resultants are:

$$n^{11}=n_\theta \qquad n^{12}=n^{21}=n_{\theta\xi} \qquad n^{22}=n_\xi$$

$$p^1=p_\theta \qquad p^2=p_\xi \qquad q^1=q_\theta \qquad q^2=q_\xi \tag{4.78}$$

and the physical ones are:

$$n_{(11)}=n_\theta \qquad n_{(12)}=n_{(21)}=n_{\theta\xi} \qquad n_{(22)}=n_\xi$$

$$q_{(1)}=q_\theta \qquad q_{(2)}=q_\xi \qquad p_{(1)}=p_\theta \qquad p_{(2)}=p_\xi \qquad p_{(3)}=p \tag{4.79}$$

the equilibrium equations become:

$$\begin{aligned} \partial n_\theta/\partial\theta + \partial n_{\theta\xi}/\partial\bar{S} + p_\theta &= 0 \\ \partial n_{\theta\xi}/\partial\theta + \partial n_\xi/\partial\bar{S} + p_\xi &= 0 \\ kn_\theta - p &= 0 \end{aligned} \tag{4.80}$$

the last equation then immediately gives the stress resultant n_θ in terms of load:

$$n_\theta=p/k=pR \tag{4.81a}$$

as it can be seen n_θ is not influenced by any edge conditions, while:

$$n_{\theta\xi}=-\int^{\xi}(\partial n_\theta/\partial\theta+p_\theta)d\bar{S}+W_1(\theta) \tag{4.81b}$$

$$n_\xi=-\int^{\xi}(\partial n_{\theta\xi}/\partial\theta+p_\xi)d\bar{S}+W_2(\theta) \tag{4.81c}$$

include functions $W_1(\theta)$, $W_2(\theta)$ which have to be determined by the edge conditions.

In a cylinder of infinite length the circumferential stress resultant equals, $n_\theta=pR_\theta$, while the contribution of the longitudinal stress resultant in balancing the normal force to the surface is small due to the infinite value of the radius(curvature equals zero).

For a finite cylinder with end plates (fig.4.7) inflated by a uniform pressure p equation (4.52) predicts the presence of a longitudinal

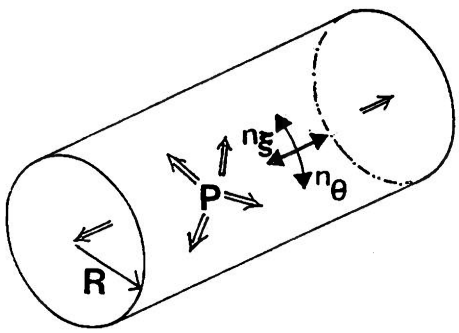

Figure 4.7:for a finite cylinder inflated by uniform pressure p, the longitudinal stress resultant(n_ξ) equals half the circumferential stress resultant(n_θ).

stress resultant which equals half the circumferential stress resultant.

4.5.3 Conclusions-Prominent Features Of Inflation.

In spite of the many differences between the various inflation tests of tables4.1,4.2 some common features exist which can be properly exploited.

There is a general correspondence between the material properties, the system of coordinates in use, and the orifice shape. At the boundary the displacements are zero, their gradients are also zero and the circumferential stretch ratio is constant and equal to unity. For a numerical method this is essentially an initial value problem and the solutions are set to converge to certain values. A circular orifice then is best expressed in cylindrical coordinates by setting the previously measured parameters to certain values at a certain radius. The Cartesian system of orthogonal axes best expresses the rectangular orifice along its orthogonal axes.
Isotropic materials or those of transverse isotropy or the radially stretched sheet are better examined by the use of a circular orifice which possesses a similar symmetry. Materials with orthotropic properties in the plane of the sheet are likely to require the use of a rectangular system of coordinates with a rectangular orifice and of course an alignment between those two, which may not be an easy task as the principal axes are not always known.

The boundary can significantly affect the shape of the whole bubble as can be seen in fig.4.8. It may well be that the shape of the orifice can be constructively used to deform the bubble at a desired shape.

In a complete mathematical solution the field of stresses and strains over the whole mebrane is usually estimated. This requires

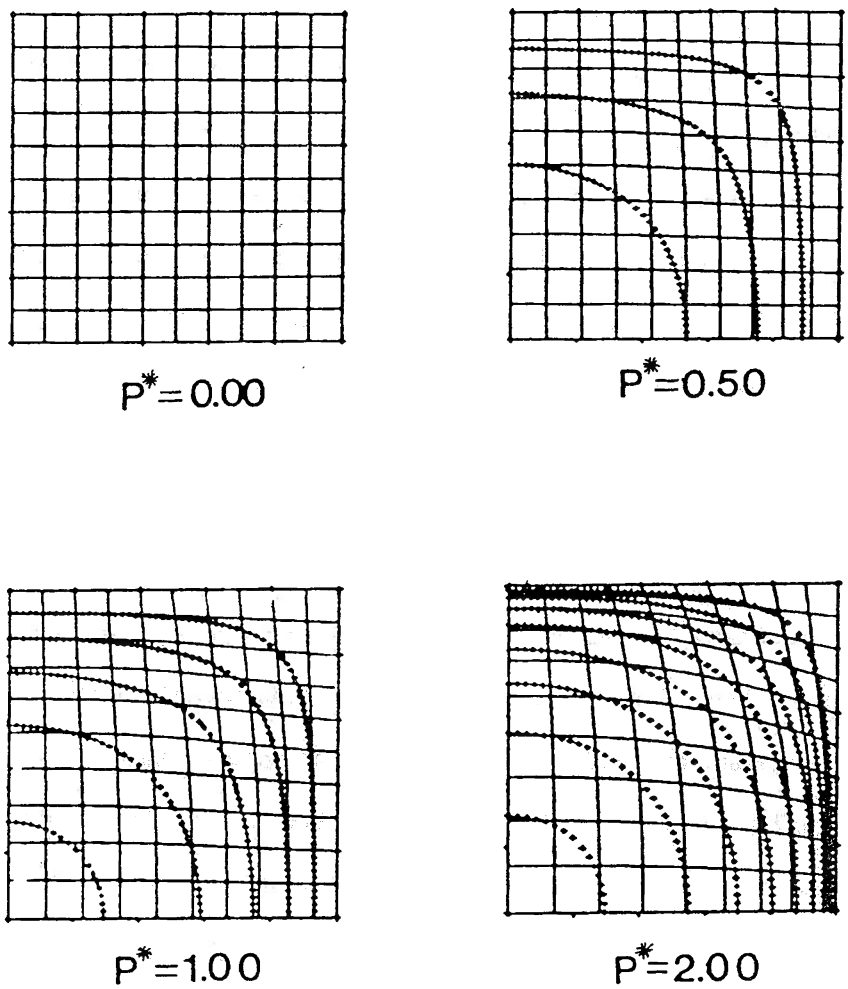

Figure 4.8:deformed configurations of an inflated plane nonlinear Mooney membrane at increasing reduced pressure (P^*) values. The constant contour lines are directly influenced by the shape of the boundary (reproduced from Feng and Huang,1974).

that a)a specific mathematical formulation has been developed, and b)that the proper S.E.F. has been fed to the elasticity conditions(Yang and Feng,1970). This, however, is never the case in the use of inflation as a testing method, because the stress/strain relations are themselves sought. In experimental cases the deformations should be recorded (direct calculation of strains), and then the stresses estimated from the geometry. The law of Laplace is a useful tool at this instance as it is the only condition which is generally applicable and with least restrictions. It can be used for evaluation of stresses where it is most convenient for the experimenter. Once the appropriate relation is obtained, the experimenter may try to compare the shape and deformation of the bubble mathematically with that predicted by the S.E.F he has already acquired.

Inflation is a non-uniform and a non-homogeneous deformation as both the magnitude and the direction of the principal stresses vary from site to site on the bubble. An elementary rectangle of the initially undeformed membrane deforms and distorts in a trapezoid or a general curvilinear parallelogram when the sheet is inflated. This, initially, has been thought to be advantageous by Joye and Poehlein(1972), if it could provide a mode where an infinite number of biaxial alternatives could exist on the same sample, but the same authors later(1973) found this to be a rather elusive possibility. The non-uniformity of the stresses(as well as stress resultants and thickness) does not appear to significantly affect the radial component of the stress resultant which attains a more or less constant value from the crown to the boundary, regardless of the material used or the particular application (fig.4.9). Nearby points on the same meridian have almost equal radial stress resultants.

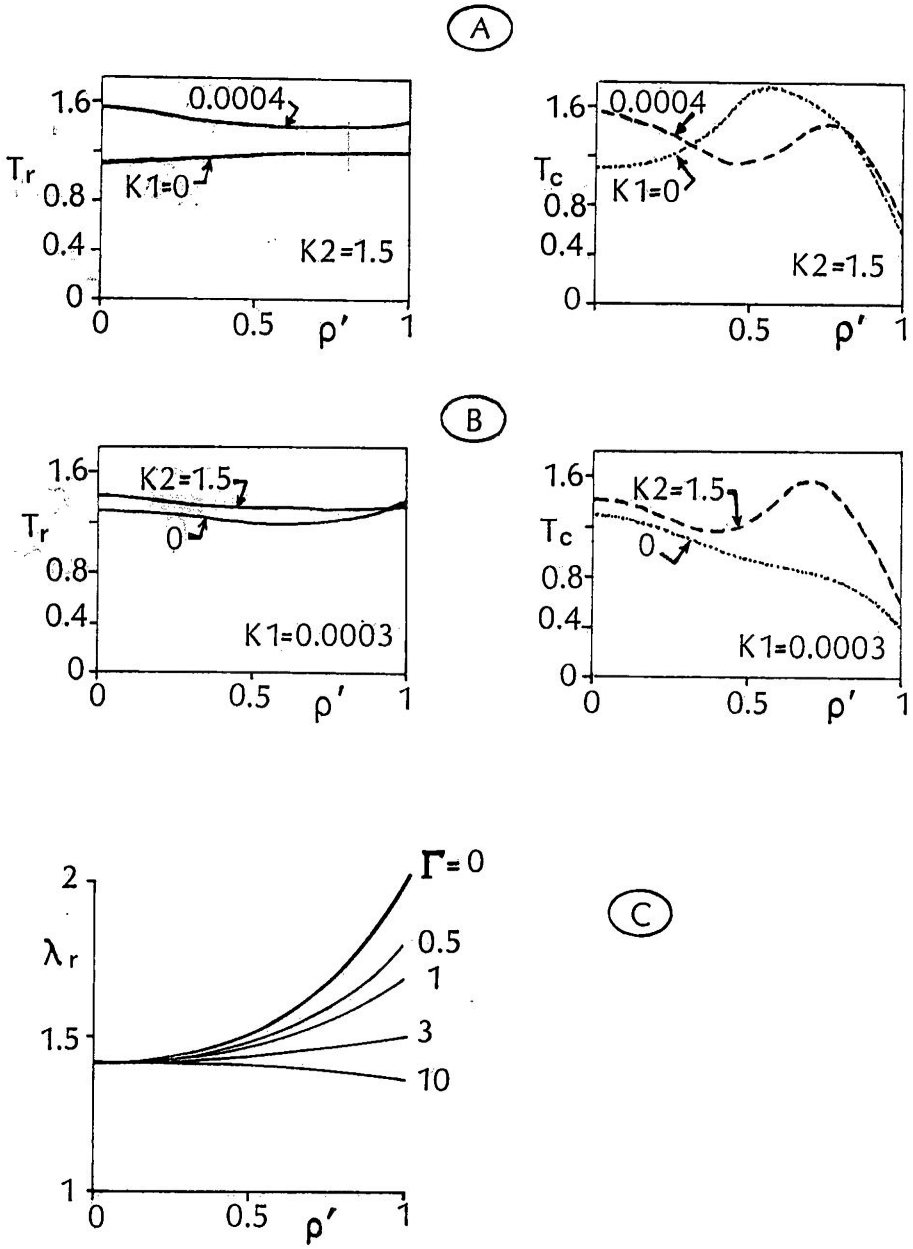

Figure 4.9:in (A) and (B) the radial stress resultant does not vary much from the centre of the bubble($\rho'=0$) to the boundary($\rho'=1$), while the circumferential stress resultant fluctuates considerably (reproduced from Hart-Crisp and Smith,1967). At (C) the stiffer the material is the more constant the radial stretch ratio λr remains along this same distance ($\rho'=0,\rho'=1$) (reproduced from Pujara and Lardner,1978).

4.6 USE OF INFLATION ON TISSUES.

Miller et al(1979) attempted characterisation of the mechanical properties of human fetal membranes by an inflation method. The basic assumption was that the kinematical behaviour of the tissue was the same as that of rubber and thus the axisymmetrical equations presented in earlier sections could be applied. The S.E.F. was of the Mooney form a function of two parameters C_1, C_2. The formulation was developed on a determination of the inflated surface at different stages of inflation by fitting to the profiles of the bubble a simple analytical expression. For determination of deflections at various radial distances the deflection of metal rods, which were attaching the specimen, was used. This must have affected their data straight from the beginning and in association with numerical computational errors resulted in them finding that the material parameters for rubber were varying with the level of inflation! The results were reported as a histogram for the distribution of the estimated values of the parameter C_1, with parameter C_2 being almost $0.1C_1$.

Wineman et al(1979) also thought that inflation has the potential of derivation of the S.E.F. for tissues and based on the same well known axisymmetric, isotropic incompressible relation they attempted to prove this claim. They tried to exploit the idea that each material point of the bubble is under different biaxial homogeneous extension along the two principal directions of the axisymmetrical deformation. In axisymmetrical conditions the crown is under uniform biaxial stretch, which gradually turns into pure shear deformation at the boundary where always $\lambda_2 = 1$. Thus certain deformation modes are common at different sites at different inflation levels and thus computational effort is reduced. Unfortunately demonstration of the method was performed on data that had been generated and not

experimentally observed. The same form of representation was used to identify the S.E.F. as was used to generate the data. These workers promised to present an application on tissues in a later report, but none has appeared in the literature. The main obstacle is probably that tissues have S.E.F. of the most diverse form and thus the good knowledge of the S.E.F. which is required to initiate the solution is also the main task of the experiment.

Kriewall et al(1983) inflated fetal dura mater and attempted to characterise the material by determining the parameters of the S.E.F. they used. One of these workers (Melvin et al,1970) had already established the anisotropic and viscoelastic nature of the mechanical properties of dura mater but in the case of inflation tests they assumed once again that the material was incompressible, homogeneous, isotropic and non-linearly elastic. The formulation of the problem then conveniently followed the mathematical analysis described in the earlier sections of the chapter and invariably used by all(Hart-Smith and Crisp,1967; Green and Adkins,1970). One further limitation was that the porosity of the fetal dura mater required the use of a rubber sheet underneath to seal the leaking air and thus the exhibited properties were a superposition of the properties of the rubber sheet and the properties of the dura mater under examination. Kriewall et al considered two possible forms for the S.E.F., that of a Mooney material and the STZC form(Skalak et al,1973) and decided that while the Mooney form was applicable to rubber properties, the combination of rubber and dura mater required the use of the STZC form. The determination of the pair of parameters used in the STZC form showed that one of the parameters could be maintained constant while the second which they called "stiffness" factor had to vary significantly to fit different samples. The only clinically important result was

that the tissue stiffness, as expressed by the stiffness factor, increased with age. However promising the fit of the behaviour by using a certain S.E.F. may appear for this particular tissue it has not been confirmed for other deformations than inflation and thus it remained very much an academic exercise.

Mohan and Melvin(1983) inflated human aortic specimens which were examined in both quasistatic and dynamic inflation rates and up to pressures which resulted in failure. The failure of aortas caused of excessive pressures or pathophysiological conditions led these workers to concentrate on failure behaviour and not the quantification of stress/strain behaviour. The anisotropy of aortas as found in uniaxial tensile tests(Mohan and Melvin,1982) was also demonstrated in the biaxial failure test by exhibiting a consistent tear in the transverse direction of the specimens. There was no statistical difference in the ultimate stresses and strains between quasistatic and dynamic biaxial tests, or in the ultimate stresses between dynamic biaxial and dynamic uniaxial tests.

4.7 INFLATION OF AN ANISOTROPIC MATERIAL.

It can be seen in tables4.1,4.2 that one possibility has not been examined or considered at all and it is exactly this class of materials that may constitute the equivalents of naturally occuring tissues; inflation of a material with orthorombic symmetry (having properties symmetrical to 3 orthogonal planes) and of a material with fibre symmetry (with the fibre axis lying on the plane of the membrane). Materials with fibre symmetry are like the ones with transverse isotropy but in the latter case the directions of identical mechanical behaviour lie on the plane of the sheet. Both the orthorombic material and the fibre symmetrical with the odd axis on the plane, are anisotropic in the plane of the sheet and it is likely

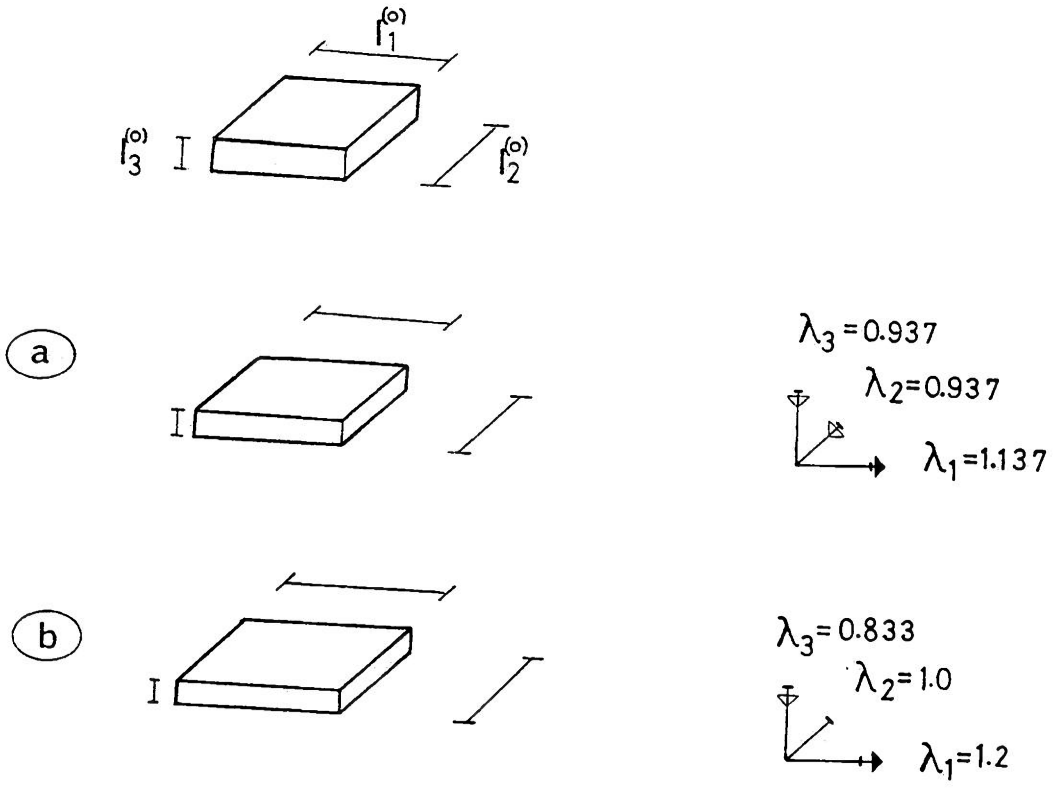

Figure 4.10:case a´ uniaxial stretch of an elemental parallelepiped with lateral contraction along the other two directions; case b´ uniaxial stretch along direction 1 may be combined by retention of the lateral dimensions along direction 2 at a stretch ratio=1.

that inflation of such materials can be expected to yield a non-axisymmetric deformation. Either of those materials has on the plane a symmetry along orthogonal directions and thus we suspect that this will lead to an "orthotropic" deformation, the shape of the inflated membrane reflecting the anisotropy of the material.

4.7.1 Search For A Suitable Material.

Suitable materials of such properties were sought to test this assumption but a)it not easy to find a material being anisotropic in its resting condition, and thus b)it was decided to "produce" an anisotropic material by prestretching an engineering material which has the additional advantage of being with consistent properties from sample to sample. Vulcanised rubber was used, which is cheap with reproducible and consistent behaviour and exhibits large deformational behaviour. Although the physics of rubber elasticity are yet not fully understood the mechanical behaviour of rubber has been extensively investigated over the years. Furthermore rubber, which is isotropic in its unstrained state can be brought into either of the anisotropic cases of orthorombic symmetry and fibre symmetry mentioned earlier, if appropriately stretched.

In the elemental parallelepiped of fig.4.10 directions 1,2 are in the plane of the membrane and direction 3 is the normal to the sheet. Associated to these directions are stretch ratios: λ_i, i=1,2,3. The undeformed parallelepiped can be deformed in either of the cases in fig.4.10a or 4.10b. We chose to create a difference $|\lambda_\alpha-\lambda_\beta|=0.2$, $\alpha,\beta=1,2$, $\alpha\neq\beta$, in the stretch ratios in the plane of the sheet.
case a':If stretched along λ_1 it will contract along λ_2, λ_3 and due to isotropy by equal amounts $\lambda_2=\lambda_3$. If the incompressibility condition is also valid then $\lambda_1\lambda_2\lambda_3=1$ and $\lambda_2=\lambda_3=(\lambda_1)^{-1/2}$. This requires a simple tensile stretching till $\lambda_1=1.137$ in respect to the undeformed

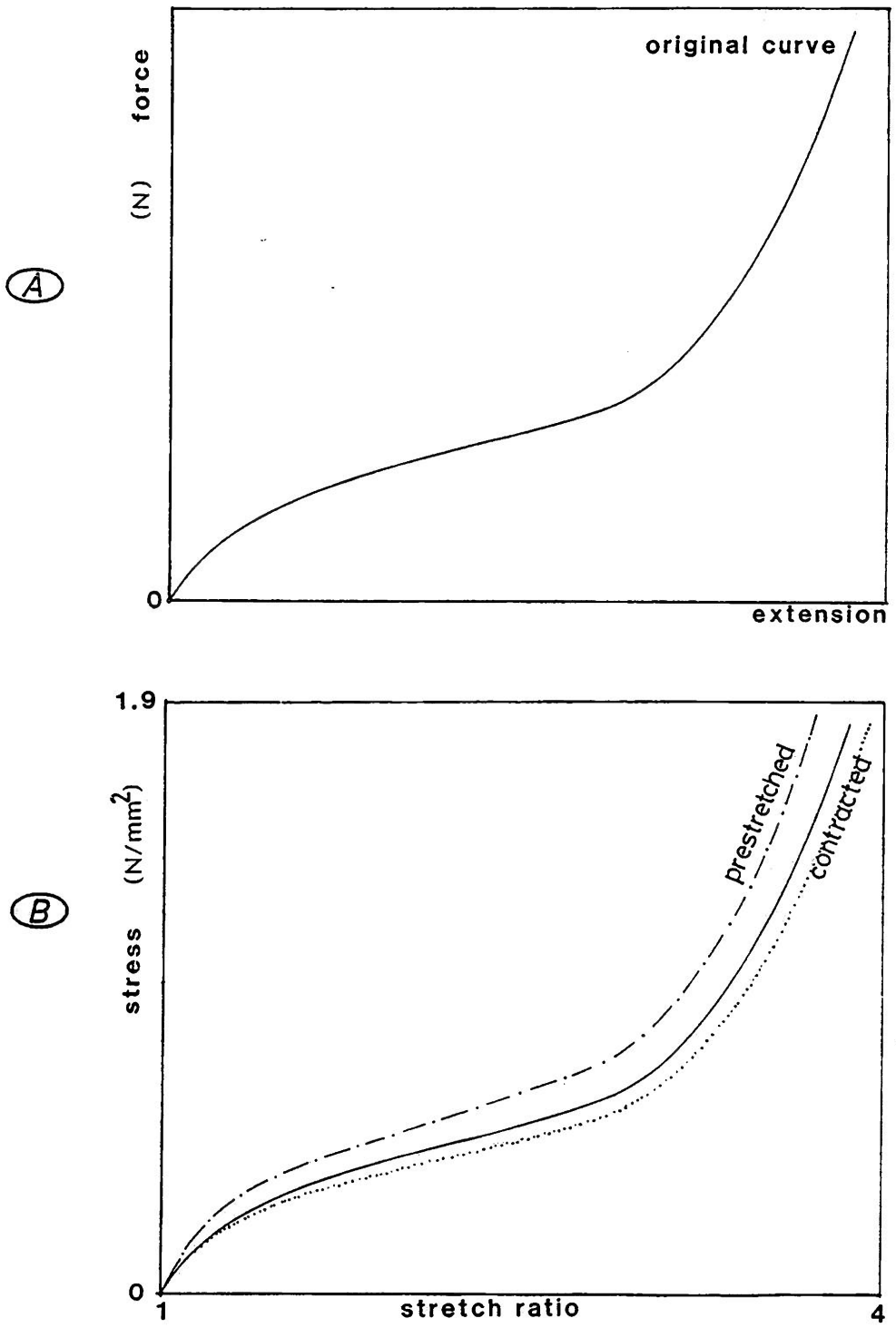

Figure 4.11: (A) typical force/extension curve produced in uniaxial stretcing rubber; (B) relation (4.83) predicts that along the prestreched direction the stresses will be increased while along the contracted direction the exhibited stresses will be reduced.

reference length $1_1^{(o)}$ and with the previous assumptions this must be followed by a contraction to $\lambda_2=\lambda_3=0.937$.

case b′:If stretched along 1, till $\lambda_1=1.2$ and held at constant $\lambda_2=1$ then this will lead to a compression $\lambda_3=0.833$. (FT)

A typical force/extension curve for vulcanised rubber is shown in fig.4.11a. It has been obtained by uniaxially stretching strips of rubber 100mm in length, 10.64mm in width and of 0.24mm in thickness at a nominal strain rate of 0.005/min. It is a markedly non-linear curve which stiffens considerably presenting an upwards turn at stretch ratios greater than $\lambda^{(t)}=3$.

The question is how the prestretch will reflect on the mechanical properties exhibited in test where stresses and strains start from a zero(0,0) point. Calculation of stresses can be made by using the principle of S.E.F can be used, where the stress $f_i^{(t)}=\partial W/\partial\lambda_i^{(t)}$ at a particular direction. If the initial reference length for relaxed rubber was $1_1^{(o)}$, an equal new reference length after prestretch is noted by $1_1^{(o)'}$, but in essence in the stretched state it includes material that was contained in $0.81^{(o)}$ of the relaxed rubber. We define $\lambda^{(t)}$, $\lambda^{(t)'}$ as the current stretch ratios calculated when testing unstrained or prestretched rubber respectively:

$$\lambda^{(t)}=x(t)/1_1^{(o)} \qquad \lambda^{(t)'}=x(t)/1_1^{(o)'} \qquad (4.82)$$

these quantities are in fact only numerically equal because the real stretch ratio when stretching the already prestretched rubber λ_R, equals $1.2\lambda^{(t)'}$ times the one exhibited in test.

(FT).Subscripts:they denote principal directions i=1,2,3; superscripts:in parenthesis is the value of time or any other suitable monotonically increasing variable, thus $^{(o)}$ denotes the reference state at the start of the test, $^{(t)}$ is any subsequent state, the prime outside the parenthesis denoting that these same variables are of the test of the prestretched rubber.

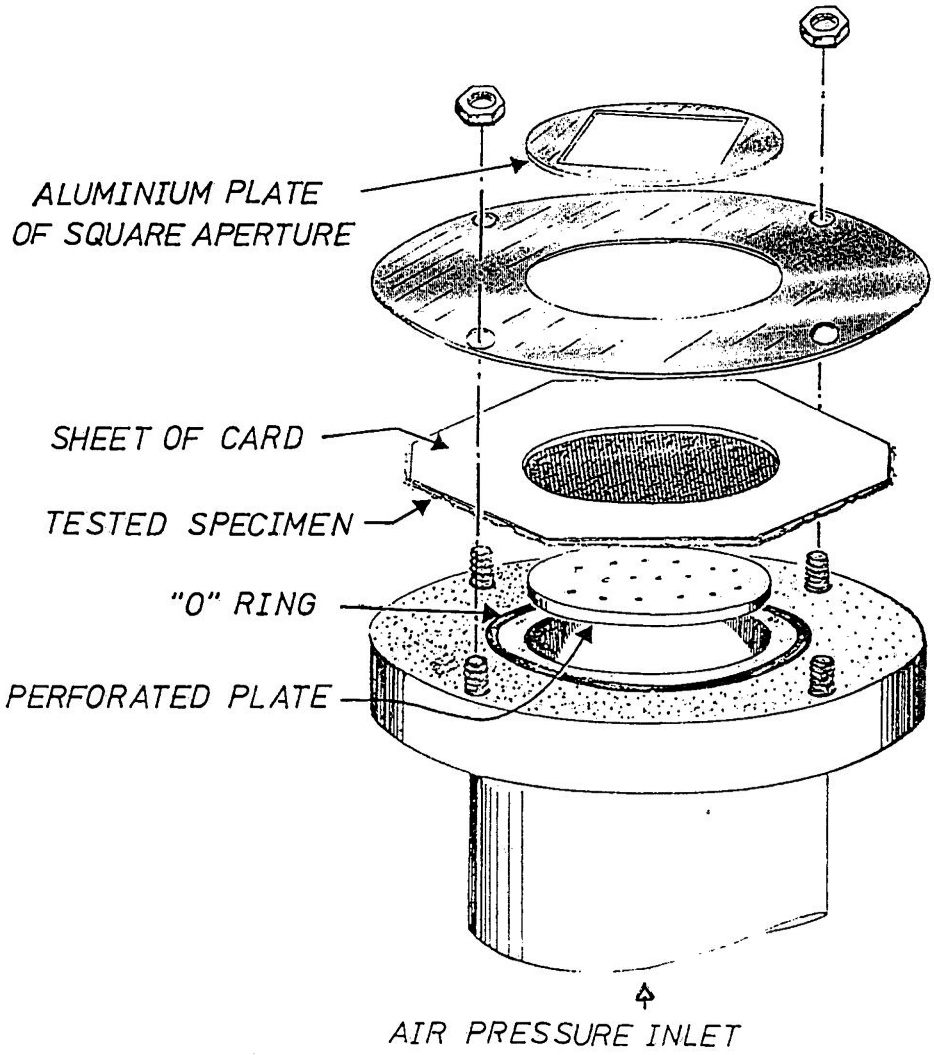

Figure 4.12: inflation apparatus.

Thus for the exhibited stresses:

$$f_i^{(t)'}=\partial W/\partial\lambda_i^{(t)'}=(\partial W/\partial\lambda_R)(\partial\lambda_R/\partial\lambda^{(t)'})=1.2(\partial W/\partial\lambda_R)=1.2f_i^{(t)} \quad (4.83)$$

and thus the stresses when testing the prestretched rubber along the prestretched direction should in fact lie at 20% higher values from the 'original' curve(rubber relaxed at its undeformed dimensions) for case a' and 13.5% for case b'. For contraction in the lateral directions we should expect the real curves to be at 6.3% (case a') and 16.7% (case b') less than the 'original' curve of fig.4.11a.

The curves of fig.4.11b start from a (0,0) origin for stresses and strains and this is particularly suitable for inflation where stresses are measured indirectly from the strains and thus no stresses can be predicted when no deformation occurs. The inflation of a flat rubber sheet is treated similarly for either prestretched and/or unstretched rubber as if the prestretched rubber is a naturally anisotropic material in its relaxed state when zero lateral pressure is applied. We suspect that the prestretched rubber sheet will produce a split of the 'original' biaxial curve into two, for the two principal directions.

4.7.2 Inflation Apparatus.

Inflation tests were carried out in the apparatus of fig.4.12. This device consists of a polymethylmethacrylate (PMMA) chamber, the top of which is made as an annulus of 90mm outside diameter and 41.5mm inside diameter, and thus provides an approximately 50mm wide annulus for clamping the samples along the perimeter between the PMMA annulus and a similarly shaped aluminium plate(fig.4.12).

The top of the annulus was covered by a layer of uniformly spread silicon-rubber to provide a surface that could be slightly compressed and of higher friction (not allowing slippage of the samples) and at

the same time not to cause any damage to the material. A recessed groove in the PMMA annulus adjacent to the central hole, housed a rubber "O" ring. The aperture of the apparatus was filled by a perforated PMMA disc which levelled with the top surface of the annulus and was there to support the undeformed specimen not allowing it to bend under gravitational forces.

Thus clamping a material or tissue on this stage allows the sample to be adequately held in its perimeter, to be subjected to air-pressure through the perforations and to deform in a shape mostly determined by the shape of the central aperture of the aluminium plate fixed on the top.

The pressure increase inside the chamber, which deformed the specimens, was created and controlled by a hand held sphygmomanometer. A large chamber (5 litres in volume) was connected to the tubing attached to the rig. This additional reservoir increased the volume capacity of the system and consequently the ratio of the air-volume pumped each time into the system by the sphygmomanometer to the total volume already present. This allows a better control of the deformation along with lower rates of inflation.

A sheet of rubber was prestretched according to case a′ by a stretch in one direction and contraction in the other two. To achieve this a wooden box was used housing a central hole of 115mm diameter. The hole had larger dimensions than the PMMA inflation annulus and could accomodate it on the inside. The unstretched sheet was stamped by a square grid and by the use of common "chinese ink", with the sides of the small grid squares being 5mm long. The sheet was stretched along one of the main directions of the grid and with the use of masking tape attached at various points along the perimeter. The use of a number of attachements of the tape onto the sheet allows

Ⓐ

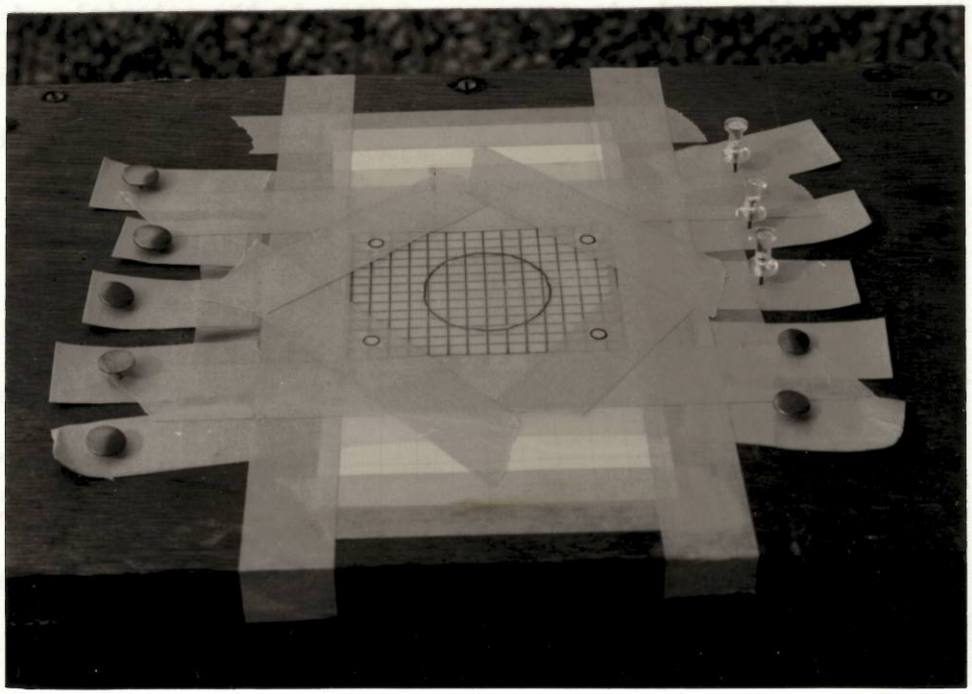

Ⓑ

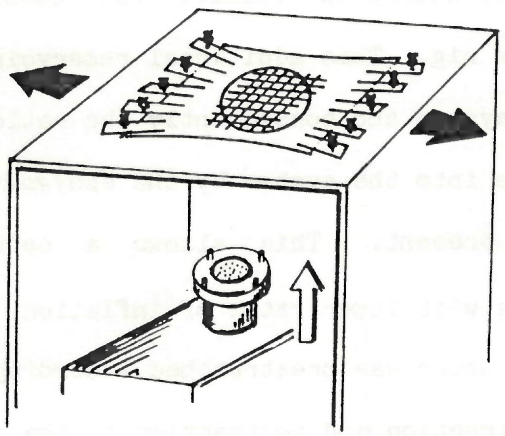

Figure 4.13:(A)preparation and maintenance of the rubber sheet in its prestretched state, (B)mounting on the rig.

lateral contraction in the free space between the tapes, while the use of a single tape all along the stretching edge would not. The rubber sheet was stretched till the appropriate stretch ratios had been achieved and in a manner that uniform deformation existed in the central area; this was easy to confirm due to the presence of the square grid. The outer edges of the tapes were pinned onto the wood and the sample appeared as in fig.4.13a ready to be mounted on the inflation rig.

The sheet was pierced in 4 sites to allow the inverted screws of the rig to pass through while ensuring that this had not affected the strain distribution around the holes, which in addition were closer to the outer diameter of the annulus and away from the central area. The rig was raised from underneath and (fig.4.13b) the specimen was mounted in its stretched state.

The pressure was increased slowly up to 2.66kPa(20mmHg) and the inflated shape was observed. It was definitely a non-axisymmetric surface which bulged outwards at 2 antisymmetrical positions.

In order to confirm this we applied the idea initially introduced by Feng et al(1974) (table4.2). They mathematically predicted that if a membrane is inflated against a constant constraint which happens to be flat, it will form an attachment boundary which, for small heights of depression, follows closely the surface contours (fig.4.14a). For larger depressions the boundary deviates significantly from the contour-shape of a freely inflated membrane (fig.4.14b). Thus a thick rigid glass plate was pressed lightly against the bubble at its crown which was inflated through the circular orifice, when it could be observed through the glass that the area of attachment had an oval boundary. At the same time it was obvious that the major-minor axes of the ovals were precisely aligned to the axes of our prestrech which

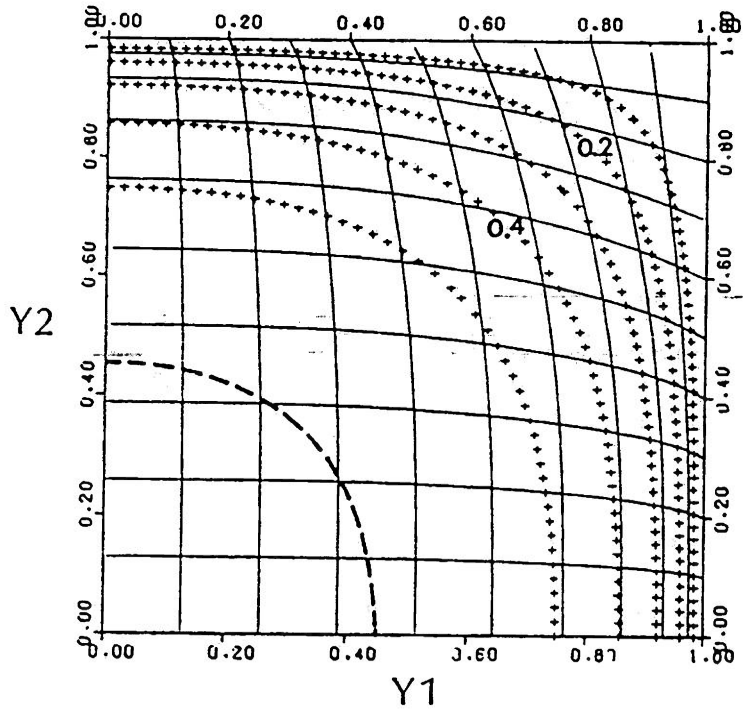

a

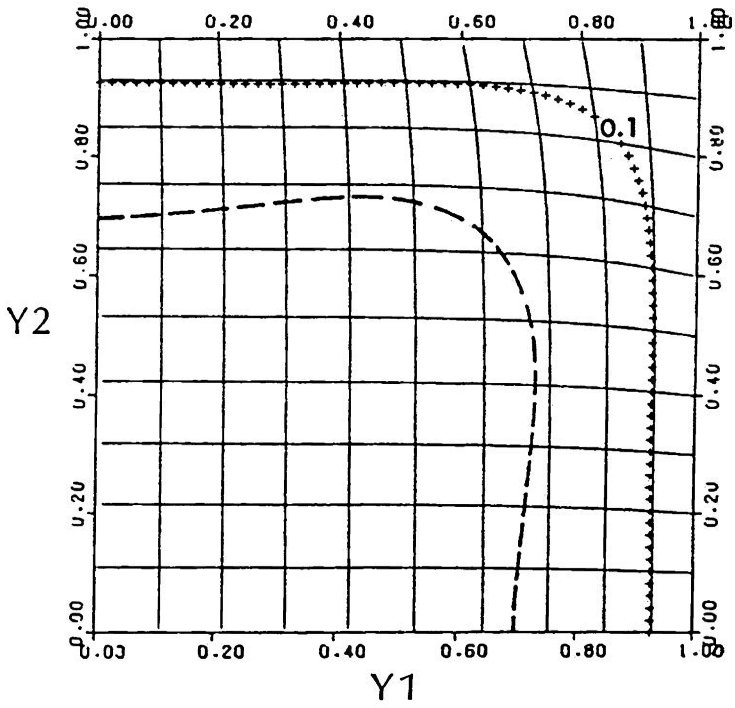

b

Figure 4.14:one quadrant of an inflated Mooney membrane against a constant constraint as predicted by Feng et al(1974). For small deflections the contact boundary follows closely the surface contours.

were along our stamped square grid.

This rather crude method is inappropriate to apply in inflation of soft tissues. It had to be substituted by another, which was stereometric and preferably non-contacting, because the contact itself distorts the shape of the bubble.

4.7.3 Shadow Moirē Technique.

4.7.3.1 Production of the fringes. The Moirē fringes are produced by the interference of a grating with its own shadow which is cast on the object's surface by the use of an intense light source. Assuming a rectilinear propagation of light (no diffraction present), gratings like the one in fig.4.15a can by superposition on their own shadow create the fringes of fig.4.15b. This phenomenon can be easily seen by superposition of two thin layers of silk(moirē) and gave its name to a technique which when applied in other forms can be invaluable in engineering strain analysis (Theocaris,1969).

The highly regular grating of fig.4.15 is not strictly necessary for the formation of the fringes. The potential of the "shadow Moirē" is that the shadow of even an irregular grid interfering with itself can form fringes. Highly regular gratings, with specified pitch are only required for a precise analytical treatment of the fringe pattern.

The three main elements for performing the "shadow Moirē" are the light source, the grid and the observing apparatus(camera). The nature of the illuminating and observing rays can either be diverging from a point light source or linear source (equivalently converging to a pin-hole observatory), or can both be parallel in their geometry (illumination and observation). That leads to the 3 cases possible of fig.4.16. If both light rays and observing rays are of the same nature (parallel or diverging) the fringes behind the screen are light

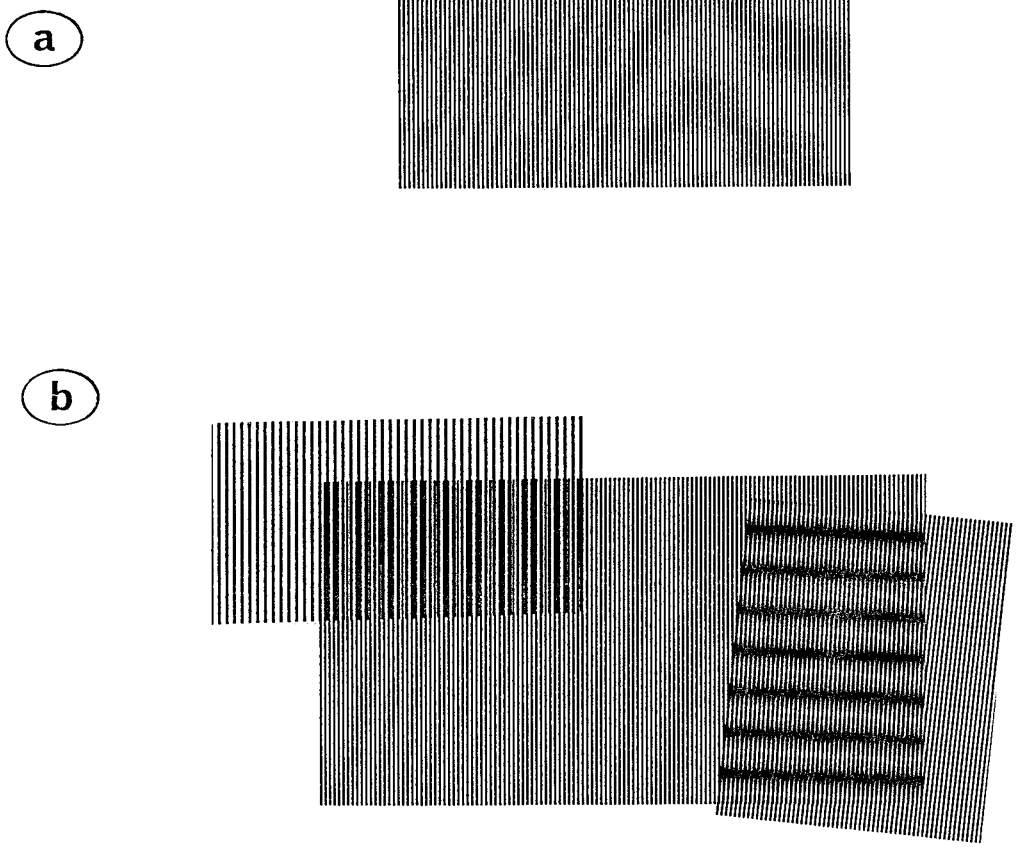

Figure 4.15:superposition of a grating with another of a larger pitch or with an angular displacement to the original creates Moiré fringes.

(a) grating of 16.75 lines/cm
(b) two gratings of 16.75 lines/cm and 9.5 lines/cm in parallel displacement and two gratings of 16.75 lines/cm in angular displacement

and dark planes parallel to the screen. Case 4.16a has the additional advantage of constant interfringe distance. For all cases the interfringe distances are constant depending only on the order of the fringe n, and not affected by the exact position of the object behind the grid. Case 4.16c has no advantages and should be avoided.

The order of the fringe gives the distance from the screen by the use of formulas:

case a) $Dh = s \cot(i)$, s:pitch, Dh:distance to screen, (4.84)

case b) $Dh(n) = nl/[(d/s)-n]$, (4.85)

using the screen to fringe depth, the 2-dimensional image information of the fringes yields a 3-dimensional reconstruction of the object's surface.

Shadow Moirē can thus provide the means for determining the general shape of the inflation bubble and ultimately lead to a spatial analysis of the surface by examination of the topographical maps as depicted in photos.

4.7.3.2 Set-up of Apparatus. The three main components of the technique are shown diagramatically in fig.4.17. The main distances have been selected so as to provide a 1mm interfringe height for all fringes according to (4.84) or 1mm screen to first fringe distance for formula (4.85).

The light source was a 800W Halogen linear filament with a cylindrical reflector. When a line-shaped filament is used (as in our application) it is necessary to align it with the rulings of the gratings in order to create the shadow. This light source could be used as both a point source (especially if used with a slit in front) or as a parallel ray illuminator if used with a light stop along the filament(fig.4.17). It is essential that in either case the light

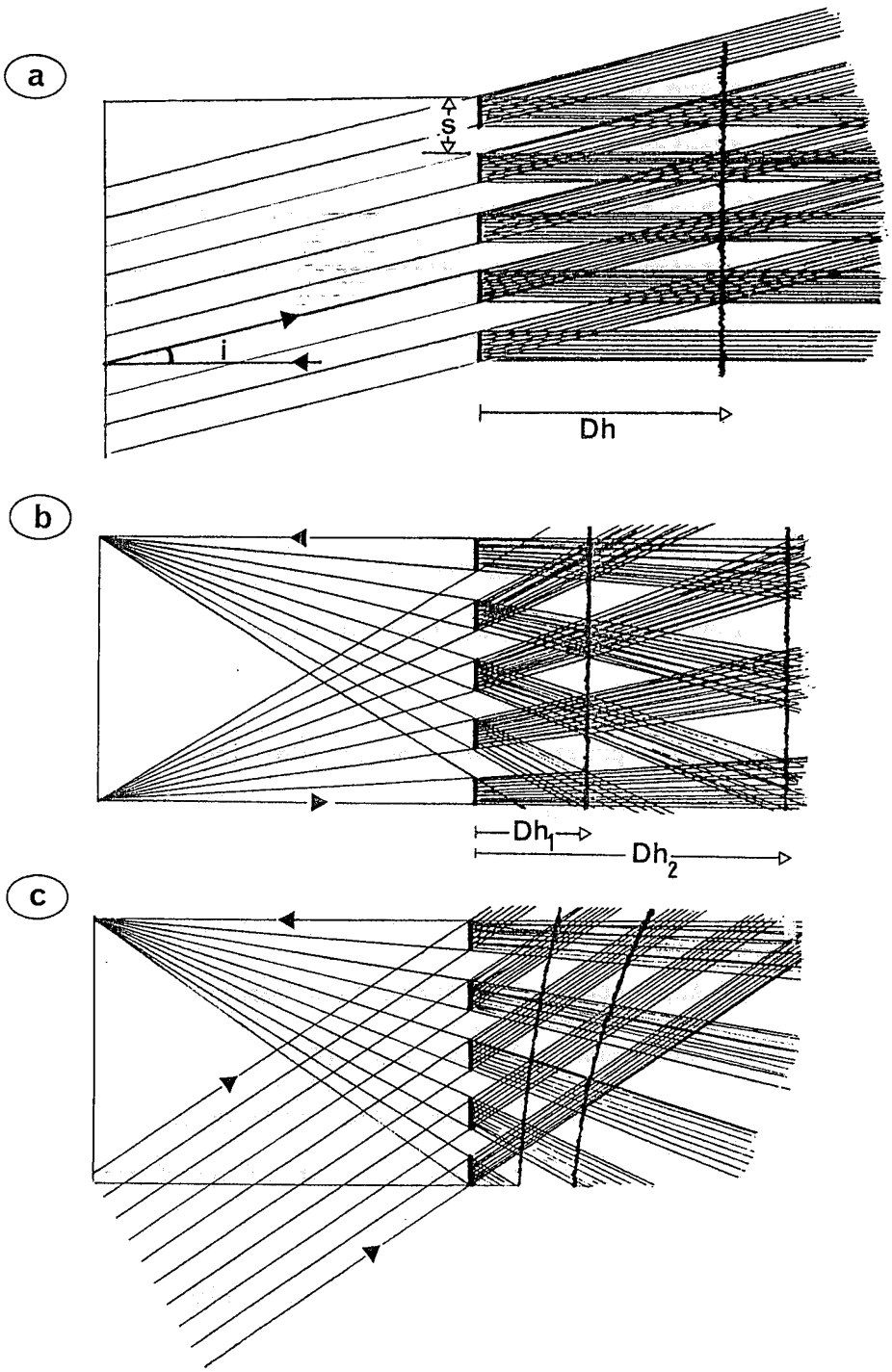

Figure 4.16:rays of illumination and observation can be either parallel or diverging leading to the three ilustrated cases. Case (a) has the main advantage of providing constant interfringe distance.

beam is collimated to avoid a blurred shadow which would prevent the formation of the fringes.

A 35mm Nikon SLR camera was equipped with a telephoto lens and an extension tube was used and could essentially fill the 35mm negative frame of the film with only the image of the central 41.5mm diameter circular aperture. Another camera, a 120mm Zenza Bronica, was set at the level of the inflation rig and could take side views of the bubble to be used in an estimation of the height of the central(maximum) deflection at the crown.

Geometrical considerations similar to those for the light source also apply to the camera. A pin-hole camera with a large aperture at a large distance l, can be considered as viewing the screen in parallel rays, while the same camera at shorter distances with a smaller aperture acts as a receiver for converging rays. In our application the distances were large and the aperture in use was of considerable size, f/8=50mm/8=6.5mm, but it is recommended that whenever it is possible formula (4.85) should be used for better precision.

In setting-up the technique it is important that: a)the camera should view the screen(grid) perpendicularly, b)the light source and the camera-lens should be in a plane parallel to the screen(grid), c)light and dark planes behind the screen are always formed in relation to the grid and parallel to it, thus a tilt of the grid results in tilted planes intersecting the object, d)the object should be placed under the screen on the optical axis of the camera for a better image, for the reason that areas in a distance of the normally viewed centre are seen through the periphery of the lens and the image could be optically distorted.

Limitations on the uncertainties Dl,Dd,Ds in the set up of the apparatus in order to achieve a specified small error in the fringe of

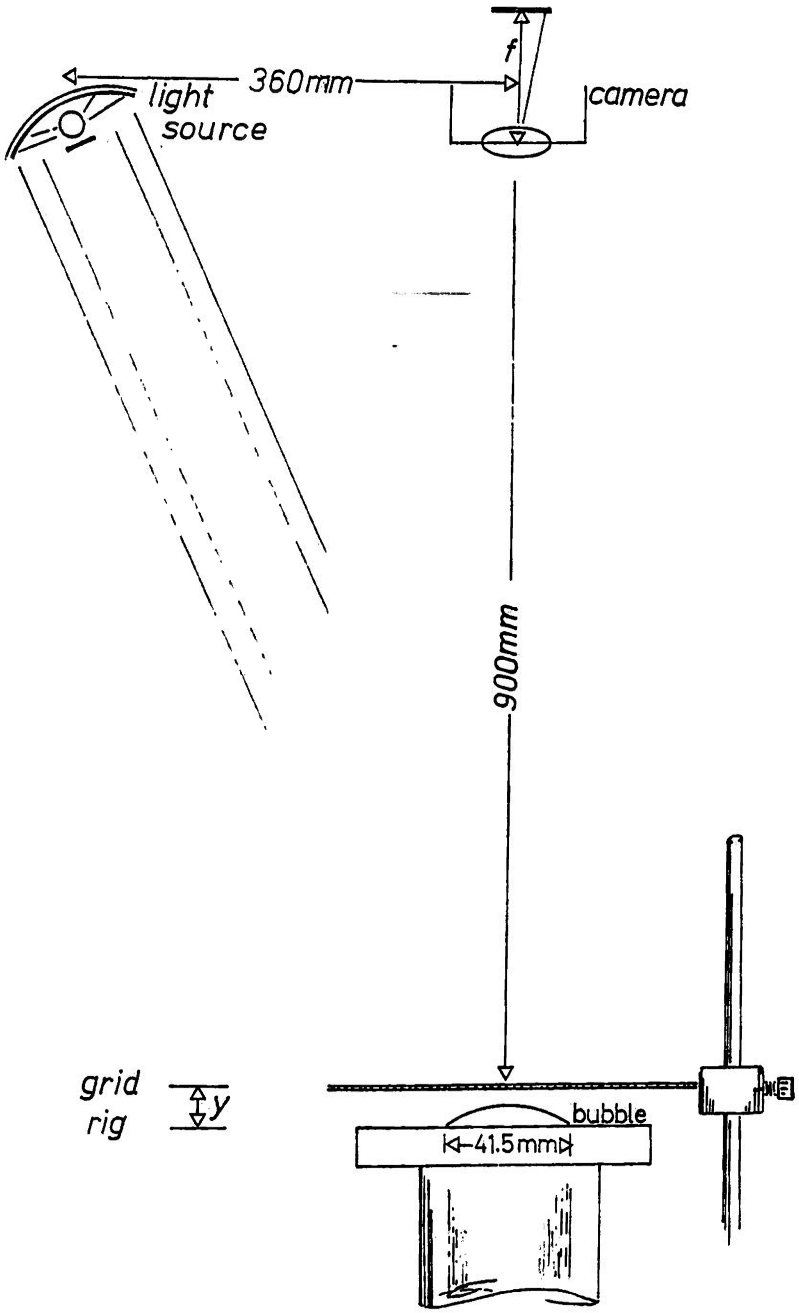

Figure 4.17:the set-up for photographic observations of the inflated samples. Distances have been chosen as to produce 1mm interfringe distances for the first fringes closer to the grid.

maximum y=3cm,
minimum y=central deflection at 0.266kPa(2mmHg)

order n have been estimated previously by Wijk(1980), who applied the rule of propagation of error in formula (4.85). For values of d,l,s scaled down to our own values the maximum uncertainty in placing the camera should be within $\pm$1cm, the uncertainty in camera to light source distance within $\pm$0.5cm accuracy in order to achieve an accuracy of half a fringe height at the depth of the 20th fringe. The values of those error bounds can relax for our application because the maximum height that the bubble attains is less than 20mm for medium pressures of less than 7.99kPa(60mmHg). Estimation of the errors is essential when accurate analytical treatment of the photos is required. It is safer to check the distances of the fringe planes with calibration objects since for this optical method small alterations of the relative place of the components can significantly affect the fringes.

The gratings used in the test apparatus were initially printed on thin films supported by a surrounding frame. It was found that they could bend slightly under their own weight and thus glass gratings were prepared similar to the ones used by Fenton(1973). Commercial gratings of translucent adhesive backings (Letratone-Letraset Ltd. U.K.) are readily available but their backings diffuse the light. If a contact print of these gratings is made on high contrast glass plates (Ilford N.60 photochemical plates,backed) the dark lines are retained while the translucent backing is replaced by the transparent glass surface.

It was found that there was a limit on the depth at which discernible fringes could be formed on the screen. It is recommended that the screen is as close as possible to the object in order to retain as much as possible of the effective depth of the field of the fringes. Experimentally it was found that 20mm was the maximum depth

Ⓐ

Ⓑ

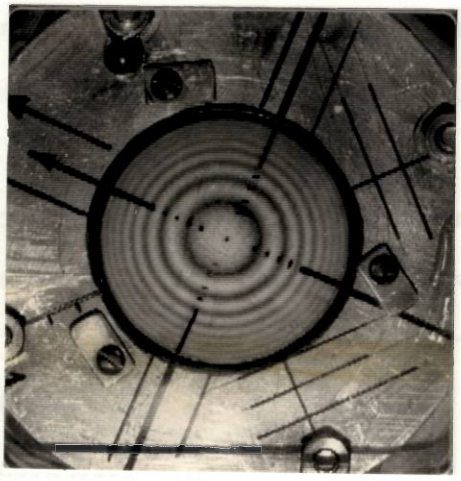

Figure 4.18: flat Ⓐ and inflated Ⓑ (20mmHg) Moiré views of the mounted prestretched rubber sample. The dark arrow on the rig platform indicates the contracted dimension; along this direction the sample is softer, thus more extensible and presenting the long axes of the ovals.

of field for forming clear fringes. This was adequate for all the following experiments.

4.7.3.3 Moiré imaging of inflated rubber specimens. The prestreched rubber sheet which had been prepared and mounted on the rig as described in section 4.7.2, was inflated and observed with the Moiré apparatus of fig.4.17. At a pressure of 2.66kPa(20mmHg) the topographic image of fig.4.18b resulted. It was found that for certain surfaces (like rubber) a paint was required to improve the contrast and produce clearer fringes. In fig.4.18 an emulsion of titanium dioxide in saline was used on the yellowish rubber surface in order to enhance the contrast. Titanium dioxide is a white pigment used in paint and it has the additional advantage of being inert and non-toxic (Deichman Gerarde,1969) and can be washed off. These features make the solution particularly suitable for subsequent use with biological tissues.

In fig.4.18b the light(alternative dark) fringes had unequal axes along the orthogonal directions which coincided precisely with the axes of prestretch and contraction and thus the axes of mechanical anisotropy. This result demonstrated that the method could indeed be used to identify the axes of mechanical anisotropy by determination of the principal geometrical directions of the surface. In order to confirm this claim the test was repeated a number of times from the prestretch stage to the Moiré views and always the arrow on the aluminium plate, which showed the direction we had expected to be more extensible, coincided with the major axes of the ovals.

The reason for the production of the ovals is demonstrated by the profiles of fig.4.19. The outer profile along the more extensible direction has a larger length and intersects horizontal planes (equal height,z) at larger radial lengths than the profile produced in the

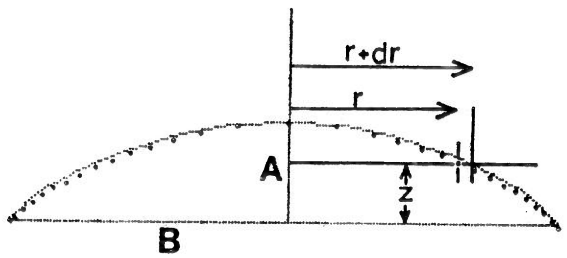

Figure 4.19:the production of the ovals is due to the unequal length of the two profiles which at a certain height z present different radial distances r and r+dr, the latter corresponding to the more extensible direction on the sample.

stiffer direction.

4.7.3.4 Analytical form for the surface. There are two reasons why it would be better if we could express the exhibited shape of the bubble in an analytical form. Firstly, in test the bubble does not deform in any of the simple axisymmetrical geometrical shapes that have been considered in tables4.1,4.2 (paraboloidal, sector of a sphere) and this may be due to the fact that a more general geometrical form had not been devised. Thus a new geometrical shape to be used with this great variety of materials could be particularly useful. Secondly, for rubber in particular which has attracted much attention in the past, it would be very helpful if we could describe its complete deformational behaviour throughout the whole test more precisely.

We started considering the general ellipsoid of fig.4.20a with the unequal axes A,B,C, participating in the implicit relation:

$$x^2/B^2 + y^2/C^2 + z^2/A^2 = 1 \qquad (4.86)$$

it becomes an ellipsoid of revolution (fig.4.20b) by putting B,C:

$$x^2/B^2 + y^2/B^2 + z^2/A^2 = 1 \qquad (4.87)$$

this form could possibly describe an axisymmetrical deformation but it does not yield different profiles along the orthogonal directions. Thus we modified it by introducing coefficients l_x, l_y as:

$$x^2/(B^2+l_x z) + y^2/(B^2+l_y z) + z^2/A^2 = 1 \qquad (4.88)$$

thinking that: 1)for $l_x=l_y=0$ it yields the previous equation(4.87), 2)for z=0 it yields the correct boundary of an ellipsoid of revolution since $B^2+l_x z=B^2+l_y z=B^2$, 3)for z=A (at the crown) it converges to a general ellipsoid with 3 unequal denominators $B^2+l_x z=B^2+l_y z=A^2$ and especially 4)it complies with our observation that the radial

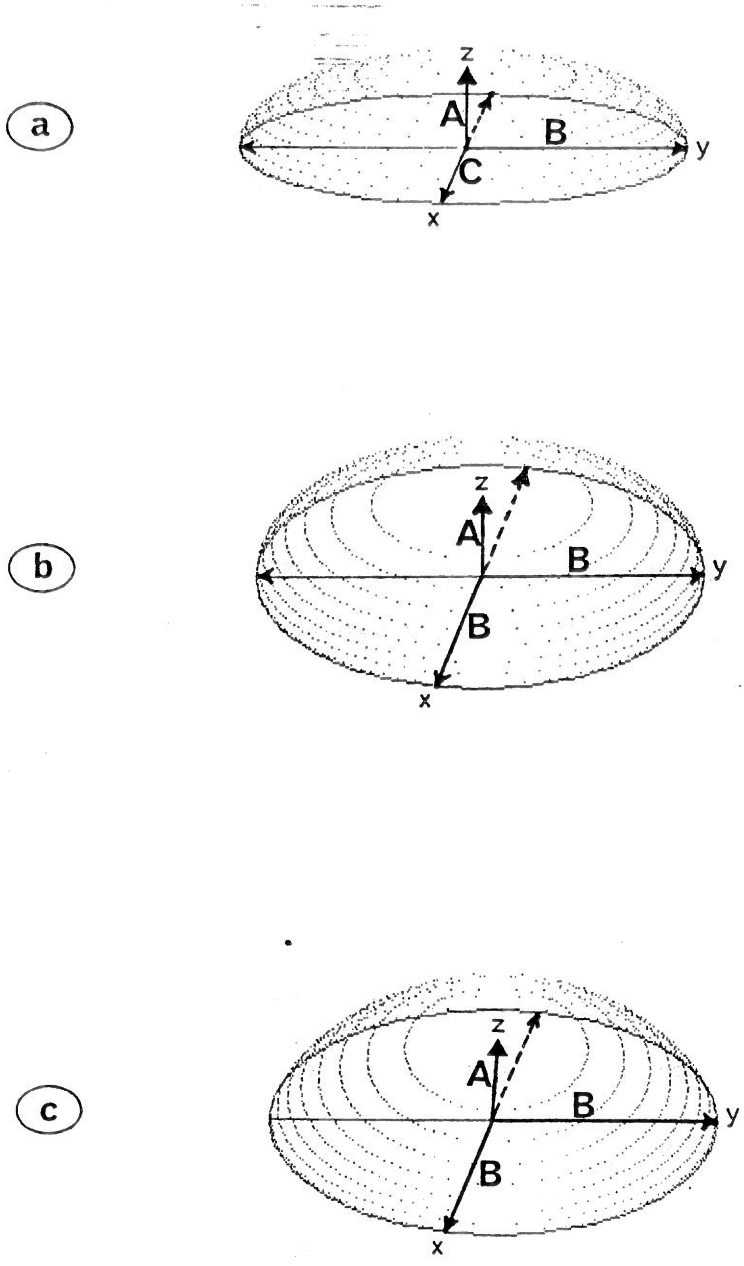

Figure 4.20: (a) a general ellipsoid of three unequal semi-axes A,B,C; (b) an ellipsoid of revolution and (c) the distorted ellipsoid of revolution resulting by use of relation (4.88).

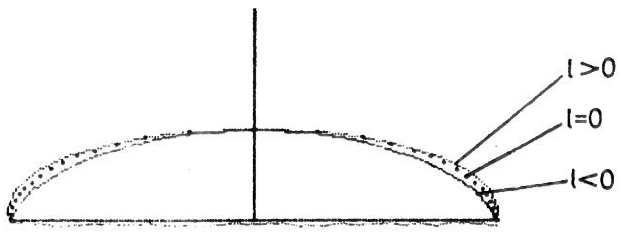

Figure 4.21:by putting the coefficient l to have positive or negative values, a profile could be drawn on the outside or the inside of the original profile of a simple ellipsoid of revolution (l=0) respectively.

difference of the two profiles of fig.4.19 is actually proportional to the height z for medium heights.

It was found (fig.4.21) that a positive coefficient 1 in (4.88) produces a profile outside that produced by equation(4.87) while if 1 is negative the profile would lie on the inside. Model (4.88) could sufficiently follow the real surface along the profiles but it was still uncertain how well it would behave in between the principal axes. It was expected that since formula(4.88) describes a smooth continuous surface which converges to the real one along the profiles, it would not differ significantly for the rest of the surface.

After repetitive trials the most probable values for the coefficients l_x, l_y were defined from the lateral views of the bubble at various inflation levels. These coefficients were subsequently fed into a computer program ("CONTOUR",Appendix Ch:4) which drew contours for height-steps corresponding to the interfringe distances of Moiré so that if the correct coefficients had been selected along with the proper interfringe heights, then the contours should predict and coincide with the light fringes of the photos.

The result for inflating the bubble with pressures of 1.33, 6.66kPa is shown in figures4.22a,b,c and on the overlying transparencies the contours have been drawn. Coincidence is good especially for the inner contours. Discrepancies could be due to the fact that the contours have been drawn to the size of the photos with a magnification factor calculated from reference points on the rig while the camera is focussed on the screen. There is a small out of focus magnification (fig.4.23) and has been accounted in the program by using formulas (4.89),(4.90) which correct the differences between the real distances X,Y and the apparent x,y. The differences are due to the projective geometry of the apparatus and the use of a pin-hole

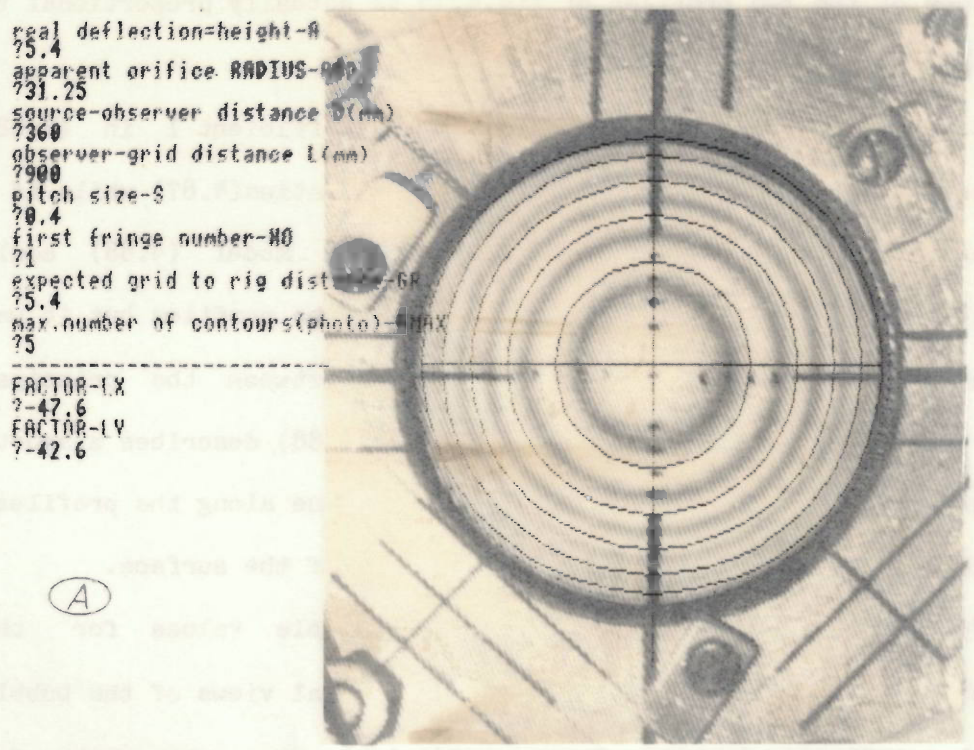

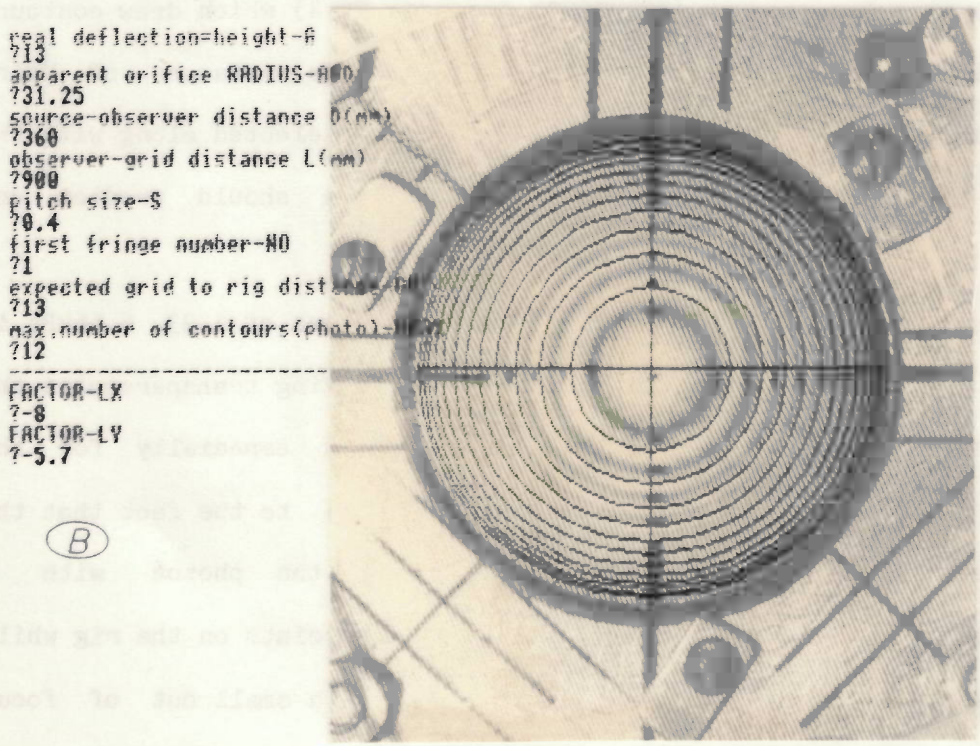

Figure 4.22:The Moirē views of the inflated sample at (A) 1.33kPa(10mmHg) and (B) 6.66kPa(50mmHg); on the transparencies the predicted contours by using (4.88) could adequately describe the surface contours especially for the inner fringes(closer to the grid).

camera.

The interfringe height is calculated with the variable depth formula(4.85) which particularly helps the deeper fringes corresponding to the outer contours of fig.4.22. Variable interfringe distance and projective geometry are factors which have been considered and implemented in Moire topography by previous workers (Takasaki,1973; Meadows et al,1970; Wijk,1980).

The good agreement between the graphical contours and the fringes of the photos shows that analytical description of non-axisymmetrical inflated caps is possible and that more complicated expressions such as formula(4.88) should be considered in the future.

4.7.4 Quantification Of Deformation.

4.7.4.1 Use of a square orifice. In section 4.6 it was suggested that there was an appropriate shape for the boundary to match the type of anisotropy of the membrane and thus form the inflated dome at a suitable geometrical shape which allows the quantification of the deformation. Having succesfully applied the "shadow Moiré" to inflation of circular specimens, the technique was applied to square specimens. An aluminium plate having a square orifice was locked into the circular aperture of the inflation rig. The sides of the square orifice were 26mm long and aligned with the orthogonal principal axes of prestretch.

Through the square aperture the sample deformed into the shape of a squared dome and with the lateral orthogonal views of the bubble shown in figures4.24a,b. The profiles of the dome could still be described by formula4.88 and the use of coefficients l_x, l_y, but now 4.88 applies only on the principal axes and not on the whole surface. The complete deformational behaviour of the material through the two orifices is compared in fig.4.25. The central deflection A is plotted

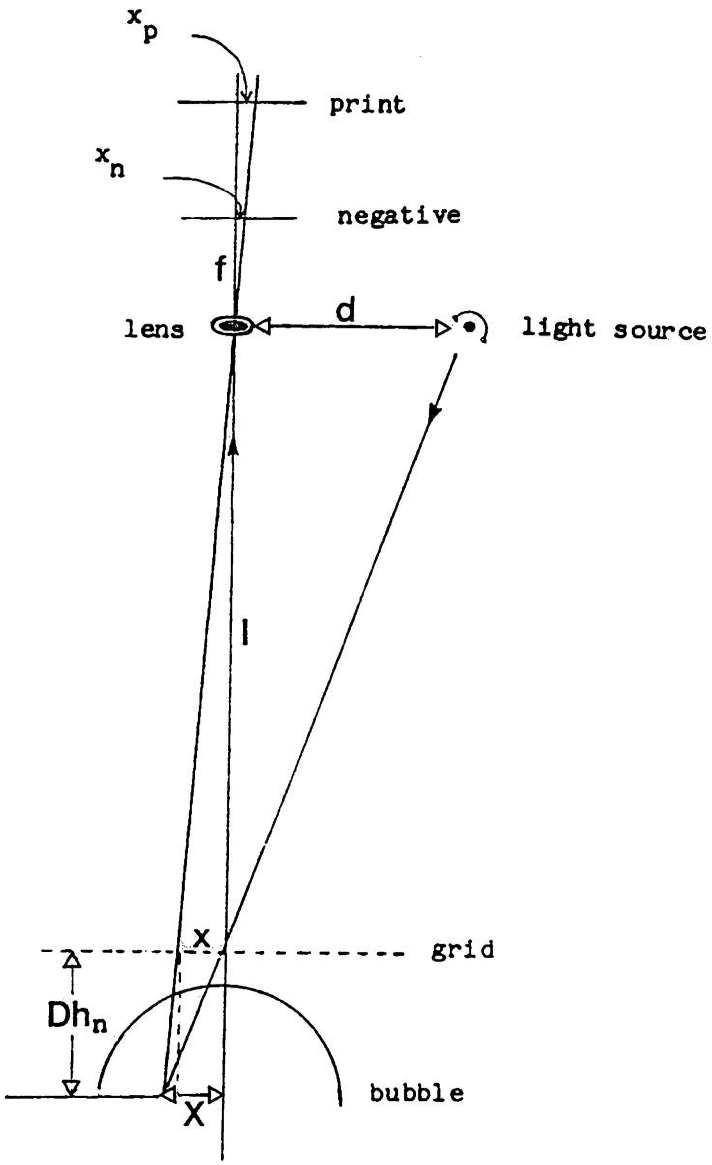

$$X = x\left(1 + Dh_n/l\right) S \quad ; \quad (4.89)$$

$$Y = y\left(1 + Dh_n/l\right) S \quad ; \quad (4.90)$$

Figure 4.23:corrections for perspective geometry and for variable interfringe height have been incorporated in the computer program which drew the Moiré contours.

against the normal pressure and it is sensibly less for the square orifice as it corresponds to a specimen of smaller initial dimensions. The plot of the coefficients against the control variable(pressure) shows a similar behaviour for both orifices with a sharper decline for the square orifice. This difference is not an adverse effect of the square orifice because the local shape of the dome is quite different for the two bubbles along the profiles. Along most of the length of the square-dome profiles a cylindrical shape exists with the generating lines parallel to the sides of the square boundary, suggesting that stress/strain relations could be obtained by the use of the Laplace formulas at those cylindrical sites.

4.7.4.2 Selection of sites. Thorough observation of the square dome of figures4.24a,b with both the lateral cameras and the Moire apparatus led to the selection of the area of the 4 neighbouring dots appearing in the photos. They corresponded to radial distances of 4,6,8,10mm from the centre and had been marked by the use of normal black ink. A number of concentric circles of similar radii had been drawn on the perforated Perspex plate which supported the sample when the specimen was flat and helped us in the marking procedure. The markers were placed at a mid-distance between the centre of the specimen and the square boundary; consequently all values of stress and stretch(strain) were calculated on those marked areas.
The camera for the lateral views was slightly above the level of the rig in order to render the markers on the profile visible.

4.7.4.3 Stress/strain formulas. The stress resultant was calculated by the use of (4.81c) which produced an Eulerian value for this variable. It was further divided by the initial thickness of the rubber sheet, h=0.25mm, to produce a semi-Lagrangian stress value.

The local value of curvature was also needed for the stretch. It

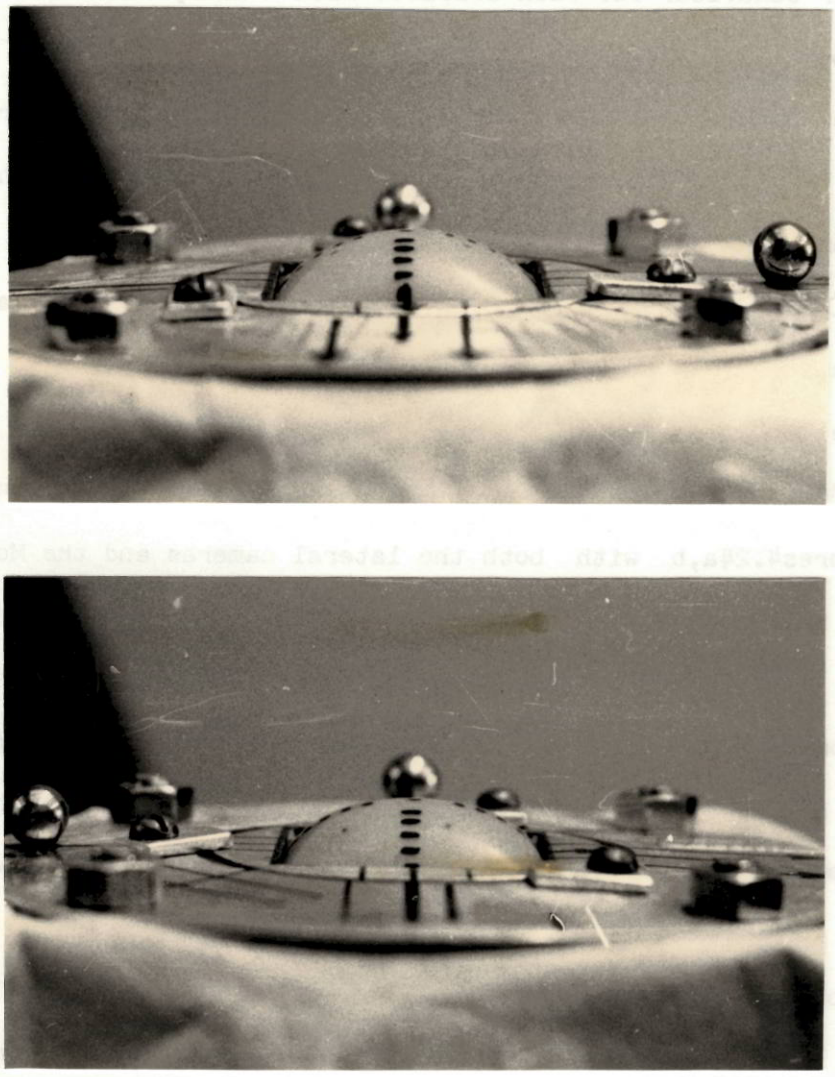

Figure 4.24:two orthogonal views of the inflated bubble to demonstrate the different profiles along the two principal directions at a 5.33kPa (40mmHg) pressure.

was calculated by measuring the quantities of tables4.3,4.4. The formula used was:

$$R=[(l^2)+(s^2)]/2s \qquad (4.91)$$

this formula applies to an arc of a circle and thus it has to be assumed that the small space between the outer dots had a circular shape.

The stretch ratio was calculated by formula:

$$\lambda = 1 + 2\,R\,[Arc(\sin(1/R))]/L_o \qquad (4.92)$$

which calculates again the stretch produced by deforming an initially undeformed length L_o into the arc of a circle of radius R. The distances were measured on a digitiser table. The estimated stretch ratio was equivalent to a Green strain since it was calculated with respect to undeformed dimensions.

All measurements were performed on enlarged photos and the values were scaled down to normal sizes by division by the magnification factor. We have used a Calcomp 9000 digitiser with 0.025mm resolution for objects in the enlarged photos. Thus real object dimensions were estimated with a resolution error of 0.001mm, leading to an error of 0.01 in the stretch ratio.

The measurements of stress/strain pairs were performed at the 5 inflation levels of the test and for pressures of 1.33, 2.66, 3.99, 5.33, 6.66kPa (10, 20, 30, 40, 50mmHg). The result is shown in fig.4.26. A pair of curves appeared which predicted that for the same stress levels a different stretch value was exhibited by the sample in the two orthogonal directions. The curve on the left which predicted higher stresses for the same strains was obtained along the prestretched direction and thus demonstrated the effect that

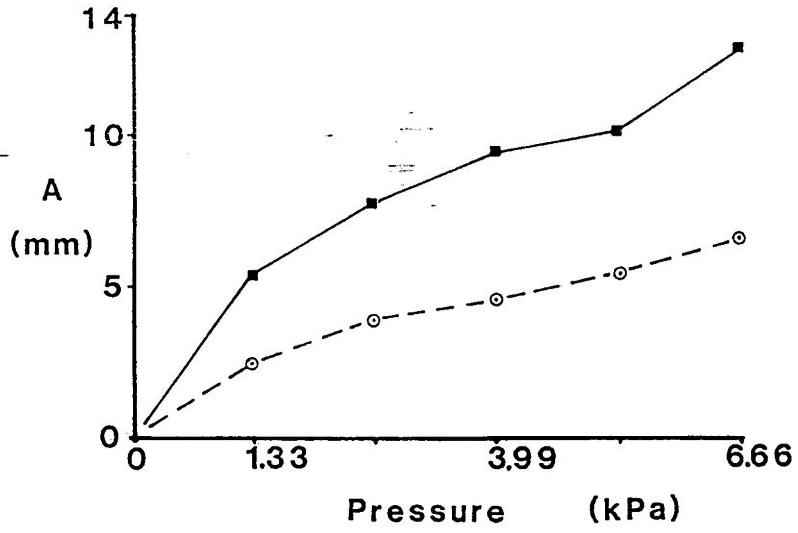

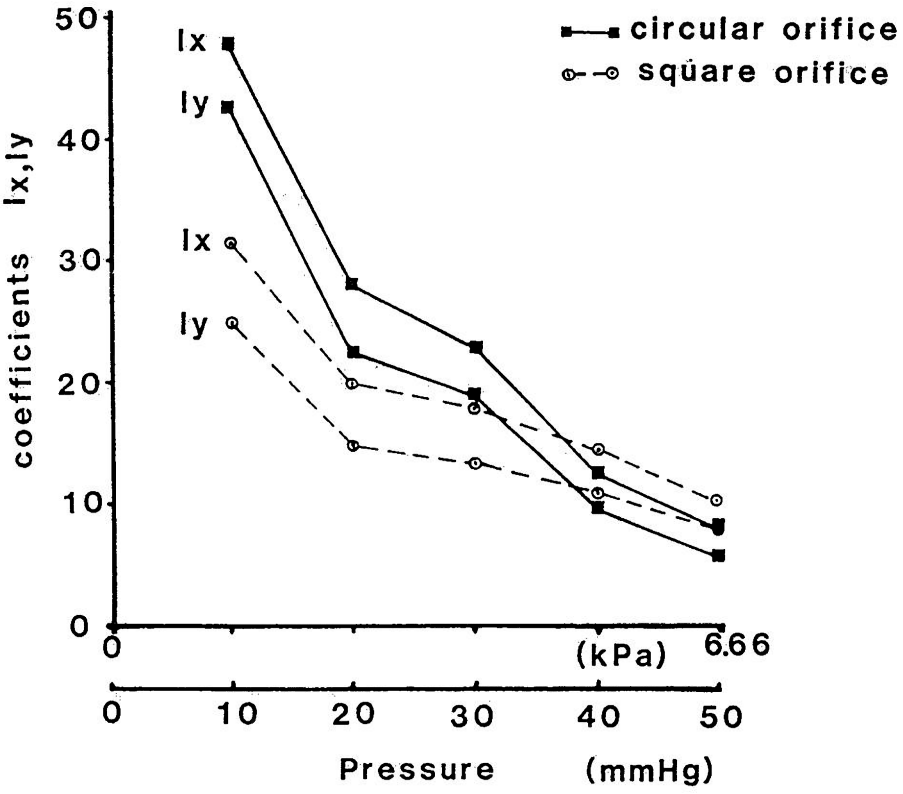

Figure 4.25:deformation through the introduced square orifice and through the initial circular orifice were very similar regarding the behaviour of the central deflection A and the variation of the surface coefficients with the applied normal pressure.

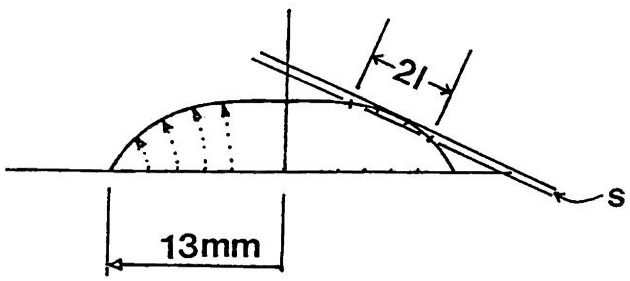

Table 4.3: profile of prestretched direction

Measured parameters			Calculated values			
pressure (133.32 N/m²)	l (mm)	s (mm)	Radius (mm)	λx	Tx (N/mm)	Sx (N/mm²)
10	6.05	0.30	31.60	1.044	0.042	0.168
20	6.20	0.50	19.99	1.072	0.053	0.213
30	6.40	0.65	16.45	1.110	0.066	0.263
40	6.50	0.90	14.23	1.130	0.076	0.303
50	6.80	1.01	12.09	1.188	0.080	0.322

Table 4.4: profile of "soft" direction

Measured parameters			Calculated values			
pressure (133.32 N/m²)	l (mm)	s (mm)	Radius (mm)	λy	Ty (N/mm)	Sy (N/mm²)
10	6.06	0.48	19.89	1.048	0.026	0.106
20	6.26	0.70	14.64	1.087	0.039	0.156
30	6.45	1.00	11.01	1.128	0.044	0.176
40	6.60	1.05	10.99	1.156	0.058	0.234
50	6.82	1.20	10.33	1.198	0.068	0.275

prestretch had in producing an anisotropic material in its reference state.

4.7.5 Validation Of The Method.

Treloar(1975) has given the mechanical behaviour for a number of different testing modes applied in rubber. The curves for uniaxial tension and pure shear tests have been reasonably confirmed by us by testing strips of rubber (of the same type that was prestretched) in an INSTRON tensile testing mashine. The resulting curves for the inflation of the anisotropic rubber sheet fell on either side of Treloar's biaxial curve with the prestretched direction lying on higher stresses and the contracted direction lying on lower stresses. In order to be able to predict the behaviour in the hypothetical case where equibiaxial stretch of an isotropic material is performed formula (4.83) was used with the S.E.F. given by Ogden(1972) for rubber. Ogden's formulation(1972) could adequately describe Treloar's data(1975) and the predicted curves are shown in fig.4.27a having been produced by using a set of coefficients in the formula:

$$W=\sum_{n}\mu_n/a_n(\lambda_1^{\alpha_n}+\lambda_2^{\alpha_n}+\lambda_3^{\alpha_n}-3) \qquad (4.93)$$

from which for biaxial mode where $\lambda_3^2=1/\lambda_1=1/\lambda_2$, and $t_1=t_2$, $t_3=0$ the nominal stress results in:

$$f=t/\lambda=\sum_{n}\mu_n(\lambda^{\alpha_n-1}-\lambda^{-2\alpha_n-1}) \qquad (4.94)$$

with the set of coefficients $a_1=1.3$, $a_2=5.0$, $a_3=-2.0$, and $\mu_1=0.63$, $\mu_2=0.0012$, $\mu_3=-0.01$ (μ in N/mm^2). The split biaxial curve alongwith the inflation data is shown in fig.4.27b. The comparison is reasonable and the discrepancies may be due to either: a)not very accurate fit of Ogden's formula to the original rubber curves, or b)experimental error in the inflation data, or c)slight differences between used rubbers, or d)to the fact that the inflation mode is not

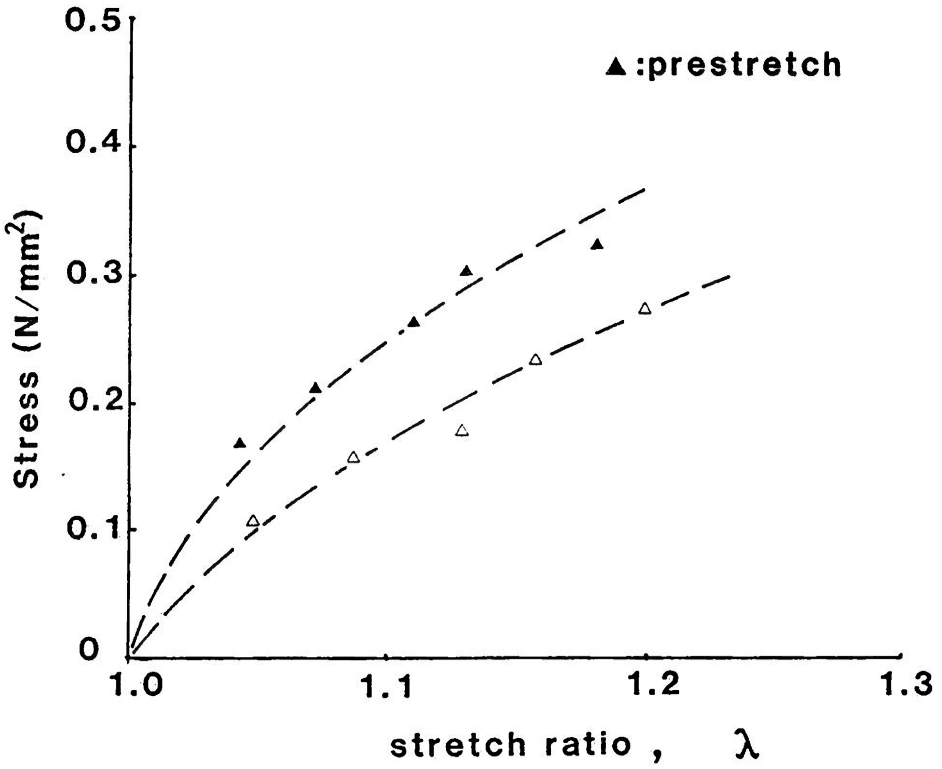

Figure 4.26:the biaxial inflation curves for the prestretched rubber specimen. The prestretched direction was both stiffer and less extensible.

a simple equibiaxial stretch and the estimated stresses and strains are calculated at two different areas on the axes of mechanical symmetry.

4.7.6 Discussion.

The arguments applying to the test and the produced data have been introduced in section4.7.1 while preparing the rubber sheet. Inflation is incapable of demonstrating the stress which is already there due to prestretch, because it treats the zero pressure state as being the reference state and for the reason that stresses in particular are calculated indirectly through the measurement of the curvature. For this reason both inflation curves converge to the true zero/zero origin for both stresses and strains without predicting any initial values.

The 20% prestretch can not also be experienced by the strains which are represented by the horizontal difference between the curves. There we observe that starting from a zero difference we end up at a value for the strain difference between the curves of approximately 50% of the initial prestretch that had been induced. This is the result of marking the sample after we had prestretched it and thus treating the prestretched geometry as our reference configuration.

In both these respects our prepared and hypothetically anisotropic material behaved as a truly anisotropic material.

A distinction should be made about the history of recording, keeping track and eventually plotting the data. The loads estimated in this method are follower loads. These loads are specified at a point of the membrane, that of the markers, and set according to the undeformed positions. Loads may change magnitudes and directions, but they act at the same material point throughout the deformation. A field load on the contrary would be specified at a position in space

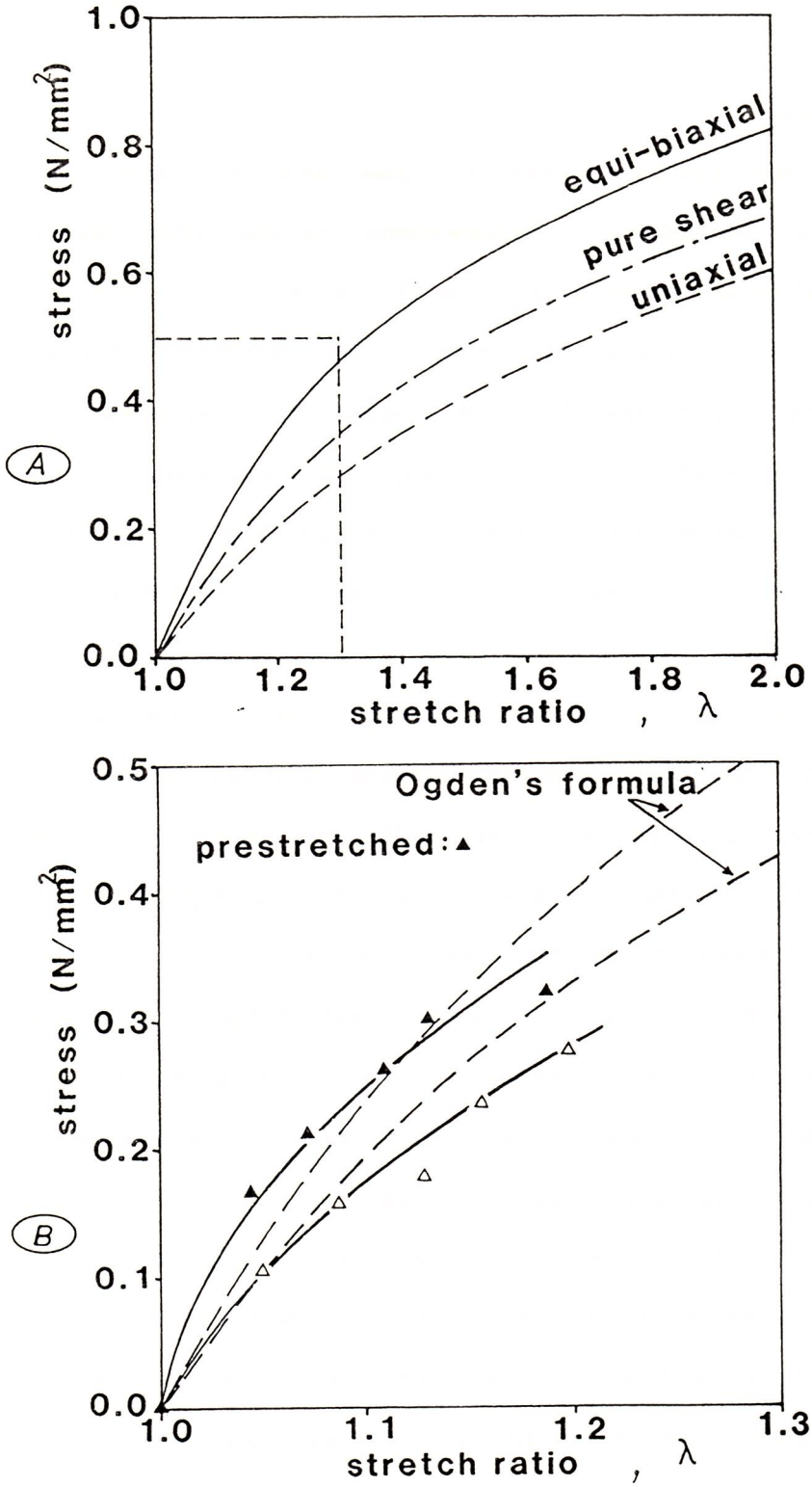

Figure 4.27:(A)the predictions for the mechanical behaviour of vulcanised rubber under three different deformation modes as produced by using Ogden's formula(1972); (B)the split biaxial inflation curve(dashed lines) produced by using relation(4.83), plotted together with the experimentally resulting curves from the biaxial inflation test developed in the present chapter.

and thus a point is subject to a load only if it occupies a particular position in space, i.e. at a certain radial distance throughout the deformation. This experimental test has the objective of determining material properties when a particular tissue area is subject to deformation and thus a follower load was adopted.

The fact that the stress values are estimated at two different points on the specimen raises a few questions. At section4.6 we saw that calculation of radial stresses(also called 'meridional' in inflation) can be done at a small distance from the centre since the meridional stress value does not vary significantly towards the boundary. It is the lateral stress resultant ('circumferential' for a circular border) which alters with the radial distance from the centre and thus may not have a constant value along the arc length over which we calculate an average value for the meridional stress. Those meridional stress values do not coexist at a particular area of the sample but at two different testing sites being at roughly the same radial distance from the centre. The lateral existing stresses at each of the two areas are in general not equal and may be a certain fraction of the meridional stress resultant itself. In inflation of a cylinder the lateral(longitudinal) stress resultant (equivalent to the circumferential in inflation) has half the value of the circumferential stress resultant on the cylinder(equivalent to the meridional direction in inflation). Despite some limitations the proposed testing mode is far simpler and more consistent than any other biaxial testing mode and thus has great value as it is offered for general use.

4.8 INFLATION OF BOVINE PERICARDIUM.

4.8.1 Introduction.

Having confirmed that inflation provides a non-destructive method

of detecting mechanical anisotropy, a test mode has been established for quantification of the biaxial stretch of an anisotropic sheet. The technique was applied to fresh bovine pericardium specimens to assess the properties of the tissue.

Soft tissue samples are easier to clamp and stretch with an inflation test and workers like Miller et al(1979), Wineman et al(1979), Kriewall et al(1983), Mohan and Melvin(1983) working on fetal membranes, soft tissues, fetal dura mater and aortic tissue respectively have found this an advantage. In these respects it is preferable to apply this mode of deformation, although non-homogeneous, than homogeneous uniaxial or biaxial tensile tests where gripping of the specimens and the application of loads pose problems.

When used simply for identification of the principal mechanical directions this non-destructive technique allows the mechanically previewed samples to be subsequently used for a different purpose, i.e.the construction of bioprosthetic valve leaflets.

The finding that a suitable boundary(square) was required to deform the inflation bubble in the desired shape is not unfamiliar to tissue mechanics. Cook(1975) used a race-track shaped border to deform skin under the application of a suction force. The cylindrical conditions produced could provide measurement of only one stress resultant per test and the test had to be repeated with the race-track orifice at a different direction in order to observe directional variations.

4.8.2 Additional Considerations.

Three more factors should be considered while dealing with inflation of a soft tissue. They are implicitly related to each other: the environment, the inflating medium and the mode of

deformation as applied in reality.

Examination of soft tissues should ideally take place in an environment similar to their physiological one. The behaviour of the tissue is sensitive to the ambient conditions (temperature, pH, electrolytes) and it would be desirable to have the tissue inflated with a liquid medium on either side of the membrane. The presence of liquid on the outer surface was for the moment ruled-out because of the optical effect of the medium which would make the Moire fringe technique more difficult to apply.

Application of physiological solution only on the inside produces another problem. In all previous applications and for the formulation of the problem we considered the applied pressure to be uniform everywhere on the bubble surface. This can be achieved if the same medium is present on both sides because it prevents the development of hydrostatic forces. The addition of such forces to the uniformly applied pressure would render the inflating pressure non-uniform and increasing from the top to the bottom of the bubble. Inflation by using a gas is always easier to pump and control. Thus the samples were inflated by air on either side with provision taken to retain them adequately moist.

The manner in which control is exerted in inflation was considered next. Joye and Poehlein(1973) suggested that if a certain mass of gas is pumped into the membrane because of the ideal gas law $PV=ct$ would predict that a specific pressure should result and thus a constant tension through Laplace law ($T=PR$). This method of control could resemble a creep test which produces a deformation under constant stress. The viscoelastic nature of the sample renders this idea dubious. The sample will creep under stress and thus increase its enclosed volume, while the gas can expand and reduce its pressure.

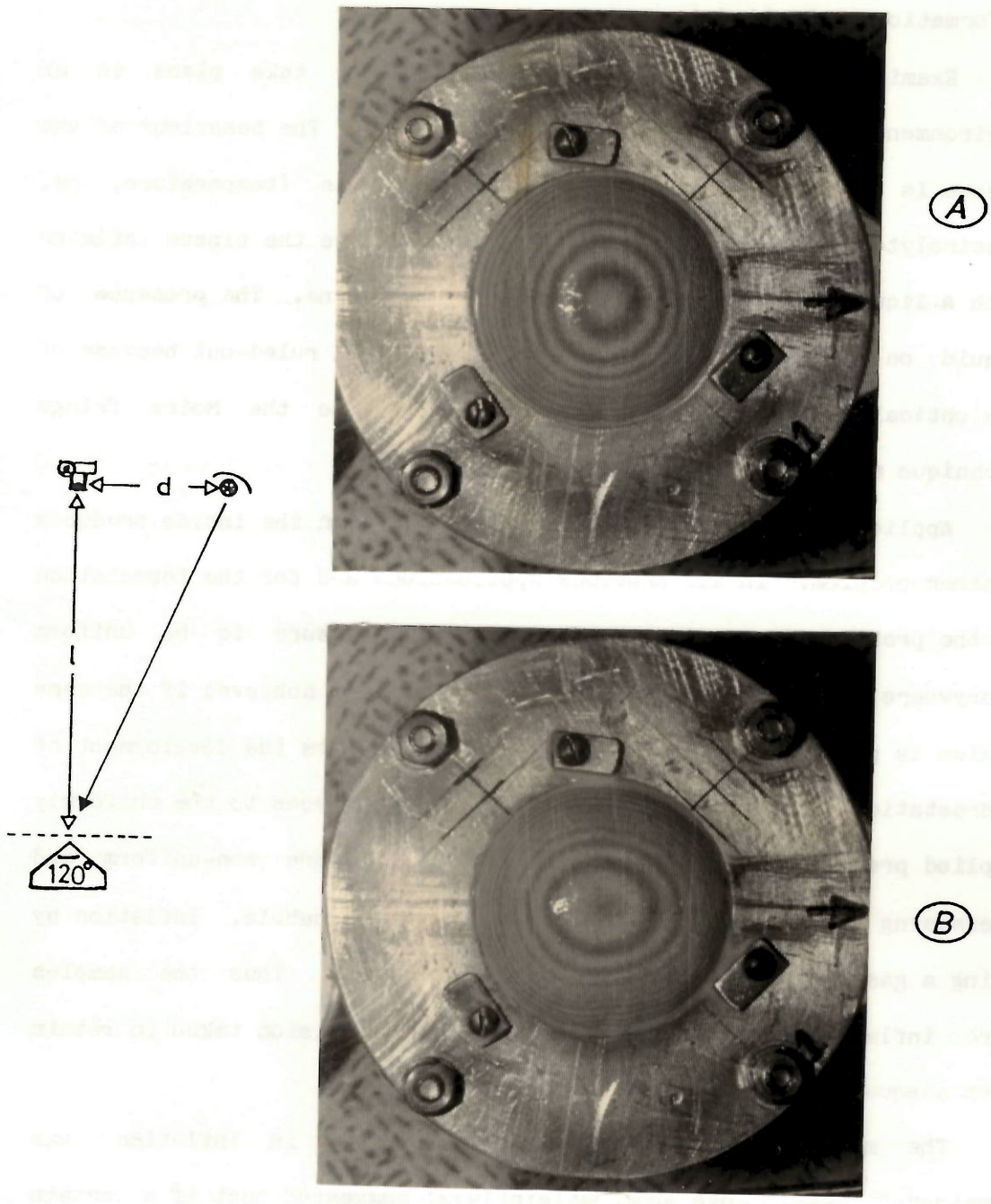

Figure 4.28:Moirē fringes on inflated fresh pericardial specimens indicated the presence of mechanical anisotropy. The specimens were mounted with the circumferential direction along the dark arrow on the aluminium plate of the inflation rig. (A) at 0.266kPa(2mmHg) the shape was rather axisymmetric or even more extensible axially, (B) at 1.33kPa(10mmHg) the circumferential direction was clearly more extensible than the axial one. A pyramide of a 120° dihedral angle was used as a calibration object to adjust the camera and the light source as to produce 1mm interfringe heights.

This pressure reduction is combined with the reduction in local radii and must definitely result in a time-dependent reduction in membrane tension.

If a constant volume of liquid is used to inflate the specimen, it would maintain the total volume of the bubble constant but due to creep and the non-homogeneity of the stress field the deformed shape of the bubble could alter locally.

It was decided, therefore to run a test using increments of pressure and maintain the pressure constant at each step for a certain time interval. This could allow additional volume to be pumped into the system to compensate for creep and also for minute leaks in the pipelines. If creep is small, changes in radii should be even smaller and thus tension would be maintained essentially constant.

4.8.3 Sample Preparation.

Exploratory tests were made on all sites identified in section 2.5.2.4, but a complete series of mechanical tests were carried out only in site-I. Test site-I is the most suitable for the construction of a valve leaflet but the fact that one can prepare only one leaflet per membrane from site-I, leads to the use of sites II, II′, III as well.

For site-I the circumference lies at a 49^{o} angle to the line connecting points B and D in the pericardial map of chapter2. There the tissue is relatively uniform with the thickness being in the range 0.30-0.40mm.

The samples were cut in a polygonal shape, with the polygon inscribed in a circle of 90mm diameter equal to the dimensions of the inflation rig platform. The polygonal shape was required in order to allow space at the perimeter for the inverted screws which clamped the top aluminium plate (see earlier fig.4.12). The pericardial sample

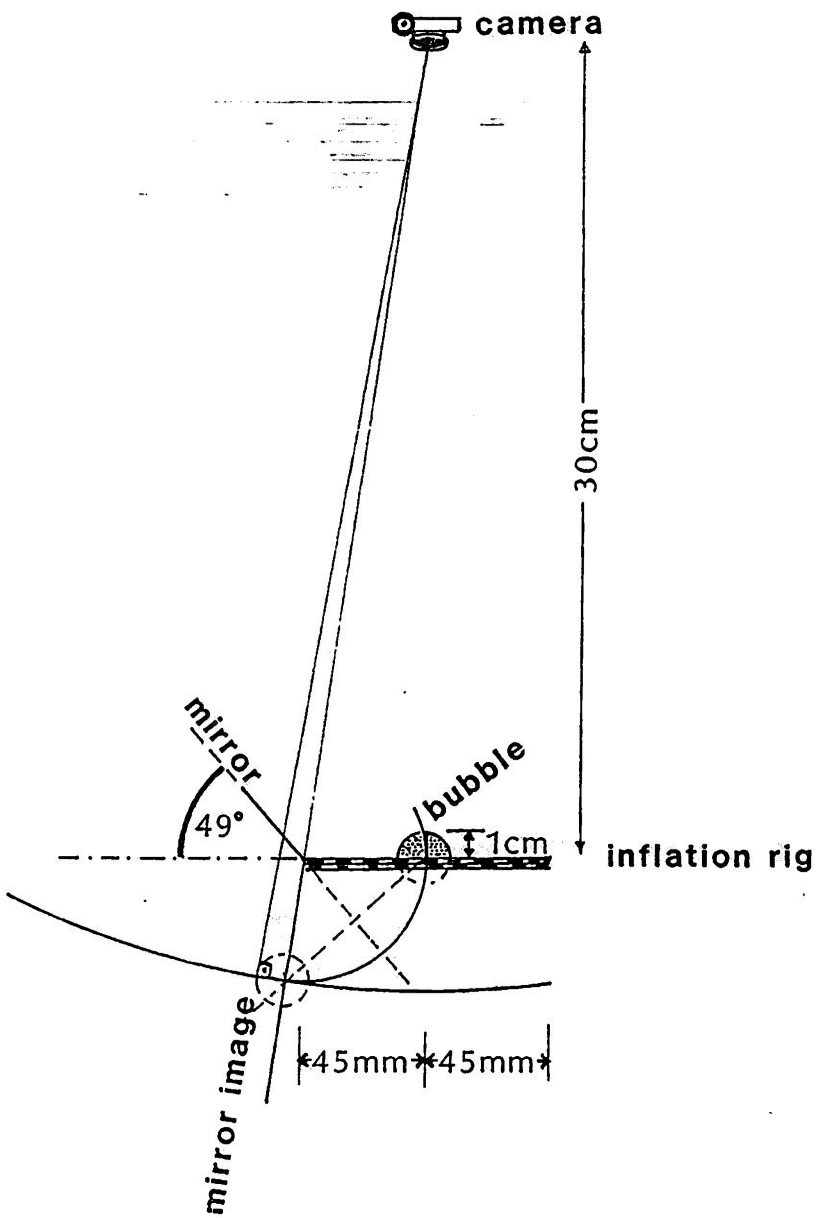

Figure 4.29: the overhead camera was put at a 30cm distance as to cover both the rig and the mirrors in its frame. The inclination of the mirrors was then adjusted to 49° in order to allow the camera to view the top of a 1cm tall bubble normally.

was initially placed in a saline bath and kept flat in a relaxed state on a saline lubricated glass with its smoother, serosal, surface downwards. An annulus of thin card with an outside diameter slightly smaller than 90mm and with a central circular hole of 41.5mm was pressed firmly onto the upper epipericardial surface which adhered to the dry card. The tissue was then gently removed by sliding the specimen along the glass surface and transferred with the adherent card to the upper surface of the test chamber and clamped between the Perspex and aluminium annuli. The card allowed reasonable handling without introducing unwanted deformations and maintained the sample dimensions along the perimeter (in contact with the card) as they were when it was lying flat in the bath.

4.8.4 Inflation Of Tissue Samples.

The pressure inside the chamber was increased to 0.66kPa (5mmHg) by the hand sphygmomanometer and the positive normal pressure was applied to the membrane through the perforations. The membrane was observed with the Moiré set-up and the deformed shape was photographed. When clear fringes (enhanced by the use of the white emulsion) formed ovals a non-axisymmetric deformation existed, and thus the anisotropic material behaviour (fig.4.28) of the tissue demonstrated.

4.8.5 Test Method.

The overhead camera was replaced by a ZENZA BRONICA (which uses a larger negative frame) and placed at a closer distance to the inflation rig (distances were worked out graphically, fig.4.29). A set of front-surface silvered mirrors (kindly supplied by the Dept. of Physics) were set on a stage to orthogonallly view the "orthotropic" bubble along its maximum and minimum extension directions.

Ⓐ

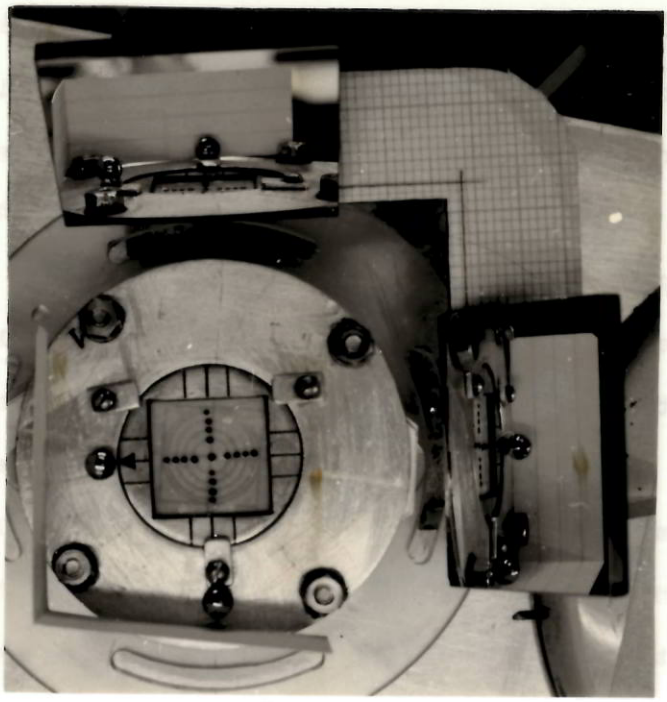

Ⓑ

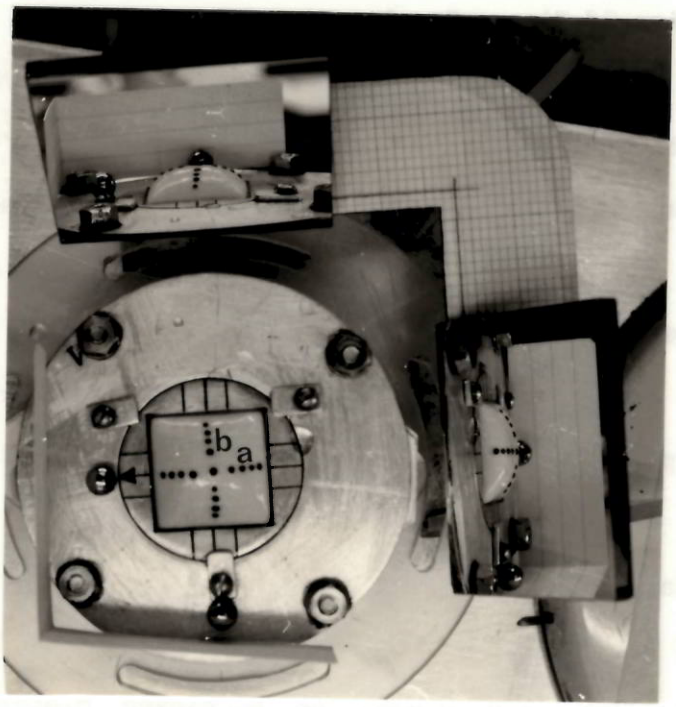

Figure 4.30: Ⓐ flat configuration of the fresh specimen(K′) marked and ready for inflation, Ⓑ the fresh pericardial specimen(K′) inflated by a 2.66kPa(20mmHg) transmembranous pressure.

The selection of the range of stresses was in reality indirect through the specification of the pressure range. An upper value of 16kPa(120mmHg) is greater than the real transmembranous pressures to which pericardium is submitted (discussed in chapter2) but in the form of fixed valve leaflets peak pressure values of even greater magnitude are normal for the systemic circulation vessels proximal to the heart.

A single test would proceed as follows:

a)the mounted sample was inflated by a 0.66kPa(5mmHg) pressure and its principal directions identified and marked on the rig,

b)the pressure was released and on the flat relaxed specimen ink droplets (ball pen ink) were placed on the axes and at radial distances corresponding to the concentric circles drawn on the underlying perforated Perspex plate. When the tissue was illuminated from beneath it is translucent enough to allow the circles to be clearly seen,

c)the square aperture was aligned with the principal directions and locked in place by three bolts, the final view before inflation being as in fig.4.30a,

d)pressure was applied in steps at 0.266, 0.666, 1.333, 2.666, 3.999, 5.333, 7.999, 10.666, 13.333, 15.999kPa (2, 5, 10, 20, 30, 40, 60, 80, 100, 120mmHg) and at each level the tissue was allowed to creep for 30s and a photo was taken which included both orthogonal views(fig.4.30b). Subsequent measurements on those photos were to be taken and used in the analysis.

4.8.6 Results.

Qualitative observations of samples of different sites and from different sacs revealed that the majority were anisotropic.

The deformation through the square aperture indicated that our quantitative approach was also applicable and thus the experimental

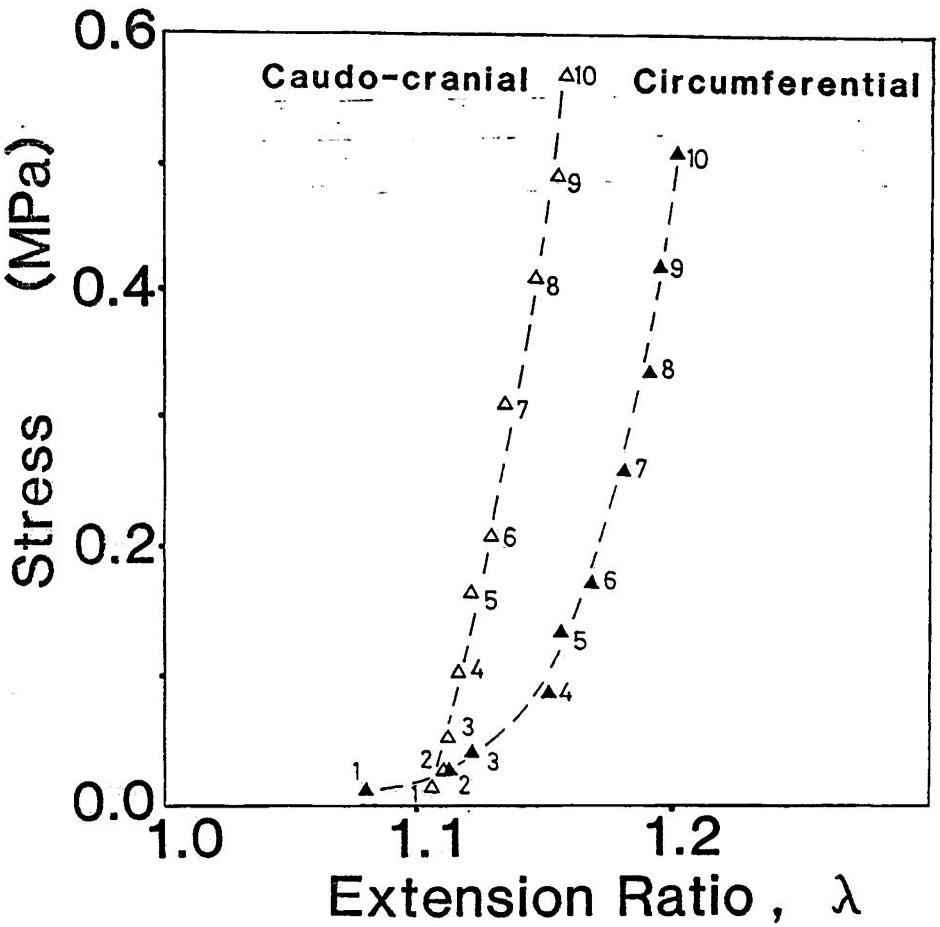

Figure 4.31:stress/stretch curves of the biaxial inflation test of specimen K'. The caudo-cranial(axial) direction was less extensible than the circumferential direction. Ten pairs of points existed, which were produced at the ten stages of inflation and are indicated by numbers 1 to 10.

and analytical preparatory work on rubber should yield meaningful results on the anisotropic behaviour of soft tissue samples by performing measurements at sites a,b, of the fig.4.30b.

For results from one site and from different sacs to be plotted on the same diagram and to be of more general usefulness, a directional consistency should exist between the samples.

All preliminary Moirē inflations of samples from site-I revealed that they were anisotropic with their more extensible direction lying within a 10^{o} angular range to the circumferential direction of the heart. This directional consistency is impressive if one considers the biological variability present and the handling and mounting difficulties of soft tissue specimens. Thus this behaviour should have a mechanical cause.

A series of 7 specimens originating from site-I, were then quantitatively examined.

With the same analysis of section 4.7.4.3 and formulas (4.91), (4.92) a single sample(membrane k′, of 0.33mm thickness before inflation test) produced the curves of fig.4.31 with the values of tables4.5,4.6.

The non-linear relationship between stress and strain for both curves is characteristic of the soft connective tissues. In both directions the tissue appears initially very compliant and then stress rises sharply to higher values. It has been mentioned earlier that the test is performed in a very slow and stepped creep mode in order to obtain the stabilised elastic phase of the tissue behaviour.

Anisotropy is also apparent in fig.4.31 with the tissue being more extensible(at higher stress levels) in the circumferential than in the axial direction, both directions being related to the heart.

The crossing of the curves at low stress levels, for pressures

Table 4.5: profile along caudo-cranial direction

Measured parameters			Calculated values			
pressure ($133.32\ N/m^2$)	2l (mm)	s (mm)	Radius (mm)	λx	Tx (10^{-2} N/mm)	Sx (10^{-2} N/mm^2)
2	13.99	1.00	14.31	1.103	0.381	1.156
5	14.03	1.06	13.56	1.107	0.904	2.739
10	14.06	1.10	13.16	1.111	1.754	5.315
20	14.07	1.13	12.85	1.113	3.427	10.384
30	14.13	1.13	12.95	1.117	5.178	15.693
40	14.25	1.15	12.94	1.127	6.898	20.904
60	14.31	1.18	12.77	1.133	10.213	30.948
80	14.44	1.21	12.69	1.144	13.530	41.023
100	14.51	1.28	12.15	1.152	16.195	49.077
120	14.55	1.33	11.78	1.157	18.851	57.125

Table 4.6: profile along circumferential direction

Measured parameters			Calculated values			
pressure ($133.32\ N/m^2$)	2l (mm)	s (mm)	Radius (mm)	λy	Ty (10^{-2} N/mm)	Sy (10^{-2} N/mm^2)
2	13.53	0.94	14.22	1.079	0.379	1.149
5	13.83	1.16	12.14	1.109	0.809	2.452
10	13.87	1.32	10.82	1.118	1.442	4.370
20	14.25	1.36	11.08	1.149	2.955	8.953
30	14.29	1.38	10.99	1.153	4.397	13.324
40	14.43	1.45	10.70	1.167	5.708	17.297
60	14.57	1.47	10.77	1.179	8.616	26.110
80	14.66	1.55	10.40	1.188	11.095	33.623
100	14.72	1.56	10.39	1.194	13.857	41.991
120	14.76	1.57	10.39	1.197	16.622	50.370

lower than 1.33kPa(10mmHg), was a typical finding for all seven pairs of curves. Descriptively speaking this crossing resulted because the membrane after it had been lifted from the stage, by the application of a small pressure, settled in a configuration which exhibited larger axial extension. This axial extension later increased only moderately while in the circumferential direction the tissue started less extensible and gradually extended to finish at a larger extension ratio at the peak pressure(120mHg).

Stresses for the first pressure levels were very similar and thus the crossing of the curves was mostly caused by the directional difference in the extension ratios. Another reason for the crossing of the curves at lower stress levels could lie in their shape. The circumferential has a prolonged loading phase with higher initial incremental moduli followed by an elbow and a rapid increase in the stresses.

For pressure levels greater than 1.33kPa(10mmHg) the axial stresses were consistently higher than their paired stresses in the circumferential direction. This was because the stresses were calculated through the geometry and the tissue exhibited different radii of curvature and extensions in the two principal directions.

This finding of higher axial stresses at each pair of stress values was significant as it applied throughout the population of paired values of all 7 samples. Since higher stresses are accompanied by lower extensions in the axial direction, while lower stresses are related to higher extensions in the circumferential, the product of the two would be roughly comparable and consequently the accumulation of the products which is related to the area under each of the curves for sample K'. If this area is equivalent to work elastically stored in the tissue during deformation, this work is comparable between the

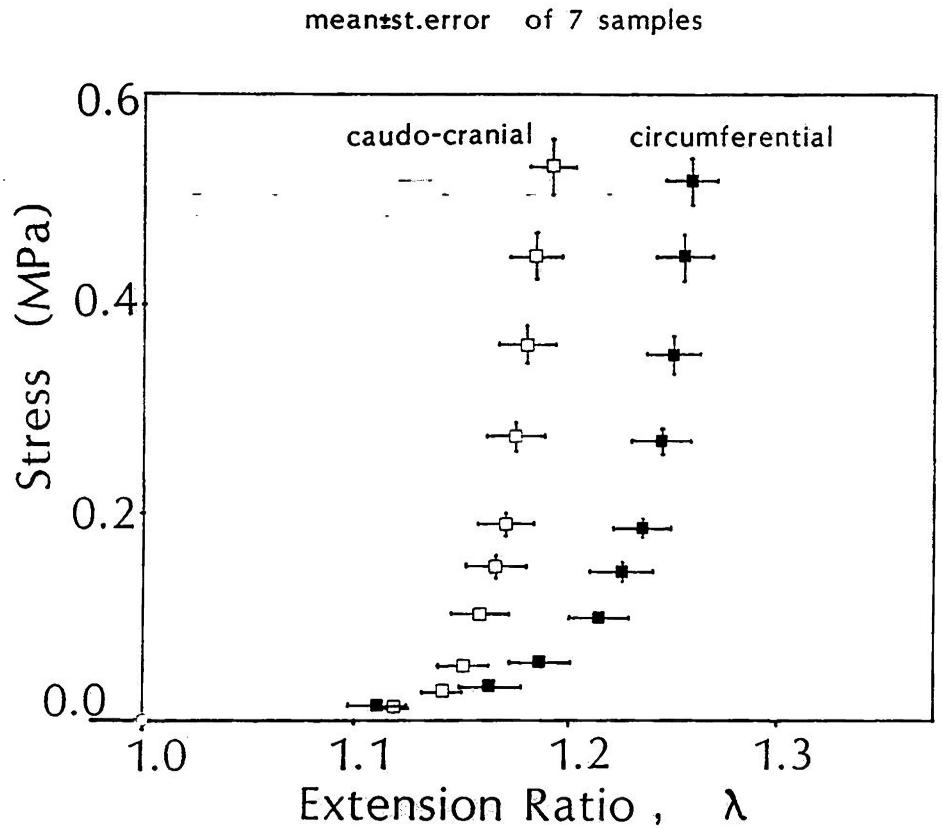

Figure 4.32:the average mechanical behaviour in biaxial inflation of all 7 specimens given as mean±st.error mean points.

two directions. There is no real need for the dissipated work along the two curves to be balanced since the pair of loading curves are produced at two different testing sites on the specimen, but it appears that inflation stretched almost equally the two directions. We checked the population of all pairs and 60% had higher axial stresses and thus favoured the idea that the work stored elastically on the tissue along the two directions was comparable. From the 7 samples, four finished at higher stress values in the axial direction one exhibited equal stresses and only two exhibited higher stresses in the circumferential direction. The ratio of the circumferential to axial energy was 1.15 for the 3 samples with the higher axial stresses, and 1.31 for the 3 samples which exhibited higher circumferential stresses. Those values were not very dissimilar and this is due to the particular shape of the curves. Circumferential curves have a longer loading length with stress building-up only in the last segments of the curve where it rises rapidly. Therefore the result depends critically on the stop point for pressure.

It should be pointed out that the curves of fig.4.31 always exist in a pair and not separately and trace the magnitude of the principal stresses along the axial and circumferential directions produced at two different testing sites.

All 7 samples exhibited the same consistent behaviour of which the general features are present in fig.4.32 as well. This is a plot of the mean values at equal pressure levels for stresses/strains of all 7 samples examined. The standard error of the mean is plotted as well with values in tables4.7,4.8. The error resulted from the deviation of the population values from their mean and was not the reading error or the calculating error of these measurements. The experimental error for measuring extension ratios was of a similar

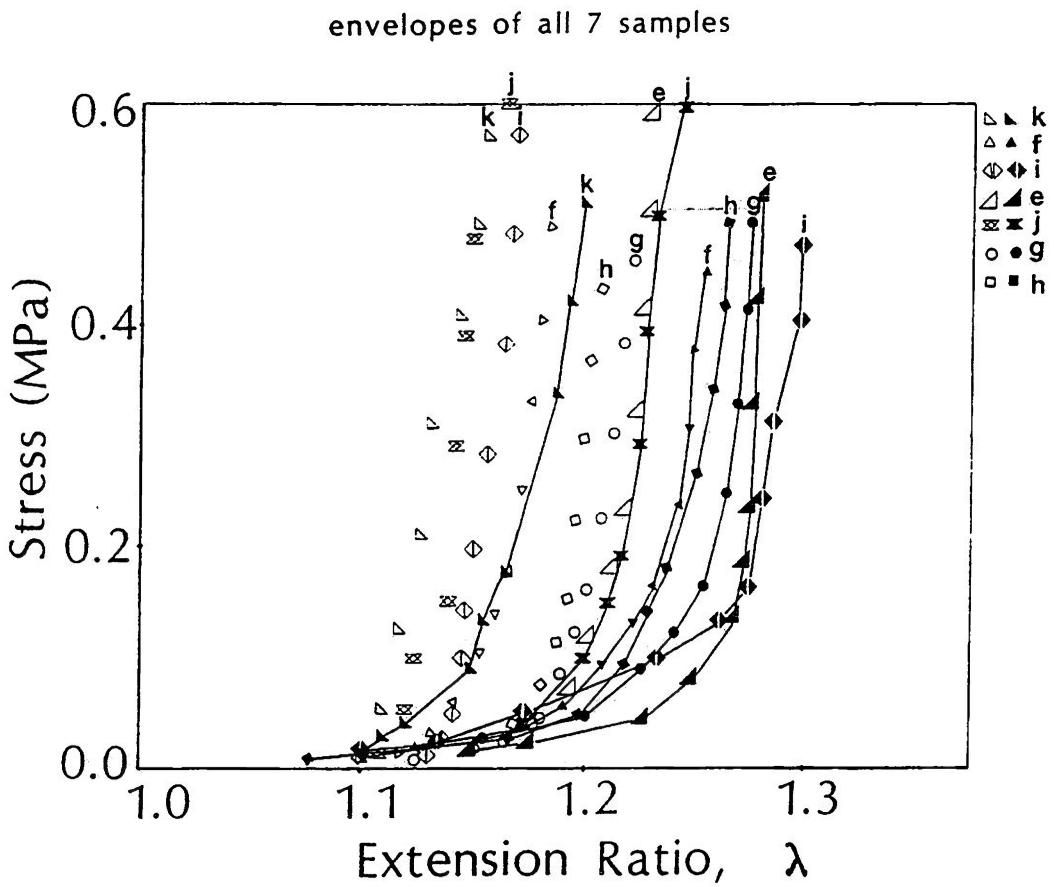

Figure 4.33:the complete data from all 7 specimens; dark symbols were used for the circumferential direction which was in general more extensible than the axial direction.

magnitude estimated at 0.01. The resulted curves were significantly different, with the circumferential being more extensible for all pressure levels above 2.66kPa(20mmHg) (Friedman test, $p<0.01$) which is after their crossing point.

The complete data obtained from all 7 samples is presented in fig.4.33. Identical symbols have been used for the curves of each of the samples, using open symbols for the axial curves and dark symbols with solid lines for the circumferential curves. The envelopes that resulted in this way are distinguishable from each other because their width is quite narrow, comparable to the mean difference in extensibility between the two directions.

It is clear that with the exception of sample K′ each of the circumferential curves is more extensible than the whole population of the axial curves. Thus one can, by just choosing the circumferential direction for a specimen from this site, be sure that this same direction is the most extensible from the whole population of samples that may be used. Sample K′ exhibited the lowest extensibility in either direction and it may have been mishandled during the preparatory stage (as by prestretching) resulting in an artefactually reduced extensibility in both directions. It has otherwise the typical response of all 7 specimens.

4.8.7 Discussion.

The mechanical behaviour of the soft bovine pericardial tissue has been examined using a novel inflation technique.

The method has been applied in a step load mode which resembles a creep test and presumably has the same effect at the specimens that preconditioning through repetitive cycling has on soft tissues, leading to a stabilized response. Deformations at very low strain rates (like this incremental test) demonstrate mostly the

Table 4.7: mean values for stress/extension ratio of all 7 samples along the caudo-cranial (axial) direction

pressure (133.32 N/m^2)	stress (N/mm^2)		extension ratio	
	mean value	standard error	mean value	standard error
2	0.0128	0.0012	1.119	0.0068
5	0.0269	0.0022	1.141	0.0097
10	0.0534	0.0044	1.152	0.0117
20	0.1002	0.0061	1.159	0.0130
30	0.1453	0.0083	1.166	0.0129
40	0.1883	0.0106	1.171	0.0126
60	0.2741	0.0146	1.175	0.0129
80	0.3609	0.0191	1.181	0.0122
100	0.4452	0.0220	1.185	0.0119
120	0.5309	0.0268	1.192	0.0107

Table 4.8: mean values for stress/extension for all 7 samples along the circumferential direction

pressure (133.32 N/m^2)	stress (N/mm^2)		extension ratio	
	mean value	standard error	mean value	standard error
2	0.0146	0.0017	1.111	0.0125
5	0.0303	0.0027	1.162	0.0138
10	0.0550	0.0051	1.186	0.0149
20	0.0989	0.0059	1.215	0.0135
30	0.1414	0.0076	1.226	0.0146
40	0.1824	0.0093	1.237	0.0143
60	0.2683	0.0127	1.245	0.0133
80	0.3502	0.0158	1.250	0.0126
100	0.4484	0.0223	1.255	0.0129
120	0.5173	0.0225	1.259	0.0124

characteristics of the elastic phase of the material.

Concerning the nature of stresses, from the Eulerian stress resultant we have derived a semi-Lagrangian by dividing by the initial thickness of the membrane before the test. To our knowledge no valid method of measuring the thickness during the test exists up to date. In any case we would prefer to have a fully Lagrangian stress than a fully Eulerian one since our deformation estimates (stretch ratios) were calculated over the undeformed length, and hence were Lagrangian.

Inflation also simulates the natural deformation protocol for this particular soft tissue, which both in its natural state as soft pericardial tissue or as a chemically fixed valve leaflet deforms under the influence of a transmembrane pressure difference.

This inflation test results in the production of a pair of stress/strain curves and developes a specific mode of biaxial stretching in which the experimenter has little (or no) control on the stretch induced. The only parameter under control is the normal pressure with the specific relation between the stretch ratios at the othogonal directions varying from specimen to specimen being a result of the local equilibrium equations and the properties of the specimen of the test. This deformational mode though is the most natural for this tissue and under these conditions the specimens exhibited a directional difference in extensibility or mechanical anisotropy.

Inflation, unlike classical biaxial tests does not need initial identification of the principal directions of elastic symmetry and can on its own cope with this problem.

The mechanical anisotropy could have resulted from structural or geometrical reasons. The heart, and the pericardium which clothes it, is curved, but the inflation specimen is constrained to be planar. The specimens thus could be slightly deformed before inflation; this

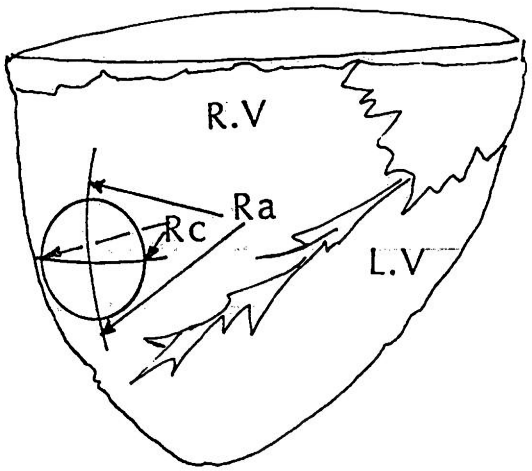

R.V :right ventricle
L.V :left ventricle
Ra :axial radius
Rc :circumferential radius

axial direction

range of:	curvature	radius	extension ratio
	dioptre	(m)	
	2	0.261	0.001
	6	0.087	0.010

circumferential direction

range of:	curvature	radius	extension ratio
	dioptre	(m)	
	7	0.075	0.013
	12	0.044	0.042

Figure 4.34:optician´s lens measure is a simple spherometer using formula (4.91) to express the curvature of a surface in dioptre(D)=one reciprocal meter=reciprocal radius of curvature. Focal power, F=(n´-n) K (n:refractive indices, K:curvature), n´=1.523 for glass, n=1 for air resulting in F=0.523 K and Radius=0.523/F. From the radius, the contraction ratio of tissue is calculated by the use of formula (4.92).

this form of anisotropy we called "geometrical". Measurements of the curvatures at the test site-I were made in the plaster cast of the heart which was prepared and already presented in chapter2, using a "lens measure" which measures the focal power of a lens in dioptres, these units were converted to mm length for the radii of curvature(formulas in fig.4.34). Formula (4.92) was used to estimate the contraction of the tissue from the curved segment of radius Ri to the straight line with the same end separation. The circumferential curvature was found to be greater than the axial one and thus may have contributed to the anisotropy shown by the specimen. The stretch ratio values differed at the most 0.03 while the difference of the mean stretch ratios of all samples along the two directions (circumferential-axial) was 0.06, at the peak pressure in tables4.7,4.8. It could thus account for some but not all of the anisotropy present.

We attempted to determine the neutral configuration of the specimens by applying a minimal pressure, to only lift the tissue from the stage by simply counterbalancing its weight. The density of a fully hydrated pericardial piece of the testing site was calculated at 2.4×10^{-3} g/mm^3. For a surface area that of the orifice of inflation only 1.02×10^{-3} (MPa) normal pressure (0.076mmHg) should be adequate for the specimen's weight. We found that control of the tissue inflation at such small pressures was impossible, with the tissue being under real stretch for our first pressure level 0.266kPa(2mmHg).

The finding, that anisotropy is present in every single specimen test is very significant because it immediately refutes the commonly accepted view arising from badly organised simple tension tests that this tissue is isotropic. In general, results of this section confirmed the anisotropy demonstrated by classical biaxial tests

conducted by other investigators (Vito,1980;Lee et al,1985;Yin et al,1986). Results obtained in inflation though, are more explicit on the question of presence of anisotropy or not.

Presence of anisotropy is of particular importance in the construction of bioprosthetic valve leaflets and this will be discussed in later chapters. It could also have some meaningful results in clarifying the role of native pericardium in-situ and thus it is absolutely necessary to confirm that the aforementioned mechanical anisotropy (in results) is indeed material anisotropy and not a geometrical one. In order to confirm that the directional variation of extensibility was a material property simple tension tests were carried out and the results are reported in subsequent sections.

5.1 MECHANICAL BEHAVIOUR IN UNIAXIAL TENSILE TESTS.

5.1.1 Introduction.

In the previous chapter4 a biaxial inflation test mode was developed and applied to a specified test site on the pericardial membrane. The response suggested, both qualitatively and quantitatively, that the specimens were orthotropic. It is possible, however, that the initial curvature of the pericardium may have influenced the result. Uniaxial tensile tests were carried out in orthogonal specimens cut from the region of inflation in order to eliminate geometrical effects. The sac-to-sac variability may make comparison of inflation and uniaxial tests difficult, unless they are made on the same sample.

As discussed already in chapter3 uniaxial tests have certain advantages but they also require considerable work for preparing the specimens. The geometry of the strips possesses a major dimension much larger than the other two and thus the tests directionally isolate the structural elements and selectively examine the material properties at the direction chosen during the preparation.

The range of stresses and extensions used were close to the levels of the inflation tests and thus close to the operational conditions expected for heart valve leaflets.

The comparison of results obtained in the two orthogonal directions and between biaxial-uniaxial test modes may consist in examination of the extensibilities at prescribed stress levels, examination of the values of specific parameters measured from the loading response and a qualitative view of the shape of the curves themselves.

Having established a satisfactory test and analytical protocol on specimens from a single site (test site-I), the influence of the site was examined by testing strips from different areas suitable for

constructing valves. The results were fed in a multifactorial statistical analysis of variance procedure to check for the influence for 3 factors: sac, area and direction.

The time dependent properties as exhibited in stress relaxation of strips were also investigated, as well as the effect that relative position within an area has on the resulting response.

5.1.2 Preparation of Samples.

The samples that have been used in producing the mean inflation curves of chapter4 were used for the present investigation. After the completion of each of the inflation tests the whole polygonal sample was returned to the saline bath and was let flat to relax overnight at 4°C. After the inflation test a significant reduction in the tissue thickness had been observed (chapter4) in the area which had been inflated, when flattened presented wrinkles an obvious sign that the area had been enlarged.

After 24 hours the tissue sample had regained its original pre-inflation thickness and assumed a plane shape over all its area. The same thickness values of the inflation tests have been used in the uniaxial tensile tests for the calculation of the initial cross sectional area and nominal stress.

A glass block was introduced into the saline bath, beneath the specimen. The specimen lying on top of the glass block was gently removed from the bath and white card was then placed on top of the smooth serosal surface of the tissue, to which it adhered. The glass was removed by sliding it along the sample's surface, leaving the sample lying on the card with its epipericardial surface upwards, bearing the markings of the previous inflation test. The small ink droplets, which were used for tracking the deformation during the inflation had been washed away easily.

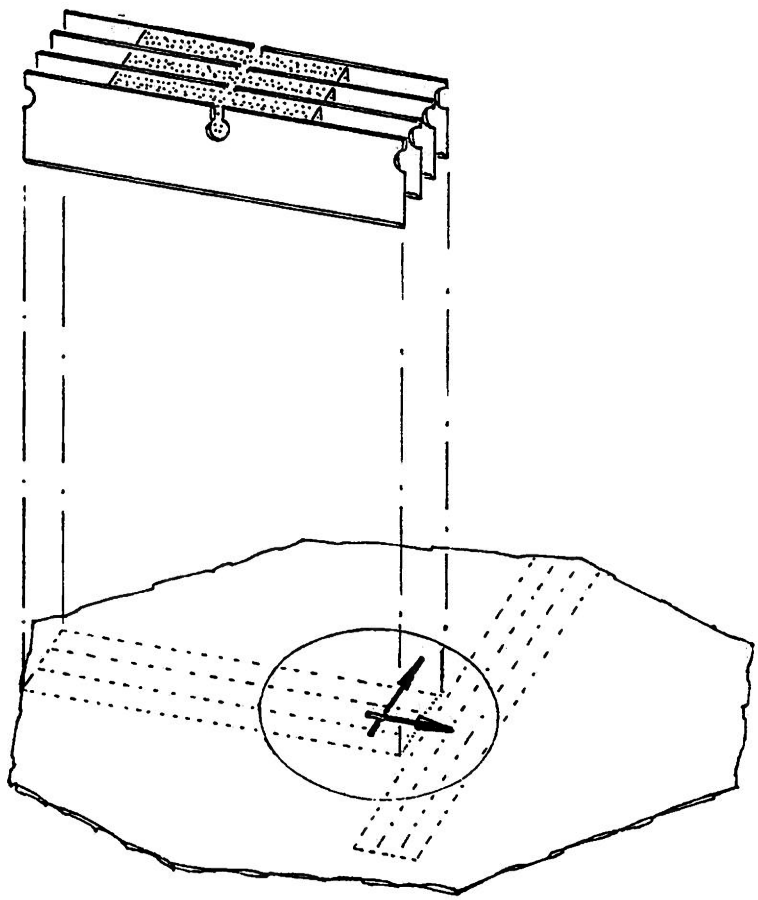

Figure 5.1:preparation of the strip specimens in two orthogonal directions.

For the preparation of the strips a block of 4 blades had been prepared with spacers between them to keep the blades 3mm apart along their entire cutting edges. With this block two sets of 3 strips each were prepared (fig.5.1), each set aligned along an axis of anisotropy as identified by the biaxial inflation test. The reason for having more than one strip per direction was to exclude possible regional variations, to avoid loss of data in a direction which is possible if a test fails and eventually to average the uniaxial tensile behaviour over a larger tested area but still performing on the same principle of uniaxial tensile testing. The strips prepared this way had a uniform width of 3mm and an almost uniform thickness. Thus the tested tissue between the grips had a relatively uniform cross sectional area along its length. This however does not mean that during the following test the nominal stress is uniformly distributed along the strip since the strip is not subjected to a homogemeous deformation along its length because it acquires a dumbbell shape.

5.1.3 Test Apparatus.

5.1.3.1 Grips. The tissue specimens supported by the underlying strip of card were mounted on a jig(Nachemson and Evans,1967) which had two pairs of jaws which were kept 15mm apart by a removable gauge block. The grips were spring loaded and the jaws had serrated surfaces to hold the specimens firmly and not allow them to slip during the test. For testing pericardium pieces of waterproof sand paper were used in the interface of the specimen and the jaws in order to avoid damage of the tissue due to gripping at those areas and at the same time still firmly hold the ends of the strips. After some preliminary tests it was found that at higher loads slipping still occured. Eastman210 cyanoacrylate adhesive was used in combination with the sand paper to eliminate this possibility.

5.1.3.2 Test Chamber. Tests were carried out in a test chamber mounted onto the cross head of a tensile testing machine. The front and back surfaces of the chamber were glass plates which allowed the viewing and photographing (if required) of the specimens during the test. The chamber had an inlet and an overflowing outlet for liquid solution to be recycled between a solution tank and the chamber. The recycling and temperature control of the solution which filled up the chamber in tests were provided by a 'Grant SU6' pump to an accuracy of 0.1°C. The temperature of the solution during the tests was set at 37°C and was constantly checked by a thermometer present inside the bath of the test chamber.

The bottom set of jaws was firmly attached to the chamber and the top set was hooked to the load cell via a thin metal rod and a universal joint coupling. The gauge block was removed and then the paper card strip which backed the specimen was gently cut by a pair of scissors. The front door of the chamber was closed and the chamber was filled with an one quarter strength Ringer's solution from the tank.

Specimens were extended by the downwards movement of the bottom grip attached to the crosshead which was driven by two lead screws housed within the vertical columns of the instrument.

The INSTRON tensile testing machine was driven by a 1195 electronic control unit and used a specially enlarged frame. It could separate the grips under either strain or load control and provide for step, ramp, trapezoidal or sawtooth inputs.

5.1.4 Protocol.

The strips were subjected to cyclic loading by imposing a sawtooth separation on the grips. The rate of separation was set at 5mm/min which resulted in a nominal strain rate of 0.0055/s. The rate relatively slow nominal strain rate was set such that a cycle could be

completed in a similar time scale to the inflation test. Initial studies were made to confirm that the response was independent of the extension rate within the range 5mm/min to 1000mm/min. For a change of two or three orders of magnitude in the strain rate the response did not alter significantly. A small and inconsistent difference was found between the results for testing at 1000mm/min and 5mm/min, but the traces of 200mm/min and 5mm/min were practically indistinguishable.

The cycles were performed between the initial 15mm separation of the grips, which from now on will be refered as the 'original' gauge length, and a peak load of 0.8N which for most of strips was equivalent to 0.8MPa nominal stress value. The peak stress value varied from sample to sample due to thickness variation. The choice of a specific peak load yielded a constant stress resultant(load per unit length) between the biaxial and uniaxial tests and this was the only physical quantity that was most accurately evaluated in the two different test modes. If a certain peak nominal stress value had been attempted to achieve(as by adopting higher peak loads for thicker strips), then both the peak stress resultant and the peak load would vary between tests of different strips. The consequences of using such set for the limits of stress and stretch at cycling with this particular material will be discussed again later on.

5.1.5 Data Recording

The machine was equipped with a potentiometric pen recorder which had an accuracy of 0.5% of the full scale, but restricted frequency responce. This chart recorder could plot load (or any other signal) as a function of time and could reverse direction as did the crosshead or run constantly in a single direction. A chart speed of 50mm/min was selected which could produce a clear drawing of a curve at the

required dimensions when the crosshead was moving at a 5mm/min speed. For the load cycling of the present test the chart was set to follow the motion of the crosshead and thus reversing at peak load to eventually yield loops of the load /deformation behaviour.

The load calibration was made by the use of a 10g dead weight at full scale deflection of the chart. The minimum subdivision on the paper was then only 0.001N but due to a slight tremor of the pen created by vibrations transmitted through the frame this reading was slightly impaired in its precision.

The stress and strain measures were Lagrangian in their nature. Strain was expressed as a stretch ratio of the strips which was the separation of the grips at any time instance (t) divided by the initial separation of the grips (gauge length=15mm). Stress was calculated as the overall load transmitted by the strip in tension divided by the initial undeformed cross sectional area of the specimen and was expressed in $Pa=N/m^2$. Area was equal to width times the thickness of the undeformed strip.

5.1.6 Response to Cyclic Loading.

The tissue exhibited a non-linear response with a large hysteresis loop on the 1st cycle. Subsequent cycles resembled the 1st unloading trace and the 2nd loading trace with the peak load point staying relatively constant, but zero load point deformation increasing. Examination of the tissue response in this low stress/strain region poses some problems which can be better appreciated from the traces of the stress/strain loops at both ends at high and zero loads.

5.1.6.1 The problem of the 'gauge length'. In fig.5.2 the initial traces of cycling of 8 pericardial strips(from a set of 10) are shown. The strips came from test site-I and were all 3mm wide and

orientated along the more extensible direction as identified by inflation. Thus they should behave very similarly but biological variability is evident by the shape of the traces with strips 1-5 being more compliant than the rest. For these recordings the initial scale corresponding to loads of 0.01N and 0.001N was 0.1N full scale deflection(F.S.D.) and at this very sensitive load scale the pen presented a tremor which resulted in the crimped tracings. The scale was subsequently increased to 1N F.S.D., producing the sudden drop from the increased load in the curves.

At a load of 0.8N a trigger reversed the crosshead motion. The numbers at the tip of each rise are the numbers of the cycles. Apart from sample3 which appeared at first cycle to rise in tension at a small distance from the axis, all the rest appeared to depart from the minimum recordable load level of 0.001N straight from the beginning. In subsequent cycles this 'first load point' appeared to travel to larger deformations indicating that, as a result of the first cycle between the original gauge length and the top load of 0.8N, the tissue acquired a new resting length. The shift was greatest for the 1st cycle and became progressively smaller. This measure will be referred as the shift in gauge length and can, through the increase in the initial tissue length, affect the measure of stretch(strain) and indirectly the expression of the modulus of elasticity at any load level.

It has been implicitly accepted that loads are the means by which such a setting of the tissue at resting length is achieved but this is not always the case. In fact in the preparation of the present pericardial strips their geometry played the most significant role. It must be remembered that it is the objective of the tests of this section to confirm the anisotropy of the biaxial inflation results

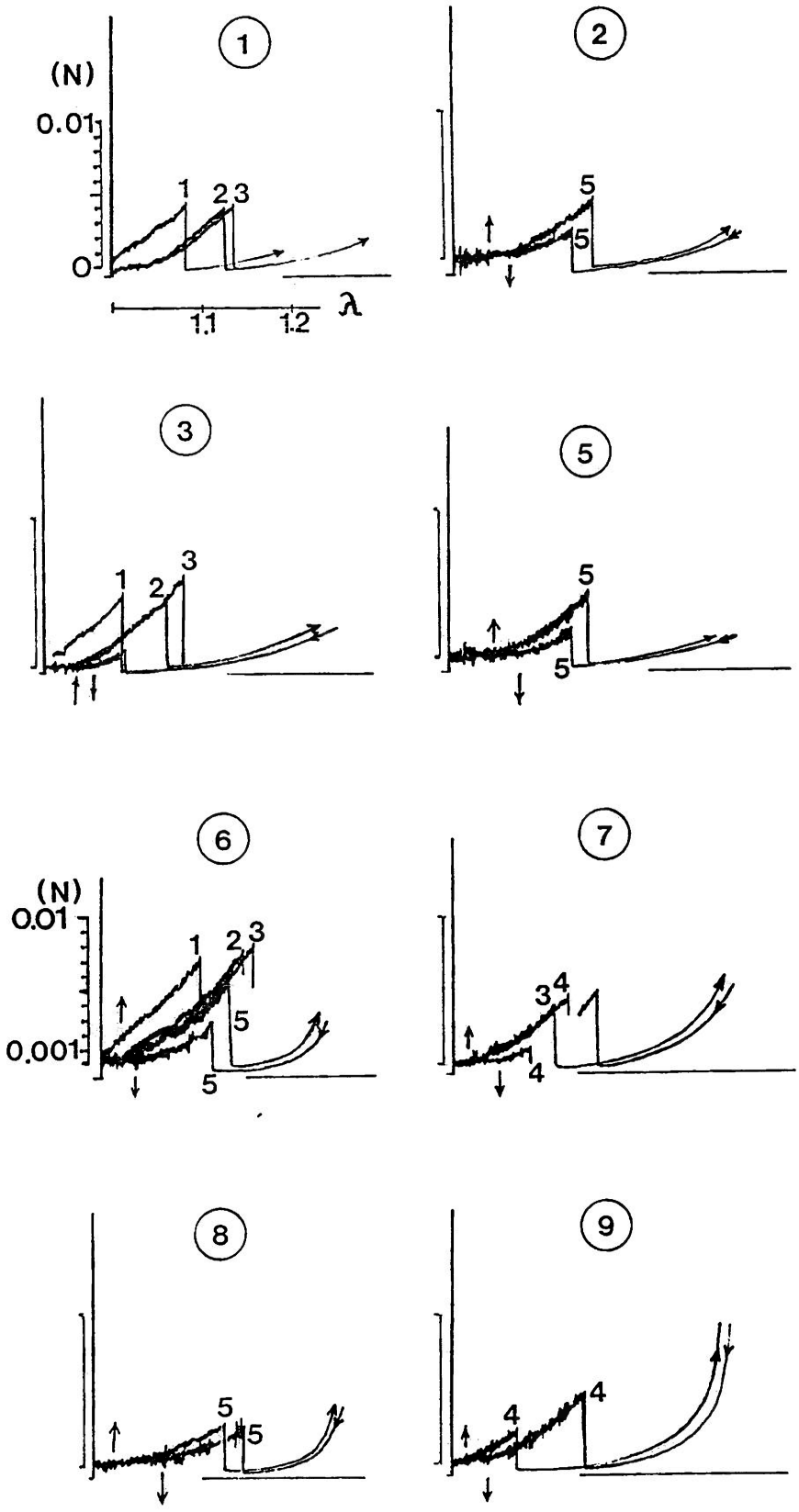

Figure 5.2:initial traces of 8 pericardial strips prepared in one direction. The arrows indicate the points where the load departs and descends to the stretch ratio axis. The difference indicated that the loop was not closed at origin.

which were particularly significant in respect to extensibilities. As it is very likely that the shape of the sample may have interfered with the biaxial data (through initial curvature), it is very possible that due to the very compliant region at the start of the tension curves a prestretch can be imposed on the strips by some short of mishandling. It is for this reason that the sample was carefully transfered from the bath on the card and was still supported by a paper card strip till it was fully mounted on the test grips. Thus both loads and deformations can be used to set a gauge length (reference initial length) and the results are always in relation to both the preparation and the convention that is to be followed.

5.1.6.2 Effect of cycling. In fig.5.2 the 2nd and subsequent cycles appear to ascend on the same curve and the more the cycling progressed the more evident it was that the tissue reached a stabilized loading phase within a small number of cycles. Both the stretch at the first load point(0.001N) and the overall behaviour up to the peak load was well preconditioned at the 5th and 6th cycle and the tracings on these cycles were used as the standard preconditioned response of the tissue in cyclic loading between those load(and/or strain) limits.

In the same fig.5.2 the sensitivity at the descending traces of some cycles has been increased tenfold as well. There was clearly a difference between the first point up and the last point down indicating that the loop did not actually close within the positive stress/stretch region of the chart recordings. The reversal of the crosshead motion to perform the cycles on either side (low region-top load) meant that the complete loop was indeed closed to a point of minimum stress/stretch. The fact that the loop was intercepting the zero stress axis at unequal stretch values indicated that the tip of

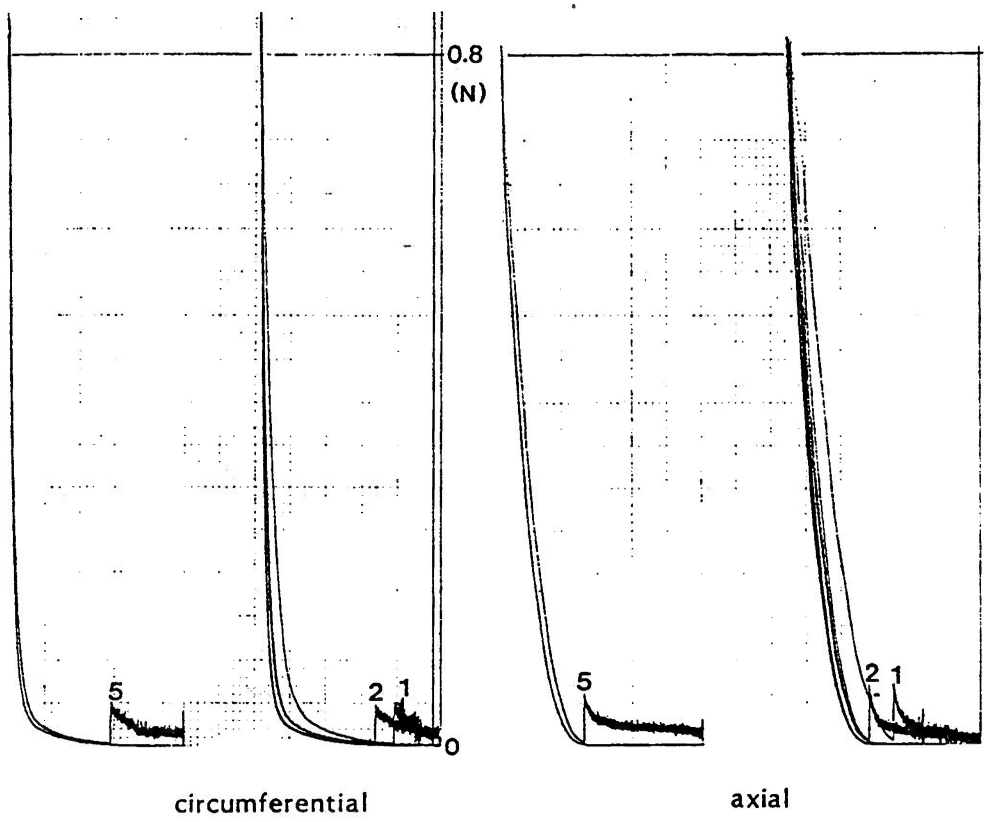

Figure 5.3:traces of the 1st and subsequent cycles of a circumferential and an axial strip from sample k'.

the loop was at the region of negative stresses. The first load point in ascent(loading) was always at a lower stretch value than the point of descent as the stress was preceding deformation in the hysteresis loop. The difference between the two could be a result of length recovered due to hydrodynamic balance of the tissue with the environment or because of the return to negative strains. However negative strains cannot be imposed on the tissue because of its lack of rigidity which resulted in a buckling of the strip as it returned to the 'original' gauge length.

Fig.5.3 includes the tracings from the 1st to the preconditioned cycle for one of the 'circumferential' and for one of the 'axial' strips. They originate from sample k' of which the biaxial curves have been presented earlier in chapter4. Those curves are typical in many respects of the expected behaviour for any 'axial' and 'circumferential' strip of this particular test site-I. The tracings have always started with the load scale of increased sensitivity and thus the points where the minimum recordable load of 0.001N appeared could be detected. Occasionally a region of lack of load could be also found on the first cycle (like in the 'circumferential' of fig.5.3) and this indicated that an amount of slackness existed when the strip was mounted in the grips and was probably related to the initial curvature of the tissue. The number at the point were the sensitivity returned to its normal scale is the cycle number. The flat crimped tracing on the 5th cycle indicates that the tissue had acquired a new resting length in both the 'axial' and 'circumferential' of the strips. This increase was 12% of the original gauge length for the 'axial' and 8% for the 'circumferential' strip. The question appears if this difference (which was consistent and significant) was an artefact caused by the fact that the initial

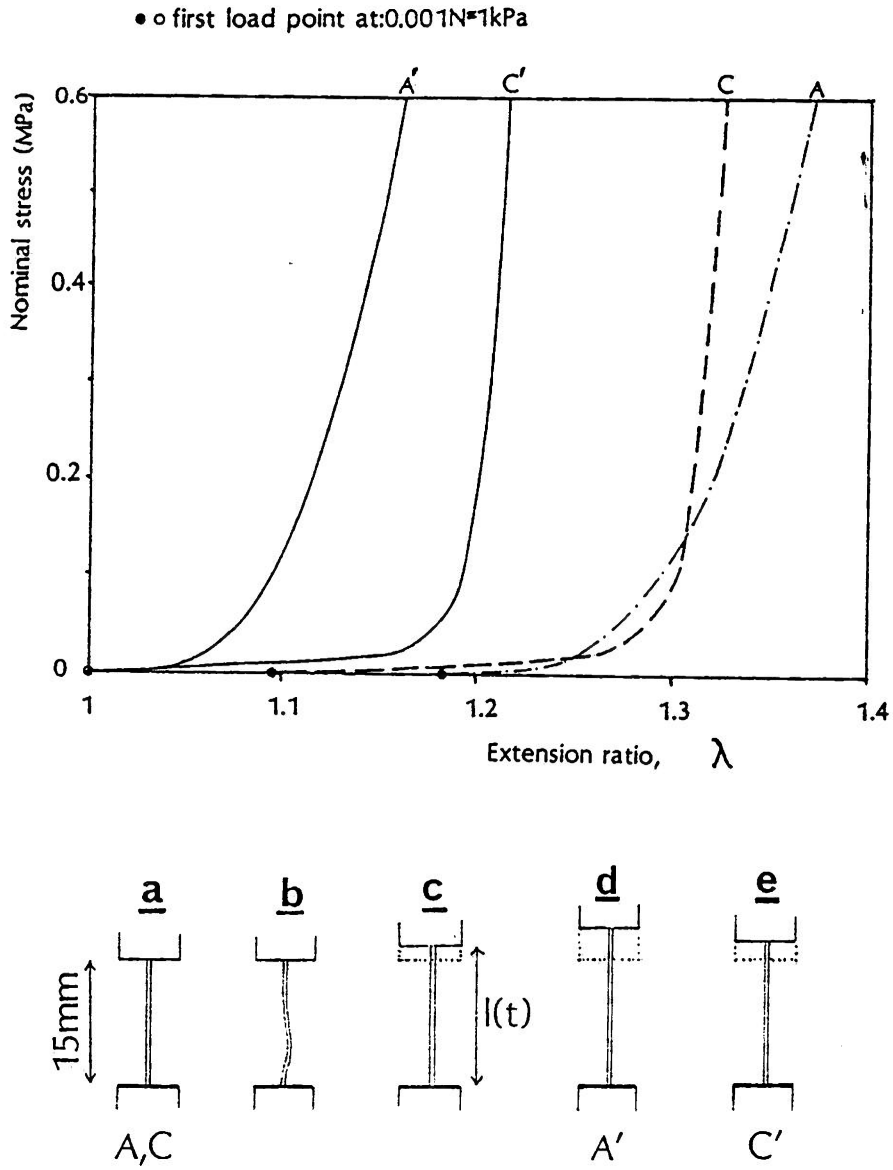

Figure 5.4:the loading response of a circumferential and an axial strip from sample k′; dashed lines are drawn by using the original gauge length which is the same for both direction as in a before the first pull and b after the initial cycles; continuous lines are drawn by the use of the shifted gauge length which was in general larger for axial strips in d, than the circumferential strips in e .

starting modulus of the 'axial' strips was lower than the starting modulus of the 'circumferential' strips, but it was visibly confirmed that the buckling of the strips (which indicated an increased length) dissapeared at the point where the first load was transmitted through the strip.

The 'circumferential' curves presented an overall increased stiffness which meant a higher initial starting modulus and a final higher tangent modulus at the peak load of 0.8N. As a result of these higher moduli on either region they presented a longer loading curve which rose to higher stresses for the same extensions (irrespectively of the gauge length used) and had an elbow with a sharp transition from the higher initial to the higher peak-load modulus.
There was some overshoot at the maximum load(0.8N) reversal point. Due to the different stiffnesses at the peak load the stiffer circumferential stips showed a greater overshoot (up to 0.84N) than the axial (0.81N) strips(fig.5.3).

At the peak load the curves had a rather stable stretch value for all cycles from the first to the preconditioned one. Like the 'axial' strip of fig.5.3, 'axial' strips presented a small shift which for n=16 had a mean value of 0.40% of the original gauge length and a standard deviation of 0.28%. 'Circumferential' strips shifted their peak-load by a mean value of 0.15% with a s.d.=0.02% (n=18).

The distortion energy irreversibly dissipated on the tissue was expressed by the size of the area of the hysteresis loop, which was a)larger in the 1st cycle than all the rest rest, for both families of strips, b)the same between the 2nd and all the rest of the cycles, c)the conditioned loop was in general larger for 'axial' than 'circumferential' strips.

The loading curve (up to peak load) altered its characteristics

only slightly after the first return so that 2nd loading/unloading and the rest did not differ much. It appeared that the structural elements of the strips had already settled to a configuration which provided a larger resting length, a reduced size for the hysteresis loop and a steeper loading curve as a result of the initial stretch up to the peak load and for the peak load level applied in the present tests.

5.1.7 A Pair of Uniaxial Tension Curves.

In fig.5.4 'axially'(A) aligned and 'circumferentially'(C) aligned uniaxial tension curves are shown. The curves were the loading portions of the preconditioned response of sample k' of which the biaxial inflation curves have been presented in chapter4 for comparison. Underneath a diagramatic presentation of the initial separation of the grips and the various gauge length options is presented. It is a side view of the mounted strip along its thickness. At the start a)the original gauge length is 15mm, b)after return from the first cycle to the original gauge length the strip buckles due to its increased length, c)the distance between the grips at any time instance l(t) if divided by the original gauge length gives as a measure the unshifted stretch ratio by use of which the dashed curves have been drawn, d)the shifted gauge length at the point where a first load of 0.001N was transmitted through the strips for the 'axial' strips gave rise to the curve A' which due to the increased gauge was less extensible and stiffer as well, e)the shifted gauge length for 'circumferential' strips by which curve C' was drawn. The shifted gauge length was in general and in average larger than the 'axial' strips, as a result the curves that initially crossed twice (for this particular specimen) were separated in the pair of A',C'.

The curves were qualitatively and quantitatively different. Like

the biaxial inflation pair of curves they crossed at low stress levels and this was not related to the gauge length in use (shifted or unshifted one). Circumferential strips presented an elongated pre-linear region where the stress increased only moderately. This region has been associated with a progressive recruitment of collagen fibres under load and usually is refered, as the 'incubation' region. When plotted from the original gauge length, the circumferential curve started with higher stresses (or reduced extensibilities at the same load levels) then the axial curve crossed the circumferential twice to finish at a higher extension for the peak load of 0.8N.

The set of the unshifted curves should confirm the anisotropic extensibility exhibited during biaxial inflation since the preparation attempted to preserve as much as possible of the initial geometry common between the two modes of test. During the preparation of the strips the sample was kept at initial(reference) dimensions similar to the ones before inflation by the use of the supporting paper card. At the same time the marking ink-dots which were used to yield the stretch in inflation were placed with the sample lying flat on the inflation rig. Thus it is suggested that if geometry (initial curvature or prestretch) had interfered with the curves obtained in inflation, this same influence should exist in the uniaxial tensile strip tests so that the results can be directly comparable.

There are other factors to consider. Firstly, absence of lateral forces allow an increased rearrangement of the fibrous components of the strips and this effect can be directionally dependent if the tissue had already an anisotropic distribution of fibres in its unstrained state. Secondly, stresses measured in inflation may reflect more accuratelly real material properties by being semi-Eulerian. This is due to the fact that the initial thickness

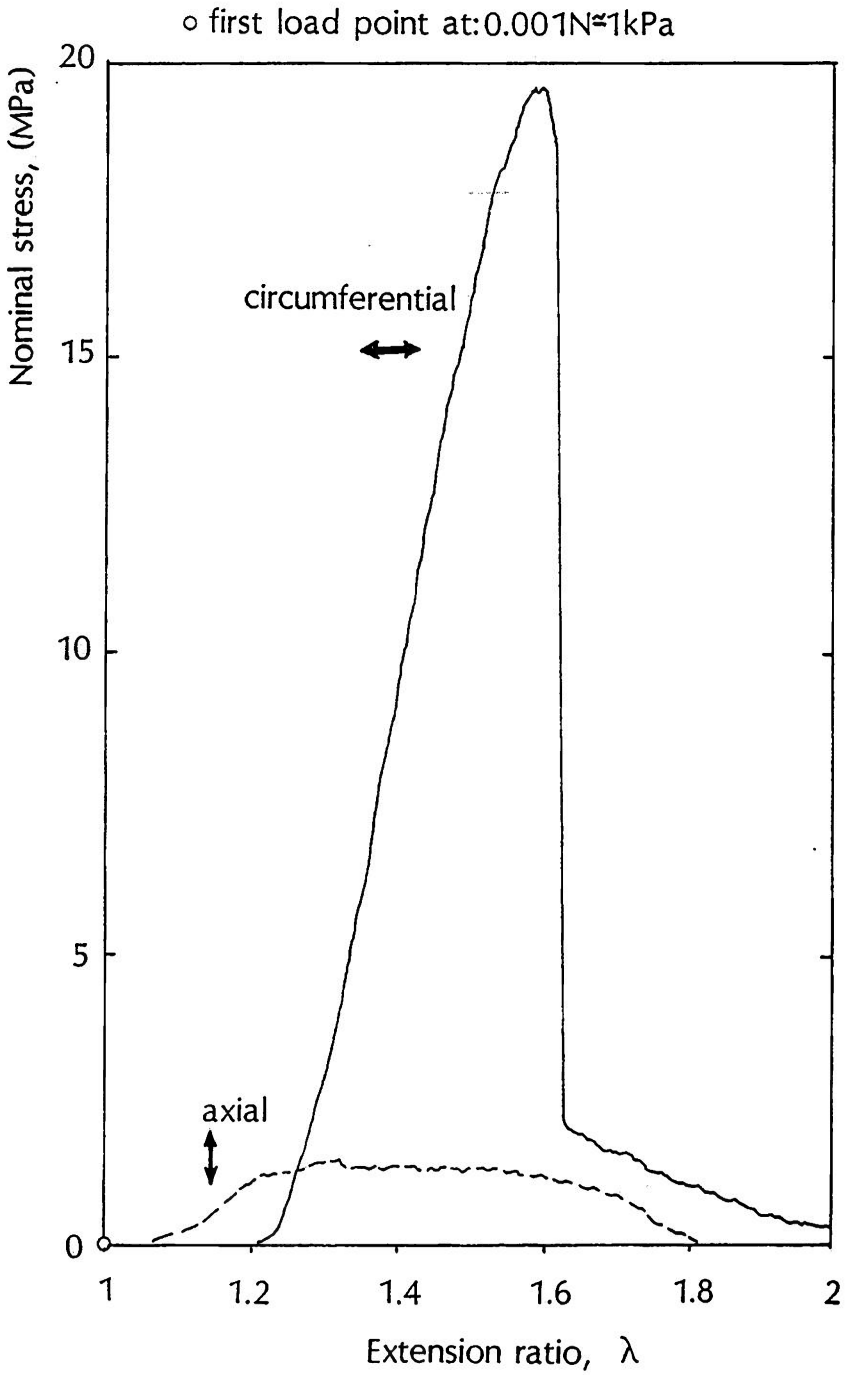

Figure 5.5:the complete curves until the failure point by the use of the shifted (redefined) gauge length. The axial direction was less extensible and weaker. (strips from sample k´).

value is used together with the stress resultant produced by use of Laplace's law which is truly Eulerian because it refers to the deformed dimensions. This may constitutes a reason why the uniaxial preconditioned tensile curves of the redefined resting strip length and thus of the shifted gauge length resemble better the biaxial inflation data.

The first of the previous suggestions will be dealt with by a test which examined the influence of the strip width on the response.

5.1.8 The Complete Loading Curves.

Fig.5.5 is an extension of the pair of curves(membrane k') drawn in fig.5.4 by using the shifted gauge length in order to cover the whole range of stresses that can be sustained by the strips. The curves have been drawn from the point where a minimum load appears till the point where complete failure occurs. Both curves in this set have the same general features up to the point where the maximum sustainable nominal stress value is reached. The first signs of stress became evident (in the full scale of 20MPa used in this chart) only after the extension ratio had reached λ=1.2 due to the very compliant initial region. Afterwards the curves turned upwards and passed into a linear region the length of which was markedly different in the two directions. The circumferential strips reached a high ultimate tensile stress(nominal), while the axial failed at lower values.

The manner at which the axial and circumferential strips behaved after the ultimate load point was different between the two directions, but consistent within each of the groups of axial and circumferential strips. The axial strips exhibited a prolonged creeping until the point where the load transmitted through the strip completely disappeared. The circumferential strips reached a high

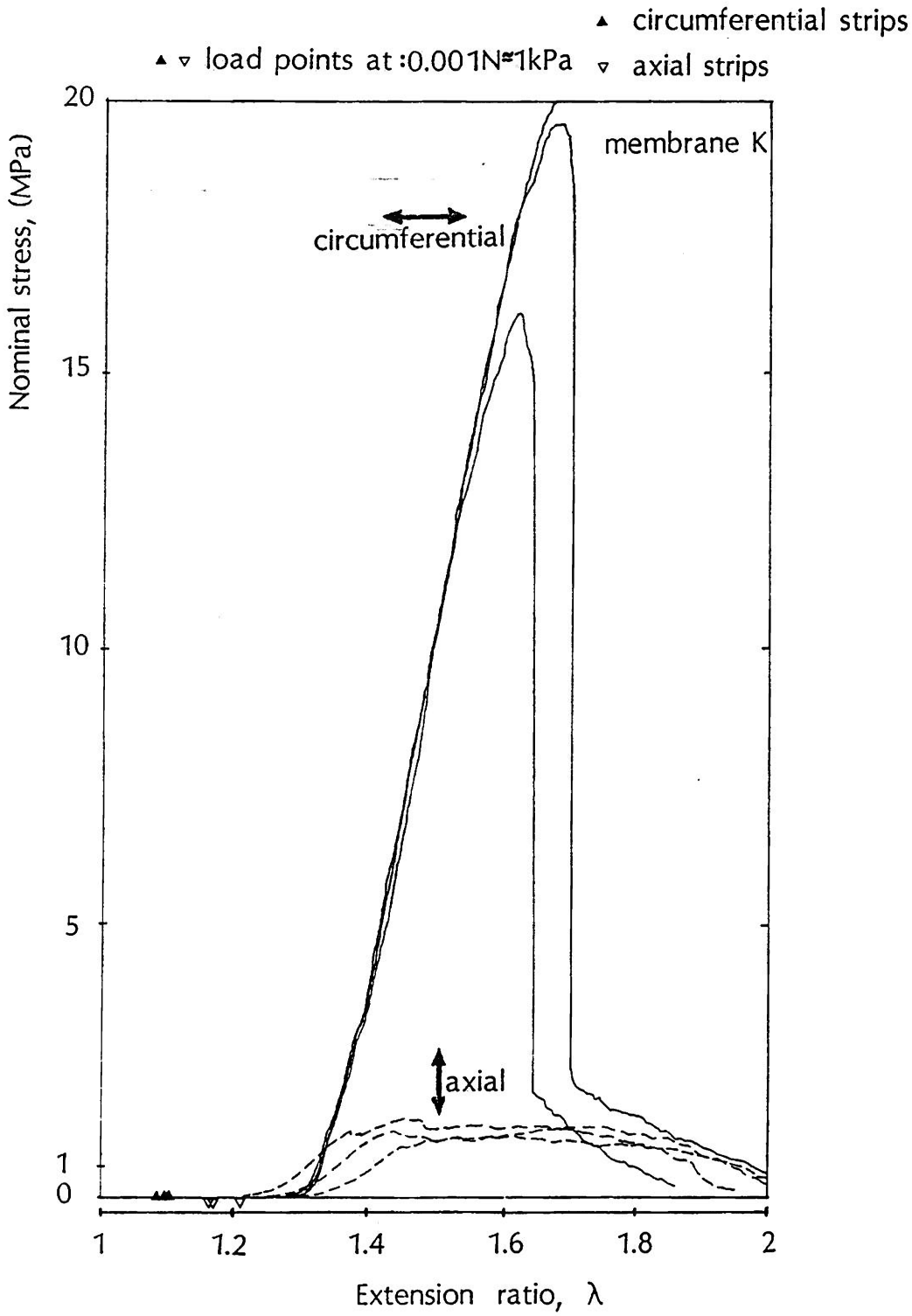

Figure 5.6:failure of all 3 strips per direction of sample k´ by using the original gauge length. The points where a minimum recordable load of 0.001N was transmitted by the strips is indicated by the triangles.

stress value which precipitously fell to levels of stress comparable to the one in the axial strips, the stress falling steadily and complete fracture occurred at higher extension ratios than in the axial strips.

The behaviour of the full loading curves to failure reflects the structure of the material. Circumferential strips have been shown to start with a higher tangent modulus in the previous section of the low stress/strain preconditioned area. These same strips in the traces of the complete curves followed a steeper rise by demonstrating higher moduli in the pre-failure linear region and ended-up at higher ultimate stress values. Both measures of moduli and ultimate stress suggest that the material structure was reinforced along this circumferential direction.

As in fig.5.4 previously plotting by use of a commom first load point was particularly helpful in stressing the anisotropy in extensibilities in the two normal directions. The axial strip in fig.5.5 were less extensible than the circumferential one at all stress levels.

In fig.5.6 the set of 3 curves per direction has been plotted from the original gauge length. The first load points have been marked by the solid and open triangles and the unequal shift in the two directions can be easily appreciated with the circumferential strips(solid triangles) having altered their resting length to a lesser extent than the axial strips(open triangles). By using the original gauge length an increased dispersity between the traces of strips at a particular direction was observed. This can particularly be seen at the axial traces of fig.5.6 where a lateral shift exists between the 3 curves.

The tissue was preconditioned to a maximum nominal stress of 0.8MPa

which is below the 1MPa mark on the stress axis. Both families of curves appear to have entered their linear region at their peak load point and thus the elastic tangent modulus at peak load of the preconditioned curves is very much the elastic modulus as calculated in the linear region.

The loads that the two sets of strips (and consequently the material) can sustain in the two directions are enormously different. One of the circumferential strips had even exceeded the maximum recordable load of 20N for the load cell in use.

In the axial direction all strips failed at an ultimate stress value below 1.5MPa. Thus the top load in preconditioning represented a substantial amount of the ultimate load that the axial strips could bear.

Assuming that the correct magnitude of stresses has been estimated for the top pressure in inflation the previous observation means that the material has to perform very close to its limits in one of the directions while it can bear substantially higher loads in the other direction.

In the series of photos around the graph in fig.5.7 the visual appearance of the strips was monitored by the use of a SLR NIKON camera equipped with an extension tube and a telephoto lens.

The strips in fig.5.7 came from sample i′. In the left row of photos, instants 1-5 came from the deformation of an axial strip. The photos on the top are from the original gauge length after the initial preconditioning cycles. The ′axial′ strip appeared slack and one can see on the plot of fig.5.7 that the first detectable load for this axial strip was at a deformation 13.3% of the original gauge length (marked by an open circle on the axis). In instant1 the extension ratio is a substantial 1.375 but on the plot this represents a small

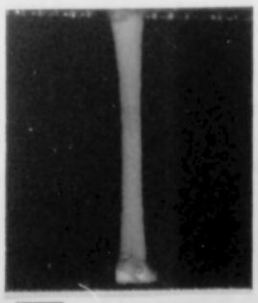

1 λ=1.375

'axial' gauge length

'circumferential' gauge length

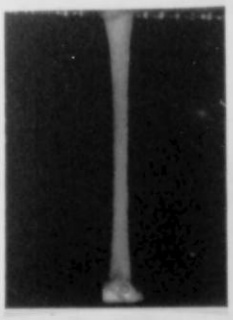

2 λ=1.452

3 λ=1.529

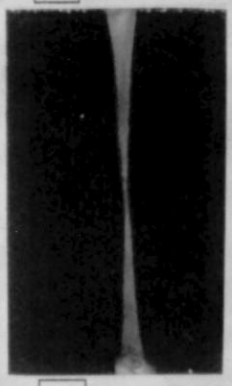

4 λ=1.666

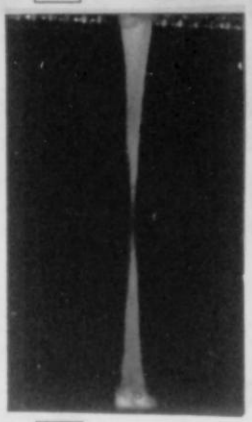

5 λ=1.951

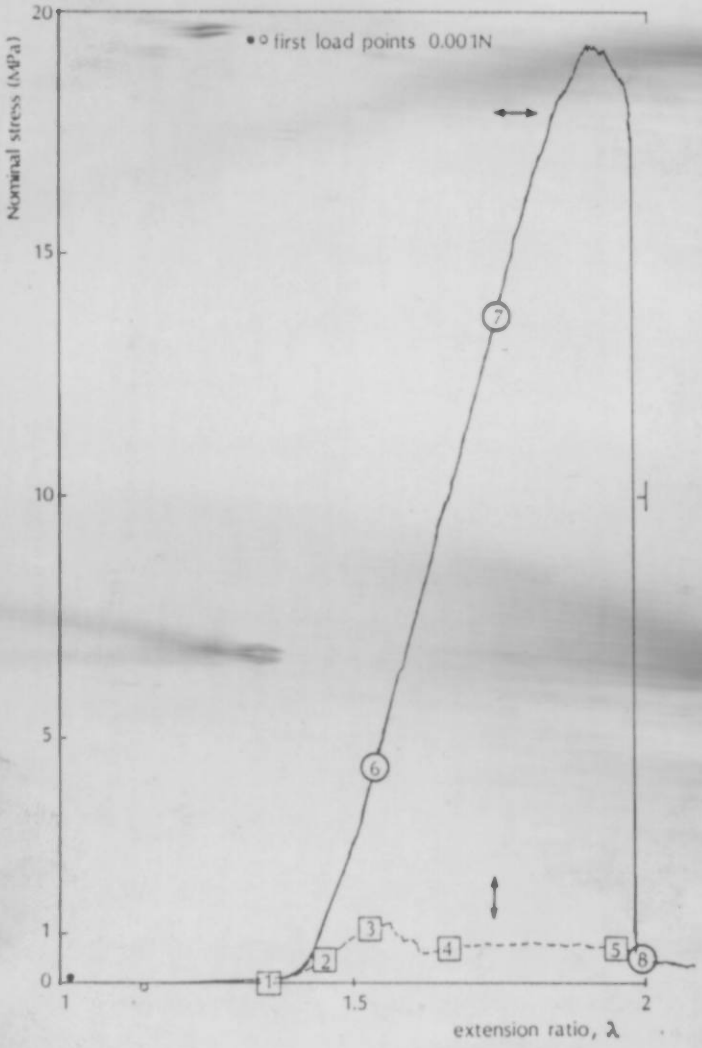

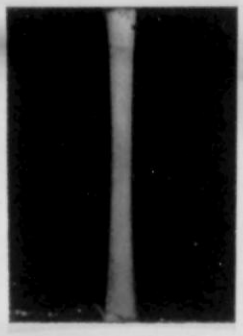

6 λ=1.537

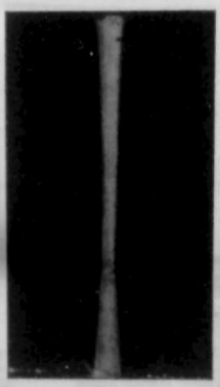

7 λ=1.759

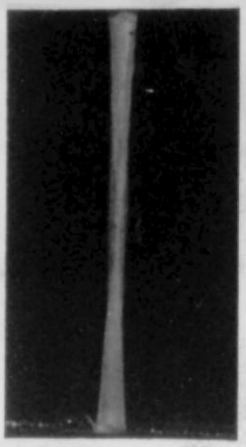

8 λ=2.0

Figure: 5.7 Photographic instants of failure of 'circumferential' and 'axial' strips.

stress value due to the compliance of the strip. Instants 2 and 3 are before the failure point of the strip where the strip was considerably narrow due to contraction in its lateral directions. At instants 4 and 5 which are after the ultimate tensile strength point the strip was flowing and failing in a ductile sense while deformation increased but remarkably it still sustained a substantial amount of the ultimate load. Failure occured in the middle of the strip and away of the grips, at an extension ratio of 1.951.

In the top row on the right hand side, photo2 shows the circumferential strip mounted after preconditioning at its original gauge length. A degree of slackness was there due to the previous cyclic loading and in the plot it is shown that the gauge length had shifted 1.86% from the original gauge length (black circle on the axis) a value much smaller than in the axial direction.

In the second row of photos, 3 instants of the failure of a circumferential strip from the same membrane I and oriented at right angle to the previous one are presented. Instant 6 was at an extension ratio 1.537 which was well within the linear region of the curve but unlike the axial strip narrowing of this strip was not prominent. Instant 7 was within the region of yield and it appeared that the previously uniformly white coloured surface of the strip had started cracking with a less uniform shade. In instant 8, which was clearly after the failure point where the strip was creeping to complete fracture, the strip appeared still intact with its lateral dimensions not significantly altered but it could now transfer only a minute fraction of its ultimate load between the grips. The photo also reveals that from within a spongylike and translucent material the image of a number of 'silky' highly stretched collagen bundles emerged which were responsible for this small amount of load

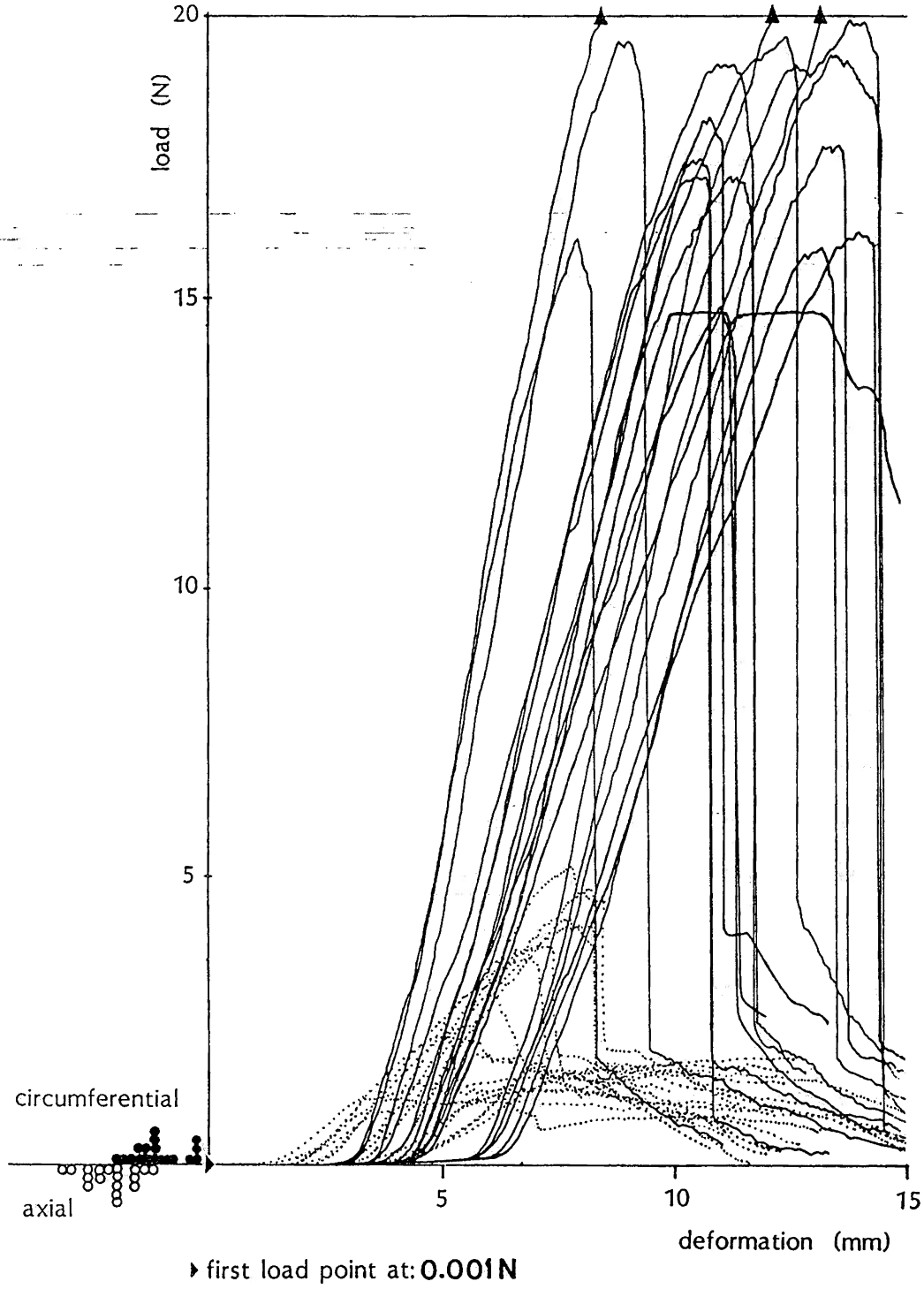

Figure 5.8:the load/deformation traces of all the strips of the 7 samples tested in test site-I. The tracings have been brought to a common first load point, the circles indicate the amounts of deformed length added to the original gauge length.
Dotted lines:axial strips, continuous lines:circumferential.

transmitted between the grips. This strip also failed with a clear snap at its middle region(fig.5.7;⑧).

5.1.9 Uniaxial-Biaxial behaviour in test site-I.

Differences in parameters should not only be statistically significant but also reflecting the reality and this can only mean that the uniaxial tensile traces should present the same consistent behaviour within each of the envelopes along the two principal directions. A complete plot of all curves brought to a common first load point is shown in fig.5.8, the dotted traces of the axial strips are clearly and distinctly different from the whole lot of complete circumferential curves.

Three strips which exceeded the maximum load recordable by the load cell in use with this test, are marked by the arrows in the figure.

Few strips failed at extensions less than 15mm and thus for a stretch ratio less than 2. Most strips although already in the post-failure region crept enough to exceed a stretch ratio value of 2.

For two strips in the 'circumferential' direction a short plateau region existed at the ultimate tensile stress and at the time of the test it was attributed to a high friction slipping from the grips. These were the only cases where the combination of the waterproof paper pads and the cyanoacrylate glue did not offer enough bonding power to firmly hold the two ends of the strips.

The dispersity between the curves in each of the envelopes was smaller than if the original gauge length had been used.

In fig.5.8 the unequal shift of the first load is obvious by the pseudo-histograms of the dark and open circles on the left of the origin. The differences in terminal slope are evident from the steep rise of the circumferential curves.

The values of Ultimate tensile strength, the unshifted and the

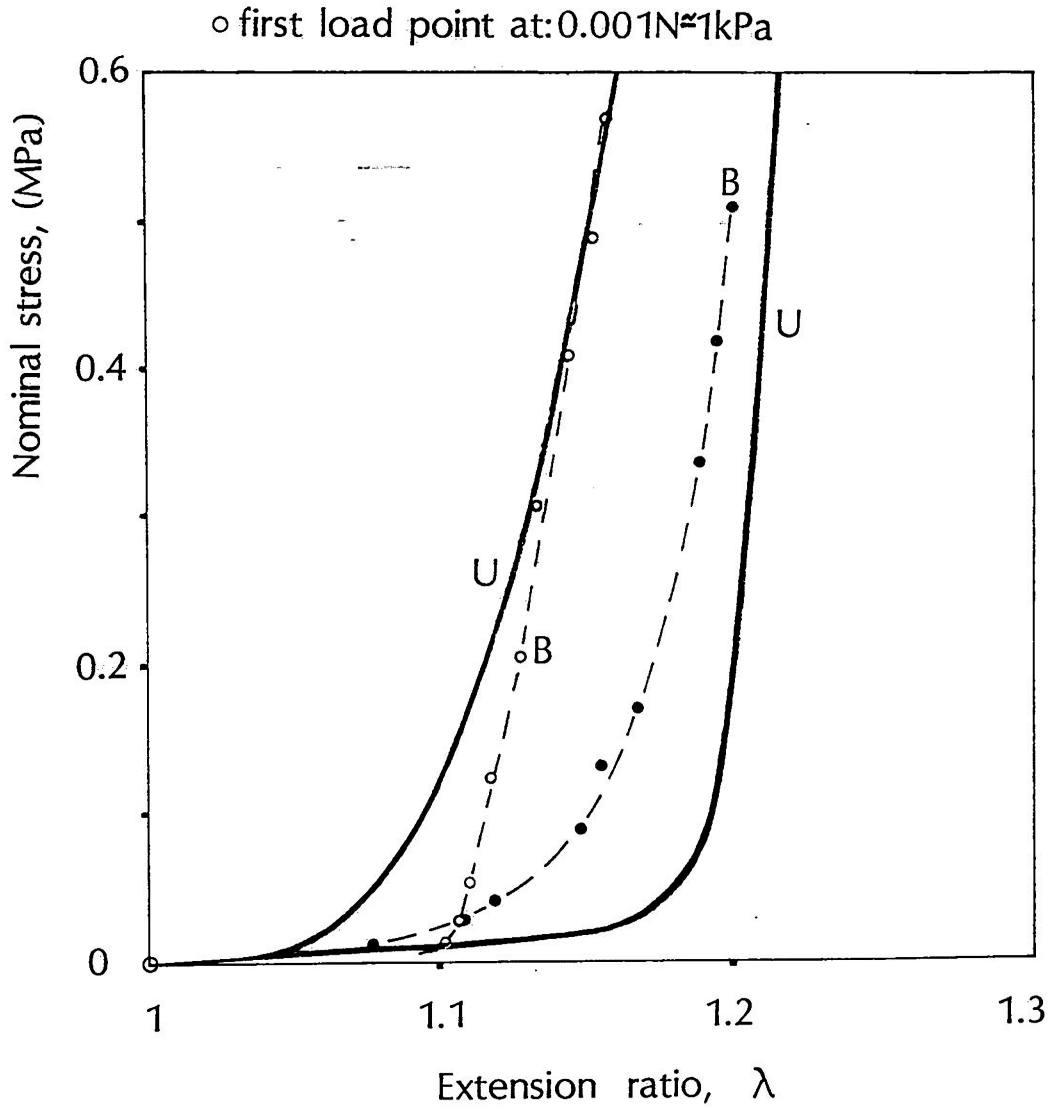

Figure 5.9:a pair of uniaxial curves(U) by using the shifted gauge length and the biaxial inflation curves(B) for sample k´.

shifted moduli of the linear region and the shift of the first load are included in a table of test site-I (table5.1).

The differences in the values of the previous parameters between the two directions were significant at $p<0.001$ (Student t-test). Statistics were performed between U.T.S.s, moduli of the linear region when using the unshifted gauge length, and moduli when using the shifted gauge length between axial and circumferential strips for all comparisons.

	MEANS	STANDARD DEVIATION	STANDARD ERROR OF MEAN
axial strips:			
U.T.S.	2.55(MPa)	1.27(MPa)	0.29(MPa)
E unshifted	13.63(MPa)	4.47(MPa)	1.05(MPa)
E shifted	15.50(MPa)	4.90(MPa)	1.15(MPa)
shift in gauge length	1.141	0.035	0.008
circumferential strips:			
U.T.S.	17.78(MPa)	1.99(MPa)	0.46(MPa)
E unshifted	46.23(MPa)	9.14(MPa)	2.10(MPa)
E shifted	49.70(MPa)	10.18(MPa)	2.34(MPa)
shift in gauge length	1.075	0.035	0.008

The comparison of the shifted loading uniaxial curves of membrane k′ and the biaxial inflation curves(chapter4) for the same membrane is shown in fig.5.9. The shape of the curves in each of the directions is very similar with the axial curves rising smoothly while the

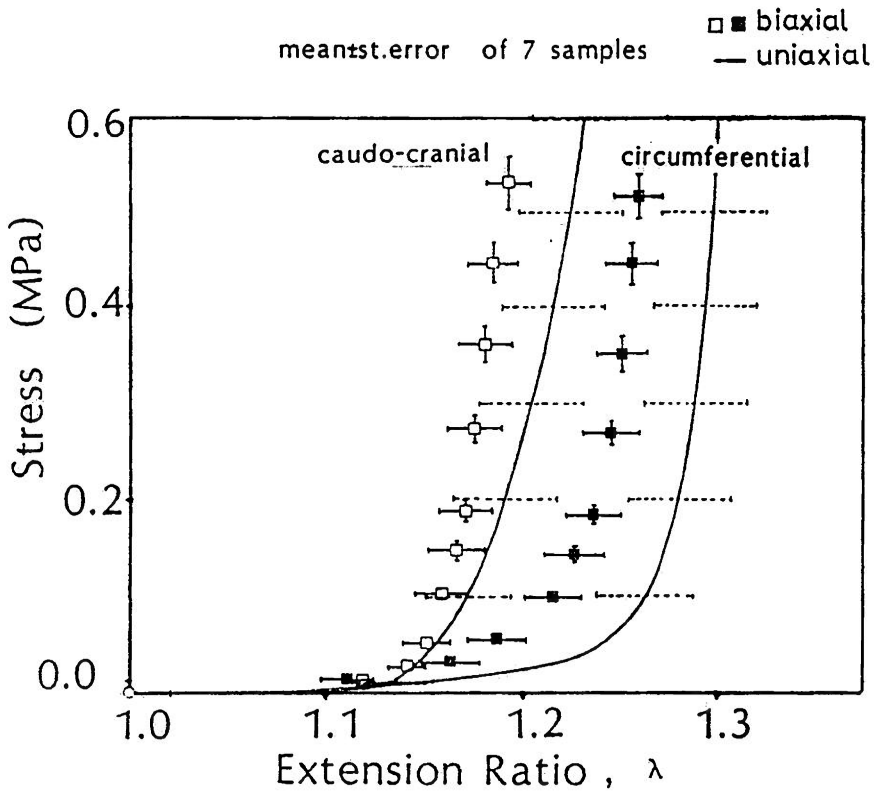

Figure 5.10:the average biaxial behaviour of all 7 samples as presented in chapter4, and the average uniaxial behaviour as exhibited in the strip tests and by using the shifted gauge length. The standard error of the mean is also shown.

circumferential curves have a prolonged loading portion at low stresses and then followed by an elbow rise to higher stresses with higher tangent moduli.

The magnitude of the difference of the extensibilities of the two curves is reasonably comparable, with the biaxial curves appearing overall less extensible due to the presence of lateral forces for each of them. For this particular membrane the 'axially' oriented uniaxial curve fell on top of the 'axially' oriented biaxial curve (fig.5.9), but this was not the case for the rest of the samples where the biaxial curves were always individually and in average less extensible than their uniaxial equivalents.

This can be appreciated in fig.5.10 where the mean behaviour of the biaxial curves previously presented in chapter4 has been plotted together with the currently produced mean uniaxial curves. The similarity between the mean curves at each of the directions is striking. The small error bars around the zero origin which have been introduced in chapter4 alongwith the considerations for the initial curvature of the tissue appear to have also found their counterpoints in the measures of the shifted gauge length in the present discussion. There is no doubt that plotting by the use of the shifted gauge length for this tissue improves the comparibility of the results and predicts only moderate shifts to lower strains from the uniaxial to the biaxial curves.

5.1.10 Standardisation of Examination of Uniaxial Tests.

In the present tensile uniaxial tests the tissue exhibited a directionally dependent behaviour which as shown in fig.5.9 for a single sample and fig.5.10 for the average behaviour can be easily demonstrated by using the biaxial inflation data.

The statistical examination of the values of the parameters

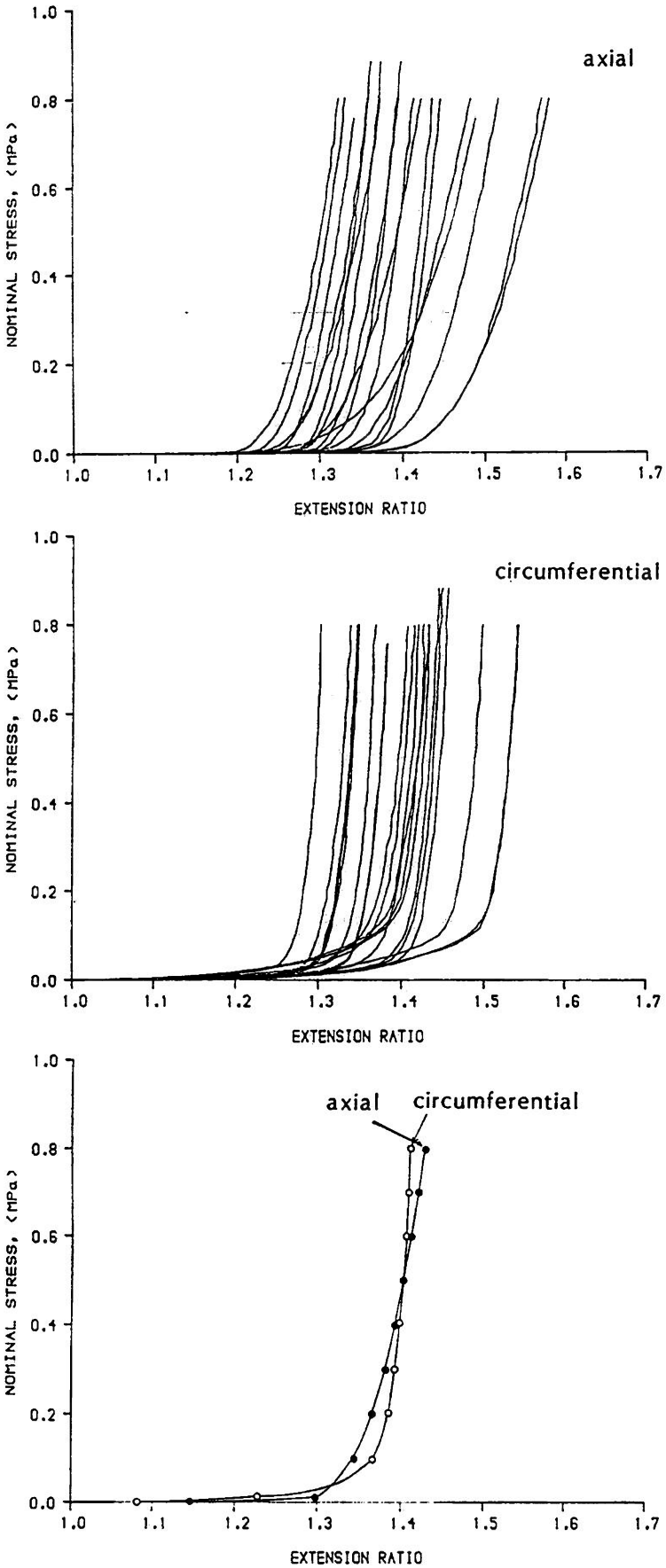

Figure 5.11:stress/stretch behaviour in test site-I (original gauge length).

Table 5.1:

SPECIMEN	A:Axial C:Circumferential	U.T.S	Young's modulus	Modulus by using the shifted gauge	Shift in loaded length
		(MPa)	(MPa)	(MPa)	(%)
e′	A	3.50	19.23	21.27	10.60
		3.80	17.54	19.85	13.20
		4.70	14.62	15.83	8.30
	C	14.60	35.71	39.85	11.60
		18.00	56.18	62.13	10.60
		14.60	46.62	52.12	11.80
f′	A	1.70	7.58	8.27	9.20
		3.00	15.55	17.19	10.60
		-	-	-	-
	C	14.80	36.05	38.79	7.60
		-	-	-	-
		-	-	-	-
g′	A	1.50	11.59	13.43	15.90
		1.60	10.36	12.15	17.33
		1.30	8.79	10.31	17.33
	C	15.80	40.08	42.75	6.66
		17.80	36.73	39.66	7.99
		16.20	34.81	38.06	9.33
h′	A	4.20	11.90	13.63	14.50
		4.60	23.72	26.85	13.20
		4.00	20.66	22.85	10.60
	C	19.50	46.77	52.66	12.60
		19.60	45.45	49.04	7.90
		20.00	36.90	39.82	7.90
i′	A	-	-	-	-
		1.20	8.74	9.90	13.33
		-	-	-	-
	C	19.20	42.86	43.66	1.86
		>20.00	44.12	44.71	1.33
		>20.00	52.19	52.81	1.33
j′	A	2.40	13.71	15.54	13.32
		2.20	13.99	15.85	13.32
		2.20	15.15	18.08	19.33
	C	17.20	45.45	47.87	5.33
		17.50	49.70	51.02	2.66
		17.20	42.61	46.01	7.99
k′	A	1.40	12.99	15.07	15.99
		1.35	9.09	11.03	21.33
		1.20	10.10	11.85	17.33
	C	19.80	62.50	67.91	8.66
		>20.00	64.50	70.08	9.99
		16.10	59.23	64.76	9.33

between directions within this test site-I showed that the specific parameters of the table5.1 accurately reflect the real situation shown in fig.5.9.

It was found that the much more prominent failure and strength features of the complete curves can be reflected to the low stress/strain region by the higher tangent moduli and the shape of the curves. As a means for qualitatively assessing the low stress/strain behaviour, charts combining graphs of all plots at each of the directions and their mean (average) behaviour have been constructed. In figures5.11a,b the whole population of loading preconditioned uniaxial curves are plotted. Fig.5.11 includes the unshifted curves for the axial strips (top plot), the circumferential strips (middle plot) and their mean behaviour (bottom plot). The mean curves have been produced by averaging the stress and stretch values at load levels of 0.0, 0.01, 0.1, 0.2, 0.3, 0.4, 0.5, 0.6, 0.7, 0.8N. It is evident immediatelly that the unshifted curves of specimens from sample k´ have a behaviour typical of the whole population as expressed by the mean curves in fig.5.11c. Within each of the envelopes of curves the resemblance between the shapes of the curves is high and this is depicted in the shape of each of their respective mean curves.

The distribution within each envelope appears normal with only a few outlying curves. These same curves which appear more extensible have a more prolonged ´incubation´ region as well, before they stiffen and enter the linear region. Thus the previously mentioned qualitative result which associated the prolonged incubation period of the circumferential strips to a larger overall extensibility, appeared to apply even within the circumferential envelope.

Fig.5.12 shows the axial, circumferential envelopes and their

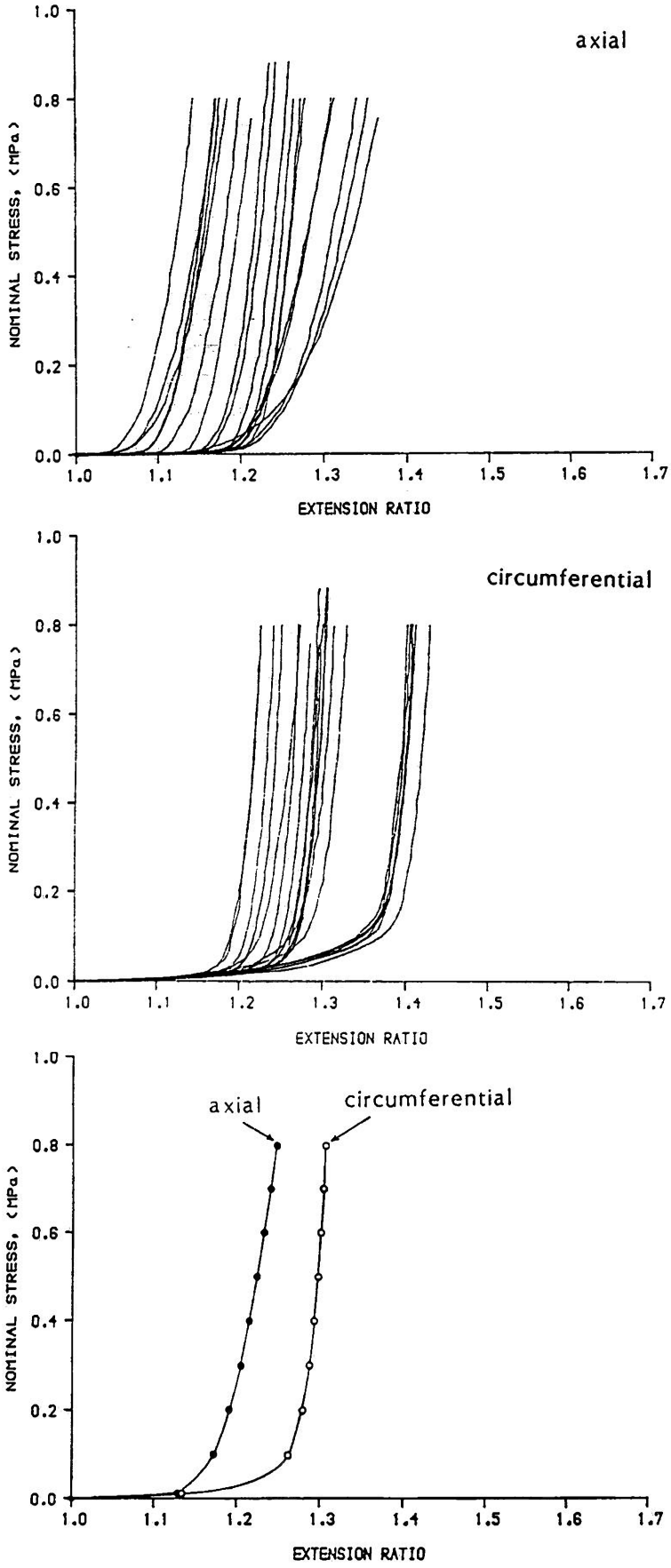

Figure 5.12:stress/stretch behaviour in test site-I (shifted gauge length).

mean responce, using the shifted gauge length at the start of the last preconditioned cycle. The extensibilities of the families of curves are significantly different above any stress level of 0.05MPa (for p=0.01 Student's t-test).

5.1.11 Factors that may Influence the Outcome.

With the present series of uniaxial tension tests a result was sought that could both validate the outcome of the biaxial inflation test and categorically decide about the anisotropy, or otherwise of the tissue.

5.1.11.1 Strip-width. It has been suggested before that the width of the strip used in uniaxial tensile tests may have a significant effect on the response obtained. Lee et al(1984) connected the ability of strips excised from porcine valve leaflet tissue to achieve a stabilized response after a number of cycles to the size of the width of the strip. It was found that a minimum 4mm width was required for circumferential 10mm long strips, while a 6mm width was required for 10mm long radial strips. It was speculated that the result of cutting a strip out of the leaflet had interfered with the integrity of the feltwork and the weave of the fibres thus resulting in a specimen with damaged texture. The highly anisotropic structure of the porcine valve leaflet with fibres running predominantly along the free edge of the leaflet in the circumferential direction meant that for the family of radial strips the blade of the cutter cut across the fibres thus leaving the loosely connected and non-organized interfibrillar collagenous network to support the tensile load.

It is possible that similar effects might occur in pericardium. The U.T.S., was thought to be the most reliable estimator of the effect of disruption of structure, and the influence of strip width was

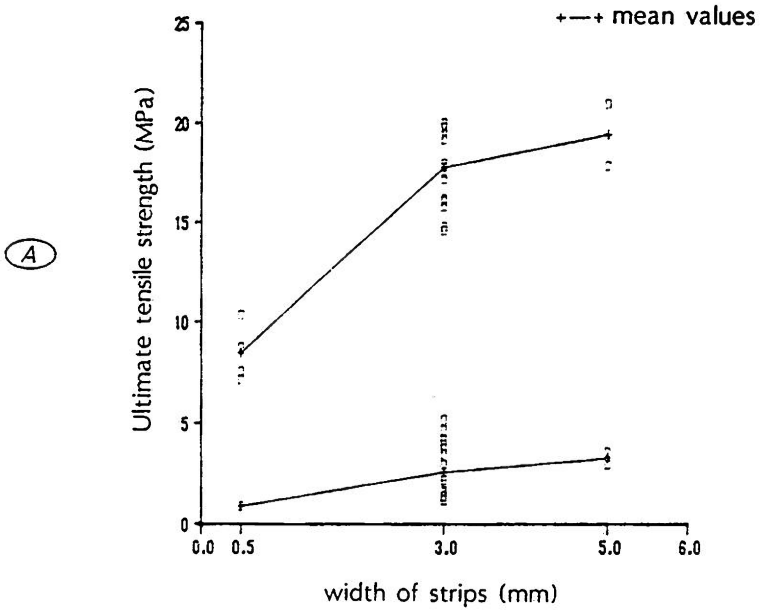

(A)

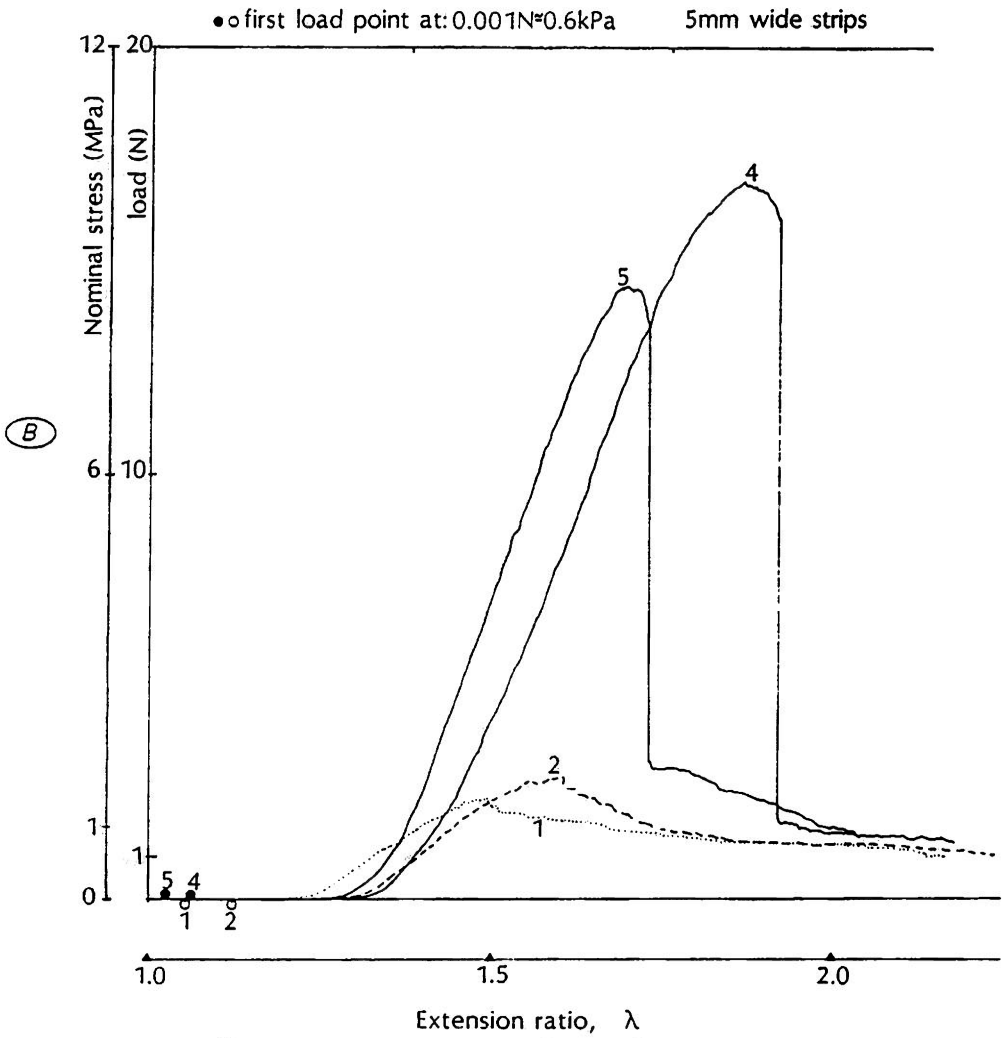

(B)

Figure 5.13: (A) plot of the U.T.S.v.the strip width; (B) the failure curves for 5mm wide strips did not differ significantly from the 3mm wide strips.

investigated for strips of 5mm, 3mm, and 0.5mm width(fig.5.13). The 3mm data points include all the strips tested in the previous section5.1.9. The 0.5mm strips were essentially strings of tissue very difficult to mount and thus for the weak axial direction only one of them has been plotted on the graph(the rest were disregarded).

The results of fig.5.13a have two main features: i)the degree of anisotropy expressed by the absolute difference between U.T.S. values in the two directions is present even in the smallest width, ii)the absolute values of the U.T.S. appear to have been reduced for 0.5mm wide strips but were not significantly different for strips of 3mm and 5mm width. From the first feature one can infer that the concept of continuity may be applicable for this tissue, but it must be accompanied by an anisotropic approach of the mechanical properties as well. From the second feature, that the strip width did not interfere with the present data and that 3mm wide strips were wide enough to yield valid data as the measurements of U.T.S. seem to have reached a stabilized response for these width values. The initial width of 3mm had been chosen by restrictions on the overall dimensions of the strips. The length of the strips was not kept the same in the trials. The 0.5mm wide strips were 15mm long, the 3mm wide were 15mm long and the 5mm wide were made 25mm long in order to preserve the ratio of length to width at least equal 5.

In fig.5.13b the traces of the 5mm wide strips are drawn. The main features as they have been established previously are again present. The behaviour is typical in either of the directions and when the traces were plotted in nominal stress .v. extension ratio with a full scale of 20MPa (in order to be directly comparable to the traces in fig.5.8) they fell inside the axial and circumferential envelopes.

Table 5.2:moduli at the origin along the two orthogonal directions.

SPECIMEN	AXIAL (MPa)	CIRCUMFERENTIAL (MPa)
e′	0.018	0.040
	0.015	0.032
	0.015	0.034
f′	0.017	0.040
	0.019	0.042
	-	-
g′	0.017	0.045
	0.015	0.040
	0.015	0.039
h′	0.030	0.076
	0.033	0.076
	0.032	0.070
i′	-	0.063
	0.011	0.054
	-	0.063
j′	0.016	0.034
	0.015	0.040
	0.015	0.036
k′	0.042	0.047
	0.025	0.042
	0.015	0.034
	n=18	n=20
mean:	0.023	0.047
st.deviation:	0.014	0.014
st.error mean:	0.004	0.003

5.1.11.2 Anisotropy at the origin. From the present series of tests and the values of the parameters in table5.1 it has been concluded that the material is anisotropic. However a group of workers (Black et al,1985; Trowbridge et al,1985)has argued that the decision about anisotropy or not should be taken by examination of the slope of the stress/extension ratio curve at the origin.

These workers proposed an isotropic, incompressible strain energy function, for describing the material properties of fixed bovine pericardium, of the Mooney form:

$$W = C1\ (I_1-3) + C2\ (I_2-3) \qquad (5.1)$$

with the material constants being C1,C2 and strain invariants I_1, I_2. By accepting a single Poisson's ratio, which only applies to isotropic materials, they suggested that the ratio of the finite strains:

$$(\lambda_2^2-1)/(\lambda_1^2-1)=f(\lambda_1^2-1) \qquad (5.2)$$

could be a second order polynomial truncated Taylor series and thus the contraction stretch ratio λ_2^2 could be a polynomial expression of the extension ratio λ_1^2:

$$\lambda_2^2=P(\lambda_1)=1+k(\lambda_1^2-1)\ +m(\lambda_1^2-1)^2+l(\lambda_1^2-1)^3 \qquad (5.3)$$

with the previous assumptions the response to load should be:

$$\sigma = 2[\lambda_1-P(\lambda_1)/\lambda_1]\ [C1+P(\lambda_1)C2] \qquad (5.4)$$

which when differentiated yields at the origin($\lambda_1\rightarrow 0$) a slope:

$$slope=4(1-k)(C1+C2) \qquad (5.5)$$

By using this analytical route, which required estimation of the parameters C1, C2, k, l, m as to best fit the data, they estimated the

slopes of a number of strips originating from different sacs and positions. Those slopes were fed into a 2WAY analysis of variance which yielded that neither of the factors (sac or position) could produce a significant difference in the response to load. On the previous evidence they claimed that fixed pericardium could be modelled as an isotropic material.

This approach has two major disadvantages: it has already adopted an isotropic model before the proof is produced, and it estimates/predicts the slopes by extrapolation at the origin instead of measuring them.

For this reason the table5.2 was constructed by measuring the moduli at the origin of our pericardial strips along the two normal to each other directions. The result was statistically significant (for $p<0.001$, Student´s t-test) with the moduli along the circumferential direction being higher than the axial moduli. This is consistent with what it has been said earlier that the circumferential curves were stiffer all along their length, from the very start to the linear pre-failure region.

On the basis of the present results which have been measured and not extrapolated it is decided that the material is anisotropic even at the origin in its relaxed state.

5.1.12 Discussion

The main problem encountered in the simple tension tests was that of the gauge length, which can influence the results and their interpretation.

The idea of a relaxed length was first introduced by Fung(´resting length´;1967) who suggested that tissues appear to possess a certain length when at a particular "environment". The term environment has a more general meaning, describing either the ambient conditions or the

loads under which the tissue operates. Depending on the presence of water and electrolytes in the environment an increased swelling of a tissue sample in its lateral dimensions may result in a longitudinal shrinkage of its length. Load cycling has also resulted in an increased length as defined by the use of some load level.

The fact that pericardium (at least in the form of strips) acquires a new length as a result of cycling must have been detected by Nelemans(1940) who, as said in chapter3, ascribed some plasticity to tissue strips. The question is if the term plasticity is appropriate as the strips of the present investigation appeared to regain their resting geometrical length when floating in a saline bath for 12hours after the completion of a cyclical loading test. Their thickness after this relaxation period did not differ significantly from the one before the test and this was consistent to the behaviour we had observed before and after the inflation test and the relaxation period that followed these biaxial tests.

Trowbridge and Crofts(1986a) have published some statistical evidence to show that both fresh and chemically modified bovine pericardium recover their main geometrical dimensions (length, width, thickness) within 10hours after being returned to their natural storage medium (saline and glutaraldehyde respectively), and later commented (Trowbridge and Crofts(1986b)) that the actual choice of the appropriate gauge length can lead to various interpretations as to the effect that chemical modification may have in altering the tissue mechanical properties from the fresh into the fixed form. These workers employed a slight initial stretch till a load 0.01N was transmitted and then unloaded the tissue till no load was recorded. Although it may seem unlikely to happen it is possible that any increase in the resting length as a result of this small stretch must

have been incorporated in the gauge length set by this procedure and thus this method was not followed in the present tests. In fig.5.2 a substantial stretch can result at such a small load due to the high compliance of the tissue. In the apparatus used in here which provided a higher load resolution the stretch at 0.001N and 0.01N can differ as much as 0.05.

There was also a small shift at the stretch ratio value of the peak load point for axial strips. For this measure there was also a clear relation between those 'axial' strips that presented the higher values of shift at peak load and the value of ultimate tensile strength sustained by those same strips. It was observed that 'axial' strips which had a low U.T.S. value, and thus the peak load represented a significant proportion of the maximum load that these strips could support, presented the higher shift with an associated difficulty to stabilize at a certain loading response. The 'axial' strip of fig.5.3 failed at 1.5N and thus the peak load represented more than 50% of the maximum load. It was suggested then that those strips had entered a region of yield. Similar observations have been made once before by Lee et al(1984) who, when working in fresh porcine valve tissue, found that ability to precondition was related to the direction (radial or circumferential) of the strip on the leaflet of the well established anisotropic valve leaflet tissue.

The native bovine pericardium exhibited anisotropy in all those parameters of table5.1 for the test site-I. Such extreme differences, as the ones present here between the ultimate tensile strength and the modulus of elasticity, have been found to exist between strips of valve leaflet tissue at their radial and circumferential directions. Lee et al(1984) reported that circumferential strips of fresh porcine valve leaflet tissue had elastic modulus and ultimate tensile strength

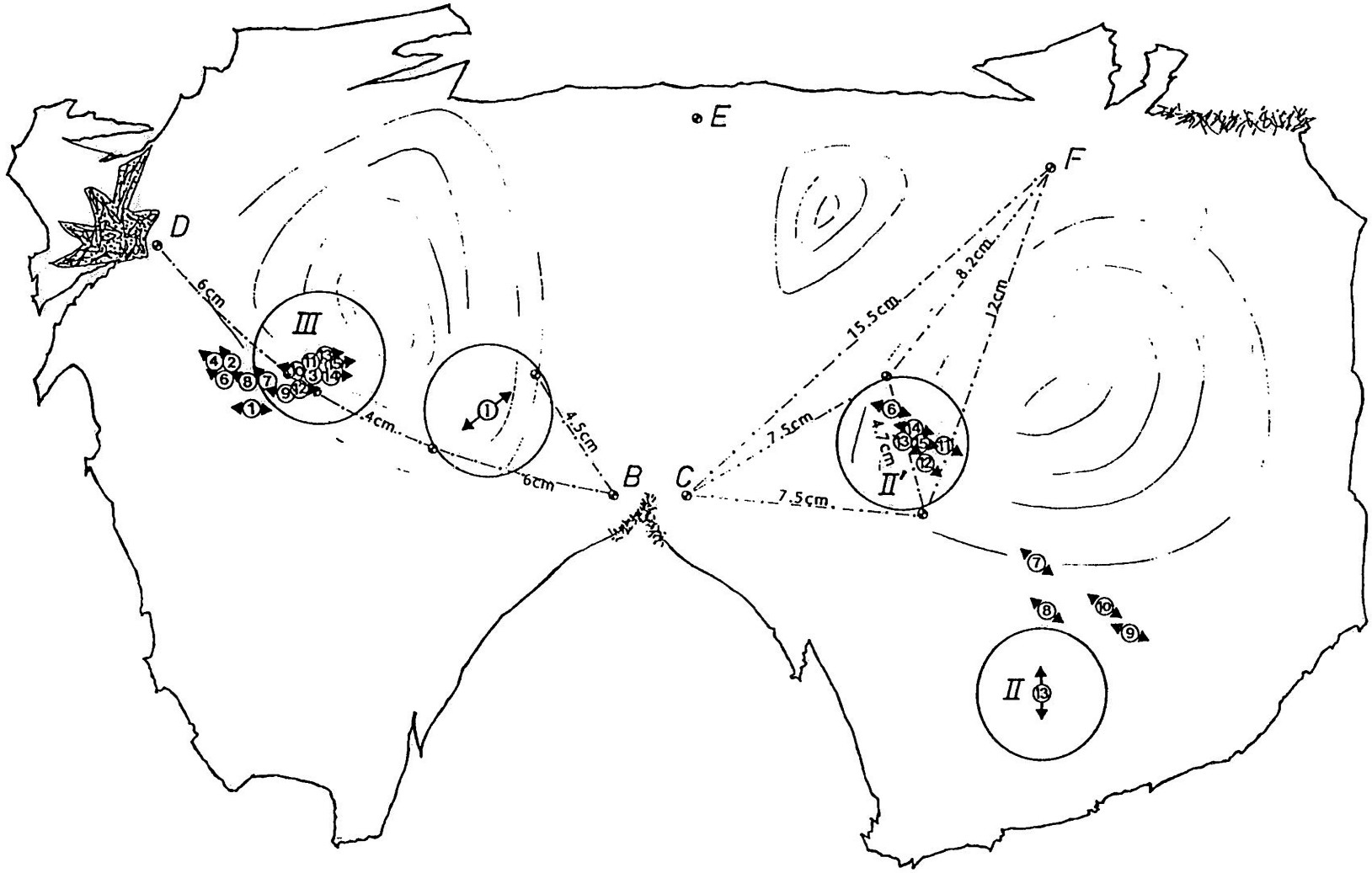

Figure 5.14:pericardial map with the test sites, the locations where samples were prepared for the tests and the directions of the maximum extensibility indicated by the arrows for each sample.

eight times that of the radial ones. The similarity which appears to exist here between the natural valve tissue and one of the candidates for replacement is encouraging.

For where the material is to be used for construction of valve leaflets it is evident that the alignment between the proper direction and the field of loads is of extreme importance for the survival of the valve for longer time limits.

The present series of tests also tested the validity of the biaxial inflation test in monitoring and quantifying biaxial deformations. The uniaxial curves were very similar to the biaxial ones when the shifted gauge length was used. The use of the shifted gauge length was based on the idea that the shift of the zero origin draws curves for a material of which the resting dimensions change with the environment and the strain history. It seems likely that the real benefit of the biaxial inflation test was that it depicted the real loading behaviour of the tissue at low stresses, while reflecting the real structural properties of the tissue at higher stresses.

The accuracy of the identification of the material axes of symmetry by the inflation test was examined by the tests included in the next chapter.

5.2 REGIONAL HETEROGENEITY IN BOVINE PERICARDIUM.

5.2.1 Introduction.

The properties of the tissue at site-I have been described in detail. Three additional sites (III, II′, II in figure of the pericardial map of chapter2) which were suitable for producing valve leaflets were also examined in order to investigate site variability in the pericardium.

From the results previously obtained in test site-I it became obvious that within an area large enough to construct at least one leaflet,

Table 5.3:parameter values for area III

AREA III

sample/direction/specimen V:vertical H:horizontal	U.T.S.	Young's modulus	as resulting from shifted gauge length	shifted gauge length ratio at a load 0.001N
	(MPa)	(MPa)	(MPa)	
1V1	13.86	27.77	32.05	1.154
1V2	17.82	25.49	29.03	1.139
1V3	19.80	41.29	46.41	1.124
1H1	19.47	35.49	38.79	1.093
1H2	21.45	42.79	44.67	1.044
1H3	21.45	35.78	38.61	1.079
2V1	7.84	27.70	29.92	1.080
2V2	7.84	24.77	26.36	1.064
2V3	9.07	23.96	25.35	1.058
2H1	12.79	32.79	35.09	1.070
2H2	11.96	38.40	41.24	1.074
2H3	16.50	42.96	45.62	1.062
3V1	7.12	25.07	27.35	1.091
3V2	6.25	22.52	25.52	1.133
3V3	6.95	24.60	26.27	1.068
3H1	15.63	43.08	48.81	1.080
3H2	15.20	34.15	37.97	1.112
3H3	15.20	40.12	44.37	1.106
6V1	4.54	16.89	18.43	1.091
6V2	5.36	19.61	20.87	1.064
6V3	10.31	22.77	24.69	1.090
6H1	16.09	29.56	31.57	1.068
6H2	19.80	36.13	38.98	1.079
6H3	18.98	45.04	48.60	1.079
7V1	3.09	13.27	14.69	1.107
7V2	4.13	11.49	12.71	1.106
7V3	4.13	10.93	12.19	1.115
7H1	11.14	26.54	28.05	1.057
7H2	11.34	25.19	26.45	1.050
7H3	13.82	22.96	24.04	1.047
8V1	1.03	8.06	8.60	1.067
8V2	1.20	7.74	8.08	1.044
8V3	1.37	8.60	8.94	1.040
8H1	17.19	39.16	40.53	1.035
8H2	14.78	29.10	31.22	1.073
8H3	16.50	49.03	52.46	1.070
9V1	7.01	23.54	26.41	1.117
9V2	7.84	33.92	35.68	1.052
9V3	6.60	21.51	22.95	1.067
9H1	18.98	33.52	35.97	1.073
9H2	18.15	31.57	33.62	1.065
9H3	19.80	33.55	35.56	1.060
10V1	1.91	9.57	10.41	1.088
10V2	2.56	9.49	10.32	1.087
10V3	2.49	13.76	15.52	1.128
10H1	12.47	21.59	22.97	1.064
10H2	15.40	26.94	28.72	1.066
10H3	11.73	22.16	23.64	1.067
12V1	4.78	23.70	25.83	1.090
12V2	4.78	23.30	26.66	1.144
12V3	7.38	26.29	29.08	1.106
12H1	7.82	20.06	21.93	1.093
12H2	6.51	17.62	19.33	1.097
12H3	9.55	16.61	18.32	1.103
13V1	5.07	17.25	19.06	1.105
13V2	6.98	24.77	27.12	1.095
13H1	9.52	30.63	32.38	1.057
13H2	15.86	36.14	37.80	1.046
14V1	3.90	16.09	17.18	1.046
14V2	3.00	13.98	14.18	1.014
14H1	9.60	37.10	37.84	1.020
14H2	8.40	37.98	38.40	1.011
15V1	2.61	18.63	19.10	1.025
15V2	2.17	16.30	17.15	1.052
15H1	16.50	69.58	71.53	1.028
15H2	18.24	65.19	69.04	1.059

significant directional differences exist which may be very important and probably should be taken into account in the following fixation procedure. Thus differences due to direction within each of the three new test sites were investigated and for such an examination the biaxial inflation tests were preceding the simple tension uniaxial tests.

5.2.2 Properties of test sites-III,II′,II.

AreasI and III were over the right ventricle, while areasII′ and II were over the left ventricle. From these areas the samples were taken at the places indicated in fig.5.14. AreaIII was near test site-I and was chosen because of its thickness value which made it suitable for the construction of leaflets. AreaII′ had a resemblance to areaI because it was lying at the belly of the left ventricle and very close to the sternopericardial ligaments, thus it resembled test site-I which was similarly sited and shaped on the right ventricle. AreaII was lying next to test site-II′ and overlying the left ventricle as well. It presented an almost uniform thickness over a substantial area.

The results obtained at the three sites are displayed as plots of the low stress stabilized loading behaviour and tables of the parameters of the complete loading curves to failure.

5.2.2.1 Methodology of Examination. In all the areas the standard method was to apply the biaxial inflation tests on appropriately prepared specimens and i)identify the axes of material symmetry, ii)quantify the biaxial deformations if directions were consistent, followed by uniaxial tests on the same samples that had been inflated along the 2 directions.

In all the new areas the qualitative biaxial inflation test indicated the presence of anisotropy in the mechanical behaviour with

Table 5.4:parameter values for area II´

AREA II´

sample/direction/specimen V:vertical H:horizontal	U.T.S.	Young´s modulus	as resulting from shifted gauge length	shifted gauge length ratio at a load 0.001N
	(MPa)	(MPa)	(MPa)	
12V1	3.71	9.11	10.11	1.110
12V2	4.54	14.08	15.36	1.091
12V3	4.55	11.91	13.09	1.099
12H1	7.01	20.98	22.28	1.062
12H2	8.66	16.80	18.41	1.096
12H3	8.25	15.86	16.86	1.063
13V1	4.54	20.13	21.48	1.067
13H1	13.20	41.65	45.65	1.096
14V1	8.25	38.14	32.21	1.028
14V2	9.99	36.51	37.49	1.027
14H1	14.76	59.40	59.46	1.001
14H2	17.33	63.28	63.28	1.000
15V1	3.66	17.89	18.34	1.025
15V2	3.60	16.89	18.25	1.020
15H1	12.83	60.22	63.29	1.051
15H2	10.54	41.58	41.62	1.001

Table 5.5:parameter values for area II

AREA II

sample/direction/specimen V:vertical H:horizontal	U.T.S.	Young´s modulus	as resulting from shifted gauge length	shifted gauge length ratio at a load 0.001N
	(MPa)	(MPa)	(MPa)	
7V1	3.95	18.27	19.99	1.094
7V2	2.51	12.88	14.09	1.094
7V3	3.59	13.85	15.15	1.094
7H1	10.04	26.93	27.79	1.032
7H2	12.20	26.27	27.64	1.052
7H3	10.76	26.93	27.66	1.027
8V1	6.75	23.98	24.94	1.040
8V2	6.00	18.77	19.88	1.059
8V3	7.12	24.48	24.90	1.017
8H1	10.88	24.01	25.21	1.050
8H2	9.75	28.15	29.90	1.062
8H3	9.75	27.21	29.36	1.079
9V1	3.12	17.54	19.26	1.098
9V2	3.57	18.75	21.00	1.120
9V3	5.80	26.04	27.81	1.068
9H1	7.31	25.36	28.43	1.121
9H2	9.81	20.26	21.88	1.080
9H3	12.49	24.27	25.60	1.055
10V1	6.60	19.37	19.74	1.019
10V2	5.87	20.92	21.69	1.037
10H1	10.27	20.64	21.14	1.024
10H2	9.16	18.35	19.87	1.083
10H3	8.07	25.33	28.39	1.121
13V1	3.39	19.79	20.52	1.037
13V2	3.39	19.12	19.75	1.033
13H1	17.42	55.06	56.55	1.027
13H2	19.25	52.76	55.50	1.052

the axes of symmetry being at right angles. The axes of anisotropy were considerably less consistent between sacs than at site-I. The new angular envelope which included each of the axes was 30^{o} to 40^{o} degrees wide. The most extensible direction for all areas formed a smaller angle to the circumference than to the base-apex direction and the strips were classified as 'Vertical' or 'Horizontal', with the latter being the more extensible in all cases.

Because of the absence of directional consistency quantitative biaxial deformation tests were abandoned and inflation was used only for identification of the normal directions as in section5.1.

The resulting most extensible directions are indicated by the arrows in fig.5.14. Samples P1 to P15 originated from areaIII, samples P12 to P15 from areaII' and samples P7-P10,P13 from areaII.

5.2.2.2 On the Parameter Values. The parameter values are tabulated in tables5.3,5.4,5.5 for all the areas.
The values of each parameter obtained in the horizontal and vertical directions were compared using Student's t-test and their descriptive statistics are included in table5.6.

Site III:comparisons between strengths, moduli and in the shift that existed in the first load point (always at 0.001N) in the preconditioned cycle of vertical-horizontal indicated that they were significantly different ($p<0.001$, Student t-test).

Site II':differences between parameters of the two groups vertical-horizontal were statistically significant for the U.T.S ($p=0.01$, t-test), significant for the moduli ($p=0.038$, t-test) and insignificant for the shift in the first load point(level of significance $p=0.055>0.05$).

Site II:for this area the statistics yielded a significant difference for the U.T.S ($p=0.01$, t-test), for the elastic moduli

Table 5.6:descriptive statistics for the parameter values.

	Test Site III			Test Site II´			Test Site II		
Parameters	Mean	St.Deviation	St.Error Mean	Mean	St.Deviation	St.Error Mean	Mean	St.Deviation	St.Error Mean
Vertical strips									
U.T.S. (MPa)	6.09	4.36	0.76	5.35	2.41	0.85	4.74	1.63	0.45
E unshifted (MPa)	19.84	7.83	1.36	20.71	10.86	3.84	19.52	3.79	1.05
E shifted (MPa)	21.64	8.76	1.52	21.67	10.88	3.85	20.67	3.73	1.03
shift in the gauge length	1.087	0.035	0.006	1.058	0.038	0.013	1.062	0.034	0.009
Horizontal strips									
U.T.S. (MPa)	14.78	4.07	0.71	11.57	3.56	1.26	11.23	3.33	0.89
E unshifted (MPa)	34.80	11.67	2.03	39.97	20.05	7.09	28.68	11.08	2.96
E shifted (MPa)	37.09	12.19	2.12	41.36	19.99	7.07	30.35	11.31	3.02
shift in the gauge length	1.068	0.026	0.005	1.046	0.041	0.015	1.062	0.031	0.008

Table 5.7:statistics on the extension ratios for all areas.

	Site III	Site II´	Site II
Load level (N)	significance level	significance level	significance level
0.001	p=0.006	p=0.55 (N.S)	p=0.97 (N.S)
0.050	p=0.140 (N.S)	-	p=0.001
0.100	p=0.029	p=0.48 (N.S)	p=0.001
0.800	p=0.043	p=0.68 (N.S)	p=0.003

(N.S):not significant at p=0.05 (Student´s t-test)

(p=0.011, t-test) and an insignificant difference for the shift in the gauge length.

5.2.2.3 Comparison of Extensibilities. Figures5.15, 5.17 and 5.19 include the response curves of the unshifted gauge length and for vertical strips(top plot), horizontal strips(middle plot) and their mean responses(bottom plot) for test sites-III, II′, II respectively. Figures5.16, 5.18 and 5.20 have been similarly constructed for the response in the same test sites by using the shifted gauge length.

Statistical analysis was performed on the extension ratio values occuring in each direction at specific prescribed loads and the significance levels of Student′s t-tests at which the comparisons would yield a statistically significant difference are shown in table5.7. The statistics was performed on the unshifted curves for all areas.

Site III:the difference in extension ratios was insignificant at a mid-low region corresponding to a load of 0.05N and this was probably due to the crossing of the curves which coincided with the elongated incubation region of the horizontal curves if compared to the smoothly rising vertical curves. For this site-III (fig.5.15) the statistical examination of the extension ratios for the curves of the shifted gauge length yields a significant difference for all load levels above 0.05N.

Site II′:the difference in extensibility between the two directions was insignificant at all load levels. The levels at which significance is attained reflect the shape of the curves which come closer together at the peak load and at the origin.

Site II:the unshifted curves were statistically different in the two directions for all load levels above 0.05N. The increase in the level of significance at the peak load reflects the shape of the

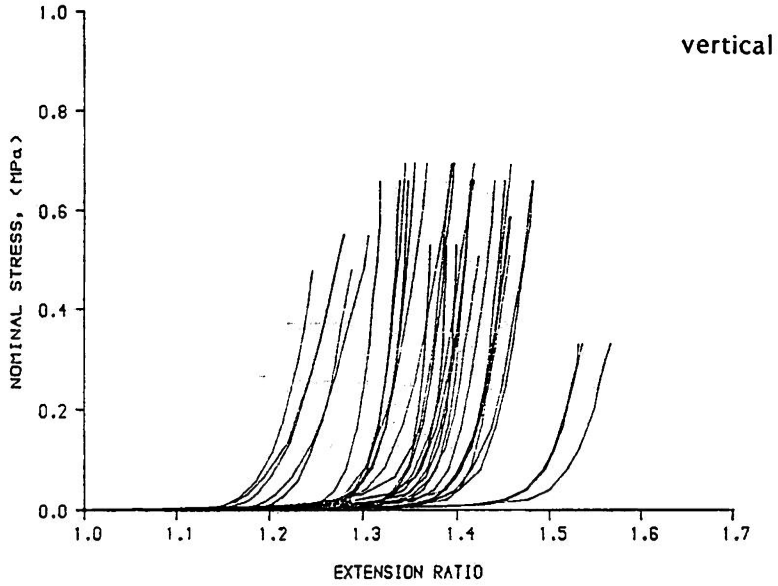

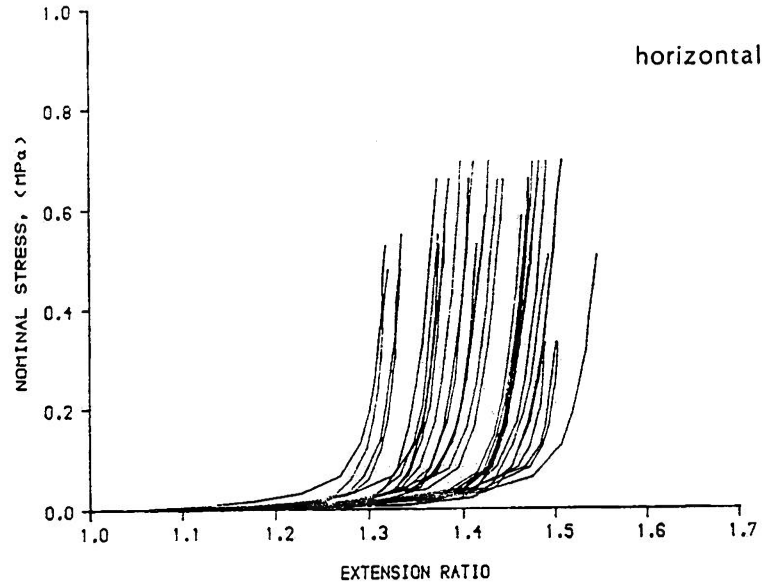

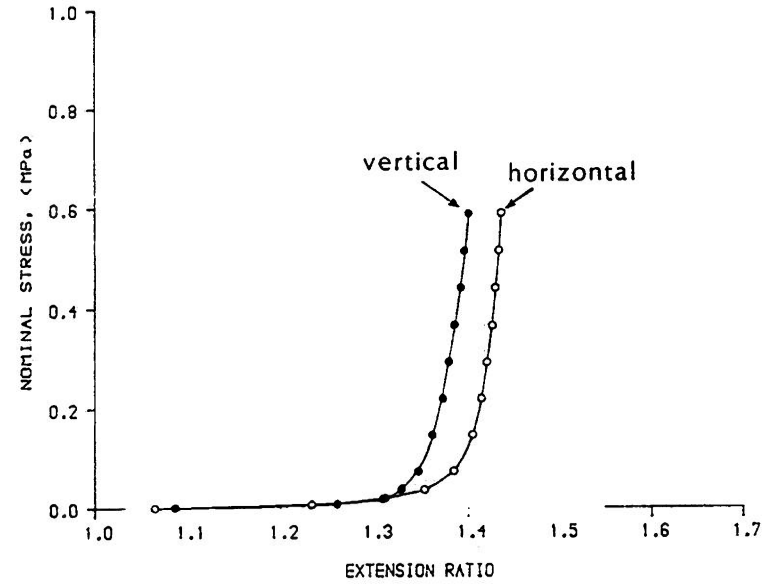

Figure 5.15:stress/stretch behaviour test site-III (unshifted gauge length)

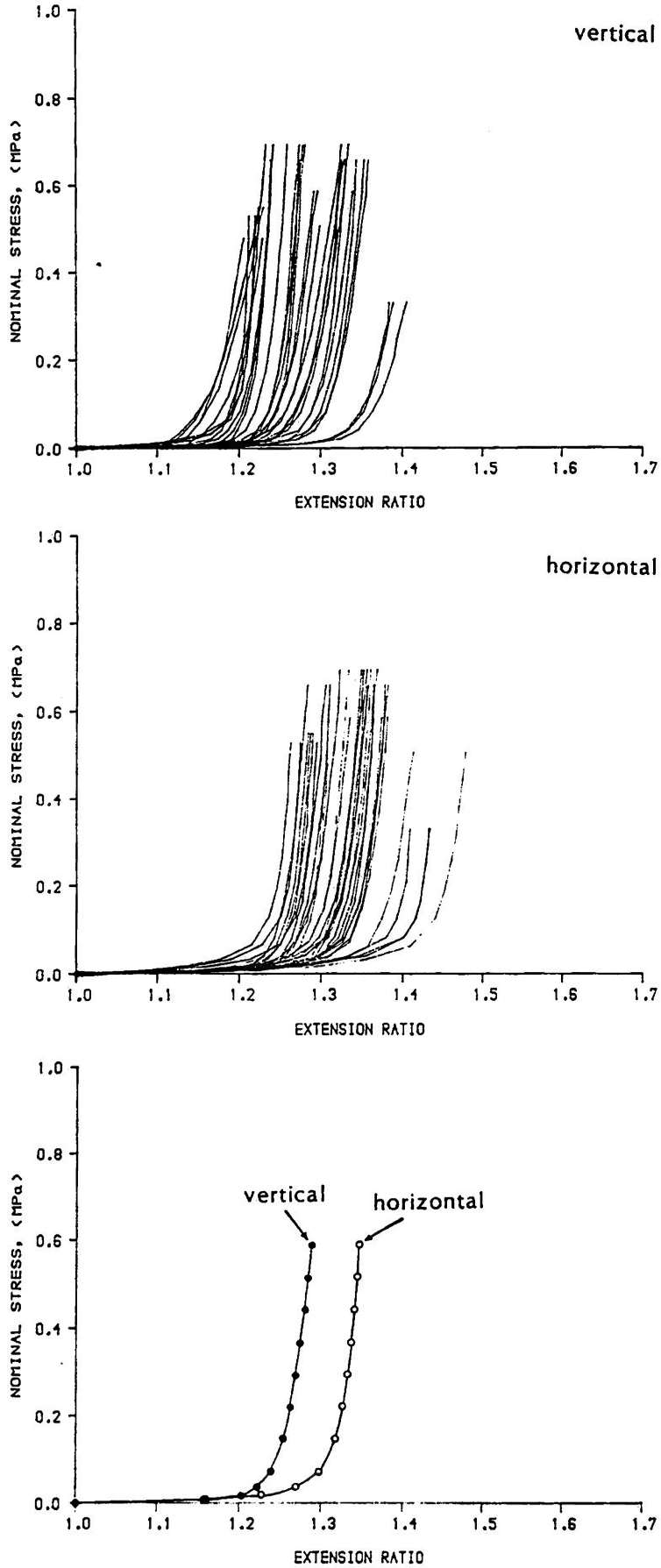

Figure 5.16:stress/stretch behaviour test site-III (shifted gauge length)

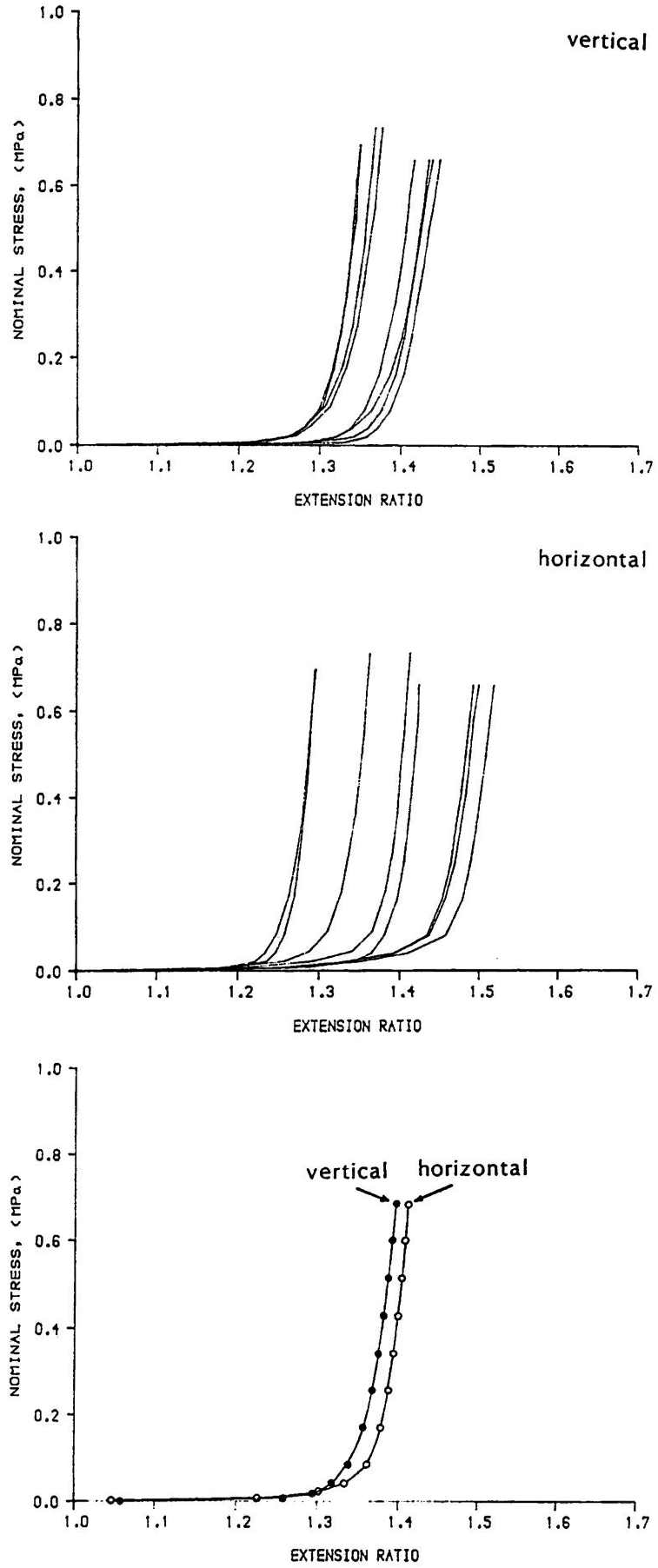

Figure 5.17:stress/stretch behaviour test site-II´ (unshifted gauge length)

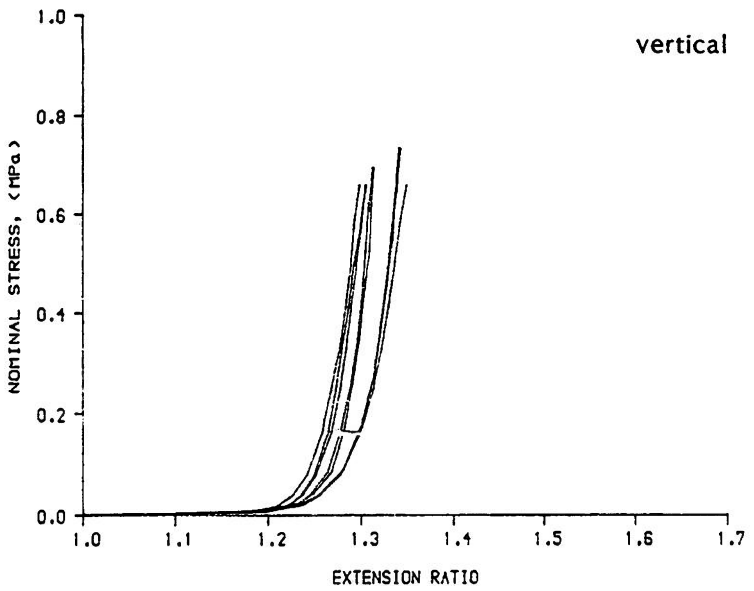

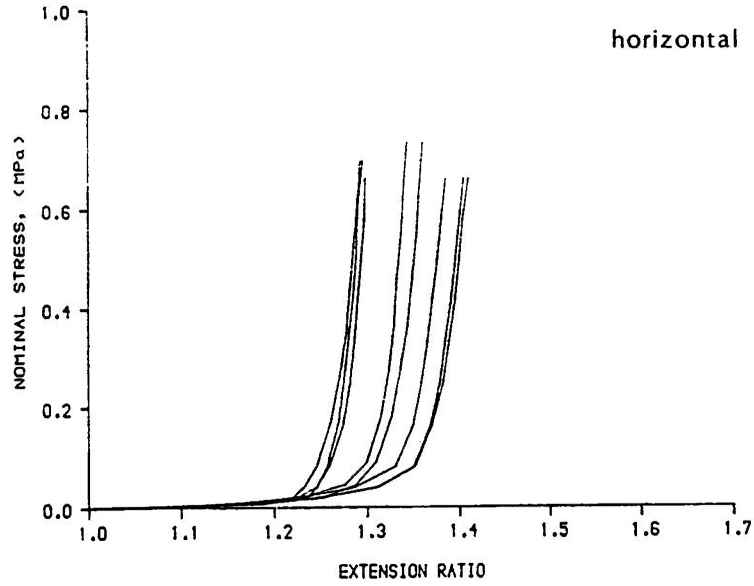

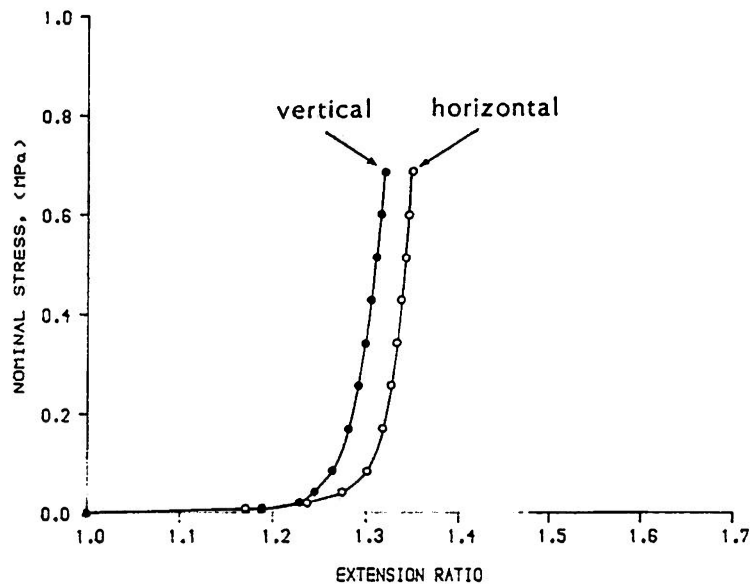

Figure 5.18:stress/stretch behaviour test site-II' (shifted gauge length)

curves which approach each other at peak load and the origin.

5.2.2.4 Qualitative view of the behaviour. Similarly to the examination of uniaxial curves of test site-I the use of the shifted gauge length had a beneficial effect in stressing anisotropy (in the extension ratios). For the present test sites the separation of the envelopes enclosing the test results increased when the shifted gauge length was used.

Redefinition of the gauge length had its influence also on the width of the envelopes which became narrower by using the shifted gauge length and to the curves which appeared more consistent within each of the shifted envelopes.

The curves within each group have the typical shapes that have been observed earlier in test site-I. Thus the prolonged incubation period of the horizontal curves and their transition to stiffer moduli at the peak load brought the curves closer together at peak load. A similar effect occured near the origin and it was reflected in the levels of significance for statistics on the extensions.

In the plots the curves end-up at various nominal stress levels because as it has been said earlier this is due to their varying initial thickness values. The cycles were performed between a peak load or maximum stress resultant point and the original gauge length. Only strips of one sample(membrane) had thickness substantially higher than the rest of the population(test site-III); the fact that the curves of this samples finished at larger extensibilities in both envelopes may not be just coincidental.

5.2.3 Variation Due to Sac, Area and Direction.

The data presented in this section can be analysed in a more general way. An analysis of variance was carried out to investigate the influence of the individual sac, the site, and the specimen

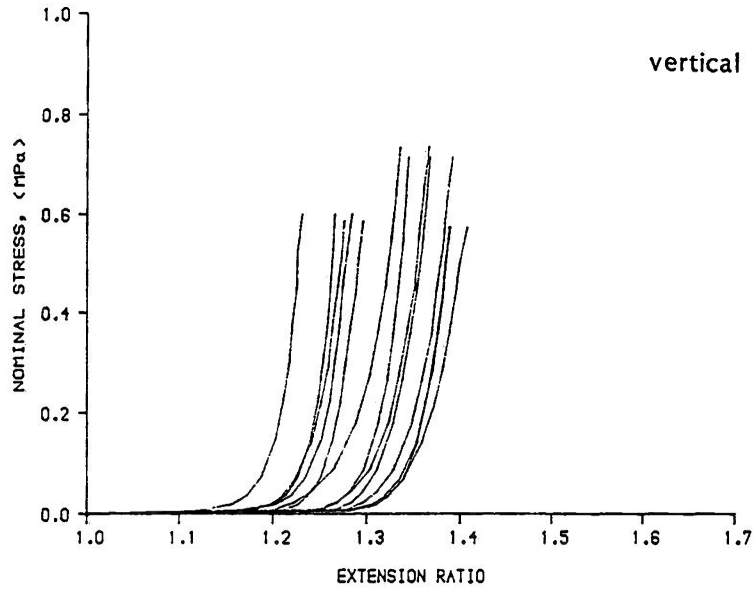

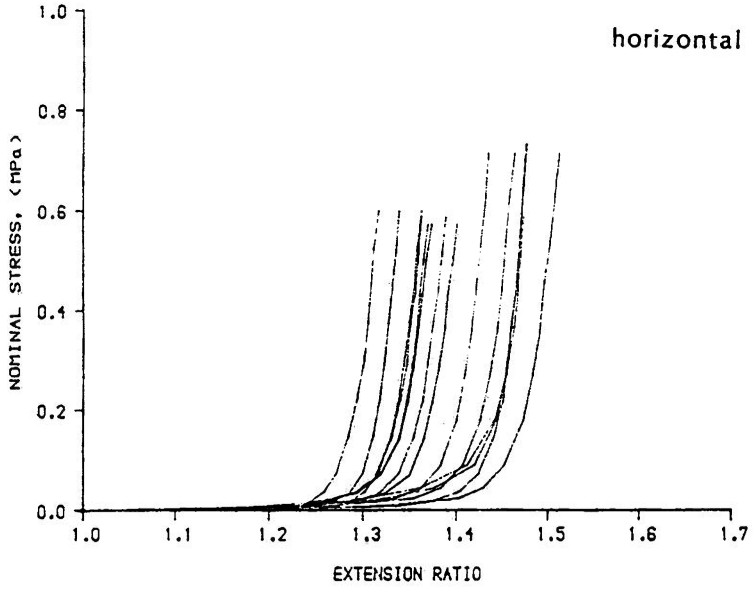

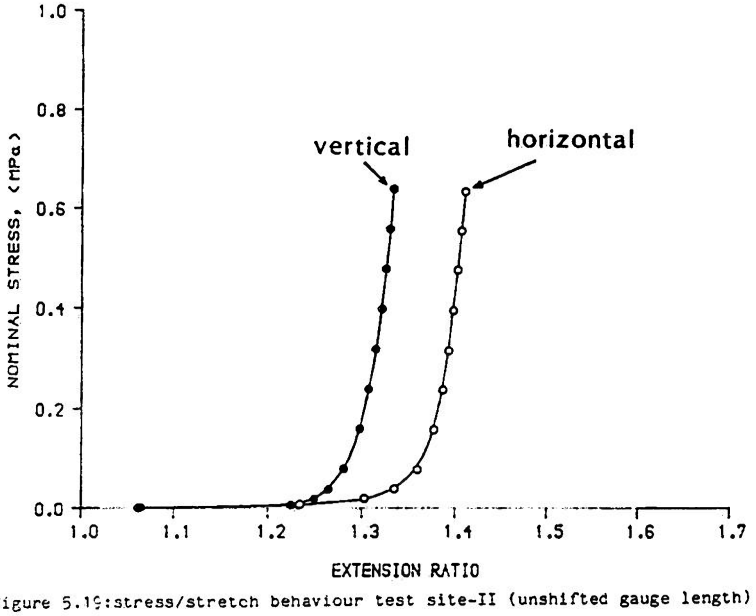

Figure 5.19:stress/stretch behaviour test site-II (unshifted gauge length)

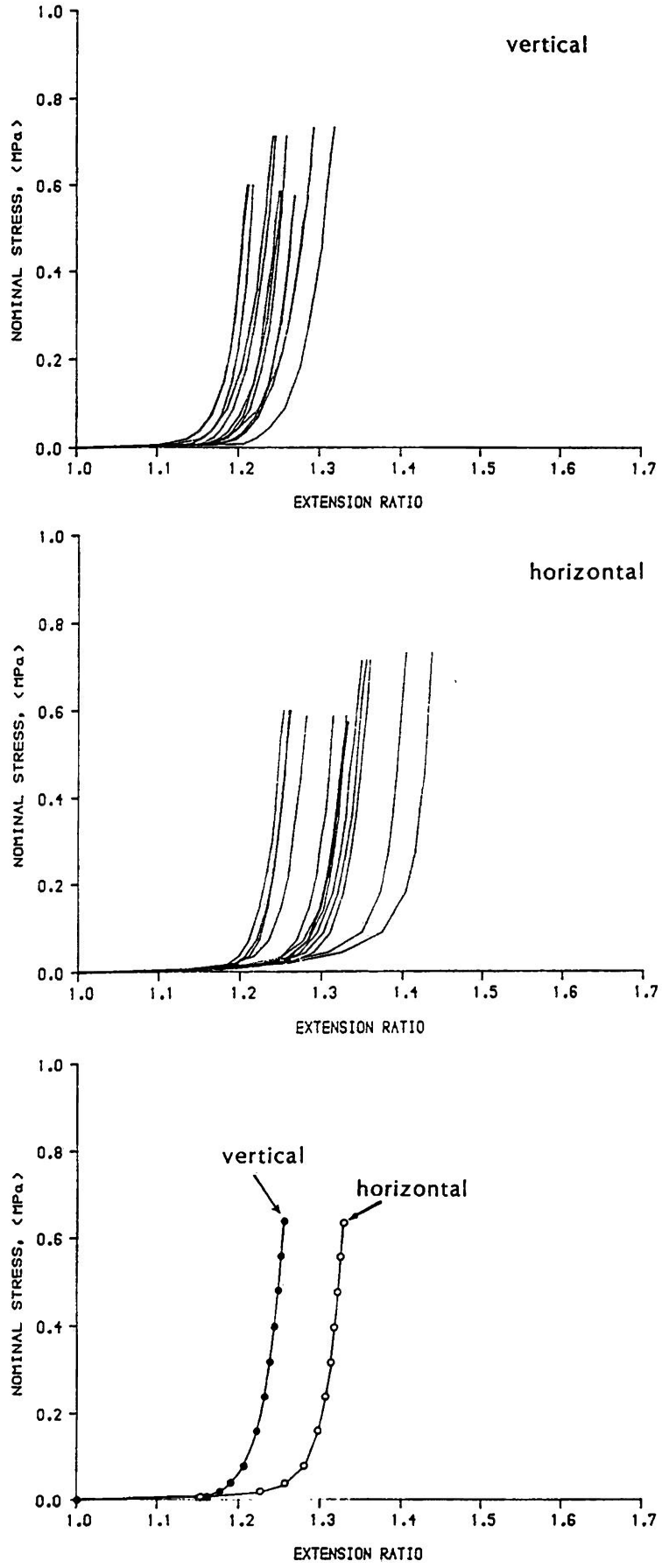

Figure 5.20:stress/stretch behaviour test site-II (shifted gauge length)

orientation on the extension ratios at the peak load point.

The 'subjects' were the measurements of the peak load extension ratio values. The number of 3 strips per direction allowed a "within group" analysis to be followed with the strips missing recorded as missing data points. The SPSS-X statistical package for social sciences was used on a main frame computer which could take care for loss of data in the analysis of variance. The factors have set to be the Area, the Direction and the Sample(sac from which specimens originated).

The results did not represent a completely balanced statistical design because preparation of samples from areas II' and II was not possible simultaneously. Thus the 3WAY ANOVA was made on pairs of sites III-II' and III-II and is presented in tables5.8 and 5.9 respectively. The results of the ANOVA can be confirmed by looking in fig.5.21 which includes the mean behaviour of the three areas with the unshifted curves in fig.5.21a and the shifted ones in fig.5.21b.

The analysis of table5.8 of areas III-II' showed that a significant difference existed between sacs and strip orientation. The influence of the area(test site) was insignificant.
Thus it was concluded that in choosing samples from areas III and II' i)attention should be taken for the direction and ii)samples should be picked-up from one and only sac.

The 2WAY interaction of area to direction was statistically significant ($p<0.01$) and this is indicating that there was a different degree of anisotropy at these two areas, something that can be seen in fig.5.21.

The other 2-WAY interactions were almost insignificant($p<0.05$). This meant that the mean for sacs was nearly indepedent on the means of either area or the direction. Thus whenever the choice is restricted

Table 5.8: AREAS:III-II´

3WAY-ANOVA for specimens from sacs P12, P13, P14, P15.

AREA(1,2) DIRECTION(1,2) SAMPLE(1,4)

Source of variation	sum of squares	DF	MSQ	F	Sign. of F
main effects	0.147	5	0.029	64.148	0.000
area	0.000	1	0.000	.020	0.890
direct	0.012	1	0.012	26.638	0.000
sample	0.134	3	0.045	97.688	0.000
2WAY interactions	0.015	7	0.002	4.682	0.004
area direct	0.004	1	0.004	8.491	0.009
area sample	0.005	3	0.002	3.742	0.030
direct sample	0.006	3	0.002	4.240	0.020
3WAY interactions	0.006	3	0.002	4.211	0.020
area direct sample	0.006	3	0.002	4.211	0.020
explained	0.168	15	0.011	24.410	0.000
residual	0.008	18	0.000		
total	0.176	33	0.005		

48 cases present
18 cases missing(29.2%)

Table 5.9: AREAS:III-II

3WAY-ANOVA for specimens from sacs P7, P8, P9, P10, P13.

AREA(1,2) DIRECTION(1,2) SAMPLE(1,5)

Source of variation	sum of squares	DF	MSQ	F	Sign. of F
main effects	0.251	6	0.042	56.303	0.000
area	0.066	1	0.066	88.170	0.000
direct	0.034	1	0.034	45.184	0.000
sample	0.154	4	0.039	51.857	0.000
2WAY interactions	0.063	9	0.007	9.390	0.000
area direct	0.010	1	0.010	13.945	0.001
area sample	0.025	4	0.006	8.489	0.000
direct sample	0.028	4	0.007	9.396	0.000
3WAY interactions	0.005	4	0.001	1.741	0.163
area direct sample	0.005	4	0.001	1.741	0.163
explained	0.319	19	0.017	22.594	0.000
residual	0.026	35	0.001		
total	0.345	54	0.006		

60 cases processed
5 cases missing(8.3%)

to control of area-sample or direction-sample with the third factor able to vary, then this produces a statistically insignificant result.

The 3WAY interaction was nearly insignificant(at p=0.01 but significant at p=0.05) showing that the outcome of the third factor could be nearly predicted by proper control of the other two.

The analysis result of table5.9 on areas III-II showed that there was a significant variation($p<0.01$) due to the area(test site) the direction and the sac which could not be explained by the overall variation of the subjects(specimens). This meant that all 3 factors(area, direction and sample) could influence the outcome in a selection of pericardial samples by using these two areas.
In this particular ANOVA the area factor was significant, something that did not happen between areas III and II′. This can be seen in fig.5.21 where the overall extensibility of curves from areaII is smaller than areaIII in each of the directions and in general.

All 2WAY interactions were significant and this is a result of all of the factors individually being able to affect the behaviour.

The 3WAY interaction was insignificant thus the means of the any factor were independent on both means of the other two. It was evident that the increased anisotropy in both those areas, the more extensible areaIII(in each direction and in general) and the always existing sac to sac variation meant that selection from those areas (with a choice being on all three factors) is more difficult than previously(areasIII, II′).

5.2.4 Variations due to Height within an Area.

Despite the results of the analysis of variance, it is still unclear if the directional variation is more important than the sample site and how uniformly the anisotropy is distributed.
Picha(1984) carried out a series of uniaxial tests on bovine

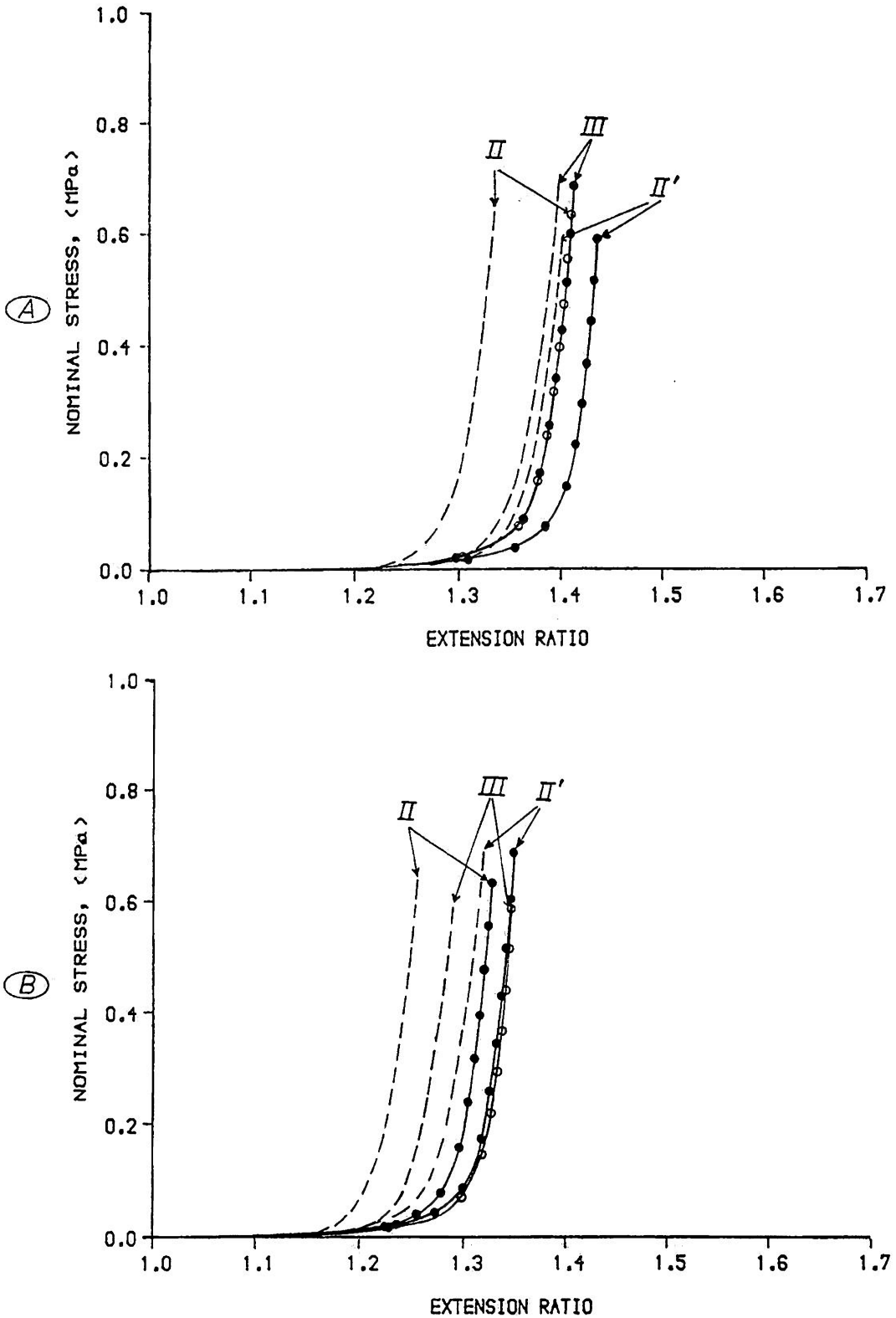

Figure 5.21:average loading behaviour by using the unshifted gauge length (A) and by using the shifted gauge length (B).

pericardium by keeping the direction of the strips constant but varying the height in a base to apex direction. The results were given as plots of the U.T.S versus the distance of travel from base to apex. They showed that a significant variation in the U.T.S. existed, with the values varying smoothly and covering the whole range of the values presented in table5.1 from our tests.

A similar idea was investigated in the present situation with strips located at varying distances from the sternopericardial ligaments lying very close to the apex of the heart, and towards the inferior vena cava, thus along the reference line of our standard map. The direction was kept absolutely constant along the strongest of the material symmetry axes (roughly circumferential). The strips came from two membranes sacrificed for the purpose of this test and with the thicknesses measured along the reference line at the site of each strip (and not averaged over a larger area like previously) in order to perform a strict normalization of the stresses. Fig.5.22b shows ultimate loads sustained by the strips and fig.5.22a the nominal stress values obtained by normalisation with respect to the initial thickness value. For membrane1 (dark circles/squares) the thickness fell almost linearly from the ligaments in the range 0.38mm to 0.33mm. For membrane2 (open circles/squares) thickness similarly fell from 0.42mm to 0.37mm. It is evident in the figure that normalization had brought the two curves close together in fig.5.22a. The values were never far away from the population of U.T.S. values for the tough circumferential strips and definitely distinctly different from the envelope of the axial U.T.S. values of our earlier tests. The lowest value of the plot should be probably rejected and must have been produced as a result of a 'traumatic' mishandling of the particular strip in the preparation.

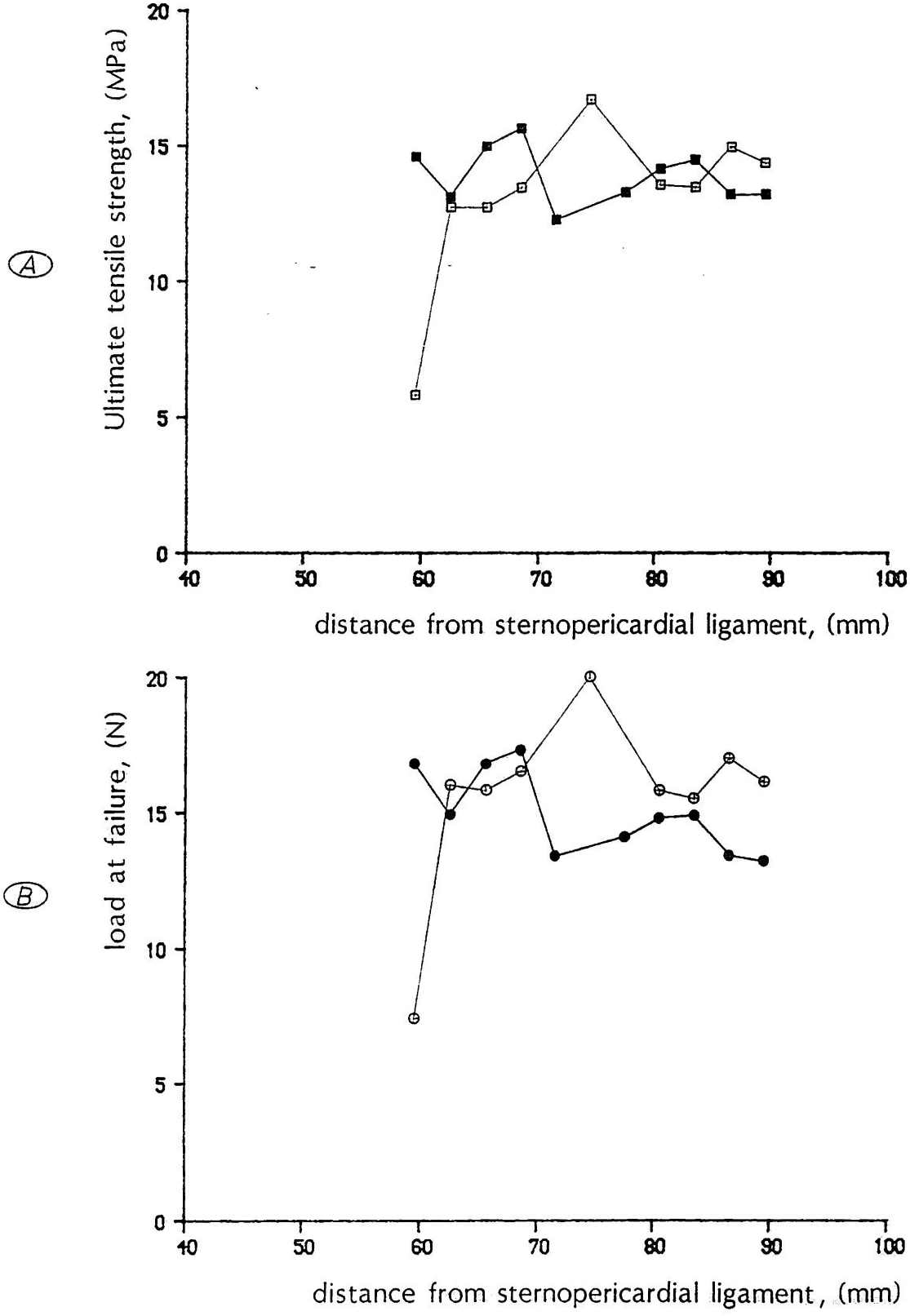

Figure 5.22: Ⓐ behaviour of the ultimate tensile strength as the location of the samples travels away from the sternopericardial ligaments; Ⓑ the behaviour of the ultimate loads. Specimens originated from two different membranes indicated by the dark and open symbols.

On the previous evidence we can conclude that, for a particular area, the direction is the most important factor of variation of the material strength and that anisotropy is consistent over an area larger even than the one needed for the construction of a single valve leaflet. This also increases the possibility of producing a greater number of leaflets from a single sac.

The present results are not necessarily in conflict with Picha(1984): i)he lacked the identification of at least one mechanical direction which was performed here with the biaxial test, ii)he travelled along the base/apex direction thus along a different reference line, iii)he covered the whole length of the sac and thus sites of different material properties.

5.2.5 Summarized Regional Response.

The analysis of variance of mechanical behaviour of fresh bovine pericardium specimens from different sites, directions and sacs showed that any of these factors can influence the possible outcome of an investigation.

It was found that sac to sac variations were significant. In addition sites can be found that behave similarly (like the present III-II′) and sites with unlike behaviour (like III-II).

Production of 3 leaflets from a single sac is possible. For the production of a leaflet it was required that i)areas of uniform properties to be identified, ii)preferably anisotropic, iii)properties should not vary greatly between different areas.

The multifactorial analysis of variance of the present section led to the following recommendations:i)alignment of the leaflet axis to be along the axes of elastic symmetry of the tissue, ii)a couple of leaflets to be made from one and the same sac from areas III-II′, and a third leaflet to be constructed from the same sac and having a

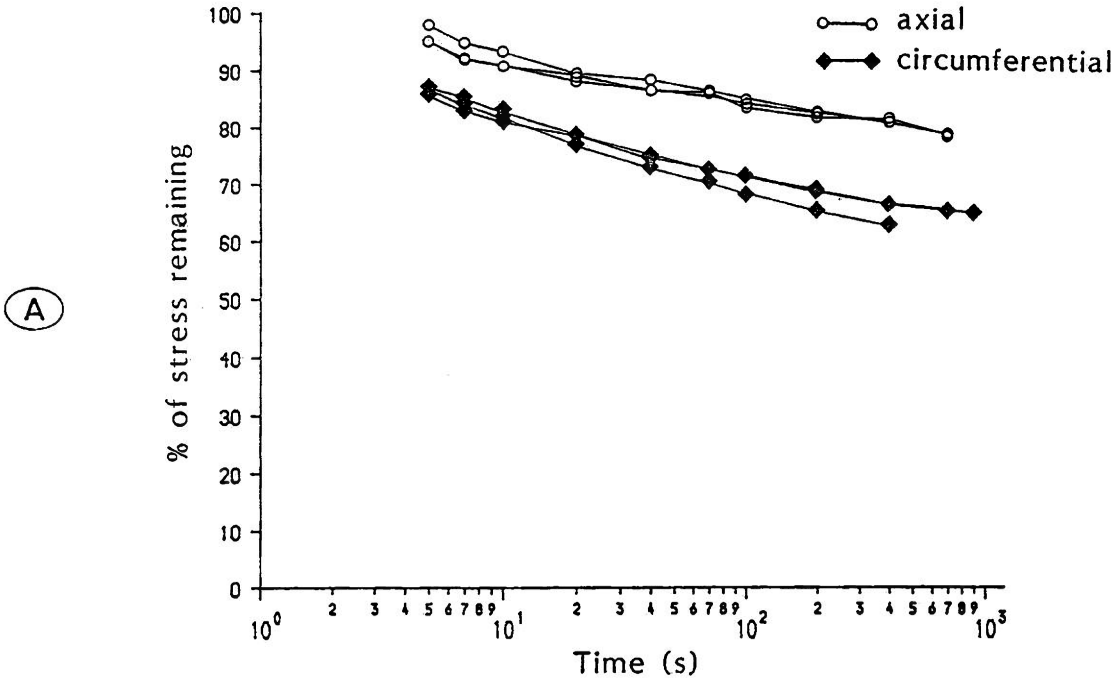

A

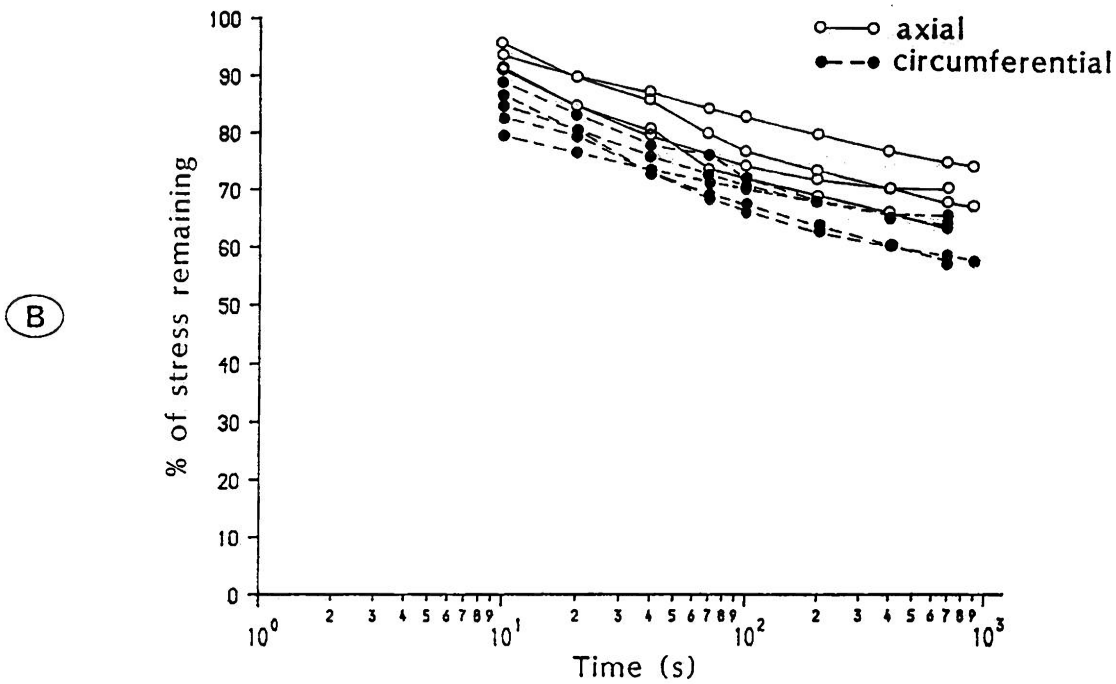

B

Figure 5.23:stress relaxation in bovine pericardium strips; (A)all strips from site-I of 1 membrane, (B)orthogonal strips from site-I from 5 different membranes.

matching thickness, or iii)three leaflets to be constructed all from a single sac with the specific tensile behaviour of the leaflet properties being appropriately modified possibly during the fixation period. The possible effects of fixation will be examined and further suggestions will follow in a later chapter.

5.3 TIME DEPENDENT BEHAVIOUR OF THE TISSUE.

In the previous uniaxial tension tests only the stabilised (preconditioned) response of the pericardial tissue was considered and the influence on this response that sac, area and direction may have. The tissue, however, has time-dependent properties which may be also directionally dependent.

Strips from natural porcine valve leaflets have been found to stress-relax significantly more in the circumferential than in the radial direction by Lee et al(1984a). The workers suggested that the behaviour in the 'along the fibres' direction is predominantly directed by the viscoelastic properties of the collagen fibres themselves that the groung substance. Viscoelastic properties have been attributed to the collagen fibres by Sanjeevi et al(1982). It is though still unclear why the behaviour of the less viscous fibre to dominate on the much more viscous ground substance which fills the innerspace between the fibres.

5.3.1 Tests.

Two types of tests were carried out. In the first a single sac was used and a single area (test site-I). Two sets of strips were prepared in orthogonal directions along the principal axes of anisotropy identified by the standard techniques introduced in earlier sections.

The strips were stretched at 20mm/min, and the stretch held constant at various load levels which were corresponding to different

extension ratios for each strip. Due to the variability in the properties of the strips between the two orthogonal directions, this method produced slightly different starting values for initial loads in the two directions and also between strips of one direction. Circumferential strips started from a higher initial load, but relaxed more. This can be easily appreciated in fig.5.23a where in a standard mode for this sort of data the percentage of remaining nominal stress has been plotted against a logarithmic time scale. The stress values and the calculated percentages have been estimated at certain time instants after the strips had achieved their starting load (5, 7, 10, 20, 40, 70, 100, 200, 400, 900s). The strips had been stretched to the peak starting load within 2-3s. The curves look reasonably linear for the range of relaxation time employed in these tests(maximum of 1000s). Within each group of curves obtained in the circumferential and axial direction the behaviour is very similar and consistent. The axial specimens relax significantly more slowly and appear to start from lower initial loads. Thus the possibility of dependence on the initial load should not be ruled out. If such dependence of the relaxation behaviour on the initial load is present the tissue has non-linear viscoelastic behaviour.

The slopes of the axial and circumferential curves have been checked by Student's t-tests on the slope values given by separate regression lines on each of the curves. Axial curves had slopes significantly different to the equivalent ones of the circumferential curves at a level of p=0.072, this means that with the standard level used (p=0.05) the difference was not statistically significant. Thus despite the fact that a visual inspection of the curves shows an increased stress relaxation circumferentially this was not statistically (although marginally) significant result. It can only

be refered as an interesting similarity to the highly anisotropic time dependent behaviour of the valve tissue reported by Lee et al(1984a).

The second series of tests had a slightly different regime. In this case 5 pericardial sacs were used to prepare 5 samples from test site-I which were mechanically identified in terms of their principal directions. Since the previous test showed a very consistent behaviour along a particular direction for strips next to one another, on these tests only one strip was prepared at each direction. This resulted in five strips examined in either direction originating from 5 different sacs. The behaviour is shown in fig.5.23b. Again two groups are clearly distinguished with the circumferential strips falling at lower remaining stress values within the same time scale but again having insignificant difference in their slopes. For the purpose of this test the strips had been pulled to a certain load and then the crosshead stopped. This resulted in almost equal initial loads for the strips but represented unequal stretch values. The initial loads were now only slightly higher for the circumferential strips due to the fact that their higher moduli produced a greater overshoot before the trigger froze the action of the machine at a particular load value.

The envelopes resulting in this way were overlapping and were spread up and down due to the biological variability between sacs.

5.3.2 Summarized Behaviour.

Bovine pericardial strips exhibited a significant reduction in the initial nominal stress value in stress relaxation tests with only 70-60%of the initial stress remaining after 1000s of initiating the test. The strips demonstrated a sufficiently linear behaviour in standard plots against a logarithmic time scale indicating that a continuous spectrum approach for the relaxation behaviour of this soft

tissue is applicable. For the features of such a spectrum: the first test showed different slopes of the almost linear curves on the semi-log paper indicating that two types of spectra should be applied for the two directions and of different heights. The difference though was not statistically significant and thus a single height for the box can be selected with different time points for its lower and upper time limits. There was the suggestion that the slope difference exhibited may be a manifestation of the non-linear viscoelastic nature of the tissue as the initial loads for the mostly decaying circumferential strips were higher. In the second test with a much more strict control on the starting loads the curves overlapped and the slopes were very similar, with still the circumferential strips having exhibited a larger relaxation at the same time points.

5.4 DISCUSSION.

A number of sites suitable for constructing bioprosthetic valves have been investigated. The suitability of the sites was judged on thickness considerations primarily looking for uniformity of thickness and of an appropriate value.

It has been mentioned in chapter3 that those workers examining properties of native pericardium of various species immediatelly faced the problem of the area from which to choose their testing samples. As examination became more and more careful, factors like the site, the size of the sac, the direction within specimens from pericardia of one species have been implicated as being responsible for the wide variations in the obtained responses. Trowbridge and Crofts(1986) implicated the position within a sac as being responsible for significant variation of the response chemically treated bovine pericardium samples. Their interpretation of the effects of fixation depends largely on the definition of some parameters and physical

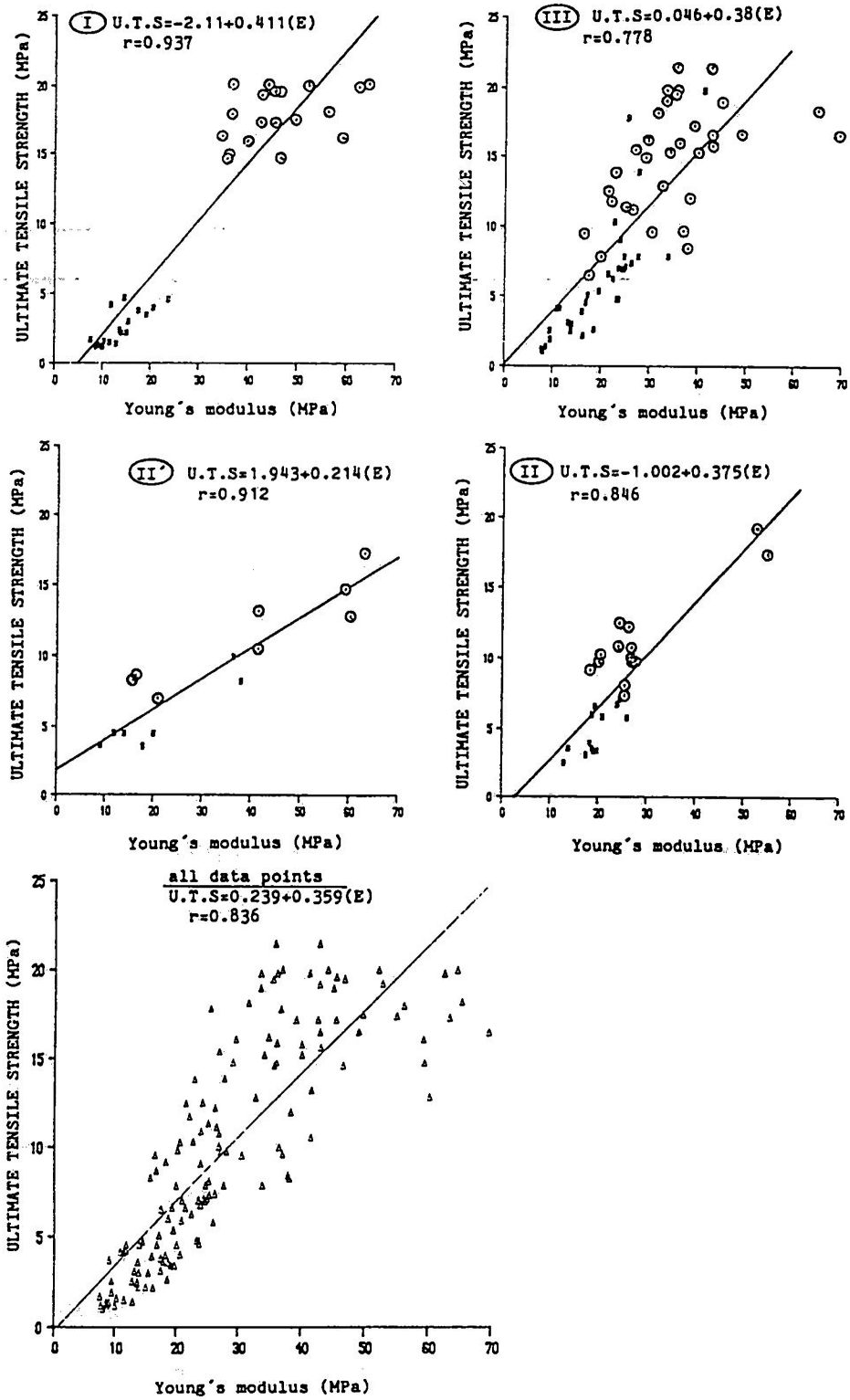

Figure 5.24:plots of the U.T.S. versus the modulus of the linear pre-failure region for all strips examined in the present study. Circles have been used for the stronger direction in each site.

quantities such as the determination of the appropriate gauge length or the amount of prestress that preceeds or accompanies fixation.

Unlike any other worker the mechanical behaviour of the specimens of the present report had been previewed by the biaxial inflation test which had identified the directions of material symmetry at each site. Biaxial inflation could also identify those directions of maximum and minimum extensibility within a site. It was found that those directions are by no means consistent from sac to sac and thus preparing specimens according to a general(and unique) reference system(as did Trowbridge and Crofts,1986a) for the whole membrane the result could be never predictable. Trowbridge and Crofts suggested that with the exception of one of their positions all sacs should behave similarly and for all other positions. These workers may have been misled by the significant variation that it has been shown here to exist within a site. The behaviour depends on direction and it is important during the preparation that the less extensible directions in one site is not compared to the more extensible of another. A single reference system for the whole membrane can not handle this problem which is essentially factor2(direction) in our analysis of variance.

Thus it is probably valid to suggest that at each test site the selection of the specimens from this site should be done on an individual basis by the determination of an individual system of reference directions for this site.

The new element in the characterisation of the properties of the native bovine pericardium tissue as resulted from both tests and methods of chapters4,5 is the mechanical anisotropy and the regional heterogeneity. There is a pictorial way to appreciate both the presence of mechanical anisotropy and the merits of the qualitative

biaxial inflation test. In fig.5.24 plots of the U.T.S values against the tangent modulus of the pre-failure region are presented. The plots can be used to demonstrate overlaping of the distributions of both parameters (projections of points on the axes) with circumferential-horizontal strips exhibiting higher U.T.S and moduli and the axial-vertical strips having statistically significant lower values.

The degree of anisotropy can also be appreciated by the two groups of the squares(axial strips) and circles(circumferential strips). In the very anisotropic test site-I the separation is absolute in the range of both parameters. In the rest of the plots the groups(populations) overlap but still the population of stiffer-tougher strips(circles) is distinct from the population of the weak-soft strips(dark squares).

The correlation of the two parameters have been questioned by previous workers studying pericardia of other species as discussed in chapter3. This may be because isotropy had been assumed in all previous reports and thus variation of either parameter has been thought to be based on random biological variability.

All plots of fig.5.24 show that U.T.S was well correlated with the modulus for all areas. The slope of the regression line in each plot signifies that regional variations probably due to structural reasons exist between sites.

The plot of all data points shows that for fresh pericardium irrespectively of direction, site and sac there is an almost linear relation of U.T.S. to modulus. Pericardium consists of structured layers of collagen fibres which by their arrangement and/or orientation are responsible for the values of both parameters. In order to confirm the structural basis of the behaviour exhibited histological examinations were made of the pericardium and are

presented in chapter7.

The work of this chapter has examined the mechanical properties of strips at the directions of the axes of elastic symmetry. The properties of the pericardium in other directions is unclear, and a multidirectional uniaxial test program is reported in the next chapter.

6.1 INTRODUCTION

The inflation of circular discs of pericardium resulted in the production of non-axisymmetric deformations. Testing the tissue in the directions of the major and minor axes of the non-axisymmetric inflated surface confirmed that the material was anisotropic.

The methodology of inflating circular discs has been validated using rubber sheets rendered orthotropic by stretching. The actual class of elastic symmetry for the pericardium is not revealed by the inflation test. Another limitation was that specimens were initially flat while it is apparent from measurements made on heart cast that the pericardium may be curved. Further tests in more than two directions are required to establish the class of material symmetry and whether the circular inflation tests actually gave the axes of mechanical anisotropy (resulting from structural features) as opposed to a global anisotropy which is both mechanical and geometrical.

In the simple uniaxial tests the most reliable parameters were found to be the U.T.S. and the modulus of the linear prefailure region. These parameters are submitted to a thorough examination in the multidirectional tensile tests of the present chapter. The chapter proceeds with an elastic approach of the material by establishing a typical stress/strain response to load of non-preconditioned strips. The results are analyzed to decide about the anisotropy of the material and to produce a general equation for failure (by using the U.T.S. data) which may be applicable under combined states of stress.

6.2 TEST METHOD

6.2.1 Preparation of Samples.

Five bovine hearts were striped of their fat, the pericardium was excised along the major vessels at the top and brought in the flat

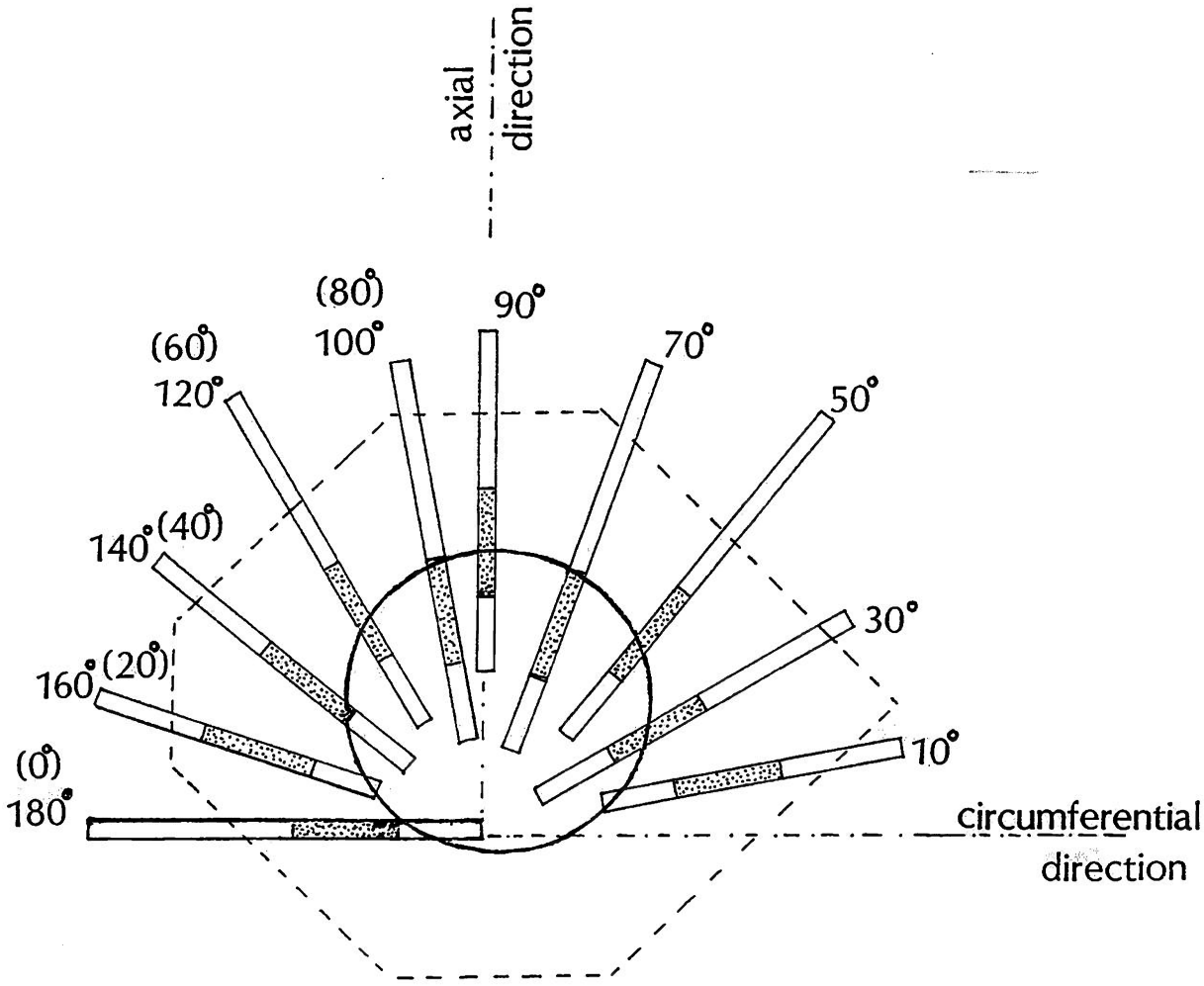

Figure 6.1:preparation of a polygonal sample along the reference axes of the heart(axial/circumferential). The tested strips were laid out at various angles in the 0°-180° range and aligned to the axes of elastic symmetry of the material as identified by the inflation test. The figure shows the case where the alignment between the axes of elastic symmetry and the reference axes would be absolute.

configuration already familiar from the tests in chapters4 and 5. From site-I of each of the 5 pericardial sacs polygonal shaped specimens were prepared and inflated in order to determine the directions of greatest and least extensibility. These directions were subsequently marked on the tissue.

The samples were subsequently transferred to a saline bath and stored at 4°C overnight, allowing them to relax flat for at least 18 hours before the uniaxial tests.

The thickness of the samples was measured with a Mitsutoyo thickness gauge and with the standard procedure described in chapter2, by allowing a 5s time interval before a reading was taken. Within the area of any of the 5 samples a general reduction of the thickness was present from the left (along the reference line) to the right (towards the left ventricular area). A typical thickness range would be between 0.45mm-0.33mm. For each of the samples a mean value of the thickness was calculated to be subsequently used for the reduction of the stress values. For samples noted as P.D.i, i=1,..5 mean thicknesses were P.D.1:0.37mm, P.D.2:0.33mm, P.D.3:0.50mm, P.D.4:0.33mm, P.D.5:0.33mm.

The samples were prepared as in chapter5 but this time an additional thin translucent polyethylene sheet was placed on top of the epipericardial surface which was facing upwards. On this translucent sheet the main directions and dimensions of the strips to be cut had been marked. The strips were prepared using the template in fig.6.1. The two main directions (reference axes) drawn on the polyethylene sheet by the use of the template at 0° and 90° were aligned to the axes of maximum and minimum extensibility(and thus of mechanical anisotropy) as identified with the biaxial inflation test. The directions of these axes were roughly circumferential/axial (with

a 5° uncertainty). Thus the strips examined for each pericardial sample were aligned relative to a set of axes specific to each test specimen according to their own mechanical behaviour as exhibited in inflation.

The template indicated the position of 10 strips around the central inflated area(marked by the circle). In order to reduce the effect of nonuniform thickness and inhomogeneity of the tissue properties the tested strips were brought as close as possible to the central area. The fact that strips had to be aligned at certain angles to each other in order to allow us to explore the directional variations in the tissue properties was responsible for the large area of tissue.

The strips were prepared by cutting through the polyethylene sheet, the tissue and the underlying card, by the use of a pair of blades which were kept apart by an inner gauge at a 3mm distance and thus were able to cut strips 3mm wide and 7cm long. The polyethylene sheet not only helped in cutting the strips but kept them adequately moist till they were mounted for testing. Just before the strips were mounted in the grips the overlying polyethylene strip was removed and the rest (tissue plus strip of card) were placed on the grips.

Our particular interest in the directional variations of the tissue properties led to the preparation of a set of 10 strips from each pericardial sample examined from test site-I. The strips as shown in fig.6.1 were generally 20° apart, and fell into two geometric quadrants 0°-90°(I) and 90°-180°(II). The reason for a 0°-180° lay out of the strips was to allow investigation of the tissue properties in both geometrical quadrants in case that non-uniformity of tissue properties existed between those two quadrants.

The systematic preparation of samples by using the template yields results at 10°, 30°, 50°, 70°, 90° in the first quadrant and at 100°,

120°, 140°, 160°, 180° in the second. It may be able to further randomised the results by using the design of the template on one or the other side. This however was not applied here, in order to keep as few factors as possible unaltered between the test of the various samples, and thus the effects of thickness variations, nonuniformity of properties and directional differences to be easier to discern.

6.2.2 Test Apparatus

The tissue specimens supported by the underlying paper card strip were mounted with a gauge length of 15mm. The same grips, test chamber and equipment as in chapter5 were used. The methodology of gripping the specimens and the liquid environment were also the same as previously.

6.2.3 Protocol

Our measures for stress and strain were Lagrangian in their nature. Strain was expressed as a stretch ratio of the strips which was the separation of the grips at any time instance (t) divided by the initial separation of the grips (gauge length=15mm). It is a reasonable measure because it accounts for both the material properties and the geometry of the tested strip by expressing the overall extension between two specific mounting points. In the form of valve leaflet substitute the tissue is suspended between constant ends at the valve posts.

Stress was expressed in $Pa=N/m^2$ and was calculated as the overall load transmitted by the strip in tension divided by the initial undeformed cross sectional area of the specimen. Area was equal to A_0=width×thickness of the undeformed strip.

The control unit of the machine was set to linearly increase the separation of the grips at a certain rate of 20mm/min which resulted in a nominal strain rate 0.022/s for the specimens. This strain rate

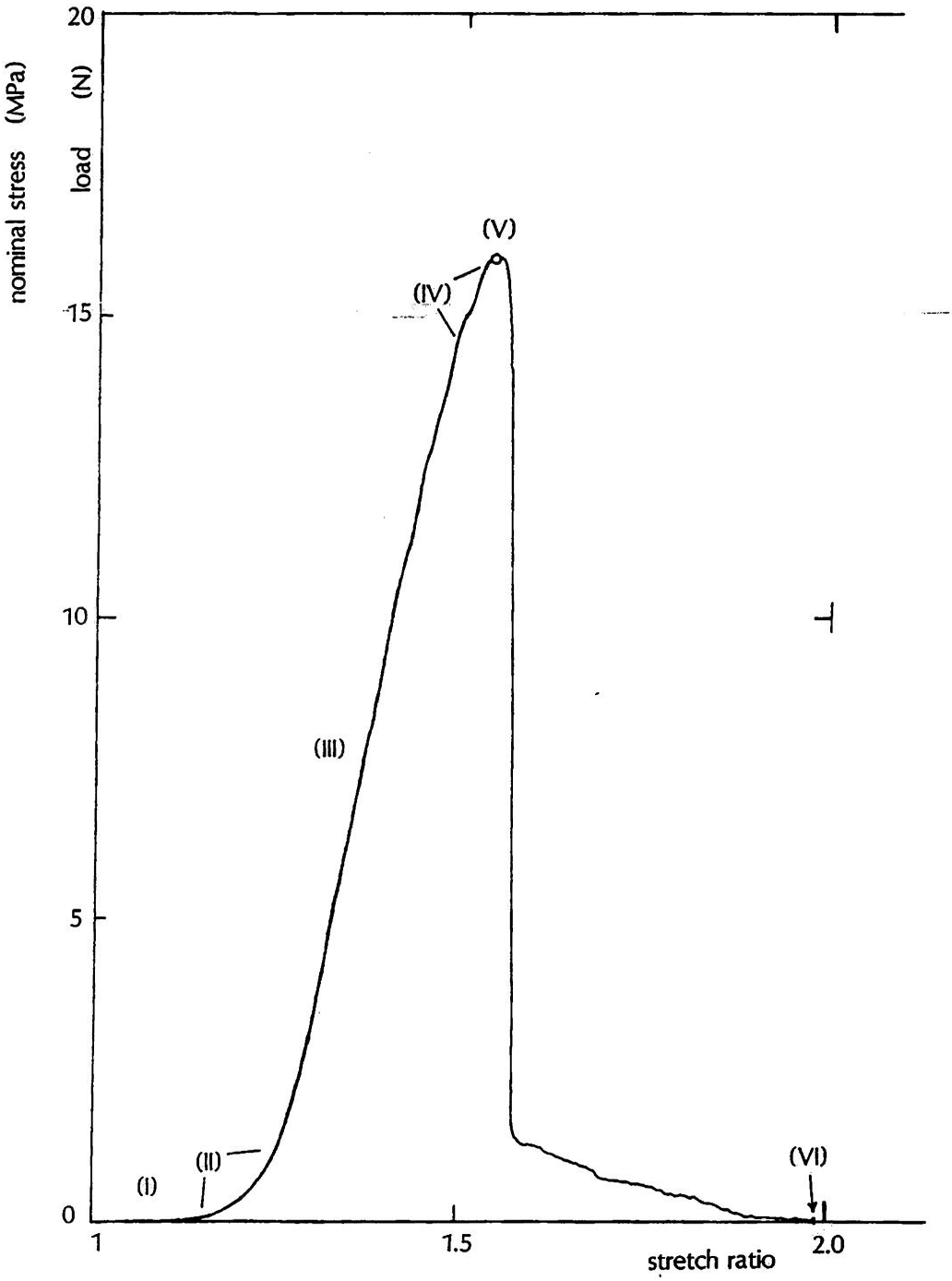

Figure 6.2:a typical stress/stretch 1st pull curve up to the complete failure for a pericardial strip originating from sample P.D.4 and being oriented at 10° to the stronger (nearly circumferential) direction.

is well within the range of strain rates previously used in similar tests.

Recognising the viscoelastic nature of the tissue strips a single pull to failure was performed at the chosen strain rate and was the same for all strips and tests, which is the usual practice in elastic materials. Reasons for preconditioning exist only in relation to the mechanics of tissues and as shown earlier preconditioning brings its own problems like the redefinition of the gauge length due to temporarily irrecoverable changes in the specimens dimensions. Preconditioning may help wiping out the previous strain history or slight errors caused by mishandling during the preparation but in the present case were the interest is focussed on the terminal properties of the tissue strips these were studied by first pull curves by pulling the strips from their relaxed 'virgin' state to failure.

6.2.4 Data Recording

The loading curves were recorded by the use of a potentiometric pen recorder which was set to run at a chart speed of 200mm/min, which in combination to the cross head motion at 20mm/min produced a clear drawing of a curve at the required dimensions.

The load calibration was made at an increasing sensitivity by the using a 10g dead weight at full scale deflection on the chart. A full scale load of 20N was used for the production of the whole failure curve without specific examination of the low stress region to take place.

6.3 RESPONSE TO LOADING.

6.3.1 Typical Simple Tension Curve.

From a population of preliminary samples was established that the maximum load required until complete failure of strips of these dimensions happens is less than 20N. A 20N load cell was used and the

full scale of the recording paper was set to be 20N.
At the start a 1N full scale was chosen and with an increase in the sensitivity in load the smallest first load point (0.002N) was marked. It was found that it practically coincided with the zero deformation point and thus all curves appear to depart from the origin.

A typical curve of the load/deformation response of the samples in the 1st pull is shown in fig.6.2. The response of the tissue to load was non-linear. It presented an initial very compliant region(I) where significant increase in the specimen's dimensions was accompanied by only small increases in load. The response of tissue to load then followed an 'elbow' with moderate increase(II) in load and then passed into a linear region(III) accounting for almost 0.3 in stretch(30% strain) for the deformation curve of this particular specimen. The tissue then entered a region resembling the state of 'yield' of a linearly elastic materials(IV) and this was followed by a drop in the load after the specimen had passed the failure point(V). The actual shape of the curve after the failure point was immediatelly appreciated that it was related to the original angular orientation of the strip on the pericardial sample. Strips at small angles to the circumference presented a drastic drop to minimum load levels while strips at small angles to the axial direction of the heart presented a ductile region as by plastic flow with some load sustained and 'creeping' for some time until the rupture occured. Rupture(VI) was defined as absence of any load because of complete discontinuity of the material between the grips.

6.3.2 Definition of Parameters.

Specimens according to their responce can be characterized as more or less extensible in respect to their stretch ratio values at certain levels of stress(as at the top pressure point in inflation) of

the nonlinear stress/strain curve. Otherwise stresses/strains can be compared at a point defined by the shape of the stress/strain curve itself independently of the human factor. Such a point can be the point of failure of the curves which occured at a particular set of values for stress-stretch for each of the specimens. From the curves 3 parameters were measured the Ultimate Tensile Strength(U.T.S) as the stress value at failure, the Ultimate Stretch Ratio(U.S.R) as the stretch ratio at failure and the slope of the linear region of the curve, which is analogous to Young's modulus(E). Specimens that can sustain significant amounts of load are characterized as strong as compared to specimens that fail at lower stresses and thus are weak. Composites, and most of the biological materials which have a composite structure, have the advantage of not propagating the failure surface and thus may be resilient to load but very tough in respect to their failure properties. On the other hand certain materials may be very stiff but they fail catastrophically by rapidly propagating failure being characterized as brittle.

From the parameters defined earlier the stretch ratio is a geometric parameter and the U.T.S which includes a stress value is a dynamic parameter. The other dynamic parameter is the tangent modulus which expresses the rate of increase of load and it is essentially the first derivative of the non-linear stress/strain at any point. In the linear region of the curve it could be taken to correspond to the Young's modulus of linear elasticity. In respect to a higher or lower modulus of elasticity specimens can be characterized as stiff or soft respectively.

Interpreting those parameters can be risky especially for biological materials, but it is acceptable to relate the ultimate stretch ratio to the general ability of the tissue to stretch along a

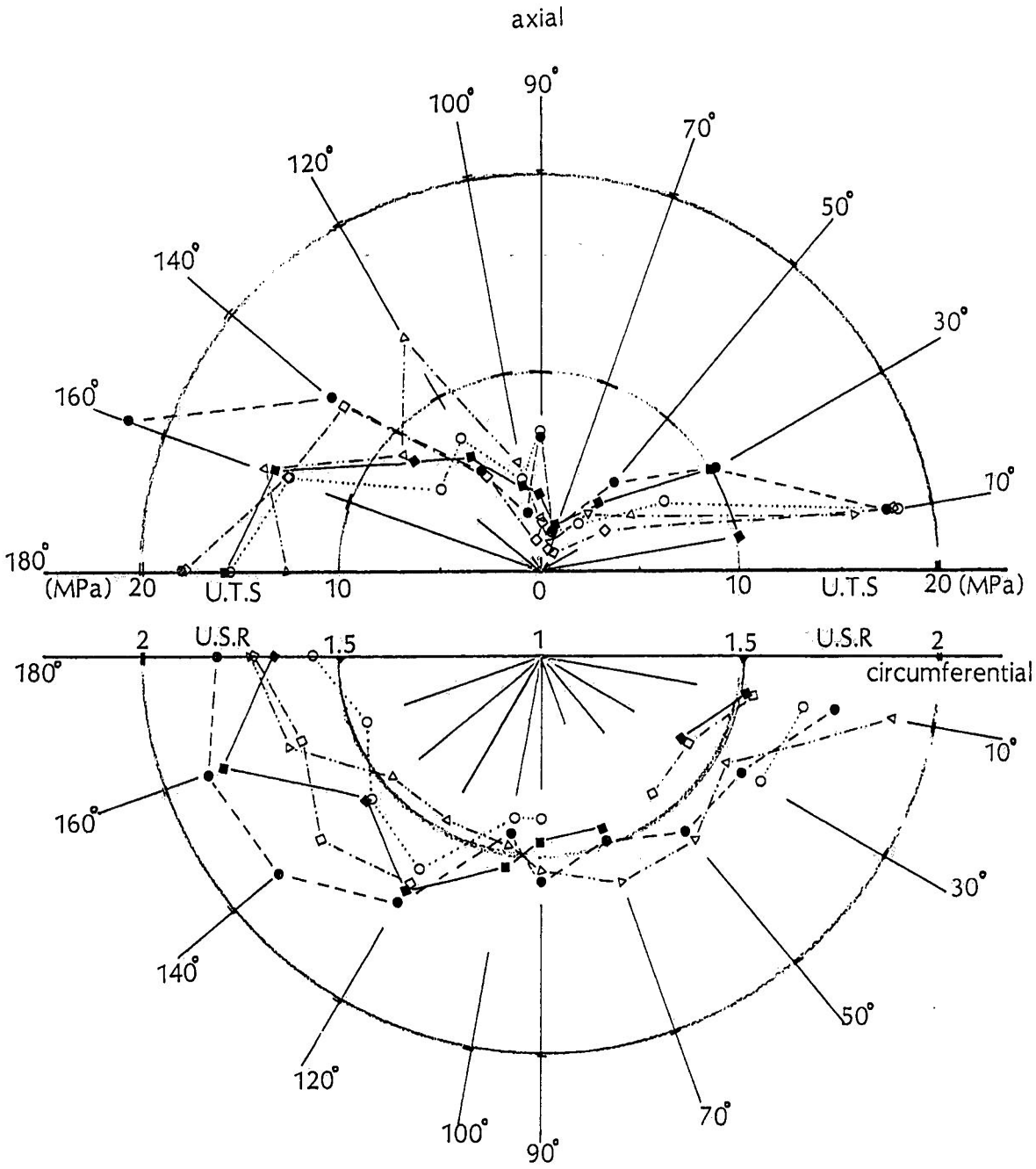

Figure 6.3:angular plots of the Ultimate tensile strength and the Ultimate stretch ratio by using all 50 strips used in the present tests.

certain direction due to a specific architecture, i.e. crimp and organisation of collagen fibres in tissues; and viewing the intensive parameters as reflecting both the quality (individual stiffness and toughness of building ingredients) and quantity (orientation and angular distribution) of the constituent elements.

6.3.3 Values of Parameters

The resulted curves of 50 specimens have been examined and the 3 main parameters U.T.S, Emodulus(Young's modulus), U.S.R(stretch ratio) as defined earlier were calculated. Their values are included in tables6.1,6.2,6.3. The angle is given in degrees as encountered in the geometrical and experimental quadrants of the test. In parentheses equivalent values of the angles within the first quadrant are given and these values which may also be used if certain symmetries apply. The parentheses at some values of the parameters in the columns indicate these values that lie away of the expected response of the tissue and may have been due to experimental error. In the two last columns the mean values of all five samples, including those for which there are some doubts, at each one of the angular orientations have been calculated and are presented and the standard error of these means is given in the last column as well. All values have been entered as columns in exactly that form in a statistical package in the computer and were used for the plots and further analytical treatment.

6.4 TREATMENT OF RESULTS.

6.4.1 Main Plots.

The results were plotted using Cartesian and polar coordinates. The angular plots are more easily comprehended and readily yield qualitative results as they relate straightway the lay out of the strips in test to the plotting axes on the paper. The human eye can

TABLE 6.1: Ultimate tensile strength(nominal stress value at failure) at various angles.

Specimen: P.D.1 Angle	P.D.2	P.D.3	P.D.4	P.D.5	Mean values	Standard error of the mean
(degrees)	(MPa)	(MPa)	(MPa)	(MPa)	(MPa)	(MPa)
180 (0)	17.8	17.6	15.8	12.6	15.8	15.92	1.04
10	17.8	17.6	10.2	15.9	18.0	15.90	1.65
160 (20)	(22.3)	13.3	13.8	14.0	13.2	15.32	1.96
30	10.0	4.0	10.2	5.8	7.2	7.44	1.34
140 (40)	13.4	12.6	8.3	8.6	6.2	9.82	1.53
50	5.7	(0.6)	4.5	3.6	3.1	3.50	0.95
120 (60)	8.9	5.5	6.5	(13.5)	7.5	8.38	1.56
70	2.0	(0.8)	2.7	1.2	1.5	1.64	0.37
100 (80)	2.7	1.2	4.2	5.4	3.8	3.46	0.79
90	7.0	2.4	3.7	2.4	7.0	4.50	1.17

TABLE 6.2: Young's modulus(modulus of elasticity in the linear region III) at various angles.

Specimen: P.D.1 Angle	P.D.2	P.D.3	P.D.4	P.D.5	Mean values	Standard error of the mean
(degrees)	(MPa)	(MPa)	(MPa)	(MPa)	(MPa)	(MPa)
180 (0)	35.13	35.65	54.65	35.98	40.40	40.36	4.13
10	52.12	35.35	31.82	61.98	34.10	43.07	6.64
160 (20)	54.05	41.32	49.99	31.98	44.07	44.28	4.24
30	31.79	10.10	33.33	28.14	30.30	26.73	4.75
140 (40)	43.44	45.45	34.99	30.30	28.41	36.52	3.83
50	19.31	(4.00)	19.09	26.52	12.99	16.38	4.21
120 (60)	27.93	19.81	21.99	50.00	32.47	30.44	6.01
70	(9.01)	(4.40)	13.33	(5.45)	(5.45)	7.53	1.84
100 (80)	15.77	(6.06)	21.25	20.20	17.32	16.12	3.02
90	25.10	12.98	18.89	11.66	27.55	19.24	3.54

TABLE 6.3: Ultimate stretch ratio (value at failure point V) at various angles.

Specimen: P.D.1 Angle	P.D.2	P.D.3	P.D.4	P.D 5	Mean values	Standard error of the mean
(degrees)						
180 (0)	1.81	1.72	1.57	1.67	1.72	1.69	0.044
10	1.75	1.55	1.67	1.53	1.89	1.67	0.074
160 (20)	1.89	1.63	(1.41)	1.83	1.66	1.75	0.073
30	1.59	1.43	1.63	1.41	1.53	1.52	0.048
140 (40)	1.85	1.72	1.56	1.57	1.47	1.63	0.075
50	1.57	(1.46)	(1.33)	(1.30)	1.60	1.54	0.052
120 (60)	1.72	1.67	1.62	1.68	1.47	1.63	0.048
70	1.48	(1.35)	(1.23)	1.47	1.60	1.47	0.058
100 (80)	1.45	(1.66)	1.42	1.53	1.47	1.51	0.047
90	1.57	1.46	1.40	1.47	1.55	1.49	0.035

easily attribute anisotropic properties to ellipsoidal schemes in angular plots than to maxima and minima in a cartesian plot.

6.4.2 Qualitative Considerations

6.4.2.1 Behaviour of strength data. In fig.6.3 all data points for U.T.S. (in the upper half) and U.S.R. (in the lower half) have been put in two polar diagrams. Points originating from the same sample have been connected with straight or dotted lines to help identification. It is evident that in the case of the Ultimate strength data the results form two 'lobes' that in quadrant II(90°-180°) being slightly larger than that in quadrant I(0°-90°). A possible explanation for this asymmetry is that it is related to the previously mentioned non-uniform thickness reduction from the left to the right in the tissue sample. The strength values have been calculated from a mean thickness value for the whole area of the sample(sheet) and thus specimens of the II-quadrant have strengths slightly overestimated(expanded in radial direction), while specimens of the I-quadrant have strengths slightly underestimated(contracted along radial direction).

Otherwise the general shape of the lobes is very similar right and left of the 90° axis. There appear to be two local minima right and left of the 90° axis at 70° and 100° respectively and thus the 90°direction does not present an overall minimum. For all 5 strips at 90° the strength was greater than the strength at 70° (also for the means) and for 3 out of the 5 strips the strength at 90° was larger than the nearby strengths at 80°(100°) and this affected the means. A possible explanation for this finding and a statistical examination of this area will follow later.

6.4.2.2 Behaviour of stretch data. From the lower diagram which depicts the ultimate values of stretch it is obvious that their polar

scheme formed an oval with the ends of its major dimension almost at the 0^o and 180^o directions. It was evident that an asymmetry existed in the shapes of the strength/stretch rosettes, and this was probably due to the non-linearity of the stress/strain curve.

The non-axisymmetric behaviour of the stretch data provided a further proof for anisotropy in the tissue extensibility.

6.4.2.3 Elastic symmetry of the material. From both of the previous polar schemes we can decide to a first approximation about the class of material symmetry. The material properties appear to reflect around the test axes and thus the material may be considered as being orthotropic with its elastic axes at normal angles, or isoclinic with its elastic axes close to the cartesian ones we used in experiment.

When working along the axes of elastic symmetry the matrix of the coefficients of deformation (Lekhnitskii,1963) for an isoclinic(6.1a) and an orthotropic(6.1b) material have the form:

$$\begin{matrix} a_{11} & a_{12} & a_{13} & 0 & 0 & a_{16} \\ & a_{22} & a_{23} & 0 & 0 & a_{26} \\ & & a_{33} & 0 & 0 & a_{36} \\ & & & a_{44} & a_{45} & 0 \\ & & & & a_{55} & 0 \\ & & & & & a_{66} \end{matrix} \quad (6.1a) \qquad \begin{matrix} a_{11} & a_{12} & a_{13} & 0 & 0 & 0 \\ & a_{22} & a_{23} & 0 & 0 & 0 \\ & & a_{33} & 0 & 0 & 0 \\ & & & a_{44} & 0 & 0 \\ & & & & a_{55} & 0 \\ & & & & & a_{66} \end{matrix} \quad (6.1b)$$

thus the main distinction between these two materials for the case of a plane tissue is due to the presence of the constants a_{16}, a_{26}.

In the present case the measures of the parameters have been made at the terminal point of the curves at the end of a long linear region. If we suggest that the results of the initial non-linear region can be disregarded in respect to the linear behaviour of the terminal region

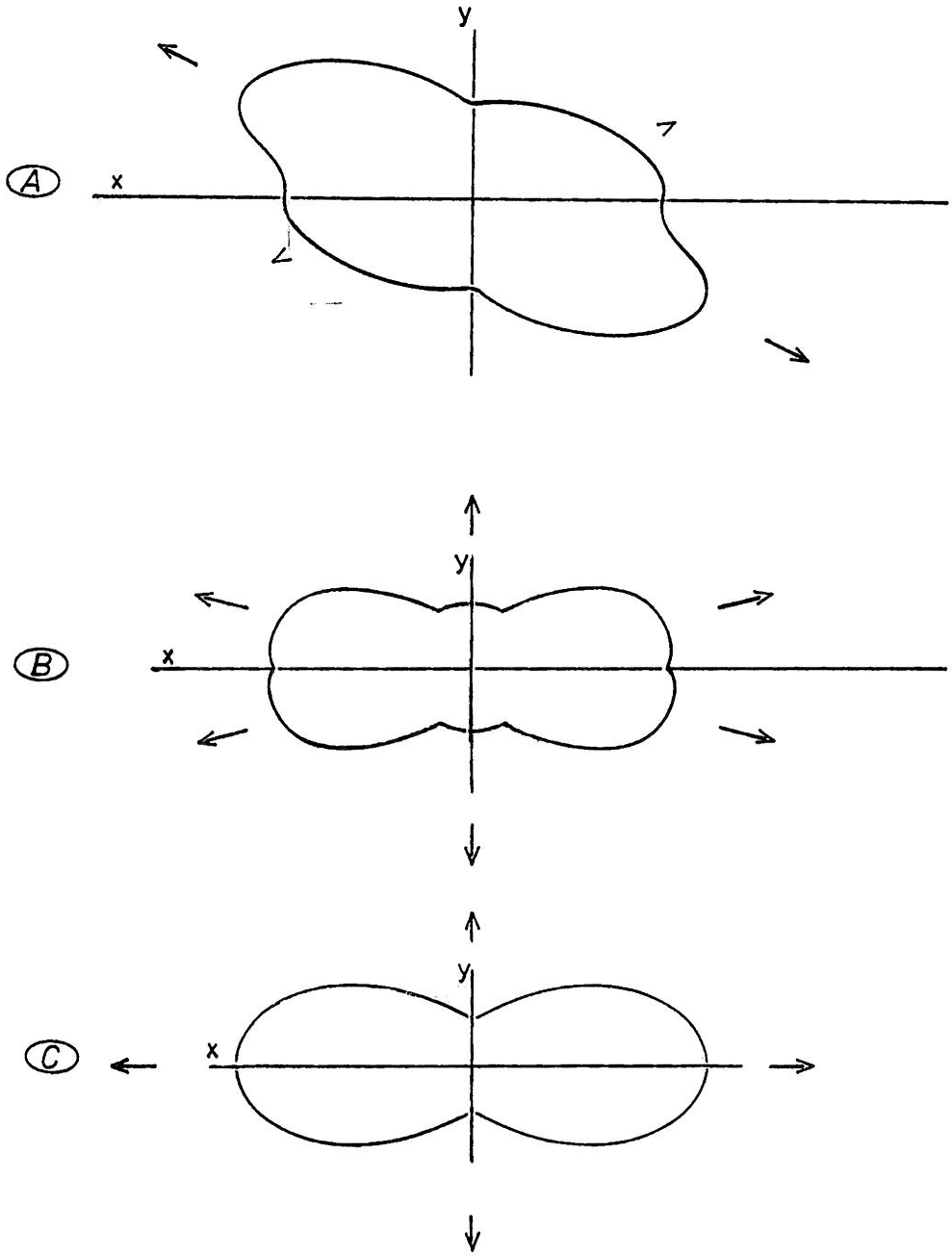

Figure 6.4:three hypothetical fibre distributions, (A)with a centre of symmetry equivalent to a second order axis of rotation at the z-direction, (B)with a centre of symmetry and a plane of symmetry (xz), (C)similar symmetry considerations as (B) but possessing only one maximum on the x-axis and a minimum on the y-axis.

we may transfer the principle of the generalised Hooke's law in the present case and apply it to finite strains and using the abbreviated notation for incremental engineering components of stress/strain. The following equations result in the plane case:

$$
\begin{aligned}
e_1 &= a_{11}\sigma_1 + a_{12}\sigma_2 + a_{13}\sigma_3 + \ldots + a_{16}\sigma_6 \\
e_2 &= a_{12}\sigma_1 + a_{22}\sigma_2 + a_{23}\sigma_3 + \ldots + a_{26}\sigma_6 \\
&\quad .\quad .\quad .\quad .\quad . \\
e_6 &= a_{16}\sigma_1 + a_{26}\sigma_2 + a_{36}\sigma_3 + \ldots + a_{66}\sigma_6
\end{aligned}
\qquad (6.2)
$$

where 1=xx, 2=yy, 3=zz, 4=yz, 5=xz, 6=xy. These relations show that the presence of the shear coupling constants a_{16}, a_{26} creates shear strain on the plane of the tissue even when $\sigma_6=0$ contributed by the normals σ_1, σ_2. If the test axes are set to the axes of the stress ellipsoid then the shear stresses vanish but shear strains would still exist if $a_{16}, a_{26} \neq 0$. The constants a_{16}, a_{26} can be present when working in a system of axes not coinciding to the axes of elastic symmetry of an 'orthotropic' material or when working along any system of axes of an 'isoclinic' material. A qualitative decision on the presence of the shear coupling constants can be taken on the degree of coincidence of the stress/strain ellipsoids (polar schemes).

From the plots in fig.6.3 it is evident that the major axes of the polar schemes were aligned close to the most extensible mechanical direction ($0^\bullet, 180^\circ$) and that both minor and major axes of the stress/strain shapes were to a great degree coinciding to each other. The qualitative conclusion of these considerations was that the material symmetry was nearly orthotropic and that the quantitative approach and further analytical treatment of the data to proceed by using these same axes as used in test.

By considering the fibrous structure of the tissue a symmetry around a

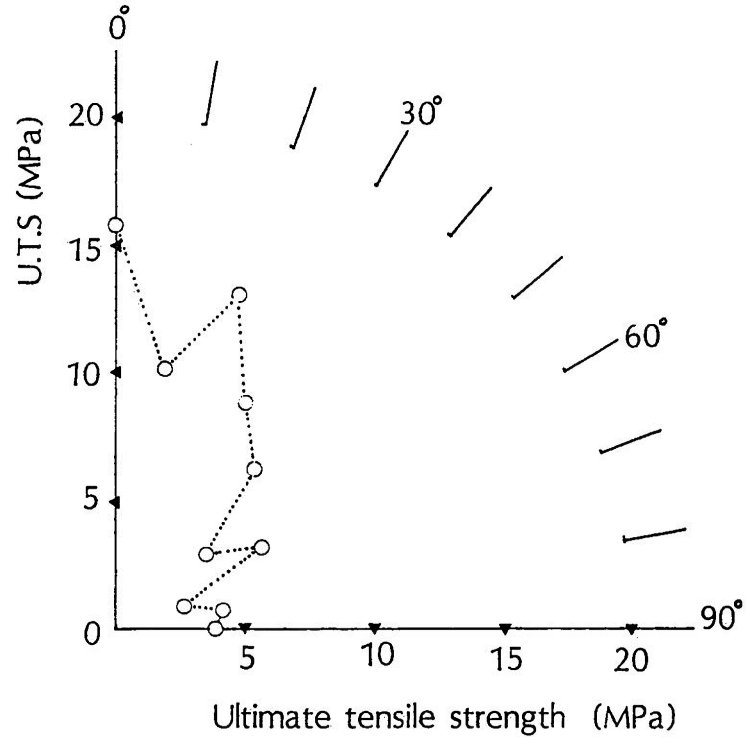

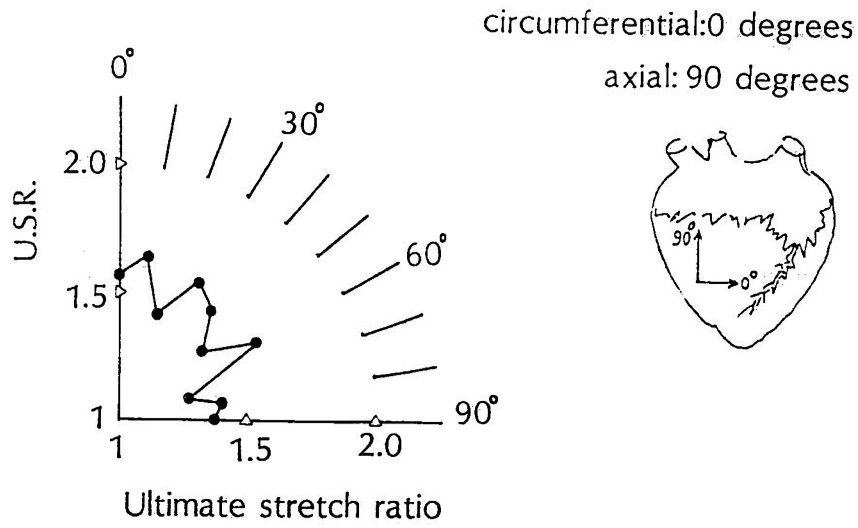

Figure 6.5:(A) U.T.S. polar graph and (B)U.S.R. polar graph for specimen P.D.3. The 0° testing direction was close but did not coincide to the heart's circumferential direction.

centre (the axes origin) is established. Fibres lying at a direction in the I-quadrant are also present in the III-quadrant. Thus a reflection around the centre exists between quadrants I-III and II-IV as in fig.6.4a of a hypothetical fibrous distribution. Fibres laid out as in fig.6.4a produce an isoclinic material with a centre of symmetry which is equivalent to an axis of rotation of the second order along the z direction(normal to the plane x,y). However if using inflation on circular discs of such a material the method would have never identified the mechanical axes (x,y) as shown in the fig.6.4a which form an angle to the axes of elastic symmetry of the material. It appears then that the use of inflation ensures also a kind of symmetry around the x-axis as shown in the hypothetical fibrous distributions of fig6.4b,c. The properties of the materials in fig.6.4b,c can be studied within the first I-quadrant and the general polar schemes(rosettes) of behaviour can result from a four times replica of the behaviour in this one and only quadrant. This resulted in a reflection of the angles of the 90°-180° range in test within the 0°-90° range of the analytical quadrant (given in parentheses in tables6.1,6.2,6.3).

6.4.3 Polar and Cartesian plots of the 3 Parameters.

Proper angular plots of strength and stretch have been prepared for all the samples with all points included in the first quadrant based on the discussion of the previous sections.

The behaviour of individual samples was like in fig.6.5 for sample P.D.3. There was a threefold larger value for strength along the axis close to the circumferential than along the axial direction of the heart. At the same time the strong-circumferential direction appeared to be more extensible (0.17 in stretch ratio values, table6.3) than the weak-axial direction when measuring the ultimate

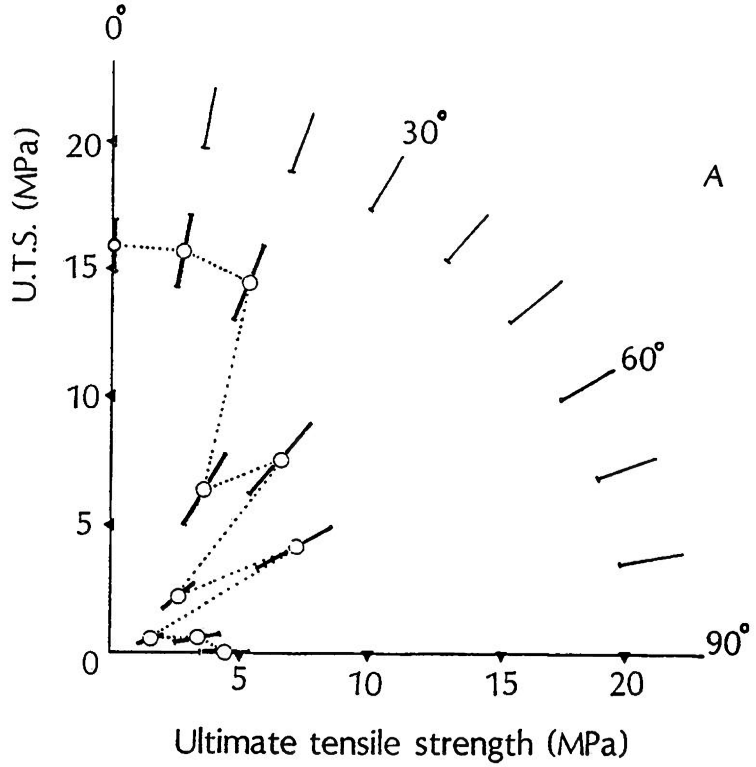

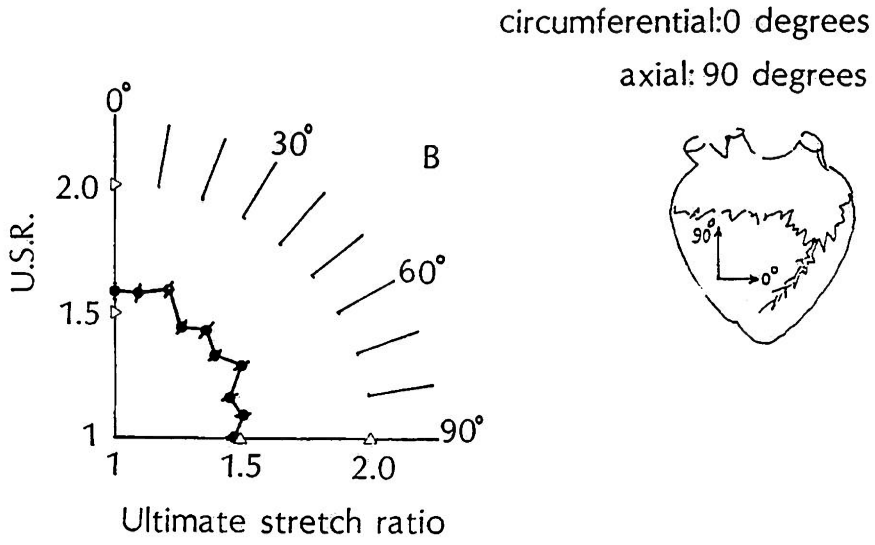

Figure 6.6 :the average behaviour of all 5 specimens in polar plots for the (A)U.T.S. and the (B)U.S.R. The 0° testing direction was close but did not always coincide to the heart's circumferential direction. (mean ± standard error of the mean points)

stretch ratio. All specimens appeared stronger, stiffer and more extensible circumferentially (tables6.1,6.2,6.3).

In fig.6.6 the average behaviour of all samples for these measures has been plotted as the mean accompanied by the standard error of the mean bar for each point.

The shape and variation of the behaviour of the mean values for strength was examined with t-tests of all possible combinations of angles. In table 6.4 the trigonal matrix(symmetric to the diagonal elements) is filled with the results of the statistics, for all t-tests the level of significance was set at p=0.05 and a positive sign indicates that there was a statistical difference between the particular row and column. At the same time the number next to the sign of positive or negative significance shows the level of p which would make the t-test significant. Negative signs are encountered close to the diagonal squares indicating that the mean values of neighbouring angular orientations were not always significantly different, while the strength values at the axes were unequivocally different and the same is true for the mean of specimens that differed 20° or more.

Points of the I-quadrant (30°, 50°, 70°) reached lower values for either parameters a possible effect of variation in thickness.

For the means at 70°, 80° which were taken very close to the axial strip(90°) and thus there was no significant influence of the thickness variation, they appeared to definitely reach lower values than the axial strip(90°) and thus produce local minima at these angles. The significance of this finding was checked with a two-way analysis of variance for the region of 70°, 80°, 90° angles. The analysis gave a F-ratio for the different angles equal 3.137 less than the critical 4.46 for a level of significance of 0.05 and thus the

TABLE 6.4:Student's t-tests were performed bu using the U.T.S. data between any two directions of the strips, significant differences (p=0.05) are indicated with a positive sign next to the level at which significance was attained. Strips at an angle greater than or equal to 20° differed significantly.

p=0.05 / p	0°	10°	20°	30°	40°	50°	60°	70°	80°	90°
0°		− 0.990	− 0.770	+ 0.000	+ 0.008	+ 0.000	+ 0.004	+ 0.000	+ 0.000	+ 0.000
10°			− 0.810	+ 0.003	+ 0.019	+ 0.000	+ 0.007	+ 0.000	+ 0.000	+ 0.000
20°				+ 0.007	+ 0.043	+ 0.002	+ 0.017	+ 0.002	+ 0.015	+ 0.002
30°					− 0.232	+ 0.032	− 0.625	+ 0.009	+ 0.029	− 0.107
40°						+ 0.008	− 0.486	+ 0.004	+ 0.006	+ 0.017
50°							− 0.025	− 0.097	− 0.972	− 0.482
60°								+ 0.009	+ 0.026	− 0.062
70°									− 0.068	− 0.059
80°										− 0.438
90°										

differences between the means when considering all 3 angles were insignificant although the strength at 70° was lower than the strength at 90° for all 5 specimens. At the same time the variation within the data in the columns(at each angle) gave a F=4.015 larger than the critical 3.84 for $F_{2,8}$ (0.05) from tables. Thus there was significant variation in the behaviour of the samples as the angle changed from 70° to 80° to 90°. This was a reflection of the previously mentioned observation that 3 of the samples presented a local maximum at 90° while the other 2 a local maximum at 80°.

In fig.6.7 in three Cartesian plots the 3 main parameters (U.T.S, Young's modulus, Ultimate stretch ratio) were plotted as a function of the angle of orientation of the samples. The whole of 50 data points has been plotted and the means were connected by straight segments. The behaviour of the 3 curves was very similar between the 3 plots indicating that there should be a significant correlation between the parameters when examined in pairs. It is apparent that points at 30°, 50°, 70° of the I-quadrant had lower values for all three parameters. In fig.6.7a the dotted lines connect the 30° 50° 70° points and the 20° 40° 60° points which originate from areas of comparable thickness. If a single curve was to describe the behaviour of the strength data over the whole range (0°-90°) then it should draw a graph in between the two dotted lines and have a parabolically decreasing form towards the 70° angle where it should flatten predicting the insignificant statistical variation in the values at 70°,80°,90°. If plotted in polar coordinates the rossette for strengths should produce a lobe along the stronger direction.

In fig.6.8 the U.T.S versus the Young's modulus values have been plotted and were found to be well correlated to each other. This shows that the relation, which was shown to exist in chapter5 for data

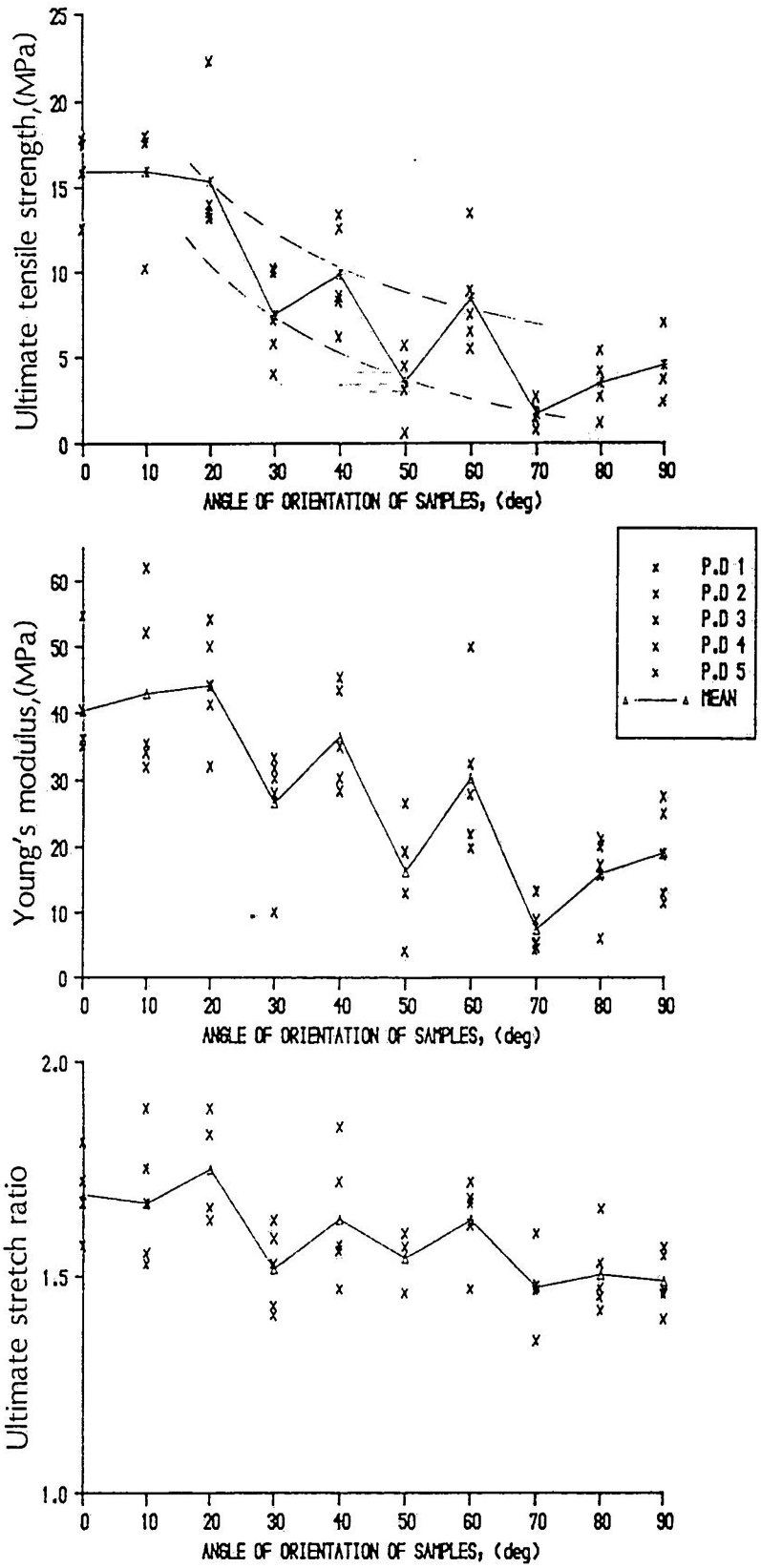

Figure 6.7:cartesian plots of the 3 main parameters(U.T.S.,Emodulus,U.S.R.)

of many samples, different areas and at only two directions, applies also within an area and at different angles. This was a solid proof that the relation between U.T.S. and elastic modulus was caused by the structure and was due to the non-axisymmetric lay out of the fibrous distribution.

Fig.6.9a,b includes plots of the same parameters against the Ultimate stretch ratio. A linear relation appears to exist between U.S.R and U.T.S and similarly between elastic modulus and U.S.R. This correlation shows that if the geometrical shape of the rossette in one of the angular plots (i.e. U.T.S.) is asymmetrical then all 3 rossettes are asymmetrical and furthermore that the alignment in their symmetry axes is absolute. This is reasonable as the same structural component is responsible for the ultimate sustainable load, for the rate of increase in load and the geometry at failure.

6.5 ANALYSIS OF FAILURE

6.5.1 Introduction.

A complete failure analysis is usually required in engineering design of elements to predict the limits of their behaviour. Here failure analysis was used to provide an insight on the architecture of the tissue, to examine the behaviour of the material at the extremities of stress and as a means of clarifying the nature of the stresses in this tissue. It is for these reasons that the route followed in the failure analysis of native pericardium is slightly different from the one followed in the analysis of engineering materials.

The well known failure theories are always based on a postulate regarding the most probable reason cause of failure. A mathematical formulation compatible with this postulate is developed which describes in terms of stresses the conditions that must exist in order

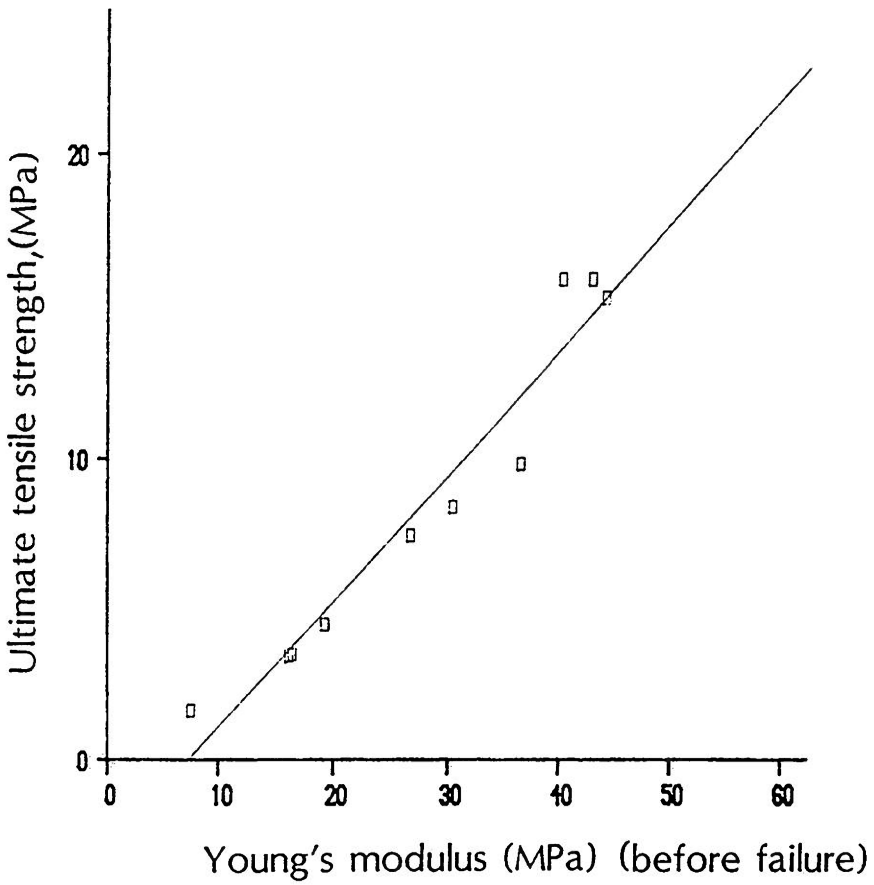

Figure 6.8:the relationship between U.T.S. and modulus of elasticity was nearly linear; r=0.971.

for failure to occur. When this formula, usually called the "failure criterion", reaches a critical value it is anticipated that conditions of failure are fullfilled and failure occurs. Data adequate to properly support the development of a failure criterion may require the use of more than one test method since the criterion should predict failure in combined states of stress and not simply in simple tension cases. A sufficient criterion can be developed from the use of only simple tension data if the failure of the material can, in reality, be dictated by the levels of normal stresses, and not shear ones.

From the failure criterion developed the experimenter should then derive the failure surface for the material, which expresses diagramatically the operational limits of the material for the infinite number of combinations of principal stresses that are able to produce failure. The last stage would be to develop a single failure equation which does not necessary require the transformation to the principal stresses in order to use the failure surface but can make use of the stresses as experienced in test.

6.5.2 Theories of Failure.

In the maximum stress theory it is postulated that failure occurs in a member subjected to combined stresses when one of the principal stresses reaches the failure value in simple tension along the principal direction. This implies that the strength of strips at an angle to the principal axes will require greater stresses to fail than that aligned along the principal axis. This is clearly not the case for this tissue which presents a reduction of strength in simple tension off the strongest axis.

In the maximum shear theory, failure is postulated to occur in a member subjected to combined stresses when the maximum shear stress

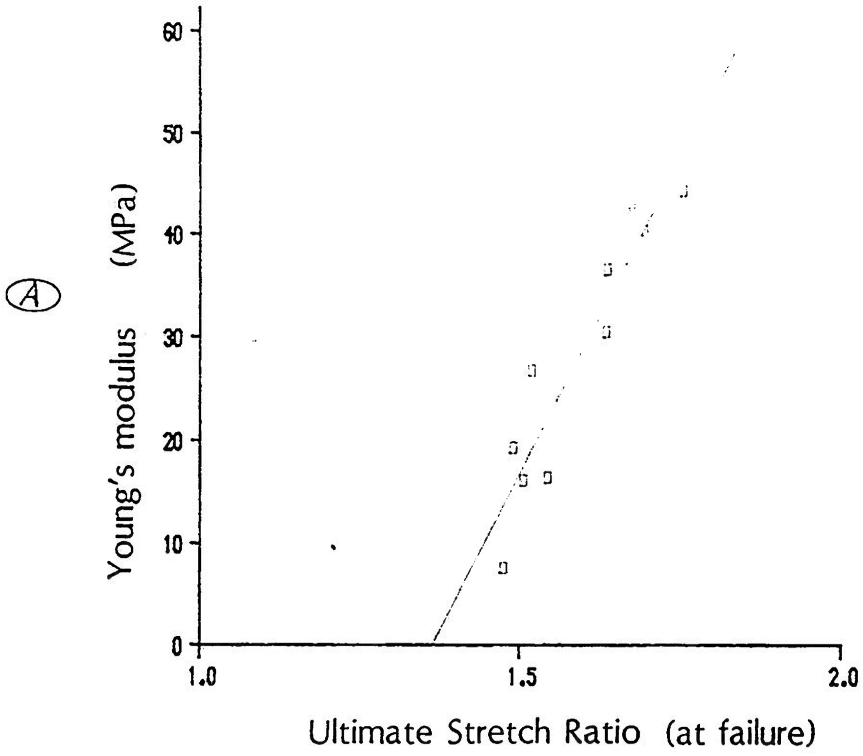

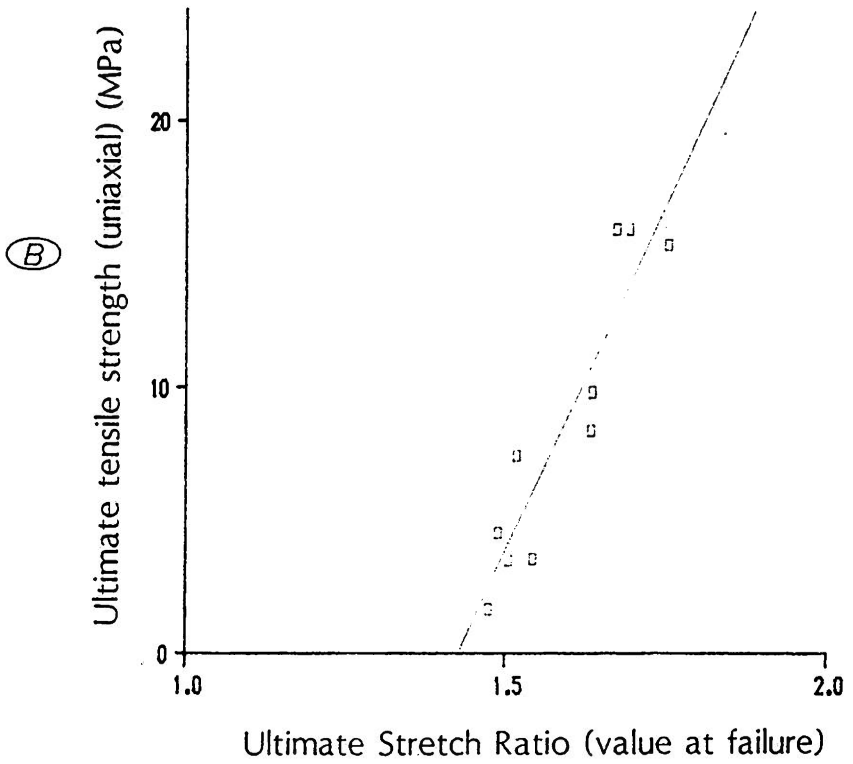

Figure 6.9:plots of (A)the ultimate stretch.v.Emodulus (r=0.930) and (B)the ultimate stretch.v.U.T.S. (r=0.923).

reaches the value of a specific failure shear stress specified in uniaxial tension tests. This theory is also not applicable in native pericardium failure which is regulated by the levels of the normal stresses and it will be shown later (in the plane of the principal stresses/failure surface) that this theory in fact underestimates the maximum sustainable combination of principal stresses.

In the distortion energy theory, failure is postulated to occur in a material subjected to combined stresses when the energy of distortion reaches the same energy as failure in tension. This theory predicts that a set of principal stresses is permissible even outside the box of the maximum principals that can be sustained. For the three-dimensional case of an linearly elastic material the distortion energy is expressed as a relation of the squares of the principal stresses and their products in pairs:

$$U_d=(1+\nu/3E)(\sigma_1^2+\sigma_2^2+\sigma_3^2-\sigma_1\sigma_2-\sigma_2\sigma_3-\sigma_3\sigma_1) \qquad (6.3)$$

E:the elastic modulus. The result is a failure surface with an oval shape with a major axis at an angle to the axes.

Criteria for yield of polymers may be applicable to failure cases as yield just preceeds failure in their deformational behaviour. The Coulomb criterion states that failure which is primarily a result of an excessive shear in some plane, occurs at a critical value for the shear stress which is a linear function of the pressure normal to this plane. The criterion has:

$$\tau=\tau_c+\sigma_N \tan\phi \qquad (6.4)$$

$\tan\phi=\mu$ being the coefficient of friction for the material, with $\tau=\sigma_1(\sin\theta\cos\theta)$ and a normal $\sigma_N=\sigma_1\cos^2\theta$ created by uniaxial compression (or tension) σ_1, the relation:

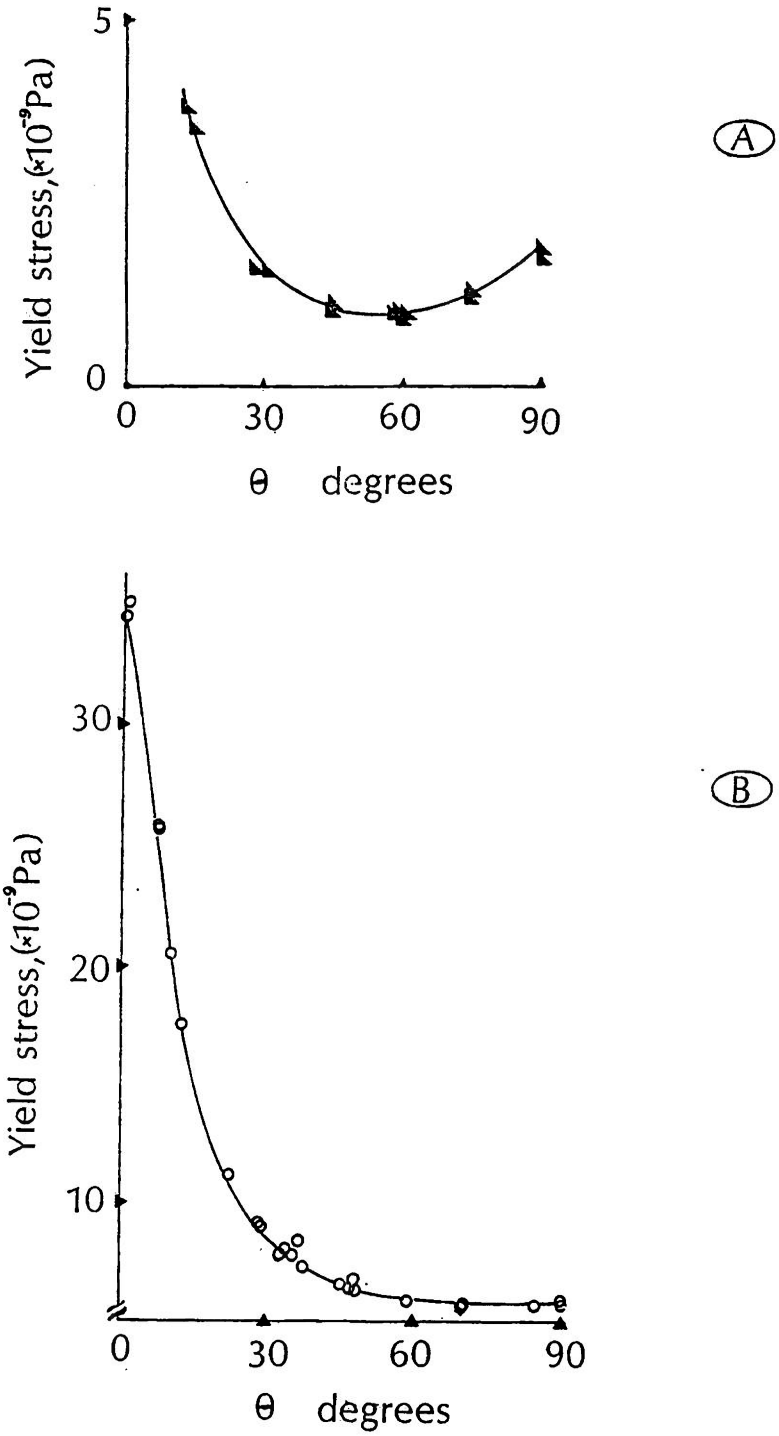

Figure 6.10: (A) yield of high density drawn poluethylene sheets described by using the Coulomb criterion by Keller and Rider(1966), (B) yield of oriented terephthalate sheets by using Hill's criterion by Brown et al(1968).

$$\sigma_1(\cos\theta\sin\theta-\tan\phi\cos^2\theta)=\tau_c \qquad (6.5)$$

results, which estimates a minimal σ_1 when the bracket is maximised. Thus the criterion provides both a condition(σ_1) and a direction(θ) of failure or yield.

With this criterion Keller and Rider(1966) described yield data of high density drawn polyethylene sheets in fig.6.10a. It is noted that the angular behaviour of the yield stress presents a minimum in between the two other extremes at 0^o, 90^o for this mechanically produced orthotropic material.

Hill(1948) presented a distortion energy based failure theory applicable to orthotropic materials and including 6 constants:

$$F(\sigma_2-\sigma_3)^2+G(\sigma_3-\sigma_1)^2+H(\sigma_1-\sigma_2)^2+2L\tau_{23}^2+2M\tau_{13}^2+2N\tau_{12}^2=1 \qquad (6.6)$$

directly relating principal stresses and shearing stresses τ_{ij}. If this formula is applied when the test axes and material axes do not coincide, transformation with Mohr's circle is needed.

Tensile yield data for oriented polyethylene terephthalate sheets was shown to obey this criterion by Brown et al(1968), fig.6.10b.

In a review of general theories of failure for anisotropic materials Franklin(1968) described the theory proposed by Radenkovic and Boschat(1962). Their postulate was that the shear strength at any plane is a function of the position of the plane $K(\theta)$. A non-axisymmetric function $K(\theta)$ could result in a theory applicable to anisotropic materials. Although it is not easily apparent, it is an extension of the maximum shear theory and is experimentally oriented, starting from a function which can be experimentally defined and can then lead to the failure surface of the material.

Hoffman(1967) proposed a criterion for orthotropic materials very

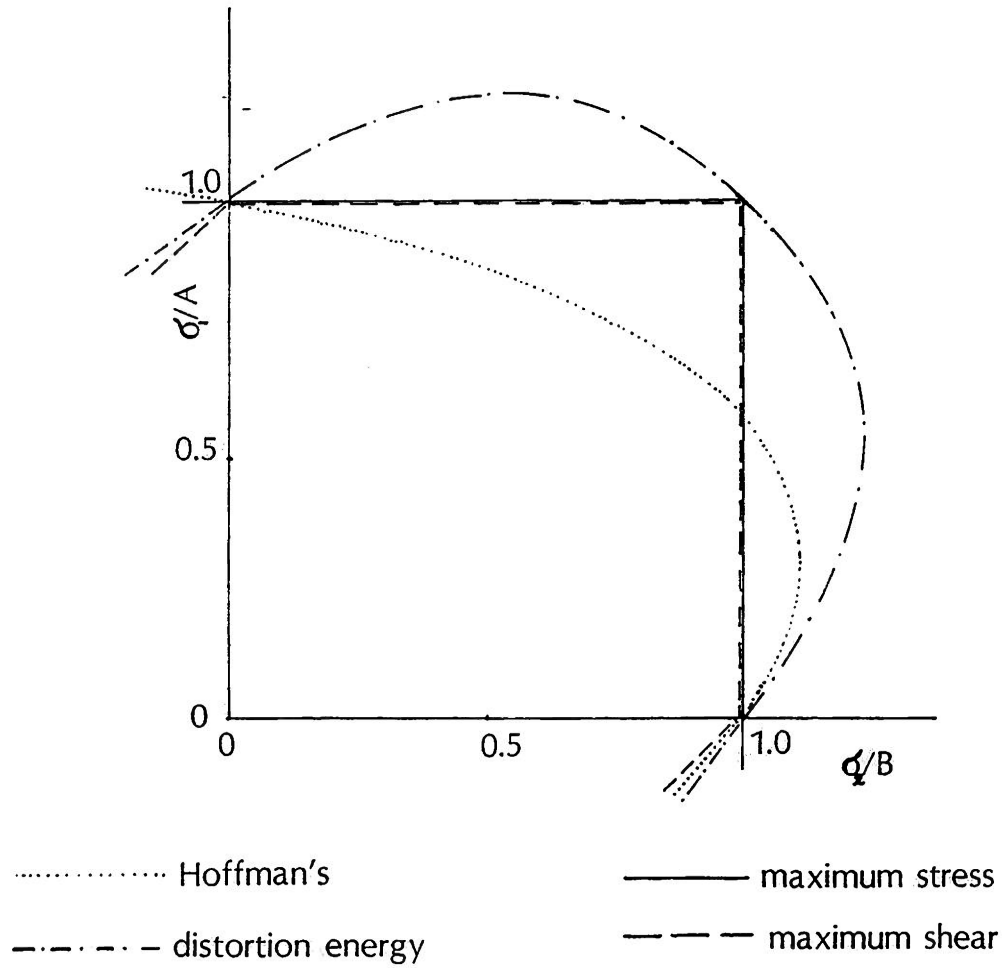

Figure 6.11:failure surfaces in the tensile-I quadrant for 4 different failure theories.

similar to the Hill's but he included first powers of the stresses. Such practice is usually avoided because it means that change in sign (and thus from tension to compression) gives a different value and thus these two cases are distinguished, most commonly called the Bauschinger effect. The surface for some of the theories is shown in fig.6.11.

All previous theories appear to be of restricted applicability for materials of a particular class and are subject to confirmation till now. Tsai and Wu(1970) suggested that a general theory may exist and started by expressing the failure surface by a scalar form $f(\sigma_K)$ of the ingredients of what they defined as strength tensors:

$$f(\sigma_K)=F_i\sigma_i+F_{ij}\sigma_i\sigma_j=1 \qquad (6.7)$$

F_i being the strength tensor of the normal stresses and F_{ij} the strength tensor of the interaction between stresses. This approach has the advantages of tensors in coordinate transformation without the $f(\sigma_K)$ itself being a tensor, it also can treat interactions indepedently and not through a closed form. It can incorporate the Bauschinger effect, and of course is applicable to combined states of stress.

6.5.3 Considerations for the Analysis.

From the previous discussion and the data acquired experimentally it was shown that any proposal:

i)should be based on an expression of stresses and not energies since the utilisation of an energy principle up to the failure point of a non-linear stress/strain curve would be difficult to set up.

ii)it must include normal stresses as the main ingredients to determine failure and not shear stresses. As a consequence of the fibrous nature of pericardium with the tension bearing collagen fibres

being able to support principally tensile forces,

iii)should accurately describe the behaviour of the tissue under test conditions like the one that produced the data,

iv)should be primarily focussed in the I-quadrant of the principal stresses diagram, thus focussing on tension cases and not on tension-compression and so forth. Extension to the compression areas is not intended and thus it may very well include odd powers of the stresses as the Bauschinger effect will not be considered.

6.5.4. Statement of the Main Postulate.

The maximum stress theory which is also developed on considerations about stresses accepts that the off axis strength is this value of a simple tension test that would, if transformed to the principal axis, yield a principal stress value equal to the principal strength of the material. This predicts larger values for strength off the strongest axis which is contradiction to the present tests.

It would be more reasonable to suggest that failure at an angular range $(\theta+d\theta)$ off the axes would occur when stresses exceed some limits which are dictated by the amount of collagen fibres aligned within this angular range $d\theta$. Assuming that the quality(properties) of collagen and elastin fibres is invariable to the angle θ, the previous proposal reduces the requirements for the analysis to an empirical description of the fibrous distribution for this particular test site.

Cox(1952) suggested the following continuous periodic function for a fibrous distribution:

$$\pi R(\theta) = 1 + a_1\cos 2\theta + a_2\cos 4\theta + a_3\cos 6\theta + \ldots + b_1\sin 2\theta + b_2\sin 4\theta + \ldots\ldots \qquad (6.8)$$

a 2-term first approximation could be:

$$\pi R(\theta) = 1 + a_1\cos 2\theta \qquad (6.9)$$

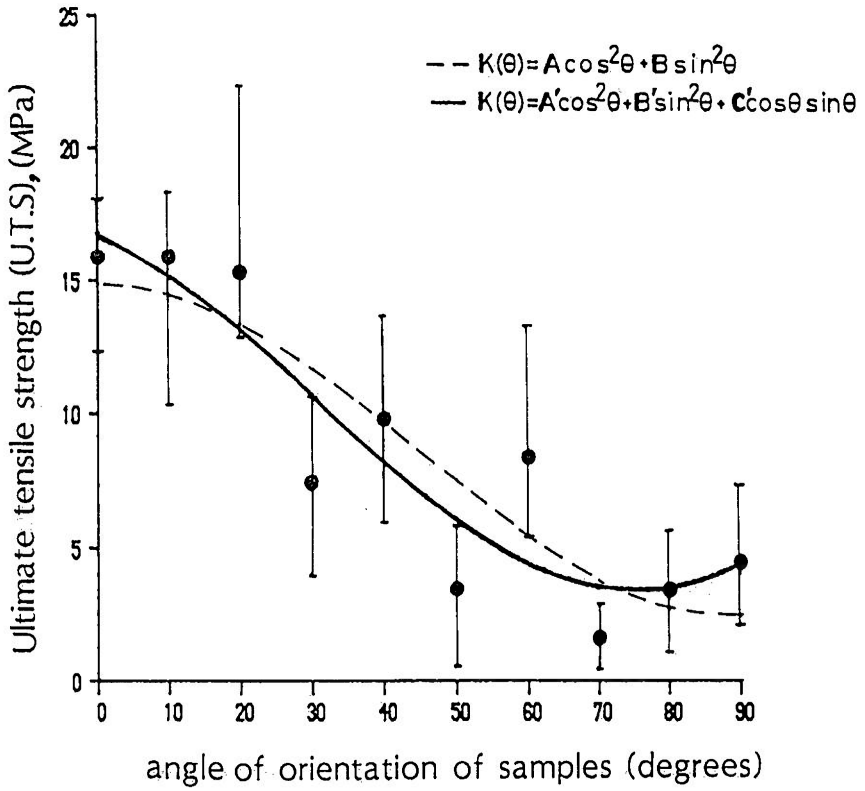

Figure 6.12:least squares best fits of the variation of U.T.S. with angle by using forms (6.10) and (6.12).
The full range of values is indicated by the bars.

which can be brought to an equivalent form:

$$K(\theta)= A \cos^2\theta + B \sin^2\theta \qquad (6.10)$$

for θ measuring the angle off the strong axis. A higher order approximation can incorporate sine forms in a 3-term formula as:

$$\pi R(\theta)= 1 + a_1\cos2\theta + b_1\sin2\theta \qquad (6.11)$$

which is equivalent to:

$$K(\theta)= A'\cos^2\theta + B'\sin^2\theta + C'\cos\theta\sin\theta \qquad (6.12)$$

The means of the U.T.S. data were fitted by a least squares technique by first using the 2-term formula (6.10) and gave: A=14.8MPa, B=2.4MPa; correlation r=0.884. The same data when the 3-term formula was used gave: A'=17.7MPa, B'=4.3MPa, and C'=-6.8MPa, with r=0.914 (fig.6.12).

Up to this point the treatment is empirical but it can result from physical reasoning and thus have an engineering equivalent. Kobayashi(1987) mentioned that the failure properties of a unidirectional lamina can be described by a longitudinal tensile strength, a longitudinal compressive strength, a transverse tensile and compressive strengths and an in-plane or intralaminar shear strength. Considering tensile strengths for the moment and that the longitudinal tensile strength is much larger than the rest, then the strength in a direction forming an angle θ to the fibres by using transformation rule equals:

$$\sigma(\theta)=\sigma_{1T}\cos^2\theta, \qquad (6.13)$$

where σ_{1T} is the longitudinal tensile strength. The classical lamination theory predicts the behaviour of a multidirectional laminate from the properties of the individual laminae. Each lamina

can be thought as quasi-homogeneous and anisotropic and obeying the previous relation (6.13). For ultimate failure of the laminate to occur, a stress must be reached which will cause failure of all plies(laminae) in the laminate. Thus the previously introduced empirical relation (6.9) can be thought as desribing angular variation of strength of a laminate consisting of two fibrous layers of different densities at right angles to each other. In engineering materials such designs have been shown to be orthotropic.

Kobayashi(1987) expressed the wish of all engineers that the presence of a failure criterion would allow a transformation of strengths as simple as a transformation of stresses. If we examine the 3-term relation (6.12) we see that $C \approx (A'-B')/2$ which is the maximum shear at angle θ as created by principal stresses equal to the strengths A', B'. Translating this into the language of strength means that the strength at an angle θ equals the transformed value of the strengths A', B' on the principal directions impaired by an amount equal the maximum shear stress developed on a plane of which the normal forms such an angle θ. Although this may be just a coincidence and the fibrous distribution simply to behaves like (6.12), the possibility can not be excluded that the real fibre distribution is given by a relation similar to (6.10) and that (6.12) is a result of the continuity in the composite structure.

6.5.5 Construction of Failure Surface.

There is a similarity in the approach followed in the previous section and what could be an application of the Radenkovic and Boschat approach mentioned earlier. Those workers presented a theory which might be applied to materials complying to a particular angular behaviour of the strengths and failing due to shear. In the previous sections a function was fitted to the angular behaviour of the tensile

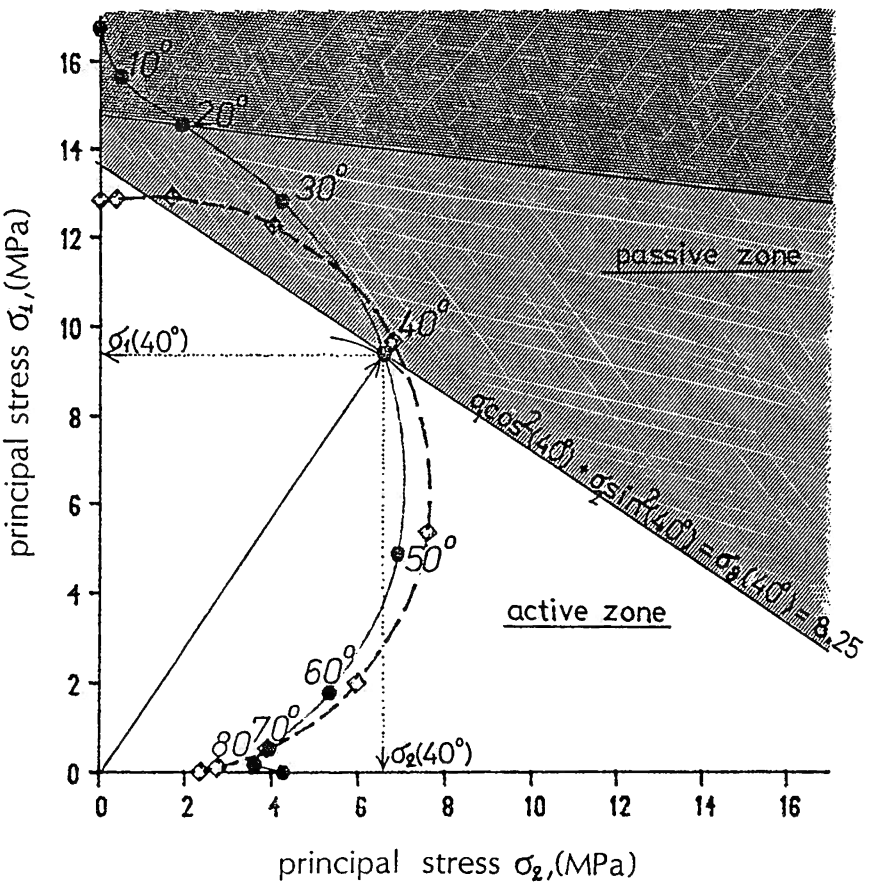

Figure 6.13:in the plane of the principal stresses equation (6.13) for a specific angle θ draws a line above which failure occurs in the shaded passive zone. The passive zones for the solution lines at 20° an 40° are shown and they overlap in the heavily shaded area. The failure surface is the innermost active area which does not consist the passive zone for any of lines drawn at angles 0°-90°.

strength of pericardial strips with a physical link and dictating the conditions of failure by considering only normal forces as being responsible. The methodology followed in the two approaches is quite similar and experimentally oriented, but unfortunately there are no desriptions in the literature of any application of their theory on any material.

In the present case in order to draw the failure surface the angular function K(θ) was resolved in the plane of the principal stresses(σ_1,σ_2). Thus:

$$\sigma_1 \cos^2\theta + \sigma_2 \sin^2\theta = K(\theta) \qquad (6.13)$$

which yields for every value of θ a straight line as the one drawn in fig.6.13 for the 3-term K(θ) at an angle θ=40°.The line gives an infinite combination of principal stresses(σ_1,σ_2) which at the particular angle would have satisfied the failure criterion of maximum tensile strength equal to K(θ). In order to minimise the failure surface the rule was applied that the pair of values sought is the one corresponding to a minimum sum of absolute values for the principal stresses. This in graphical representation is shown in the fig.6.13 to be the distance of each line from the origin of the diagram. The resulting 10 point (for angles 0° to 90°) were subsequently joined in order to produce the failure surface. However each line according to Radenkovic and Boschat divides the plane in an operational active zone and a forbidden passive zone. Overlapping between passive zones further reduces the active area.

6.5.6 Failure Equation.

It should be mentioned that those criteria that utilise principal stresses as part of their formula in a closed form yield readily the failure surface which is drawn on the plane of the principals. The

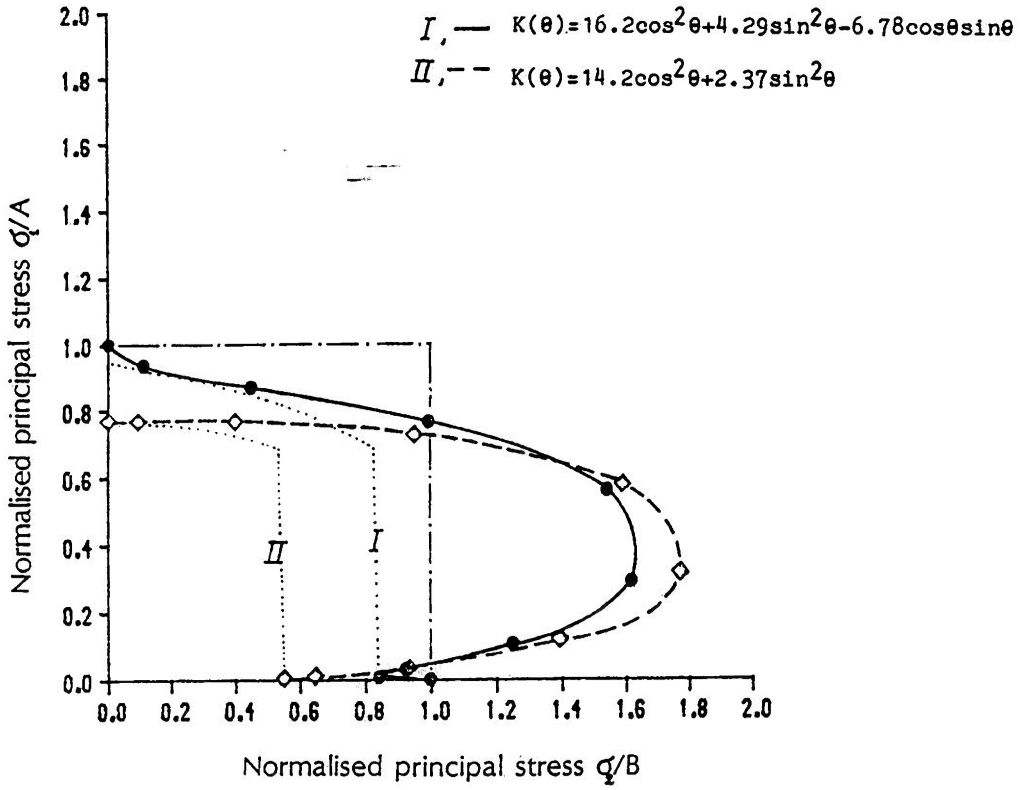

Figure 6.14:in the plane of the normalised principal stresses(by using the maximum strength value on the axes(A′,B′)) the failure surface(I) of the 3-term formula permits substantially greater domain of values for the principal stresses in the tensile I-quadrant.

formula in use in here needed the application of a specific graphical rule in order to draw the surface but it has a great advantage in the following respect.

If the maximum strength acceptable at an angle θ is to be produced by a combination of normal stresses $\sigma x, \sigma y$ and the presence of a shear stress τxy then the transformation rule gives:

$$\sigma x \cos^2\theta + \sigma y \sin^2\theta + 2\tau xy \cos\theta\sin\theta = K(\theta) \qquad (6.14)$$

the importance of this equation is that it predicts the case of failure when a pair of normal stresses and a shear stress exist in a system of coordinates in a plane, without requiring the use of Mohr's circle to find the principal ones.

6.5.7 Summary

The development of a failure theory is based on some postulate. From the many that could be attempted on the angular behaviour of the present material, one that requires the least assumptions was adopted. It is basically an empirical form of trigonometric functions but it could have a link to mechanics of both composites and continua. This function was equated to the proper set of stresses for the failure surface to be drawn and as such stresses only normals were considered. The most important result of the development of a failure theory is considered to be the graph of the failure surface. In fig.6.14 the surface has been drawn in a standard mode encountered in the literature in two axes of the normalised principal stresses. The normalization has been performed by the maximum strengths at each of the principal directions A and B respectively. A direct comparison can be done with the failure surfaces of general theories of failure in fig.6.11. There is an apparent similarity between the general shape of one of the many possible Hoffman surfaces and the one

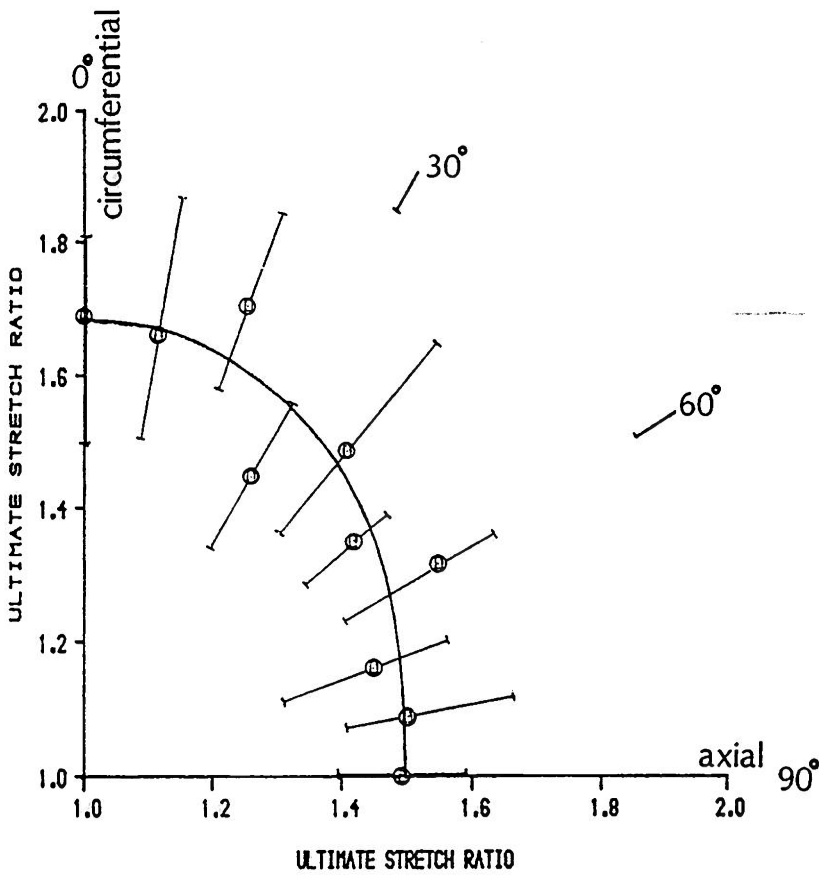

Figure 6.15:description of the angular variation of the ultimate stretch ratio by assuming that these extension values can be transformed as finite strains $E=(\lambda^2-1)/2$. In this respect the tissue was more extensible along the 0° testing direction which for this site was almost circumfential on the heart. The full range of values is indicated by the bars.

developed for pericardium. They both apply for anisotropic and include first powers of the stresses thus predicting a different behaviour in tension-compression. Hoffman's theory can easily be extended to the rest of the quadrants through his formula while the experimentally determined pericardial surface would require additional tests to take it into the compression region.

In the region off the strongest axis only reduced strengths are permissible since the dashed line is drawn below the unit square predicted by the maximum stress theory.

In the region off the weak axis strenghts are increasing in magnitude outwith the unit square. However the overalpping of the passive zones further restricts the active areas for the two functions in the dotted inside the dotted lines I,II for the 3-term and the 2-term $K(\theta)$ respectively. The small inflection area near the weak axis is due to the presence of reduced strength for strips at 70^{o}, 80^{o} and is accounted by the 3-term $K(\theta)$. The irregular shape of the failure surface as produced by the 3-term $K(\theta)$ raises some doubts for the validity of this formula for use.

6.6 ANGULAR BEHAVIOUR OF THE EXTENSIBILITY.

The very early polar plot of the ultimate stretch ratios versus their angles of orientation over the 0^{o}-180^{o} range shows a qualitative difference between angular behaviour of the strength and stretch data. The stretch formed an oval scheme of whic the major axis was roughly along the transverse experimental direction. Although the possibility that the material is isoclinic would also meant that the stress and strain directions do not necessarily coincide, for reasons of convenience we can describe the stretch data along these same principal directions.

For the description the possibility that the stretch can be treated

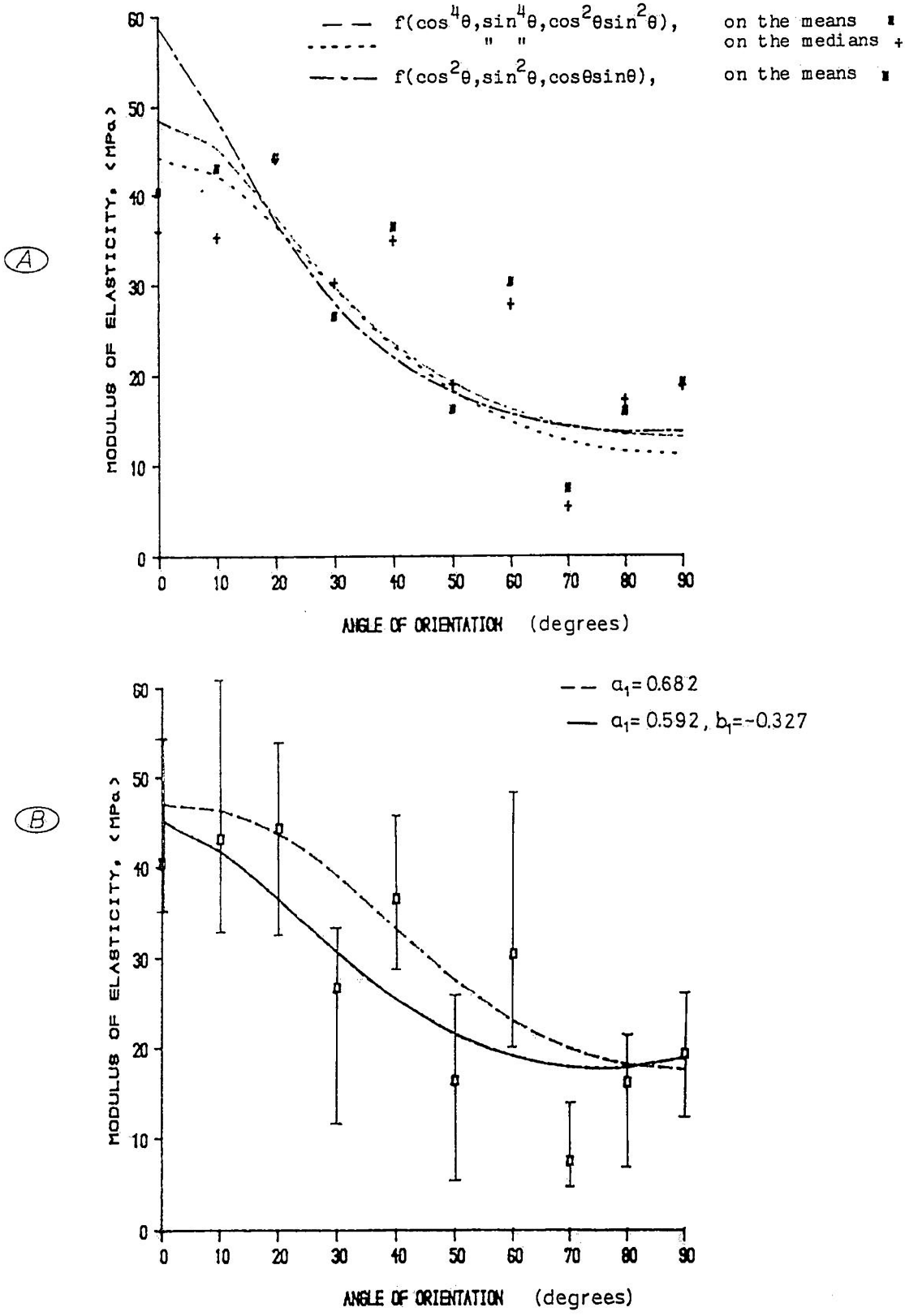

Figure 6 16: Ⓐ 3 regression fits of the means and the medians of the tensile elastic modulus at a testing direction θ, Ⓑ the theoretically predicted behaviour of the elastic tensile modulus by using Cox's theory and the 2-term (dashed line) or the 3-term(continuous line) formulas for the fibre distribution. The full range of values is indicated by the bars.

and transformed as a strain measure was examined. The stretch values were turned into finite strains equal to $(\lambda^2-1)/2$. The resulted values which were the finite strains at an angle θ were regressed with $\cos^2\theta$, $\sin^2\theta$ to yield:

$$(\lambda^2-1)/2 = 0.922 \cos^2\theta + 0.617 \sin^2\theta \qquad (6.15)$$

the intercepts on the axes were translated as principal finite strains and were turned into stretch ratios giving $\lambda c=1.69$ on the most extensible direction and $\lambda a=1.49$ on the least extensible direction. Anisotropy is again signified by the difference in these two values. By using (6.15) the graph in fig.6.15 was prepared. The correlation between predicted and experimental finite strains was only r=0.772 but in fig.6.15 the fit to the data appears to be good.

6.7 ANGULAR BEHAVIOUR OF THE ELASTIC CONSTANTS.

6.7.1 Modulus of Elasticity.

The loading behaviour of the pericardium is non-linear and time-dependent but in the present investigation we shall treat the multidirectional results as produced on a linearly elastic material capable of undergoing finite deformations. This assumption is probably valid for higher strains into the linear region of the pericardial stress/strain response where the modulus of elasticity was measured.

For a three dimensional isoclinic material there are 13 independent elastic constants, for an orthotropic material the constants reduce their number to nine and for a two dimensional orthotropic material are just 5.

The results obtained in tests refer to the technical constants like the moduli in tension or shear and the Poisson's ratios which can be experimentally measured. However transformation of the these measures

can only be performed if they are turned into the elastic constants which are components of either the stiffness or compliance matrices. Where experimental determination of some of the constants is attempted the two general systems of coordinates: this of the test axes and the other of the material symmetry may not coincide but form angles between any of the 6 axes. If a_{ij} (i,j=1,2,3) are the cosines of the angles between any of the axes (1,2,3) then any of the constants s_{ijkl} in the one system of coordinates can be transformed to another system which has resulted by a rotation around the z axis as:

$$s_{1'1'1'1'}=a_{1'1}a_{1'1}a_{1'1}a_{1'1}s_{1111}+a_{1'2}a_{1'2}a_{1'2}a_{1'2}s_{2222}+$$
$$+a_{1'1}a_{1'1}a_{1'2}a_{1'2}s_{1122}+a_{1'2}a_{1'2}a_{1'1}a_{1'1}s_{2211}+ \quad . \ . \ .$$
$$. \ . \ . \ . \ . \qquad +a_{1'1}a_{1'2}a_{1'1}a_{1'2}s_{1212} \qquad (6.16)$$

if $a_{11}=\cos\theta$ and $a_{12}=\sin\theta$ and depending on the class of the elastic symmetry of the material these relations reduce to polynomial expressions of $\cos^4\theta$, $\sin^4\theta$, $\cos^2\theta\sin^2\theta$, $\cos^3\theta\sin\theta$, $\sin^3\theta\cos\theta$ and so forth. The mean values of the moduli in table6.2 were reversed to yield measures of the compliances and these were regressed by using $\cos^4\theta$, $\sin^4\theta$ and $\cos^2\theta\sin^2\theta$ which is applicable to an orthotropic material. The regression equation was:

$$s(\theta) = 0.0206\cos^4\theta + 0.0757\sin^4\theta + 0.0915\cos^2\theta\sin^2\theta \qquad (6.17)$$

with a correlation coefficient=0.823 and predicting maximum modulus along the circumference of 1/0.0206=48.54MPa and minimum modulus along the axial direction of 1/0.0757=13.21MPa. These predictions can be well compared to the mean moduli along the circumferential direction in test site-I chapter5 which was 46.25MPa with a standard deviation of 9.14Mpa and the one along the axial direction which was 13.63Mpa with a deviation of 4.47MPa.

For this particular test where the sample size was small at each particular angle (n=5) the behaviour of the medians could be more reliable. Thus the same method was applied to the medians of moduli data. The correlation was poorer at r=0.796 and the predicted maximum modulus at 0^o angle Emax=44.25MPa while the Emin=11.29MPa at axial direction.

The possibility was also examined if a lower power form of $\cos^2\theta$, $\sin^2\theta$, and $\cos\theta\sin\theta$ can describe the data, based on the idea that the material is essentialy a two dimensional structure. The correlation was worse indicating that this oversimplification should be avoided. All 3 fits of can be seen in fig.6.16a.

Cox(1952) presented a theory for a fibrous composite without a matrix. The elements were linearly elastic and the theory was ideally applicable for infinitesimal strains. Cox expressed the compliances as functions of the coefficients of periodic function which describes the fibrous distribution and was presented earlier in (6.8).

$$
\begin{aligned}
s_{11} &= [(2-a_2)(6-4a_1+a_2)-(2b_1-b_2)^2]/D \\
s_{22} &= [(2-a_2)(6+4a_1+a_2)-(2b_1+b_2)^2]/D \\
s_{12} &= -[(2-a_2)^2- 4b_1^2+b_2^2]/D \\
s_{16} &= -4[(2-2a_1+a_2)b_1+(2-a_1)b_2]/D \\
s_{26} &= -4[(2+2a_1+a_2)b_1-(2+a_1)b_2]/D \\
s_{66} &= 16(2+a_2-a_1^2)/D
\end{aligned}
\qquad (6.18)
$$

where $D= K[(2+a_2-a_1^2)(2-a_2-b_1^2)-(a_1b_1-b_2)^2]$

and K is a constant the product of the fibre modulus and density of fibres. This theory has the great potential of providing a link between the structure and the elastic behaviour if the fibrous distribution has been sufficiently described.

The 2-term and 3-term approximations to the fibre distribution by

using relations (6.9) and (6.11) were used to yield material constants a_1=0.682 for the 2-term and a_1=0.592, b_1=-0.327 for the 3-term expression.

The single constant a_1=0.682 gives the set of compliances:

$$s_{11}=0.021,\ s_{22}=0.057,\ s_{12}=-0.0130,\ s_{66}=0.0800 \text{ for } K=100 \qquad (6.19)$$

the values of s_{11}, s_{22} and $2s_{12}+s_{66}$=0.106 are reasonably compared to the coefficients of (6.17) which are the regressed estimates of these same quantities. The presence of only a_1 resulted in only 4 non-zero constants which apply to an orthotropic material.

If the 3-term expression is used then a_1, b_1 produce:

$$s_{11}=0.0222,\ s_{22}=0.0529,\ s_{12}=-0.0116$$
$$s_{16}=0.0035,\ s_{26}=0.0135,\ s_{66}=0.0857 \qquad \text{for } K=100 \qquad (6.20)$$

which by the presence of $s_{16}\neq 0$ and $s_{26}=0$ indicates the presence of an isoclinic material if the constants are expressed for the axes of elastic symmetry.

The use of the structure produced set of constants (6.19) and (6.20) gives the angular behaviour of the elastic moduli by using the relations:

$$(6.19):\quad s_{11}(\theta)=s_{11}\cos^4\theta + s_{22}\sin^4\theta + [2s_{12}+s_{66}]\cos^2\theta\sin^2\theta \qquad (6.21)$$

$$(6.20):\quad s_{11}(\theta)=s_{11}\cos^4\theta + s_{22}\sin^4\theta + 2s_{16}\cos^3\theta\sin\theta + 2s_{26}\cos\theta\sin^3\theta + [2s_{12}+s_{66}]\cos^2\theta\sin^2\theta \qquad (6.22)$$

where the abbreviated notation has been applied. These entirely theoretical and structure produced fits are shown in fig6.16b. The correlation coefficients were r=0.845 for relation (6.21) and r=0.822 for relation (6.22). Both these correlations of the fully predicted curves of fig.6.16b were better than the regressed ones of

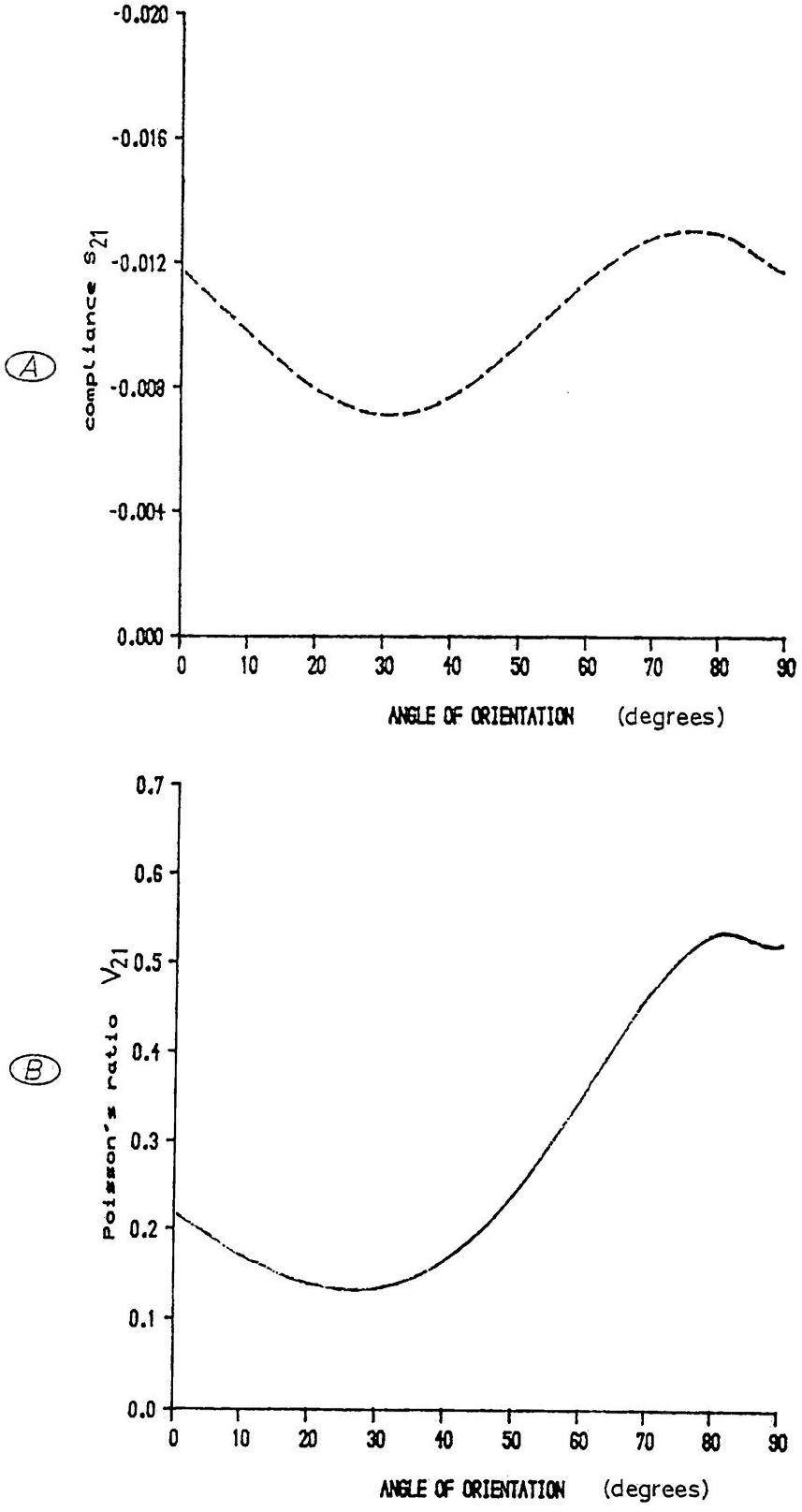

Figure 6.17: theoretically predicted variations with the angle of orientation of the strip for (A) the compliance constant s_{21}, and the (B) Poisson's ratio ν_{21}.

fig.6.16a. The prediction curve which resulted from the 3-term structural relation was qualitatively better in describing the variation of the tensile modulus with the angle of orientation of the strips.

6.7.2 Poisson's Ratio.

The successful application of the theory to the angular description of at least one technical constant raises hopes that the rest of the technical constants can to a certain extent be predicted by the use of the same route. By using the general rule for transformation (6.16) the angular behaviour of the compliance constant s_{12} is given as:

$$s_{12}(\theta) = s_{12}(\cos^4\theta+\sin^4\theta) + [s_{11}+s_{22}-s_{66}](\cos^2\theta \sin^2\theta) + \\ + [s_{16}-s_{26}](\cos\theta\sin^3\theta) + [s_{26}-s_{16}](\cos^3\theta\sin\theta) \qquad (6.23)$$

from which by also using (6.22) we can predict the angular behaviour of the Poisson's ratio $\nu_{21}(\theta)$ at any direction θ. The prediction of the variation of the elastic constant s_{12} and of the Poisson's ratio ν_{21} with the angle of orientation of the strip can be seen in fig.6.17.

6.8 DISCUSSION AND CONCLUSIONS.

Examination of the failure properties of a material provides a qualitative view of the composite nature of the soft biological tissues which present a complex rheological behaviour. In this particular application it was proved that the biaxial inflation test can sufficiently identify the axes of material symmetry. In achieving this the effect that geometry (as by initial curvature) has on the biaxial test has to be of a secondary role. Significant curvature of the tissue can result in false identification of the directions of the axes of elastic symmetry. In general the biaxial inflation test is of

great qualitative importance but it may have its limitations in identifying axes lying close but not exactly on the two normal directions, and this may be the case for isoclinic materials of which the principal directions are not in general normal to each other.

The pericardial material was undoubtedly anisotropic. The rubber sheets which were rendered anisotropic by prestretch in chapter4 for validation of the inflation test, were thought of possesing at their reference state both a stress and strain rosette aligned to the prestretch direction. Depending on the uniformity of prestretch the strain rosette can be a perfect ellipse with the shape of the associated stress oval being modulated by the degree of linearity between the stress and strain. Independently of the shape of those rosettes one thing was certain with rubber; their axes were absolutely aligned as the production of one was causing creation of the other. In the case of the pericardium this claim which would result in a simple form of orthotropy had to be proved by the complete alignment of its respective stress/strain rosettes. Such an alignment existed to a certain degree but the use of Cox's theory and the 3-term formula to describe the fibre distribution strongly indicated that the material is isoclinic and thus any alignment of the axes is only relative.

By the use of the angular simple tension test of this chapter it became feasible to predict the behaviour of the material outwith the axes for the 3 parameters examined. It is also interesting to notice that the complete multidirectional behaviour could result from tests in only the orthogonal directions.

The U.T.S.(nominal stress value) was roughly a third of the terminal modulus along the stronger direction, and roughly a quarter of the terminal modulus along the weaker direction. A theoretical

prediction based on interatomic bonds for engineering materials predicts a strength=E/5, with detailed consideration of interatomic forces it reduces to E/20, while efficient composites reach only E/50, ductile materials a ratio E/100 and brittle materials only E/1000(Wainwright et al,1976). By all these standards the present biological composite (pericardium) has unmatched failure features in either direction if compared to any manmade material.

The nearly linear relationship between any two of the parameters especially of the modulus versus the U.T.S. may be of practical interest. It showed that the behaviour of one of the parameters can be predicted by another, and thus for the construction of valve leaflets it signified that the Young's modulus (a measure of the stiffness) of the material, which can be also measured by a non-destructive test, can sufficiently predict the value of the U.T.S and the stronger direction.

The anisotropic properties of pericardium make it an even better candidate for the construction of bioprosthetic valve leaflets. The properties of the natural leaflets are examined in chapter8. With the present investigations it is reasonable to suggest that alignment of the material on the moulds for the production of the leaflets should be made along the axes of geometrical symmetry for the mould and with the stronger direction being aligned to the direction of maximum stresses expected in operation of the valve.

7.1 NON-INVASIVE OPTICAL OBSERVATIONS.

7.1.1 Introduction.

In the previous chapters the pericardial samples when examined at two different modes of deformation exhibited mechanical anisotropy. The external macroscopic appearance of the tissue did not reveal any features which would indicate that preferential directions should exist in the mechanical characteristics of the tissue. This must have been the reason why most workers in the past have treated pericardia from all species as isotropic although some results of mechanical tests had indicated that anisotropy should be seriously considered(chapter3). Both the biaxial inflation test and the multidirectional uniaxial tensile test gave results which suggest the existence of an anisotropically structured tissue without specifically proving this assumption.

In order to provide insight into the tissue structure, optical microscopy on whole tissue specimens was employed. Unlike the uniaxial tests which irreversibly damaged the tissue structure by cutting it in strips, optical microscopy was non-destructive of the samples and thus the pieces of tissue could always be available for subsequent tests. A simple biaxial test also preserved a specimen intact but still affected the strain history of the material. In these respects optical examinations were thought to be both non-invasive and non-destructive means for observations.

The technique was based on the natural birefringence by collagen fibrils when the specimens are placed between crossed polarizers. The report by Diamant et al(1972) on tendon suggested that the incorporation of individual birefringent elements within the tendon structure gives rise to different optical patterns as observed on the surface of the larger organised tendon subunits. Depending on the

level and the form of organisation Diamant et al were able to predict that the fibrils inside a fibre bundle had a planar three dimensional configuration while the fibre bundle had a cylindrical shape. A later report by Kastelic et al(1978) revised the tendon structure and used polarised optical microscopy as a consistent examination method of the tendon structure up to the level of the fascicles of fibrils.

Of special importance were the observations of Broom(1977,1978a,b) on fresh, frozen and fixed heart valve tissue by the use of polarised light microscopy. There, it was shown that optical observations can be related to structural features, the fibrous organisation and the state of deformation of the structure. These reports were the first on a two-dimensional soft tissue and the growing confidence on such observations led Orberg et al(1983) to build a possible model for the organisation of collagen fibrils in the intestine by simply examining the optical pattern viewed from the tissue's submucosa surface. Deformations of the tissue were also shown to relate to alterations in the morphology of the pattern. Unfortunately this report was not followed by a histological examination of the tissue, nor were the mechanical properties of the material correlated to the observed pattern.

7.1.2 The Optics of Birefringent Fibrils.

All previous workers decided after the first observations that the angle formed between the plane of polarisation of light and the direction of the long axis of the collagen fibrils determines the creation of the optical effect. The physics behind this was never examined in detail probably because the final result was more than satisfactory.

Birefringence is an optical property of anisotropic crystals in which the electrons can move with different amounts of freedom in different

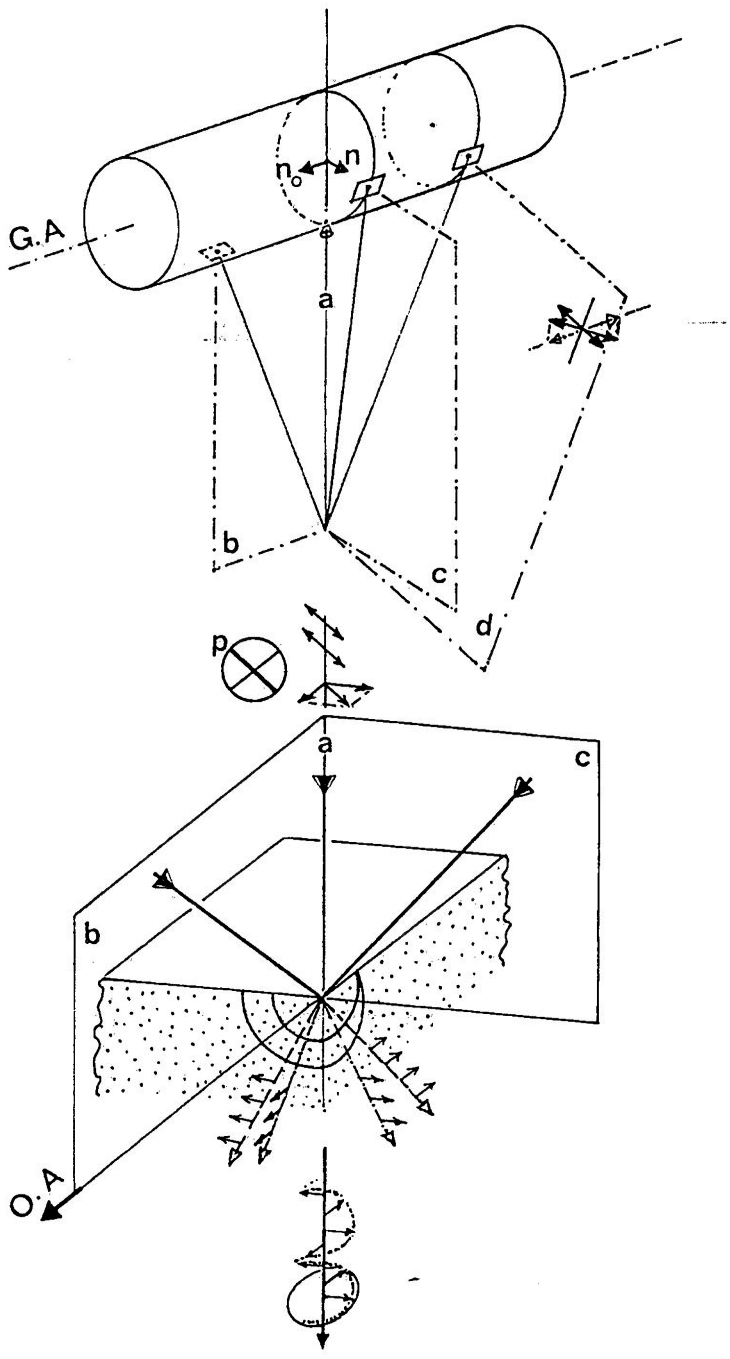

Figure 7.1: Illumination of a differential segment of a fibril which is made of a positive uniaxial birefringent material.

directions. This means that the material has an action on any light beam passing through it which depends on the direction of the beam and on the orientation of the plane of vibration with the axis of the crystals. The direction within the crystal along which the effect does not occur is known as the optic axis. Occasionally, as in the case of the Calcite($CaCO_3$) crystals, one can immediately tell the direction of the optic axis because it coincides with an axis of symmetry of the external shape of the crystal.

The collagen fibre is an assembly of thread-like macromolecular units, which are laterally glued to form a microfibril, a subfibril, a fibril, a bunch of fibrils and the other higher forms of collagen organisation (Eyre,1980). Up to the level of the fibril collagen possesses a cylindrical geometry with the subfibril constituents being arranged around its long geometric axis. For reasons of symmetry we can assume that the main geometric axis of the fibril is also its only optic axis(uniaxial). The anisotropy takes the form of two refractive indices one along the optic axis and the second perpendicular to it. For collagen the refractive index along the fibril is the larger of the two(Hukins,1984) and thus the fibril behaves as a positive uniaxial birefringent crystal. The difference between the two indices is called the intrinsic (material) birefringence(Dn) and takes generally small values (i.e $(6\pm1)\times10^{-4}$ for articular cartilage; Yarker et al,1983).

In fig.7.1 illumination of a fibril with polarised white light is considered. The geometric axis(G.A) is considered the optic axis(O.A) of the crystal as well. Instead of a collimated parallel beam a point source can be considered in order to examine the different possible cases. In each case the planes of incidence for the light were drawn and numbered a,b,c,d. For the description of the behaviour of the

beams and the propagation of wavefronts in anisotropic media the principle of the wavelets (Huygens) can be employed. A beam forming an angle of incidence with the surface of an element of the material will refract into two, of which the ordinary ray is constructed from spherical wavelets and the extraordinary beam from wavelets which are ellipsoids of revolution and are included in the spheres (positive crystal). Ellipsoids coincide to the spheres on the optic axis where their velocities are equal. The split original beam gives two, which are polarised in two mutually perpendicular planes which are the plane of incidence for the original ray and a plane normal to it. The amount of light split in each of the two rays depends on the plane of polarisation of the original ray.

In case-a light falls normal to the optic axis and along the normal to the surface. There is no split in the beams but the component which is parallel to the optic axis follows the ellipsoid wavelet and is retarded compared to the component of the spherical wavelet and this will in general produce elliptical polarised light which will pass through the analyser. The only condition for light not to pass the analyser would be the alignment of polariser and the optic axis.

In cases b,c light will be transmitted through the second polariser (analyser) unless the polariser is parallel to the optic axis of the material. This inhibits the production of the ordinary beams which are aligned in the direction of the analyser and thus would allow a fraction of the original ray to pass through the analyser.

The last case-d is the most general of all and applies in illumination of any differential fibre segment even in fibres of three dimensional wavy configuration. In this case the ray may be considered as one of many possible combinations of two rays like b and c. It will create two rays which are polarised along and perpendicular to its plane of

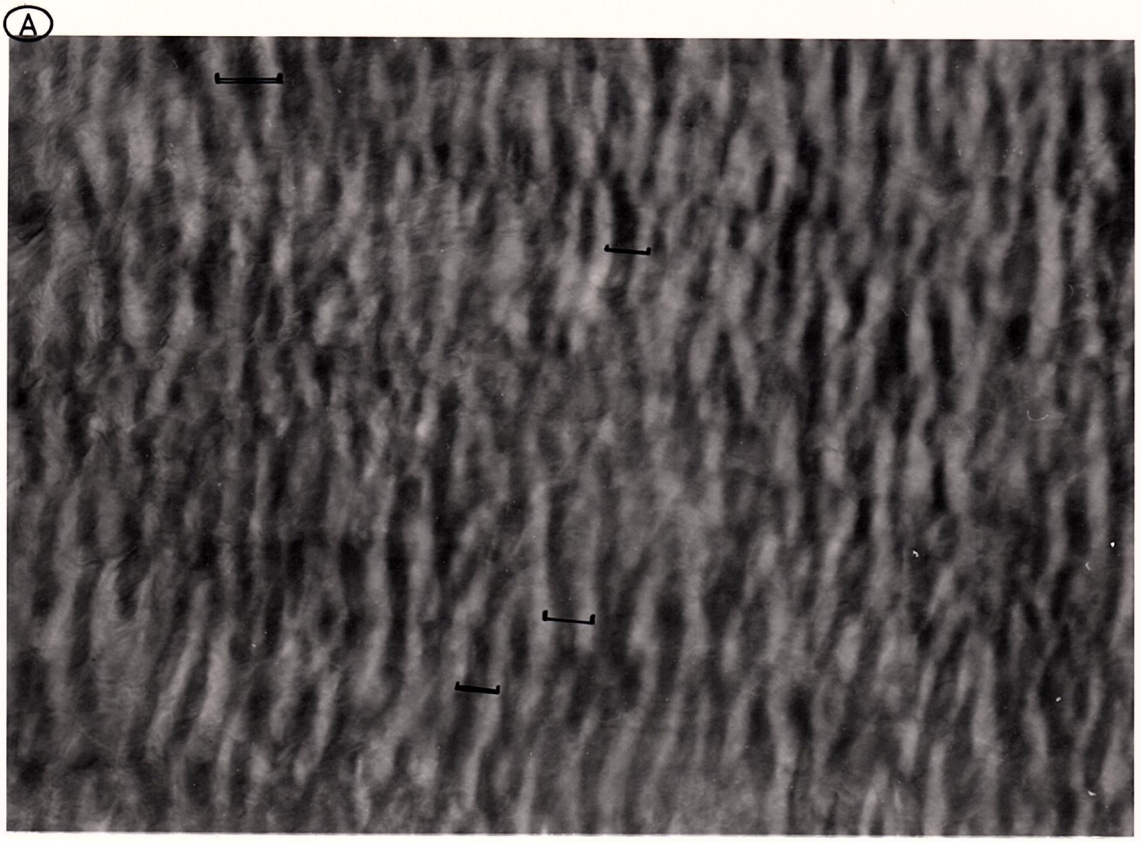

Figure 7.2: Photomicrograph of optical pattern; a)as seen from the epipericardial surface, b)as seen from the serosal surface.

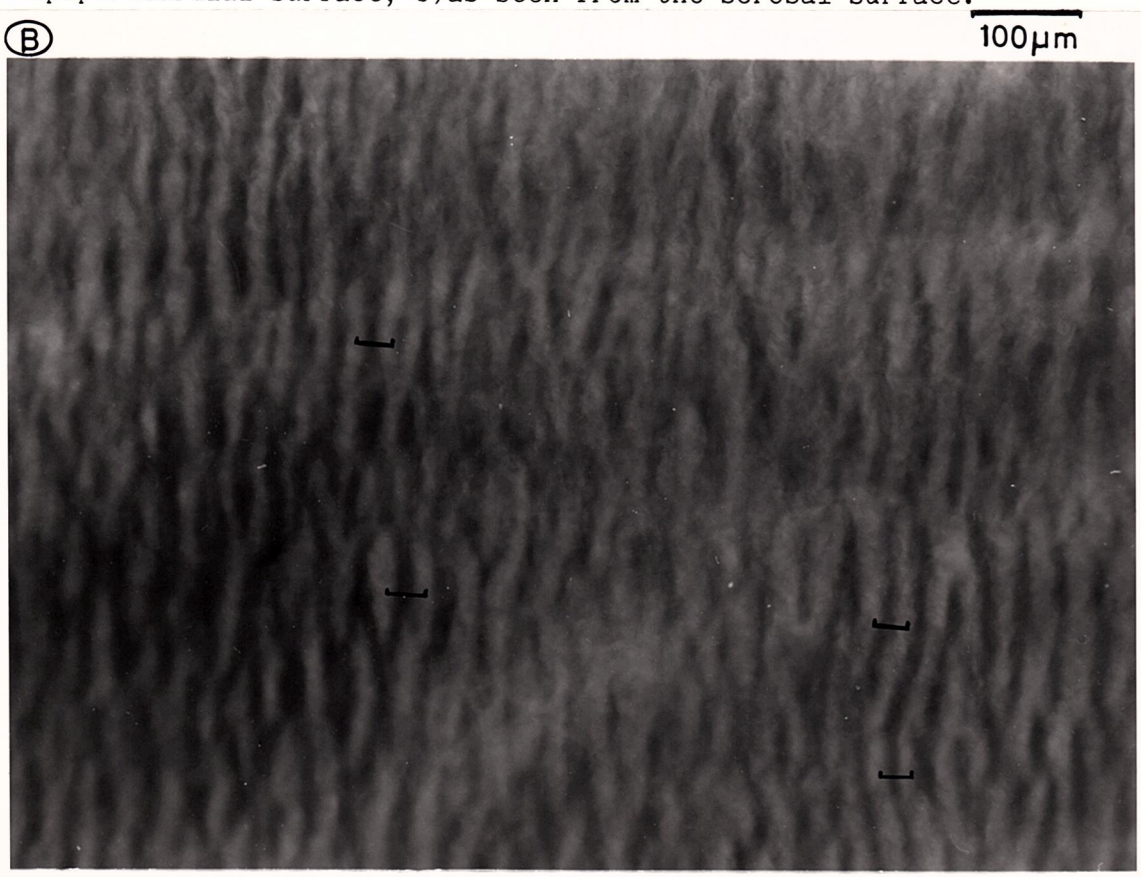

incidence and can be projected in components along and normal to the optic axis to yield exactly the same prediction: that unless the polariser is parallel to the optic axis, light will pass through.

7.1.3 Inspection of the Pericardial Membrane.

Samples of fresh pericardium were examined in polarised light using an Ortholux-Leitz Wetzlar optical microscope equipped with a photographic camera and a set of polarisers.

The samples showed (fig7.2a,b) relatively regular array of light and dark bands. The image was qualitatively different when views were taken from the two surfaces. The epipericardial pattern (fig7.a) when not obstructed by fat globules was sharper and present everywhere on the specimen's surface, while the serosal pattern (fig7.2b) was more indistinct and dissapeared at some points. Both were surface patterns as checked by focussing to produce a clear image. However the epipericardial pattern was produced directly from the superficial fibres which could also be viewed with polarised reflected light, while the serosal pattern could only be seen with transmitted light.

The spacing or periodicity of the light/dark banding also depended on the surface viewed. The histograms in table7.1 are measurements of the size of this periodicity in μm. Photos from three pericardial samples from test site-I were used and 4 measurements of the period of the pattern were performed in each photo. The periods were significantly different confirming the visual impression that the serosal pattern had closer banding.

It appeared in all specimens that the direction of the banding of the optical pattern was directly related to the direction of the mechanical axes of anisotropy as identified by the biaxial inflation test. In particular it was aligned along the axial direction and thus dark and light zones were normal to the circumferential direction of

Table 7.1: There was a significant difference in the size of the periodicity of the optical pattern between the epipericardial and serosal views.

Histograms: Epipericardial view			Serosal view	
Midpoint	Count		Count	
22.0	0		1	*
25.5	1	*	1	*
29.0	1	*	2	**
32.5	4	****	6	******
36.0	4	****	5	*****
39.5	10	**********	5	*****
43.0	8	********		
46.5	3	***		
50.0	1	*		

periodicity of optical pattern measured in μm

Epipericardial pattern: mean ± st.error mean=38 ± 1.0 μm

Serosal pattern : mean ± st.error mean=33 ± 0.9 μm

the sample. This was consistent in all mechanical tests(chapters4,5) and thus the optical pattern soon became an optical result which could reliably help to preview the axes of mechanical anisotropy before the test and identify their directions even without a test.

The coincidence to the mechanical axes was not absolute and consistent from the serosal surface, but it was unmistakable from the epipericardial site.

The method was used to examine the specimens prepared to test mechanical properties of the rest of the areas (II,II′,III) on the sac. Areas thicker than 0.5mm were uniformly translucent without any particular pattern being formed at any depth of focussing. With the exception of these thicker areas which did not transmit enough plane polarised light to form this birefringent pattern, all other areas exhibited an alignment of the direction of the dark/light bands with the weaker axis at each site. A map of the direction of the optical pattern was constructed (fig7.3) similar to the map of mechanical anisotropy (chapter5). In fig.7.3 the map contains the average directions of the optical banding seen in all the membranes which have been mechanically tested in chapters4,5,6. The single arrows indicate a predominant direction of banding for both the epipericardial and the serosal pattern, while two arrows indicate that either the two patterns did not coincide or that there was a sac to sac variation at these particular sites. The structural basis of both the optical and mechanical anisotropy was investigated by histological examination of the tissue.

7.2 HISTOLOGICAL EXAMINATION

7.2.1 A Review of the Previous Work.

The most salient features of the structure of mammalian pericardium have been adequately described in reports by Ishihara et

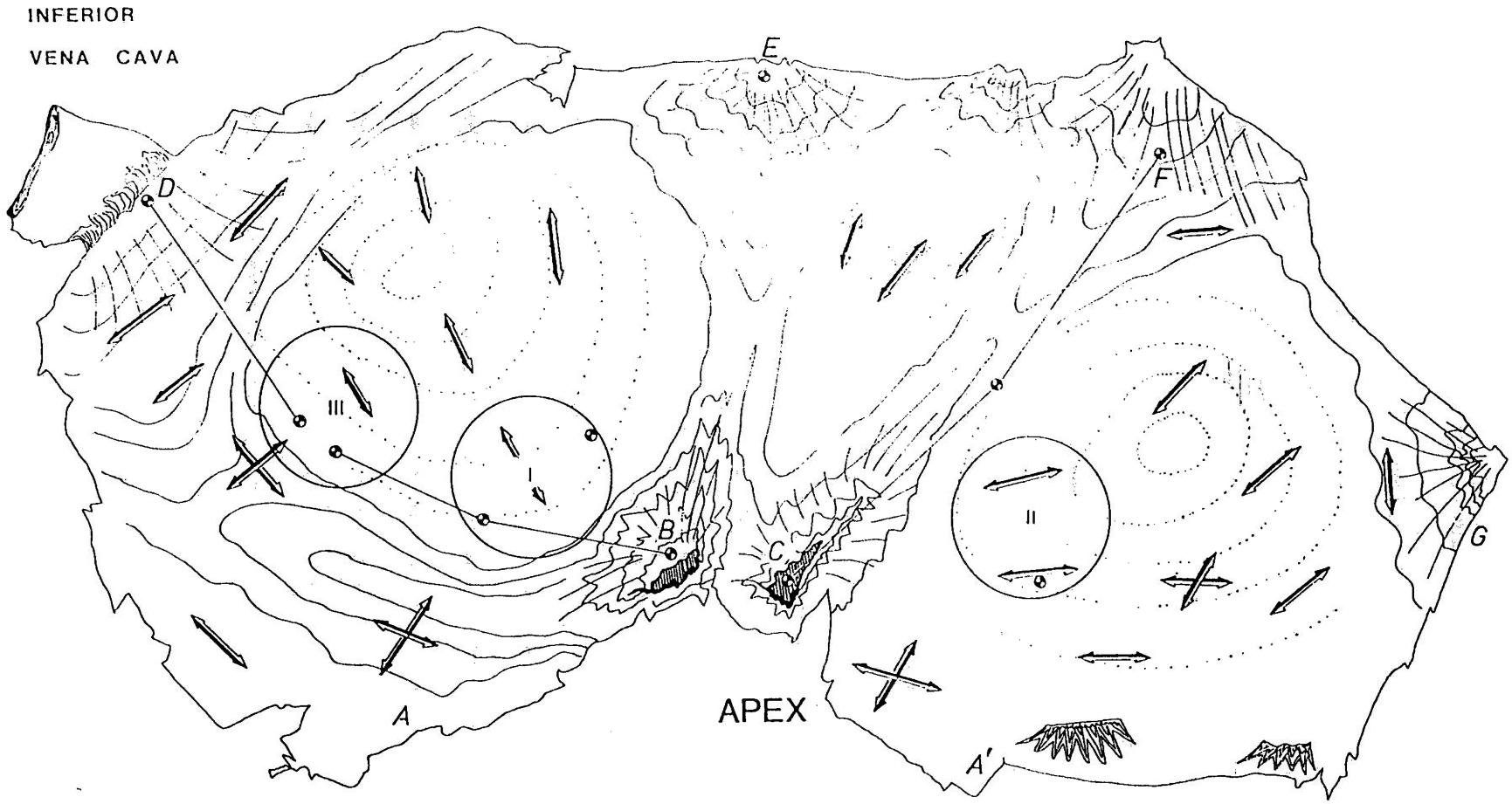

AREA : I II III
Thickness : (0.33±0.03)mm (0.38±0.03)mm (0.40±0.03)mm

: Optical Pattern

: Sternopericardial Ligaments

Reference points

lines of initial curvature

Figure 7.3: Pericardial map.

al(human,1980; bovine,1981), Allen et al(1984) and Fentie et al(1986). The impetus for the histological examination of bovine pericardium in particular was the potential of this tissue to become a useful biomaterial. These workers examined the ultrastructure and microstructure of the tissue by performing purely histological examination. The examination was isolated from the mechanics of the tissue and its macrostructure as defined by the arrangement and orientation of the fibrous elements.

Isolated pericardium which has been cleaned from the fat deposits overlying its epipericardial surface, consists of the tunica fibrosa (fibrous layer) and the tunica serosa(layer of mesothelial cells). Ishihara et al(1981) distinguished the fibrous contents lying on the epipericardial surface as a separate epipericardial layer, but this is not generally accepted. The fibrosa consisted of collagen bundles which varied in diameter across the tissue thickness and averaged 10 to 15μm on the epipericardial side. Each bundle was made up of fibrils which, when examined with transmission electron microscopy had diameters varying from 300 to 1400Å. Elastic fibres were also present being relatively larger at 0.05μm to 2μm in diameter. The space between the collagen bundles was filled by water and a matrix of proteoglycan granules and spicules which occasionally formed a loosely arranged network extending between the fibres. Tissue cells were abundant being mainly fibroblasts, histiocytes and mast cells. Neural and vascular elements were also present. The serosa consisted of a single layer of flattened mesothelial cells approximately 10μm in size. The cells formed intercellular junctions, had a surface covered by numerous microvilli and were anchored on a thin basal lamina. The lamina, at the interface of the cells and the fibrosa, was also fibrillar consisting of disorganised microfilaments firmly anchoring

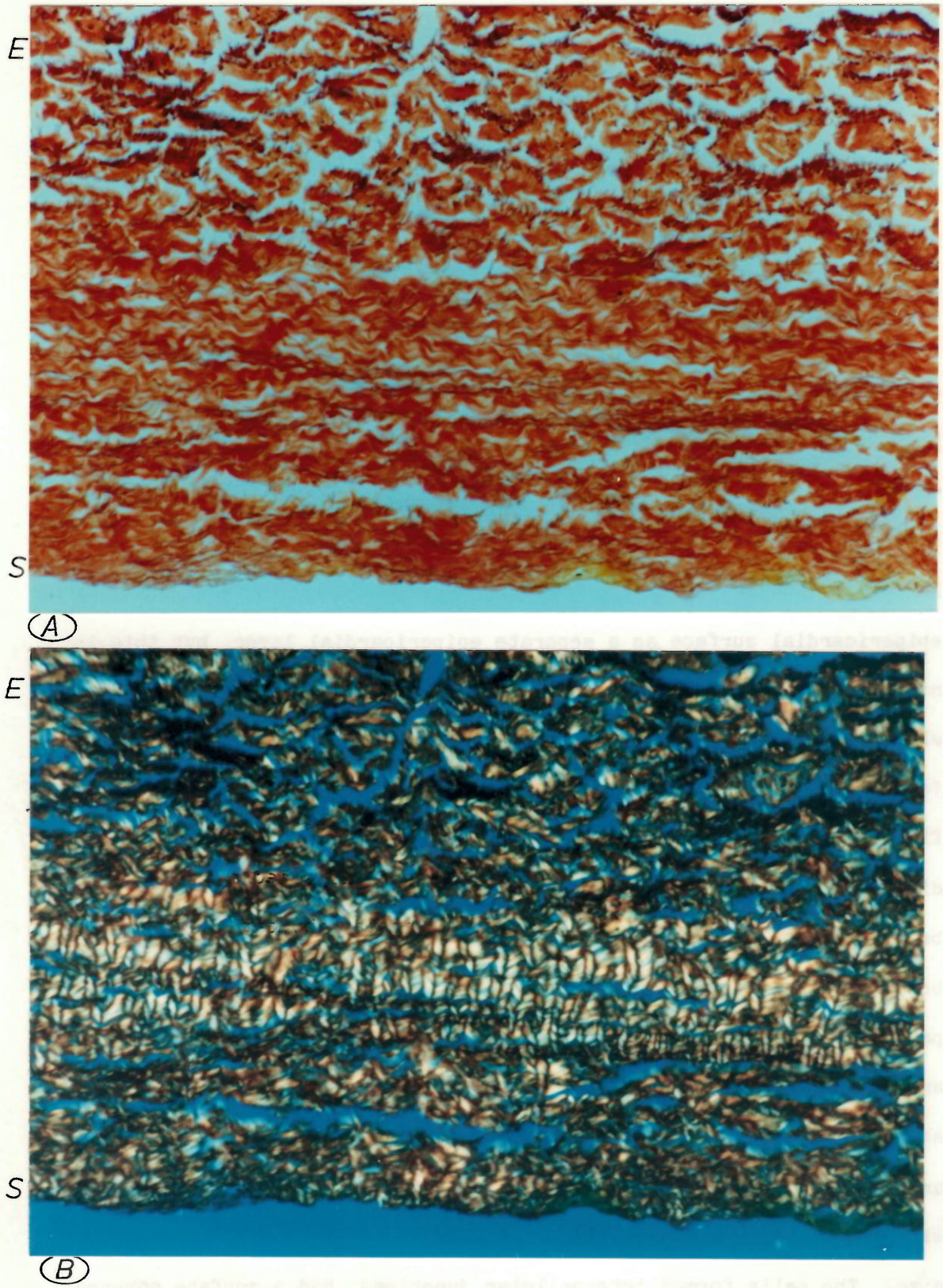

Figure 7.4: Transverse section of bov. pericardium sample. Stained by picric acid and orcein. (E)epipericardial surface, (S)serosal surface. a)polarisers in parallel, b)crossed polarisers.

the epithelial cells. During deformation of the tissue the cells became elongated along the direction of load without being detached from the membrane.

7.2.2 General Structure as seen in Transverse Sections.

Fig.7.4a,b show transverse sections of bovine pericardium. Prepared as 5μm thick paraffin mounted sections originating from test site-I. In fig.7.4a the section was stained with orcein and subsequently counterstained by a picric acid solution(Drury et al,1967,p.44) to differentiate the fibrous elements. As a result the elastic fibres have been stained brown while all other fibrous constituents counterstained yellow. The structure appeared to be laminar and consisting of more than 3 layers. The middle layer(b) was cut at a small angle to the long axis of the fibres which appeared running from left to the right side of the section. Layers in region (a)-above and (c)-below have been sectioned at a higher angle to the long axis of their fibres and thus it was more difficult to discern between different layers inside these regions. At the top epipericardial region the bundles were more dispersed resulting in a less dense structure. The elastic fibres appear abundant and seem to aggregate in numbers to the outer side of the bundles and be more coarse in size. Towards the serosal side they tend to be thinner and concurrent to the collagen fibrils. The epipericardial fibrils have been cut in clusters here and there, this must have been a result of either them having a three-dimensional arrangement (by forming angles to both the plane of the section and also diving to be integrated in the fibrosa), or having a three- dimensional waveform at this level of organisation.

By the use of polarised light(fig7.4b) the middle layer(b) exhibited a periodic extinction pattern running along the length of the fibres.

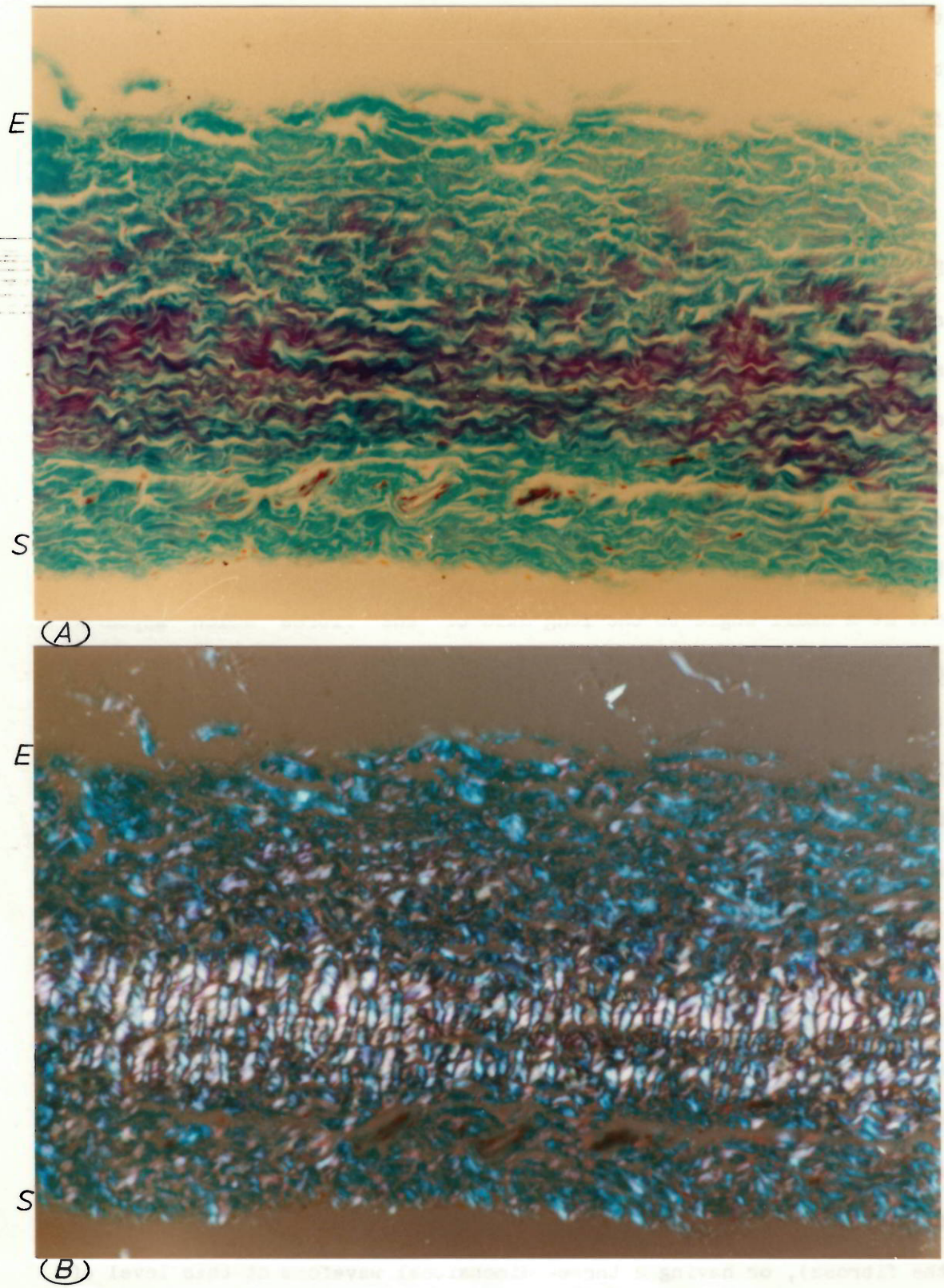

Figure 7.5: Transverse section of bov. pericardium. Stained with a picro-polychrome technique(Shoobridge,1983). (E)epipericardial, (S)serosal. a)parallel polarisers, b)crossed polarisers.

The layers at (a) and (c) demonstrated irregular birefrigence indicating that they had been cut short by the microtome blade. The use of polarised light was very helpful in recognising the presence of a greater number of layers within this section. Elias and Boyd(1960) claimed that the pericardial fibrosa included 3 basic layers. In view of section in fig7.4 a possible explanation for the cause of their conclusion could be the presence in every section of a layer sectioned at a small angle to the direction of its fibres and thus simply by its different appearance from the rest yielded an optical image where the fibrous structure had 3 optically different regions.

In fig.7.5a,b another transversely cut section has been stained with a picro-polychrome technique which has been suggested for routine use by Shoobridge(1983). This technique could clearly differentiate constituents in complex structures and had the great advantage that fixation of the tissue could be performed at the first stages of the staining procedure and thus even sections that had been prepared fresh could be treated. The multilayer structure was again present with fibres belonging to different layers being differentiated by colour(fig7.5a) as well as by their birefrigent image(fig7.5b). There was an uncanny relationship between the amount of birefrigence demonstrated in some areas(judged quantitatively) and the red appearance of these same regions. In this circumferential strip and by some yet unknown mechanism the fibres aligned closer to the circumferential direction and of which longer birefrigent segments have been included in the section, also stained red on a blue/green background. The cytoplasm of the mesothelial cells in the serosal layer had been stained red/orange and the same was true for the other cells in the interior of the fibrosa. The basal lamina(d) was detached at places and at a relatively small distance above the

serosal surface a number of transversely cut blood vessels were present. In the vicinity of the vessels there was a complete lack of birefrigence in the surrounding collagen as checked with polarised light(fig7.5b). In contrast with the valve leaflet tissue which is mostly avascular(Ishihara et al,1981) the pericardial tissue had blood vessels dispersed along its entire thickness. In view of the fact that these vessels pass into the tissue from the mediastinum it was easier to explain why in a number of sections they appeared to follow a diving course from the epipericardial surface to the serosal one. The blood vessels entered from above, from the rough epipericardial surface where larger fibre bundles existed which can been seen projecting away from the section in fig.7.5a. Closer to the serosal surface the vessels became parallel to the surface, reduced in diameter and gradually disappeared.

From an overall point of view the pericardial fibrosa seemed to consist of densely packed collagen fibres stack together to form what appeared to be a homogeneous structure. The porcine valve leaflet tissue has in comparison (Ishihara et al,1981) a distinct 3 layer structure with the middle layer being loose and bound by dense fibrous layers on either side. From a mechanical point of view it was clear that the pericardial fibrosa is the dominant element in the mechanical response of the tissue in loading, with the role of the cellular and vascular components being insignificant. It was also clear that although transverse sections could include the full range of the constituent materials, which is primarily the interest of the histologists, they could not be used to clarify the orientation of the fibres in the plane of the membrane. Such investigation would require the production of sections which would include an image of the fibres along their length and because the layers were presumably running

parallel to the surface it was decided that sequential sections be prepared parallel to epipericardial surface.

7.2.3 Histology on Parallel to the Surface Sections.

The fresh pericardial samples were very flexible and thin plane specimens were extremely flexible and thus difficult to manipulate. Initial efforts using the standard method of embedding the samples in paraffin blocks showed that orientation of the sample within the wax bath was crucial if sections were to be cut parallel to the tissue surface.

7.2.3.1 Frozen sections. The first method for preparing the necessary specimens was the use of frozen sections of the fresh material. Specimens were cut from the pericardial membrane in an asymmetrical trapezoidal shape and laid flat on the flat top surface of a cryostat with the epipericardial surface upwards. The stage of the cryostat bearing the specimen was levelled by appropriate adjustment and thus the microtome knife travelled in planes parallel to the epipericardial surface, cutting the tissue in parallel sections. The trapezoidal shape of the specimens was chosen because it allowed identification of the margins(right/left) and the surfaces(upper/lower) of the prepared sections in the floatation bath and for mounting on the slides.

With this technique rapid freezing with liquid CO_2 rendered the sample under examination rigid within seconds. The fibrous structure of the tissue itself determined the thickness of the sections. The mounting medium in this case was the frozen watery ground substance which thawed upon contact with the warmer solution of the floatation bath and thus turned the sections flaccid and difficult to handle. It was found that sections had to be at least 30μm thick if they were not to to disintegrate in smaller pieces and be mountable. The critical

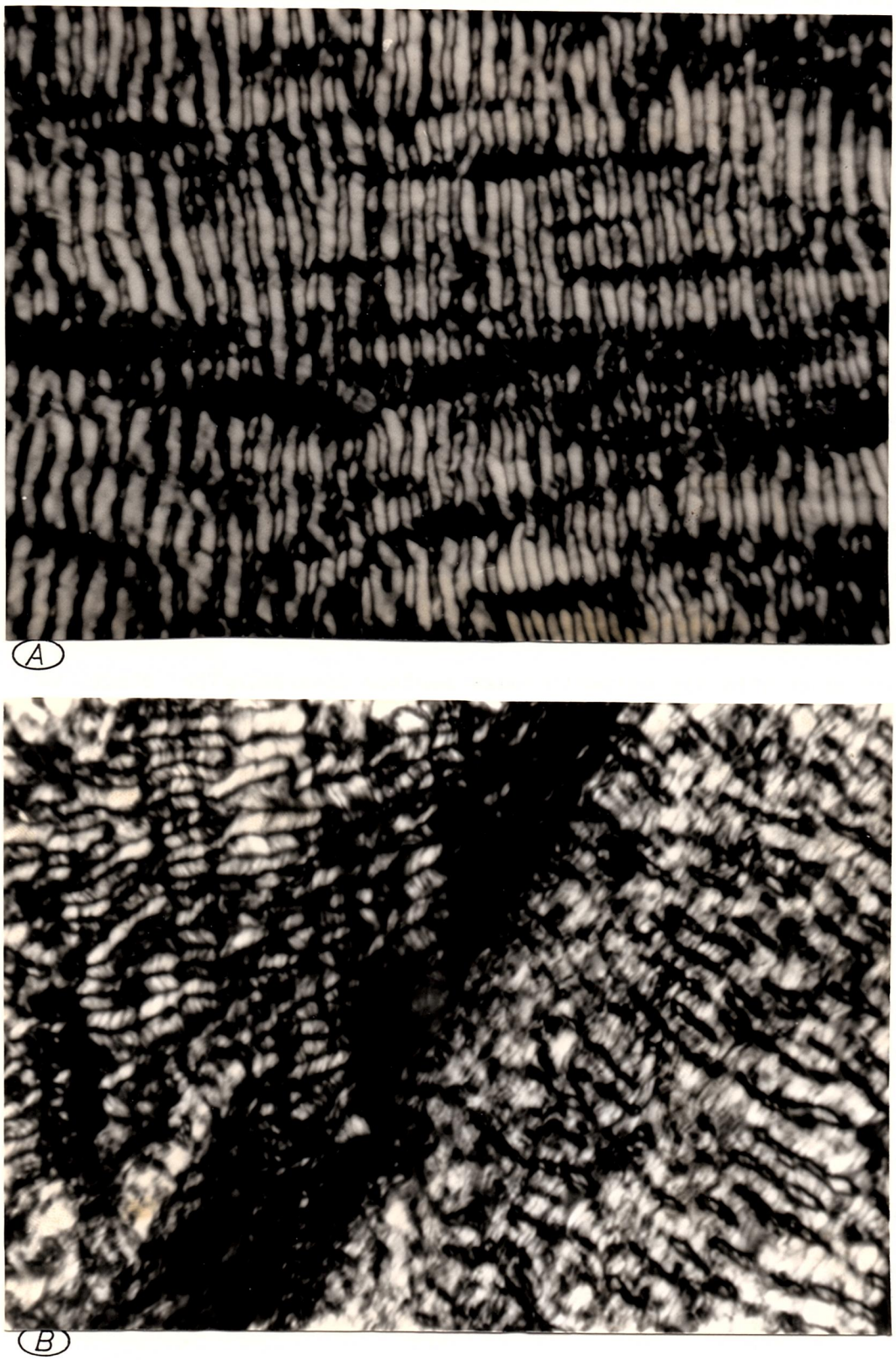

Figure 7.6: a)a fixed/frozen section of the inner fibrosa mounted in xylene, b)two differently oriented layers of the pericardial fibrosa.

thickness of the sections with this technique is very much a matter of the rigidity of the sectioned material. The presence of an increased number of native or even artificially induced cross-links may allow the preparation of even thinner sections. Bovine pericardium samples fixed in formalin for 7days allowed 20μm thick sections to be cut. A frozen section of the fixed material is not without its artifacts which can be caused by frozen crystals of the fixative or by shrinkage accompanying fixation of any fresh tissue. A particular problem of those preparations was the adherence of the section to the glass slide. Fresh sections adhered sufficiently and remained adequately flat upon dehydration but they washed off the slides when put through the different staining solutions. The fixed sections used to unstick at places even during dehydration probably due to shrinkage of the section. Dissolving gelatin in the water bath did not solve the problem because the forces which developed upon dehydration appeared to be much stronger than the adhesive action of gelatin. A thin layer of albumin spread on the glass slide was necessary to solve the problem. Care was required to apply a very thin layer of albumin because occasionally stains also stain albumin and may obstruct the view of the section.

Fig.7.6a shows a fixed/frozen 20μm thick section, mounted in xylene beneath a coverslip. Kastelic et al(1978) noted that collagen fibres may appear opaque, translucent or transparent depending on the index difference between the fibres and the surrounding medium. The presence of xylene enhanced the clarity of the polarised light image. When the dry sections were uncovered and surrounded by air there was considerable diffusion of light, especially at places were collagen fibres had been cut and their free ends were loose. There was a fine parallel arrangement of collagen fibres in bundles 15-20μm wide, which

were crimped in register. Along the waveform of a single fibre there were alternative dark and bright segments which because of the lateral registration of neighbouring fibres in synchronous crimp created dark and light zones normal to the long axis of the fibre bundle. Rotation of the crossed polarisers caused the dark and light zones to travel along the bundles' length, coinciding with the long segments of the waveform or with the peaks and troughs of the crimp. This was strong evidence that the birefrigent collagen fibre remained dark only at those segments which were parallel to the direction of one of the polarisers. This was perfectly in accord with the speculations made earlier in this chapter. There was no doubt that the optical pattern seen across the thickness of the whole mebrane was a result of superposition of successive extinction patterns of the parallel sections. The extinction pattern within each of the sections was not always consistent and presented patches of fibres coming together at different orientations as in fig7.6b. In areas of some sections where fibres from two successive layers were overlapping their extinction patterns contributed destructively to an overall optical pattern across the 30μm thick section.

Scanning electron microscopy(S.E.M) was used to examine the morphology of the surface of the inner fibrous layers of the tissue. The S.E.M samples originated from the same test site-I and where fixed/frozen cut in sequential sections. Albumin was used to stick them firmly on small round glass slides which were less than 1cm in diameter and could fit on the top flat surface of the aluminium stubs used to carry the specimens in S.E.M. The specimens underwent the standard preparation of critical point drying and covering with a thin surface layer of gold-palladium alloy. In fig.7.7a-d layers(sections) 1, 3, 6, and 8 (from a series of 9 sections) are presented in an

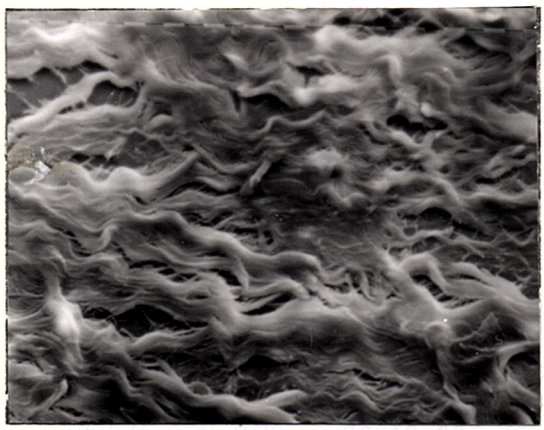

a-section 1, x320

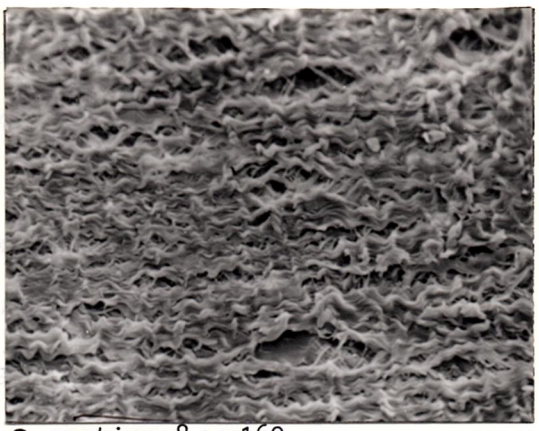

e-section 8, x160

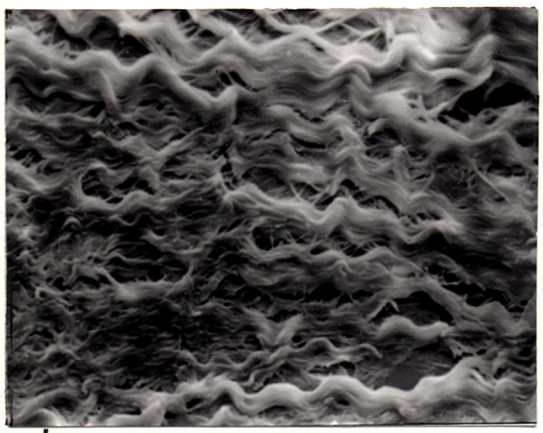

b-section 3, x320

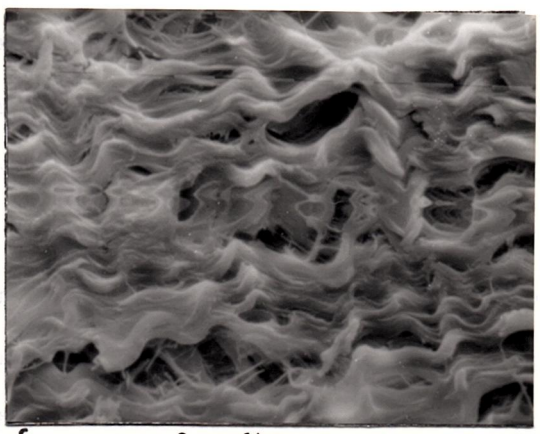

f-section 8, x640

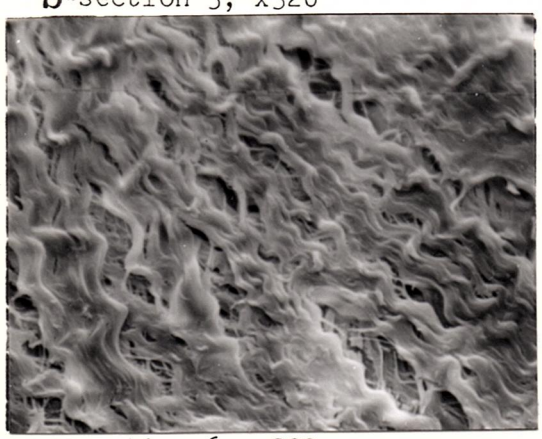

c-section 6, x320

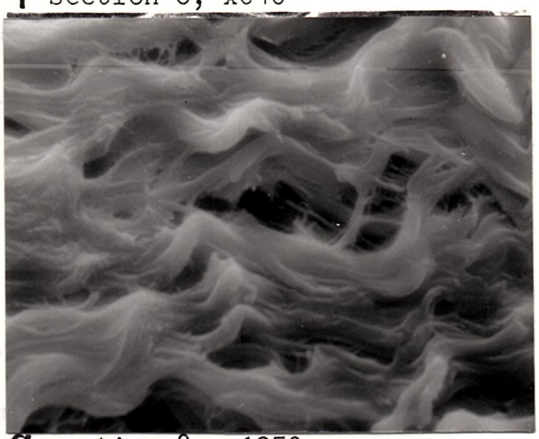

g-section 8, x1250

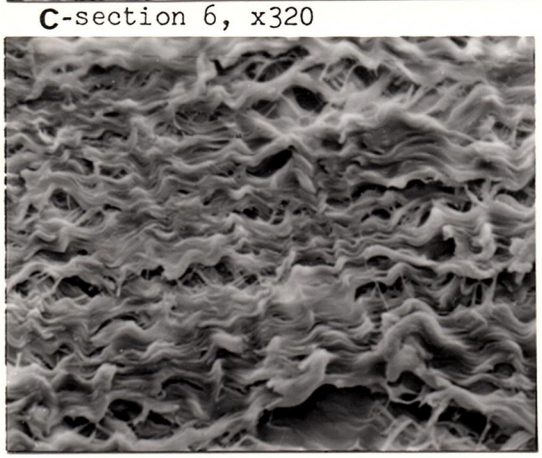

d-section 8, x320

Figure 7.7: S.E.M. photomicrographs of successive layers from the epipericardial to the serosal surface of the tissue. Sample originating from test site-I, the circumferential direction is from left to right. The gap in photo-g is probably site of depleted fibroblast in preparation.

original magnification of x320. The layers in between (2,4,5,7,9) were kept for light (polarised and reflected) microscopy. Fig.7.7e-g are close-up views of a single layer-6.

The structure appeared to consist almost entirely of fibres with some areas where nerve trunking and the sheaths of blood vessels had been sectioned. The main fibrous constituent elements were collagen and elastin and at least in the present S.E.M photos no real identification and/or distiction between these fibres could be seen. There was a controversy about the level of organisation of collagen and elastin and especially their respective orientations since Ishihara et al(1980) reported that elastic fibres had been seen to cross collagen fibres at right angles. This appeared to be adopted by other workers who did not commit their own experiments (Reece et al,1974). Such a relationship was not observed here, while the detailed examination of the orientations of these two constituents was planned to take place later by differential staining and light microscopy on parallel sections.

The series of S.E.M photomicrographs suggested that an organised fibre arrangement occurred at the macrostructural level. Fibre bundles inside each layer showed a predominant orientation along one direction. In layers1,3,8 for this sample from site-I this direction was almost circumferential. Fibre bundles in layer-6 were at an angle of 50°-70° to the circumference. The preferential orientation was evident in particular at lower magnifications (i.e.photo-e, fig7.7). At the level of the fibrils as seen by T.E.M observations Allen et al(1984) described a tight parallel packing of the fibrils inside a bundle and a relatively larger average dimension for the bundles of the epipericardial than in the serosal side. This is evident in the a comparison of fig7.7a with fig7.7d. Bundles on the epipericardial

side were coarser and more diversely oriented with their general orientation from left to right in the photo(circumferential). Bundles on the serosal side were more densely arranged presenting a smaller crimp and were more uniformly and consistently oriented along their preferential orientation for this layer which was again circumferential.

The crimp was measured from the present photos and at 5 sites in each photo and found to be section1:30.1±1.6μm, section3:28.5±1.6μm, section6:26.2±2.8μm and section8:22±1.9μm. The differences were significant between any two of the sections(Ttest, p=0.05) and not only between the top epipericardial and the bottom serosal section. This favourably compares with the previously existing difference between the optical patterns (table1) as viewed from either surface. In the present case the difference between the size of the epipericardial and serosal crimps was relatively larger than the difference between the respective periods of the optical patterns. This was probably in accordance with the previous suggestion that the pattern reflects the fibril orientation of more than one superficial layer on either side. The equivalent of this idea is considering the epipericardial optical pattern to result from a superposition of extinction patterns of sections1 and 3 and the serosal optical pattern from a similar superposition of sections6 and 8. This would have reduced the difference between the two periodicities to the levels observed earlier(table7.1).

The actual values of the crimp measured from the S.E.M photos are significantly smaller than the periodicity of the optical pattern. Although the S.E.M samples and the optical pattern measurements were made on different specimens and thus biological variation may account for the difference, it is more likely that this was due to the

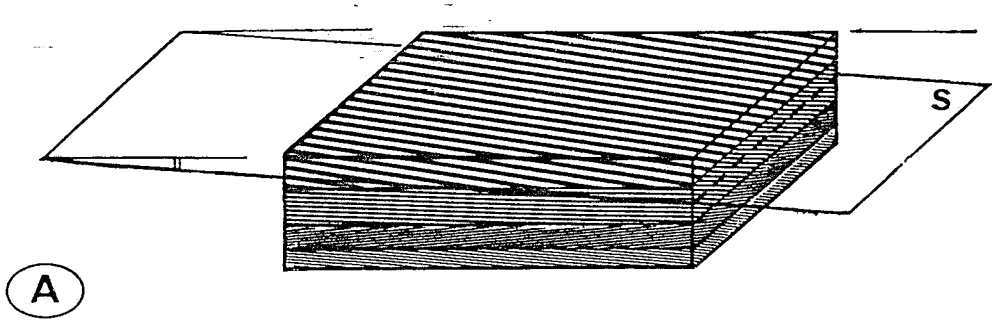

A

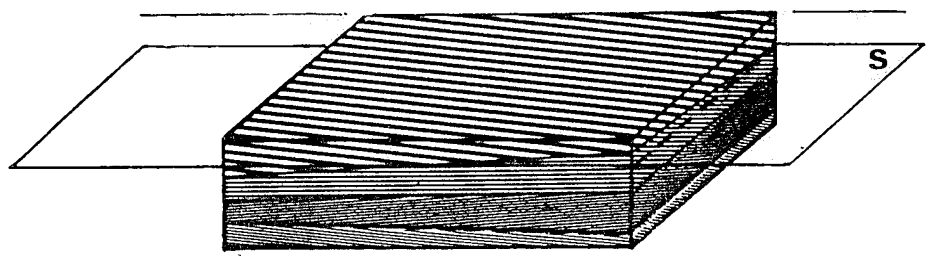

B

Figure 7.8: In either of the cases section(s) will produce the same extinction pattern in the polarised light. a)an inclined section cutting through layers of uniform thickness, b)a parallel section cutting through layers of non-uniform thickness.

shrinkage of the samples introduced in the S.E.M preparation.

The scanning microscope is most suitable for observing shape and surface patterns of the constituent elements as well as giving a stereometric view of the specimen's structure. A pseudo-three dimensional image is produced by photographing the primary electron image with the microscope being like a simple camera. Bright areas and shadows give a first qualitative stereographic view of the specimen under examination. The specimens shown in fig7.7 and especially those at higher magnification suggest that the waveform of the fibre bundles in the pericardial layers was not planar. As well as having a right/left crimp the bundles had a periodic tilt up and down from the plane of their major waveness. Assuming that the bundles were wavy and crimped in two normal planes with the amplitude of the waveform being larger in one of the planes then the bundle would have an oval outline if viewed longitudinally. This was strongly suggested by photos in fig7.7. In addition the bundles in fig7.6 possess a waveform with sharp angles at the peaks and troughs of the wave and this may have resulted as a two dimensional image (projection on a plane) of a helical form which is smoothly curved along its length. This would allow a greater potential volume for the ground substance matrix of the tissue and may explain the abundant gaps and holes which appeared in the S.E.M photos. In the earlier transverse sections the tissue had demonstrated a very dense structure with bundles tightly packed. For the S.E.M observations specimens were treated in a 0.95%(w/v) saline solution which washed off any loosely bound cells and matrix. Most of the mucoid substance which covers the fibres remained there after the preparation and could always mask the view of the fibres. It is believed that the gaps appearing in the photos at higher magnification are a result of the

Table 7.2: predominant orientation of fibrils as seen by the use of polarizers and in frozen sections at different sites on the tissue. The examined samples were cut from two different membranes and the location of the sites is shown on the map of the membrane. Angles were measured in degrees from the circumferential direction.

	membrane 1				membrane 2
site:	a	b	c	test site-I	test site-I
	0	0	0	60	-60
	-60	90	60	0	60
	90	0	0	-60	0
	60	90	-60	0	-60
	90	0	0	70	0
	0			0	

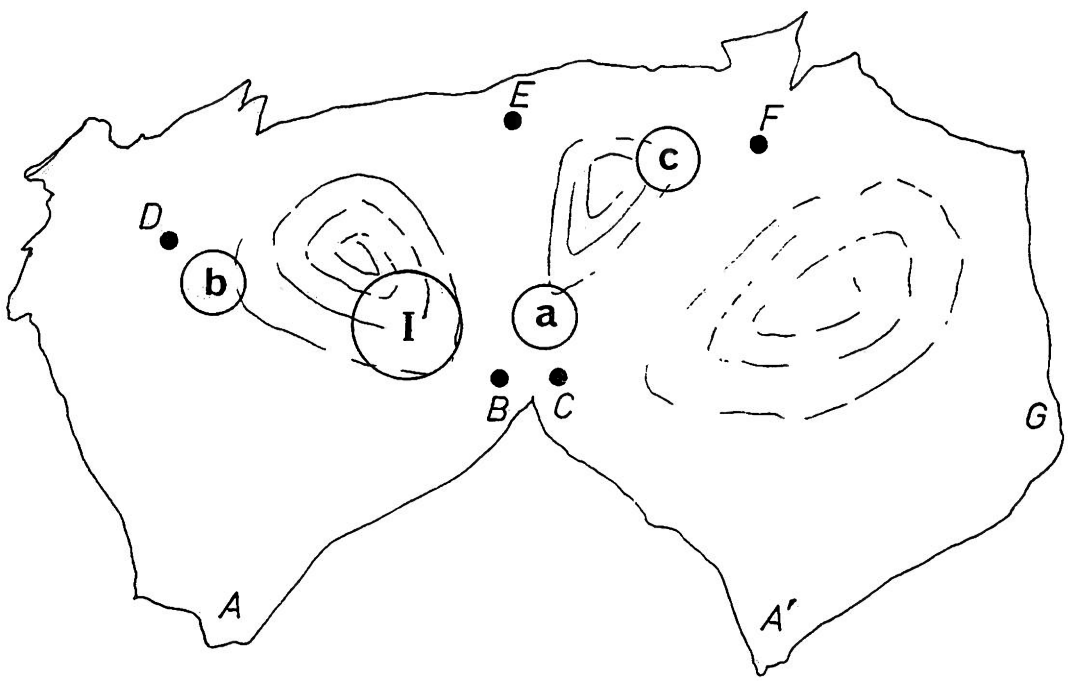

saline treatment while the fissures appearing between the fibrils of a bundle or the separation between bundles were due to the action of the knife during sectioning.

The geometric arrangement of the bundles appeared to follow some pattern as well. The superficial epipericardial layer (section-a, fig7.7) presented a shorter average length and this was probably related to the fact that they appeared to be inclined towards the lower layers of the structure and thus they had been cut shorter by the microtome blade. This was also apparent in some transverse sections and happens because through these superficial fibres the tissue blends with the surrounding mediastinum. Fibrils could occasionally be seen to migrate between the bundles of a single layer and the same must be true for fibrils and/or bundles between differently oriented layers. This migration of fibrous elements presumably holds together the differently oriented adjacent layers providing lateral strength and continuity of the structure. It is also required in order to bring compatibility between the mechanical properties of the different and highly anisotropic layers.

Discontinuities in the fibre orientation within a section may be due either to the section being at an angle to the free surface of the tissue, cutting through layers of uniform thickness(fig7.8a), or, to a section parallel to the free surfaces cutting through layers having a non-uniform thickness (fig7.8b). By observing the orientation at particular areas inside the samples at the successive sections a minimum number of 5 differently oriented extinction patterns were observed to exist and for samples from various sites on the membrane(table7.2). It was also concluded that the case of fig.7.8a was more likely to be true for a tissue with layers of uniform thickness and thus the degree at which accurate observations were made

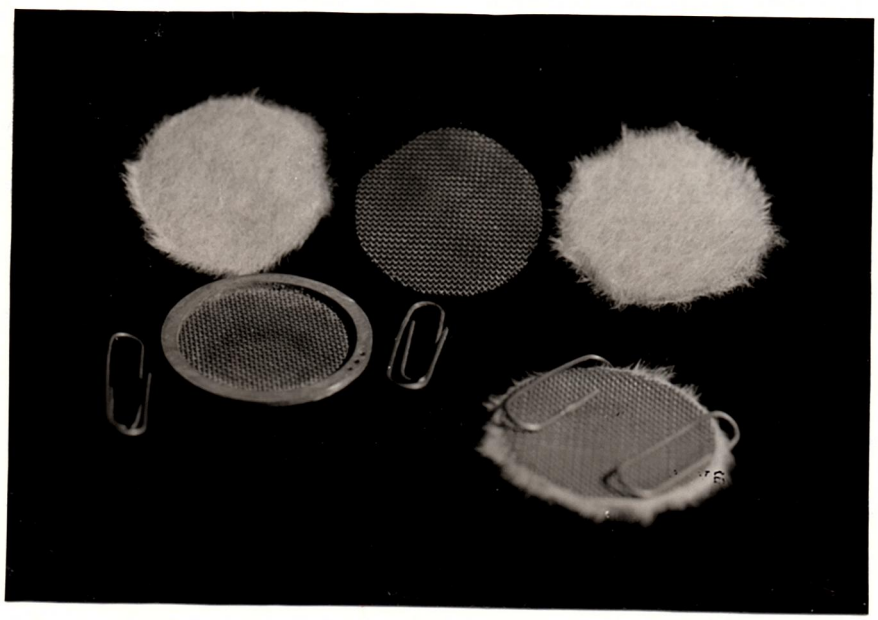

Figure 7.9: The metal cases which were used to retain the pericardial samples at a flat configuration during impregnation in paraffin wax. Sheets of filter paper were placed on the inside to prevent direct contact between the samples and the grid.

was dependent on a careful alignment of the knife and the thickness of the sections themselves. For whole membrane thickness of 0.33mm at test site-I the existence of at least five layers indicated that the thickness of frozen sections was too great approaching the thickness of a single layer. Since the thickness of the sections by this method had reached its critical minimum value, paraffin mounted samples were prepared.

7.2.3.2 Paraffin sections. For the paraffin wax method the metal cases shown in fig.7.9 were made. They consisted from two copper-alloy grids on either side, kept at least 0.5mm apart by the ring at their perimeter which was acting as a gauge. The sample was placed between two sheets of filter paper which allowed the processing to occur but protected the sample from contact with the metal grids. The specimens were thus fixed, dehydrated, cleared and wax impregnated at a flat configuration and remained flat and rigid at the end of the procedure. They could then easily be placed and moulded in wax blocks. From the blocks prepared this way sections as thin as 3μm could be made. Sections no-thinner than 5μm were made in order not to disrupt the structure of the individual bundles of fibrils within the layer. Very thin sections of less than 3μm disrupted the waveform of the bundles thus interrupting the continuity of the bundle along its length. The primary interest was still on the macrostructure of the tissue and the orientation of fibres in each layer, with the optimum thickness of the sections only considered as the factor which could allow the different layers to be adequately distinguished from each other.

Fig.7.10a,b show a paraffin wax section 8μm thick. The section has been stained with a routine orcein method which demonstrates elastic fibres by selectively staining them brown, leaving other

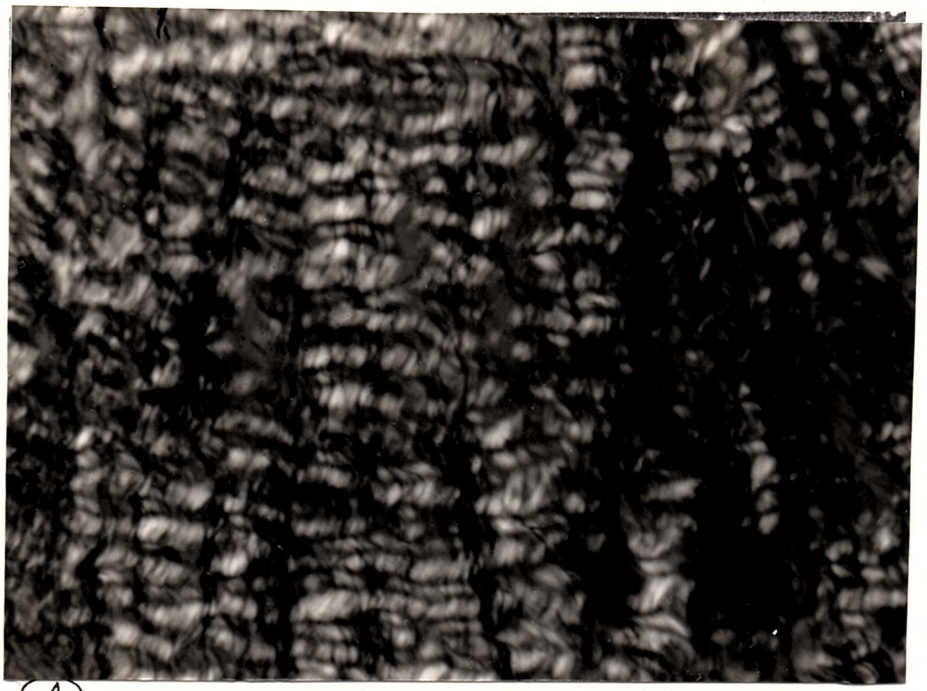

A

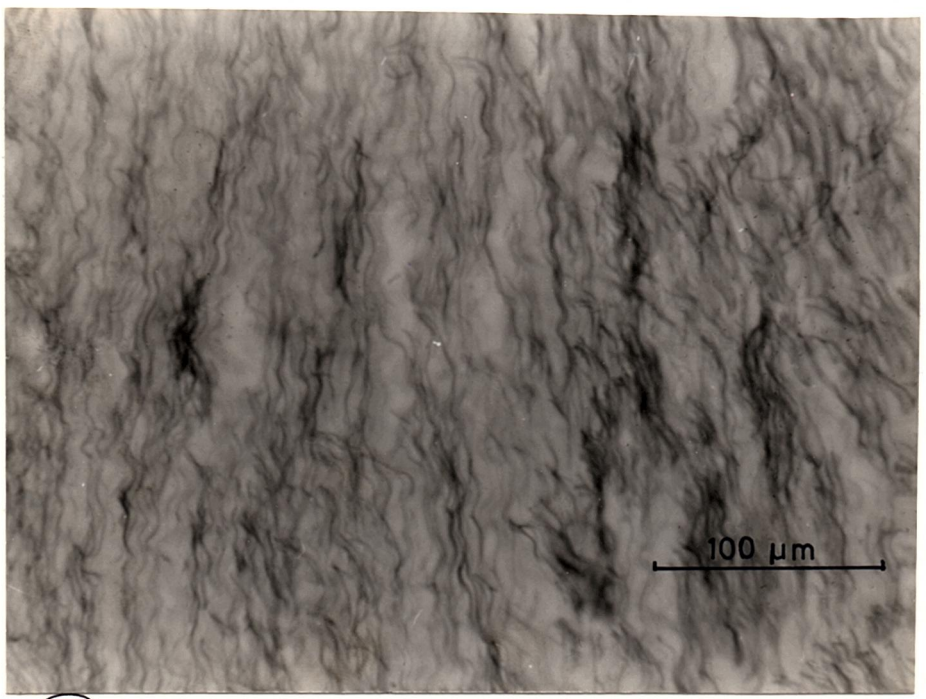

B

Figure 7.10: Parallel section, orcein stained. a)crossed polarisers demonstrate the birefringent collagen bundles, b)parallel polarisers the elastic fibres ran in parallel to the collagen bundles.

components unstained. In order to have a clearer view of the elastic fibres the section was not counterstained. The direction of the unstained collagen fibres could be determined by their birefringence when viewed by polarised light. The result of fig7.10a,b was typical of all the sections made and treated in this manner. There were no sections in which elastin was running at a large angle to the collagen fibrils. The previous claim of Ishihara et al(1980) which may have influenced the decision making on pericardial mechanics of a number of workers was not substantiated. All sections made in this study showed a clear and strong association of the elastic and collagenous elements with elastic fibres following even the undulations of the collagen fibrils. In respect to their orientation they appeared to be absolutely concurrent. This is not novel in the organisation of collagen and elastin in connective tissues and is probably the rule for a great number of tissues as collagen and elastin are laid down in fibres by the fibroblasts (Goldberg and Rabinovitch,1983). The particular case of heart valve leaflet tissue where elastin runs normal to the great majority of collagen bundles (Broom,1977) is probably an exception with specific functional implications.

Fig.7.11a,b is a presentation with crossed and parallel polarizers of a section 5μm thick, which has been sectioned at a small angle to a blood vessel lying in the inside layers of the fibrosa. The stain was orcein for the elastic fibres followed by a haematoxylin/eosin preparation to differentiate and demonstrate the remainder of the constituent. Fibroblast cells were abundant in the space between the fibre bundles. In the vessel's walls the enthothelial cells and the elastic fibres of the tunica interna, the elastic and collagen fibres of the tunica media and externa can be seen. Inside the lumen there are a number of red blood cells(R.B.C).

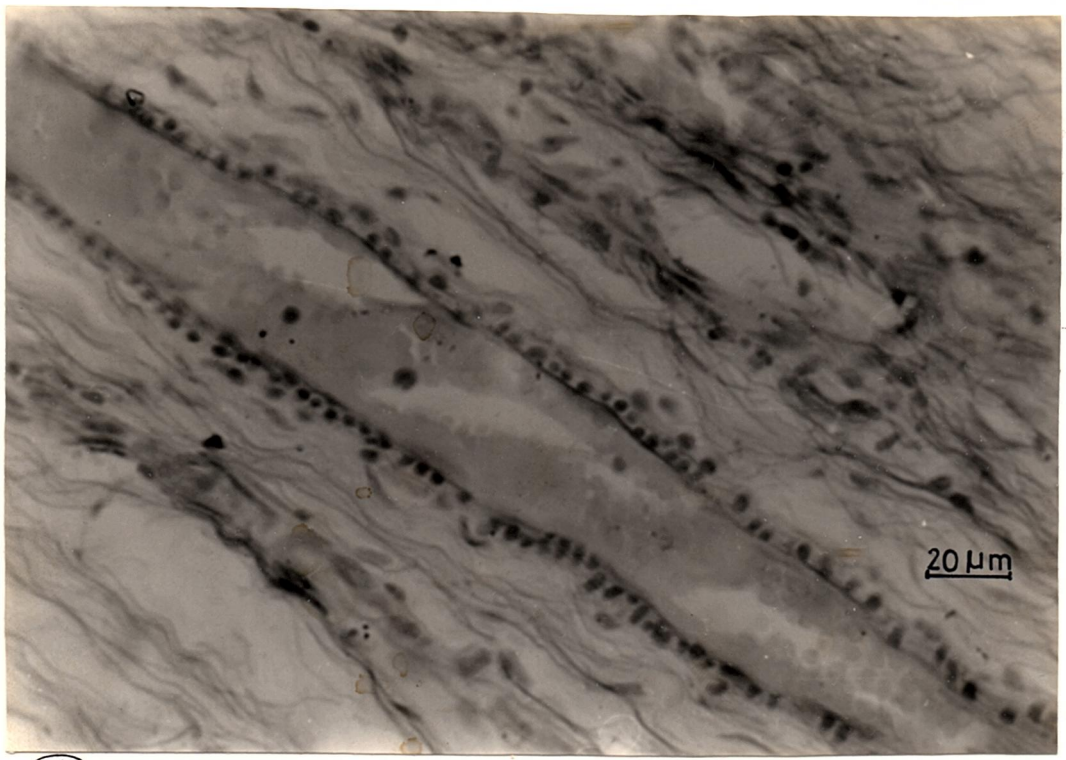

A

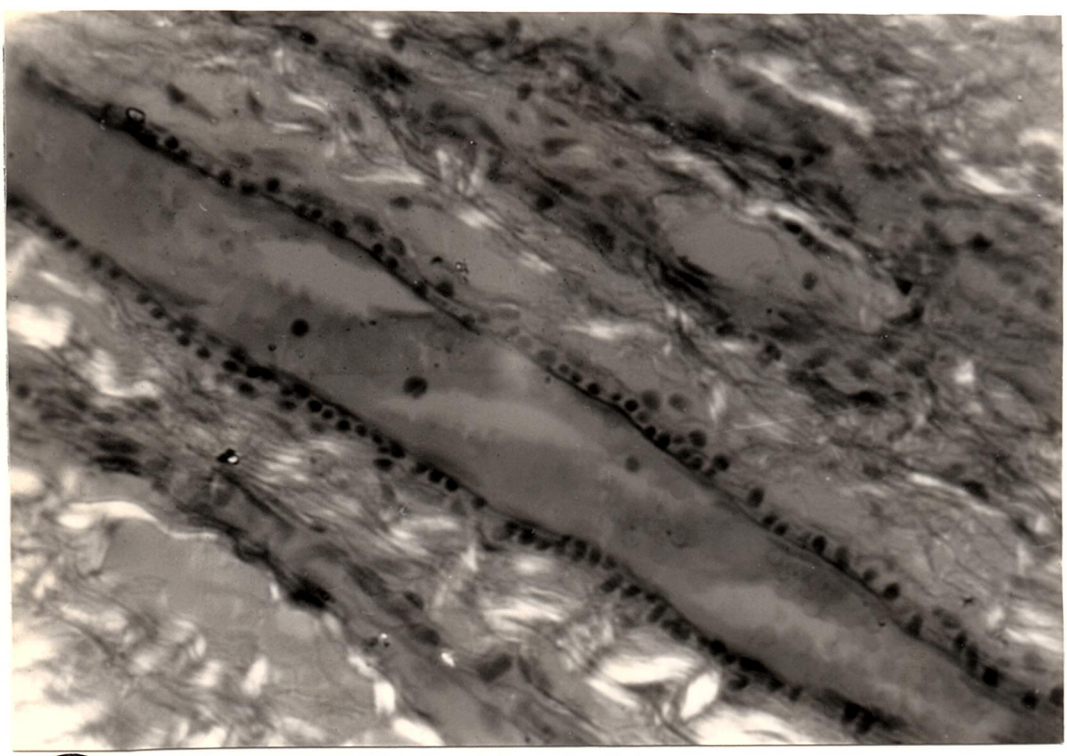

B

Figure 7.11: Blood vessels were also aligned to the direction of the collagen bundles within a layer. Haematoxylin-eosin stain. a)polarisers in parallel, b)crossed polarisers.

The collagen in the vicinity of the vessel ran parallel to the vessel itself and this may be easier to discern when the polarizers were crossed (fig7.11b) to produce an extinction pattern along the fibres. From a great number of sections it appeared that the arterial tree which entered the pericardium from the epipericardial surface, branched and followed successive layers along their respective fibrous orientations till it dissapeared completely above the serosal surface. The consistency by which the blood vessels and the adjacent collagen bundles ran in parallel was such, that after a short time it became apparent that the orientation of the superficial epipericardial layers could be identified by simply observing the red coloured course of the vessels along the surface. Provided that the fresh membrane is not thoroughly washed in saline and thus the vessels are not fully depleted from their R.B.Cs, this observation may constitute a useful trick for the early detection of the course of the fibres in native freshly excised pericardium.

7.2.4 The Fibrous Elements after Deformation.

The previous investigations regarded material which was unstrained after excision and were exploratory of the tissue structure at a relaxed state. The state of the fibrous bundles of the tissue after a significant amount of stretch had been imposed on tissue strips, was also examined.

Tissue strips were driven to failure according to the regime of chapter5 after they had been mechanically preconditioned. Then following fixation in formalin they were paraffin wax impregnated in blocks. Sections were prepared both in transverse and parallel planes.

In the first series of tests a number of circumferentially aligned strips were subjected to preconditioning cycles and then were

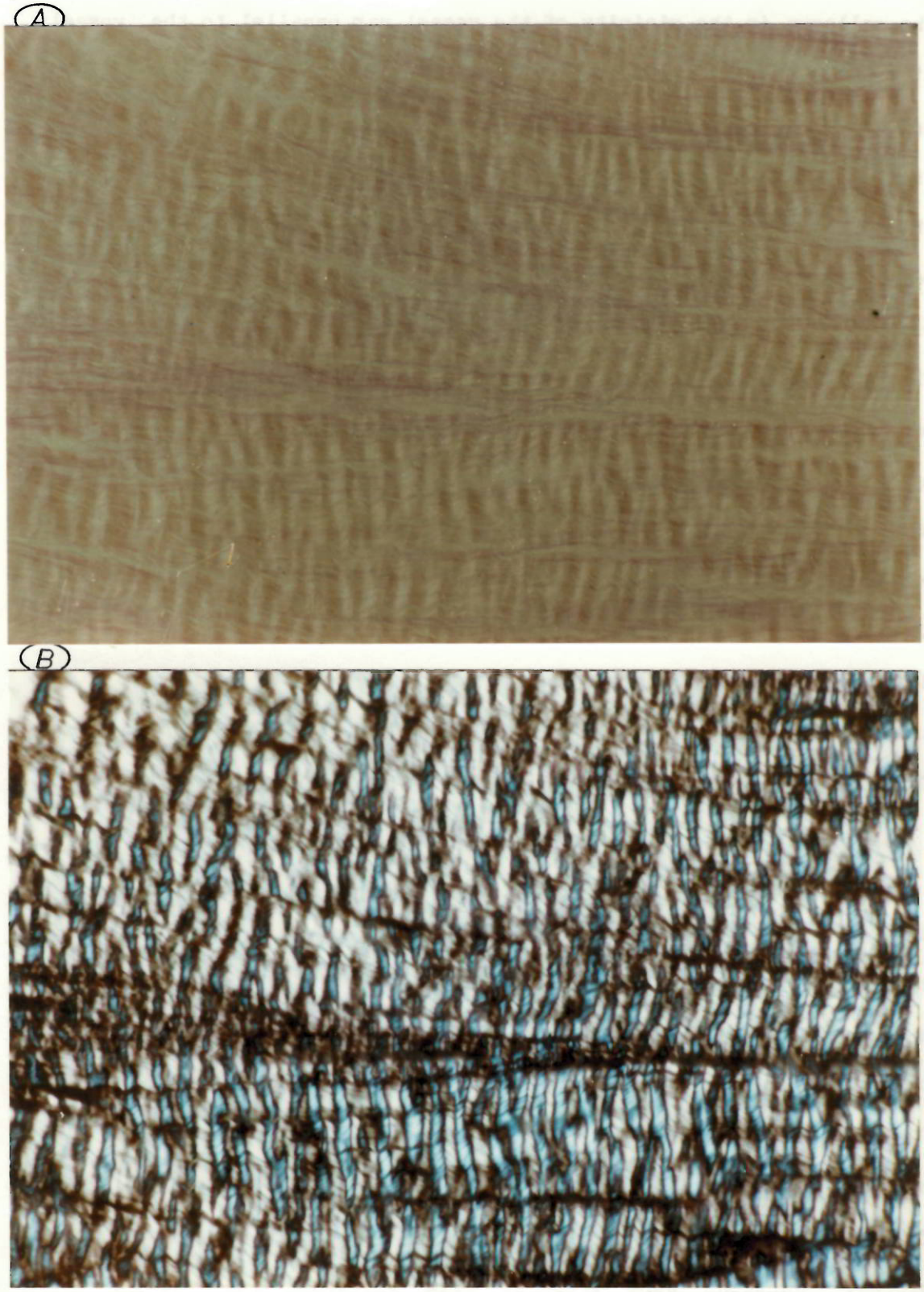

Figure 7.12: Parallel section of a failed circumferential strip. a)parallel polarisers, elastic fibres are mostly straightened out; b)crossed polarisers, collagen pattern appears non-uniform and irregular.

driven to failure. The strips were subsequently fixed, paraffin wax processed and orcein stained for the demonstration of the elastic fibres. In fig.7.12a the parallel section is sited close to the central area of failure for the strip and came from the interior layers of the fibrosa. The brown elastic fibres are exhibited on the slightly birefrigent substrate of the collagen bundles of fibrils. Unlike most previous sections of unstretched tissue which had showed a close association of elastin to collagen, in the present case the majority of the elastic fibres were stretched and appeared detached from the collagen bundles. The collagen bundles themselves, which are easier to observe in the fig7.12b with the crossed polarizers, retained a degree of recoverable crimp which though was irregular. Fibres were registered with crimps that did not match and thus the crimp could be seen at places to bifurcate from the previously well established clear periodic pattern to a pattern of a disorganised shorter periodicity. Although the fibres were highly aligned along a single direction (from right to left in photo, circumferential direction and also the direction of load) the previously experienced dark/light banding was non-uniform and irregular. The external dimensions of the strip were definitely larger post the failure point and an irrecoverable macroscopic deformation had been imposed on the strips. On these considerations one would expect that a similar elongation would have been imposed on the fibrils themselves and that the optical pattern would have enlarged its periodicity by dark/light zones moving apart from each other as the fibres were extended. The stretched elastic fibres showed that there was a permanent deformation at the microstructural level, but the behaviour of the collagen fibrils and their associated optical pattern was still waiting for an explanation.

In the second series of tests which were carried out in collaboration with Dr.Judith Foster a number of axial and circumferential strips were driven to failure and then paraffin wax processed and examined in transverse sections. The strips were as usually preconditioned and their response was confirmed to be typical along the two normal directions. The strips were driven past the failure point and then the test was discontinued in order to keep the strip in one piece and thus the two ends of the strip were still attached in the central thinned area. The strips were cut in both ends and underwent the histological preparations.

Sections of these samples were stained with the Masson's thrichrome technique which has been said to be able to stain according to the strain history of the material. Previous reports on skin (Craik and McNeil,1965, 1966) and tendon (Flint et al,1975; Flint,1976) have shown that collagen fibres will stain red or green depending on whether they have been stressed or relaxed prior to fixation. A more recent report by Lanir(1984) claims that such results have not a biochemical cause but are due to a mechanical reason. Lanir's suggestion was that those areas that appear to retain the red stain are indeed stressed, but as a result of the mechanical deformation they have an increased fibre thickness at these same sites and thus penetration by the second green stain is hindered by the more dense structure. Although due to one or the other of the reasons the stressed fibres will retain some red dye and thus the technique is extremely useful, Lanir concluded that it did not consist a reliable tension probe.

In the present experiments the technique was firstly standardised and optimised for the particular tissue (appendix7) and then applied to groups of tissue specimens. Thus a distinction was made between axial

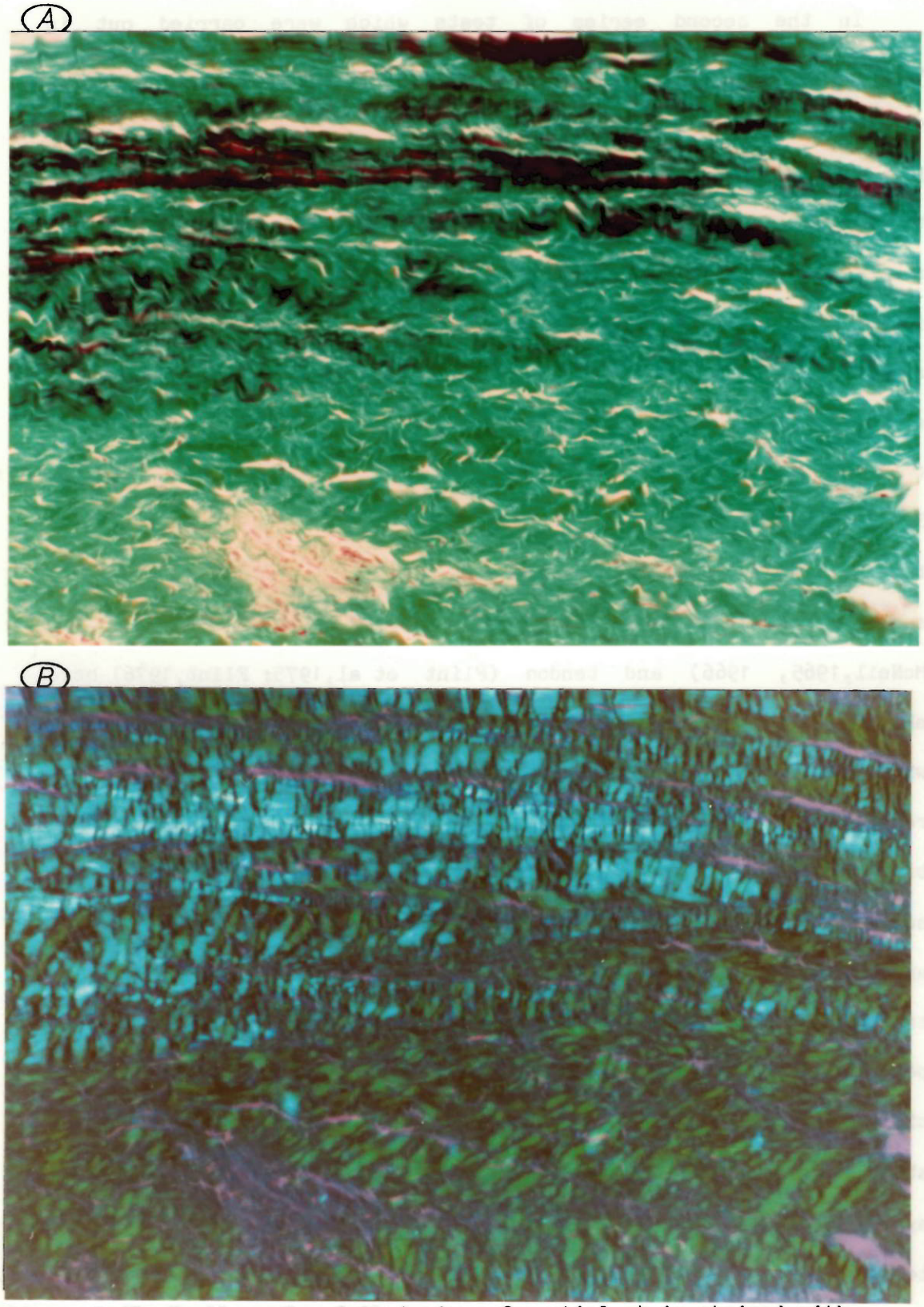

Figure 7.13: Section of a failed circumferential strip stained with Masson's trichrome method. Collagen fibrils which retained the red stain, also appeared having a permanently deformed waveform.

and circumferential samples and also between fresh, frozen and fixed tissue.

The results were a matter of subjective assessment and could only be expressed qualitatively. A certain amount of red existed in some sections and for deciding if its presence constituted a significant proportion of the section or not, a ranking system of three grades was invented. The assessment was consistent when the same experimemter was to decide about the presence of red by viewing all slides and award one, two or three crosses of redness to a section. The actual number of crosses is very much depending on the judgement of the experimenter but a few conclusions could be drawn irrespectively of this personal factor involved. Firstly, it was concluded that freezing the fresh material and storing it for some time after the completion of a mechanical test and before it undergoes the histological preparation was not seriously affecting the presence of red in the sections. Both fresh and frozen sections showed the same ability to react according to their strain history. This is particularly important when human or other rare specimens have to be examined and allows them to be retained and transported till the histological examination takes place. Secondly, it was decided that fixation should be avoided as the technique appeared incapable of producing the same results (presence of red) on fixed tissue. Thirdly regarding the strip orientation, a number of circumferential strips stained sufficiently red but there was complete absence of red from sections of the axial strips.

In fig.7.13 a section of a circumferential strip shows areas where the red stain had been clearly retained by the fibres. This was a section which best stained red with the stain being uptaken by whole fibril bundles or in patches here and there. By a thorough observation of

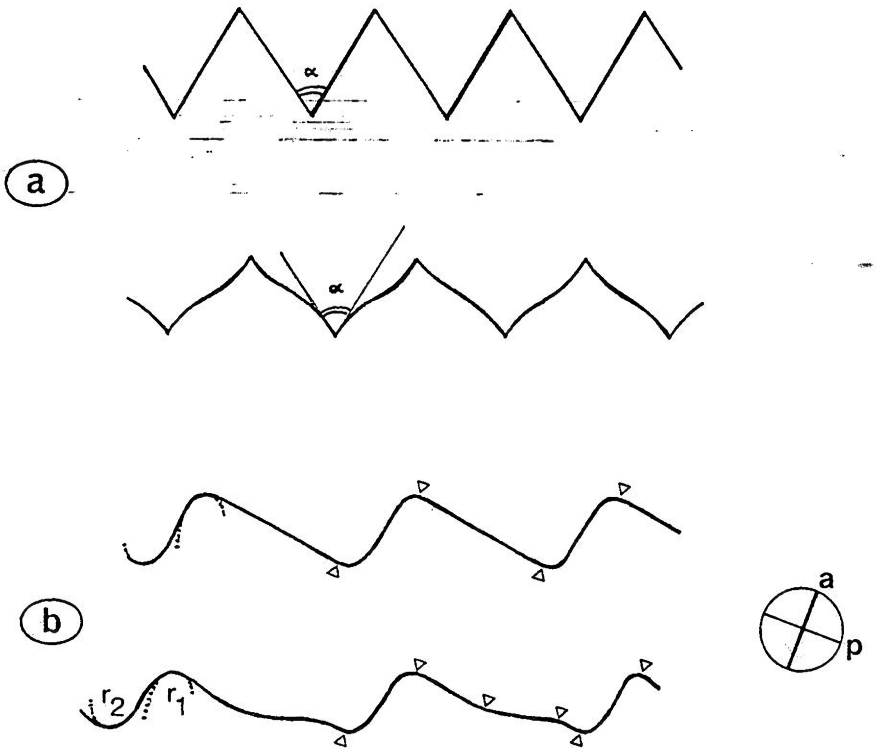

Figure 7.14: a)relaxed and extended zigzag waveform for rat tail tendon fibrils as proposed by Diamant et al(1972),
b)relaxed and extended form of the tilted waveform of pericardial fibrils as observed here.

such sections a few things became evident. There was a definite relation between the ability to stain red and the waveform of the stained fibrils. Fibrils which had been stretched enough had been permanently deformed since they had retained their new shape without being under stress during fixation. Those fibrils had been straightened out and presented lateral buckling at periodic intervals. This showed that the original waveform had not stretched by simply unwinding, but instead it had retained its peaks and troughs of the crimp and had extended significantly in the intermediate segments. This was not such a novel finding; similar observations had already been made during stretching of tendon fibrils (Diamant et al,1972). The elastic equation that was then developed described the extension of a zigzag waveform (fig7.14a) by treating the points of crimp as sites of infinite rigidity and the intermediate segments as elements capable of elastic bending. In the present case the original waveform was more of a tilted sinusoidal wave (fig7.14b) which deformed by keeping its edges at certain curved geometries and extended its middle segments considerably. Of course such description applies on a planar originar waveform; if according to the S.E.M photos the fibrils have a native helical geometry then upon deformation the fibril helix (spiral) would unwind and stretch by subjecting differential segments along its length in torsion rather than extension.

This mechanism for deformation of individual fibrils does not make any clearer the reason why the deformed fibrils retain the red stain and it is compatible with more than one of the speculations that have been already made. Lanir's speculation, that an increased density as resulting from stretch is responsible for the result, seems unlikely at least at the level of the fibril bundles. In the present thin sections there was no doubt that all areas could rapidly and the same

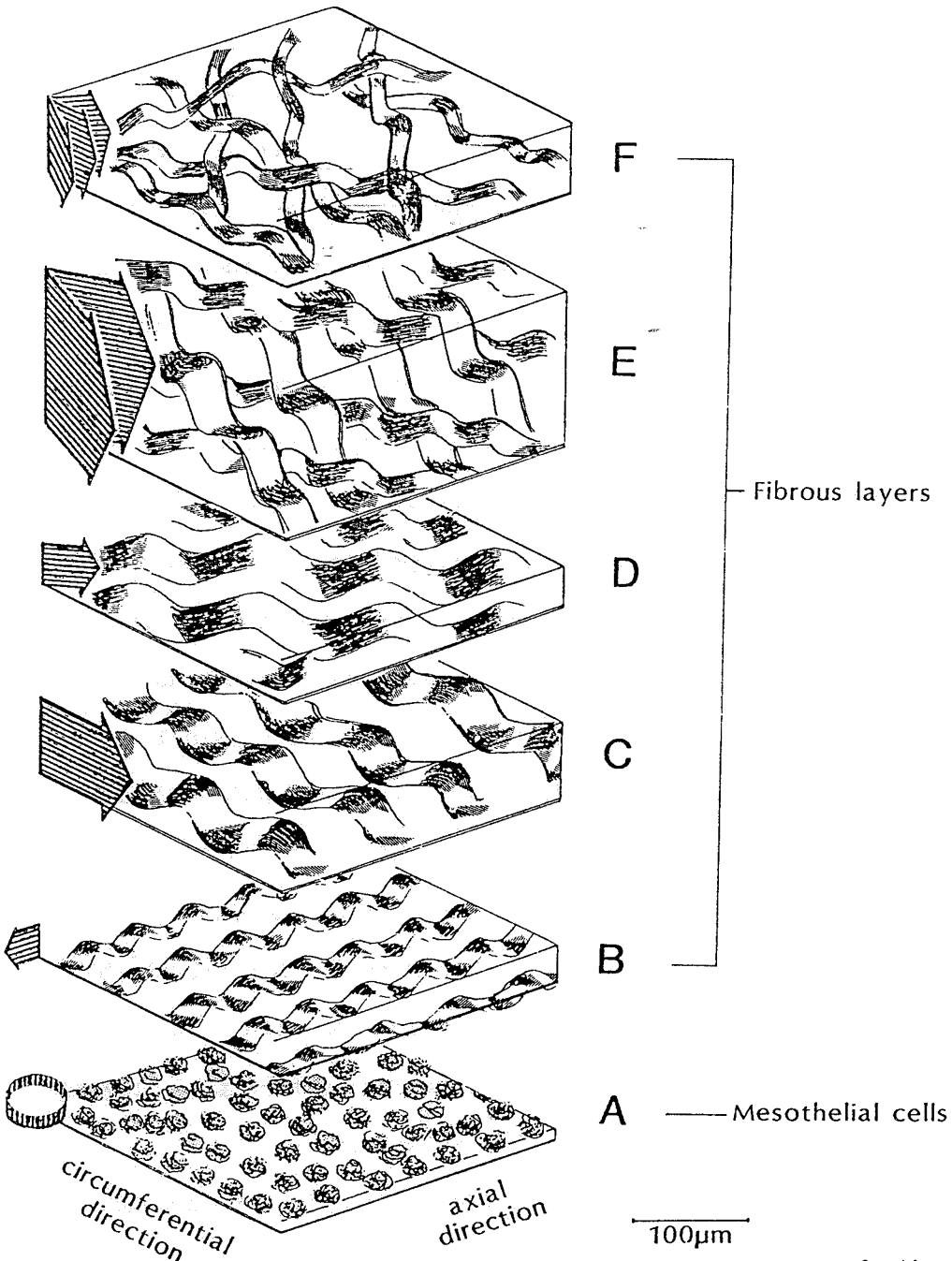

Figure 7.15: Graphical reconstruction of a tissue sample from test site-I based on a series of parallel sections.

as easily be accessed by the stains and despite this the distorted fibres stained red. An increased density at a sub-fibril level though could result from torsion along the fibril segments according to the previous suggestion and thus retain the red on the fibril interior. This would still require binding sites on the fibril to be exposed to the action of the dye. It had been originally thought that a blanket of mucopolysaccharides may cover the fibres and prevent their staining by covering possible active binding positively charged sites, but this was rejected by Flint(1976). He proposed instead that positive charged sites become available by the geometric distortion of the fibre as a result of strain.

7.2.5 Reconstructing the Tissue.

Fig.7.15 is a reconstruction of the appearance of a single bovine specimen. It was based on 16 slides made from a series of 45 paraffin wax sections from a sample from test site-I. Each section was 8μm thick and every third section was mounted on a slide. From the original sample five blocks were made. The four were sectioned in succession in parallel to the surface sections and the fifth was intentionally cut at an angle to the epipericardial surface including both free surfaces at the two ends of the same section. The single fifth block which was cut at an angle gave sections which were of great help in identifying how many layers were present and their individual thicknesses.

Fig.7.15 was drawn as realistically as possible. The thickness of the separate layers is in scale and if all layers are stacked together the tissue is 0.33mm thick. The dimensions of the size of the bundles, their wavelength of crimp and their orientations and inclination are established from the sections and are in scale. Even the shades which attempt to show the light and dark segments of the fibril bundles are

according to the rule by which the fibre segments in parallel to either of the polarizers are dark. The polarizers have been assumed to be directed along the axial and circumferential directions.

From a mechanical point of view the bundles have been shown to be an assembly of both collagen and elastin which are the dominant elements in the mechanical response of the tissue. Nevertheless neural and vascular elements have been found to be similarly positioned and oriented and thus follow these same lines. The arrows show the orientation of the fibrils for each of the layers which is also the direction of the axis of mechanical anisotropy. The mesothelial cells are attached to the basal lamina which should be isotropic but its mechanical role is considered to be insignificant.

7.3 DISCUSSION

In the early parts of this chapter transmitted polarised light was used to examine the pericardium and was found to be a non-destructive and non-invasive optical method for examining the tissue structure. The optical pattern was shown to be consistently related to the mechanical anisotropy of the tissue at each site and thus constituted a simple non-destructive method of mechanical identification and proved to be a valuable tool in the examination of the tissue properties throughout this research study.

Histological studies of the tissue structure showed that an extinction pattern was created by the natural birefringence of the collagen fibrils and their fine unidirectional arrangement next to one another in each of the layers within the structure. A great number of layers assuming a general direction created the optical pattern seen across the whole native membrane and thus the histological examination suggested that the optical pattern was due to a superposition of the extinction patterns of the individual layers, with the more

superficial ones having the greatest influence. Thus the optical pattern which had been related to the tissue's mechanical anisotropy was also related to structural features of the pericardial tissue and as a technique presented a potential for predicting the mechanical behaviour of pericardial specimens.

For the detailed examination of the pericardial structure histological methods were employed. Unlike other workers who examined transverse sections of the tissue, a method was developed which allowed sections parallel to the surface to be prepared. Using this method it became clear that in these areas which had been previously identified as being mechanically anisotropic the fibres in the interior of the tissue were not randomly oriented but assumed a general direction along the strong axis of the anisotropy.

The fibrosa of pericardium consists of tightly packed layers of fibres which create a very strong fibrous composite, especially along the direction of their preferential orientation. This explains the results of chapter6 where the strength of strips tested in uniaxial tests were found to have a 6 to 1 ratio in two normal directions. Of the two normal directions the one of preferential fibrous orientation is considerably reinforced. This is only one of the techniques that nature utilises in order to produce a directionally reinforced composite. This 'plywood' technique (Wainwright et al,1976) employs unidirectionally reinforced laminae with angular difference between laminae. This offers advantages in that there is always a layer aligned in the direction of load, but there is the danger of delamination if properties of different laminae do not match. This may explain the observed migration of fibres between layers as being a necessity of the mechanics of the tissue. The progressive manner in which the size of the crimp changes from the epipericardial to the

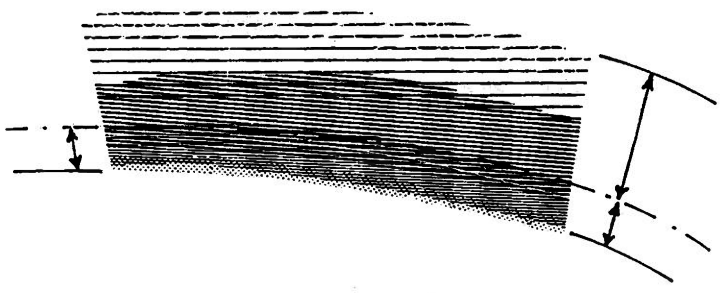

Figure 7.16: In simple bending the position of the neutral axis lies closer to the serosal surface as a result of an increased material density on the serosal side of the tissue. This may potentially reduce the level of the maximum compressive stresses experienced by the tissue.

serosal surface may also be related to a gradual change in the properties between layers. The second natural method of reinforcement employs three directional arranged fibres crossing layers and directed randomly(i.e. skin) and resembles a sponge with a fibrillar net inside. The problem it is that is not possible to achieve efficient packing of fibres if they have random orientations; low packing fractions lead to low stiffness and hence poor reinforcement in isotropic fibre-composite materials. However both designs can be either isotropic or anisotropic depending on the distribution of the reinforcing element, the fibres. The great difference is that in the first case reorganisation of the fibres is more restricted and occurs inside each lamina as the tissue is specialised to accept loading in a predominant direction, while in the design of skin the loads can come from any direction and the very action of loading reorients and reinforces the tissue along the loading direction.

Nature has apparently optimised the built-up of pericardium to accept loads in its plane, being reinforced at directions which lead to the points where the tissue attaches to the mediastinum of the thorax while at the same time being thin in order to flex easily. The behaviour of the tissue under flexion has not been considered seriously but it seems that the it may be related to the greater density of the fibres observed in transverse sections at the inner serosal surface. As seen in fig7.16 this may result in translation of the neutral axis in simple bending towards the serosal surface. In life the pericardium has only to flex towards the heart with the serosal surface being concave and thus this design seems appropriate to reduce compressive stresses which have been implicated in the failure of heart valve tissue(Broom,1978). Natural heart valve leaflet tissue has a structure which is built slight differently

across its thickness and has to flex on either side. The suitability of pericardium for valve construction and also the design and structure of a heart valve are examined in the next chapter.

8.1 INTRODUCTION.

In the present chapter the importance of the pericardial tissue in the construction of artificial heart valves is shown clearly and the benefits that can be gained by the further understanding of pericardial mechanics are highlighted as well.

The anatomy, structure and function of the natural valves alongwith the solution and design that nature has provided is examined and is followed by the human attempts in producing a valve substitute of either the mechanical or bioprosthetic form. In subsequent sections observations on the wear and fatigue of bioprosthetic valve substitutes lead to recommendations for the better use of pericardium for the particular use of construction of valve leaflets. All suggestions have been based on the knowledge of the mechanics and structure of pericardium acquired during the work of the previous chapters.

8.2 NATURAL VALVES.

8.2.1 Physiological Function.

There are four valves in the human heart all working on the same principle and providing unidirectional flow of the blood as it passes through the major heart compartments (atria-ventricles). Two valves provide an entrance and exit to the right ventricle (tricuspid and pulmonary valves respectively) and another two, similarly sited, operate on the left ventricle (mitral and aortic respectively).

The valves open and close according to the pressure gradient across their orifice. The sequence of closing and opening of the valves can be seen in fig.8.1 where the pressure gradients during the cardiac cycle are created by contraction and relaxation of the myocardial walls. Atria are in prolonged diastole with the pressure in them steadily increasing as blood flows into them continuously from their

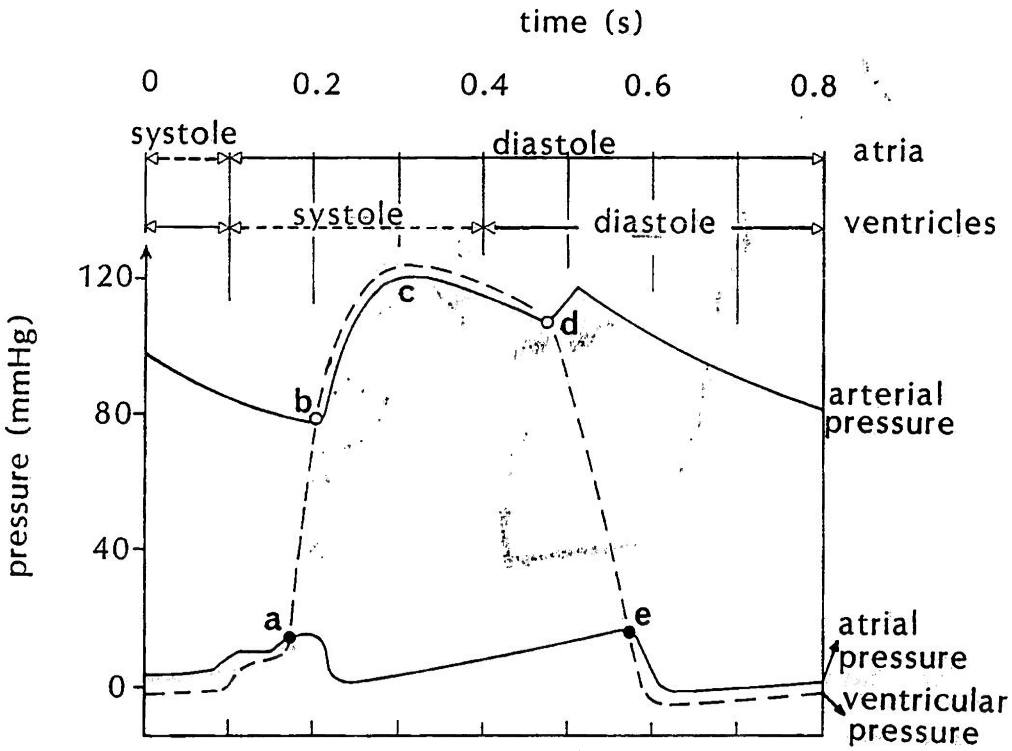

Figure 8.1: Arterial, atrial and ventricular pressure during the cardiac cycle. Valves open and close when the curves intersect at a,b,d,e.

vessels. Ventricular systole starts simultaneously and the ventricular pressure rises sharply. At a the ventricular pressure exceeds the atrial one and a backflow of blood closes the atrioventricular valves. The ventricles keep on contracting but both the pulmonary and aortic valves remain closed until the ventricular pressure exceeds the arterial pressure. This happens at b where both valves open for approximately 0.5s. Once the ventricles eject the blood the ventricular pressure falls below that of the great vessels and the pulmonary and aortic valves are closed by a backflow of blood created by the recoil of the elastic walls of the arteries(d). At e the ventricles are in diastole their pressure drops below the atrial pressure and the atrioventricular valves open. The atria subsequently contract and send the remaining blood into the ventricles. A new cycle starts then at a.

8.2.2. Anatomy and Geometry of the Leaflets.

All of the valves comprise three flaps except the mitral valve which has only two. The flaps grow out of the wall of the heart and are covered with endocardium. In the atrio-ventricular valves the flaps end in cords (chordae tendineae) which are attached to the ventricular myocardium and work in two ways. Firstly by opening the flaps when the ventricle dilates (Rushmer,1976) and secondly by supporting some of the load exerted on the flaps (Ghista and Rao,1973) when the ventricles contract and thus not allowing them to bulge inside the atria.

Chordae tendinae do not exist for the pulmonary and aortic valves which are shaped as in the simplified fig.8.2. Increased pressure in the arteries has brought the three leaflets of this valve together and sealed the blood flow through the vessel. An engineering substitute for a valve should be shaped in the form of the valve in fig.8.2 since

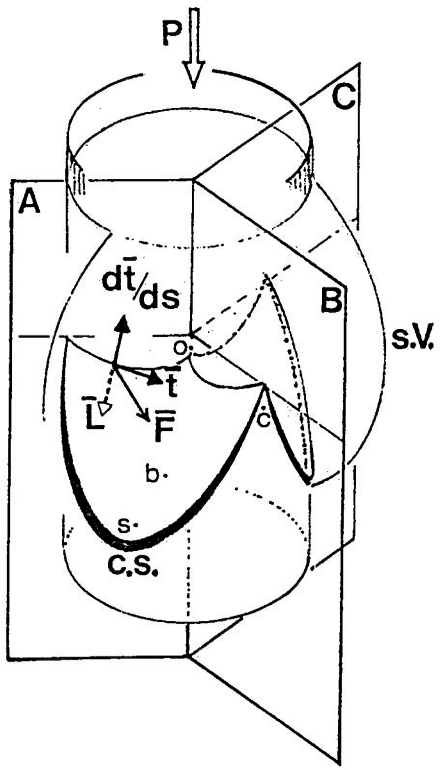

Figure 8.2: Geometry of a trileaflet valve.

chordae tendinae can not be attached to the leaflets of a substitute valve. For this reason the shape(Mercer,1973), mechanics(Clark,1973) and architecture(Clark and Finke,1974) of the natural human aortic valve has attracted early attention.

The aorta bulges outwards behind each of the leaflets where it forms the sinuses of Valsalva (s.V.). Sinuses and flaps form three pockets which by their shape help to shut the leaflets when flow reverses and blood is driven inside them(Bellhouse and Talbot,1969). The fibrous leaflets hang from the aortic walls and come together at three points called the commissures (c). The shape of the flaps forms a belly (b) and has a U-shaped cartilaginous supporting ring (c.s.) which is symmetric around its bottom the scallop (s). The surface of the leaflets has been described as a)a circular cylinder(Swanson and Clark,1974), b)an elliptical paraboloid(Christie,1982) or c)an inclined paraboloid of revolution(Mercer,1973). The three leaflets come together at the centre point of coaption (o) along three arcs of attachment which are also parabolic(Mercer,1973) and each one of them is symmetrical around a plane passing through the middle line (s.b.o.). At the centre point of coaption the leaflets are thicker forming the nodule of Arantius.

Natural human leaflets are not absolutely identical and thus the three planes A,B,C of fig.8.2 only approximately form 120^{o}dihedral angles between themselves. Artificial valve substitutes are not restricted by any geometrical reasons and it is better if they are constructed in a fully axisymmetrical manner by three identical leaflets at 120^{o}.

When pressure from underneath is higher(fig.8.2) the three leaflets open and the blood flows through the valve orifice. This aspect of viewing the valve is called the inflow one. When pressure reverses and the valve shuts the blood flow is facing the outflow aspect of the

valves as it diverts away from the centre (o).

Directions on the leaflets are defined as either circumferentially that is parallel to the free edge of the leaflet along the line c.o.c between two commissures and passing from the centre; and radially (similarly to line s.b.o) belonging to any plane which contains the central axis of symmetry and flow of the valve.

8.2.3 Structure of the Leaflets.

The fibrous structure of the natural leaflets is mainly collagenous, elastin fibres in a non-ordered form are also scattered in the interfibrillar space and with both those load bearing components being embedded in a soft matrix of mucopolysaccharides (Clark,1974). Human leaflets have been found to have a multilayered structure (Missirlis,1973). The load bearing fibres are directionally organized and run mostly circumferentially on the leaflet densely packed along the free edge. Further down at the leaflet belly the directions of the collagen bundles are more diverse, but there is a definite orientation towards and normal to the cartilaginous supporting ring all along its length.

Like with all living organisms of which the load bearing elements are fabricated and deposited under stress, the ordered structure of the collagen fibres in the leaflet could be a blueprint of the design requirements.

8.2.4 Stresses on the Leaflets.

The accurate estimation of the stresses experienced by healthy or diseased natural valve leaflets is dependent on an accurate description of the geometry of the leaflets. Transleaflet pressure difference yields tensile and shear stresses in the leaflets very much like inflation. The normal forces exerted on the leaflet by the blood have to be transmitted to the walls of the myocardium or the aorta.

It looks like a suspension along the cartilaginous ring with a contact attachment to the other leaflets at the osculating planes A,B,C (fig.8.2). Fig.8.2 shows the loading of an aortic leaflet(non-supported by chords along its edge). Fibres act as suspension cables under tension along the free edge. The force $\bar{F}$ is exerted by the membrane on an elemental length along the edge with $\bar{t}$ being tangent to the edge line. If $\bar{F}$ is resolved along the normal vectors $\bar{L}$ and $\bar{t}$ ($\bar{L}$ lies along the direction of principal curvature of the line of attachment) it can be shown(Peskin,1974) that the three leaflets are tangent to each other at the three osculating planes A,B,C, forming sharp edges(cusps). Equilibrilum yileds also that the tension along the edge line is constant. This tension can only be supported by a thickening of the leaflet along its edge and this dense collagenous built-up is indeed present. By further use of differential geometry Peskin(1974) showed that the families of load bearing fibres lie along geodetic lines of the surface. He suggested that if the leaflet is practically inextensible (early at closure and at higher pressures) then the surface forms possible are under a certain constraint which requires that the metric of the surface (first fundamental form;Stoker,1969)

$$I = Edu^2 + 2Fdudv + Gdv^2 \qquad (8.1)$$

is invariable. For a single family of load bearing fibres (as by one direction being much stiffer than the other) this would mean that E=1 and F,G arbitrary and thus giving an infinite number of possible leaflet shapes. For 2 families of load-bearing fibres only the intresections of the parametric lines(u,v) stay constant with the angles of the lines varying similarly to a Tchebychef net(Stoker,1969) resulting in a restricted number of possible surfaces. This

constitutes a geometric reason why the leaflets should rapidly and accurately approximate consistent shapes at valve closure by simply being under controlled motion from within the leaflet.

The stress analysis of the leaflets is not only a matter of the magnitude of stresses but of their distribution and their direction as well. Chong et al(1973) mentioned stress distribution but instead he employed an analytical method to calculate single values for the pair of stresses along the principal geometrical directions (radial -circumferential). Silicon rubber moulds provided the geometrical data regarding the two principal radii of curvature of normal aortic leaflets and the range of their subtending angles. Membrane analysis was applied by using Laplace's law and boundary conditions and led to a calculation of a larger tension in the radial direction. The result appeared to be in agreement with a single example they gave of a ruptured aortic valve coming from an autopsy. The results of the analysis are doubtful since the radial tension along the annular attachment (reaction at the boundary) was thought to be constant, uniformity of thickness was assumed, as was uniformity of properties and isotropy for the tissue.

The second analytical report by Clark and Sutera(1974) examined mitral leaflets and confined the analysis along an idealised infinitesimal strip in the mid-zone of the leaflet at the radial direction because it was assumed that this was the primary curvature of the leaflets. At 130mmHg pressure the stress value was estimated at 0.24MPa.

The report by Missirlis and Armeniades(1976) was another analytical attempt which has been discussed already in the inflation chapter. They introduced two different moduli for the radial and circumferential direction in a thin shell theory of an anisotropic

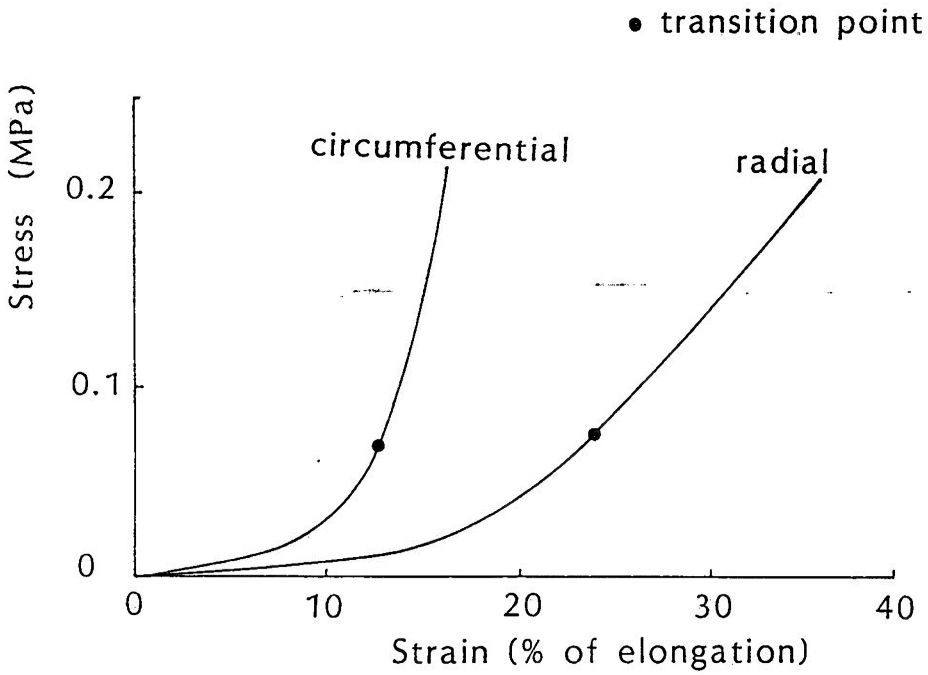

Figure 8.3: Averaged stress/strain curves for fresh human aortic leaflet tissue along the principal directions. Reproduced from Clark,R.E,1973.

material which deforms to hypothetical axisymmetric shapes and showed that the stress resultants are unequal.

Clark et al(1975) and Cataloglu et al(1977) used silicon rubber moulds of human aortic valves and close range stereophotogrammetry to examine the geometry of the leaflets under changing pressures and finite element analysis to calculate the stress distribution in the leaflets.

It should be said that all these attempts are quasistatic treatments (by neglecting any inertial forces) of the leaflet loading which is essentially a dynamic problem.

8.2.5 Leaflet Mechanical Properties.

The ordered structure of the fibres in the natural leaflet influences the mechanical properties of leaflet. The collagen network bears the load on the leaflet and transmits it to the aortic wall by means of the bundles directed perpendicular to the supporting ring. In the transverse direction (circumferential) the load-deformation behaviour of the leaflet tissue is largely that of the collagen bundles. In the radial direction the load-deformation characteristics of the elastic meshwork will be the more influential factor.

Clark(1973) examined the mechanical properties of fresh and frozen human aortic and mitral leaflet tissue strips. The strips were directed along the radial and circumferential directions on the leaflet. The results are shown in fig.8.3 for fresh tissue. Clark defined a low pre-transition modulus for both curves with the values being radially: (0.012 ± 0.005)MPa and circumferentially: (0.019 ± 0.007)MPa. He also defined a higher post-transition modulus for both curves with mean values radially: (17.4 ± 6.98)MPa and circumferentially: (59.8 ± 30.1)MPa. In either of the directions there was a high degree of elastic recovery which accounted for 98-99% of

the original gauge length and thus permanent deformation as a result of the tests was minimal. These were the values for the aortic tissue, mitral tissue behaved similarly. In all cases the leaflet tissue was far more compliant in the radial direction than in the circumferential direction with compliance refering to extensibility at a particular stress level while in terms of stiffness the circumferential direction had a significantly higher elastic modulus than the radial direction either in the pre- or the post-transition region. The tensile strength in the circumferential direction was estimated to be three times greater than in the radial one although actual values were not quoted.

As a result of cycling the material became more compliant regarding both its extensibility at the transition point and the pre/post-transition moduli in either direction.

The structure based reason for this anisotropic behaviour was confirmed by the fact that his tensile tests on chordae tendineae, which consist of uniaxially densely arranged collagen bundles, produced results very similar to the circumferentially aligned strips. Clark(1973) also noted that there was a difficulty in defining the stress free state of the strips and that the tensile strength of the material was 500 to 1000 times higher than the stresses at which valve leaflets operate in-vivo. He suggested that the observed anisotropy may permit a larger amount of kinetic energy to be stored as potential energy within the leaflet tissue than if it behaved linearly bidirectionally throughout the deformation. He eventually concluded that the heart valve tissue combines a high elastic recovery with a phenomenal durability(4 billion cycles) and an anisotropy like no-other known man-made material.

This report on the static in-vitro properties of the leaflet

tissue was complemented by another by Ghista and Rao(1973) on the dynamic analysis of the mitral leaflets. The authors suggested that analysis of the acoustic frequencies of the heart sounds as the valves close may allow determination of the elastic modulus in-vivo and thus diagnose degradation of the structural state of the valve material as expressed by its modulus. From such an analysis for healthy leaflets they finally decided that the mitral valve operates up to the point of transition into the stiff region.

8.2.6 Valve Mechanics and Leaflet Kinematics.

The collagen network has a geometry defining function especially when the leaflet is unloaded by retaining the leaflets curved shape. The valve has two phases in its motion(Bellhouse and Talbot,1969). In the first phase during the deceleration of the aortic flow the leaflets have almost come together and a small backflow is required to shut them completely. The pressure difference across the leaflets at this point is almost zero and the leaflets are stress free. The geometry of the leaflets at the nearly closed position is determined by the arrangement of the collagen fibres and their unstressed length. In phase two under a severe reverse pressure difference the leaflets behave as inextensible membranes due to the exponentially stiffening properties they possess. Once again the collagen network defines the leaflet geometry in this stressed state.

The flexibility of the leaflet is significantly affected by the collagen architecture. Both Mohri et al(1972) and Clark and Finke(1974) noticed the striations caused by the position and orientation of the collagen bundles which were macroscopically visible below the enthothelial cell layer. Sauren et al(1980) suggested that the leaflet tissue hinges around the collagenous invaginations and flexes in the space between them and he thought that this was

consistent with Mercer's(1973c) observations from cineangiographic analysis of the movements of canine leaflets. Mercer(1973a) also noted that the efficiency of the valve leaflets depends on their being constructed so that lines of strength alternate with lines of flexion and that flexibility of the leaflet attachments permits essential changes in valve geometry during the cardiac cycle.

The properties of the U-shaped cartilaginous support have been linked to the valve and leaflet kinematics. The U's are more flexible at their top near the commissures and this may constitute a stress reducing mechanism. The more rigid bottoms of the U's are able to move on the plane of the orifice and expansion of the base of the valve (aortic ring) has been observed by many(Brewer et al,1976; Thubrikar et al,1979).

The outwards expansion of the aortic ring may also initiate the leaflet motion when the valve is about to open. If the base of the valve is rigid a clear pressure difference is required so that the created wave pushes the leaflets apart. If the base is moving outwards the base of the leaflets experiences a buckling which drives up to the free edge of the flaps and clears the orifice. The latter mechanism requires smaller transvalvular pressure differences to achieve the same basic effect which is the opening of the valve with a central washout and minimal turbulence.

8.3 VALVE REPLACEMENT.

8.3.1 Introduction.

Normal human healthy valves are mechanically very efficient presenting minimal resistance to forward flow and rapid closure with little reverse flow (regurgitation). Malfunctioning human valves are mechanically characterised as incompetent while clinically the occurence of incompetence is called valvular heart disease. Valvular

insufficiency can be caused by rheumatic fever which leads to fibrosis of the leaflets and results in a mechanically stenotic and/or regurgitant valve. Infective endocarditis may cause degeneration of the valvular tissue which, under mechanical stresses, produce holes and tears on the leaflets resulting mainly in regurgitation. Calcification of leaflets may be initiated by rheumatic fever or an autoimmunologic reaction and results in a valve being both stenotic and regurgitant.

Valvular malfunction on the right heart will result in lung congestion, while stenosis of the aortic valve will increase the left ventricular pressures in systole and will cause left ventricular hypertrophy. It is not certain that those conditions will lead to symptoms which can diagnose valvular insufficiency by external examination. Auscultation can detect murmurs caused by a prolapsed mitral valve leaflet. Radiological means are also used in diagnosing valvular problems as well as nuclear medicine imaging, echocardiography and cardiac catheterisation.

If not the cause of a disease, valves may require replacement due to congenital abnormalities, i.e. like the congenitally bicuspid aortic valve which presents high incidence of early in-vivo calcification resulting in valve incompetence. Implantation of a valve may be required when the natural valves are malformed or even absent.

8.3.2 Possible Valve Substitutes.

The use of man-made devices to assist circulation has been reported as early as 1954 (Hufnagel,1979). There are two basic groups of heart valve substitutes, namely the mechanical and tissue valves. The standard mechanical designs are the ball (usually silastic) and cage valve (Starr and Edwards,1961) and the tilting disk design

(Bjork,1969).

The tissue valves fall in a class of their own usually called bioprosthetic valves. The first valves were not man-made but homografts (presently called allografts) implanted in 1962 (Ross,1962; Barratt-Boyes et al 1965). These transplants between humans were followed by an autograft implantation at 1967(Ross et al,1979) which was a pulmonary valve transferred to the aortic position and replaced at its original site by another tissue valve. Autografts or allografts have been thought to be better accepted by the human body but their durability is doubtful. They were usually implanted in their fresh condition (treated only with antibiotics) and were found to be prone to degeneration of their fibrous structure and to develop holes and tears.

Xenografts are bioprosthetic valves with leaflet tissue originating from species other than human. They are subdivided into xenografts constructed from valvular tissue and xenografts with leaflets constructed from other biological material. In the former category fall the porcine valve xenografts first introduced in 1970 (Jones,1975). They are aortic porcine valves chemically treated with glutaraldehyde and mounted inside a cloth covered frame. In the latter category belong the pericardial xenografts which utilise three leaflets fabricated from glutaraldehyde treated bovine pericardium, first introduced in 1976 (Ionescu et al,1977).

Allograft valves with fabricated leaflets have also been made by using dura mater and fascia lata (Ionescu et al,1972) with uncertain results.

8.3.3 Performance and Assessment.

Mechanical and tissue valves each have advantages and disadvantages and the selection of the valve to be used in each case

is considered in respect to these factors and the clinical condition of the individual in particular. Mechanical valves have long-term durability due to the use of engineering materials which present consistency in manufacture. These materials have well defined properties which also make their design by analytical means more meaningful. They have only a few mechanical disadvantages because unlike the natural valves they don't provide central flow and don't have natural shape. Their many disadvantages though, are in the biological field where their rigid components may cause blood haemolysis by crushing or harming erythrocytes, immunological reaction, blood thickening (coagulation) or formation of thrombus which may produce emboli. Thus they require long-term (usually life-time) anticoagulation therapy which may not be possible to provide in some countries(third world). Formation of thrombus and tissue ingrowth may also interfere with their, otherwise asymptomatic, mechanical performance by obstructing the operation of some moving parts.

Bioprosthetic valves have better hydrodynamic performance providing less obstructive and less turbulent central flow and are very close to the natural form of valve. They do not require any form of anticoagulation treatment and do not cause blood trauma. Their soft tissue leaflets are better accepted by the body's system but deterioration of the leaflet properties and/or structure due to in-vivo calcification, thrombus formation and fibrous ingrowth may occur. Efforts have been made to incorporate anticalcification agents in the chemical treatment in the preparation of the leaflet material. The main concerns are for their long-term durability and for the consistency of manufacture because of the use of biological materials with unpredictable properties. Research in this field will probably

continue for many years to come.

An advantage, not usually mentioned by many, is the slow and gradual process of failure for the bioprosthetic valves (unlike the rapid failure of mechanical prostheses) which allows for safe elective re-replacement surgery, thus resulting in a higher overall survival rate.

Comparisons of the many variations of valve substitutes available within each of the previous groups is a controversial matter as the number and kind of tests to which a valve must be subjected is not generally agreed.

In-vitro tests are either hydrodynamic, measuring pressure drops and pulse duplicator studies, or tests for structural integrity such as accelerated fatigue tests. The pulse duplicator studies give valuable information on the hydrodynamic performance of a valve and it is likely that the valve which performs well in the laboratory will exhibit satisfactory haemodynamic performance in-vivo. The accelerated fatigue tests though may allow assessment of the time to failure and also characterisation of some modes of failure, but the result may not reflect accurately biological durability due to the reactions within the body which may retard some modes of failure while enhancing some others.

Animal tests can provide preliminary and basic data on a new valve design but they are in general short follow-up studies of only up to three months post implantation. The validity of the tests depends on species differences and on the animal model chosen in particular (MacIver and Howarth,1985). At the same time the choice of the species may be beneficial in studying a specific factor. Sheep have been widely used for studying calcification and thus operate as accelerated calcification models (Fisher et al,1988). Dogs are

probably suitable for studying the effects of thrombosis on valves as incidence of thrombosis and infection has been reported after implantation of a pericardial prosthesis (Gabbay et al,1984a). Calves are restricted to only young animals because of their size and then the period of follow-up is definitely reduced as the animal can double its size within 3months. In calf-trials (Boncheck et al,1967) exhibited calcification of implanted prostheses.

The clinical assessment of the prostheses after implantation (Taylor,1986) can be done by recatheterisation haemodynamic data, echocardiography Doppler non-invasive examination, longitudinal patient follow-up studies (at one clinical centre or many utilising the same prosthesis) and finally by valve explant data.

8.4 SUCCESSFUL BIOPROSTHETIC VALVES.

Bioprosthetic valves consist of three approximately equal tissue leaflets sutured to a tricornute frame, the stent. The stent is needed because it provides both reliability of function and convenience of insertion. The frame may be rigid or flexible (Reis et al,1971) and always is covered by a tight cloth, usually Dacron, which provides a firm substrate for suturing and also prevents the direct and possibly thrombogenic contact of the blood and the stent material.

8.4.1 The Porcine Bioprosthesis.

The porcine xenograft consists of an entire porcine aortic valve preserved in a solution of glutaraldehyde and mounted on a stent. It possesses the shape, the size, and the design of a natural heart valve but not the viability of its native counterpart. Thus while the living valves are able to self-maintain for a lifetime the porcine xenografts are subject to unrepairable injuries and wear.

The success of the prosthesis is very much dependent on knowledge about the mechanical properties (Broom,1977; Sauren et al,1983;

Rousseau et al,1983) and the structure (Broom,1978a,b) of its soft material. Studies of native porcine valves have been extensive for two main reasons. The first is that they resemble the human valves more than those of other animals (Sands et al,1969) and they can easily be obtained and in large numbers. Thus it is convenient to study the functional behaviour of the human valve by using the abundant porcine valves. The second reason is that because of this similarity they are serious candidates as replacement valves and thus they should be thoroughly examined in order to optimize such variables as stent, geometry and fixation conditions.

There are some differences between porcine and human valves. The porcine are less symmetric with uneven leaflets one of which has a myocardial shelf protruding in the leaflet's surface. The porcine leaflets are slightly thicker and with the noduli of Arantius being less distinct. The structure of the porcine leaflets is very similar with only one exception regarding the presence of a layer of loose connective tissue underlying the dense collagenous layer which exists in human and porcine valves. It has been suggested that the presence of the loose layer has a mechanical significance by allowing the collagenous layer to move over the elastic layer(Mohri et al,1972). It is more likely that this architecture allows a reduced second moment of area by having a dense structure around the neutral plane at flexion and by having components of lower stiffness value(loose tissue layer) at a distance to the neutral plane. Its absence from the human leaflet tissue does not seem to have any serious effect on the performance of the natural healthy human heart valves and thus all the previous speculations about its mechanical role are of reduced importance.

The mechanical properties of the leaflets are qualitatively but

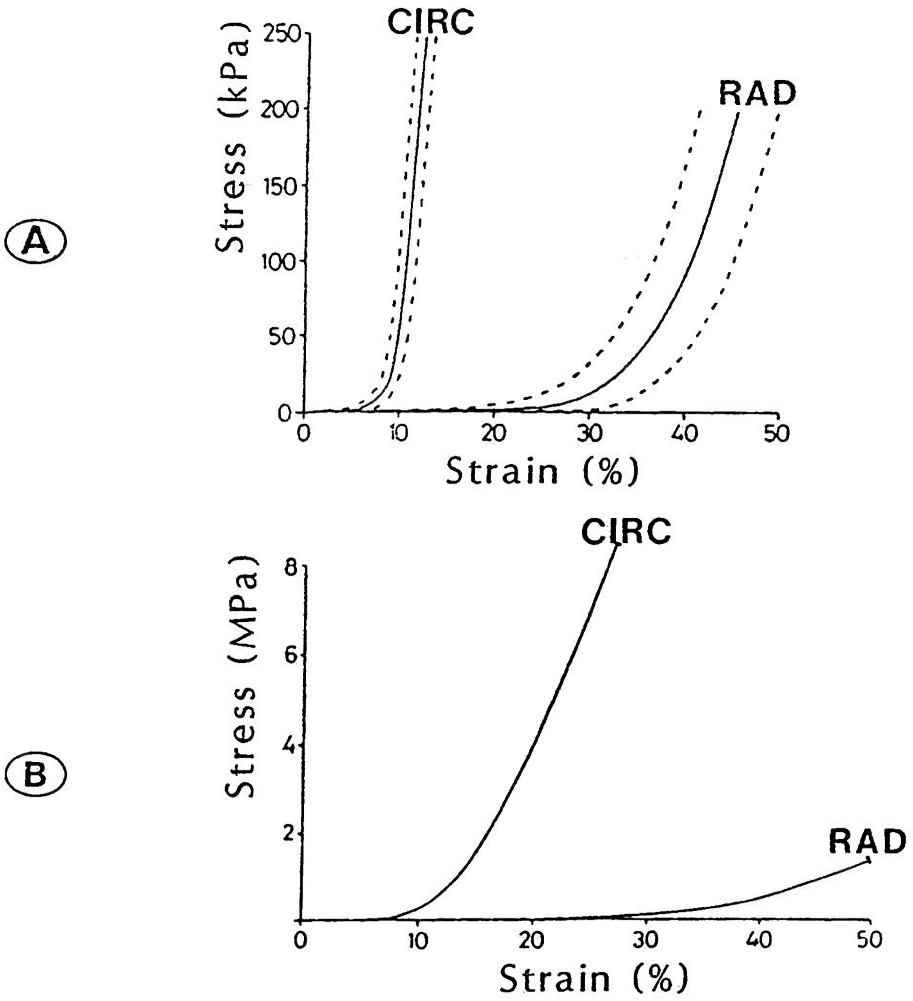

Figure 8.4: (A) Mean stress/strain curves for radial and circumferential strips from fresh porcine valve leaflets. Mean strain+stand.error for n=20 circumferential and radial. Significantly different at all stress levels with $p<0.01$. (B) Stress/strain curves to fracture for a typical radial(RAD) and a typical circumferential(CIRC) strip. Reproduced from Lee et al,1984a.

not quantitatively similar to the human leaflets. In fig.8.4 the response to load of native porcine aortic valve tissue(Lee et al,1984) is shown along the two principal directions on the leaflet. As in the human leaflet tissue, anisotropy is markedly present. The complete curves to failure are included in fig.8.4b. It is evident that the circumferential direction is less extensible, overall stiffer and stronger than the radial one. The tissue modulus (prefailure linear region) was circumferentially: (54.6±7.4)MPa and radially: (7.82±0.58)MPa. If those values are accurate it means that the porcine tissue is slightly less stiff in either direction from the human leaflet material values presented in section8.2.5. The ultimate tensile strength of the porcine tissue was given by the same authors to be circumferentially: (6.25±0.90)MPa and radially: (1.18±0.09)MPa. These values are lower than the equivalent ones measured for bovine pericardium from any area in the sac as presented in chapter5.

The design and whole construction of a porcine bioprosthesis suffers from some inherent limitations. The leaflet material is collected as a whole valve and thus is subject to significant variations from animal to animal. Furthermore as some of the natural human valves are susceptible to failure (for reasons that are not yet clear), the same may be true for the animal valves some of which may have undertaken a failure course before removed from the animal. Thus the control exerted by the manufacturer on the material is very much restricted. Improved recent designs have at least tried to eliminate the asymmetry of the leaflets by removing the leaflet having the muscular shelf, but it is uncertain how much the substitute leaflet matches the other two. The only promising improvements have been in the conditions at fixation, where fixation under lower pressures seems

to result in softer leaflets of increased durability.

In construction the whole porcine valve has to fit inside the stent and thus the valve orifice is inevitably reduced. The result of those limitations can be demonstrated by in-vitro tests where porcine valves have overall lower opening areas at the same flows than the pericardial bioprostheses and also exhibit higher presssure drops for the same forward flowrates than the pericardial ones (Reul et al,1986).

8.4.2 The Pericardial Bioprosthesis.

This xenograft has leaflets manufactured from glutaraldehyde treated bovine pericardium. The leaflets are prepared separately or from a single piece of tissue and then are firmly attached by sutures onto a cloth covered frame.

The great potential advantage of this design is the high degree of intervention that the manufacturer has on the construction of the prosthesis. Modifications and improvements of the design can be introduced in all the components. Firstly, the shape of the stent is not restricted by anatomical factors such as having to accommodate a porcine valve. It can be made to the shape that has the best possible hydrodynamic and durability performance. Secondly, the choices for treating the leaflet tissue are virtually unrestricted regarding its leaflet geometry, the fixation regime which is followed, the attachment method on the stent which is adopted and the specific choice of the soft tissue material. Control on those factors can again result in better performance and increased durability of the prosthesis.

There are many modifications of the original Ionescu-Shiley valve (Ionescu and Tandon,1979) which was released for general use in 1976 and have led to significant improvements over the years, although the

original design has shown satisfactory clinical follow-up results. Primary tissue failure such as tearing close to the edge of the cloth covered frame has been reported(Brais et al,1985; Cosgrove et al,1985; Gabbay et al,1984b). Since 1980 four new pericardial valves have been commercially available: the Ionescu-Shiley Low Profile (ISLP), the Hancock Pericardial valve (HP), the Mitral Medical valve (MM), and the Edwards Pericardial valve (EP). They have already undergone clinical trials (Ionescu et al,1986) and comparative in-vitro tests on their design function and durability (Fisher et al,1986b). The valves incorporated a lower post height or profile in order to reduce the risk of damaging the ventricular wall when implanted in the atrio-ventricular position. Gabbay et al(1984c) and Walker et al(1984) suggested that abrasion of the leaflet on the cloth of the stent is the most common cause of failure but while this is a usual finding in laboratory studies it may be not as common in-vivo where the tissue at exactly those sites is invested by blood deposits and tissue ingrowth(Spyt et al,1988). Placement of sutures close to areas of tissue flexion can significantly reduce the durability of the valve(Black et al,1984).

Fisher et al(1986b) studied the leaflet dynamics of Ionescu-Shiley standard valves(ISU), ISLP, HP and MM. It was seen that in the open position ISU and HP had symmetrical orifices unlike the ISLP and MM. The difference was caused by the presence of stitches at the top of the posts in ISU and HP. In the closed position the posts of the flexible frames deflected inwards thus reducing the tension at the free edge of the leaflets. The HP and MM valves required higher flowrates to fully open than the ISU and ISLP. This was a result of the method of fixation which also affected the way the leaflets transposed from the closed to the open position. In the ISU and ISLP

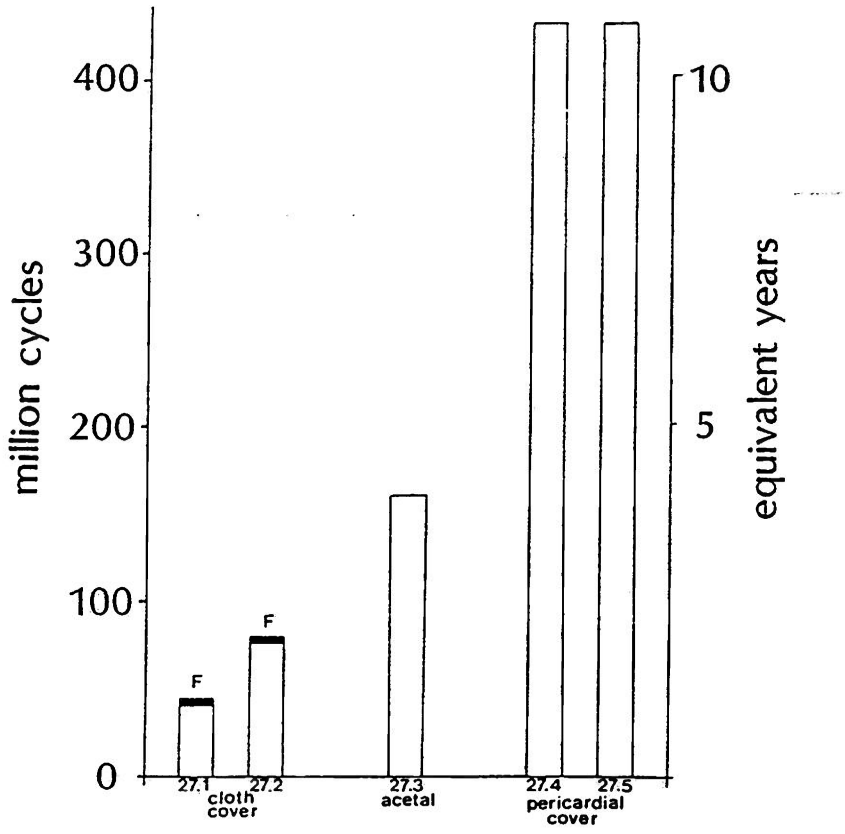

Figure 8.5: Results from fatigue tests for valves with different covering materials of the frames. All valves are 27mm diameter. Reproduced from Fisher and Wheatley,1987.

the tissue buckled circumferentially across the leaflet, while in the HP and MM the tissue reversed its curvature in the base of the leaflet, first buckling in the radial direction.

The new pericardial valve developed in Glasgow has incorporated basically four innovations (Fisher and Wheatley,1987). Firstly, a new flexible frame design manufactured from acetal polymer. Secondly, the frame consists from two parts; an inner frame with radially projecting pins on which the leaflets are mounted, and an outside sleeve covered with polyester cloth which clips over the frame and radial pins to maintain the leaflets' position on their retaining pins. Thirdly, the inner frame is covered with glutaraldehyde treated pericardium. Fourthly, the leaflets have been moulded in a shape of mixed cylindrical and circular geometry and has been developed on the basis of extensive in-vitro testing.

The objectives of the previous modifications were respectively: a)to reduce stresses at the top of the posts, b)to allow for easiness of interchange of leaflets during manufacture in order to obtain accurate leaflet matching (in respect to both operation and properties) as well as avoiding the need of suturing anywhere on the leaflet, c)to reduce the incidence of failure caused by abrasion on the frame by covering it with the soft pericardial tissue, d)the shape has been chosen such that it achieves the most stable closed position, the most symmetric open position, improved transposition from one position to another with minimal turbulence induced on the flow, with a geometry that it is less affected by mismatching between the leaflet properties, it provides a good wash-out in the outflow surface and with improved hydrodynamic parameters like the minimal flow to open, lower transvalvular pressure drops at certain RMS flowrates, lower closing regurgitation volumes and lower closed valve leakage volumes.

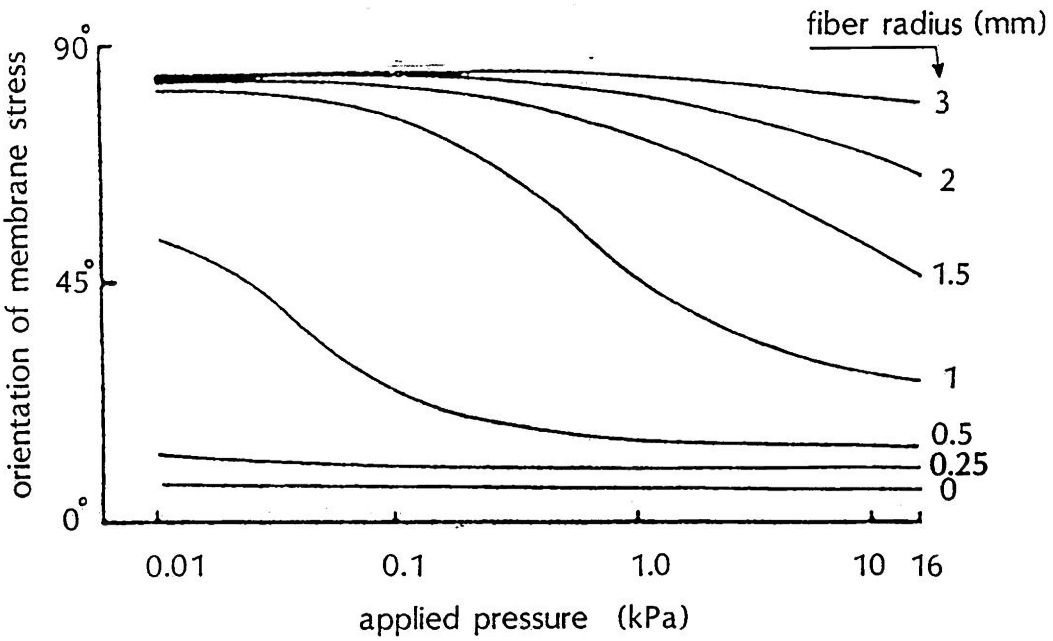

Figure 8.6: Orientation of the membrane stress field relative to the fibre direction in the leaflet belly as a function of pressure. Reproduced from Christie and Medland, 1982.

This valve design has succeeded in producing favorable results in the hydrodynamic tests against any other commercial valve and exhibited a greatly improved durability (fig.8.5) mainly due to the pericardial covering of the inside frame.

All these efforts are of the "observe and correct" form regarding the function of the valve, and of "report and eliminate" regarding the valve durability. The state of the art in valve manufacture and the most elegant method is the use of finite element stress analysis for predictions of the valve behaviour and the design of an improved valve. It is always easier to change the shape of the leaflet on the screen than produce a series of prototypes in order to investigate the same effect. In some cases where the field of stresses over the whole leaflet is sought finite elements are the only method available, provided of course that the formulation has been made on the correct assumptions.

Christie (1982) developed an analysis of the mechanics of bioprosthetic valves by using a finite element formulation. Two possible cases were considered. In the first one the leaflet tissue was modelled as a thin isotropic membrane, while the second model allowed the tissue to have anisotropic properties as would be the case for allografts and porcine xenograft valves. The anisotropy was achieved by embedding circumferential hyperelastic fibres into the isotropic membrane.

The analysis of the isotropic model suggested that the maximum stress existed at the leaflet belly, which was consisted with observations of Carpentier et al(1976) about common sites of failure in valves. The stress concentration was high at the commissures where a number of valves do develop tears and this condition required the introduction of the flexible stent posts to reduce the stresses. The stress field

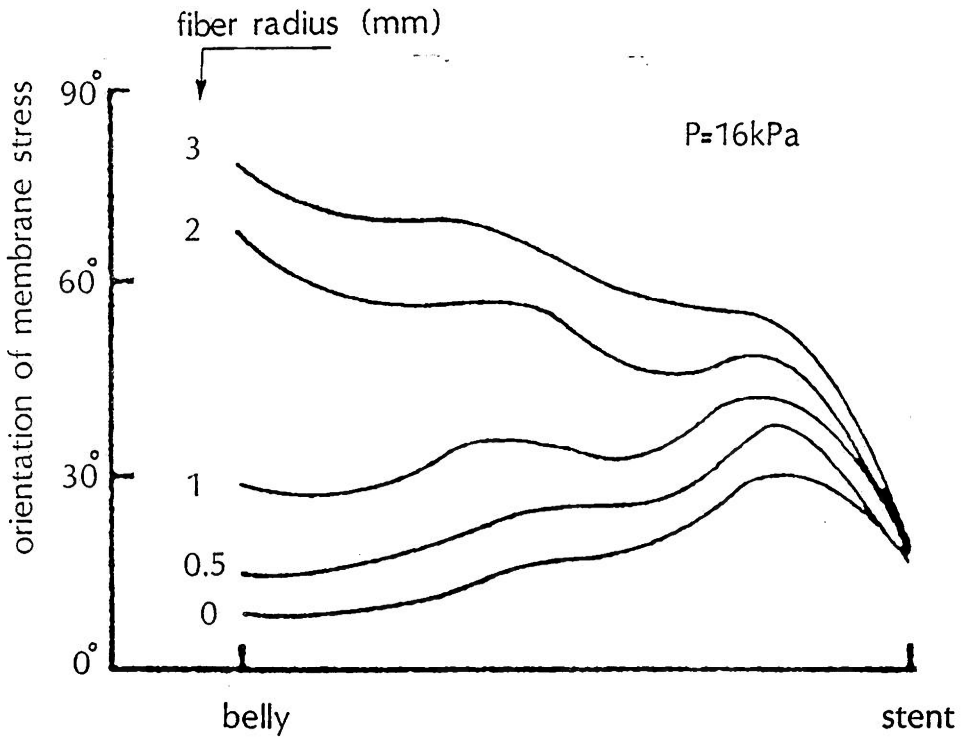

Figure 8.7: Orientation of the membrane stress field relative to the fibre direction across the leaflet at P=16kPa. Reproduced from Christie and Medland, 1982.

was closely aligned in the circumferential direction over most of the leaflet surface and this alignment was pressure independent. The maximum stresses increased with decreasing tissue compliance and this fact should be seriously considered during the fixation procedure. The leaflet shape deformed mainly by moving downwards as pressure increased and not by increasing its coaptation area with the other leaflets. The reaction along the stent boundary was not uniform and presented peaks at the commissures and at a 32^{o} angle from the centre line of the leaflet.

The anisotropic model showed that a)stress reduction was observed everywhere on the leaflet but it was not as pronounced as in the area of the commissures where stress was reduced by a factor of ten, the reason for this being that the stress field was almost uniaxial at the commissures and the existence of the circumferentially aligned fibres was more effective there. The orientation of the stress field is shown in figures8.6-8.7, higher fiber radii symbolised a higher degree of anisotropy and it is evident that for higher anisotropy the field of stresses was virtually always aligned to the radial direction for all ranges of pressure. In fig.8.7 the field alignment at a pressure of 16kPa for various degrees of anisotropy was presented along a line from the centre of the belly to the scallop, the greatest changes were observed in the belly and thus presence of anisotropy brought relief to the area of the leaflet prone to failure. The downwards movement of the leaflets with an increase in pressure was retarded and the movement towards the coaptive area was increased when pressure was increasing as well as when the degree of anisotropy was increasing, because the net movement of the leaflet is towards the coaptive area in the anisotropic membrane, this area of coaption was found to increase with both the pressure and the anisotropicity of the

leaflets. The reaction force at the leaflet boundary was found to be distributed further down the post and not at the commissures but it was still not uniform and probably only a proper fibre adjustment like the one existing in the leaflets could lead to a uniform distribution of load onto the stent post.

Hamid et al(1986) also carried out finite element analysis on leaflets and concentrated their efforts on the influence of the stent height on the distribution of stresses on the closed cusp of the bioprosthetic valve. The model was based on the following assumptions. The initial geometry of the leaflet was thought to be an elliptic paraboloid. The tissue was isotropic which may be the case for the leaflets of commercial pericardial xenografts but not for the particular case of procine valves on which the model was applied. The material properties were non-linear by a discretisation in five regions of constant Young's modulus. The leaflet thickness was assumed to be uniform all over the surface. The stent was modelled as being rigid, which may not be the case with the latest flexible stents.

The results showed that, as in Christie's isotropic case, the higher normal and shear stresses occurred at the commissures and their magnitude was increasing as post height was reduced. Coaptation areas were not significantly increased upon deformation but they were higher for lower post heights. The reaction force along the boundary was slightly more uniform for lower struts.

We said earlier that the latest designs reduce the height of the posts in order to gain haemodynamic advantages, but on the basis of this report it seems likely that this will result in mechanical disadvantages.

8.4.3 Optical Observations on Leaflets.

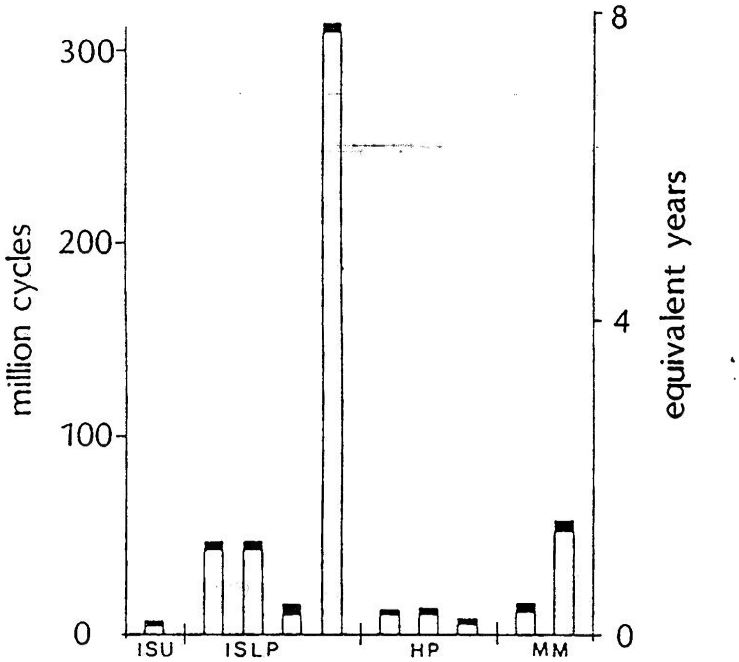

Figure 8.8: Durability of 4 commercial pericardial valves in accelerated fatigue tests. Reproduced from Fisher et al,1986b.

8.4.3.1 Commercial Pericardial Valves. As part of the design project of the Glasgow-pericardial valve currently manufactured by Biomedical Systems ltd., the leaflets of a number of commercially available pericardial bioprosthetic valves have been examined with the polarising optical method introduced in chapter7. The method has a great potential in identification of the direction of alignment of the collagen fibres in pericardium and consequently in the leaflets.

None of the commercially available bioprosthetic pericardial valves claims to have incorporated and utilize anisotropic leaflets in its product. In order to confirm this opinion a great number of different brands of commercial valves were dismantled and their leaflets were viewed with the polarised microscope.

During the development of the Glasgow valve some of the valves were subjected to extended fatigue studies in a pulse duplicator rig(Fisher,1986) and preliminary results on the function, design and durability(fig.8.8) of these commercial valves has already been reported(Fisher et al,1986). The conclusions drawn contributed invaluably to the functional behaviour of the improved Glasgow pericardial valve(Fisher and Wheatley,1987). The dimensions of the valves were only marginally different (table8.1), but the more updated Hancock pericardial and Mitroflow valves had an altered construction and design from the original Ionescu-Shiley valves.

The tissue leaflets of valves fatigue-cycled in laboratory tests were examined in the polarised microscope and the primary interest was the appearance of the tissue at the sites of failure as well as the alignment of anisotropy axes in those leaflets.

The valves were cycled in Rowan Ash accelerated fatigue testers at 12Hz with a closed back pressure of between 100 and 130mmHg and peak forward flow of between 330 and 450ml/s. Valves were inspected

Table 8.1:key dimensions in mm for the size 29 and size 23mm valves.				
Valve size	ISU 29	ISLP 29	HP 29	MM 29
outside diameter Do	31/30	31/30	29	29
internal diameter Di	25	24.5	24	24.5
overall height H	20	19	17	16.5
leaflet height h	16	15	12.5	12.5
coaption depth hc	4	3	2.5	2.5
Valve size	ISU 23	ISLP 23	HP 23	MM 23
outside diameter Do	28/25	26/25	24	22.5
internal diameter Di	19.5	19.5	20	19
overall height H	18.5	17	16	15

every 160million cycles but the first signs of failure defined as a tear of at least 2 to 3mm in the leaflet were noticeable earlier.

The results are presented for each one of the leaflets which are numbered as 1,2,3 with the number being of no-significance since the 3 leaflets of the axisymmetric pericardial bioprostheses are identical.

IONESCU-SHILEY No.34 (29mm) showed: leaflet 1, failed close to the rim by developing a hole which was obviously due to abrasion with the Dacron cloth which covered the stent. The optical pattern had a random orientation evidence of an isotropic leaflet.

Leaflet 2, had two long holes on either side close to the rim, developed similarly because of abrasion between tissue and stent. The optical pattern was double (crossing itself) and inconsistent to the leaflet's axes. Near the holes it was obvious that only those fibrous layers which ran across from one side to the other and thus were aligned normally to the stent rim were still intact and could sustain stresses.

Leaflet 3, had an optical pattern indicating that fibres mostly ran circumferentially and had complete absence of any signs of failure.

IONESCU-SHILEY No.22(29mm) fatigue cycled in a similar fashion gave: leaflet 1, serosal view(outflow aspect) of leaflet had fibres aligned at a large angle to the circumference and epipericardial view of fibres aligned circumferentially. The leaflet had developed a hole along the stent rim (near the leaflet edge midway the top-post and the leaflet scallop) and careful inspection with the microscope revealed that delamination of the fibrous layers had occurred where fibers were aligned parallel to the stent and not normal to it.

Leaflet 2, had fibres running at 20°-30° angle to the circumferential direction of the leaflet and with a crossed optical pattern on either surface. There were no areas or signs of failure in this leaflet.

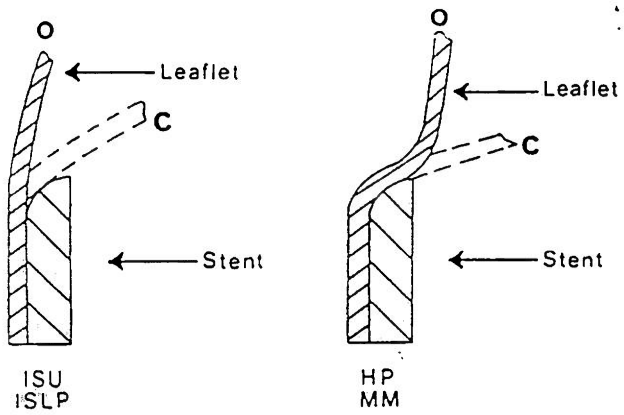

Figure 8.9: Geometry at the base of the open and closed leaflet at the edge of the frame for two different commercial valve designs. Reproduced from Fisher et al,1986b.

Leaflet 3, demonstrated an optical pattern which varied grossly in direction along the leaflet when viewed from its serosal surface. On the epipericardial side the alignment was 0^{o}-30^{o} to the circumference. As a result of fatigue cycling a small hole had developed at one side close to the rim and, there, fibrous layers were found to align along the hole.

IONESCU-SHILEY No.43(29mm) showed: leaflet 1, superficial fibres aligned radially on either side(serosal- epipericardial). Near the stent wear had resulted in a hole on one side and the onset of a developing hole on the other. At this area where the hole had not progressed to a clear perforation it was found that the inner layers of the tissue had fibres with diverse orientations which were still sustaining the load and keeping the leaflet intact.

Leaflet 2, showed identical abrasion pattern with one fully developed hole and one starting. The deeper fibrous layers at the site where abrasion had not result in a complete perforation were again multidirectionally oriented.

Leaflet 3, had circumferential alignment of fibres along the free edge and a crossed optical pattern further down the leaflet belly. Two holes had developed on either side along the rim away from the commissures.

The geometry around the stent was different between the ISLP and the HP or MM valves. In fig.8.9 the result of different manufacturing procedures is shown, ISLP leaflets were prefabricated in their natural shape and then mounted on the stent while both HP and MM are fixed in a shape which follows the contour of the stent. This results in different position and behaviour of the leaflet at this site when the valve is open or closed. The ISLP valves mostly abrade on the stent

than flex. HP and MM valves are attached to the contoured boundary and flex at a higher site by reversing their curvature during the complete cycle of operation of the leaflet.

From a number of HANCOCK pericardial valves, valve No.23 (29mm) showed: leaflet 1, a pattern running at 45° to the free edge(circumference) on either surface. The leaflet was intact with no signs of failure.

Leaflet 2, had developed a tear started at the free edge close to the commissure and going down parallel to the rim. The superficial fibres appear to run at 70° to the circumference on the serosal surface, and at various directions on the epipericardial surface.

Leaflet 3, had a crossed optical pattern on either of the viewed surfaces and was thicker than the other two leaflets. No signs of failure were there on any site.

HANCOCK No.32 a 29mm valve showed: leaflet 1, a crossed optical pattern at 45° on either surface. The leaflet was in good condition with no signs of fatigue-failure.

Leaflet 2, was in a very good condition and had a crossed epipericardial optical pattern and a serosal pattern which varied in direction locally on the leaflet's surface.

Leaflet 3, had fibres at a small angle to the circumference on the serosal surface and almost uniformly circumferentially oriented fibres on the epipericardial surface. It was thinner than the other two and had started to develop a groove along the rim of the stent due to abrasion of the leaflet with the Dacron cloth of the stent.

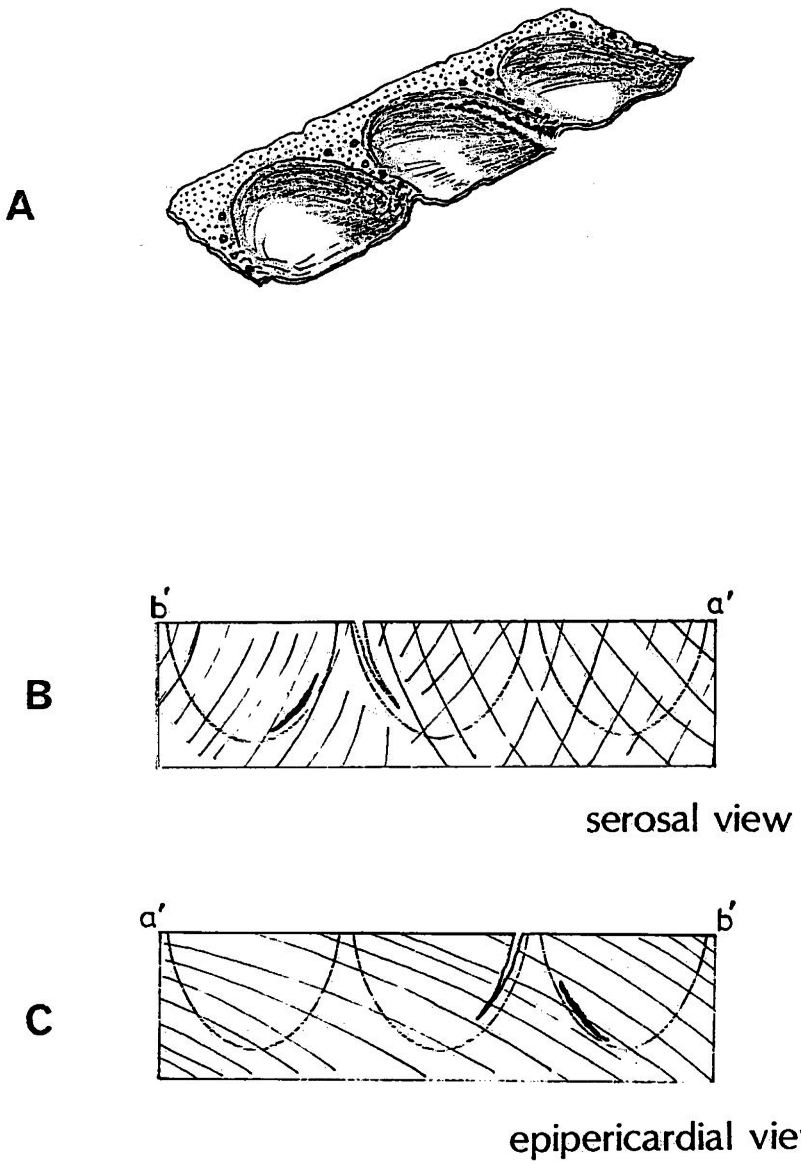

Figure 8.10: The single pericardial piece of a MITROFLOW valve bioprosthesis. Valve No.44 was cycled in accelerated fatigue-tests and developed a tear along the rim of the middle leaflet. B and C are the two views by using transmitted polarised light microscopy, showing the orientation of the fibres in those leaflets.

The MITROFLOW (manufactured by MITRAL MEDICAL Canada ltd.) consisted by a single piece of pericardial sheet which was attached and sutured to the outside of the stent posts and was wrapped around the perimetry of the valve orifice. Thus on dismantling the valve an elongated rectangularlike piece of tissue was obtained which included the three leaflets (fig.8.10a). As a result of this manufacturing procedure it may be possible to manufacture leaflets with similar properties if the tissue presents uniform properties over a substantial length l_o.

MITROFLOW No.45 a 29mm valve presented:

a serosal surface with fibres running at 10°-20° to the circumference from the left to right side and facing the pericardial piece. A small hole had developed in the middle leaflet at a site where fibres aligned along the hole, and other areas were starting to produce holes with the progression of the wear always starting from the epipericardial surface.

The epipericardial surface had a pattern absolutely aligned to the one on the serosal surface and again it was rotating from small angles to the circumference to larger angles as the examination proceeded from end a′ to end b′ of the pericardial piece.

MITROFLOW No.44 a 29mm valve showed:

a serosal surface (fig.8.10b) with fibres running in diverse directions. It had developed a tear along the rim starting from the commissure downwards the leaflet belly in the middle leaflet and had a hole at the usual position near the leaflet rim for one of the side leaflets

The epipericardial surface (figue8.11c) had superficial fibres aligned mostly circumferentially along the whole length of this pericardial piece.

The conclusions that can be reached by such investigations are: i)the various manufacturers follow different procedures in collecting and manufacturing leaflets, with the Mitroflow valve being the only one which forms three adjacent leaflets from a single piece of pericardium. This procedure could result in uniform interleaflet properties if the pericardial piece of tissue has uniform properties over a larger area; ii)none of the commercially available valves claims to have incorporated leaflet tissue of anisotropic properties and it is very unlikely, that by randomly positioning the tissue on the mould, leaflets with fibres running circumferentially will be produced; iii)the valves fatigue-cycled in the present investigation showed the classic weaknesses reported in the literature, by failing along the rim of the stent as a result of abrasion on the rough Dacron cloth covering the stent itself and in combination with the bending stresses developed in those areas as a result of repetitive flexion of the tissue. The improved design of the Glasgow pericardial valve, which comprises an inner frame covered also by pericardium and thus provides an elastic smooth boundary, hopes to eliminate this failure mode. iv)a number of tears developed as a result of excessive tensile stresses near the commissures and this was in agreement with the high values of stresses calculated for these sites by all stress analyses for valve leaflets. The frequency of occurence of these two modes of failure i.e.along the rim and at the commissures, appears to be different for valves operating in-vivo. v)Connection of those sites prone to failure and the fibre-orientation has been established by the occurence of holes and tears; at points of higher stresses missalignment of the fibres to the direction of maximum tensile stresses was more likely to result in failure. To avoid such failure the fibres had to run circumferentially at the commissures and at a

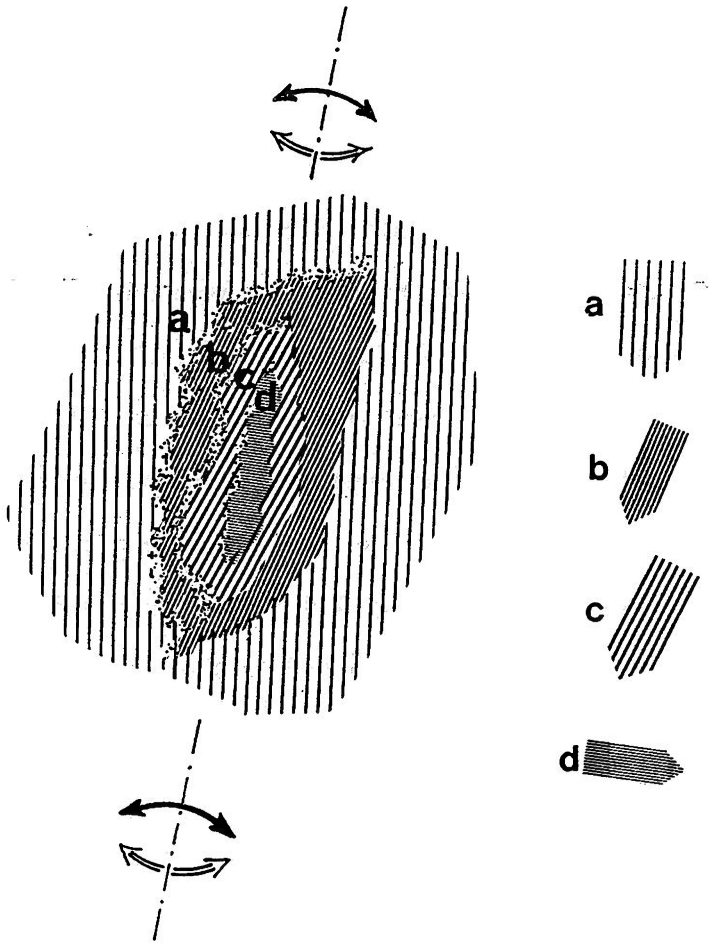

Figure 8.11: Delamination of pericardium due to abrasion. From a number of successive layers only those which ran across the hole were able to withstand the wear.

large angle (if possible normal) to the rim along the boundary very much like the optimum fibre orientation existing in the natural valves. At those cases where failure was encountered the previous rule did not apply. The reason being that a hole progresses as in fig.8.11. Abrasion had induced mechanical wear of the material while cyclic flexion resulted in bending stresses which have already been shown to exist in the fixed leaflet tissue of bioprosthetic valves (Thubrikar et al,1980; Thubrikar et al,1982a) and induce failure especially by compressing the tissue (Broom,1978c). From a number of successive layers of the "plywood" structure of pericardium (chapter7) only those that run across the elongated hole(groove) can sustain the mechanical stress. Delamination of the tissue starts on the epipericardial surface (attaching onto the stent) and continues till complete perforation occurs. It is likely that some areas with non optimum fibre alignment may elude complete failure, probably due to a greater thickness, but prolonged operation would result in failure there as well. It was found that thicker leaflets which at the same time appeared more isotropic (by having a great number of multidirectionally directed fibres) remained intact and in a good condition, but this can not be used as a suggestion for an optimum leaflet construction as thicker leaflets are overall stiffer and thus require higher transvalvular pressures for opening of the valve.

8.4.3.2 Glasgow Pericardial Valve. During the development of the improved Glasgow valve the validity of the assumption that the fibre orientation in a valve leaflet can be effectively controlled and the results that it may have on modes of failure were examined. A number of Glasgow pericardial valves have been cycled in the pulse duplicator testing rig described elsewhere (Fisher,1986) and those valves that presented signs of failure were inspected and examined in the

microscope.

Valve 17.11 was in the pulse duplicator for 5 months and because of the accelerated nature of cycling this was equivalent to a period of 4 years in the life of a normal individual (75 beats per minute). Leaflet 1 presented a tear running along the central area and starting from the free edge and progressing towards the belly. It was the point of coaption between all 3 leaflets of the valve where the leaflet formed an angle when the valve was shut. The fibres there were found to run predominantly in the radial direction and thus failure had occurred in the matrix and the interfibrillar material which was keeping the fibres together. In manufacture the collagen fibres in the leaflet were aligned to the radial direction of the leaflet on purpose. This practice was followed because the initial results on the mechanical properties of the tissue showed that the axial direction in area-I was less extensible in the fresh pericardium. The intention was that leaflets manufactured in such a way would exhibit an anisotropy in extensibilities similar to the one of the natural leaflet. Unfortunately this meant that the fibres were aligned radially and thus unlike the fibres of a natural valve leaflet. As a result flexion and tension induced shearing stresses across the fibres in the centre of the coaption area and resulted in a tear of the leaflet.

Leaflet 2 had a similar orientation of the fibres along the radial direction and as a result early signs of failure appeared in the central area of coaption between all 3 leaflets. The tissue was very thin and a delamination of the structure had started by wear of the collagen layers on either side of the leaflet.

Leaflet 3 was positioned with its fibers running at an angle roughly

45° to the free edge of the leaflet and showed no signs of commencing or progressing failure.

Valve 27.11 was similarly cycled and the intention during manufacture was to position the fibres at a radial direction. Again the emphasis was put on the mechanical behaviour sought from the leaflet and not on the proper alignment of the stress bearing elements(collagen fibres) along the circumference. Upon inspection the valve showed:

Leaflet 1 had fibres running radially and exhibited a tear at the centre of the coaption area starting at the free edge and progressing to the leaflet belly. The optical pattern was identical on either side (serosal- epipericardial) and the tissue had obviously failed by a separation of the fibres right and left of the tear.

Leaflet 2 had fibres also aligned on the radial direction and had developed a hole along the rim of the stent midway the distance between the commissures and the bottom of the leaflet. Failure of a leaflet of this kind was a common feature of the early pericardial valve and was due to the abrasion of the leaflet on the Dacron cloth covering the stent. In the Glasgow valve this was unlikely to have happened because one of the innovations introduced has been the covering of the inside frame with a pericardial sheet. The reason for this failure must have been then the fatigue flexion of the tissue along the hole (at a site of an initial wrinkle formed during fixation) which had clearly destroyed the interfibrillar bonding at this area. Natural valve leaflets again have a structure comprising fibres running normal to the rim all along its length and thus avoid this sort of failure.

Leaflet 3 presented a double pattern on either side which indicated a

diversity of orientation of the fibres along its thickness. No apparent damage was there present on this leaflet at any site.

From such investigations it was concluded that

i)preferential orientation of the fibres of a leaflet along the leaflet's radial or circumferential direction was possible with a high degree of accuracy during manufacture as confirmed by the optical pattern of the leaflets after fixation, and

ii)alignment of the fibre-direction along the radial leaflet direction does not guarantee that the leaflet will be less extensible circumferentially, but it has the highly possible result of interfibrillar break-down as the elements which hold the fibres together are subjected to considerable stresses produced by the stress field of the valve as described in earlier sections. For this reason circumferential alignment of the fibres is recommended because it results in suitable alignment of the fibres to the stress field for a larger area of the leaflet.

8.5 DISCUSSION.

In the present chapter the function, geometry and properties of the natural human valves were reviewed with an emphasis given on the leaflets and their role in valve mechanics. The idea was that a better understanding of the engineering requirements for the construction of a successful valve prosthesis can come from analysis of the structure and deformations of human or porcine aortic valves. If the natural design and shape of valve is the optimum then the reasons for the anisotropy (both mechanical and structural) of the native leaflets should also be found. Use of finite element methods together with logic can be very helpful in clarifying the conditions. The leaflet must exist in a suspended mode from its boundary and

sustain a significant normal pressure by transmitting it to the walls. Finite elements showed that these loading conditions yield an almost circumferential field of stresses. The structural effect of anisotropy is then to help sustain increased loading in the circumferential direction and thus increase valve durability. The analysis also showed that there is a functional reason behind the different stiffnesses and extensibilities of the stress/strain curves, according to which a leaflet more compliant radially would coapt better to the other two. However in bioprosthetic valve design the coaptation area can be controlled at will, as in the new Glasgow valve by suitable adjustment of the leaflet geometry at the coaptation site. Therefore from the two conditions the one which is more important in the manufacture of an aortic-type valve bioprosthesis, is the fibre-reinforcement along the circumferential direction.

The present optical observations that commercial leaflets show no consistency in fibre-orientation confirm that manufacturers of pericardial xenografts do not treat the pericardial material as anisotropic. The use of polarised light was very helpful in identifying the local fibre-orientations in the leaflets. Further inspections of fatigue-cycled leaflets showed a connection between sites of failure close to where the leaflets abraded on the stent and the local fibre direction. This indicated that the fibre-orientation may be correlated even with classical modes of failure by abrasion and local bending stresses.

The mechanical tests on native bovine pericardium showed that the anisotropy of this tissue compares favorably with porcine valve material and even the human valve tissue. Two more factors should also be investigated. These are the effect that fixation has on the anisotropy of the fresh tissue and the effect that the body

environment may exert on the mechanical behaviour of the pericardial tissue. Information on both these topics may allow prediction of the pericardial behaviour after implantation and recommendations for the better use of the tissue.

9.1 INTRODUCTION.

The work of the previous chapters has dealt with the properties, structure and anisotropic elasticity of fresh bovine pericardium. Chemical stabilisation of the tissue by aldehyde-treatment is required prior to the use of the tissue for the construction of the bioprostheses. This treatment results in modification of the tissue properties and the mechanical properties may be significantly altered after fixation.

In the present chapter the mechanical behaviour of fixed bovine pericardium is examined and the research that has been performed is presented in two sections.

The first examines the effect that fixation has on the mechanical anisotropy of fresh tissue.

In the second section a series of tests is described which were performed on fixed pericardial tissue currently used for the construction of valve leaflets. This is the only part of the whole thesis where there could be no examination of the properties of the tissue prior to fixation and thus both the approach and the treatment of the results had to be isotropic. There is no information in the literature about the long term effects of mechanical conditioning on this tissue and the modification of the original mechanical response after implantation in the human body. The influence of these factors had to be examined to allow prediction of the valve behaviour (or even performance) following the design and manufacture.

9.2 FIXED BOVINE PERICARDIAL TISSUE.

9.2.1 Fixation, Reasons and Fixatives.

One of the first biological reactions after the death of a cell is the release of enzymes which attack the proteins of the cell itself and the surrounding tissues, initiating the decay. Preservation

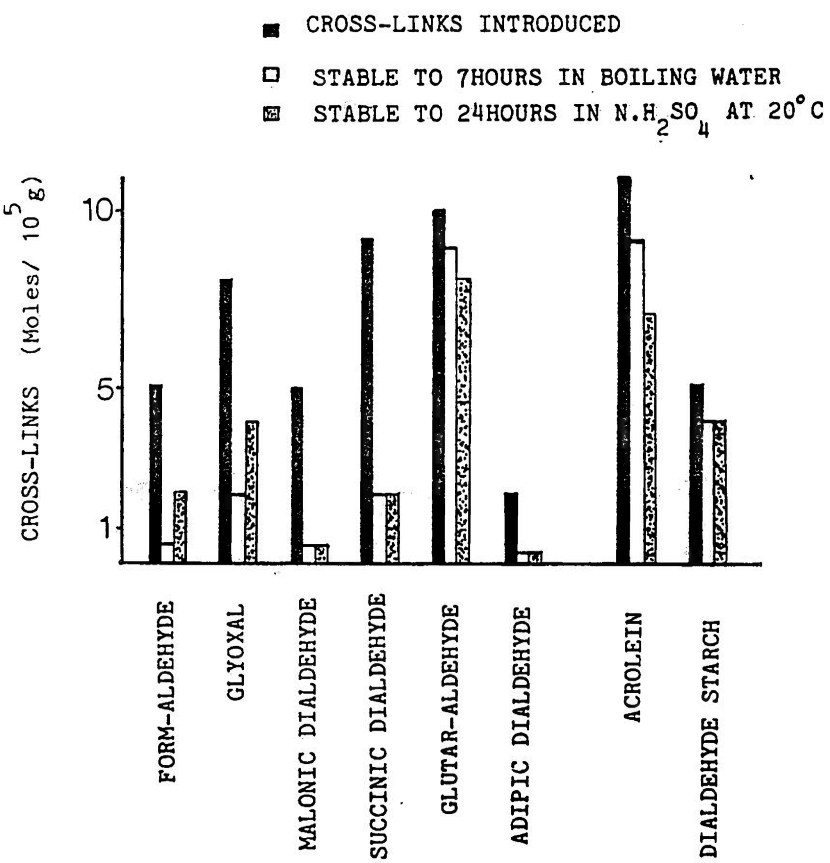

Figure 9.1: Performance and stability of a number of dialdehydes. Glutaraldehyde bonds have been found easier to introduce and also more stable in boiling water and treatments in acid solutions. The authors also suggested that acrolein appears quite competitive especially where fixing in vapour phase is indicated. Reproduced from Bowes & Cater,1965b.

employed various methods including heating to boiling which unfortunately destroys the cellular and structural proteins in addition to the autolytic proteins. Glycerol can substitute the water inside the cells and thus prevent their decay (like preserving fruits in syrup); deep freezing at -70°, -196°C which is very effective otherwise is not applicable here, while when storing at 4°C retarded autolysis exists which can be kept acceptable for a couple of days but does not stop the whole process. The possibility of microbial contamination is also there and methods like freezing will definitely preserve microbes as well as tissue. Irradiation can kill some microbes but fungi may survive, while anti-biotics and anti-fungal agents still are considered to offer low level sterilization. Immunological reactions tend to be lower for tissue implants that have low vascularity or develop no specific revascularization but they will be there as long as viable microbes and untreated tissue proteins exist. Immunogenic reactions in association with mechanical load will result in long-term or late onset of degeneration.

Fixation of biological tissues has then the primary objectives of stabilizing the structure, reducing solubility and increasing the resistance to enzymes and bacteria. From the many chemical substances which would at first appear suitable to use, dialdehydes are the most appropriate because they present two chemically active sites which can react on either side with amino groups of proteins and thus bridge the gap between fibrous elements. Structural stability depends on various cohesive forces such as ionic-hydrostatic contacts, hydrogen bonds, covalent bonds and covalent crosslinks, the number and the quality of which are equally important. The stability of the protein-aldehyde bonds varies with the aldehyde, some aldehydes being better than others (fig9.1).

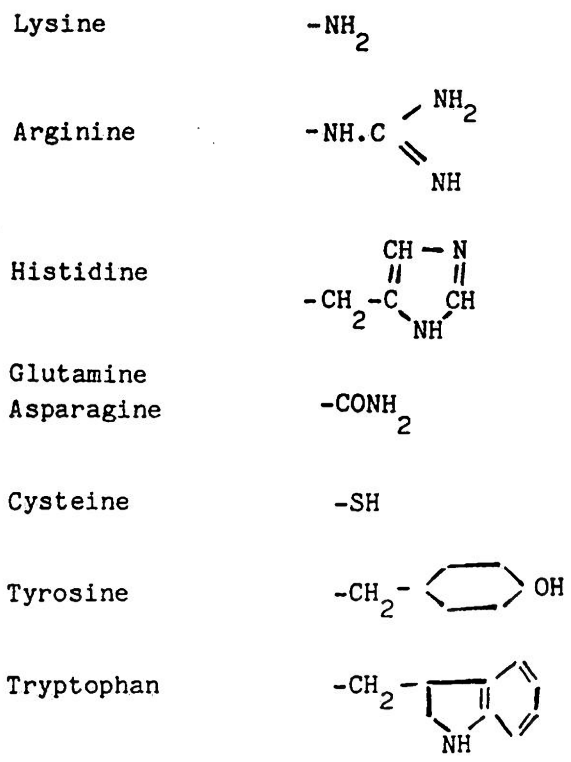

Figure 9.2:Reactive groups of proteins. Reproduced from Bowes & Cater,1965a.

In dialdehydes one or both groups may react, giving either an aldehydic group to participate in subsequent reactions or the direct cross-linking of the polypeptide chains. The actual mechanism of glutaraldehyde reaction is not clear yet. It has been suggested that it involves either Schiff's base formation, unsaturated addition reactions (Cheung and Nimni,1982a) aldol condensation(Richards and Knowles,1968) or pyridinium type cross-links (Hardy et al,1976). The kinetics of the incorporation of the fixative in the tissue have been found to be unpredictable as well. At low concentrations first order kinetics utilising only one exponential coefficient are required (Gavilanes et al,1984), but at higher concentrations a multiexponential formula was required. The need for different formulas at different concentrations indicated the presence of two populations of lysyl and hydroxylysyl residues which may be reacting as Cheung and Nimni(1982a,b) suggested; they proposed that at lower concentrations intramolecular bonds are more likely to form while at higher concentrations a rapid coating of the collagen fibrils by glutaraldehyde may prevent penetration of the fibril itself and thus only intermolecular bonds were formed.

Glutaraldehyde tends to polymerise in higher pH; in a monomeric or polymeric form the reaction being with amino groups(fig.9.2) some of which may not be physically accessible to aldehydes of higher molecular weight and thus larger size. From a number of 34moles amino-groups per 10^{-5}g collagen approximately 26moles appear to be available for binding with glutaraldehyde, 20-22 under favourable circumstances are involved in cross-linking, leaving only 4-6 moles involved in uni-point fixation (Bowes et al,1965). The final performance depends also on the conditions and the degree of polymerisation of glutaraldehyde at each particular instant.

Polymerisation may appear at even small amounts of water. In acidic environment polymerisation is retarded for long time periods, but as the pH is raised polymerisation is rapid but so are the fixation reactions some of which only occur at pH 9 or 10, e.g.the guanidino groups of arginine. Some reaction occurs at pH3 with the optimum being around pH8; at higher values increased polymerisation reduces the efficiency of the cross-linking (Bowes and Cater,1965a). It may be possible to exploit these features by impregnating the tissue in an acidic solution of glutaraldehyde and then, following the equilibration, rising the pH to initiate the reactions through the whole tissue depth. This technique is claimed to be followed by at least one valve manufacturer (Mitral Medical,Ltd).

Temperature, time, concentration and pH are all important in the glutaraldehyde's kinetics its stability and purity(Gillett and Gull,1972). These factors also influence the number and the quality of the cross-linking achieved.

The interactions of any aldehyde binding on collagen can be assessed by chemical means and radio-isotope techniques(Bowes et al,1965), or by determination of the loss of lysine and hydroxylysine (Cheung and Nimni,1982b). Physical means such as the measurement of shrinkage temperature (Gavilanes et al,1984) may be used, as may the very uncertain method of estimating the cross-links by stress/strain measurements of thermally shrunk collagen which assumed that the material behaved according to simple rubber theory (Cater,1963). The last one, applied after temperature shrinkage, presumes that the collagenous structure behaves like rubber and thus rubber polymer equations can be used.

The assessment by these means is not without questions. Shrinkage temperature depends on the nature of the tissue in question. The

level of organisation of the collagen is also important as the work of Cheung et al,(1982abc) has shown. These workers while working on soluble collagen, reconstituted fibres and fixation of whole tissue observed that the glutaraldehyde's action is based on the ability of the fixative to reach the active amino-groups. It is easily appreciated that the degree of alignment and entanglement of the fibres is different in different tissues, that the cross-linking entities may not be uniformly stable at higher temperatures and thus quantification of the cross-links may be difficult, and that once one cross-link has bridged 2 molecules further cross-links may be impossible to detect. Amino acid analysis of hydrolysates also depends on the geometric form and the lay-out of the active sites. Although almost invariably (Cheung et al,1982abc; Gavilanes et al,1984) higher concentrations yield lower percentages of lysyl residues recovered, this was only because an outer protective glutaraldehyde coating was formed which prevented penetration to the inside of the fibre. Solubilisation of previously denatured collagen gave higher percentages of recovered material and thus indicated that fibrous form presented reactive groups that were better accessed to the dialdehyde molecules.

The use of glutaraldehyde, in particular, was found to have good sterilising effects (Woodroof,1979), it being able to kill a wide range of micro-organisms. However unlike the optimum conditions for fixation and glutaraldehyde stability, higher concentrations were more effective for sterilisation than lower ones. It was found that spores were more difficult to destroy and cells with a higher lipid content in their cell membrane were better protected. This is in accordance with Gavilanes et al(1984) observation that a more effective fixation could be achieved by delipidation of the collagenous tissue. The

protective role of lipids fortunately did not apply to proteoglycans which are perfectly permeable to glutaraldehyde. This is particularly important for the tissue matrix not to hinder the action of the fixative at deeper layers.

9.2.2 Current Fixation Conditions.

The previous considerations were all taken in account when setting the fixation regime for the Glasgow leaflets which aimed to produce a tissue with reduced biodegradability and antigenicity, but with a high mechanical stability and consistency in its mechanical properties. A solution of well monitored constitution was used. A variety of glutaraldehyde solutions were examined and the presence of monomeric forms absorbing at 280nm and polymeric alpha-beta unsaturates absorbing at 235nm were monitored using U.V spectroscopy(Fisher,1986). The solutions were purified prior to tissue treatment by extraction of the polymeric forms by distillation and filtration. The effect of adding pericardial tissue to the glutaraldehyde solution was also monitored. It was found that tissue induced polymerisation by formation of alpha-beta unsaturates. When the solutions were diluted and buffered to pH7.4 rapid polymerisation occured. In order to have standardised fixation conditions, a pure commercial solution was used, which was freshly diluted and buffered and which was only used once.

A further study was undertaken to examine the shrinkage temperature of different layers at different depths in the tissue to investigate any variation due to the penetration of the fixative. No difference was detected, showing that the penetration was uniform. The rate of increase of shrinkage temperature was the same for 0.5% and 0.25% concentrations and appeared to stabilize within two hours of fixation. The lower concentration produced higher shrinkage temperatures after

Table 9.1: thickness values of the fixed samples used in the present chapter and of the fresh samples used in chapter5. Measurements expressed in (mm). There is no relation between samples noted by the use of the same letter, i.e.fixed sample-E and fresh sample-e′.

thickness values of the samples in mm (average values over the tested area)			
sample	FIXED TISSUE	sample	FRESH TISSUE
D	0.40	e′	0.30
E	0.36	f′	0.35
F	0.44	g′	0.33
G	0.43	h′	0.33
H	0.38	i′	0.30
I	0.38	j′	0.33
		k′	0.34
n :	6		7
mean :	0.398		0.326
st.error mean:	0.007		0.013

longer exposures but this did not necessarily reflect the quality of the cross-links formed because it is known that glutaraldehyde continuously polymerises. It was hoped that the low initial concentrations would initially result in reaction of monomeric forms, preferably inside the fibrils before coating the outside.

9.2.3 A First Approach of the Fixed Tissue.

Nine pericardial sacs were prepared fresh as described in chapter2. From each pericardial sac a sample was dissected from test site-I which presented typical structural anisotropy as indicated by the optical pattern. The thickness values of the samples were typical of this area. The samples were identified as being anisotropic by the use of both the optical pattern and the well established geometrical references, and the principal axes of anisotropy were marked on the fresh tissue prior to fixation.

Fixation was completed in solutions prepared according to the specifications set previously, with the tissue sample being allowed to float in the glutaraldehyde bath free from any constraints. The samples were retrieved after 7days. The thickness was measured and is reported in table9.1. The average thickness value of these fixed samples was markendly higher than the thickness of the fresh specimens in chapters5,6. The samples have been numbered D to I with the first three been wasted in exploratory tests till a standardise test routine was established.

The fixed samples were firstly viewed in the polarising optical microscope from either surface. The optical pattern was still apparent although less light was transmitted through the tissue. The only difference between the optical patterns of the fresh and fixed samples was the yellowish appearance of the latter. Apart from that the directions of the banding had remained the same between the fresh

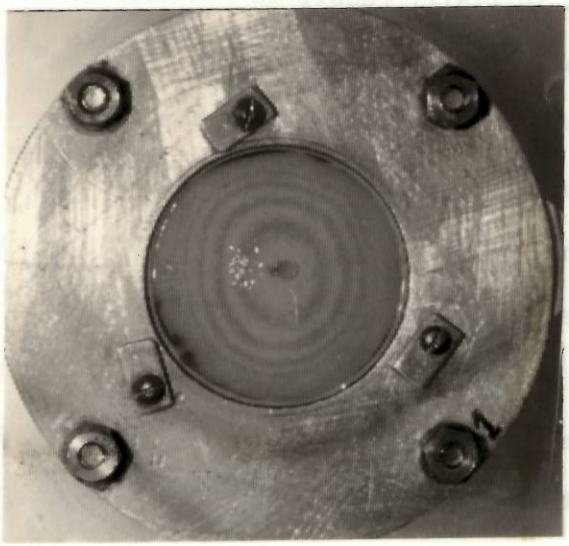

Ⓐ

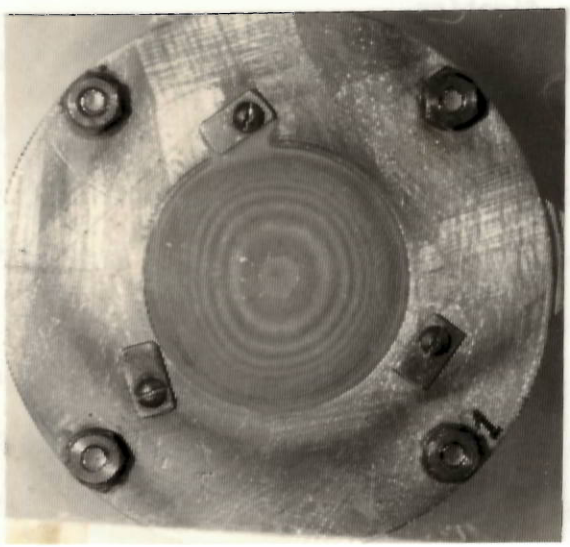

Ⓑ

Figure 9.3:Moiré views of inflated fixed tissue at Ⓐ 2mHg and Ⓑ 10mmHg the circumferential direction, from left to right in the photos, was less extensible; compare with the Moiré views on fresh specimens in Figure 4.28.

and fixed sample.

The samples were subsequently inflated and were viewed by the use of the Moiré shadow technique, when a large qualitative difference was evident, compared to the usual behaviour of the fresh samples. The fresh tissue was more extensible circumferentially at low to medium pressure levels (between 0 to 60mmHg), but in the fixed tissue the circumferential direction had become less extensible (fig.9.3). The ovals presented a major axis along the axial direction.

9.2.4 Uniaxial Mechanical Tests.

The deflated samples were returned to the glutaraldehyde solution and allowed to relax for 24hours. Before preparation of the uniaxial strips the thickness of the tissue samples was again measured and found to have completely recovered pre-inflation values.

The strips were prepared along the principal axes of anisotropy as identified when fresh, 3 being produced in each direction with a 3mm width. The strips were supported by a postcard and were mounted and handled as were fresh strips (chapter5).

The testing protocol and the testing equipment were also the same as in the fresh tissue strip tests. The nominal strain rate was 0.0055/s and five preconditioned cycles were performed and recorded along with the conditioned sixth cycle. The treatment of the results was also similar to the fresh tissue tests, to aid any comparisons.

The response of fixed pericardial tissue to load was typical of collagenous tissues in presenting an initial high compliant region (the incubation area) and then rapidly rising to higher loads or stresses.

The tissue dissipated more energy within the first cycle as indicated by the area of the hysteresis loop included between the loading and unloading curves. The size of the loop was decreased from the first

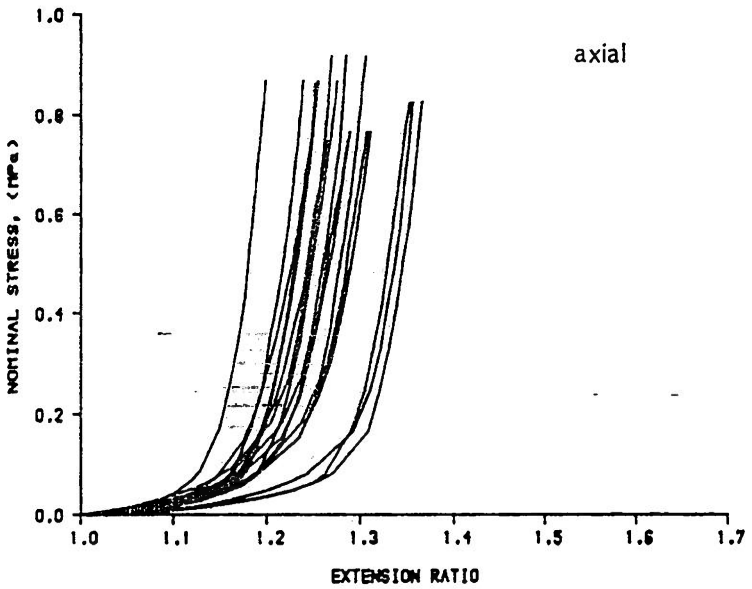
axial
NOMINAL STRESS, (MPa)
EXTENSION RATIO
1.0
0.8
0.6
0.4
0.2
0.0
1.0
1.1
1.2
1.3
1.4
1.5
1.6
1.7

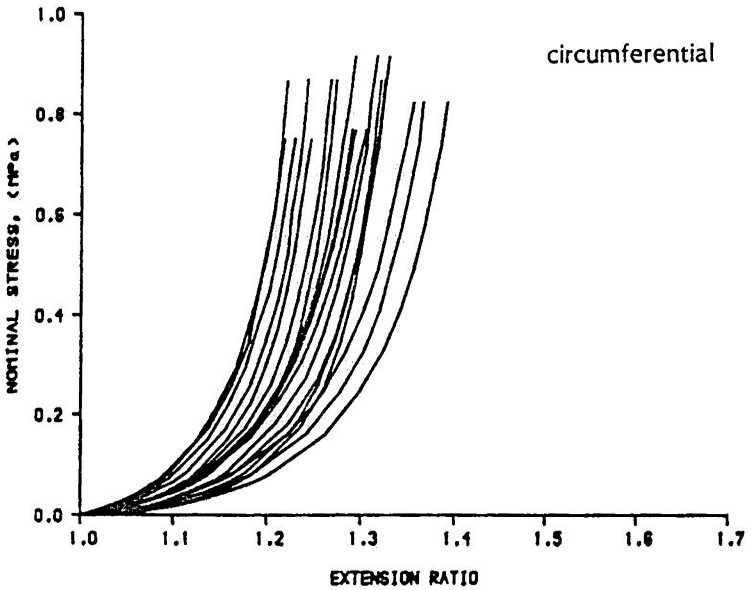
circumferential
NOMINAL STRESS, (MPa)
EXTENSION RATIO
1.0
0.8
0.6
0.4
0.2
0.0
1.0
1.1
1.2
1.3
1.4
1.5
1.6
1.7

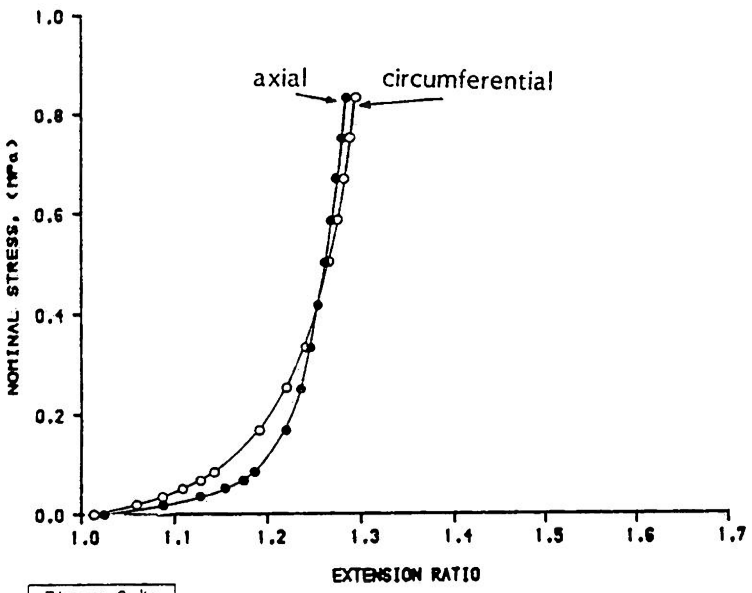
axial
circumferential
NOMINAL STRESS, (MPa)
EXTENSION RATIO
1.0
0.8
0.6
0.4
0.2
0.0
1.0
1.1
1.2
1.3
1.4
1.5
1.6
1.7

Figure 9.4:

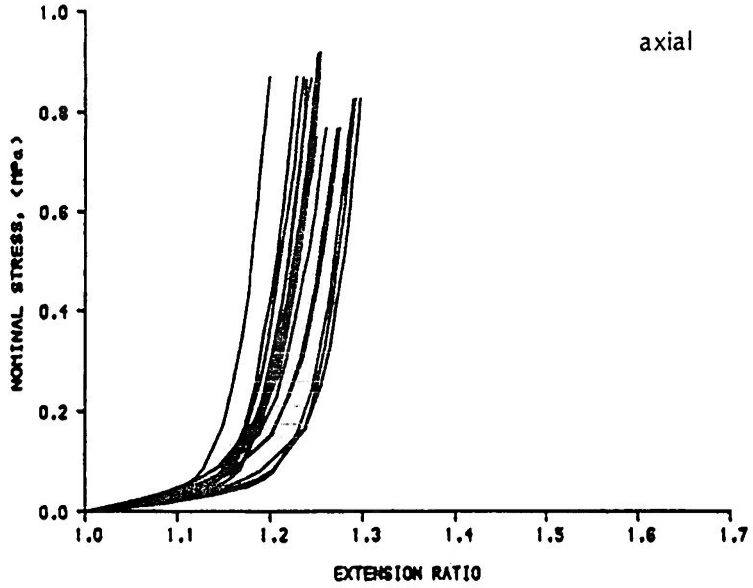
axial
NOMINAL STRESS, (MPa)
EXTENSION RATIO

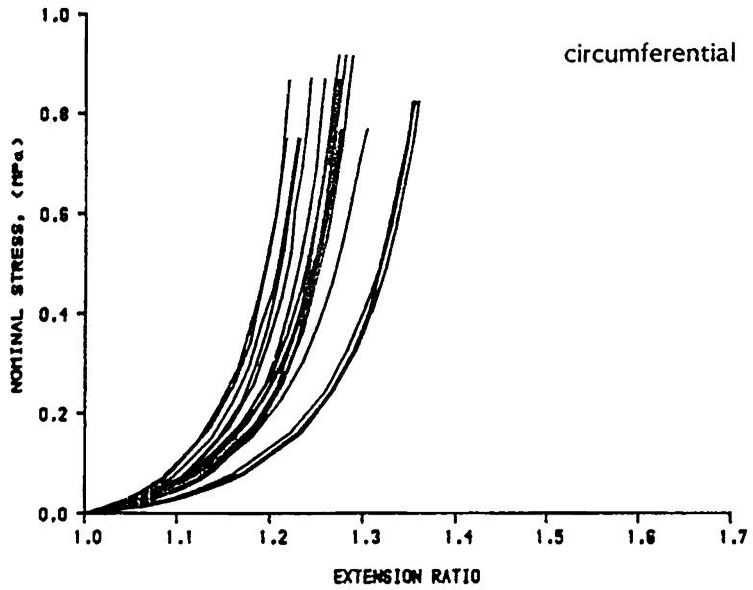
circumferential
NOMINAL STRESS, (MPa)
EXTENSION RATIO

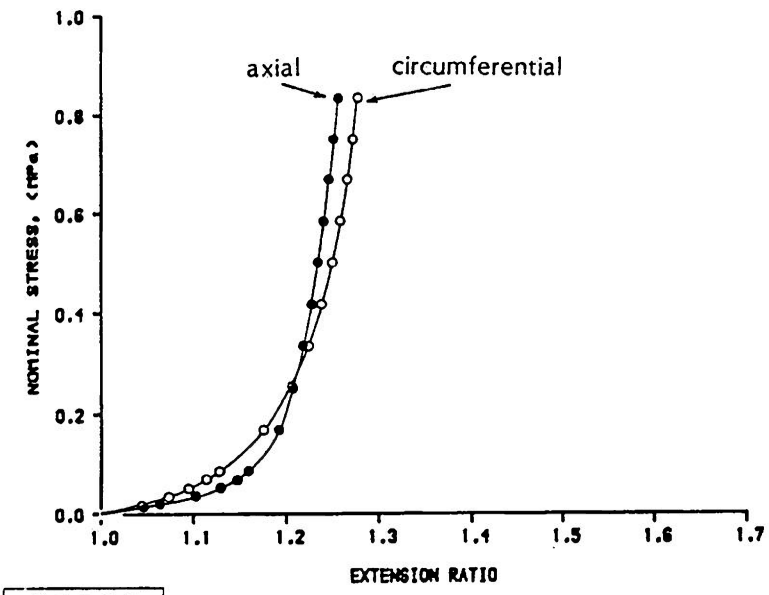
axial
circumferential
NOMINAL STRESS, (MPa)
EXTENSION RATIO

Figure 9.5:

to the conditioned cycle. The greatest change was between the first and second cycles, with little subsequent change.

The loading response of the tissue was almost stabilised from the second pull onwards and the same was true for the return curves, which after the first pull to the peak load were almost invariable for all cycles following the first one.

The shift of the first load point, where a minimum load of 0.001N could be transmitted, was a very small measure unlike the fresh material which had acquired a significantly longer 'natural' length after preconditioning.

The first aspect of anisotropy to be examined was the stress/strain behaviour at the low load region below a peak load of 1N. In fig.9.4 the envelopes of the stress/strain curves along the axial direction (fig.9.4a), the circumferential direction (fig.9.4b) and their mean behaviour (fig.9.4c) at prescribed 0.02, 0.04, 0.06, 0.08, 0.1, 0.2, 0.3, 0.4, 0.5, 0.6, 0.7, 0.8, 0.9, 1N load levels have been plotted. The nominal stress values have been calculated by the use of the load and the initial cross sectional area. The extension ratio is the ratio of the current length of the strip over the initial gauge length.

Qualitatively speaking there was a difference in shape between the curves of the two envelopes; the circumferential ones appearing to rise gradually, while the axial curves presented a sharp transition to a stiffer region. From the six different samples that have been used, samples D, G and I had loading axial and circumferential curves that finished at the same extensibilities at the peak load point. Samples E and H had a more extensible circumferential direction at peak load and sample F had a more extensible axial direction. Averaging all the curves together yielded the mean behaviour of fig.9.4c. The shape of

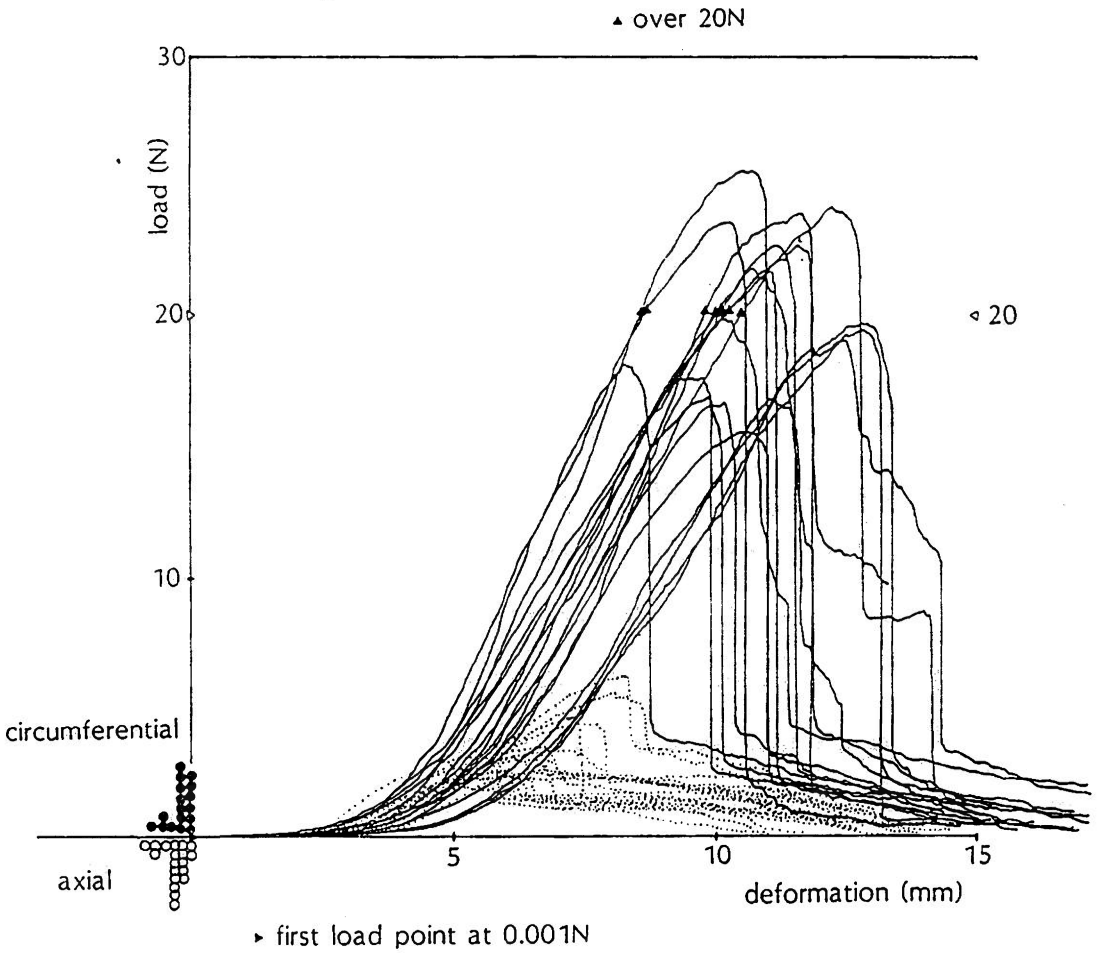

Figure 9.6: The complete load-deformation curves. Dotted lines draw the traces of axially oriented strips, continuous lines for the circumferentially oriented strips. The curves have been brought to a common first load point of 0.001N. The histograms at the left of the origin indicate where the actual gauge length started for the strips, there was not any significant difference in this measure(t-test, $p<0.05$) between the two normal directions.

the curves resulted in their intersection at a load level of 0.5N (approximately 0.42MPa). The differences in extensibilities at the load levels below the intersection point where significant between the 0.02N and the 0.25N load levels. In particular the significance levels at Student's t-tests were:

load level	level of significance	
0.02 N	p=0.0006	
0.08 N	p=0.0004	
0.20 N	p=0.0420	
0.30 N	p=0.29	NOT significant

thus the circumferential direction in average appeared to be less extensible at the intermediate load levels which was in accordance with the inflation test as well.

As when examining the fresh strips, a chart including the stress/strain response curves drawn by the use of the shifted gauge length has also been prepared (fig.9.5). There was not a dramatic shift to lower extensibility because the shift in first load point was small. Nevertheless as in the fresh strips, this method resulted in narrower envelopes with the curves being very similarly shaped within each envelope but with evident differences between the two normal directions. The mean behaviour (fig.9.5c) did not alter significantly from that previously presented for the original gauge length (fig.9.4c) indicating that either of the gauge length definitions could be equally well used. The slightly higher shift of the first load point for the axial direction resulted in a higher value for the redefined gauge length and thus the shift of the axial curves was greater and consequently the averaged curves intersected at a point

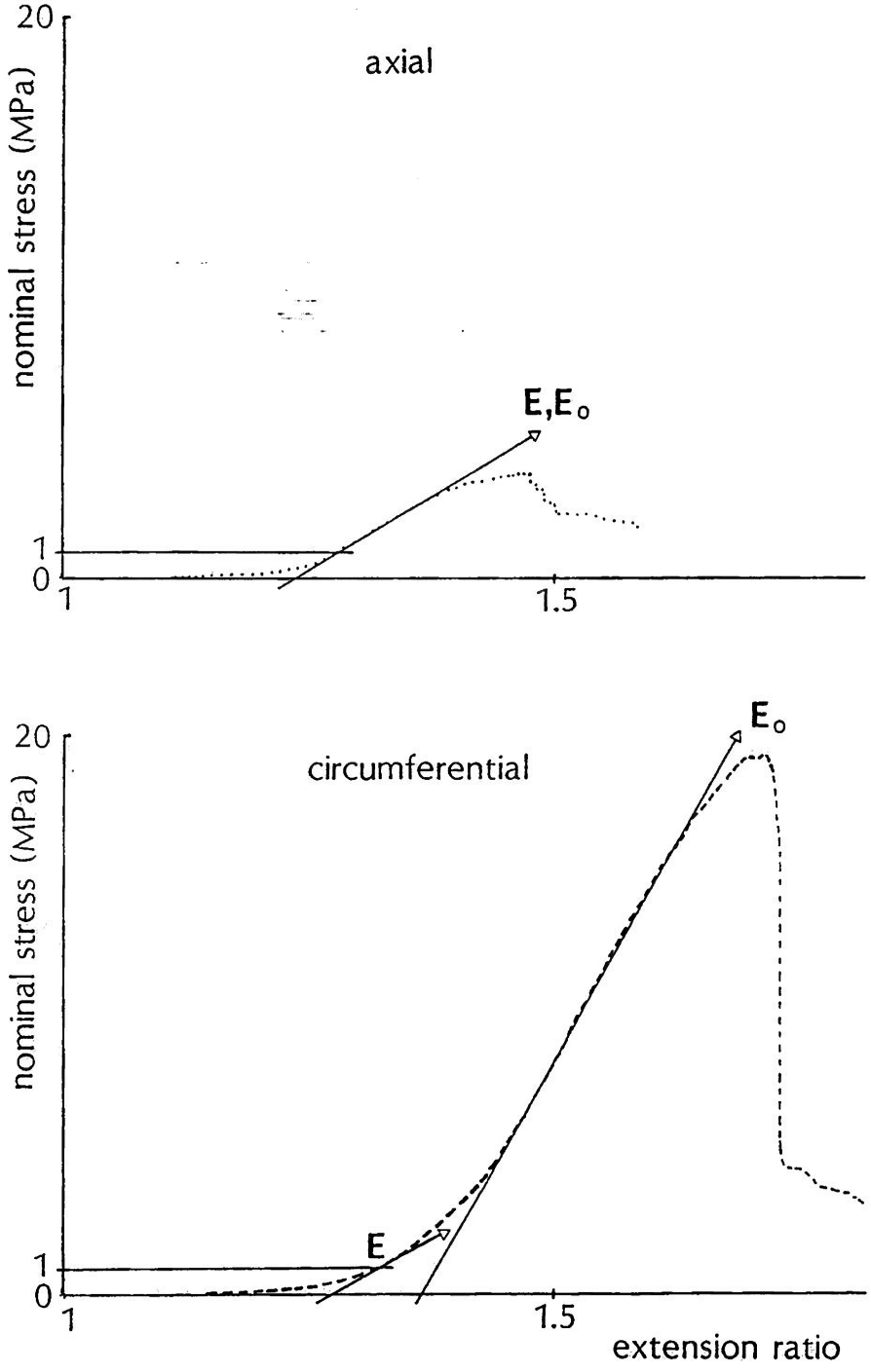

Figure 9.7: The incremental modulus(E) at the peak load of 1N was also the Young's modulus for the linear region(Eo) of the axial strips which had entered their linear region. Circumferential at a peak load of 1N were still in their incubation region and thus the incremental modulus (E) was less than the terminal modulus (Eo).

corresponding to a load level of approximately 0.35N. The circumferential direction was less extensible at lower load levels, while the axial direction was less extensible at higher load levels up to the peak load point.

In the fresh tissue tests the full curves to failure provided an accurate reflection of the structural anisotropy of the tissue and also gave a general idea of the behaviour for the whole range of stresses that can be sustained. The complete curves to failure for the present fixed tissue strips have been drawn in fig.9.6. It is evident that: i)structural anisotropy is always present, the comparison of the ultimate tensile strengths at each direction and between fresh and fixed should be performed separately, ii)the level of loads sustained by the tissue strips was higher than in the fresh tissue in either direction, with 8 out of 18 strips(44% of the samples) exceeding the 20N load, iii)it is evident that the tissue extensibility is indistinguishable at loads lower than 1N, which has already been examined with statistics, iv)the marked difference in the nature of failure for the two principal directions was still there, with axial strips creeping till complete failure and the circumferential presenting an abrupt drop in load after the U.T.S point, v)the linear region for either group of curves appeared to be less smooth than in the fresh tissue, vi)the axial strips appeared to have entered the linear region at the 1N peak load, while the circumferential entered their linear region at roughly a load level of 3N, vii)the pseudo-histograms of the distribution of the shift in the first load points for either direction overlapped significantly with the axial shifts being a little higher.

Introduction of fig.9.7 helps to clarify both the features of the curves and the definition of the parameters. Unlike the fresh tissue

Table 9.2: parameters of the fixed strips and their descriptive statistics in the two normal directions.

axial direction

sample	U.T.S.	incremental modulus at peak load 1 N	Young's modulus at linear region	shift in first load point
	(MPa)	(MPa)	(MPa)	(%)
D	5.12	16.96	21.76	4.5
	4.54	17.83	18.93	5.7
	2.06	15.77	14.29	4.8
E	2.93	16.73	19.00	2.5
	2.29	17.83	14.23	4.4
	2.75	19.71	18.77	1.2
F	1.77	14.97	11.26	0.0
	1.91	13.05	10.62	1.1
	1.91	13.18	11.73	3.0
G	2.68	16.89	14.40	2.3
	3.26	14.88	18.73	2.8
	2.88	14.30	12.64	2.7
H	2.60	26.46	12.78	0.9
	1.56	20.83	13.43	1.6
	2.60	19.59	17.00	0.0
I	3.90	23.62	16.30	1.0
	2.17	14.03	14.17	1.9
	2.61	19.64	15.16	1.0
mean	: 2.75	17.57	15.29	2.30
st.deviation	: 0.95	3.61	3.15	1.67
st.error mean	: 0.22	0.85	0.74	0.39

circumferential direction

sample	U.T.S.	incremental modulus at peak load 1 N	Young's modulus at linear region	shift in first load point
	(MPa)	(MPa)	(MPa)	(%)
D	13.61	14.25	42.23	2.4
	16.08	13.81	38.40	0.1
	16.08	17.09	37.16	1.0
E	14.66	18.89	48.17	3.2
	15.58	13.49	49.89	1.0
	15.13	15.84	48.75	3.4
F	16.66	13.67	40.22	0.0
	17.34	14.77	37.54	0.1
	17.30	18.65	36.92	1.2
G	14.58	10.95	36.01	0.1
	15.34	13.35	48.00	1.2
	16.64	11.72	53.35	1.3
H	22.14	17.40	61.51	0.8
	15.19	22.26	54.58	4.5
	15.63	19.41	61.77	0.0
I	20.40	20.91	54.58	0.1
	20.84	20.06	50.06	0.1
	20.84	22.79	45.44	3.5
mean	:16.89	16.63	46.93	1.33
st.deviation	: 2.49	3.61	8.27	1.44
st.error mean	: 0.59	0.85	1.95	0.34

the circumferential fixed strips did not enter their linear region at the peak load of 1N and thus the incremental Young's modulus at the peak load (E) was much less than the elastic modulus of their linear region (Eo). On the contrary the axial strips had already entered their linear region and thus the incremental modulus as measured at peak load was very much the elastic modulus of the linear region. This distinction indicates that measurements of the modulus of elasticity within the low stress region can lead to wrong conclusions if someone does not have the whole picture of the tissue loading behaviour till its failure point.

In table9.2 some relevant parameters have been tabulated: the U.T.S values, the incremental modulus(E) at 1N, Young's elastic modulus at the linear region(Eo) and the % of shift in the first load point. At the bottom of the tables mean values are given with standard deviations and standard errors. Student's t-tests gave that there were significant differences between: i)U.T.S. values along the axial(2.75MPa) and circumferential(16.89MPa) directions, ii)the Young's modulus of the linear region along the axial (Eo=15.29MPa) and circumferential (Eo=46.93MPa) directions, iii)the circumferential incremental modulus at peak load (E=16.63MPa) if compared to the elastic modulus (Eo=46.93MPa) of the linear region for this direction. There was not significant difference between: i)in the axial (E=17.57MPa) incremental modulus at 1N and the linear region elastic modulus (Eo=15.29MPa) in the same direction (justifying the previously introduced qualitative description of the behaviour of the curves in fig.9.7), ii)the moduli(E) at peak load between the two directions, and i)the shift in the first load point was also insignificant (Student's t-test, $p=0.072>0.05$).

Fig.9.8 shows the U.T.S values versus the Young's elastic modulus

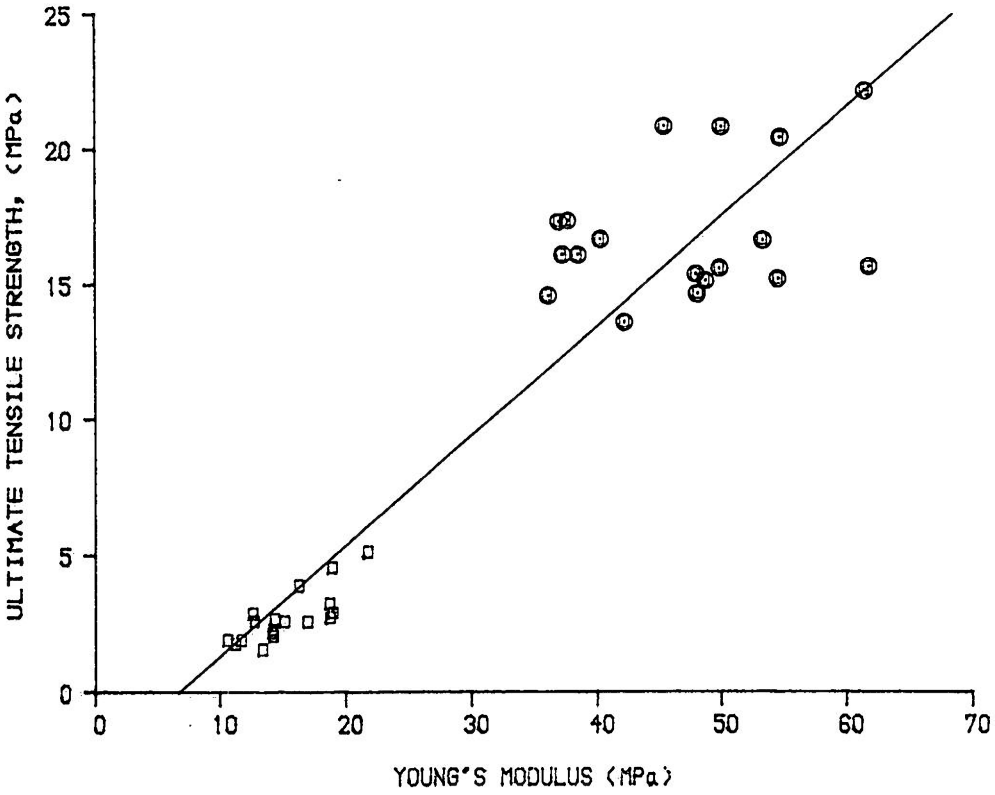

Figure 9.8: Plot of nominal U.T.S .v. Young's modulus of the linear pre-failure region. (⊙) circumferential, (□)axial.

of the pre-failure linear region for the fixed tissue. It has been shown (chapters5,6) to be the plot best reflecting the structural properties of the tissue. Very much like the fresh tissue of area-I there was an absolute separation of the strength and stiffness parameter values between the two groups along the two normal directions. Thus the first conclusion is easily drawn; that no matter what the effect of fixation is in the loading behaviour at the low stress region, the pronounced directional anisotropy in strength of the fresh bovine pericardium is retained after glutaraldehyde fixation.

If we recall the equivalent U.T.S and elastic modulus values for fresh from chapter5 a comparison can be performed for the specific influence at each direction.

		U.T.S (MPa)	Young's modulus (MPa)
FRESH	axial	: 2.6 ± 0.30	13.6 ± 1.05
	circumferential	:17.8 ± 0.46	46.2 ± 2.10
FIXED	axial	: 2.8 ± 0.22	15.3 ± 0.74
	circumferential	:16.9 ± 0.59	46.9 ± 1.95

Thus the equivalent parameters for fresh and fixed tissue were not significantly different.

The existence of anisotropy in the mechanical behaviour in the low stress initial loading region was examined(at the origin). When examining the slopes at the origin of the fresh tissue it had been found that the circumferential direction had roughly twice the value of the axial direction; in particular: axial 0.023 ± 0.004(MPa), circumferential 0.047 ± 0.003(MPa). These experimentally measured values disproved then the hypothesis made by Black et al(1985) that

Table 9.3: values and descriptive statistics for the experimentally measured slopes of the present fixed samples in the two normal directions. The difference was significant (t-test, $p<0.0001$).

SPECIMEN	AXIAL (MPa)	CIRCUMFERENTIAL (MPa)
D	0.216	0.239
	0.217	0.249
	0.185	0.268
E	0.318	0.432
	0.372	0.488
	0.384	0.488
F	0.259	0.536
	0.304	0.572
	0.268	0.384
G	0.276	0.343
	0.296	0.459
	0.292	0.471
H	0.229	0.431
	0.469	0.370
	0.290	0.458
I	0.179	0.647
	0.209	0.369
	0.223	0.382
mean :	0.277	0.421
st. deviation :	0.075	0.109
st. error mean:	0.018	0.026

native bovine pericardium is isotropic in its unstrained state. The initial moduli for fixed tissue are tabulated in table9.3. In a Student's t-test the two distributions were significantly different ($p<0.00001$) and thus rejecting the null hypothesis that the slopes at the origin of even the fixed bovine pericardium are directionally invariant. Two more things are evident: i)the slope along the circumferential direction is again (as in fresh) almost double the slope along the axial direction, and ii)the new slopes after fixation represented a tenfold increase in the values of the slopes at the origin for either of the directions. The isotropic grand mean value of the extrapolated slopes of fixed bovine pericardial tissue at the origin were given by Black et al(1985) as 0.224 ± 0.118(MPa) which is not significantly different from our present value along the weak axial direction.

The behaviour of the Incremental Elastic Moduli over the whole length of the stress/strain curve below the peak load point(1N) was examined then. The curve appears to be rather exponential and plots of the Incremental Modulus against the stress at each load level were constructed, and found to be linear. In fig.9.9a the three axial and three circumferential curves from a single sample have been drawn and linearly regressed. The previous qualitative description was that below the intersection point of the two curves, the circumferential curve shows higher moduli and thereafter the axial curve which has already entered its linear region appears stiffer. As a result a single regression line for the whole curve up to 1N(almost 0.8MPa) gives higher slopes for the axial curves drawn for all the samples in fig.9.9b, than do the circumferential ones included in fig.9.9c. The non-significant difference in the peak load Incremental Moduli between the two directions can be appreciated by the points of the two

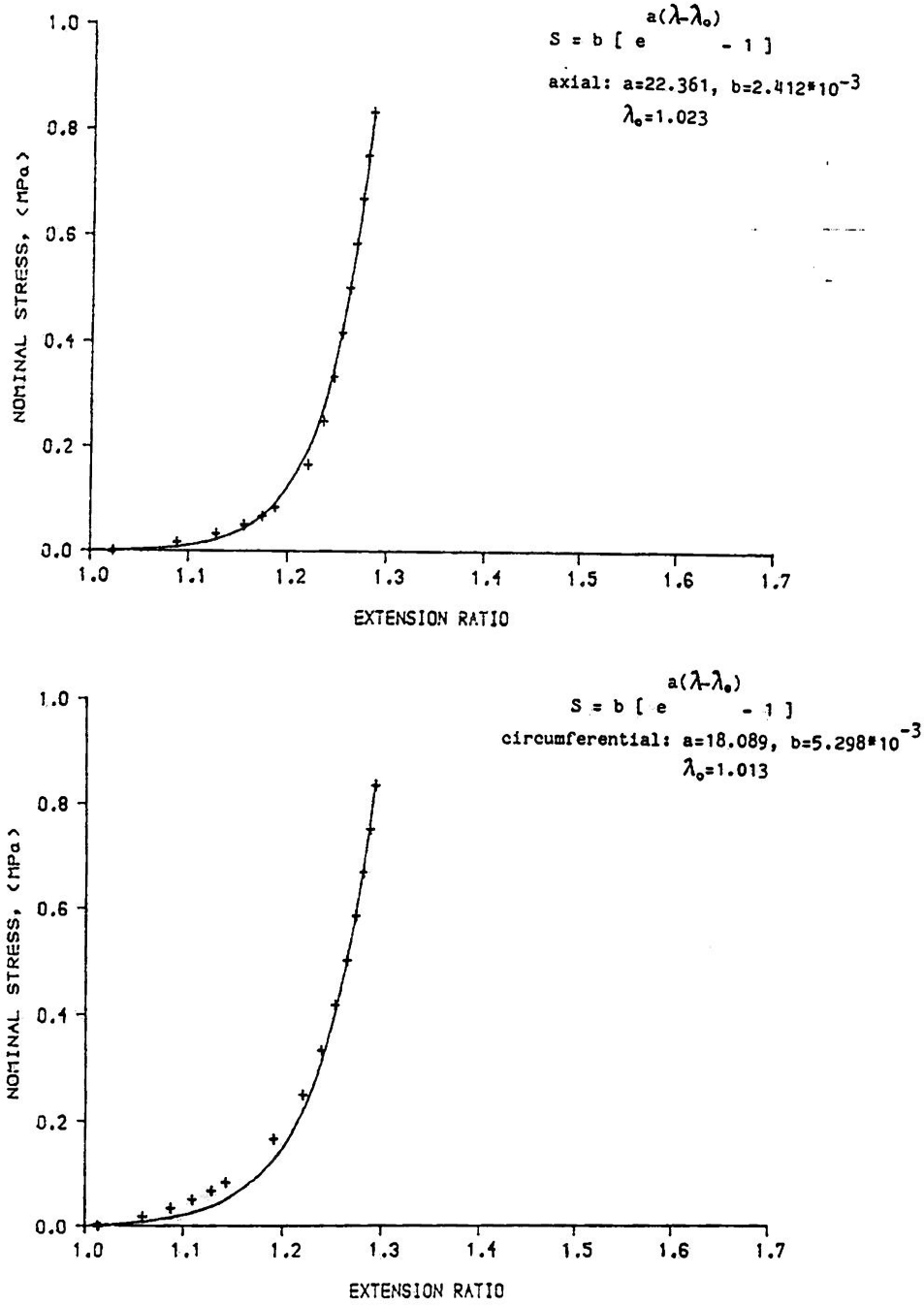

Figure 9.10: (+)average loading behaviour along the two normal directions. Continuous line is the best fit by the use of the exponential formula. Parameters a, λ_o, take the average values of the population of the strips in each of the directions.

envelopes coming together at the peak load. There the axial curves have reached their linear region and thus reached a constant value of the incremental elastic modulus, while the circumferential curves stiffened rapidly to enter their linear region.

In order to be used in subsequent sections, where the behaviour of 'isotropic' tissue will be examined, a simple two-parameter exponential formula was fitted to the curves to investigate if it was capable of describing this type of behaviour and reflecting the qualitatively different behaviour along the two directions. In fig.9.10a,b the mean behaviour along the two directions by using the original gauge length has been fitted with the exponential formula. The slopes of the Modulus.v.Stress regression lines of fig.9.9b,c were averaged at each direction and gave the mean values a=22.361 for the axial and a=18.089 for the circumferential. A function $s'(\lambda)=[\exp(a(\lambda-\lambda_0))-1]$ was estimated at each load level by using the previous value for a and λ_0. The outcome was an array of predictions for stress at the prescribed load levels and behaved exponentially. The exponentially behaving predictions ($s'(\lambda)$) were then linearly regressed to the experimental mean stress values at these same load levels and this produced a parameter b which is a multipication factor which scales down the predictions to the level of the observed stresses.

The fit appears good above the 0.2MPa stress level for both curves. This reflects the previously introduced argument that above the intersection point the axial curves are stiffer because they have already entered their linear region. Thus the formula, which produces a higher value a for the axial direction, accurately describes both curves in this region. In the region below 0.2MPa the circumferential curves increase more rapidly than the axial curves and thus the

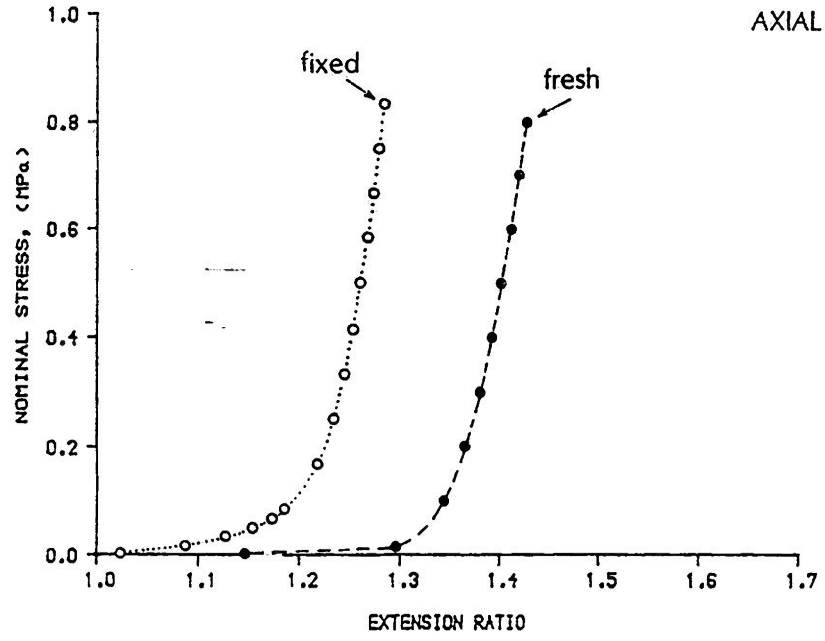

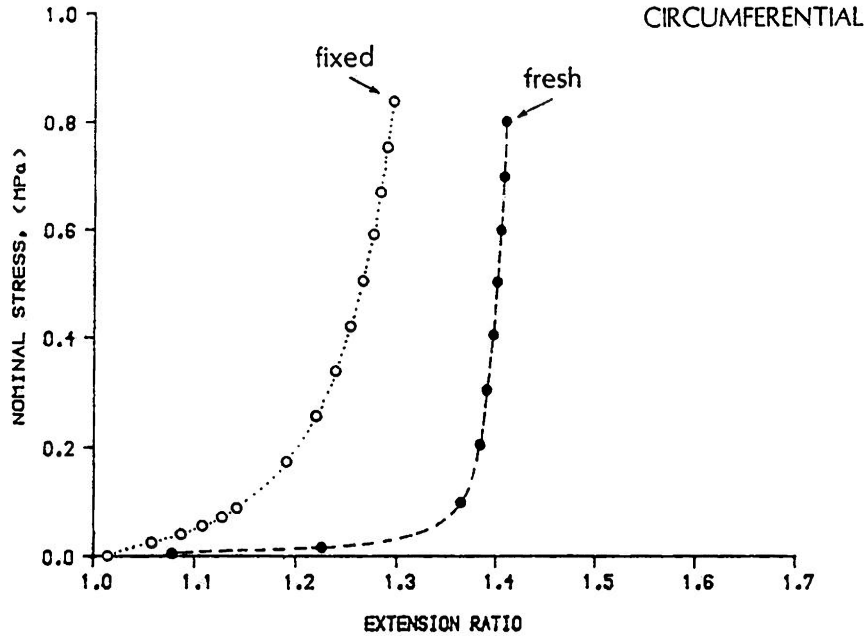

Figure 9.11: average behaviour in two normal directions for the fixed samples of this chapter as compared to the average response of the fresh tissue already presented in chapter5. The original gauge length has been used.

formula which draws a stiffer curve for the axial, lacks accuracy in describing the circumferential behaviour. It appears that for the description of the smoothly rising circumferential behaviour which is all within the incubation region along this direction a biphasic approach would be more successful. Such could be an application of this same formula with a set of constants(a,b) up to the intersection point and subsequently a new set of constants for describing the behaviour up to the peak load point.

Figures9.11a,b 9.12a,b present what is a standard examination of a fixation regime by comparing the preconditioned tissue loading behaviour between fixed and fresh tissue. The curves are the mean behaviour for 6 fixed samples and for 7 fresh samples(chapter5). It should be remembered that the fixation was with no constraints and by using the solutions and time scales described earlier. In fig.9.11a,b the fixed strips demonstrated a reduced extensibility at the same stress levels than the fresh strips. The fixed axial strips had a loading behaviour similar to the fresh but the curve was shifted much to the left by 0.144 of the extension ratio (14.4% nominal strain) and the circumferential curve by 0.117 (11.7% nominal strain). Qualitatively speaking the axial fixed curve was less compliant over the whole length, while the circumferential fixed curve was stiffer at the origin but had a lower peak load incremental elastic modulus than the fresh curve which had already entered its linear region.

The first load point of the conditioned response in fig.9.11a,b was encountered at very small nominal strains for the fixed, but it was of substantial magnitude for the fresh strips. This could be due to one of many reasons. It could be just the fact that the tenfold increase in the incremental elastic modulus at the origin (between fresh/fixed) made it easier for a first load(0.001N) to be detected.

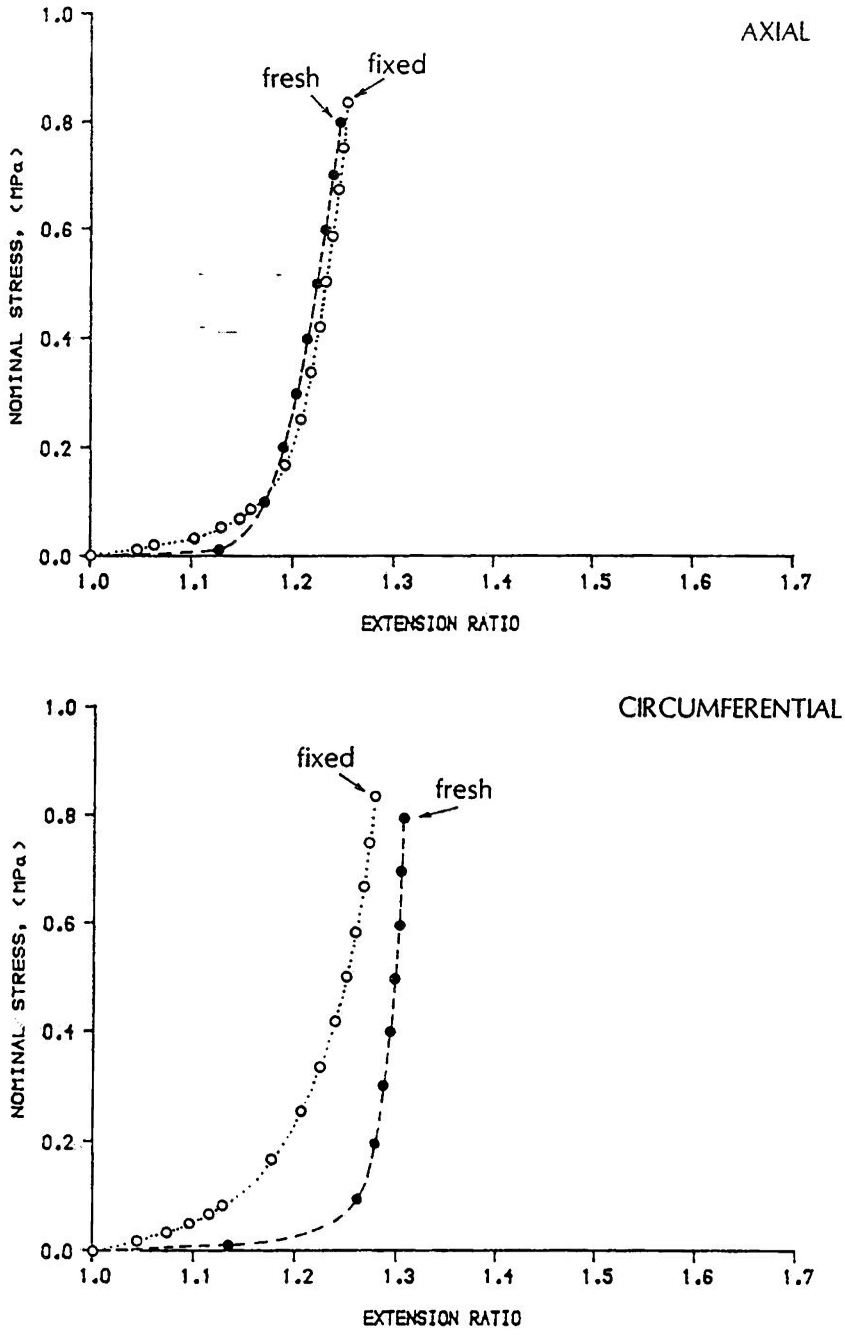

Figure 9.12: average behaviour along the axial and circumferential directions for fresh and fixed tissue by the use of the preconditioned gauge length.

Alternatively, it could be due to the introduction of an increased number of crosslinks in the fixed tissue, which inhibit the rearrangement of the fibres inside the soft matrix and thus do not allow the tissue to acquire a new increased length. Indication that the second idea was more likely to be true than the first was the observation during the tests that the fresh tissue had indeed acquired an increased 'natural' length by presenting strips that were buckled when returned to the original gauge length, while the fixed tissue strips retained their initial dimensions.

In fig.9.12a,b the current mechanical behaviour of the preconditioned strips is shown by the use of their conditioned (extended) gauge length. The severe critisism earlier in chapter5 on the use of the shifted gauge length was that it should only be used when a 'new' material is present and thus its 'natural' (relaxed) length should be redefined. But in the case where the current deformation of the strip is recoverable within short time periods of the stress being removed, is not quite clear if this redefinition is valid or just yields artifactual results. At the same time it was said that the geometry of the specimens in tensile uniaxial tests (strips) may be connected to the plastic deformation of the specimens by allowing an increased degree of fibre rearrangement in the absence of lateral constraints. Thus plots by using the shifted gauge length should only be used for the advantages they possess in demonstrating the current loading characteristics of the tissue and should be carefully interpreted.

Thus in fig.9.12a where the fresh and fixed axial loading curves have been brought together to a common extension at a first load point (0.001N) it is evident that fixation has resulted in an upwards shift of the stresses mostly affecting the initial incubation region which

Table 9.4:Glutaraldehyde's chemistry

MECHANICAL ASPECTS BIO-CHEMICAL ASPECTS

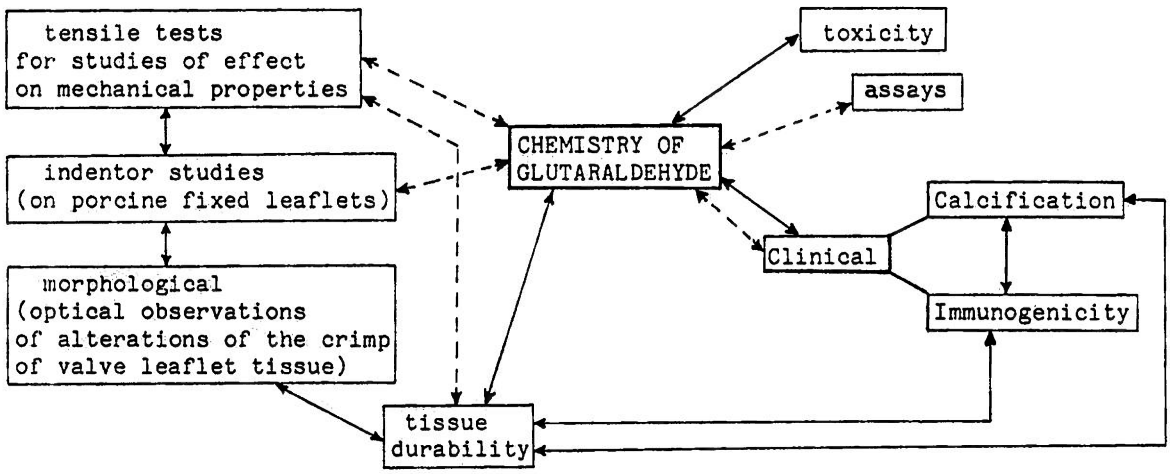

<----> assessment
<——> relation

has been extended up to a stress value of 0.2MPa (qualitative assessment). In the circumferential direction the effect of fixation is more pronounced with the fixed curve being both less extensible at all stress levels and less compliant.

The only valid way of describing the fixed curves if compared to their fresh counterparts is by saying that increased levels of stresses, or loads are encountered at the same strains in the fixed tissue irrespective of the definition and measurement of strain and the specimen's relaxed dimensions.

9.2.5 Discussion.

The present chapter started with an introduction to the chemistry of glutaraldehyde where it was said that the specific conditions regarding the constitution of glutaraldehyde and the mechanical constraints during the period of fixation may drastically influence the outcome. How complicated the matter is can be appreciated in table9.4. The central issue is the chemistry of glutaraldehyde as refering to the general use of this fixative and its effects on tissues, around which the literature up to date has been gathered.

The mechanical aspects of fixation include standard tensile tests before and after treatment like the ones presented here. Indentor studies were qualitative observations made by Broom and Thomson(1979) to assess the influence of fixation under various pressures on the rigidity of the fixed leaflets of porcine valves. They also observed the effect of constraints (application of pressure or fixation under strain) on the crimp of the collagen fibres of leaflet tissue and suggested that fixation essentially "freezes" the geometry of the fibres at the state of deformation currently occurring during fixation. There may also be a relationship between conditions at fixation and durability. The stiffer the leaflets are, as a result of

prestrain or higher glutaraldehyde concentrations, the more prone they are to concentrate stress at localised points of the valve leaflets and fail. Sabbah et al(1985) predicted that overall stiffening increases the stresses in valve leaflets. The effect and assessment of fatigue-cycling on the tissue by tensile tests will be described in later sections of this chapter.

On the other side biochemical assays have been a standard method for examining the specific sites of reacting amino-acid residues and the influence of different solutions. Toxicity is both biochemical and clinical aspect and a number of workers pointed out that biocidal effects(Gendler et al,1984) of residual glutaraldehyde leaking out of the tissue can only be avoided by thorough rinsing of the fixed tissue before implantation. Control of any of the conditions at fixation has not been shown clinically to reduce calcification; instead modern fixation treatments attempt to incorporate anticalcification agents. It has been suggested that calcification may be related to immunogenic reactions by the fact that autograft valves(Ross et al,1979) have not been seen to calcify, while allografts and heterografts undoubtedly do. Thus it seems that the body recognises proteins coming from a foreign body not only of a different species but from the same species as well. The absence of calcification of autografts suggests that an immunogenic reaction may be behind the early onset of calcification. It is obvious that both calcification and immunogenicity may dramatically influence the durability of a tissue prosthesis.

Occasionally the mechanical and biochemical aspect must be considered together. Low concentrations of glutaraldehyde have been found to yield a better mechanical result by first fixing the inside of fibres, but the sterilizing effects of glutaraldehyde are better at higher concentrations. Similarly the mechanical properties stabilise within

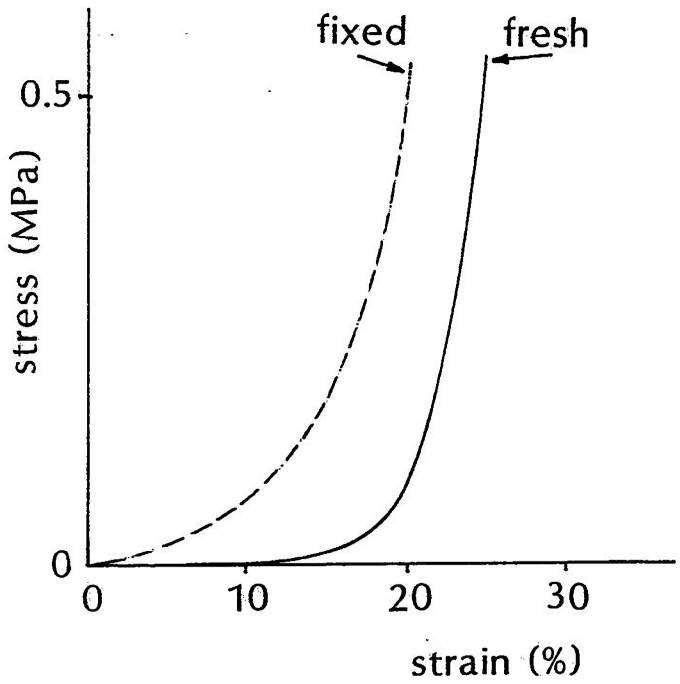

Figure 9.13: comparison of the mechanical characteristics of fresh and fixed bovine leaflet tissue along its circumferential direction. Reproduced from Broom,1977.

a couple of hours of treatment but more subtle properties like blood compatibility and immunogenicity may require prolonged exposures.

The effects of fixation on the mechanical properties of the tissue have been discussed briefly. It was very clear that the loads at any strain level were increased as well as the incremental elastic moduli over the whole stress/strain curve. In fig.9.13 the mechanical characteristics of fresh and fixed bovine valve leaflet tissue along its circumferential direction are compared(Broom,1977). The similarity between fig.9.12b and fig.9.13, which report the results of fixation on different tissues, indicates that the result of fig.9.12b should be considered as being typical of the effect of fixation in collagenous structures along the collagen fibres. It also indicates that if the gauge length is accuratelly defined and correctly reported, results from different sources may be comparable and yield proper conclusions.

It was found that a distinction should be made between the anisotropy in the low stress region where the material is expected to operate in a functioning valve, and its behaviour outwith this region till the failure point. In the low stress region, fixation has been found to mask the anisotropic features of the tissue. The qualitative difference between the curves is very subtle and strain differences are small (envelopes are overlapping significantly). Thus if the principal directions of material mechanical anisotropy have not been identified by other means such as the inflation test(when fresh) or the optical microscope(for fresh or fixed), it is very likely that the existing anisotropy will not be detected. This proves the great value of examining mechanical properties of the tissue in its fresh state and then extending the investigations on the fixed material. The reason for the masking of the anisotropy in the low stress region must

be the shape of the curves along the principal directions of the fresh tissue. These curves (chapter5) had been seen to cross each other at a low stress point and then intersect again at a higher level. Between the origin and the first intersection point a loop was formed. This was caused by the overall stiffer circumferential direction starting with a higher modulus and having a more abrupt turn into a more stiff linear region. In the fixed tissue the overall increase of the stresses at all strain levels resulted in both an enlargement and an upwards shift of the loop formed between the two intersection points. Thus within the range of zero to 1MPa stresses, the curves did not differ much. If the mechanical behaviour is examined in uniaxial strip tests with strips not exactly aligned at the principal mechanical directions, it is possible that the results will point towards an 'isotropic' behaviour.

The pronounced differences between the two directions are evident at higher stresses and their behaviour at failure. In both directions the fixed curves were slightly and non-significantly stiffer in their linear region than the fresh curves. The increased number of crosslinks had increased the loads required to achieve the same deformations but the effect was only obvious in the low stress region and not in the sharply rising linear portion of the curve. The actual loads at failure were increased in both directions, but because of an increase in thickness the normalised values of U.T.S and Incremental Elastic Modulus(in the linear region) were not statistically different ($p=0.05$) from the fresh material. The mean values in each of the direction were slightly higher for the axial direction and slightly lower for the circumferential direction. It has already been mentioned that this is related to the geometrical lay-out of the fibres and the mechanism of failure. Along the axial direction and

across the fibres the loads are sustained by the cohesive elements of the tissue, the naturally crosslinking ground substance and the randomly scattered fibres migrating between layers. Thus the effect of an increased number of crosslinks is an increased U.T.S value of the reinforced material. Along the circumferential direction the crosslinks cause a 'riveting' of the fibres which may not be just a lateral anchoring but it may affect the carbon-carbon backbone as well and thus prevent the stretching of the individual fibres. If this is true the effects of controlled intrafibrillar or interfibrillar fixation are linked to the failure properties of the fixed pericardial tissue. A simple 'riveting' of the fibres may inhibit uniform distribution of stress and thus cause the early failure of some fibres and initiate the complete tissue failure. In chapter6 it has been said that a stiffer material it is not necassary stronger. In fact the great strength of the generally very compliant animal tissues is due to their ability to rearrange their fibrillar elements through the soft matrix along the direction of load. This has been shown here where the increased number of crosslinks, which would have reinforced an amorphous rubber, have not reinforced the direction along the fibres which has weakened. This is similar to the reduction of strength along the circumferential direction of porcine valve leaflet tissue after fixation reported by Lee et al(1984). Although in the particular case of porcine leaflets a disruption of the spongiosa layer by fixation may also have caused some reduction in strength, these workers mentioned that experiments by Mohanharandhakrishan and Ramanathan(1965) also showed reduced strength in tendons after fixation.

When examining the application of the exponential formula on the tissue loading response it has been suggested that a biphasic approach

to the description of the circumferential curves may be required. This is in agreement with Black, Trowbridge et al(1985) who suggested a biphasic isotropic strain energy function for describing the behaviour of fixed pericardial tissue which was split in two regions with separate sets of constants for the strain energy function for each region. A formula with a potential of describing both anisotropic and biphasic behaviour will be discussed in chapter10.

9.3 PERICARDIAL-VALVE TISSUE.

9.3.1 Introduction.

The problems with the construction of a successful bioprosthetic valve and the role of pericardium have been already highlighted in the earlier sections of chapter8. Even if the problems regarding abrasion and wear of the leaflets with the stent have been overcome by the use of improved valve designs, like the Glasgow valve (chapter8), there are still problems of the short or long term performance and condition of the pericardial tissue itself.

Geometric measurements and morphological observations show that fatigue-cycled leaflets exhibit a permanent sagging. Repetitive cycling of the pericardial leaflet may have drastic effect on the usual response of this tissue to load and thus result in the transformation of the original manufacture material in a 'new' material.

By examining the stress/strain characteristics of strips from leaflets of fatigue-cycled valves, possible alterations in the mechanical properties of the post fatigue-cycled material can be established. The alterations in the leaflet geometry (sagging) may also be reflected on these same stress/strain curves.

It was impossible to examine valve material before and after fatigue-cycling due to the destructive nature of the uniaxial test

when producing the strips. Instead two populations were examined: a control group of the normal uncycled virgin valve material and the group of the fatigue-cycled valve material.

Examination of the condition and the material properties of bioprosthetic valves leaflets after long-term mechanical conditioning has not been performed before either for the pericardial or porcine valves. Pericardial bioprostheses allow the greatest degree of intervention and control in the construction of the frame and the leaflets (chapter8). Thus the present study is of great potential importance for the manufacture of such valves.

Assuming that a well designed valve has been developed, which takes care of the alterations that occur to the material after extended cycling and is able to survive long periods of operation under in-vitro laboratory conditions, there is still one more factor to be examined, which is the effect of a non-inert environment like the human body on the valve leaflet properties. The living body is a reactive environment which is hostile to foreign body implants and may accelerate the wear of the tissue or modify the leaflet tissue properties in a different way. Deterioration of the quality of the leaflet tissue can occur mainly due to: host tissue ingrowth and calcification. Host tissue ingrowth invests and thickens the leaflets thus increasing their rigidity and consequently affecting their ability to flex, open and close as easily as after manufacture. Calcification will occur almost inevitably in any tissue valve (Lawford et al,1987) and depending on its severity will result in either rapid leaflet failure by development of leaflet tears and holes, or result in valve malfunction by drastically changing the leaflet properties. In the presence of severe calcification the valve leaflets do not flex at all and the valve has to be replaced. If

Table 9.5: THICKNESS VALUES prior to tensile tests in (mm). Leaflets originated from 4 valves for each of the uncycled and fatigued-cycled groups, and from 3 valves for each of the implant and explant groups. One leaflet was lost in the uncycled group and two leaflets from each of the implant-explant groups.

Groups:	un-cycled	fatigue-cycled	implants	explants
	0.50	0.45	0.64	0.75
	0.47	0.48	0.64	0.72
	0.37	0.45	—	—
	0.45	0.38	0.40	0.48
	0.49	0.42	0.40	0.55
	0.48	0.42	—	—
	0.44	0.54	0.45	0.70
	0.42	0.45	0.45	0.80
	—	0.44	0.45	0.80
	0.44	0.41		
	0.45	0.46		
	0.44	0.38		
	n=11	n=12	n=7	n=7
mean :	0.45	0.44	0.49	0.69
st.deviation :	0.036	0.044	0.105	0.124
st.error mean :	0.011	0.013	0.040	0.047

t-tests:

between	un-cycled/fatigue-cycled: not significantly different, level of significance p=0.56
	Glasgow un-cycled/Ionescu control: not significantly different, level of significance p=0.37
	implants/explants: significantly thicker explants, level of significance p=0.008<0.05

calcification is retarded or reduced possibly by some chemical pretreatment of the material it would be useful to know the after implantation material properties for leaflets that have been modified by deposition of blood elements(thrombotic loci) and tissue ingrowth. Once again the examination of mechanical properties of leaflets of valve explants as compared to a control population of leaflets from (non-implanted) valve implants is the first of this kind for any type of tissue valve.

9.3.2 Materials.

The control group of uncycled leaflets were standard Glasgow pericardial leaflets prepared for 27mm valves according to the specifications set for the production of the improved Glasgow valve. They were completely un-cycled after fixation and thus possessed no history of deformation. The leaflets were formed by fixation on a acetal mould of which the geometry and dimensions are described elsewhere(Fisher,1986). Following fixation the leaflets assumed the shape of the mould as it can be seen in fig.9.14a,b. The intention was to produce a leaflet with a variable thickness distribution over its area, having a thinner belly and being thicker at the free edge. Thinner areas on the leaflet are expected to experience lower bending stresses during operation which is especially important for areas where the curvature reverses during cycling, i.e.the leaflet belly. Variability of thickness had been achieved to an extent by suitable tissue selection and leaflets were slightly thicker at the free edges. The thickness values reported in table9.5 are the average values over the whole leaflet. Leaflets had been matched in thickness during manufacture and thus leaflets originating from the same valve had similar thickness values.

The fatigue-cycled group consisted of 12 leaflets from 4 Glasgow

Figure 9.14: fixation of a leaflet on an acetal mould, after removal the tissue has taken the form of the mould (f:leaflet´s free edge, b:leaflet´s belly).

27mm pericardial valves that had been cycled in accelerated durability tests in a Rowan Ash fatigue tester at 12Hz for at least 400 million cycles (equivalent to 10 years in life). The valves were dismantled, the leaflets inspected and only those valves/leaflets which had no signs of wear and/or tear were subsequently subjected to tensile tests.

Thickness values averaged over the leaflet area are reported in table9.5. A normal distribution of the thickness values existed for those fatigued leaflets with the average fatigued leaflet being slightly thinner compared to the uncycled leaflet. However this difference was not significant. There was still some correlation of the thickness values of the 3 leaflets of each valve.

The population of explant valve leaflets was very much a result of a selective procedure. Twenty seven pericardial valves implanted for periods between 13 to 84 months were explanted in the Glasgow Royal Infirmary since 1986. From this number 19 were Ionescu-Shiley pericardial (Fisher et al,1987) and from these only the ones which satisfied the following criteria were subjected to tensile tests. Valves that had not failed due to leaflet tear or calcification were considered. These valves had been replaced in double valve reoperations for reasons of precaution alongwith the failed valve. These valves were considered to have normal function when examined clinically with Doppler ultrasound and echocardiography prior to reoperation. The selected leaflets were from valves size 29/31mm that had been implanted in the mitral position for time periods between two and seven years.

The group of implants consisted of valve leaflets of standard Ionescu-Shiley (ISU) valves the size of which was chosen to match the size of the explant valves. These leaflets were the control group

population for the implant/explant study. The idea was that comparison should be attempted between similar valve leaflets.
The thickness of the ISU(Ionescu Shiley Standard) leaflets within a valve was perfectly matched to each other(table9.5) and their average value was not significantly different from the mean thickness value of the Glasgow leaflets. However the average thickness of the control leaflets was significantly lower than those of the explants as seen in table9.5.

9.3.3 Methods.

The population of fatigue-cycled leaflets was prepared by using the facilities already existing from the development of the improved Glasgow pericardial valve(Fisher,1986).

All explant valves were morphologically examined, photographed, their macroscopic description recorded and stored in physiological saline at $4^{o}C$.

All leaflets from all four groups were viewed by polarised transmitted light microscopy in order to determine the fibre orientation for each particular leaflet and if there was any consistency in this direction of fibres in respect to the two main directions on the leaflet(radial or circumferential).

Valves of all types have been hydrodynamically tested in a pulsatile flow simulator(Fisher et al,1986c) at a normal cardiac output of 4 l/min and rate of 70beat/min. The evaluation of their hydrodynamic performance was assessed on standard parameters identically to the comparative performance of the commercial valves(Fisher et al,1986b) reported in chapter8. The hydrodynamic features of each valve were only to be compared with other valves of the same type (Glasgow or ISU). Root mean square forward flow, mean pressure difference, regurgitant volumes during closure and when fully

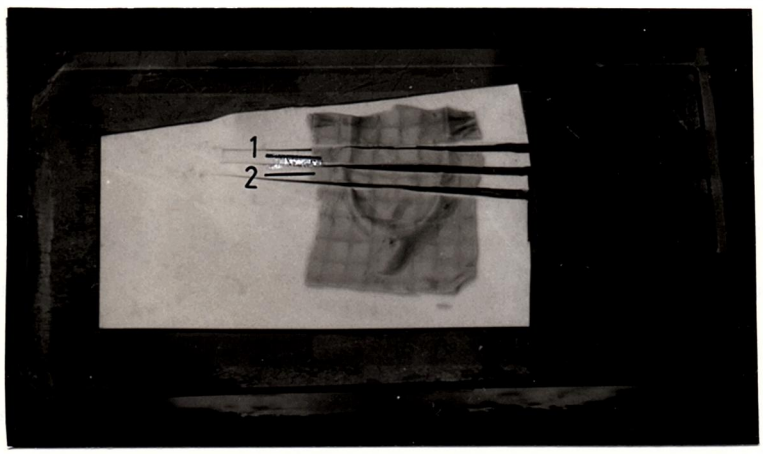

Figure 9.15: preparation of the strips along the circumferential direction of the leaflet and near the free edge.

closed and effective orifice area were all measured. The leaflet dynamics were studied using a video camera and recorder.

Tensile tests were undertaken using the standard procedures of chapters5 and 6 and of the previously reported tests on fixed tissue. Special attention was paid in the preparation of the strip specimens because all fixed valve leaflets were curved. The Glasgow leaflets are fixed on a mould and at manufacture the free edge of the leaflet (fig.9.14, point f) was allowed to descend on the mould towards the belly to prevent stretching the radial direction at the leaflet belly. This may have prestretched the tissue a little along the free edge and this possibility was checked by stamping fresh tissue by a grid of 5x5mm squares and observing the distortion of these reference squares after the tissue had been placed on the mould for fixation. The resulting leaflets showed that the squares along the free edge had turned into parallellograms nearer the posts indicating the presence of shear caused by the descent of the centre of the free edge towards the belly. Thus the strips along the edge were neither flat nor straight. At the post-attachment areas all leaflets formed an edge which, however, did not participate in the tensile tested area because the 15mm gauge length was less than the post to post distance of the leaflet. These edges were accommodated between the jaws of the grips. The leaflets were placed on a postcard after they had been allowed to relax on a flat piece of glass and then covered with a thin translucent polyethylene sheet. The blade cutter cut through the sheet and the tissue and the underlying card. Before mounting on the grips the polyethylene strip on top was removed, the tissue strip with the card backing the tissue was placed on the intergrip supportive stage and the jaws of the grips were closed by pressing the edge shaped corners from their oblique side. This specific procedure was

necessary in order to ensure that the tested area between the grips was flat and unstretched at the end of preparation.

Two 3mm wide strips per leaflet were prepared by the use of a blade cutter. The strips were in a circumferential direction close to the free edge of the leaflet (fig.9.15). Strip1 was closer to the free edge than strip2 which was closer to the leaflet belly. When the strips were cut they could assume a much more flat and straight shape. A nominal strain rate of 0.0055/s was used during the preconditioning cycles and the recorded cycle. The minimum recordable load was 0.001N. Cycling was performed between the original gauge length and a maximum load of 1.0N.

For the analysis various estimators were considered, like the extension ratio values at certain load levels, the stiffness of strips as expressed by their Incremental Elastic Modulus and a plot of the extensions against these moduli as used in previous sections of this chapter. A formula to describe the mean loading behaviour in all four groups was also considered as well as the significance in the changes of the formula's parameters between groups under comparison.

Apart from the elastic aspect of the response the viscous aspect was also considered. The main features of the response to load of fresh or fixed pericardial strips were already established in chapter5 and earlier in chapter9. The highest percentage of the work done during loading is dissipated in the first cycle and this percentage is rapidly stabilised to a smaller value almost from the second cycle till the stabilised conditioned cycle. Although there is no firm theoretical foundation, the size of the stress/strain loop has been considered to be a reliable measure and has even been used to test strain rate independence and the degree of fading memory for fixed pericardial strips(Trowbridge and Crofts,1987b), who found that the

Table 9.6: changes in the hydrodynamic performance of explanted valves as compared to the standard performance of valves of the same type which have not been implanted.

Valve	Size	Position	Implantation Duration	RMS Flow	Mean Pressure Difference	Effective Orifice area	Regurgitation Closing/Closed
				ml/s	mm Hg (133.32 N/m^2)	cm^2	ml/ml
HP	23	A	Not implanted	185	3.2	2.0	4.5 3.0
HP	23	A	20 months	185	6.0	1.4	1.1 2.2
ISLP	21	A	Not implanted	185	4.5	1.7	4.1 2.3
ISLP	21	A	56 months	185	15.9	0.9	0.8 3.1
ISU	19	A	Not implanted	193	6.0	1.5	1.7 3.0
ISU	19	A	73 months	186	10.7	1.1	2.0 1.6

HP: Hancock pericardial, ISLP: Ionescu-Shiley Low Profile, ISU: Ionescu-Shiley Standard, A:aortic

work done on loading, the energy lost in loading/unloading (size of the loop) and the percentage energy dissipated for the two different strain rates was not different. However both the work done on loading per unit volume and the energy lost per unit volume were higher in the first test than on subsequent tests with the strips allowed to relax 24hours between the tests. Some dependence on the position on the sac was also noted.

Thus it may be possible in the present case to detect the effects of long term conditioning by such energy based principles.

9.3.4 Results.

Observations of the leaflets in the optical microscope revealed that there was no consistent fibre orientation, proof that all leaflets had been formed and treated as if they were isotropic.

Morphologically the fatigue-cycled leaflets appeared to be permanently extended (sagged). They presented larger dimensions than after manufacture and thus an enlarged leaflet area.

The explanted valves were free from macroscopic calcification and leaflet tears. When viewed with x-rays they also appeared free of calcification in the body of the leaflet. They presented extensive host fibrous ingrowth. The outflow surface of the explanted leaflets adjacent to the frame was covered with a thin layer of fibrous tissue which extended about 1 to 2 mm onto the flexing portion of the valve leaflet. This reduced the area of leaflet that could move and produced a restricted asymmetrical orifice for forward blood flow. The unloaded explant leaflets also appeared permanently extended and thickened.

In the hydrodynamic performance no major changes were seen in the function of valves after cycling in durability tests in the laboratory for 400 million cycles, although the geometry of the individual

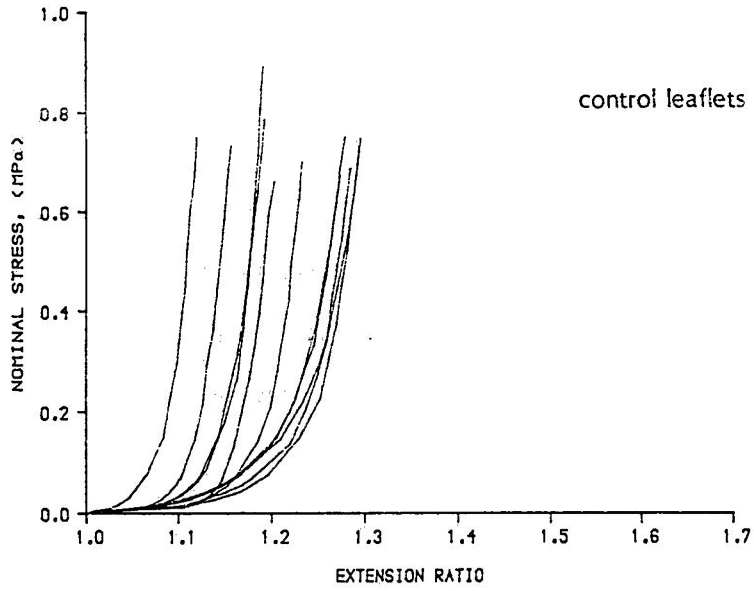

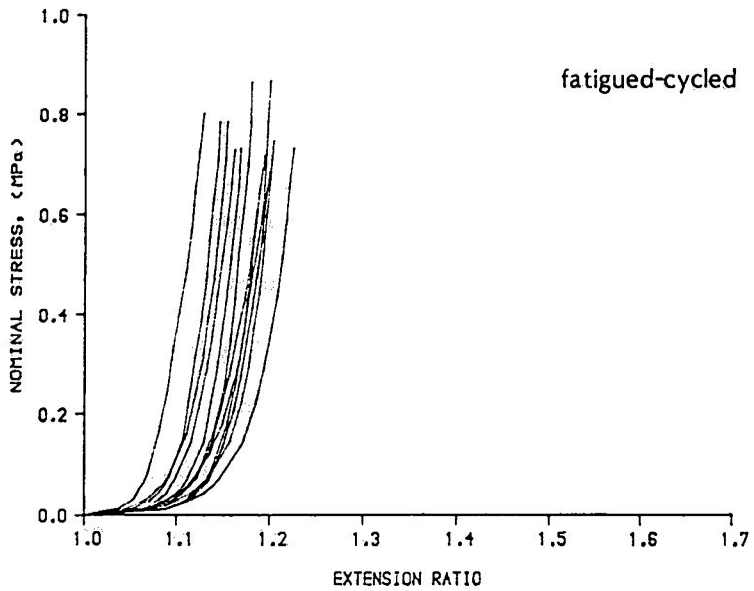

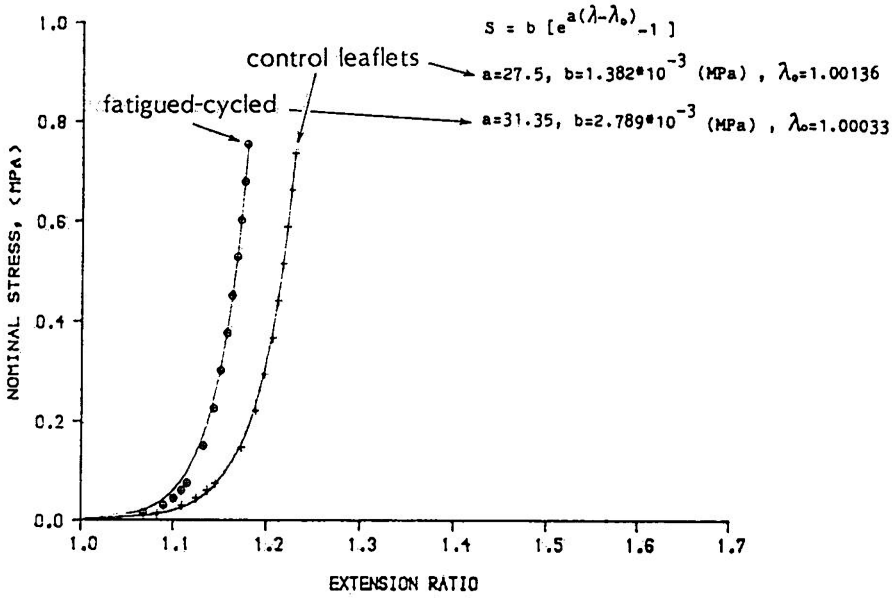

Figure 9.16: stress/stretch behaviour of uncycled and fatigue-cycled leaflets.

leaflets had been altered by the permanent sagging.

The changes in the hydrodynamic function of the explanted pericardial valves were significant. It is shown in table9.6 that the mean pressure difference during forward flow was increased. The effective orifice area was reduced as a result of both the increased transvalvular pressure drop and the reduced geometric orifice. The regurgitation volumes were improved by presenting lower volumetric values but this was a result of either incomplete opening or the reduction of the valvular leaks due to the sealing of minute openings by the development of the fibrous ingrowth.

The tensile curves of nominal stress versus extension ratio for the un-cycled and the fatigue-cycled leaflets are shown in fig.9.16a,b for strip2. It is evident that the envelope of the control tissue was wider than the one of the fatigue-cycled tissue, in average the fatigue-cycled leaflets appear less extensible than the control leaflets and the shape of the fatigue-cycled curves appear to rise more steeply and thus indicate the presence of a stiffer material.

The parameters to express this behaviour were chosen to be the Incremental Modulus of Elasticity and the extension ratio values at prescribed load levels.

The behaviour of the extensibilities of the strips nearest to the free edge(strip1) and the strips below towards the belly(strip2) and for both uncycled/fatigued populations were all compared. The results are summarised:

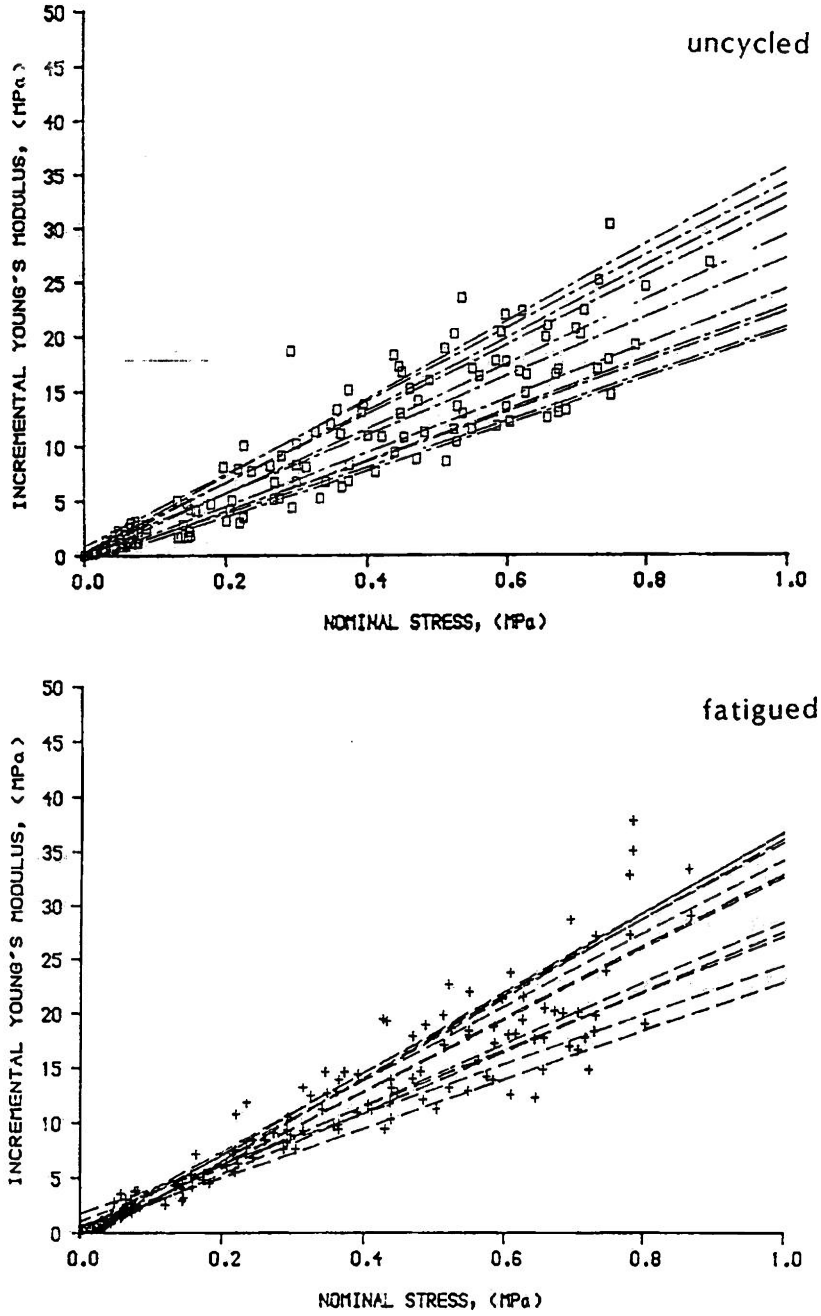

Figure 9.17: linear regression lines on Incr.Modulus.v.Nominal Stress plots. The fatigue-cycled tissue was in general stiffer, thus presented higher slopes.

		EXTENSION RATIO at peak load 1N		
	Position of strip	mean	st.deviation	st.error of mean
uncycled	1	1.221	0.061	0.019
"	2	1.229	0.061	0.018
fatigued	1	1.214	0.044	0.013
"	2	1.179	0.028	0.008

a reduction at peak load extensibility (by 0.05=5%nominal strain) was evident for strips2 between uncycled and fatigue-cycled, while strips1 also had a reduced average value but to a lesser degree. The significance of the findings was checked with Student's t-test between these samples. Significant differences are noted by a (+) and had $p<0.05$, while non-significant differences have a (-) next to their level of significance:

p=0.05 / p		uncycled		fatigued	
	position	1	2	1	2
uncycled	1		-/p=0.75	-/p=0.75	
	2				+/p=0.025
fatigued	1				+/p=0.038
	2				

the statistics showed that: i)at manufacture properties of strip1 did not differ from strip2 and ii)that fatigue cycling induced a significant difference only in the properties of strip2 between uncycled and fatigue cycled leaflets. Statement i) suggests that strips 1 and 2 were made identical at manufacture and thus either of the positions can be used for inferring the effect that

fatigue-cycling has on the tissue properties, but because strip1 was close and included in the leaflet coaption area it was protected from the effects of fatigue-cycling and thus only strips at position 2 nearer the belly were adequately stretched during cycling

It was then decided that only strips2 would be further considered in the analysis for the comparisons on extension ratios, moduli for uncycled/fatigued and for the implants/explants.

Fig.9.17 shows the Incremental Modulus before and after fatigue. The exponential nature of the original stress/strain curves suggested that a linear relation may exist if Modulus values were plotted against the nominal stress values. Fig.9.17 confirms that to a reasonable extent this was true, separate regression lines gave correlation coefficients between 0.954 and 0.989 for the uncycled and 0.948 to 0.989 for the fatigue-cycled. It is clear that the envelope of the regression lines for the fatigue-cycled leaflets is shifted upwards indicating the presence of an overall stiffer material after fatigue-cycling. However the mean values of the slopes (hereafter to be called Fung's moduli) were(mean$\pm$st.error) for uncycled a=27.5$\pm$1.57 and for the fatigued a=31.4$\pm$1.63 producing a non-significant difference between these populations (t-test, p=0.10 >0.05).

A much better fit in the modulus versus stress plots could be achieved by a segmented curve preferably of sequential linear segments. It could be also seen that most of the alteration in the shape of the stress/strain curve occured at the low stress region below 0.2MPa. Separate regression lines were performed for all uncycled and fatigued strips and resulted: uncycled a=27.1$\pm$3.54, fatigued a=36.7$\pm$2.49. Thus the Fung's moduli for the low stress, which previously has been called the incubation region, were statistically different(t-test, p<0.05).

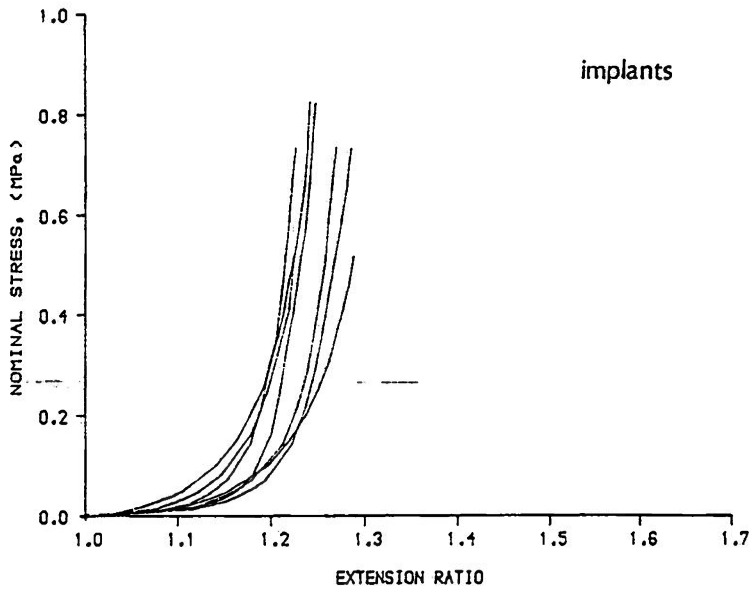

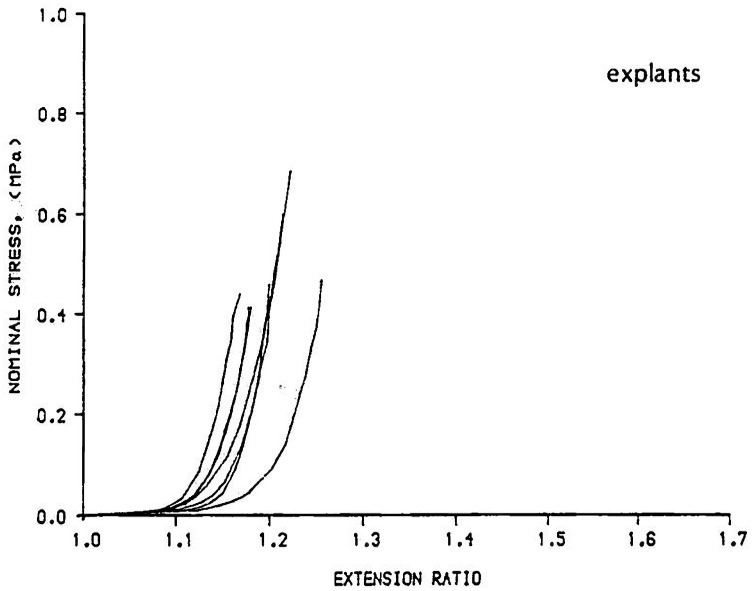

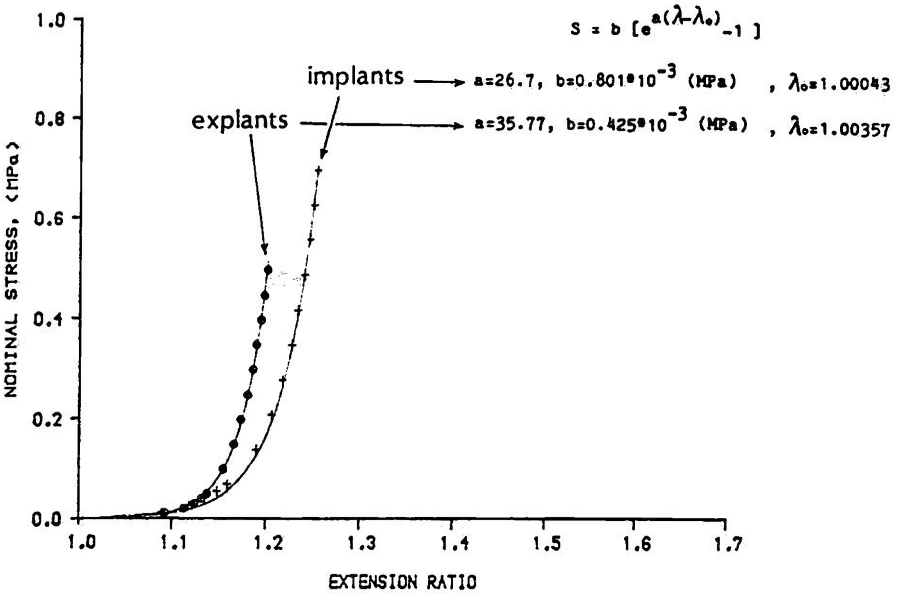

Figure 9.18: stress/stretch behaviour of implant and explant leaflets.

When comparing the terminal elastic moduli of the stress/strain curves the result was nonsignificant like the comparison of the Fung's moduli for the whole modulus/stress curves. In particular uncycled had an Incremental Elastic Modulus of 20.3±1.61MPa, compared to the fatigued values of 25.5±2.03MPa ($p>0.05$; t-test) and thus rejecting the idea that the terminal moduli had been significantly altered.

The satisfactory linear fit of the moduli to the stress values was translated to a stress/strain relation by the use of the exponential formula:

$$S = b\,[\,\exp(a(\lambda - \lambda_o)) - 1\,] \qquad (9.1)$$

which is the smooth curve drawn in fig.9.16c. The steps to apply the formula were: i)a pool of the slopes a in fig.9.17a,b was created and the mean values were calculated to be 27.5 and 31.4 for uncycled/fatigued respectively; ii)the exponential function of the bracket ($[\exp(a(\lambda-\lambda_o))-1]$) was estimated for all the extension ratio values at the stress/strain points of the curve expressing the mean behaviour of the population; iii)the resulting predictions of stress were linearly regressed with nonconstant (intercept being zero) against the mean stress values of the tests; iv)the estimated constant b with units of stress(MPa) scaled down the predictions of the bracket to fit the data and resulted in the smooth curves of fig.9.16c.

The formula yields a zero stress value at a certain extension ratio λ_o which is calculated as the average of the values λ_o at which the first load that could be detected (0.001N) was transmitted through the strip. The shift in the first load point was minimal, less than 1.4%, and was slightly bigger for the uncycled control strips. In the present case it was thought that it had incorporated both a slight error from the preparation (mounting the strip) and any amount of

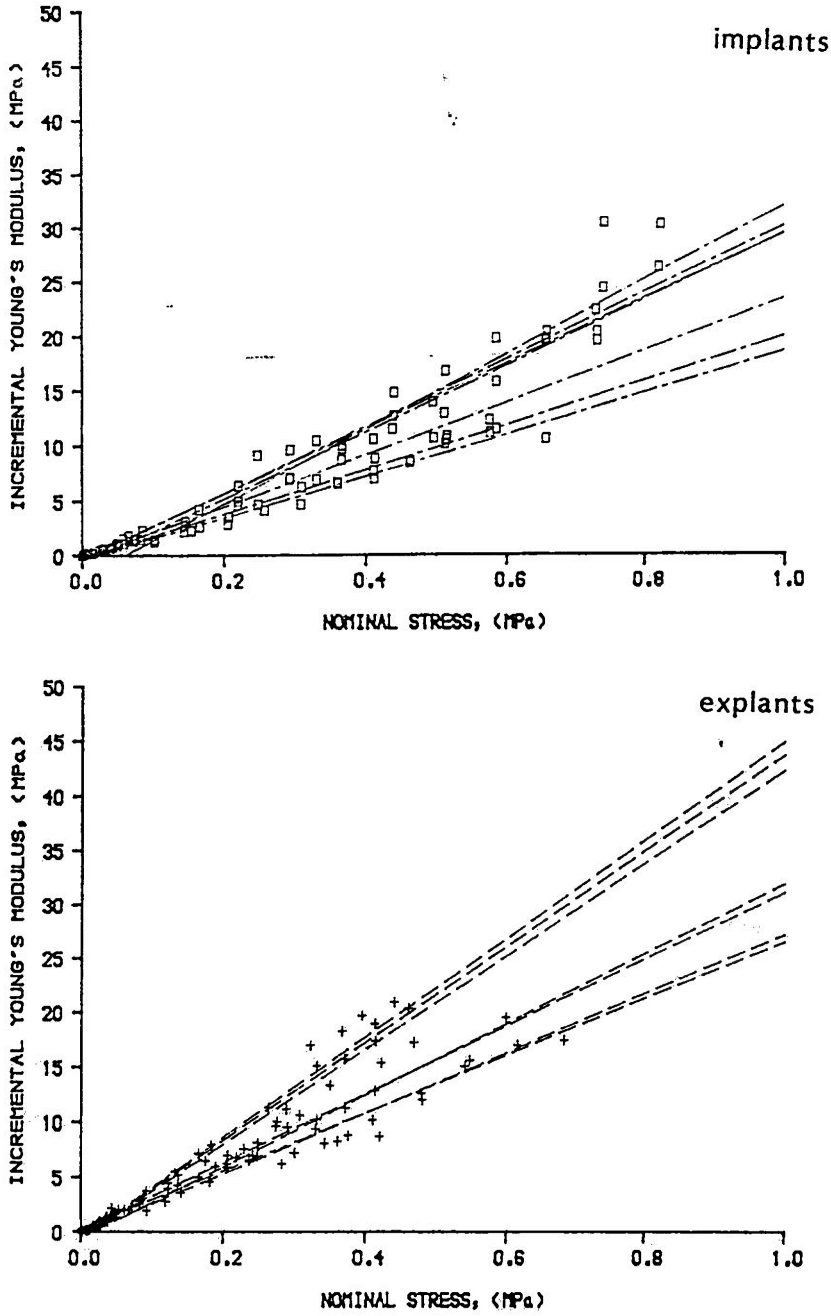

Figure 9.19: linear regression lines on Incr.Modulus.v.Nominal Stress plots. The explant tissue appeared stiffer, presenting higher slopes.

plastic deformation caused by the preceding preconditioning cycles.

Comparison between implants/explants was performed only on strip2. The loading curves for those strips are shown in fig.9.18a,b. The explants reached lower nominal stress values at peak load as a result of an increased initial thickness value and of them being cycled up to a specified load of 1.0N. The explant response appeared stiffer and reached lower extensions at peak load.

The statistics for implant/explant peak load extension ratios were:

	EXTENSION RATIO at peak load point 1N		
	mean	st.deviation	st.error
implants n=7	1.2543	0.0266	0.101
explants n=7	1.2019	0.0305	0.012

resulting in a significant difference(t-test, $p<0.05$).

In fig.9.19a,b the modulus versus nominal stress plots are presented. The upwards shift of the explant curves is again evident. The Fung's moduli(slopes of the regression lines) for the implants had an average value (mean+st.error) $a=26.7\pm2.20$ and the explants had $a=35.7\pm3.16$. This produced a significant statistical difference at a t-test with $p=<0.05$. As previously the change was more pronounced at the low stress region while as in the uncycled/fatigued comparisons the terminal Incremental Elastic Moduli were not significantly different: implants=20.0 ± 2.77 MPa, explants=18.2 ± 1.04 MPa and producing ($p>0.05$; t-test). This is not unexpected and was due to the marked increase in thickness for the explants.

By the use of the average values for the Fung's moduli for each of the linear regresssion envelopes (fig.9.19a,b) and the average first load (0.001N) extension ratio values, the smooth curves of fig.9.18c were

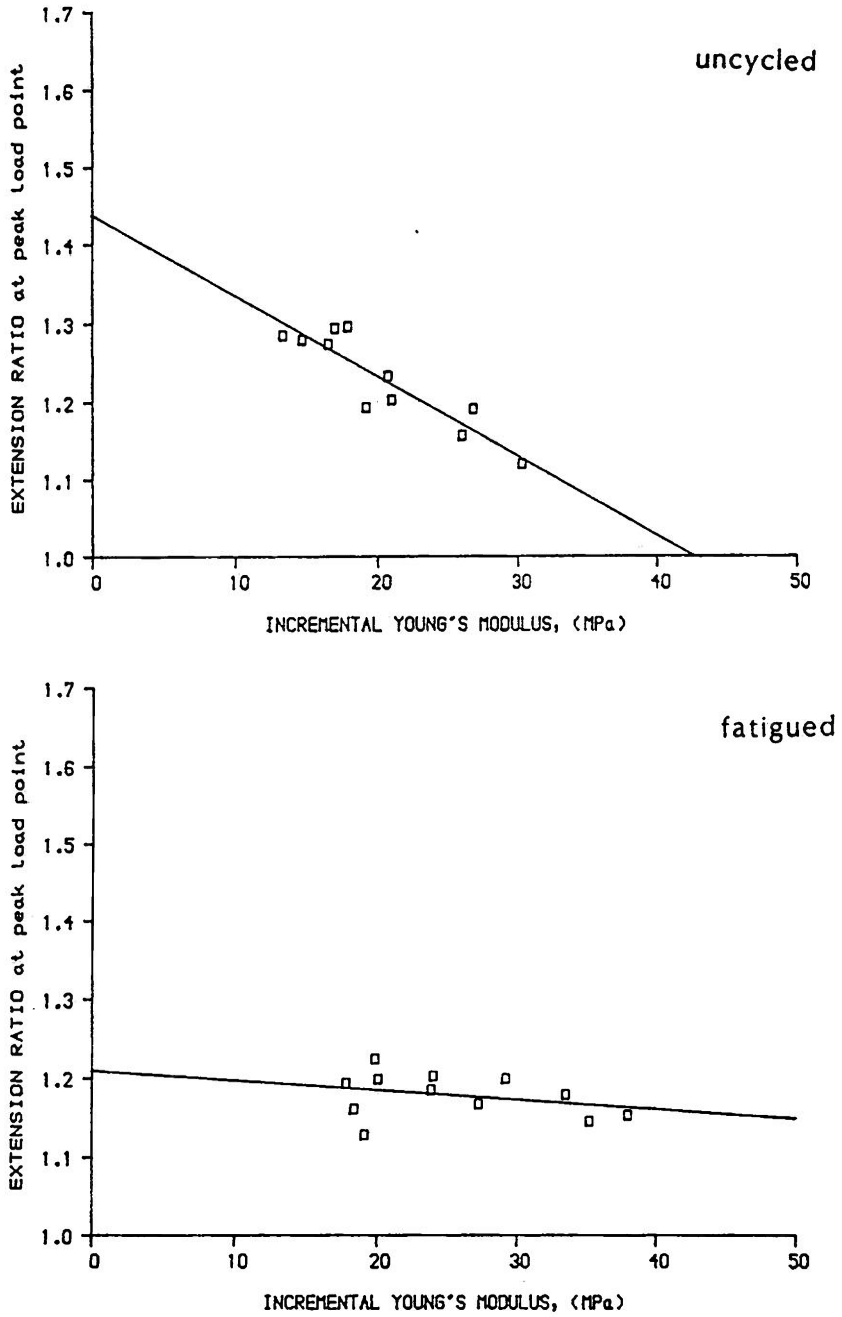

Figure 9.20: The plot of the incremental modulus at peak load.v.extension ratio atpeak load for the Glasgow leaflet tissue had a negative slope suggesting that the tissue had been under variable amounts of stretch during fixation.

fitted to the mean behaviour for the implants and explants. Constant b was a result of regression of the precalculated function $[\exp(a(\lambda-\lambda_o))-1]$ against the observed mean stress values for implants/explants and passing from zero which was literally the point where the minimum detectable load(0.001N.) could be recorded. The values for λ_o were small, less than 1% nominal strain values for either of the groups.

The fit appeared good at higher stress levels but poor in the low incubation region. The linear regression of $[\exp(a(\lambda-\lambda_o))-1]$ against the mean stress values was performed by a least squares method which minimises the deviations of the stress values up and down the line. As a result the curve estimates stresses with the same consistency over the whole range. At low stresses the deviations appear large as the rise of the curve is slow, while at higher stresses the rise is exponential and there deviations of the same order appear small.

It has been suggested that fixation under stretch produces a stiffer material by extracting some of the tissue's early extensibility in the incubation region. If there is a consistency between stiffness and degree of extension it may be possible to show by plotting the extension ratio against the Incremental Elastic Modulus at a particular stress level. Figures9.20, 9.21 include such plots of the extension ratio versus the Incremental Young's Modulus at the peak load points for uncycled/fatigued and implants/explants respectively. What was common between all plots is that there was a negative slope in all populations. Those strips that were more extensible at the peak load (1N) were also more compliant and this was a proof that in general the overall stiffness of the strips was related to the levels of prestretch. However from all plots only the Glasgow uncycled leaflet tissue presented a satisfactory correlation

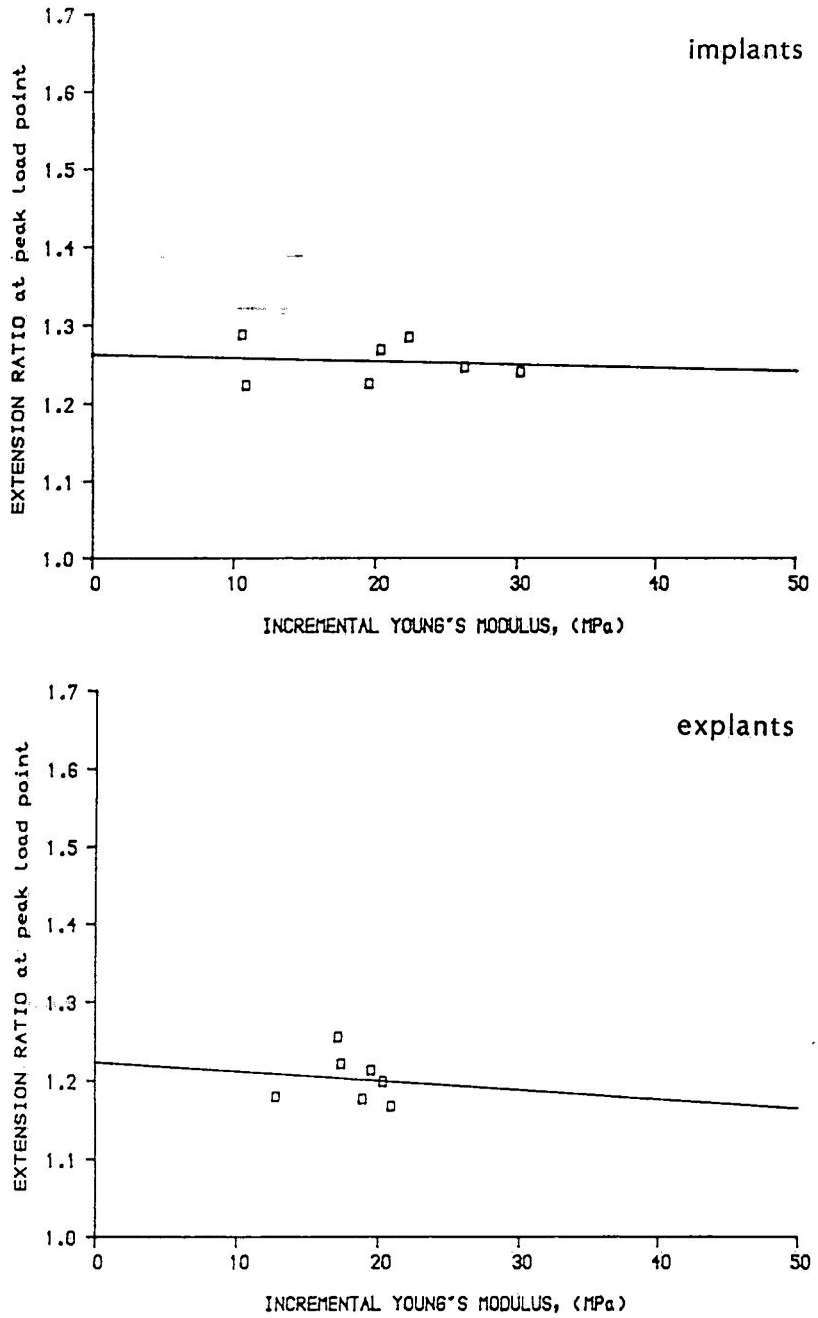

Figure 9.21: the extension ratio at peak load point were not related to the stiffness (incr.modulus) at peak load for the ISU leaflet tissue suggesting a different way of manufacture for those leaflets.

coefficient. In Fig.9.20a the Glasgow uncycled showed a gradual reduction in extensibility as the stiffness at the peak load points was increasing. These points are the ending points of the loading curves(ends of loops in fig.9.18a). In Fig.9.20b of the fatigue-cycled the shift of the moduli to higher values, the reduction in the spread of the extension ratios and the reduction in extensibility of the fatigue-leaflets can be appreciated. In Fig.9.21a the ISU implants presented a very small slope showing an independence of the terminal extension ratios to the material stiffness while they all ended up to a very small range of terminal extensibilities. In chapter8 it has been said that the way of manufacture of ISU leaflets is different from the Glasgow leaflets. This difference shows up in the loading behaviour. The Glasgow leaflets have been made by variable amounts of prestretch at manufacture which created i)the broad envelope of the loading behaviour of the material in fig.9.16a and ii)the negative slope of the modulus versus extensibility plot in fig.9.20a. The ISU leaflets are prepared with i)consistent loading characteristics at manufacture (all curves within a narrow envelope, fig.9.18a), but because of the variability in the peak load moduli ii)from a material having variable properties at manufacture.

The result of mechanical conditioning appears in figures9.20b and 9.21b. There the fatigued cycled leaflets which had escaped stretch at manufacture (and thus were compliant) have undergone larger extensions than the leaflets which had been made less compliant at manufacture. As a result the envelope of the loading behaviour of the fatigued cycled leaflets appears narrow and their loading characteristics very consistent (fig.9.16b) reaching a small range of peak load extensibilities, while the peak load material moduli cover a

Table 9.7: descriptive statistics of the energy parameters for all four groups of tissue strips.

uncycled	N	MEAN	STDEV	SEMEAN
1	11	43.46	16.54	4.99
2	11	32.83	11.01	3.32
3	11	26.86	8.85	2.67
4	11	0.4500	0.0361	0.0109
5	11	1.2295	0.0607	0.0183
6	11	0.3681	0.0524	0.0158
7	11	0.17911	0.02400	0.00724
8	11	12.17	5.73	1.73
9	11	4.380	1.617	0.488

fatigued	N	MEAN	STDEV	SEMEAN
11	11	32.47	4.19	1.26
12	11	28.18	4.38	1.32
13	11	20.56	4.64	1.40
14	11	0.4428	0.0449	0.0136
15	11	1.1834	0.0239	0.0072
16	11	0.3638	0.1334	0.0402
17	11	0.2710	0.1293	0.0390
18	11	9.03	3.65	1.10
19	11	5.863	3.306	0.997

implants	N	MEAN	STDEV	SEMEAN
21	7	51.80	9.43	3.56
22	7	38.03	6.77	2.56
23	7	30.34	5.22	1.97
24	7	0.4900	0.1046	0.0395
25	7	1.2543	0.0266	0.0101
26	7	0.4122	0.0339	0.0128
27	7	0.20154	0.02552	0.00965
28	7	14.72	3.42	1.29
29	7	5.210	0.838	0.317

explants	N	MEAN	STDEV	SEMEAN
31	7	34.03	8.54	3.23
32	7	26.23	5.30	2.00
33	7	20.47	3.90	1.47
34	7	0.6853	0.1238	0.0468
35	7	1.2019	0.0305	0.0115
36	7	0.3876	0.0817	0.0309
37	7	0.2178	0.0372	0.0141
38	7	6.587	2.446	0.924
39	7	2.799	0.740	0.280

i1 :work input in first pull (kJ)
i2 :work input in conditioned pull (kJ)
i3 :work given back in the return (kJ)
i4 :thickness values (mm)
i5 :extension ratio at peak load points (λ_0)
i6 :% of energy dissipated from total energy input during 1st pull
i7 :% of energy dissipated from total energy input during conditioned cycle
i8 :energy per unit volume dissipated in 1st cycle (kJ/m^3)
i9 :energy per unit volume dissipated in conditioned cycle (kJ/m^3)

i=0 Glasgow uncycled, i=1 Glasgow fatigue-cycled, i=2 ISU implants, i=3 ISU explants.

wide range of values.

The ISU explants show in fig.9.21b that (with the exception of a single point) mechanical work had induced a negative relation between material stiffness and extension which the manufacture process had been attempted to avoid.

As mentioned earlier it is more difficult to reach clear conclusions about changes in material properties and behaviour of different populations by simply working on energy principles. In table9.7 columns 1 to 3, 11 to 13, 21 to 23 and 31 to 33 included: the actual work done on loading the strip in the first pull, the conditioned pull and the work given back in the return from the conditioned pull. Columns 6,7, 16,17, 26,27, 36,37 included the percentage of energy irrecoverably dissipated in the first loop and the conditioned loop respectively. Columns 4,14,24,34 included a thickness factor which turned the values of work done on loading into work per unit volume in columns 8,9, 18,19, 28,29, 38,39. Columns 5,15,25,35 included the peak load extension ratio values. Columns i6 to i9 (i=0,1,2,3) in all groups were normalised energy measures reflecting material properties.

From this data the correlation matrices of table9.8 were calculated. Some correlations although statistically strong, have no useful physical meaning and therefore have been omitted from the table, i.e.in Glasgow uncycled leaflet tissue the more work done in the first pull the more work is done in the conditioned and the more the return work was. However the percentage of energy lost in the conditioned loop was not correlated with the amounts of work input in the tissue (columns i1,i2 against i7 for all groups). Thus the %of energy of the conditioned loop was probably a consistent measure of properties of all materials when the loop is performed up to the same stress points.

Table 9.8: correlation matrices for the columns including the values for the energy parameters of table9.7, only correlations with some physical meaning have been kept in the matrix.

	1	2	3	4	5	6	7	8
2								
3								
4	0.181	0.204	0.211					
5	0.935	0.918	0.899					
6				0.035	0.884			
7	0.376	0.361		-0.016	0.608			
8				-0.008	0.915			
9				-0.043	0.914			

	11	12	13	14	15	16	17	18
12								
13								
14	-0.150	-0.316	0.095					
15	0.410	0.628	0.645					
16				-0.197	-0.408			
17	-0.012	-0.024		-0.352	-0.317			
18				-0.451	-0.296			
19				-0.590	-0.051			

	21	22	23	24	25	26	27	28
22								
23								
24	0.722	0.856	0.835					
25	0.345	0.378	0.357					
26				-0.170	0.120			
27	-0.085	0.198		0.213	0.114			
28				-0.418	0.166			
29				-0.180	0.371			

	31	32	33	34	35	36	37	38
32								
33								
34	0.487	0.637	0.700					
35	-0.084	-0.018	0.018					
36				-0.149	-0.061			
37	0.581	0.316		-0.107	-0.108			
38				-0.141	0.073			
39				-0.201	0.219			

The statement that the energy per unit volume or the percentage of energy dissipated in the first loop reflects the degree of conditioning of the material(Trowbridge and Crofts,1987b) was not confirmed; the mean value for this measure was slightly higher for the uncycled tissue, but a t-test between column 8(uncycled) and 18(cycled) gave a non-significant ($p=0.144$) difference in the energy per unit volume dissipated in their first loop.

The size of the conditioned loop was nonsignificantly smaller for the uncycled ($4.4\pm0.49(kJ/m^3)$ than the fatigue-cycled ($5.9\pm0.99(kJ/m^3)$). The greater size of the conditioned loop area for fatigue-cycled material was accompanied by a significantly (t-test; $p<0.05$) greater % of dissipation of energy in the conditioned loop the values being 27.1% for fatigued compared to the equivalent 17.9% for the uncycled. Thus the case was that the stiffer and less extensible fatigue-cycled tissue dissipated more energy during each conditioned cycle.

There was a strong correlation between the extension ratio values at peak load and all the energy based variables of the tissue for the uncycled Glasgow valve. This correlation was positive and once again reflected the manufacturing procedure for these leaflets (column 5 versus 1,2,3, 6,7,8,9). This showed that more extensible strips which had not been stretched during manufacture presented large amounts or percentages of energy which is either input, lost or returned. However after fatigue-cycling all coefficients were reduced and the normalised ones (percentage of energy lost and energy per unit volume) had negative signs indicating that the more extensible the strip the less viscous the material was. This indicated that not only the less extensible fatigue cycled tissue was in general more viscous, but within the envelope of the fatigue-cycled tissue the less extensible tissue strips (of which the extensibility had been mostly affected by

fatigue-cycling) dissipated more energy during each cycle.

The thickness was weakly correlated with the work either input, lost or return of Glasgow uncycled or fatigue-cycled. The coefficients for these same variables were larger for the ISU valves indicating that thicker strips presented larger amounts of work which was either input, lost or return. When correlated to the normalised energy variables (columns i6,i7,i8,i9) the only consistent finding was that for all materials most signs were negative and especially those of the energy/unit volume(kJ/m^3) (columns i8,i9) for the first and conditioned loop. This indicated that thicker tissue dissipated less energy/unit volume.

9.3.5 Discussion.

The statistical comparison of the effects of cycling and implantation presented some difficulties. It was not possible to examine the same sample under two conditions e.g.pre/after implantation. Therefore comparisons were undertaken between parameters describing the populations of the specimens.

Frequently the choice of the parameters is done per se, in order to express the qualitatively appreciated differences. Problems arise from the sample size and the robustness of the parameters. Robustness of a statistical estimator can be easily checked by throwing out(excluding) data and observing the influence on the outcome of the same estimator.

The most consistent measure to indicate alterations due to mechanical conditioning or implantation was found to be the tissue extensibility at a specified load level. The strips that originated from the free edge of the leaflet were protected by coapting to each other and showed minimal changes compared to their properties at manufacture, but the strips closer to the leaflet belly showed marked

stiffening. This suggests that the stress field during function of the valve was inhomogeneous and non-uniform.

The reduction in peak load extensibilities is related to the definition (or even redefinition) of the gauge length in chapter5. There the stress/strain response of the fresh tissue could be different when the unconditioned or the preconditioned natural strip length was used for the calculation of the extension ratio. It has been observed in pericardial strips that repetitive cycling produced a small deformation which was irrecoverable in the time scale of the tensile tests. This deformation shifted the minimum load point by a substantial amount, while the peak load occurred at almost the same extension cycle after cycle. This plastic deformation resulted in increase of the natural length for the fresh strip and it was recoverable when the strip was allowed to relax after it had been cycled for a limited number of cycles. If a redefinition of the gauge length is performed as by remounting the elongated strip the tissue appears less extensible (in Lagrangian terms) at the same load levels. This was inevitably the case for mounting the present pericardial valve strips. They were treated as a 'new' material when laid onto the supporting intergrip gauge length. The fatigue leaflet tissue indeed constituted a 'new' material as the permanently 'sagged' leaflets showed no signs of recovering any of their earlier smaller dimensions for the time period before the tensile tests which could be as long as weeks.

The increased natural tissue length was reflected in the reduced extensibility of the fatigued and explant strips. An early application of this method must have been the tests on fatigue-cycling of valve tissue strips by Broom(1977). Mechanical conditioning of individuals strips resulted in reduction of tissue compliance

(extensibility) but the author did not show the proper attention to the fact that this reflected a permanent elongation of the strips. However Broom(1977) noticed that the modification was mainly in the low incubation region and was structurally related to reduced crimping and waviness of the collagen.

The present study confirms these previous results. The Elastic Incremental Modulus of uncycled and fatigued tissue showed an insignificant increase at the peak load point, but the increase in the elastic moduli for the fatigue-cycled tissue was dramatic in the low stress(<0.2MPa) region.

In the explant tissue which had also been subjected to extensive mechanical conditioning, the reduced extensibility was combined with the effect of deposition of thrombotic particles and the thickening fibrous ingrowth. The explants had both reduced extensibility and significantly higher Elastic Moduli at all stress levels. In the absence of any mechanical conditioning material stiffening could have resulted from the simple deposition of rigid elements on the tissue. Theory of composites claims that a means of increasing the elastic modulus of a material is by encapsulation of grains of a material of much higher elastic modulus.

An attempt was made to describe the loading behaviour of the materials in all four groups by the use of an exponential formula. The choice of the exponential function was made empirically, it being simple and flexible in describing a number of samples showing similar behaviour. It is also a two parameter model thus reducing the number of unknown constants that have to be defined in order to adequately describe a set of data. Parameter a the non-dimensional Fung's modulus determined the convexity of the curves and possessed higher values for fatigue-cycled and explanted tissue strips. Parameter b

Table 9.9: a,b parameter values as estimated by fitting the exponential formula to each one of strip2 from all leaflets which have been tested.

parameters: a	b	a	b
	(MPa)		(MPa)
uncycled		fatigue-cycled	
31.413	0.0011700	27.8	0.0014342
29.500	0.0006985	28.3	0.0024441
33.000	0.0023429	34.1	0.0023028
33.300	0.0038786	37.1	0.0010416
23.300	0.0011406	37.2	0.0025647
22.800	0.0010110	35.7	0.0042646
24.700	0.0005096	38.0	0.0005322
26.800	0.0043855	26.2	0.0104708
35.300	0.0106000	33.5	0.0008201
21.200	0.0014273	22.7	0.0435720
21.200	0.0020296	22.4	0.0093869
		33.2	0.0011132
implants		explants	
20.1	0.0058555	44.4	0.0002960
18.9	0.0022332	45.6	0.0000826
30.5	0.0004456	26.2	0.0031154
34.0	0.0002306	27.4	0.0018122
29.6	0.0008884	32.6	0.0001140
30.2	0.0002250	43.1	0.0002006
23.6	0.0008838	31.1	0.0010924

was a multiplication constant with units of stress and estimated by a fitting routine based on a least squares method.

Two factors could also be considered for a better fit: i)a multiparameter model or ii)the use of a routine other than least squares method for calculation of the constants.

A better fit is almost certain to be achieved by the use of more parameters but this does not justify their use because a single multiparameter formula is able to describe any behaviour by the simple fact that it offers more degrees of freedom without this proving its superiority. Besides the experimenter for a single set of data can choose between a greater number of differently built and structured models(polynomial or exponential or others) many of which may perform adequately, but only some have a physical relation to the underlying mechanisms of deformation and thus are reasonable to use. An exponential formula implicitly accepts that an ever increasing stiffness will occur as stress increases, which can be the result of recruitment of more fibres and their reorientation along the direction of load. On the other hand the fewer the parameters the better. Thus the choice of an exponential two parameter formula resulted.

The model itself by no means restricts the method of parameter estimation to be followed. An alternative to the least squares method could also be used. Choice of an unsatisfactory method, or failure to appreciate that at higher strains the stresses rise fast, and thus deviations are expected to be larger, may lead to hilarious conclusions like the ones proposed by Yin et al(1986) who, in attempting to explain the larger deviations between predicted and observed stresses at higher strains, discovered fictitious non-existing experimental factors which influenced the recorded loading response.

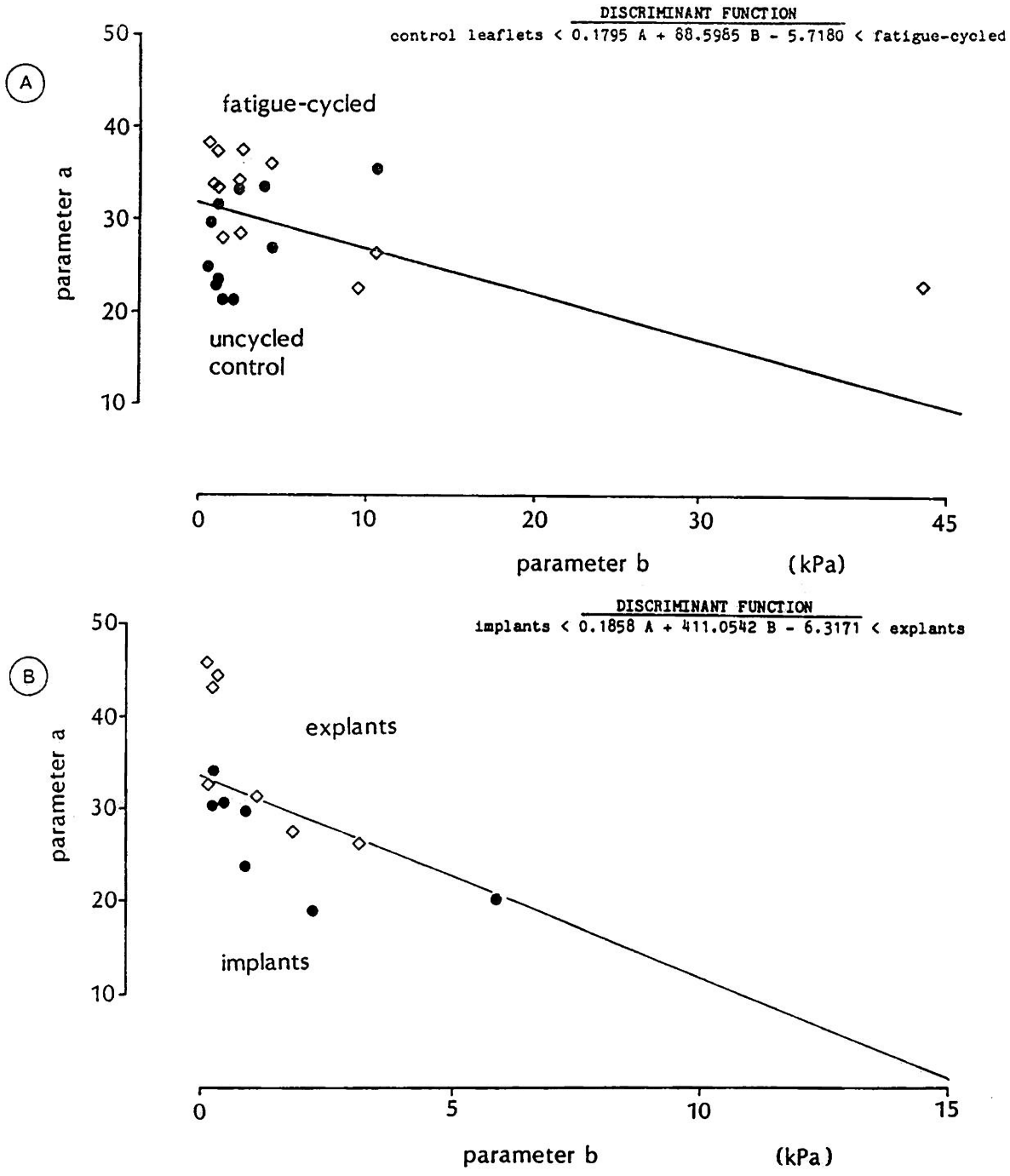

Figure 9.22: (A) discrimination between uncycled and fatigue-cycled, (B) discrimination between implant and explant tissue, by using a linear discriminant function on the actual values of the parameters.

The degree of precision of estimation achieved by the formula is important, but it is also preferable that small changes in the predicted behaviour require large changes in the values of the parameters of the formula. This makes distinction between populations easier. Unfortunately the exponential behaviour of the curves results in exactly the opposite, with only small changes in the parameter values being able to produce major alterations in the curves. This became obvious when the ranges of values of the parameters appropriate for the different groups of tissues under examination had to be defined. The distributions of the values were significantly overlapping and this yielded a statistically non-significant change of parameters a or b between the groups under comparison.

Since there was a definite difference in response to load between un-cycled to fatigue-cycled and implants-explants we would expect a separation of the parameter values which described the response within each group. For this reason discriminant statistical analysis was employed. It was the simple observation that the parameters do in fact exist in pairs and not in arbitrary combinations that led to the plots of fig.9.22a,b. An acceptable separation of the populations of the descriptive parameters would be the one that could discriminate between dark and white symbols as by splitting the domain of their values in two separate territories. At the start the situation looked a little confusing with an evident overlapping existing between the dark and white symbols, but if one considered the significant overlaping of the actual envelopes of the loading curves the idea appeared promising.

Discriminant statistical analysis was performed and the resulting discriminant function can be seen in fig.9.22. The extended description for the analysis is included in Appendix9, where some of

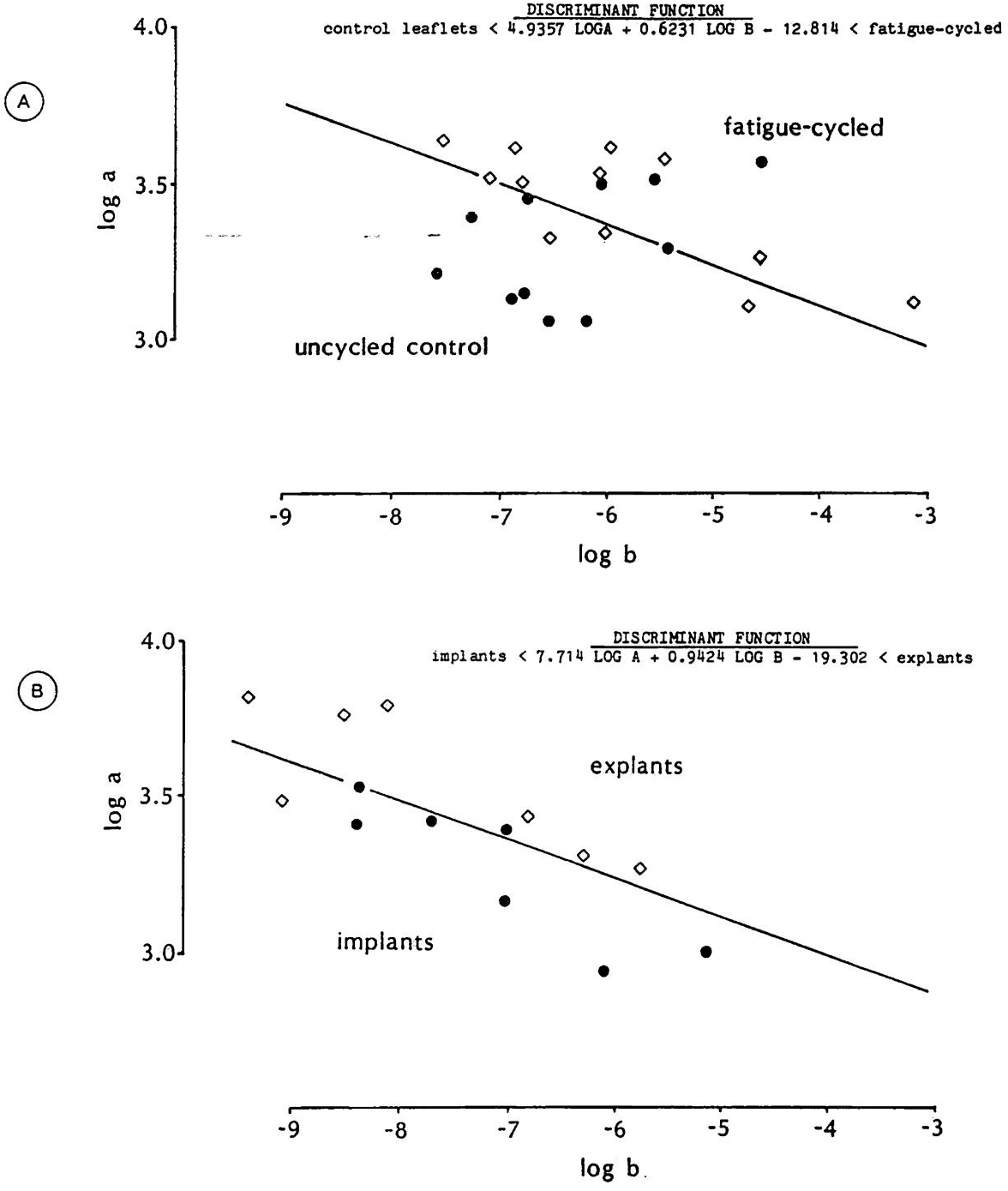

Figure 9.23: (A) discrimination between uncycled and fatigue-cycled, (B) discrimination betweeen implant and explant tissue, by using the logarithmetic values of the parameters a,b.

the problems encountered when discriminating between uncycled/fatigued and between implants/explants are discussed.

Discriminant analysis is always calculated from the observed data and does not require knowledge of the underlying probability mechanisms; it may be proposed though that suitable transformation of the original data can improve the performance of the function. This was accomplished by using the logarithmetic values of the parameters a,b (fig.9.23) and thus rendering linear the initial non-linear envelopes of fig.9.22. The discrimination of implant/explants by using the logarithmetic parameter values was greatly improved, but the same was not true for the uncycled/fatigued discrimation. This was probably due to the 3 data points of the uncycled tissue which invaded the fatigue-cycled territory. If a strict quality control had been applied at manufacture these leaflets might have been excluded.

Discriminant analysis has usually a diagnostic role for classifying future unlabelled cases in either of the groups depending on which side of the linear boundary they fall.

In the present case the analysis can serve differently by using it in a prediction role. It can become a powerful tool in computer-aided design of valves because it provides two separate, distinct and adequately different pools from which the future bioengineer can draw pairs of values. These parameter values describe different loading behaviours and thus help simulating and in essence predicting future conditions regarding work-hardening (discrimination-1) or implantation effects (discrimination-2).

Another estimator which may prove useful in valve construction are the Elastic Modulus versus extensibility plots. A number of workers claimed that fixation under stress or stretch produced a stiffer material (Reece et al,1982; Rousseau et al, 1983; Lee et

al,1984). The validity of this claim and the differences in the manufacture of different bioprostheses were both confirmed by the use of the Modulus .v. extensibility plots. The leaflets manufactured for the Glasgow valve are constrained to have the geometrical shape of an acetal mould. Although they were not under specific tension, they were kept at a certain length and overall dimensions during fixation. Fig.9.20a showed that this procedure resulted in the manufacture of leaflets for which the stiffer they were at peak load the less extensible they were at peak load extension ratios. Apparently when handling the tissue, before it was placed on the mould, a variable degree of prestretch had been imposed on the leaflet. After mechanical conditioning the negative slope of the plots was greatly reduced indicating that as a result of the mechanical conditioning, those strips that had not been stretched before, did so during fatigue-cycling and thus the narrow consistent envelope of mechanical response to load of fig.9.16b resulted. The ISU leaflets were made to have a certain extensibity at a certain load level and this resulted in the narrow unconditioned envelope of fig.9.18a at manufacture. This was probably the result of a selective procedure at manufacture which matched properties and thicknesses of the leaflets to each other. Fig.9.21a indicates that this resulted in strips with a wide range of Elastic Moduli at peak load, suggesting the presence of qualititatively different materials. As a result after implantation the envelope spread (fig.9.18b) and there was an indication that stiffer strips were less extensible (fig.9.21b); once again mechanical conditioning affected mostly leaflets less constrained at manufacture. From the previous observations it is difficult to suggest which rules should be kept at manufacture of leaflets. Obviously one wishes to have the loading behaviour as the ISU at manufacture (fig.9.18a) and

the loading behaviour of Glasgow valve leaflets after long-term conditioning (fig.9.16b), and if possible the same degree of leaflet sagging (alteration in geometry) to accompany these mechanical alterations for all leaflets.

One more idea worth considering in the future would be to construct bioprosthetic leaflets with heterogeneous properties over the leaflet area by successfully controlling local constrictions at fixation.

The mechanical behaviour as exhibited in the tensile tests showed a marked stiffening of the fatigued leaflets which however did not produce any significant change in the hydrodynamic performance parameters of the valve. It would be reasonable to think that a larger leaflet area will be more restrictive in forward flow or cause other problems because it deviates from the original valve design, but these fears did not materialize. The explant valves had significantly different hydrodynamic performance which is easier to understand because they had thicker and more rigid leaflets and a reduced valve orifice due to the tissue ingrowth.

9.4 CONCLUSIONS.

The tests of the present chapter present basic knowledge on the main component of a pericardial bioprosthesis; the fixed pericardial material.

In the first section the degree in which the anisotropy in the load-extension behaviour and strength is retained after fixation by treatment in glutaraldehyde was examined. It was found that although elastic behaviour at the low stress region, where valve leaflets are mostly loaded, depended on the mechanical conditions during fixation, the anisotropy in strength was preserved. Using the strength as a criterion there should be no doubt that the stronger fibre reinforced direction of a pericardial sample should be always directed along the

circumferential direction of the bioprosthetic leaflet.

In the second section the long term performance of the fixed pericardial tissue was examined under the influence of a mechanical factor (fatigue-cycling) and biological environment (implantation in the human body).

It was found that the pericardial material will continue to operate satisfactorily for longer(>10 years) time periods with no obvious changes in the hydrodynamic performance of the valve provided that the material escapes the classic modes of primary tissue failure such as the development of holes and tears caused by poor valve design. However the quality of the material itself deteriorates, producing leaflets with altered geometry which are permanently sagged, with increased stiffness and increased dissipation of energy per cycle. After implantation these same mechanical changes will occur plus a biological modification which includes fibrous tissue ingrowth and leaflet thickening which adversely affect the hydrodynamic performance parameters of the valve. Application of discriminant analysis on the parameters expressing the stress/strain behaviour of the tissue before and after the modification showed that the course of modification may be predictable and this is valuable for valve design in the future.

"... to a scientist a mathematical model is as a stethoscope to a physician, or a trowel to a bricklayer. The model is an image of reality, an abstraction, which touches upon reality in such a manner as to render some of its characteristics visible. It is the expedient relating complex systems to more trivial and simple systems, which last then represent the former. The development of models enables us to compensate for the limits of our imagination and descriptive abilities; by refraining from the details and concentrating on the essentials, the complex reality becomes surveyable, controllable, and comprehensible."

Figure 10.1:Hooft,J.P.,1979 reproduced in its translated form.

10.1 INTRODUCTION.

There have been numerous attempts to model the load/deformation behaviour of soft tissues and pericardium in particular, but the 'ideal' constitutive equation has not yet been produced. Modelling of soft tissues poses special problems arising from the non-linear, time-dependent and almost invariably anisotropic nature of these materials. Additional to the characterisation of these features Kenedi et al(1975) pointed out that a constitutive equation should also have general applicability for more than one tissue and be able to describe multiaxial situations. The problem becomes simpler if attention is focussed on some features as in the present case where the interest is restricted on the elastic phase of the tissue response rather than on the time dependence.

The need for modelling of biological tissues has been stressed by many workers. Fung(1967) indicated that models may help in data collection as well as in analysis of boundary value problems. Lanir(1983) pointed out that models may facilitate the understanding of the function of the tissues and also provide an insight into their response to a given deformation, while others (Hooft,1979; fig10.1) proved to be even more elegant in describing the merits of a theoretical approach.

Three major approaches can be distinguished. The continuum approach applies general material theories to tissues generally assuming the tissues to be hyperelastic and to possess a stored(strain) energy function(S.E.F), but the rationale behind such an application is questionable because soft tissues have complex rheological behaviour which arises from their composite and multiphased structure(Fung,1973). The phenomenological approaches are empirical descriptions which are not restricted by any physical

reasoning. They are in general easier to apply but they lack any relation with the tissue structure and mechanics. The third group includes the structural approaches which include the tissue structure as an intrinsic key factor. This group has been subdivided in the 'structure inspired' models and the 'structure based' models(Barbenel,1979). Structure based models are more difficult to produce because they require detailed knowledge of the tissue structure and are appropriate only for specific tissues while the structure inspired models can be both simple for mathematical analysis and still retain their structural features relating to physical quantities.

The mathematical functions relating stress/strain in use with all models appear to be either of a power law form or of an exponential form. Polynomial power forms are usually related to classical finite elasticity theories which incorporate powers of the stretch ratios, while the exponential polynomial forms are usually encountered with empirical/phenomenological approaches.

Both mathematical functions have been employed earlier in models describing the mechanical behaviour of mammalian pericardia. Hildebrandt et al(1969a,b) employed the principle of a strain energy function(S.E.F) and applied relations arising from finite elasticity theories to describe the load/deformation behaviour of three tissues, one of which was canine pericardium, under uniaxial and uniform biaxial stretch. In doing so they had to assume that the tissues were isotropic and incompressible and also that the S.E.F principle could be applied. The model had a great simplicity and presented a link to elastomer theories but the assumptions that had to be made and the lack of any relation to the tissues' structure were its major drawbacks. Rabkin and Hsu(1975) used a simple empirical exponential

formula for describing the uniaxial stress/strain behaviour of canine pericardial samples. Collagen and elastin were thought to combine like springs in parallel capable of producing the non-linear response exhibited by the tissue. Non-linearity and anisotropy are obviously two features that are structure related and these workers at least made a first attempt in attributing non-linearity to the presence of the constituting elements. In a later report on fixed bovine pericardium Trowbridge et al(1985) used an isotropic, compressible S.E.F to model the fixed bovine pericardium tissue. Although at the time there was no firm evidence that pericardium was anisotropic these workers did not present any histological evidence that it is isotropic. Their assumption about isotropy was arbitrary and merely reflected the inadequacies of their experimental techniques in detecting and quantifying anisotropy. The latest report on canine samples (Yin et al,1986) addressed the question of anisotropy in fresh pericardial samples and attempted to prove that a reasonable quantification of the tissue's biaxial stress/strain data may be possible by the using an earlier exponential empirical formula introduced by Tong and Fung(1976) to describe the mechanics of skin. Anisotropy in the mechanical response of individual specimens could be adequately reflected in changes of the parameters of the empirical function, but since there was no relation to the structure of the tissue their work remained rather inconclusive.

10.2 A STRUCTURE BASED MODEL.

10.2.1 Introduction.

The previous section which highlights the drawbacks and failures of earlier models suggests that all models should have some relation to structure or at least consider the tissue's structure as a key factor in the mechanical behaviour of the tissue. Such models are

always more comprehensive and if correctly built they should anticipate various loading conditions and thus describe the loading response of the tissue under different deformation modes.

Lanir(1979) produced a general theory which can provide a framework for the development of structure related models. It considers the tissues as fibrous composites and not as continua and suggested that a detailed description of the configurational alterations of the fibres during deformation may be able to accurately predict the overall mechanical behaviour of the tissue. In fibrous composites the mechanical role of the fibres is dominant while the role of the soft matrix(ground substance) is generally insignificant. The analysis is based on geometrical and equilibrium analysis of the fibrous structure and Lanir(1979) demonstrated that it could produce loading curves of the correct non-linear shape and suggested that it can be further used to produce the values of the structural features of the tissue by following a specific loading protocol employing uniform biaxial stretch. Lanir developed the model after his own experience with skin and tendon, but he did not attempt to apply the theory on any tissue, neither has any other worker since. This may be due to the fact that application of this theory required a detailed knowledge of the tissue's structure and this can only be done as a part of an extensive investigating project.

10.2.2 Setting-up the Model.

Pericardium is a flat almost two-dimensional tissue consisting of collagen and elastin fibres. The model assumes that the actual structure may be idealised as consisting of a network of planar collagen fibres, which in their resting state are coiled and contorted, and will not support a tensile load until they are extended and straight. A second network consists of elastin fibres which are

straight in their resting configuration and capable of transmitting load immediately. The initial load-extension behaviour of the model is controlled entirely by the elastin network, the bending stiffness of the fibres being negligible. Collagen dominates the load-extension response at high loads (or extensions), when the collagen fibres are straightened and may be aligned in the direction of the load. The transitional behaviour between the initial elastin controlled and the final collagen controlled phases is determined by the mechanical association of collagen fibres to the elastic fibres. The collagen fibres under stretch obey the principle of progressive recruitment, an idea which was firstly introduced by Wiederhielm(1965). Anisotropy is introduced by assuming that the fibres are not randomly distributed, but according to a polar distribution $R(\theta)$.

Lanir proposed two conceptual models in both of which elastin was straight and prestretched in the relaxed state.

In the first version the collagen undulations are induced by the prestressed elastin fibres which are attached to the collagen fibres at numerous points. This idea probably originated from earlier observations on skin made by Finlay(1969). The crosslinks between collagen and elastin subdivide the collagen fibre along its length into segments which are considered as being mechanical subunits. The ratio of the length of the collagen fibre in each unit to the distance between the two crosslinks which bound the unit equals the stretch ratio (λs) at which the collagen will become straight and starts transmitting load itself. A great number of units exist of different stretch ratios(λs) characterised by a distribution function $P(\lambda)$. In this model there is a strong association of collagen with elastin leading to a single $R(\theta)$ describing the angular distribution of both elastin and collagen. For pericardium the histological observations

of chapter7 indicated that the directional association of the two elements was correct but there was no proof that the whole of elastin was prestretched causing the undulations in collagen. Thus this version was rejected and the consequent loading behaviour of the mechanical subunits resulting from this idealisation was also dismissed.

In the second version the collagen undulations originate from the subfibrillar or macromolecular organisation within the collagen fibre. Elastin was prestretched and formed an independent network. Thus collagen obeyed an angular distribution Rc(θ) while elastic fibres were laid-out according to a function Re(θ).

The version which was developed for the present model accepted that there was a strong association between collagen and elastin making it reasonable to assume a simple angular distribution R(θ) to describe both fibres. The angular density distribution function R(θ) describing the geometrical arrangement of the fibres dictates that the fraction of fibres between θ and θ+dθ is given by R(θ)dθ. The total of the fibrous population is included in a $-\pi/2,\pi/2$ interval and thus the overall fibre density is:

$$\int_{-\pi/2}^{\pi/2} R(\theta)\, d\theta = 1 \qquad (10.1)$$

while the distribution R(θ) and the density of fibres is considered to be constant throughout the tissue thickness.

Elastin was thought to exist in both straight and undulating forms in the relaxed state of the tissue. The straight elastin was thought of transmitting load immediately upon deformation while the undulated elastin and collagen only from the point where they had been straighten out. The load required to straighten the collagen was

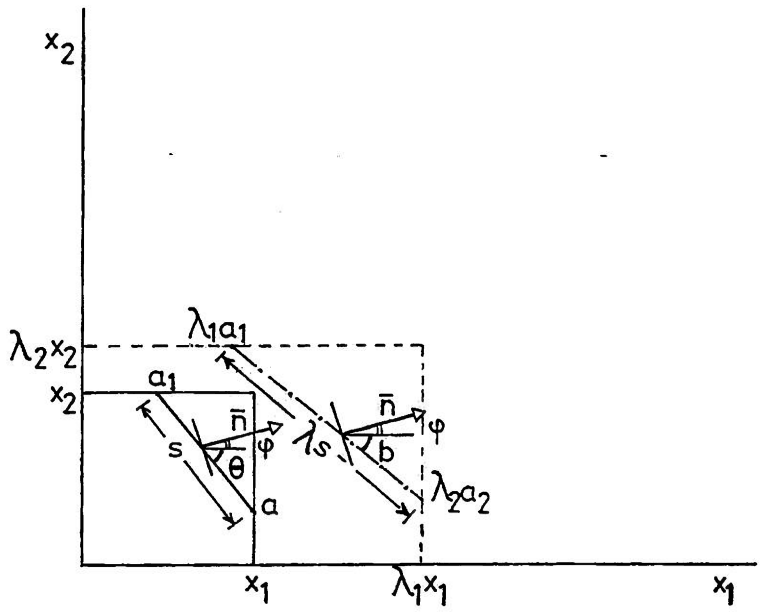

Figure 10.2:A square specimen under general homogeneous deformation turns into a rectangular. Fibres which formed an angle θ to the axis x1 before deformation, form an angle b after deformation. A unit area of which the normal vector $\bar{n}$ forms an angle φ to the axis x1 is also shown.

negligible compared to the load transmitted by the elastin fibres or that of the stretched collagen.

The fibres were assumed to possess only extensional rigidity, while their compressive and bending rigidities were negligible. Both elements were linear with moduli of elasticity K'e for elastin and K'c for collagen, their contribution being weighted to effective moduli Ke,Kc by their active volume fractions Ve,Vc respectively. The active volume fraction for elastin was the product of the bulk volume fraction for elastin and the proportion of elastin fibres which were straight at their resting state. The active volume fraction for collagen was the product of bulk volume fractions of collagen, the proportion of undulating elastin fibres attached to collagen and the proportion of collagen fibres already recruited under load.

A first approximation to the loading function $S(\lambda)$, which is the constitutive relation for the elements interacting as described previously, is:

$$S(\lambda) = Ke\ Ee(\lambda_1,\lambda_2) + Kc\ Ec(\lambda_1,\lambda_2) \qquad (10.2)$$

where Ee,Ec are the effective strains for elastin and collagen and are functions of the current stretch ratios λ_1,λ_2 for a case of general biaxial stretch. Estimation of the precise form of the loading function requires considerable analytic work which first considers the kinematics of a single fibre.

A single fibre which was initially at angle θ to the axis x1 (along which the stretch ratio λ_1 applies) upon deformation will rotate by an angle a and stretch along its length to a stretch ratio λ. In the present case only homogeneous biaxial deformations are considered(fig10.2) which in the absense of shear(γ=0) become:

$$y1=\lambda 1x1+\gamma y2=\lambda 1x1, \quad y2=\lambda 2x2 \tag{10.3}$$

Each fibre is subjected to a uniaxial strain which is the tensorial transformation of the overall strain in the fibre direction(affine transformation) and thus:

$$\lambda^2 = \lambda^2(\theta) = \lambda 1^2 \cos^2\theta + \lambda 2^2 \sin^2\theta \tag{10.4}$$

a fibre of a length s before deformation extends to a length λs after deformation when the angle that the fibre forms to the axis x1 equals b. If the fibre ends were at a1,a2 before deformation, they settle at $\lambda 1a1, \lambda 2a2$ after the deformation. Then the following relations can be produced:

$$(x1-a1)/s = \cos\theta, \quad (x1-a1)/s = \lambda \cos b/ \lambda 1,$$

from both of which: $\cos b = \lambda 1 \cos \theta / \lambda$ (10.5)

similarly it is shown that:

$$\sin b = \lambda 2 \sin \theta / \lambda \tag{10.6}$$

After the application of loads the fibres are under a state of equilibrium in which the internal load applied to a unit area is equal to the sum of the contributions of the tension of all the fibres that cross this unit area. Lanir pointed out that for planar fibrous configurations the effect and presence of hydrostatic pressure p would be negligible if compared to the tension of the fibres and thus it can be neglected.

Consider a unit area, the normal unit vector $\bar{n}$ of which forms an angle φ to the axis x1. At equilibrium this unit area is crossed by a number of fibres equal to:

$$R(\theta)\, d\theta \cos(\varphi - \theta) \tag{10.7}$$

upon deformation fibres at angle θ will rotate to an angle b and stretch to a stretch ratio λ as described earlier. If we assume that the loading function $S(\lambda)$ for these fibres is known, then the stress exerted by all fibres originally at an angle θ which cross the unit area which had original normal unit vector $\bar{n}$ will be:

$$Sn = S(\lambda)\cos(\varphi-\theta)\,R(\theta)\,(\bar{i}\cos b+\bar{j}\sin b)\,d\theta \qquad (10.8)$$

the unit vectors i,j are along the directions 1,2 respectively. The resultant of this stress in any other direction $\bar{s}$ at an angle ψ will eventually be (using relations(10.5)):

$$Sns = [S(\lambda)/\lambda]\cos(\varphi-\theta)R(\theta)[\cos\psi\lambda_1\cos\theta+\sin\psi\lambda_2\sin\theta]d\theta \qquad (10.9)$$

thus the total stress at a direction $\bar{s}$ resulting from the total load on the fibres over the initial unit area is:

$$Ss = \int_{-\pi/2}^{\pi/2} [S(\lambda)/\lambda]\cos(\varphi-\theta)R(\theta)[\cos\psi\lambda_1\cos\theta+\sin\psi\lambda_2\sin\theta]d\theta \qquad (10.10)$$

and thus the tensile stresses along the testing directions1,2, which have ($\psi=0, \varphi=\pi/2$) and ($\psi=\pi/2, \varphi=0$) respectively, are:

$$S1(\lambda_1,\lambda_2) = \lambda_1 \int_{-\pi/2}^{\pi/2} [S(\lambda)/\lambda]R(\theta)\cos^2\theta d\theta \qquad (10.11)$$

$$S2(\lambda_1,\lambda_2) = \lambda_2 \int_{-\pi/2}^{\pi/2} [S(\lambda)/\lambda]R(\theta)\sin^2\theta d\theta \qquad (10.12)$$

the next step being the production of the appropriate loading function $S(\lambda)$ and the choice of the parameter values wherever they are encountered.

The loading function consists from two parts for the elastin and

the collagen networks. We consider fibres at an initial angle θ to the axis x1 for which direction the stretch ratio is $\lambda(\theta)$ given by relation(10.4).

For elastin then its own loading function would simply be:

$$Se(\lambda 1,\lambda 2,\theta) = Ke\ [\lambda(\theta) - 1] \qquad (10.13)$$

where all elastin fibres included in the formula were initially straight and thus loaded immediately upon deformation.

The collagen and its attached elastic fibres would possess a distribution of the stretch ratios λs under which the fibres become straight. This distribution is P(x) and for the present model it was assumed to be a normal distribution of mean μ and standard deviation s.d.. The loading function for all collagen fibres and the attached elastic fibres not originally stretched would be:

$$Sc(\lambda 1,\lambda 2,\theta) = Kc \int_{1.0}^{\lambda(\theta)} P(x)\ [(\lambda(\theta)-x)/x]\ dx \qquad (10.14)$$

the upper limit $\lambda(\theta)$ is a function of the original angle θ which a fibre had at the relaxed state of the tissue, and the current stretch ratios along the testing directions.

As stated earlier in the equilibrium analysis these forms have to be integrated between $-\pi/2$ and $\pi/2$ in order to include the contribution of all elastin and collagen fibres that cross a unit area of original normal vector $\bar{n}$.

The combined loading function is given by the sum of (10.13) and (10.14) i.e:

$$S(\lambda) = Ke\,[\lambda(\theta)-1] + Kc \int_{1.0}^{\lambda(\theta)} P(x)[(\lambda(\theta)-x)/x]\,dx \qquad (10.15)$$

which when substituted into equations (10.11),(10.12) yields the tensile stresses in directions x1 and x2:

$$S1(\lambda_1,\lambda_2)=\lambda_1 \int_{-\pi/2}^{\pi/2} \{\, Ke[\lambda(\theta)-1] + Kc \int_{1.0}^{\lambda(\theta)} P(x)[(\lambda(\theta)-x)/x]\}\{R(\theta)/\lambda(\theta)\}\cos^2\theta\,d\theta \qquad (10.16)$$

$$S2(\lambda_1,\lambda_2)=\lambda_2 \int_{-\pi/2}^{\pi/2} \{\, Ke[\lambda(\theta)-1] + Kc \int_{1.0}^{\lambda(\theta)} P(x)[(\lambda(\theta)-x)/x]\}\{R(\theta)/\lambda(\theta)\}\sin^2\theta\,d\theta \qquad (10.17)$$

where: $P(x)= (\exp[-(x-\mu)^2/2(s.d.)^2]) / s.d.\sqrt{2\pi}$ (10.18)

and $\lambda^2(\theta)=\lambda_1^2\cos^2\theta + \lambda_2^2\sin^2\theta$

as given in (10.4).

For application in uniform biaxial and constrained biaxial deformations the only requirement is to feed the appropriate stretch ratios λ_1,λ_2 into (10.4), (10.16) and (10.17). For the uniaxial case where one of the two stretch ratios is negative some of the fibres will contract and because they bear no load and they should be excluded from the calculation of the stresses. The fibres that contract have equation(10.4) less than 1. If this inequality is

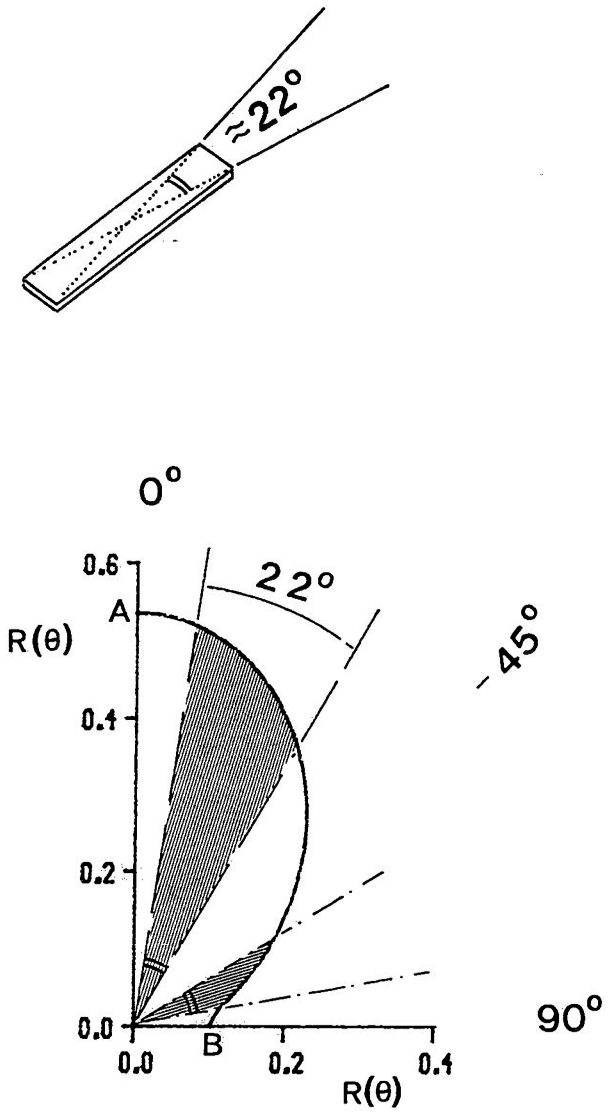

Figure 10.3:Strips 15mm long and 3mm wide isolated a 22°angular sector from the total angular fibre distribution. The U.T.S. value exhibited at each angle $\theta\in(0^\circ,90^\circ)$ was assumed to be linearly related to the value $R(\theta)$. A and B were rescaled as to give a total density of fibres between $[-\pi/2,\pi/2]$ equal 1.

solved, the critical angle turns out to be:

$$\theta o = \text{Arc tan}([(1 - \lambda^2 1)/(\lambda^2 2 - 1)]^{1/2}) \qquad (10.19)$$

and the limits $(-\pi/2,\pi/2)$ for integration in equations (10.16),(10.17) are then substituted by $-\theta o, \theta o$.

For the implementation of this model the distribution $R(\theta)$ and a number of structural, geometrical and material parameters have to be defined; these were obtained from the experiments reported in previous chapters.

Structural parameters. From the histological observations of chapter7 it was concluded that the pericardial tissue has a multilayered structure with the fibres within each layer being directed along a single direction and the various layers assuming a more general direction along which the tissue has one of its axes of mechanical anisotropy. For use in the model the angular fibrous distibution should be expressed as a continuous function of the angle θ. The data obtained in the failure tests of chapter6 was used to produce this angular distribution. The assumption was made that the function obeyed the same angular behaviour as the U.T.S. values given in chapter6. The rationale behind this is based on figure10.3 which shows that the geometry of the test strips always resulted in isolating all fibres of the distribution within a 22° angular sector which ran from one set of grips to the other and were therefore load bearing. It was assumed that the U.T.S. value measured in any direction reflected the amount of fibres traped between the jaws of the grips and thus there was a linearly proportional relation between the angular variation of U.T.S. and the fibre density distribution function $R(\theta)$. The distribution function was found to be (equation(6.10)) of the form:

$$R(\theta) = A\cos^2\theta + B\sin^2\theta \qquad (10.20)$$

For average U.T.S values in the principal directions of 17.34MPa and 3.28MPa, the coefficients of the function $R(\theta)$ were rescaled as to yield a total density of 1 according to relation (10.1). This produced A=0.535 and B=0.101 and an $R(\theta)$ of the form:

$$R(\theta) = 0.535\cos^2\theta + 0.101\sin^2\theta \qquad (10.21)$$

which is the function drawn in fig10.3. Form(10.21) in cartesian coordinates is bell-shaped resembling a normal (Gaussian) distribution for fibres aligned along a direction of mean value(θ_o) and with a standard angular deviation like the one that Lanir(1979) used as an example.

Geometrical parameters. These are the mean (μ) and the standard deviation (s.d.) of the recruitment process. In an earlier report Decraemer et al(1980) used the previous quantities in their literal physical meaning assuming that some collagen fibres started stretching immediately (λ=1.0) which meant that the mean was almost 3 st.deviations from the origin. Lanir(1979) on the other hand related the st.deviation to the level of geometrical uniformity along the collagen/elastin fibres. In both these applications the parameters were only geometrical equivalents to the real physical quantities and should be chosen in such a manner as to best reflect the loading behaviour of the tissue. The association with the natural equivalents probably led these workers to believe that there was only one possible pair of values for the mean(μ) and the st.deviation(s.d.) for each tissue.

In the present work we disengage our parameters from any direct relationship to the natural equivalents. Thus firstly the fibre mean

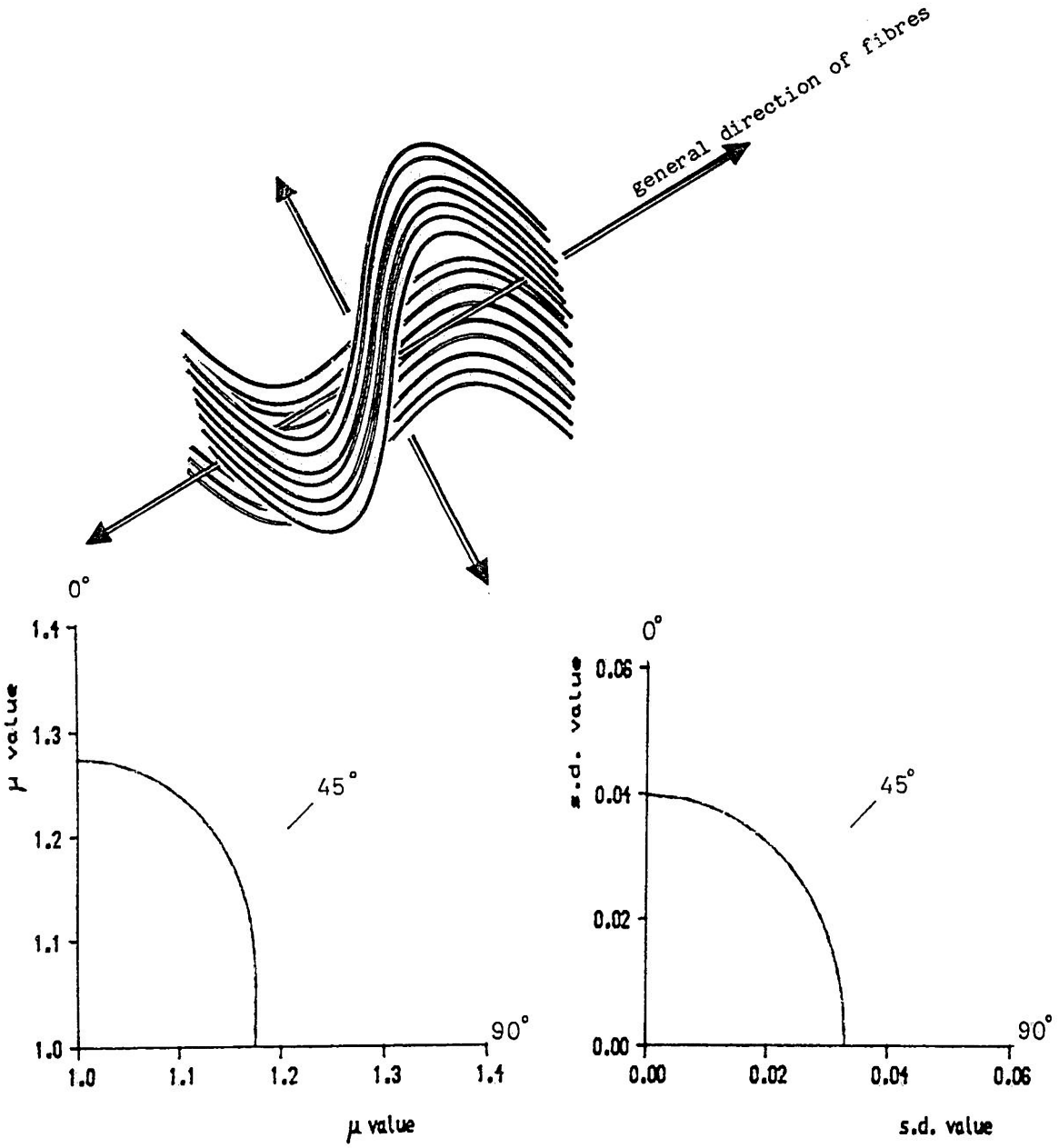

Figure 10.4:Top; the tissue consisted of a great number of fibrous layers assuming a general direction along the strong axis of mechanical anisotropy. The structure can be viewed as an idealised spring which possesses a greater potential of expansion along the general fibre direction than across the fibres.
Below; postulated behaviour of the fibre distribution mean(μ) and the standard deviation (s.d.) off the axes according to:

$$[(\mu^2-1)/2]=[(\mu_c^2-1)/2]\cos^2\theta+[(\mu_a^2-1)/2]\sin^2\theta, \quad \text{s.d.}= \text{s.d.}_c\cos^2\theta+\text{s.d.}_a\sin^2\theta$$

c:circumferential, a:axial, angle θ is measured from the stronger 0° direction. The intercepts on the axes of the μ and s.d. values are chosen as to best fit the uniaxial data.

is the stretch at which 50% of the collagen fibres have entered their linear region and started bearing load. This is the natural outcome of modelling the collagen fibres as being linear with a modulus (K'c) while they probably possess non-linear loading characteristics. Secondly we consider that both parameters express geometric properties of the tissue rather than its fibres and thus reflect the tissue's ability to stretch anisotropically in its plane. The rationale behind this idea is shown in figure10.4. The tissue is depicted as an idealised spring with its fibres assuming a general direction. Such a tissue possesses a greater potential for expansion along the fibre than in the direction perpendicular to the fibres. Unlike skin where fibres entangle and have a three dimensional layout, the immediate response to load of the tightly packed pericardial fibres are only moderate rotations within their own laminae. According to the preconditioned uniaxial tests of chapter5, the biaxial inflation tests of chapter4 and the failure analysis of chapter6 the loading curves in the axial direction present the same characteristics (i.e incubation region, linear region, failure point) at lower strains than the circumferential curves. Thus although in microscopical level parameters μ and s.d. have values which are directionally independent, as a result of the macroscopic packing of the fibres the parameters should be functions of the angle θ and thus directionally dependent. In chapter6 in particular the ultimate stretch ratio of tissue strips in different directions treated as a finite strain measure and was transformed at directions off the axes. In fig.10.4 the postulated angular variation of fibre mean(μ) and the standard deviation(s.d.) are given. The fibre mean has been treated as a finite strain and the s.deviation as a strain value. The fibre mean has a higher value at the circumferential direction and we consider

(A)

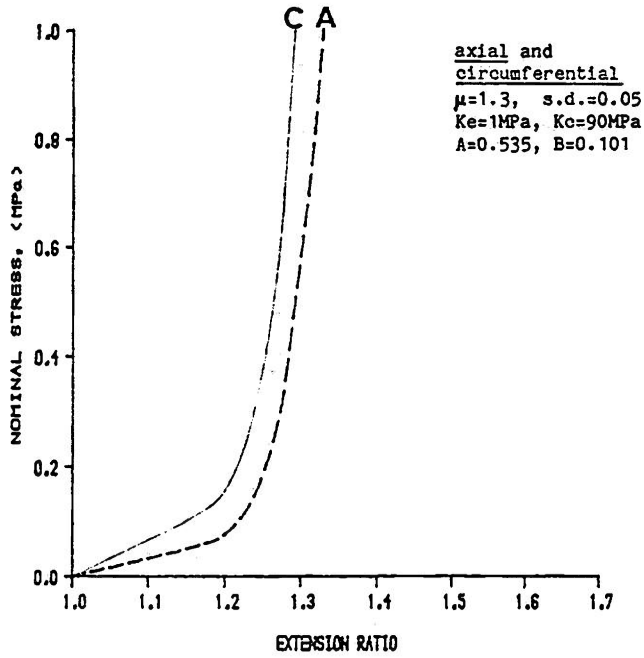

(B)

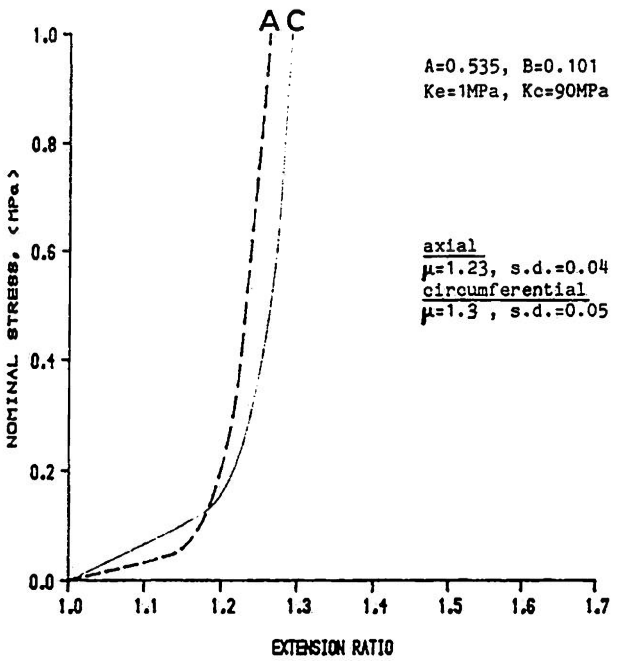

Figure 10.5:Demonstration curves. (A) all parameters are the same in the two normal directions, axial(A) and circumferential(C). The difference is due to the anisotropic fibre distribution introduced by R(θ). (B) curves having the required features can be produced by an anisotropic choice of the geometrical parameters μ,s.d.

this to reflect the tissue's greater potential for deformation along this direction. The direction dependent μ and s.d. can be incorporated in the model with lower values along the axial direction. The actual values on the axes are chosen as to best fit the data.

The beneficial consequences of the previous assumptions for the structural and the geometrical parameters can be seen in the demonstration curves of figure10.5a,b. All 4 curves in fig10.5a,b have the same structural parameters A,B and distribution function R(θ) defined earlier. As a result of this choice the following integrals take the values:

$$\int_{-\pi/2}^{\pi/2} R(\theta)\cos^2\theta d\theta=0.67, \qquad \int_{-\pi/2}^{\pi/2} R(\theta)\sin^2\theta d\theta=0.33 \qquad (10.22)$$

In the case of uniform biaxial stretch these integrals can be isolated in the forms (10.22) in relations (10.16),(10.17) and thus act as multiplication factors for the tissue loading response over the whole length of the loading curve. In the case of the uniaxial tests significant lateral contraction happens only at higher strains and thus near the origin equations (10.22) predict a 2:1 ratio in their slopes. Such a 2:1 ratio for the slopes at the origin was measured in experimental data of both fixed (chapter9) and fresh (chapter5) material and strongly suggests that the structural parameters A,B and the proposed function R(θ) were correct.

The geometrical parameters have been altered between fig10.5a and fig10.5b. In fig10.5 the axial and circumferential curves both have the same μ and s.d producing a circumferential curve both stiffer and less extensible. If μ and s.d. are set to follow anisotropic behaviour by having lower values along the axial direction fig10.5b is produced. The circumferential curve was stiffer along its whole

length but demonstrated an increased extensibility after the incubation region at the same stress levels as did the experimental results.

Material Parameters Ke,Kc were chosen to best fit the uniaxial curves. The initial region in the model is described by suitable choice of Ke which is the effective modulus for elastin fibres multiplied by the product of the volume fraction of elastin and the proportion of elastin straight in the resting state of the tissue. A convenient choice for Ke that would fit curves in either of the directions was Ke=0.15MPa.

It was a little more difficult to chose an effective value for the modulus Kc. The material properties of collagen fibres have been said to be non-linear, but both Diamant(1972) and Comninou and Yannas(1976) have shown that an inherently linear collagen can exhibit non-linearity due to the wavy resting fibre configuration. Christensen and Waals(1972) obtained effective moduli for linearly elastic phases when examined composites with two and three dimensional randomly oriented fibres. It may be possible to model the non-linear stress/strain curve of collagenous tissues as a bilinear curve of two linear segments and use two constant values for the Young's modulus of collagen for the low and the high stress regions respectively. The problem is that the modulus of elasticity exhibited in the linear region of the stress/strain curve in uniaxial tests is a result of contribution of an unknown number of fibres which have been recruited at a variety of stretch. The value of Kc for the model may be chosen by trial and error till the proper response is achieved but we may also make a reasonable estimate of this modulus by using the theory of Cox(1952) which was presented in chapter6. The theory was applicable for infinitesimal strains and was developed for a fibrous composite

without a matrix with the elements being linearly elastic. Cox(1952) expressed the angular fibrous distribution as a periodic function $R(\theta)$

$$\pi R(\theta) = 1 + a1 \cos 2\theta + a2 \cos 4\theta + a3 \cos 6\theta + \ldots + b1 \sin 2\theta + b2 \sin 4\theta + \ldots\ldots \quad (10.23)$$

and then he found that the stiffnesses equal:

$$c11 = (K/16)(6+4a1+a2), \quad c22 = (K/16)(6-4a1+a2) \quad (10.24)$$

$$c12 = (K/16)(2-a2) \quad (10.25)$$

where K was the product of the fibre modulus and volume ratio of the fibre material, and for the compliances:

$$s11 = [(2-a2)(6-4a1+a2)-(2b1-b2)^2]/D \quad (10.26)$$

$$s22 = [(2-a2)(6+4a1+a2)-(2b1+b2)^2]/D \quad (10.27)$$

$$s12 = -[(2-a2)^2-4b1^2+b2^2]/D \quad (10.28)$$

where: $$D = K[(2+a2-a1^2)(2-a2-b1^2)-(a1b1-b2^2)] \quad (10.29)$$

the distribution $R(\theta)$ already proposed in (10.21) can be brought in the form (10.23) by setting a1=0.682 and all other coefficients set to zero. By using the only remaining a1 into equations (10.24) it was found that stifnesses, compliances, effective Young's moduli and effective Poisson's ratios have a relationship:

$$\frac{c11}{c22} = \frac{0.545K}{0.205K} = 2.67, \quad \frac{s22}{s11} = \frac{E1}{E2} = \frac{5.686/K}{2.132/K} = 2.67, \quad \frac{s12/s11}{s12/s22} = \frac{\nu 12}{\nu 21} = \frac{0.61}{0.23} = 2.67, \quad (10.30)$$

In the uniaxial tests for site-I presented in chapter5 and 6 the modulus in the linear region was estimated to be around 45MPa for the circumferential strips and around 14MPa for the axial strips, an almost 3:1 ratio. Thus by using the distribution function (10.21), constant a1 was estimated which resulted from the behaviour of the tissue strips at the failure region. This failure related structural

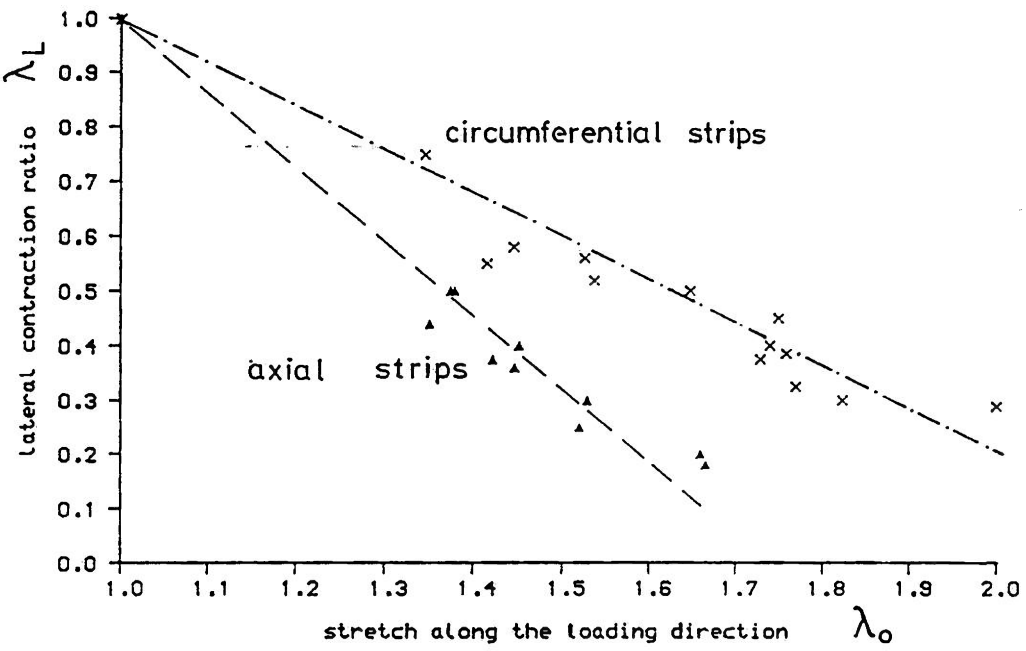

Figure 10.6:Longitudinal stretch and lateral contraction of strips aligned along the axial and circumferential directions as resulting from photographic observations.

constant a1, was used in a developed model which averages the effect of all fibres that are under tensile load and produced the accurate 2:1 ratio for the slopes of the curves near the origin. When this same constant a1 was used in Cox's theory, assuming the theory to be applicable to the final prefailure linear region of the curves, it predicted a 2.67:1 ratio between the two terminal Young's moduli. This value is smaller than the 3:1 ratio exhibited in uniaxial tests and this is probably due to a larger number of fibres being under contraction in the axial strips than in the circumferential strips. Nevertheless the use of Cox's theory, applicable to linearly elastic materials under small strains, by inserting a parameter calculated from the failure characteristics of the material gave an estimate for the ratio of the moduli which compares reasonably with the one exhibited in tests. Once again this was a strong indication that the structural parameters were set-up correctly and that they would yield the right value for the moduli if constant K is carefully chosen. Constant K is in the range (80-100)MPa.

10.2.3 Applications for different deformation modes.

10.2.3.1 The uniaxial case. Application of the previous theoretical model for uniaxial stretch needed a further exploratory step. Equation (10.19) calculates the angular range $(-\theta o, \theta o)$ within which the fibres stretch and thus exclude the fibres which contract, and this requires the relationship between the two principal stretch ratios $\lambda 1, \lambda 2$ to be established. In the present study the experimental longitudinal stretch and lateral contraction of axial and circumferential strips were photographed and measured. The behaviour was described to a first approximation by linear relationships(fig10.6) which differed for strips along the axial and circumferential directions. This qualitative difference in the

lateral contraction of axial and circumferential strips was described in chapter5 and can be seen in the failure photos which have been included there. The axial strips continuously thinned until complete failure occured while the circumferential strips presented less lateral contraction. With the development of the present model and especially by anticipating that a number of fibres will contract upon deformation this finding is easier to explain. Circumferential strips have the majority of fibres aligned along the strip axis with only a small proportion of fibres at right angles in the axial direction. For the axial strips the majority of fibres are aligned along the normal circumferential direction which is also the direction of contraction and thus a greater portion of a fibres contract. This mechanism provides in the present case a physical reason for what is a fundamental property of orthotropic bodies where the ratio of Young's moduli equals the inverse ratio of the Poisson's ratios (Hearmon,1961). There is a different way of handling the contraction data. The present deformations are large and thus we could consider the relation that the finite elastic normal strain components B11/B22=$(\lambda_1^2-1)/(\lambda_2^2-1)$ have. This relation appeared reasonably linear and gave:

for axial strips, $(\lambda_2^2-1) = -0.10 - 0.613(\lambda_1^2-1)$ (10.31)

and circumferential strips, $(\lambda_2^2-1) = -0.07 - 0.360(\lambda_1^2-1)$ (10.32)

The slopes, which represent the effective Poisson's ratios for the material should be comparable with the predictions obtained previously by using Cox's theory. The effective Poisson's ratio which is applicable when stretching axial strips was 0.613 compared to the predicted 0.611, while the Poisson's ratios for circumferential strips was experimentally observed to be 0.36 and was predicted at 0.23.

In figure10.7a the mean behaviour of the first pull curves of the

(A)

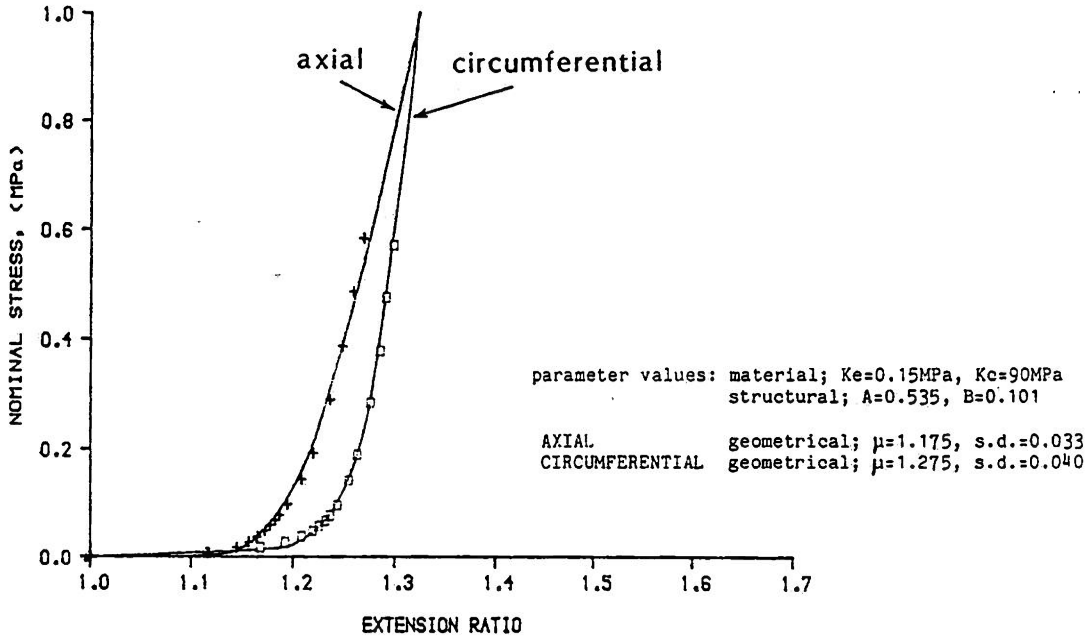

(B)

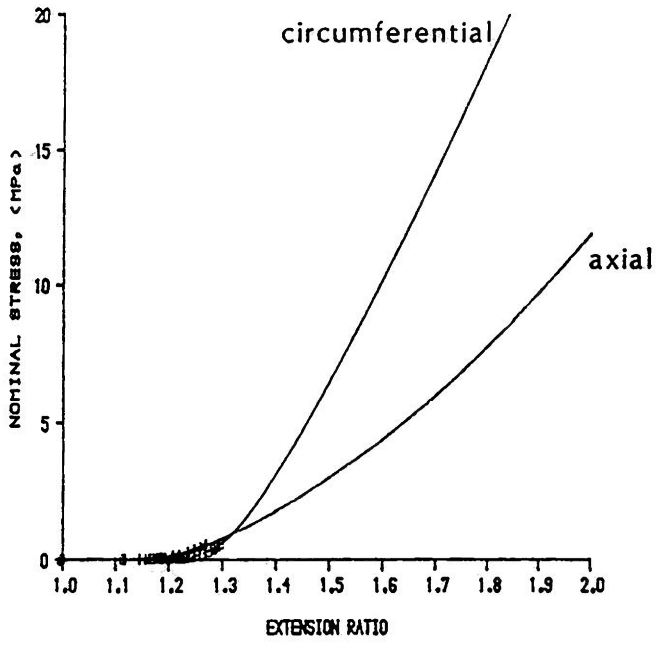

Figure 10.7 (A) best fit to the average behaviour at the low stress region of the test samples in chapter6 by the using relations (10.16),(10.17). (B) expansion of the formula to higher strains to describe the complete curve up to the failure point.

failure analysis data presented in chapter6 have been fitted by relations (10.16), (10.17). The structural and material parameters were used as experimentally produced by following the reasoning of previous sections. The geometrical parameters were chosen as to yield a good fit to the data. An empirical way to obtain a first approximation of the geometrical parameters (μ,s.d.) was to set μ to the extension ratio at which a line tangent to the linear portion of the curve would intercept of the stretch axis, and to set the incubation region of the stress/strain curve having approximately the length of two standard deviations(s.d.). The fitting procedure was based on trial and error because the constitutive equations included single and double integrals which could not be expressed in an analytic form in order to perform a suitable minimisation routine.

The fit in the low stress region(fig10.7a) appeared good for the circumferential curve, but underestimated the stresses at the peak stress(0.5-0.6MPa) points of the axial curve. The axial predicted curve did not rise steeply enough to fit all the data points within this range of stresses. The reason for this must have been either that a greater number of fibres have been excluded due to contraction in the model than in the real situation, or that some other yet unknown mechanism(i.e crosslinking) could account for the reinforcement of the axial strips in test.

The predicted curves crossed each other at a point near the origin and this was a consequence of the circumferential curve having a higher slope but stretching to greater extension ratios. The predicted curves then once again intersected at a stress of 1MPa and continued with different slopes into their linear regions(fig10.7b).

The predicted behaviour at higher stress levels can be compared to the experimental tensile failure traces of all the samples in

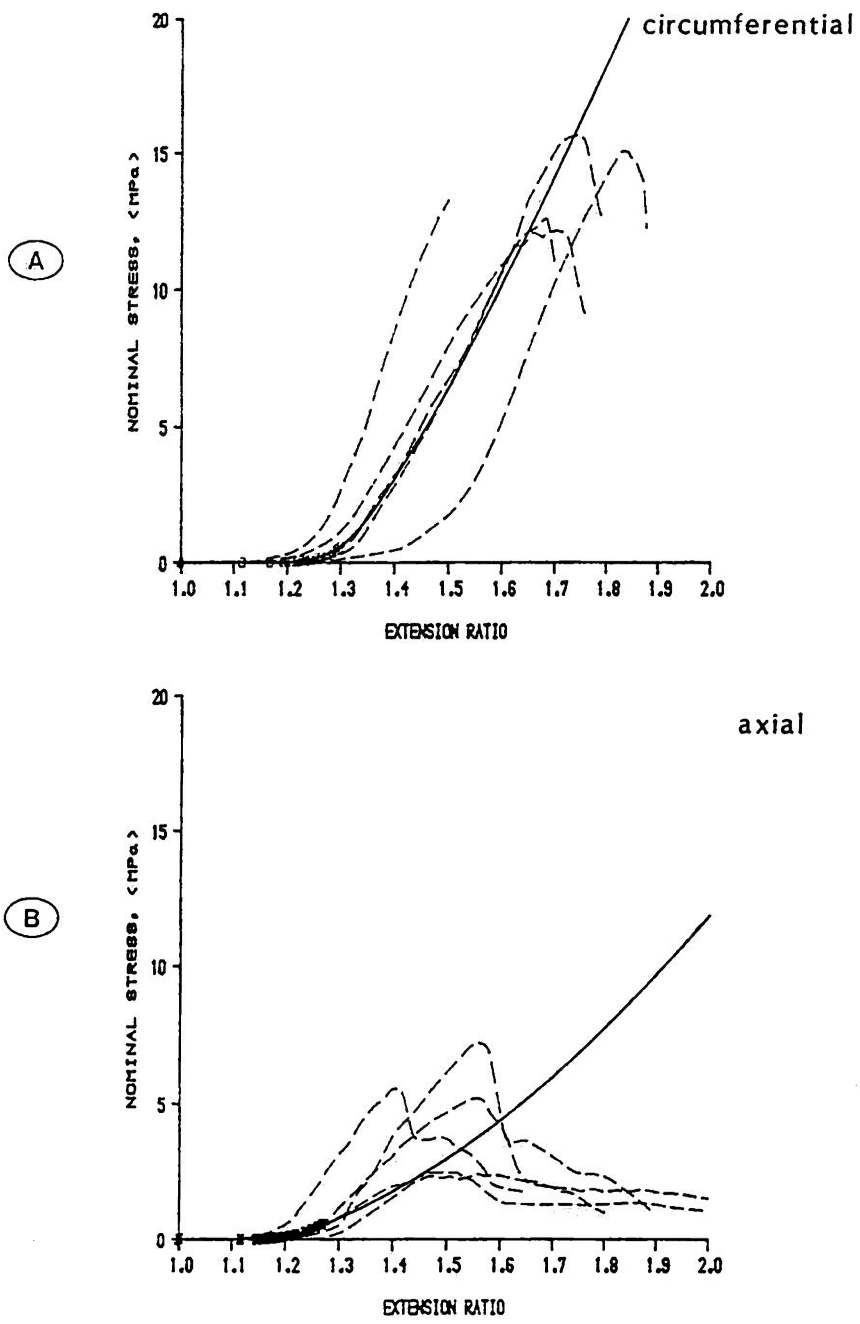

Figure 10.8:Comparison of the predicted behaviour (continuous lines) to the exhibited behaviour (dashed lines) in uniaxial tensile tests of chapter6. The fit of the formula in the low stress region(<0.8MPa) could adequately describe the complete tensile curve over the whole range of deformation.

figure10.8a,b. Those are the samples used in chapter6 and the curves were fitted to their average behaviour in the low stress region(<0.8MPa). It can be seen in fig10.8a,b that the model described the anisotropic behaviour of bovine pericardium strips sufficiently over the whole range of the deformation that the strips can undergo. The curves predicted by the model describe an ever increasing loading but they should in fact terminate at the failure point for each of the directions. A failure mechanisms has not been built into the model but it could probably be easily implemented if this is required. It could account for a number of fibres snapping for the ever increasing stretch after the linear region. A failure mechanism which could account for a region of yield would be similar to the progressive recruitment which produced the incubation region,

10.2.3.2 Biaxial stretch. In the introduction of the present chapter it was said that a constitutive equation should be able to describe different deformation modes. In chapter4 inflation of 7 bovine pericardial samples was described and the average results presented for mechanical behaviour of pericardium at test site-I. For this same test site-I we have now developed a model which adequately describes the uniaxial tests in the two normal directions. For the prediction of the uniform biaxial case equations 10.16,10.17 were used with all fibres being under stretch. The structural material and geometrical parameters were the same for both the uniaxial and the biaxial tests. The result is shown in figure10.9a,b. The predicted curves for uniform biaxial stretch were not significantly different from the average behaviour in inflation at any stress level and thus could not be rejected as describing the inflation data. In fig10.9 the inflation data has been given as the mean points with their standard error of the mean. This practice is followed when mean

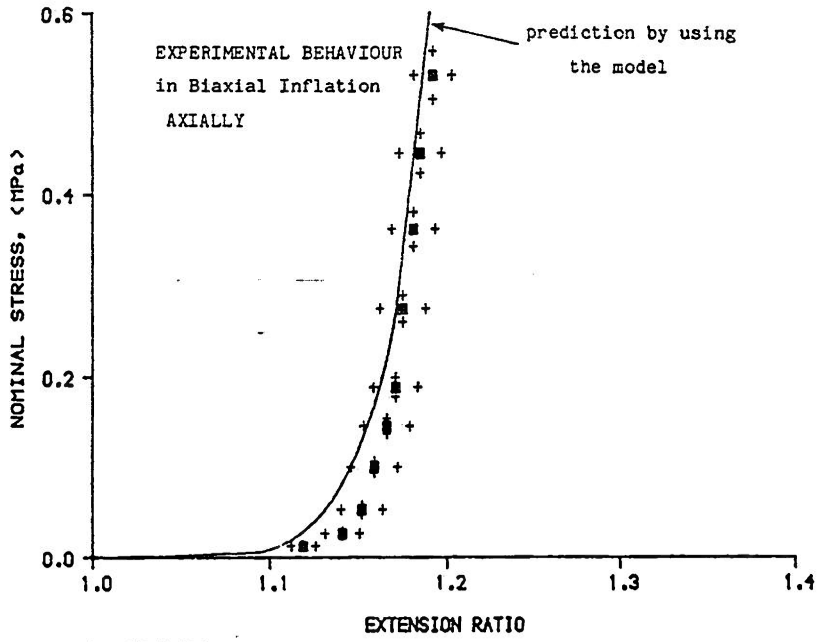

parameter values:

material; K_e=0.15MPa, K_c=90MPa
geometrical; μ=1.175, st.d.=0.033
structural; A=0.535, B=0.101

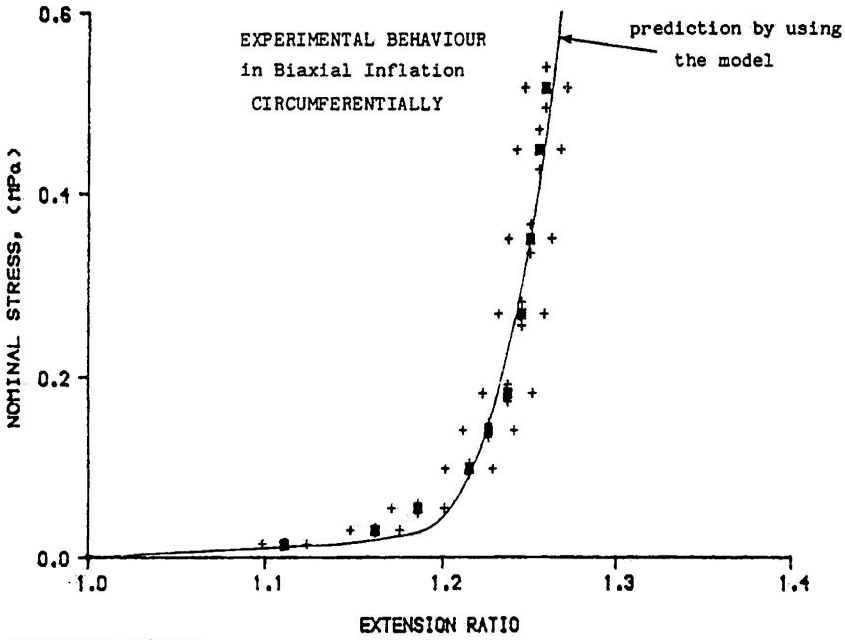

parameter values:

material; K_e=0.15MPa, K_c=90MPa
geometrical; μ=1.275, st.d=0.04
structural; A=0.535, B=0.101

Figure 10.9:Continuous lines are the predictions for the uniform biaxial stretch by using the set of parameters chosen to fit the uniaxial tensile curves. Dark squares are the average behaviour in the biaxial inflation tests presented in chapter4. Crosses indicate the standard error of the mean at each point.

behaviours of two different populations have to be compared. In the present case the single prediction curve should be compared with the envelope of the standard deviation of the seven inflated samples. Otherwise the prediction curve which resulted from description of the uniaxial tests for five different samples should be bound from either side by its own standard error of the mean limits. By using either of the statistical rules the difference between the prediction for uniform biaxial stretch and the experimental results in biaxial inflation tests was not significant.

Data from strip biaxial tests has not been collected in the present study. The model allows the prediction for the behaviour under this homogeneous constrained biaxial test. In equations 10.16,10.17 the lateral stretch ratio can be simply put to equal 1.0 over the whole deformation; the predictions are shown in fig10.10. The uniaxial and uniform biaxial predictions which have been experimentally confirmed are also presented. The curves comply with the general features of biaxial stretch of flat tissues. They rise exponentially and because of anisotropy in each deformation mode they were produced in pairs. Lanir and Fung(1974b) in stretching rabbit skin observed this duality of response in different directions and also that the greater the amount of lateral stretch the stiffer the curves were. This particular feature is easy to appreciate in fig10.10 from the uniaxial to the uniform biaxial stretch. The greater the lateral constraints, the stiffer and less extensible the curves are.

10.3 DISCUSSION.

In the present chapter a structural model is developed for the mechanical behaviour of native bovine pericardium based on the principle of load equilibrium and kinematics of its fibres which are

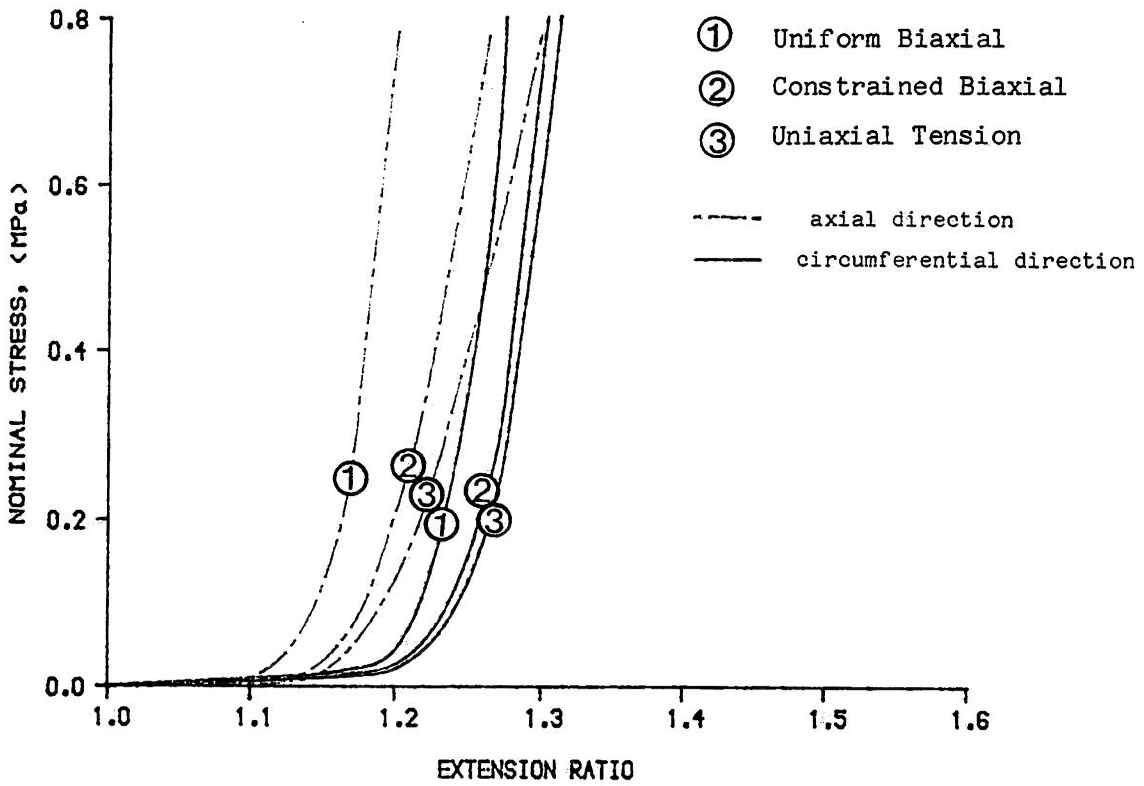

Figure 10.10:Predicted stress/strain behaviour under uniform biaxial stretch, constrained biaxial stretch and strip uniaxial stretch. Cases 1 and 3 have been confirmed by the experiments in chapters4 and 6 respectively.

embedded in the soft matrix.

A structural approach has a number of advantages. It facilitates the understanding of the tissue function and provides an insight into the deformation. All its mathematical functions are physical quantities and thus if there is an understanding of the way that individual elements work and interact by appropriate mechanical reasoning one can have an idea on the expected mechanical behaviour. Parameters and functions have their natural equivalents, but their meaning is not literal. Parameters and constants are refered as effective to indicates that they take the values by which they are experienced, while elements and structures are being idealised in behaving in a convenient manner.

For the implementation of the model the knowledge obtained in the failure analysis of the tissue in chapter6 was used. In essense it was shown that by using the characteristics and description of the failure region, the loading behaviour of the tissue can be described over the whole range of deformation. Features like the slope at the origin, the length of the incubation region, the extensibility at certain levels, the terminal modulus of the linear prefailure region can be adequately predicted and described. It can also explain some 'odd' findings of the uniaxial tests, like the continuous thinning of the axial strips when pulled to failure, while circumferential strips retained much of their original width.

The finding that Poisson's ratios as seen in tests were comparable to the predictions of Cox's(theory) was very important. If indeed Cox's theory can yield reasonable estimates of the two Poisson's ratios sought, then knowledge of the single structural parameter a1 could result in full description of the lateral contraction behaviour of the material which is required for

application of the model for the uniaxial case. Constant a1 may be produced by multidirectional uniaxial tests as in chapter6 or histological observations and can be used to produce the general behaviour between λ_1 and λ_2 in the absence of photographic observations of the lateral contraction. Furthermore a1 can estimate or be estimated by the structural parameters A,B which are responsible for producing the anisotropic stiffness along the two normal directions. Cox's theory may also be used to give a first estimate of the stiffness parameter Kc by adjusting constant K as to yield appropriate slope at the linear region. In this way a first approximation for the full implementation of the present model for all test modes can result.

The attempt to predict the behaviour of the biaxial test by using the parameters chosen to fit the uniaxial behaviour was successful. For uniaxial data the 1st pull curves of chapter6 have been used. It was thought that after load cycling the fibres would have retained some degree of alignment along the stretch direction as indicated by the elongation of the strips after the 1st cycle and thus the deformation could not be possibly described by the same set of initial parameters. In this respect the biaxial inflation test was also a 1st inflation test. Successful fit to different modes was performed despite the presence of biological variability. The uniaxial data of five samples has been fitted by the model and the model then has been used to predict the biaxial behaviour of seven different samples. The importance of this finding can be appreciated if it is compared with the findings of Tong and Fung(1974b). They employed a multiexponential empirical formula to describe the mechanical behaviour of skin and concluded that even when using a single specimen "no single set of parameters can fit all the tests".

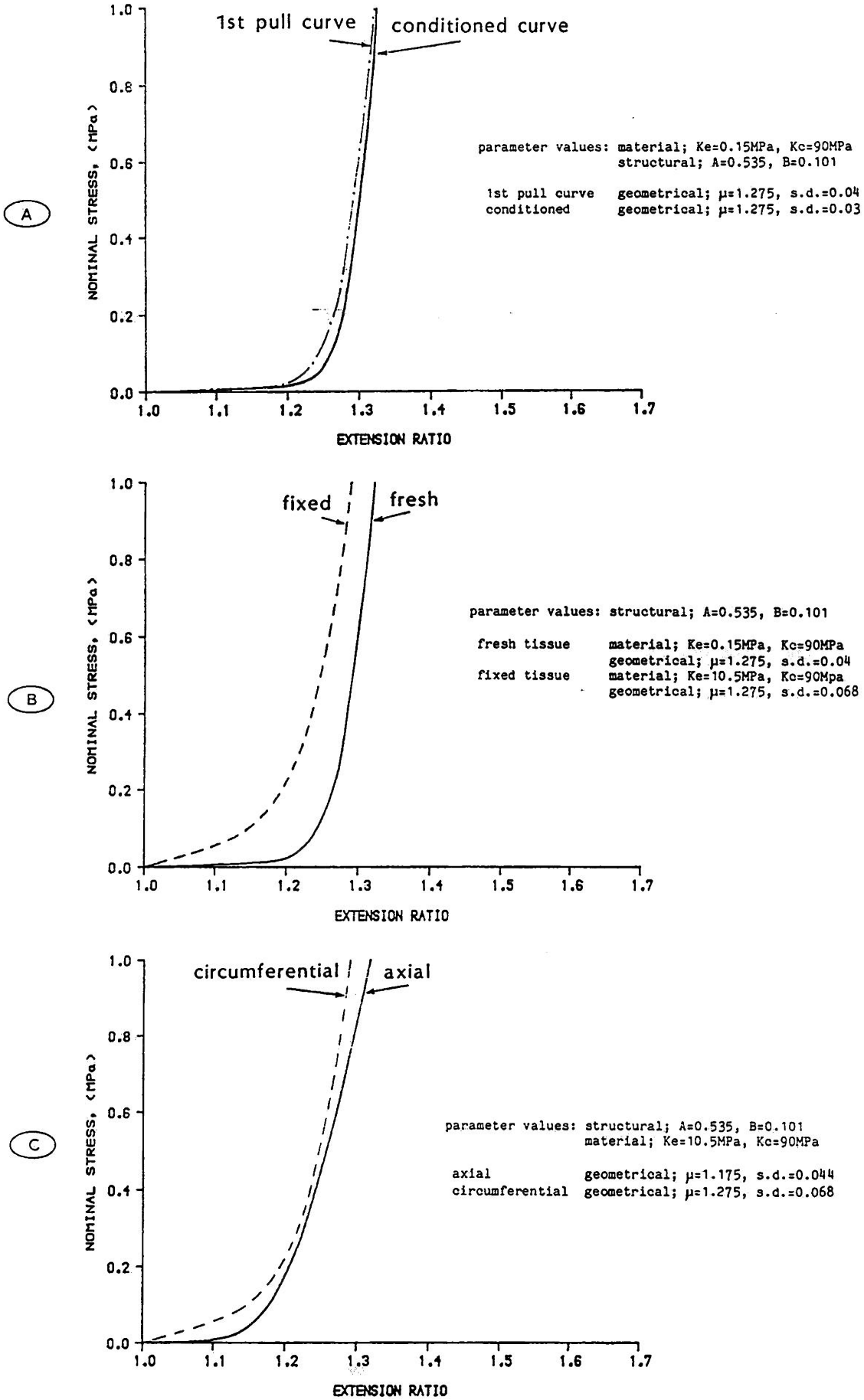

Figure 10.11:the flexibility of the model may allow description of different 'materials', like (A) the mechanically conditioned material and (B) (C) the glutaraldehyde fixed material.

The prediction of the uniform biaxial stretch reasonably described the inflation tests. This was not surprising as the test sites, where the stress/strain values were calculated in inflation, lay on the axes of elastic material symmetry and thus the tissue along these directions was under pure deformation in the absense of shear. The inflation curves were produced by a pair of stress/strain points travelling to higher stresses as the normal pressure was increased. Thus although at each particular time instant the two areas on the bubble were under unequal amount of stretch, each of the areas may have been under equibiaxial stretch. The fit to the biaxial data was poor in the low incubation region and we suspect that this was due to the incorporation and recruitment of linear collagen elements. If the behaviour of the individual collagen fibres had been modelled as non-linear this would have led to a smoother rise in the incubation region.

At the start of this discussion it was mentioned that a good knowledge of fibre interactions and mechanics may enable us to anticipate various other situations. An example is given in fig10.11. It may be possible to describe the conditioned behaviour by only altering the geometrical parameters. As a result of the initial cycles the fibres have settled at a slightly larger mean(μ) and slightly reduced st.deviation(s.d.).

The effect of fixation was to introduce an increased number of crosslinks which in general and indiscriminantly stiffen the material elements. This may be simulated by a tenfold increase in the effective elastin modulus according to the tenfold increase in the slope at the origin between the fresh and fixed tissue. Increased number of crosslinks was also translated in a recruitment of fibres starting at λ=1.0 due to an increased fibre-fibre interaction. Thus

the standard deviation was increased to such a value that the fibre mean(μ) was at 4 standard deviations from the origin. The similarity between the predicted behaviour for the fixed in fig10.11b and figures9.12,9.13 is striking.

The degree in which anisotropy is retained in the low stress region(<1MPa) can also be checked. In fig10.11c the tenfold increase in the initial slopes in both directions was sufficient to reverse the extensibility of the curves and render the circumferential curve less extensible than the axial. Suitable choice of parameters for curves in fig10.11c would have resulted in fig9.5 and fig9.6. This demonstrates the great advantage of the structural model over any empirical or phenomenological model.

CONCLUSIONS

The examination of the anatomy and shape of the tissue suggested that there are significant differences between the pericardia of different species and from site to site within single pericardial membranes. These arise from different functional needs and thus the results from the pericardium of one species can not by any means be generalised for the rest of the mammalian pericardia.

It was shown that inadequate testing methods and preparations together with lack of criticality of some workers have resulted in some important features of the mechanical behaviour of the pericardium (i.e.anisotropy) being overlooked.

The non-destructive biaxial inflation test developed as part of this study has a unique feature in demonstrating the anisotropy (asymmetry) of the mechanical properties on the plane of the tissue. This test could yield a qualitative important result in all cases but the quantification of the behaviour is more complicated and best limited to the two principal axes of elastic symmetry.

The uniaxial tensile tests confirmed that anisotropy of a greater or smaller magnitude existed in all 4 sites suitable for the construction of bioprosthetic valve leaflets making the production of 3 anisotropic leaflets for a valve from only one sac feasible. Related to this was the conclusion that study of the tissue properties should be done at each site and according to reference axes applying to the site, preferably the axes of elastic symmetry, and not according to a global set of reference axes applying to the whole membrane. This may be the reason for the descrepancy occuring between the results obtained here and the recommendations of other groups of workers. Trowbridge and associates suggested that there are significant variations of the properties within a sac but not from sac to sac. This may be so

because he compared the fibre reinforced direction of one site to the weak direction of another site. In the present study clearly the differences between sacs were significant but the differences between sites were not.

It was also found that the structure induced anisotropy which is reflected in angular variations of the strength and the stiffness, could be predicted by a structure based theory which has been developed earlier for man-made materials(Cox,1952).

The histological observations showed that the anisotropy is indeed structure-based, showing that differently oriented fibre layers are directed with small angles to the mechanically stronger and stiffer direction. The anisotropy in strength, stiffness and structure resembles that of the natural valve leaflets and makes bovine pericardial tissue an even better candidate for the manufacture of bioprosthetic valve leaflets.

Specific properties of the natural leaflets like the increased extensibility along the more compliant direction, which much improves the kinematic behaviour of the leaflet, may be incorporated in the future to a reasonable degree by suitably controlling the conditions at fixation. However the recognition of the anisotropy in structure and strength should on its own improve the durability of valve leaflets if appropriately exploited.

The prolonged durability of the pericardial leaflets and alterations in their mechanical properties have been demonstrated in in-vitro tests. Alterations in the mechanical properties and the geometrical dimensions of the leaflets due to the presence of the host environment (in-vivo) were also examined and it was shown that explanted leaflets were permanently extended and thicker, presenting stiffer and less extensible stress/stretch behaviour. The course of this in-vivo

modification was shown to be predictable and could be accounted for in all future valves from the design level.

The anisotropic model proposed which accounts for the non-linear and anisotropic elastic phase of the tissue loading response may also be of help in the future design of pericardial valves. The incorporation of the relevant features into a finite element method may lead to the production of a fully anisotropic and computer designed bioprosthetic pericardial valve.

BIBLIOGRAPHY

Adkins,J.E.,Rivlin,R.S.,(1952)
Large elastic deformations of isotropic materials IX.The deformation of thin shells,Phil.Trans.A,244,pp:505-531.

Alexander,H.,(1968)
A constitutive relation for rubber-like materials,Int.J.Engng. Scien.,Vol.6,pp:549-563.

Allen,D.J.,Didio,L.J.A.,Zacharias,A.,Fentie,I.,McGrath,A.J.,Puig,L.B., Pomerantzeff,P.N.A.,Zerbini,E.J.,(1984)
Microscopic study of normal parietal pericardium and unimplanted Puig-Zerbini pericardial valvular heterografts,J.Thorac.Cardiov. Surg.,Vol.87,(6),pp:845-855.

Ashdown,R.R.,Done,R.,(1984)
"The Ruminants",Vol.1,Bailliere Tindall-Gower Med. Publishing,1984.

Banchero,N.,Rutishauser,W.J.,Tsakiris,A.G.,Wood,E.H.,(1967)
Pericardial pressure during transverse acceleration in dogs without thoracotomy,Circ.Res.,20,pp:65-77.

Banks,P.,Bartley,W.,Birts,L.M.,(1976)
"The Biochemistry of the tissues",John Wiley&Sons,1976.

Barbenel,J.C.,(1979)
Time dependent mechanical properties of skin,Ph.D.thesis, University of Strathclyde,1979.

Barbenel,J.C.,Evans,J.H.,(1986)
Soft Connective Tissues:Mechanical properties, in:McAinsh(Ed), "Physics in Medicine Encyclopedia",Pergamon Press,Oxford,pp:780-783.

Barnard,H.L.,(1898)
The functions of the pericardium,Proceed.Physiolog.Soc.J.Physiolog., 22,pp:43-48.

Barratt-Boyes,B.G.,Lowe,J.B.,Cole,D.S.,Kelly,D.T.,(1965)
Homograft valve replacement for aortic valve disease,Thorax,1965, 20,pp:495-504.

Bartle,S.H.,Hermann,H.J.,Cavo,J.W.,et al,(1968)
Effect of the pericardium on left ventricular volume and function in acute hypervolemia,Cardiovasc.Res.,3,pp:284-289.

Bellhouse,B.J.,Talbot,L.,(1969)
The fluid mechanics of the aortic valve,J.Fluid Mech.,35,pp:721-735.

Benedict,R.,Wineman,A.L.,Yang,W.H.,(1979)
The determination of limiting pressure in simultaneous elongation and inflation of nonlinear elastic tubes,Int.J.Solids Struct., Vol.15,pp:241-249.

Berglund,E.,Sarnoff,S.J.,Isaacs,J.P.,(1955)

Ventricular function. Role of the pericardium in regulation of cardiovascular hemodynamics,Circ.Res.3,pp:133-139.

Bjork,V.O.,(1969)
A new tilting disc valve prosthesis,Scan.J.Thorac.Cardiovasc.Surg., Vol.3,pp:1-10.

Black,M.,Drury,P.J.,Tindale,W.B.,(1984)
A construction technique for minimising valve leaflet failure in pericardial valves,Life Support Systems,1984,2,Suppl.;pp:89-91

Black.M.M.,Daniel,C.L.,Lawford,P.V.,Stoves,J.L.,Trowbridge,E.A.,(1985)
The properties of natural tissues used for heart valve substitutes,in: Biocompatibility of tissue analogs,Vol.II,Ed:Williams,D.F.,CRC Press,1985.

Black,M.M.,Drury,P.J.,Tindale,W.B.,(1985)
The clinical performance of bioprosthetic heart valves,in:Bio compatibility of tissue analogs,Vol.II,Ed:Williams,D.F.,CRC Press, 1985..

Boncheck,L.I.,Tatooles,C.J.,Braunwuld,N.S.,(1967)
Experimental Cardiac Surgery in the Calf,Ann.Thorac.Surg., 3,pp:211-217.

Bowes,J.H.,Cater,C.W.,(1965a)
Cross-linking of collagen,J.Appl.Chem.,15,p.296.

Bowes,J.H.,Cater,C.W.,(1965b)
The reaction of glutaraldehyde with proteins and other biological materials,J.Royal Micr.Soc.,Vol.85,pt(2),pp:193-200.

Brais,M.P.,Bedard,J.P.,Goldstein,W.,Koshal,A.,Keon,W.J.,(1985)
Ionescu-Shiley pericardial xenograft:follow-up of up to six years, Ann.Thorac.Surg.,39,pp:105-111.

Brewer,R.J.,Deck,J.D.,Capati,B.,Nolan,S.P.,(1976)
The dynamic aortic root:its role in aortic valve function,J.Thorac. Cardiovasc.Surg.,Vol.72,(3),pp:413-417.

Brookhart,J.M.,Boyd,T.E.,(1947)
Local differences in intrathoracic pressure and their relation to cardiac filling pressure in the dog,Am.J.Physiol.,148,pp:434-444.

Broom,N.D.,(1977)
The stress/strain and fatigue behaviour of glutaraldehyde preserved heart-valve tissue,J.Biomech.,1977,Vol.10,pp:707-724.

Broom,N.D.,(1978a)
The observation of collagen and elastin structures in wet whole mounts of pulmonary and aortic leaflets,J.Thorac.Cardiovasc.Surg., Vol.75,No.1,1978,pp:121-130.

Broom,N.D.,(1978b)
Simultaneous morphological and stress/strain studies of the fibrous components in wet heart valve leaflet tissue,Conn.Tiss.Res.,1978, Vol.6,pp:37-50.

Broom,N.D.,(1978c)
Fatigue-induced damage in glutaraldehyde-preserved heart valve tissue, J.Thorac.Cardiovasc.Surg.,Vol.76,No.2,1978,pp:202-211.

Brown,N.,Duckett,R.A.,Ward,I.M.,(1968)
The yield behaviour of oriented polyethylene Terephthalate,Phil.Mag., 18,p:483,(1968)

Bylski,D.I.,Kriewall,T.J.,Akkas,N.,Melvin,J.W.,(1986)
Mechanical behaviour of fetal dura mater under large deformation biaxial tension,J.Biomech.,Vol.19,No.1,pp:19-26.

Carleton,H.M.,(1929)
The delayed effects of pericardial removal,Proc.Royal Soc.London, sB 105,pp:230-247.

Carpentier,A.,Deloche,A.,Relland,J.,Dubost,C.,(1976)
Valvular xenograft and valvular bioprosthesis:1965-1975 The Mitral Valve:a pluridisciplinary approach,(ed.D.Kalmanson),Edward Arnold, London,pp:505-518.

Cataloglu,A.,Gould,P.L.,Clark,R.E.,(1976)
Refined stress analysis of human aortic heart valves,J.Eng.Mech. Divis.,1976,pp:135-149.

Cataloglu,A.,Clark,R.E.,Gould,P.L.,(1977)
Stress analysis of aortic valve leaflets with smoothed geometrical data,J.Biomech.,Vol.10,pp:153-158.

Chater,E.,Neale,K.W.,(1983a)
Finite plastic deformation of a circular membrane under hydrostatic pressure-I,Rate-Independent behaviour,Int.J.Mech.Scien.,Vol.25,No.4, pp:219-233.

Chater,E.,Neale,K.W.,(1983b)
Finite plastic deformation of a circular membrane under hydrostatic pressure-II,Strain-Rate effects,Int.J.Mech.Scien.,Vol.25,No.4, pp:235-244.

Cheung,D.T.,Nimni,M.E.,(1982a)
Mechanism of crosslinking of proteins by glutaraldehyde I:Reaction with model compounds,Conn.Tiss.Res.,Vol.10,pp:187-199.

Cheung,D.T.,Nimni,M.E.,(1982b)
Mechanism of crosslinking of proteins by glutaraldehyde II:Reaction with monomeric and polymeric collagen,Conn.Tiss.Res.,Vol.10,pp:201-216.

Cheung,D.T.,Nimni,M.E.,(1982c)
Mechanism of crosslinking of proteins by glutaraldehyde III:Reaction with collagen in tissues,Conn.Tiss.Res.,Vol.13,pp:109-115.

Chew,P.H.,Zeger,S.L.,Yin,F.C.P.,(1986a)
Determination of Material Properties of Biological Tissues: Pericardium, in Schmid-Schonberg,G.W.;Woo,S.L-Y.;Zweifach,B.W.(Eds) "Frontiers of Biomechanics",Springler-Verlag Inc.,New York,1986, pp:86-97.

Chong,K.P.,Wieting,D.W.,Hwang,N.H.C.,Kennedy,J.H.,(1973)
Stress analysis of normal human aortic valve leaflets during diastole, BIOMAT.MED.DEVIC.ART.ORG.,1,(2),pp:307-321.

Chong,M.,Missirlis,Y.F.,(1978)
Aortic valve mechanics part-II:A stress analysis of the porcine aortic valve leaflets in diastole,BIOMAT.MED.DEV.ART.ORGANS,6,pp:225-244.

Christensen,R.,Waals,F.,(1972)
Effective stiffness of Randomly oriented fibre composites,J.Compos. Materials,6,p:518.

Christie,C.W.,(1982)
Analysis mechanics of Bioprosthetic heart valves,Ph.D.thesis University of Auckland,1982.

Christie,C.W.,Medland,I.C.,(1982)
A Non-linear Finite Element Stress Analysis of Bioprosthetic Heart Valves, in:Finite Elements in Biomechanics,(Ed):Gallagher,R.H.,Simon, B.R.,Johnson,P.C.,Gross,J.F.,JOHN WILEY & Sons Ltd,Chichester,1982, pp:153-179.

Clark,R.E.,(1973)
Stress-strain characteristics of fresh and frozen human aortic and mitral leaflets and chordae tendinae,J.Thorac.Cardiovasc.Surg.,Vol.66, No.2,Aug.1973,pp:202-208.

Clark,R.E.,Sutera,S.P.,(1973)
Methods of design of leaflet valvular prostheses:I.Stresses in the mitral valve leaflets in health and disease,J.Thorac.Cardiovasc.Surg., Vol.65,(6),pp:890-896.

Clark,R.E.,Finke,E.H.,(1974)
Scanning and light microscopy of human aortic leaflets in stressed and relaxed states,J.Thorac.Cardiovasc.Surg.,Vol.67,No.5,pp:792-803.

Clark,R.E.,Karara,H.M.,Cataloglu,A.,Gould,P.L.,(1975)
CLose-range stereophotogrammetry and coupled stress analysis as tools in the development of prosthetic devices,Trans.Am.Soc.Artif.Intern. Organs,21,pp:71-77.

Comninou,M.,Yannas,I.V.,(1976)
Dependence of stress-strain non-linearity of connective tissues on the geometry of collagen fibres,J.Biomech.,Vol.9,pp:427-433.

Cook,T.H.,(1975)
The mechanical characterisation of human skin in vivo,Ph.D.thesis, Stevens Institute of Technology,New Jersey,1975.

Cossgrove,D.M.,Lyttle,B.N.,Gill,C.C.,Golding,L.A.R.,Stewart,R.W.,Loop,F.D., Williams,G.W.,(1985)
In-vivo haemodynamic comparison of porcine and pericardial valves, J.Thorac.Cardiovasc.Surg.,Vol.89,pp:358-368.

Cox,H.L.,(1952)
The elasticity and strength of paper and other fibrous materials, Br.J.Appl.Physics,Vol.3,pp:72-79.

Craik,J.E.,McNeil,I.R.R.,(1966)
Microarchitecture of skin and its behaviour under stress,Nature 209, pp:931-932.

Craik,J.E.,McNeil,I.R.R.,(1965)
Histological studies of stressed skin,in "Biomechanics and Related Bio-engineering Topics",ed:Kenedi,R.M.Pergamon press,Oxford,1965.

Cunningham,D.J.,(1972)
"Textbook of anatomy",New York,MacMillan,London,1972.

Danielsen,C.C.,(1981)
Mechanical properties of reconstituted collagen fibrils,Conn.Tiss. Res.,Vol.9,pp:51-57.

Decraemer,W.,Maes,M.A.,Vanhuyse,V.J.,VanPeperstraete,P.,(1980)
An elastic stress-strain relation for soft biological tissues based on a structural model,J.Biomech.,Vol.13,pp:559-564.

Dehoff,P.H.,(1978)
On the nonlinear viscoelastic behaviour of soft biological tissues, J.Biomech.,Vol.11,pp:35-40.

Deichman,W.B.,Gerarde,H.W.,(1969)
"Toxicology of drugs and Chemicals" Academic Press,New York.

DeLahunta,A.,(1986)
"Applied Veterinary Anatomy",2nd Ed.,Philadelphia,1986.

Dewanjee,M.K.,Singh,S.K.,Wooley,P.H.,Mackey,S.T.,Solis,E.,and Kaye,M.P.,(1986)
Identification of NewCollagen Formation with 125I-labeled Antibody in bovine Pericardial Tissues valves Implanted in Calves,Nucl.Med. Biol.,Int.J.Radiat.Appl.Instr.,partB,Vol.13,No.4,pp:413-422.

Diamant,J.,Keller,A.,Baer,E.,Litt,M.,Arridge,R.G.C.,(1972)
Collagen;ultrastructure and its relation to mechanical properties as a function of ageing,Proc.R.Soc.Lond.B,180,pp:293-315.

Dickey,R.W.,(1974)
On the transformation of the Foeppl membrane equations to ordinary Differential equations,J.Math.Analysis and Appl.,47,pp:169-177.

Dong,R.G.,(1974)
Tensile Failure of viscoelastic Materials under multiaxial loading at various temperatures,Trans.Soc.Rheol.,18,(1),pp:45-63.

Dunn,M.G.,Silver,F.H.,(1983)
Viscoelastic Behaviour of human connective tissues:Relative contribution of viscous and elastic components,Conn.Tiss.Res., Vol.12,pp:59-70.

Elias,H.,Boyd,L.,(1973)
Notes on the anatomy,embryology and histology of the pericardium, J.N.Y.MED.COLL.,Vol.2,pp:50-75.

Evans,J.H.,(1973)
Structure and Function,Ph.D.thesis,Univ.of Strathclyde,1973.

Eyre,D.R.,(1980)
Collagen:Molecular Diversity in the Body's Protein Scaffold, Science,Vol.207,pp:1315-1322.

Feng,W.W.,Huang,P.,(1974)
On the inflation of a plane non-linear membrane,J.Appl.Mech.,Trans. ASME,pp:767-771.

Feng,W.W.,Tielking,J.T.,Huang,P.,(1974)
The inflation and contact constraint of a rectangular Mooney membrane,J.Appl.Mech.,Trans.ASME,pp:979-984.

Feng,W.W.,(1976)
Inflation of a viscoelastic ellipsoidal neo-Hookean membrane, AIAA J.,Vol.14,No.5,pp:672-675.

Fentie,L.H.,Allen,D.J.,Schenck,M.H.,Didio,L.J.A.,(1986)
Comparative electron microscopic study of bovine,porcine and human parietal pericardium, as materials for cardiac valve bioprostheses, J.Submicrosc.Cytol.,18,(1),pp:53-65.

Fenton,T.R.,Vas,R.,(1977)
A kinetic analysis of heart motion,J.Biomech.,Vol.10,pp:789-797.

Fenton,T.R.,Cherry,J.M.,Klassen,G.A.,(1978)
Transmural myocardial deformation in the canine left ventricular wall,Am.J.Physiolog.,Vol.235,(5),H:523-530.

Filonenko-Borodich,M.,(1965)
"Theory of elasticity",translated by M.Konayeva,DOVER Publ.,New York.

Fincham,W.H.A.,Freeman,M.H.,(1980)
"Optics",9th Ed.,Butterworths,p:74,1980.

Finlay,J.B.,(1969)
Scanning electron microscopy of the human dermis under uniaxial strain,Bio-med.Engng,4,pp:322-327.

Finlay,J.B.,(1970)
Biodynamic studies of human skin,Torsional characteristics in relation to structure,Ph.D.thesis,Univ.of Strathclyde,1970.

Fisher,J.,(1986a)
Design Development and Evaluation of a Improved Pericardial Bioprosthetic Heart valve,Ph.D.,University of Glasgow,1986.

Fisher,J.,Reece,I.J.,Jack,G.R.,Cathcart,L.,Wheatley,D.J.,(1986b)
Laboratory assessment of the design, function and durability of pericardial bioprostheses,in:Heart Valve Engineering, Mech.Eng.Publ. Ltd,for I.M.E.,1986.

Fisher,J.,Wheatley,D.J.,(1987a)
An improved pericardial bioprosthetic heart valve. Design and laboratory evaluation,Eur.J.Cardio-thorac.Surg.,1987,1,pp:71-79.

Fisher,J.,Gorham,S.D.,Howie,A.M.,Wheatley.D.J.,(1987b)
Examination of fixative penetration in glutaraldehyde-treated bovine

pericardium by stratigraphic analysis of schrinkage temperature measurements using differential scanning calorimetry,Life Support syst.,5,pp:189-193.

Fisher,J.,Wheatley,D.J.,Douglas,I.,Spyt,T.J.,Reece,I.J.,(1987c)
Failure modes in pericardial and porcine Bioprostheses,in:"Calcification and Degeneration of Heart Valve Bioprostheses".Proceedings 1st Scient. Meeting of Int.Assoc. for Cardiac Biological Implants,(Eds):Gabbay,S., Cabrol,C.,Publ.Dr.A.AMEUR,Commun.Medicale.

Flint,M.H.,(1976)
The basis of the histological demonstration of tension in collagen, ed:LONGACRE,J.,Ch.4,Springfield,Illinois:Charles Thomas.

Flint,M.H.,Lyons,M.F.,Meaney,M.F.,Williams,D.E.,(1975a)
The Masson staining of collagen-an explanation of an apparent paradox, Histoch.J.,Vol.7,pp:529-546.

Flint,M.H.,Lyons,M.F.,(1975b)
The effect of heating and denaturation on the staining of collagen by the Masson trichrome procedure,Histochem.J.,Vol.7,pp:547-555.

Flint,M.H.,Merrilees,M.J.,(1977)
Relationship between the axial periodicity and staining of collagen by the Masson trichrome procedure,Histochem.J.,Vol.9,pp:1-13.

Flugge,W.,(1960)
"Stresses in Shells",Springler-Verlag Berlin,1960.

Foster,H.O.,(1967)
Very large deformations of axially symmetrical membranes made of neo-Hookean materials,Int.J.Engng.Scien.,Vol.5,pp:95-117.

Franklin,H.G.,(1968)
Classic theories of failure of anisotropic Materials,Fibre Science and Techn.,Vol.1,No.2,pp:137-150.

Frasca,P.,Buchanan,J.W.,Soriano,R.Z.,Dunn,J.M.,Marmon,L.,Melbin,J.,Buchanan, S.J.,Golub,E.E.,Shapiro,I.M.,(1985)
Moprhological observations of mineralizing pericardium cardiac grafts,Scan.Electron Microsc.,pt(3),pp:1253-1258.

Fung,Y.C.B.,(1967)
Elasticity of Soft Tissues in simple elongation,Am.J.Physiol., Vol.213,No.6,pp:1532-1544.

Fung,Y.C.B.,(1973)
Biorheology of soft tissues,Biorheology,1973,Vol.10,pp:139-155.

Fung,Y.C.,(1981)
"Biomechanics",Springer Verlag,New York-Heidelberg-Berlin.

Gabbay,S.,Bortolotti,U.,Cipolletti,G.,Wasserman,F.,Frater,R.W.M.,(1984a)
The Meadox Unicusp Pericardial bioprosthetic heart valve,Ann.Thorac. Surg.,1984,37,pp:448-456.

Gabbay,S.,Bortolotti,U.,Wasserman,F.,Tindel,N.,(1984b)

Long-term follow-up of the Ionescu-Shiley Mitral pericardial xenograft,J.Thorac.Cardiovasc.Surg.,Vol.88,pp:758-763.

Gabbay,S.,Bortolotti,U.,Wasserman,F.,Factor,S.,Strom,J.,Frater,R.W.M., Bronx,N.Y.,(1984c)
Fatigue-induced failure of the Ionescu-Shiley pericardial xenograft in the mitral position,J.Thorac.Cardiovasc.Surg.,1984,Vol.87,pp:836-844.

Gavilanes,J.G.,DeBuitrago,G.G.,Lizarbe,M.A.,Municio,A.M.,Olmo,N.,(1984)
Stabilisation of pericardial tissue by glutaraldehyde,Conn.Tiss. Res.,Vol.13,pp::37-44.

Ghista,D.N.,Rao,A.P.,(1973)
Mitral-valve mechanics-stress/strain characteristics of excised leaflets, analysis of its functional mechanics and its medical application,Med.Biolog.Engin.,Nov.1973,pp:691-702.

Ghista,D.N.,(1976)
Toward an optimum prosthetic trileaflet aortic-valve design,Med. Biol.Eng.,pp:122-128.

Ghoshal,N.G.,(1975)
Ch.33,in:Sisson and Grossman's"The anatomy of the domestic animals" Vol.1,Robert Kelly,D.V.M.,Ph.D.,5th ed.,W.B.Saunders Co,1975.

Gilbert,S.G.,(1983)
"Pictorial Anatomy of the fetal Pig",Univ. of Washington Press Seattle,1983.

Glantz,S.A.,Misbach,G.A.,Moores,W.Y.,Mathey,D.G.,Lekven,J.,Stowe,D.F.,Parmley, W.W.,Tyberg,J.V.,(1978)
The pericardium substantially affects the left vebtricular diastolic pressure-volume relationships in the dog,Circ.Res.,42,pp:433-441.

Gleason,M.N.,Gosselin,R.E.,Hodge,H.C.,Smith,R.P.,(1969)
Clinical Toxicology of Commercial products,Williams and Wilkins Co., Baltimore,1969.

Goldberg,B.,Rabinovitch,M.,(1983)
Connective tissue, in "Histology,Cell and Tissue Biology", 5th edt.,Ed. by Weiss,L. The MacMillan Press.

Grahame,R.,(1968)
Elasticity of human skin in-vivo,Ann.Phys.Med.,Vol.10,3,pp:549-559.

Green,A.E.,Zerna,W.,(1968)
"Theoretical elasticity",2nd Ed.,Clarendon Press,Oxford,1968.

Green,A.E.,Adkins,J.E.,(1970)
"Large elastic deformations",2nd. Ed.,Clarendon Press,Oxford,1970.

Hamid,M.S.,Sabbah,H.N.,Stein,P.D.,(1986)
Influence of stent height upon stresses on the cusps of closed bio-prosthetic valves,J.Biomech.,Vol.19,No.9,pp:759-769.

Harris,B.,(1980)
The mechanical behaviour of composite materials,in:"The mechanical

properties of Biol.Materials",Cambridge Univ.Press,1980.

Hart-Smith,L.J.,Crisp,J.D.C.,(1967)
Large elastic deformations of thin rubber membranes,Int.J.Engng. Scien.,Vol.5,pp:1-24.

Hayashi,K.,(1982)
Fundamental and applied studies of mechanical properties of cardiovascular tissues,Biorheology,19,pp:425-436.

Hearmon,R.F.S.,(1961)
"An introduction to Applied Anisotropic Elasticity",Oxford Univ. Press,1961.

Hefner,L.L.,Coghlan,C.H.,Jones,W.B.,Reeves,T.J.,(1961)
Distensibility of the dog left ventricle,Am.J.Physiolog.,201,H:97-101.

Hess,O.M.,Bhargava,V.,Ross,J.,Shabetai,R.,(1983)
The role of the pericardium in interactions between the cardiac chambers,Am.Heart J.,106,p:1377.

Hilbert,St.L.,Ferrans,V.J.,Swanson,W.M.,(1986)
Optical methods for the non-destructive evaluation of collagen morphology in bioprosthetic heart valves,J.Biomed.Mat.Res.,Vol.20, pp:1411-1421.

Hildebrandt,J.,Fukaya,H.,Martin,C.J.,(1969a)
Completing the length-tension curve of tissue,J.Biomech.,Vol.2, pp:463-467.

Hildebrandt,J.,Fukaya,H.,Martin,C.J.,(1969b)
Simple Uniaxial and Uniform Biaxial deformation of nearly isotropic incompressible tissues,Biophysical J.,Vol.9,pp:781-791.

Hill,R.,(1948)
A theory of the yielding and plastic flow of anisotropic metals,Proc. Royal Soc.,193,pp:281-297.

Hoffman,O.,(1967)
The brittle strength of orthotropic Materials,J.Compos.Mat.,1,Apr.1967.

Holt,J.P.,Rhode,E.A.,Kines,H.,(1960)
Pericardial and ventricular pressure,Circ.Res.,8,pp:1171-1181.

Holt,J.P.,(1970)
The Normal Pericardium,Am.J.Cardiol.,Vol.26,Non.1970,pp:455-465.

Hooft,J.P.,
"De Ingenieur",91,p.289,translated by Huiskes,R.,Biomechanics of bone-Implant Interacions, in:"Frontiers in Biomechanics",Springler-Verlag Inc.,New York,1986,p.248.

Hooley,C.J.,McCrum,N.G.,Cohen,R.E.,(1980)
The viscoelastic deformation of tendon,J.Biomech.,Vol.13,pp:521-528.

Hort,W.,Braun,H.,(1962)
Untersuchungen uber Grosse,Wandstarke und mikroskopischen Aufbau des

Herzbeutels unter normalen und pathologischen Bedingungen,Arch. Kreislauffosch,38,pp:1-22.

Hufnagel,C.A.,(1979)
Basic concepts in the development of cardiovascular prostheses, Am.J.Surg.,1979,137,pp:285-300.

Hukins,D.W.L.,(1984)
Ch.8:Collagen Orientation,in "Connective Tissue Matrix" London MacMillan,1984.

Humphrey,J.D.,Vawter,D.L.,Vito,R.P.,(1987)
Quantification of strains in biaxially tested soft tissues,J.Biomech., Vol.20,No.1,pp:59-65.

Ingels,N.B.,Daughters,G.T.,Davies,S.R.,MacDonald,I.B.,(1971)
Stereo-photogrammetric studies on the dynamic geometry of the canine left ventricular epicardium,J.Biomech.,Vol.4,pp:541-550.

Ionescu,M.I.,Pabraski,B.C.,Holden,M.P.,Mary,D.A.S.,Wooler,G.H.,(1972)
Results of aortic valve replacement with frame supported fascia lata and pericardial grafts,J.Thorac.Cardiovasc.Surg.,1972,Vol.64,pp:340-355.

Ionescu,M.I.,Tandon,A.P.,Mary,D.A.S.,Abid,A.,(1977)
Heart valve replacement with the Ionescu-Shiley pericardial xenograft, J.Thorac.Cardiovasc.Surg.,1977,Vol.73,pp:31-42.

Ionescu,M.I.,Tandon,A.P.,(1979)
The Ionescu-Shiley Pericardial Xenograft Heart Valve,in "Tissue Heart Valves"Butterworths publ.Ltd,1979,London-Boston.

Ionescu,M.I.,Tandon,A.P.,Silverton,N.P.,(1986)
Long-term durability of the pericardial valve,in Yacoub,M.,Bodnar,E., (Eds)"Biological and Bioprosthetic Valves"Yorke Medical Books, New York,pp:165-175.

Ishihara,T.,Ferrans,V.J.,Jonès,M.,Boyce,S.W.,Kawanami,O.,Roberts,W.C.,(1980)
Histologic and Ultrastructural Features of Normal Human Parietal Pericardium,Am.J.Cardiol.,Vol.46,pp:744-753.

Ishihara,T.,Ferrans,V.J.,Jones,M.,Boyce,S.W.,Roberts,W.C.,(1981)
Structure of Bovine parietal pericardium and of unimplanted Ionescu-Shiley pericardial valvular bioprostheses,J.Thorac.Cardiov.Surg., Vol.81,pp:747-757.

Janicki,J.S.,Weber,K.T.,(1980)
The pericardium and ventricular interaction, distensibility and function,Am.J.Physiolog.,238,H:494-503.

Janicki,J.S.,Weber,K.T.,Gochman,R.F.,Schroff,S.,Geheb,F.J.,(1981)
Three-dimensional myocardial and ventricular shape:a surface representation,Am.J.Physiolog.,241,H:1-11.

Jenkins,A.,White,H.E.,(1976)
"Fundamentals of Optics",4th Ed.,McGrawHill book Co.,1976.

Jones,E.L.,(1975)

Haemodynamic and clinical evaluation of the Hancock xenograft bioprosthesis for aortic valve replacement,J.Thorac.Cardiovasc.Surg., 1975,Vol.75,pp:300-308.

Jones,R.,(1974)
A simplified approach to the large deflection of membranes,Int.J. Non-Linear Mech.,Vol.9,pp:141-145.

Joye,D.D.,Poehlein,G.W.,(1972)
A bubble inflation technique for the measurement of viscoelastic properties in equal biaxial extensional flow,Trans.Soc.Rheol.,16, (3),pp:421-445.

Joye,D.D.,Poehlein,G.W.,(1973)
A bubble inflation technique for the measurement of viscoelastic properties in equal biaxial extensional flow II,Trans.Soc.Rheol., 17,(2),pp:287-302.

Kastelic,J.,Galeski,A.,Baer,E.,(1978)
The multicomposite structure of tendon,Conn.Tiss.Res,Vol.6, pp:11-23.

Katz,J.L.,(1976)
"Advances in Bioengineering",Eds.Mates,R.E.,Smith,C.R.,ASME,New York,p.18.

Keller,A.,Rider,J.G.,(1966)
On the tensile behaviour of oriented polyethylene,J.Mater.Sci.,1, pp:389-398,1966.

Kenedi,R.M.,Gibson,T.,Evans,J.H.,Barbenel,J.C.,(1975)
Tissue Mechanics, Physic.Med.Biol.,20,pp:699-717.

Kingsley,J.S.,(1926)
"Outlines of Comparative Anatomy of Vertebrates",3rd Ed.,Philadelphia, P.Blakiston's Son&Co.,1926,pp:18-20,304-307.

Kobayashi,A.S.,(1987)
"Handbook on Experimental Mechanics",Society for Exp.Mechanics Inc., Prentice Hall,Inc.,New Jersey(1987).

Kraus,H.,(1967)
"Thin elastic shells",John Wiley&Sons,Inc.,New York-London-Sydney.

Kricheyskaya,I.P.,(1962)
The effect of reflexes from receptors in the pericardium on blood filling in the spleen,Bull.Exp.Biolog.Medic.,52,pp:1119-1961.

Kriewall,T.J.,Akkas,N.,Bylski,D.I.,Melvin,J.W.,Work,B.A.Jr.,(1983)
Mechanical behaviour of fetal dura mater under large Axisymmetric Inflation,J.Biomechanical Eng.,Vol.105,pp:71-76.

Kuno,Y.,(1916)
The significance of the pericardium,J.Physiol.,50,pp:1-36.

Lanir,Y.,Fung,Y.C.,(1974a)
Two-Dimensional Mechanical Properties of Rabbit Skin-I. Experimental

System,J.Biomech.,Vol.7,pp:29-34.

Lanir,Y.,Fung,Y.C.,(1974b)
Two-Dimensional Mechanical Properties of Rabbit Skin-II. Experimental Results,J.Biomech.,Vol.7,pp:171-182.

Lanir,Y.,(1979)
A structural theory for the homogeneous Biaxial stress-strain relationships in flat collagenous tisues,J.Biomech.,Vol.12,pp:423-436.

Lanir,Y.,(1983)
Constitutive equations for fibrous connective tissues,J.Biomech., Vol.16,No.1,pp:1-12.

Lanir,Y.,Walsh,J.,Soutas-Little,R.W.,(1984)
Histological Staining as a Measure of stress in collagen fibres, Trans.ASME,Vol.106,pp:174-176.

Lawford,P.V.,Black,M.M.,Drury,P.J.,Bilton,G.,(1986)
The in vivo durability of bioprosthetic heart valves-modes of failure observed in explanted valves,in:"Heart Valve Engineering",Mech.Eng. Publ.,Ltd.,for I.M.E.,London,1986,pp:65-74.

Lee,J.M.,Boughner,D.R.,(1981)
Tissue mechanics of canine Pericardium in different Test Environments, Circ.Res.,49,pp:533-544.

Lee,J.M.,Courtman,D.W.,Boughner,D.R.,(1984a)
The glutaraldehyde-stabilised porcine aortic valve xenograft I:Tensile Viscoelastic properties of the fresh leaflet material,J.Biomed.Mat. Res.,Vol.18,pp:61-77.

Lee,J.M.,Boughner,D.R.,Courtman,D.W.,(1984b)
The glutaraldehyde-stabilised porcine aortic valve xenograft II:Effect of fixation with or without pressure on the tensile viscoelastic properties of the leaflet material,J.Biomed.Mat.Res.,Vol.18,pp:79-98.

Lee,J.M.,Boughner,D.R.,(1985)
Mechanical properties of Human Pericardium. Differences in Viscoelastic Response when compared with Canine pericardium,Circ.Res.,Vol.57,No.3, pp:475-481.

Lee,M.C.,LeWinter,M.M.,Freeman,G.R.,Shabetai,R.,Fung,Y.C.,(1985)
Biaxial mechanical properties of the pericardium in normal and volume overload dogs,Am.J.Physiolog.,249,:H222-230.

Lim,K.O.,Boughner,O.R.,(1975)
Mechanical properties of human mitral valve chordae tendinae:Variation with size and strain rate,Can.J.Physiol.Pharmacol.,53,pp:330-339.

MacIver,A.G.,Howarth,W.S.,(1985)
The fate of prosthetic leaflet heart valves implanted in animals, in:Williams,D.(ed)"Biocompatibility of Implant Materials",London: Sector Publishing,(1985),pp:211-215.

Markenschoff,X.,Yannas,I.V.,(1979)
On the stress-strain relation for skin,J.Biomech.,Vol.12,pp:127-129.

Maurer,F.W.,Warren,M.F.,Drinker,C.K.,(1940)
The composition of mammalian pericardial and peritoneal fluids. Studies of their protein and chloride contents,and the passage of foreign substances from the blood stream into these fluids, Am.J.Physiolog.,129,pp:635-644.

Meadows,D.M.,Johnson,W.O.,Allen,J.B.,(1970)
Generation of surface contours by Moire patterns,Appl.Optics,Vol.9, No.4,pp:942-947.

Melvin,J.W.,McElhaney,J.H.,Roberts,V.L.,(1970)
Development of a mechanical model of the human head-Determination of tissue properties and synthetic substitute materials,Proceeding of the 14 Stapp Car Crash Conf.,Society of Automotive Engineers,Inc., New York,1970.

Mercer,J.L.,Benedicty,M.,Bahnson,H.T.,(1973a)
The geometry and construction of the aortic leaflet,J.Thorac. Cardiovasc.Surg.,Vol.65,pp:511-518.

Mercer,J.L.,(1973b)
The functional characteristics and behaviour of the normal aortic valve, and their relevance to the design of trileaflet prostheses, MSc thesis,St.Thoma's Hospital Med.School,(1973).

Mercer,J.L.,(1973c)
The movements of the dog's aortic valve studied by high-speed cine-angiography,Brit.J.Radiol.,46,pp:344-349.

Minns,R.J.,Soden,P.D.,Jackson,D.S.,(1973)
The role of the fibrous components and ground substance in the mechanical properties of biological tissues:A preliminary investigation,J.Biomech.,Vol.6,pp:153-165.

Miller,C.E.,Lavery,J.P.,Donnelly,T.A.,(1979)
Determination of elastic parameters for human fetal membranes, J.Rheol.,Vol.23,pp:57-78.

Mirsky,I.,(1970)
Effects of anisotropy and nonhomogeneity on left ventricular stresses in the intact heart,Bull.Math.Biophysics,Vol.32,pp:197-213.

Missirlis,Y.F.,(1973)
In-vitro studies of human aortic valve mechanics,Ph.D.Thesis,Rice University,Houston,Texas.

Missirlis,Y.F.,Armeniades,C.D.,(1976)
Stress analysis of the aortic valve during diastole:important parameters,J.Biomech.,1976,Vol.9,pp:477-480.

Missirlis,Y.F.,Chong,M.,(1978)
Aortic valve mechanics-part I:Material properties of natural porcine aortic valves,J.Bioeng.,2,pp:287-300.

Mohan,D.,Melvin,J.W.,(1982)
Failure properties of passive human aortic tissue I-uniaxial tension tests,J.Biomech.,Vol.15,pp:887-902.

Mohan,D.,Melvin,J.W.,(1983)
Failure properties of passive human aortic tissue II-Biaxial tension tests,J.Biomech.,Vol.19,No.1,pp:27-37.

Mohri,H.,Reichenbach,D.D.,Meredino,K.A.,(1972)
Biology of homologous and heterologous aortic valves, in "Biological Tissue in Heart Valve Replacement"Ed.Ionescu,M.I.,Ross,D.N.,Wooler,G.H., pp:137-142,Butterworths,London.

Morgan,B.C.,Guntheroth,W.C.,Dillard,D.H.,(1965)
Relationship of pericardial to pleural pressure during quiet respiration and cardiac tamponade,Circ.Res.,16,pp:493-498.

Nachemson,A.C.,Evans,J.H.,(1967)
Some mechanical properties of the third lumbar interlaminar ligament, J.Biomech.,Vol.1,pp:211-220.

Neal,H.V.,Rand,H.W.,(1936)
"Comparative Anatomy",The Blakiston Co.,1936.

Ogden,R.W.,(1972)
Large deformation isotropic elasticity-on the correlation of theory and experiment for incompressible rubber-like solids,Proc.R.Soc.,A, 326,p:565.

Orberg,J.,Baer,E.,Hiltner,A.,(1983)
Organisation of collagen fibres in the intestine,Conn.Tiss.Res., Vol.11,pp:285-297.

Pahl,G.,Beitz,W.,(1984)
"Engineering Design",Ed:Wallace,K.,London Design Council,1984.

Paraux,C.,(1982)
"A color Atlas of Bovine Visceral Anatomy",Wolfe Med.Publ.Ltd.,1982.

Pegram,B.L.,Bishop,V.S.,(1975)
An evaluation of the pericardial sac as a safety factor during tamponade,Cardiovasc.Res.,9,pp:715-721.

Peskin,C.S.,(1974)
The differential geometry of heart valves,J.Franklin Institute, Vol.297,No.5,May1974,pp:335-343.

Phillips,V.A.,(1971)
"Modern Metallographic Techniques and Their Applications",Willey-Interscience,John Wiley&Sons,Inc.,New York,1971.

Picha,G.J.,(1974)
(on pericardium),MSc.thesis,CASE Western Univ.,1974.

Picha,G.J.,Gibbons,D.F.,(1976)
Effects of formaldehyde and glutaraldehyde on pericardium,in:Bio-compatibility of implant materials,(ed)Williams,D.,Sector Publ.Ltd., London,1976,pp:193-201.

Pujara,P,Lardner,T.J.,(1978)
Deformations of elastic membranes-Effect of different constitutive

relations,ZAMP,Vol.29,pp:315-327.

Rabkin,S.W.,Berghause,D.G.,Bauer,H.F.,(1974)
Mechanical properties of isolated canine pericardium,J.Appl.Physiol., Vol.36,No.1,pp:69-73.

Rabkin,S.W.,Hsu,P.H.,(1975)
Mathematical and mechanical modelling of stress-strain relationship of pericardium,Am.J.Physiol.,Vol.229,No.4,pp:896-900.

Radenkovic,Boschat,(1966)
Integrated research on carbon composite materials,Technical report, AFML-TR-66-310,Part-I,Union Carbide corp. in Association with Case Inst.Techn. and Bell Aerosystems Company,Oct.1966.

Radjeman,A.,Liew,S.C.,Lim,K.O.,(1985)
Anisotropic elasticity of bovine pericardial tissues,Jpn.J.Physiol., 35,(5),pp:831-840.

Reece,I.R.,VanNoort,R.,Martin,T.R.P.,Black,M.M.,(1982)
The physical properties of bovine pericardium. A study of the effects of stretching during chemical treatment in glutaraldehyde,Ann.Thorac. Surg.,Vol.33,No.5,pp:480-485.

Reis,R.L.,Hancock,W.D.,Yarbrough,J.W.,Glancy,D.L.,Morrow,A.G.,(1971)
The flexible stent:a new concept in the fabrication of tissue valve prostheses,J.Thorac.Cardiovasc.Surg.,Vol.62,pp:683-689.

Reul,H.,Giersiepen,M.,Knott,E.,(1986)
Laboratory testing of prosthetic heart valves,in "Heart Valve Engineering" Mech.Eng.Publications Ltd,for I.M.E.London 1986.

Rivlin,R.S.,Saunders,D.W.,(1951)
Large elastic deformations of isotropic materials VII.Experiments on the deformation of rubber,Phil.Trans.Royal Soc.,Ser.A,Vol.243, pp:251-288.

Rivlin,R.S.,Thomas,A.G.,(1951)
Large elastic deformations of isotropic materials VIII.Strain distribution around a hole in a sheet,Phil.Trans.Royal Soc.,Ser.A, Vol.243,pp:289-298.

Romer,A.S.,Parsons,T.S.,(1977)
"The vertebrate body",5th Ed.,W.B.Saunders Co.,1977.

Ross,D.N.,(1962)
Homograft replacement of the aortic valve,Lancet,1962,2,p:487.

Ross,D.N.,Martelli,V.,Wain,W.H.,(1979)
Allograft and Autograft Valves used for Aortic Valve replacement, in "Tissue Heart Valves",Ed.:Ionescu,M.I.,1979,Butterworths, London-Boston.

Ross,J.Jr.,Sonnenblick,E.H.,Covell,J.W.,Kaiser,G.A.,Spiro,D.,(1967)
The architecture of the heart in systole and diastole,Circ.Res., Vol.21,No.4,pp:409-421.

Rousseau,E.P.M.,Sauren,A.A.H.J.,VanHout,M.C.,VanSteenhoven,A.A.,(1983)
Elastic and Viscoelastic material behaviour of fresh and glutaraldehyde treated porcine aortic valve tissue,J.Biomech.,Vol.16,No.5,pp:339-348.

Rushmer,R.F.(1976)
"Cardiovascular Dynamics",4th edition,Saunders,1976.

Sandler,H.,(1970)
Dimensional analysis of the heart-A Review,Am.J.Med.Sciences,Vol.260, pp:56-70.

Sands,M.P.,Rittenhouse,E.A.,Mohri,H.,Meredino,K.A.,(1969)
An anatomical comparison of human,pig,calf,and sheep aortic valves, Ann.Thorac.Surg.,8,(5),p:407-414.

Sanjeevi,R.,Somanathan,N.,Ramswamy,D.,(1982)
A Viscoelastic model for collagen fibres,J.Biomech.,Vol.15,pp:181-183.

Sauren,A.A.H.J.,Kuijpers,W.,VanSteenhoven,A.A.,Veldpaus,F.E.,(1980)
Aortic valve histology and its relation with mechanics-preliminary report,J.Biomech.,Vol.13,pp:97-104.

Sauren,A.A.H.J.,VanHout,M.C.,VanSteenhoven,A.A.,Veldpaus,F.E.,Janssen,J.D., (1983),The mechanical properties of porcine aortic valve tissues, J.Biomech.,Vol.16,No.5,pp:327-337.

Schmidt,L.R.,Carley,J.F.,(1975)
Biaxial stretching of heat-softened plastic sheets using an inflation technique,Int.J.Engng.Scien.,Vol.13,pp:563-578.

Schoen,F.J.,Tsao,J.W.,Levy,R.J.,(1986)
Calcification of Bovine pericardium used in Cardiac Valve Bioprostheses Implications for the mechanisms of Bioprosthetic tissue mineralization, Am.J.Pathology,Vol.123,(1),pp:134-145.

Shabetai,R.,(1981)
"The pericardium",Grune and Stratton Inc.,New York,1981.

Shoemaker,P.A.,Schneider,D.,Lee,M.C.,Fung,Y.C.,(1986)
A constitutive model for two-dimensional soft tissues and its application to experimental data,J.Biomech.,Vol.19,No.9,pp:695-702.

Shoobridge,M.P.K.,(1983)
A new principle in polychrome staining: a system of automated staining, complementary to hematoxylin and eosin, and usable as a research tool, Stain Technology,Vol.58,pp:245-258.

Sisson and Grossman's
"The anatomy of the domestic animals",Vol.1,Robert Getty,D.V.M., Ph.D.,5th Ed.,W.B.Saunders Co.,1975.

Skalak,R.,Tozeren,A.,Zarda,R.,Chien,S.,(1973)
Strain Energy Function of red blood cell membranes,Biophysics J., Vol.13,pp:245-264.

Spotnitz,H.M.,Kaiser,G.A.,(1971)
The effect of the pericardium on pressure-volume relations in the

canine left ventricle,J.Surg.Res.,11,pp:375-380.

Spyt,T.J.,Fisher,J.,Reid,J.,Anderson,J.D.,Whealey,D.J.,(1988)
Animal Evaluation of a New Pericardial Bioprosthetic Heart Valve, Artificial Organs,12,(4),pp:328-336.

Starr,A.,Edwards,M.L.,(1961)
Mitral valve replacement:Clinical experience with the ball valve prosthesis,Ann.Surg.,154,pp:726-737.

Stoker,J.J.,(1969)
"Differential Geometry",Wiley,1969.

Storåkers,B.,(1983a)
Small deflections of linear elastic circular membranes under lateral pressure,J.Appl.Mech.,Vol.50,pp:735-739.

Storåkers,B.,(1983b)
A viscoelastic correspondence principle for plane membranes subjected to lateral pressure,J.Appl.Mech.,Vol.50,pp:740-742.

Storakers,B.,(1983c)
Variation principles and bounds for the approximate analysis of plane membranes under lateral pressure,J.Appl.Mech.,Vol.50,pp:743-749.

Swanson,W.M.,Clark,R.E.,(1974)
Dimensions and geometric relationships of the human aortic valve as a function of pressure,Circ.Res.,35,pp:871-882.

Takasaki,H.,(1973)
Moire topography,Appl.Optics,Vol.12,No.4,pp:845-850.

Taylor,K.M.,(1986)
The clinical aspects of heart valve replacement:an overview,in "Heart Valve Engineering"Mech.Eng.Publications,Ltd for I.M.E.,London 1986.

Theocaris,P.S.,(1969)
"Moire fringes in strain analysis",Pergamon Press,1969.

Thubrikar,M.,Harry,R.,Nolan,S.P.,(1977)
Normal aortic valve function in dogs,Am.J.Cardiolog.,40,pp:563-568.

Thubrikar,M.,Bosher,L.P.,Nolan,S.P.,(1979)
The mechanism of opening of the aortic valve,J.Thorac.Cardiovasc. Surg.,Vol.77,No.6,1979,pp:863-870

Thubrikar,M.,Piepgrass,W.C.,Deck,J.D.,Nolan,S.P.,(1980)
Stresses of Natural versus prosthetic aortic valve leaflets in-vivo, Ann.Thorac.Surg.,Vol.30,No.3,Sept.1980,pp:230-239.

Thubrikar,M.J.,Skiner,J.R.,Eppink,R.T.,Nolan,S.P.,(1982)
Stress analysis of porcine bioprosthetic heart valves in-vivo, J.BIOM.MAT.RES.,Vol.16,pp:811-826.

Tong,P.,Fung,Y.C.B.,(1976b)
The stress/strain relationship for the skin,J.Biomech.,Vol.9, pp:649-657.

Tortora,G.J.,Anagnostakos,N.P.,(1983)
"Principles of Anatomy and Physiology",4th Ed,Harper and Row,Publ. New York

Treloar,L.R.G.,(1975)
"The physics of rubber elasticity",3rd Ed.Clarendon Press,Oxford,1975.

Trowbridge,E.A.,Black,M.M.,Daniel,C.L.,(1985)
The mechanical response of glutaraldehyde-fixed bovine pericardium to uniaxial load,J.Mat.Science,20,1985,pp:114-140.

Trowbridge,E.A.,Crofts.C.E.,(1986a)
Pericardial heterografts:a method for leaflet mechanical property control,in: "Heart Valve Engineering",publ.Mech.Eng.Public.Ltd, for I.M.E.,London,pp:103-107.

Trowbridge,E.A.,Crofts,C.E.,(1986b)
Evidence that deformations which occur during mechanical conditioning of bovine pericardium are not permanent,Biomaterials,Vol.7,pp:49-54.

Trowbridge,E.A.,Crofts,C.E.,(1986c)
The standardisation of gauge length: Its influence on the Relative Extensibility of natural and chemically Modified Pericardium, J.Biomech.,Vol.19,No.12,pp:1023-1033.

Tsai,S.W.,Wu,E.M.,(1970)
A general theory of strength for anisotropic materials,J.Compos. Mat.,Vol.5,pp:58-80.

Turvey,G.J.,(1979)
Large deflexion of prestressed/prestrained circular membranes,Proc. Inst.Civ.Engnrs,pt(2),67,pp:1121-1126.

Ueng,C.E.S.,Sun,Y.S.,(1974)
Large elastic deformation of an inflatable membrane of revolution, AIAA J.,Vol.12,No.6,pp:761-766.

Valanis,K.C.,Landel,R.F.,(1967)
The strain-energy function of a hyperelastic material in terms of the extension ratios,J.Appl.Physics,Vol.38,No.2,pp:2997-3002.

VanDenBroek,J.H.J.M.,VanDenBroek,M.H.L.M.,(1980)
Application of an ellipsoidal heart model in studying left ventricular contractions,J.Biomech.,Vol.13,pp:493-503.

VanNoort,R.,Yates,S.P.,Martin,T.R.P.,Barker,A.T.,Black,M.M.,(1982)
A study of the effects of glutaraldehyde and formaldehyde on the mechanical behaviour of bovine pericardium,Biomaterials,Vol.3,pp:21-26.

VanWijk,M.C.,(1980)
Moire contourgraph-An accuracy analysis,J.Biomech.,Vol.13,pp:605-613.

Vaughan,H.,(1980)
Pressuring a prestretched membrane to form a paraboloid,Int.J.Engnrs. Scien.,Vol.18,pp:99-107.

Viidik,A.,Danielsen,C.C.,Oxlund,H.,(1982)

On fundamental and phenomenological models,structure and mechanical properties of collagen,elastin and glycosaminoglycan complexes, Biorheology,19,pp:437-451.

Vito,R.,(1979)
The role of pericardium in cardiac mechanics,J.Biomech.,Vol.12, pp:587-592.

Vito,R.,(1980)
The mechanical properties of soft tissues-I:A mechanical system for Biaxial Testing,J.Biomech.,Vol.13,pp:947-950.

Wainwright,S.A.,Biggs,W.D.,Currey,J.D.,Gosline,J.M.,(1976)
"Mechanical Design in Organisms",1976,Edward Arnold.

Walker,D.K.,Scotten,L.N.,Nugent,A.H.,Brownlee,R.T.,(1986)
In-vitro assessment of the Ionescu-Shiley III,Mitral Medical and Edwards pericardial valves,in:Yacoub,M.,Badnar,E.,(eds)"Biomedical and Bioprosthetic valves".

Ward,I.M.,(1971)
"Mechanical properties of solid polymers",Wiley-Interscience,John Wiley&Sons,Ltd.,1971.

Wasil,B.A.,Merchant,D.C.,(1964)
Plate-deflection measurement by photogrammetric methods,Exp.Mech., pp:77-83.

West,E.S.,Todd,W.R.,(1961)
"Textbook of biochemistry",The MacMillan Comp.New York,1961.

Wiegner,A.W.,Bing,O.H.L.,with S.E.M. by:Borg,T.K.,Caulfield,J.B.,(1981)
Mechanical and Structural correlates of canine pericardium,Circ. Res.,Vol.49,No.3,pp:807-814.

Wiederhielm,C.A.,(1965)
Distensibility characteristics of small Blood Vessels,Fed.Proc.,24, pp:1075-1084.

Wineman,A.,Wilson,D.,Melvin,J.W.,(1979)
Material identification of soft tissue using membrane inflation, J.Biomech.,Vol.12,pp:841-850.

Yarker,Y.E.,Aspden,R.M.,Hukins,D.W.L.,(1983)
Birefringence of articular cartilage and the distribution of collagen fibril orientations,Conn.Tiss.Res.,Vol.11,pp:207-213.

Yang,W.H.,Feng,W.W.,(1970)
On axisymmetrical deformations of non-linear membranes,J.Appl.Mech., Trans.ASME,pp:1002-1011.

Yang,W.H.,Lu,C.H.,(1973)
General deformations of neo-Hookean membranes,J.Appl.Mech.,Trans. ASME,pp:7-12.

Yin,C.P.,Chew,P.H.,Strumpf,R.K.,Zeger,S.L.,(1985)
Biaxial stress/strain properties of myocardium and pericardium,

Proc.Inst.Physics Conf.:Material properties and stress analysis in Biomech.Brunel Univ.,pp:3-8.

Yin,F.C.P.,Chew,P.H.,Zeger,S.L.,(1986b)
An approach to quantification of biaxial tissue stress-strain data, J.Biomech.,Vol.19,No.1,pp:27-37.

Young,J.T.,Vaishnav,R.N.,Patel,D.J.,(1977)
Non-linear anisotropic viscoelastic properties of canine arterial segments,J.Biomech.,Vol.10,pp:549-559.

Yung,C.E.S.,Sun,Y.S.,(1974)
Large elastic deformation of an Inflatable membrane of revolution, AIAA J.,Vol.12,No.6,pp:761-766.

APPENDIX Ch:4.

The computer program which was used to draw the Moiré contours in chapter4.

```
10 REM:"CONTOUR"plots contours,PROSPECTIVE correction and MAGNIFICATION
15 REM:is accounted
20DIM DLN(30)
30 REM: 18/04/88
40CLS
50MODE0
60PRINT"real deflection=height-A"
70INPUT A
80PRINT"apparent orifice RADIUS-AOD"
90INPUT AOD
100B=20.75
110MAG=B/AOD
120PRINT"source-observer distance D(mm)"
130INPUT D
140PRINT"observer-grid distance L(mm)"
150INPUT L
160PRINT"pitch size-S"
170INPUT S
180PRINT"first fringe number-NO"
190INPUT NO
200FOR I=1 TO 30
210DLN(I)=(I*L)/((D/S)-I)
220NEXT
230PRINT"expected grid to rig distance-GR"
240INPUT GR
245 IF (GR-A)>=DLN(NO) THEN 230
260PRINT"max.number of contours(photo)-NMAX"
270INPUT NMAX
280PRINT"-------------------------"
290PRINT"FACTOR-LX"
300INPUT LX
310PRINT"FACTOR-LY"
320INPUT LY
330 S%=B DIV 1
340 K%=S%+5
350DIM X(K%)
360PROC_CALC
370PROC_Z
380*SDUMP
390END
400DEF PROC_CALC
410FOR I=NO TO NMAX
420 Z=GR-I*DLN(1)
430 O=1-(Z*Z/(A^2))
440 W=B^2+(LY*Z)
450 YE=SQR(O*W)
460 R=B^2+(LX*Z)
470 PROSPECT=1+I*DLN(1)/L
480FOR Y=0 TO YE
490 Q=Y*Y/W
500 P=O-Q
510 X(Y)=SQR(P*R)
520NEXT
530 XSCALE=9.455/MAG/PROSPECT
540 YSCALE=11.35/MAG/PROSPECT
550 MOVE 800,500
560FOR Y=0 TO YE
570 DRAW 800+X(Y)*XSCALE,500+Y*YSCALE
580NEXT
590 DRAW 800,500+YE*YSCALE
600 MOVE 800,500
610 DRAW 800,600+YE*YSCALE
620 MOVE 800,500
630FOR Y=0 TO YE
640 DRAW 800-X(Y)*XSCALE,500+Y*YSCALE
650NEXT
660 DRAW 800,500+YE*YSCALE
670 MOVE 800,500
680FOR Y=0 TO YE
690 DRAW 800+X(Y)*XSCALE,500-Y*YSCALE
700NEXT
710 DRAW 800,500-YE*YSCALE
720 MOVE 800,500
730 DRAW 800,400-YE*YSCALE
740 MOVE 800,500
750FOR Y=0 TO YE
760 DRAW 800-X(Y)*XSCALE,500-Y*YSCALE
770NEXT
780 DRAW 800,500-YE*YSCALE
790NEXT I
800ENDPROC
810
820DEF PROC_Z
830 Z=0
840 O=1-(Z*Z/(A^2))
850 W=B^2+(LY*Z)
860 YE=SQR(O*W)
870 R=B^2+(LX*Z)
880 PROSPECT=1+(GR/L)
890FOR Y=0 TO YE
900 Q=Y*Y/W
910 P=O-Q
920 X(Y)=SQR(P*R)
930 XSCALE=9.455/MAG
940 YSCALE=11.3/MAG
950NEXT
960 MOVE 800,500
970FOR Y=0 TO YE
980 PLOT 69,800+X(Y)*XSCALE,500+Y*YSCALE
990NEXT
1000 PLOT 69,800,500+YE*YSCALE
1010 MOVE 800,500
1020 PLOT 69,800,600+YE*YSCALE
1030 MOVE 800,500
1040FOR Y=0 TO YE
1050 PLOT 69,800-X(Y)*XSCALE,500+Y*YSCALE
1060NEXT
1070 PLOT 69,800,500+YE*YSCALE
1080 MOVE 800,500
1090FOR Y=0 TO YE
1100 PLOT 69,800+X(Y)*XSCALE,500-Y*YSCALE
1110NEXT
1120 PLOT 69,800,500-YE*YSCALE
1130 MOVE 800,500
1140 PLOT 69,800,400-YE*YSCALE
1150 MOVE 800,500
1160FOR Y=0 TO YE
1170 PLOT 69,800-X(Y)*XSCALE,500-Y*YSCALE
1180NEXT
1190 PLOT 69,800,500-YE*YSCALE
1200ENDPROC
```

APPENDIX Ch:9.

The discriminant analysis applied in chapter9 was performed in an SPSSextra statistical package which provided a linear discriminant function for the two groups to be separated in each case, the number of functions being one less than the numbers of existing groups and equal to the degrees of freedom.

The fact that the discriminating boundary is linear tacitly assumes that the covariance matrix is the same for both populations. By looking in the plots we can say that this is basically correct with only one case of the fatigue-cycled leaflets falling far away from the ensemble of the other points. In tableA9.1 and A9.2 the coefficients of the discriminant functions are given and below the scores of each particular point if this discrimination is followed. When separating Glasgow uncycled from fatigue-cycled 4 cases per population would rather belong to the opposite population by scoring higher propabilities on the other side of the curve (in the foreign territory). The overall performance of the particular discriminant functions can be seen in tableA9.2 and A9.4 where it is shown that on average 66% of the cases are correctly classified by the adopted discriminant curves. The histograms of all groups together can readily illustrate the frequency of points right and left of the discriminant boundary when the populations are viewed along the boundary's dimension. At the bottom of the histograms the centroids of the canonical discriminant functions are noted, which are evaluated at the mean vectors of the groups.

The performance of the discriminant function for the implant-explant domain appeared to be odd. If a discrimination was performed by hand a line can be found which can only misclassify one case of each population. The difference is that the classification performed by the numerical routine of the computer was the result of a minimisation performed for a line passing in between the positions of the mean vectors of the two populations. This can be appreciated by values of the group centroids which were:

CANONICAL DISCRIMINANT FUNCTIONS EVALUATED AT GROUP MEANS:

	GROUP	FUNCTION
UNCYCLED:	1	-0.54578
FATIGUED:	2	0.50030
IMPLANTS:	1	-0.72391
EXPLANTS:	2	0.72391

while the values were equally balanced for the implants/explants, the line was pulled towards the fatigued leaflets and thus provided more territory to the uncycled leaflets. This was a result of the uncycled leaflets participating with 11 points and thus with less degrees of freedom than the fatigued cycled leaflets(12 points). The implant/explants had 7 points each and equal covariances and thus the linear boundary dissected their inter-mean vector segment.

In essence the position and direction of the linear boundary was a function of mainly three factors (Norusis,1979); i)the position of the mean vectors and the distributions of the data vectors around them (in the explants one 'odd' datum is pulling the mean to higher b values), ii)the number of data vectors per populations (affecting the degrees of freedom), and iii)the weights given to each datum which was assumed 0.5 for either group in the present analysis(a more thorough approach would have assigned lower prior probability to the 'odd'

explant datum). Linear discrimination was also found to be a robust estimator with only the 'odd' point in the population of the explant samples being able to produce a noticable difference when it was excluded. There were no grounds why this datum should be rejected and thus it was kept in the population.
The actual performance of 66% on the present data has nothing to do with the expected performance of the discrimination analysis. The Wilk's lambda (Λ) testing the significance of all the discriminating functions (only one in here) had a level of significance of a=0.0731 (>92%) for uncycled/fatigue and a=0.0725 (>92%) for implants/explants both having two degrees of freedom estimated for two variables(parameters a,b) and two groups in each of the discrimination analyses. With the percentages of confidence limits being higher than 92% the possibility of having a discriminating function in the domain of values for the parameters a,b appeared quite optimistic.

When examining the performance of a discriminating function for the logarithmetic values of the parameters, tables: A9.5, A9.6, A9.7, A9.8 resulted.
The performance was the same for uncycled/fatigued (tableA9.6), but it was greatly improved for the implants/explants (tableA9.8).
The Wilk's lambda(Λ) which are not included in the tables had a level of significance a'=0.13 (87%) for uncycled/fatigued and a'=0.03 (97%) for implants/explants. Thus having a discriminant function between implant and explant tissue was justified with a 97% confidence limit.

STATISTICAL DISCRIMINATION ANALYSIS

Table A9.1:

ON UNCYCLED CONTROL LEAFLET TISSUE _ FATIGUE CYCLED LEAFLET TISSUE

UNSTANDARDIZED CANONICAL DISCRIMINANT FUNCTION COEFFICIENTS

	FUNC 1
A	0.1795222
B	88.59849
(CONSTANT)	-5.717990

CASE SEQNUM	MIS VAL	SEL	ACTUAL GROUP		HIGHEST PROBABILITY GROUP	P(D/G)	P(G/D)	2ND HIGHEST GROUP	P(G/D)	DISCRIMINANT SCORES...
1			1	**	2	0.6346	0.5125	1	0.4875	0.0250
2			1		1	0.8528	0.5873	2	0.4127	-0.3602
3			1	**	2	0.9311	0.6122	1	0.3878	0.4138
4			1	**	2	0.9176	0.6582	1	0.3418	0.6037
5			1		1	0.3744	0.8140	2	0.1860	-1.4341
6			1		1	0.3224	0.8295	2	0.1705	-1.5353
7			1		1	0.4884	0.7811	2	0.2189	-1.2386
8			1		1	0.9780	0.6268	2	0.3732	-0.5182
9			1	**	2	0.2901	0.8394	1	0.1606	1.5583
10			1		1	0.2150	0.8634	2	0.1366	-1.7857
11			1		1	0.2354	0.8567	2	0.1433	-1.7323
12			2	**	1	0.9566	0.6466	2	0.3534	-0.6002
13			2	**	1	0.9007	0.6027	2	0.3973	-0.4210
14			2		2	0.9144	0.6592	1	0.3408	0.6077
15			2		2	0.5932	0.7514	1	0.2486	1.0346
16			2		2	0.4920	0.7801	1	0.2199	1.1875
17			2		2	0.5697	0.7580	1	0.2420	1.0688
18			2		2	0.5152	0.7734	1	0.2266	1.1510
19			2	**	1	0.6463	0.5167	2	0.4833	-0.0868
20			2		2	0.8953	0.6010	1	0.3990	0.3687
21			2		2	0.0859	0.9124	1	0.0876	2.2176
22			2	**	1	0.7495	0.7070	2	0.2930	-0.8650
23			2		2	0.8733	0.5939	1	0.4061	0.3408

Table A9.2:

ALL-GROUPS STACKED HISTOGRAM

CANONICAL DISCRIMINANT FUNCTION 1

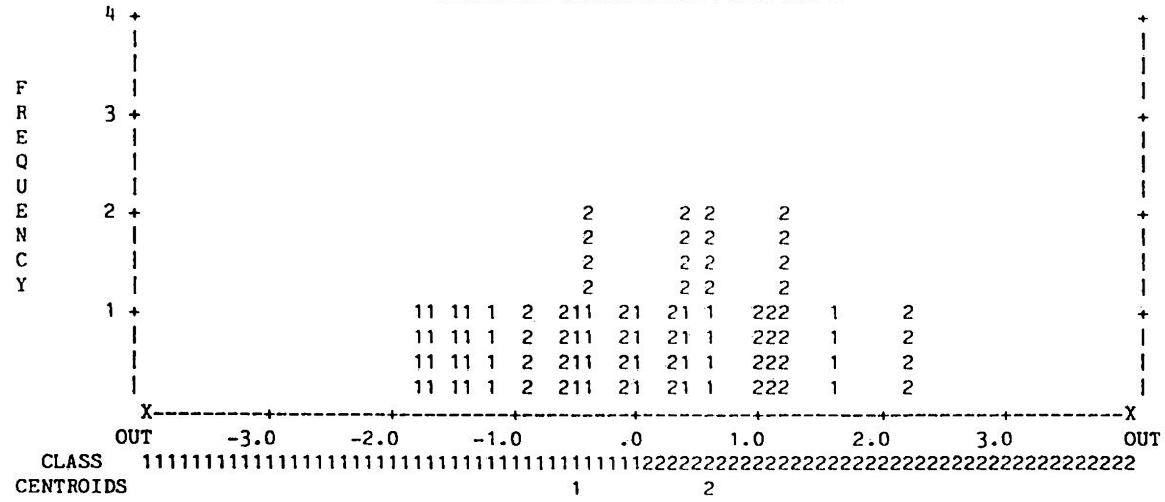

CLASSIFICATION RESULTS -

ACTUAL GROUP		NO. OF CASES	PREDICTED GROUP MEMBERSHIP 1	2
GROUP	1	11	7 63.6%	4 36.4%
GROUP	2	12	4 33.3%	8 66.7%

PERCENT OF "GROUPED" CASES CORRECTLY CLASSIFIED: 65.22%

STATISTICAL DISCRIMINATION ANALYSIS

Table A9.3:

ON IMPLANT _ EXPLANT VALVE TISSUE

UNSTANDARDIZED CANONICAL DISCRIMINANT FUNCTION COEFFICIENTS

	FUNC 1
A	0.1858119
B	411.0542
(CONSTANT)	-6.317060

CASE SEQNUM	MIS VAL	SEL	ACTUAL GROUP		HIGHEST PROBABILITY GROUP	P(D/G)	P(G/D)	2ND HIGHEST GROUP	P(G/D)	DISCRIMINANT SCORES...
1			1		1	0.5833	0.5631	2	0.4369	-0.1753
2			1		1	0.2447	0.9389	2	0.0611	-1.8872
3			1		1	0.7970	0.6628	2	0.3372	-0.4666
4			1	**	2	0.5296	0.5345	1	0.4655	0.0953
5			1		1	0.7856	0.6580	2	0.3420	-0.4518
6			1		1	0.9117	0.7084	2	0.2916	-0.6131
7			1		1	0.3983	0.9065	2	0.0935	-1.5686
8			2		2	0.1833	0.9514	1	0.0486	2.0547
9			2		2	0.1426	0.9597	1	0.0403	2.1899
10			2	**	1	0.5784	0.5606	2	0.4394	-0.1682
11			2	**	1	0.8080	0.6674	2	0.3326	-0.4809
12			2	**	1	0.6092	0.5764	2	0.4236	-0.2127
13			2		2	0.2937	0.9288	1	0.0712	1.7739
14			2	**	1	0.5257	0.5323	2	0.4677	-0.0893

Table A9.4:

ALL-GROUPS STACKED HISTOGRAM

CANONICAL DISCRIMINANT FUNCTION 1

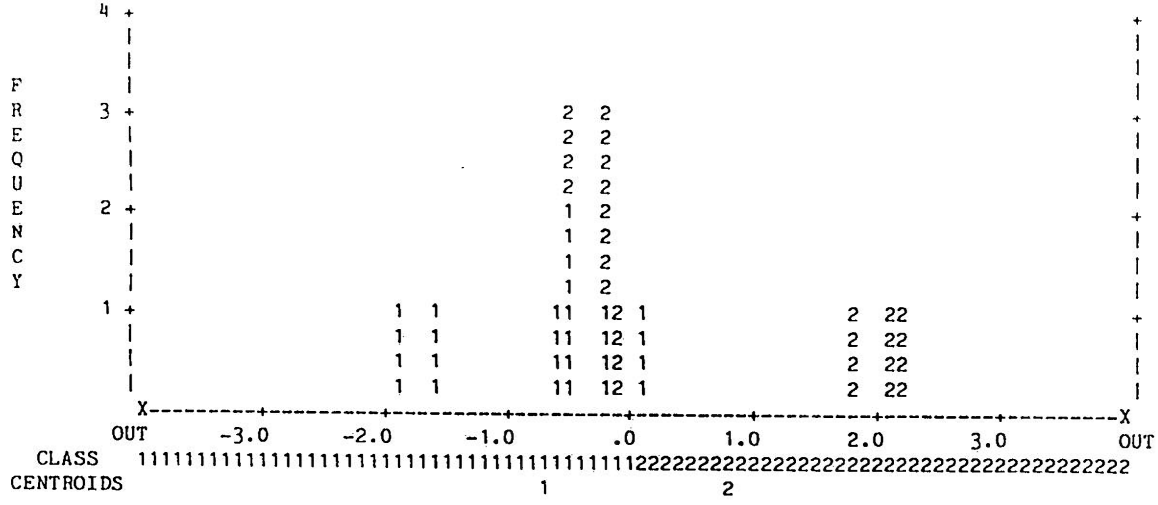

CLASSIFICATION RESULTS -

ACTUAL GROUP		NO. OF CASES	PREDICTED GROUP MEMBERSHIP 1	2
GROUP	1	7	6 85.7%	1 14.3%
GROUP	2	7	4 57.1%	3 42.9%

PERCENT OF "GROUPED" CASES CORRECTLY CLASSIFIED: 64.29%

Table A9.5:

STATISTICAL DISCRIMINATION ANALYSIS

ON UNCYCLED CONTROL LEAFLET TISSUE_FATIGUE CYCLED LEAFLET TISSUE
USING THE LOGARITHMETIC VALUES OF THE PARAMETERS a,b.

UNSTANDARDIZED CANONICAL DISCRIMINANT FUNCTION COEFFICIENTS

	FUNC 1
A	4.935688
B	0.6230968
(CONSTANT)	-12.81350

CASE SEQNUM	MIS VAL	SEL	ACTUAL GROUP		HIGHEST PROBABILITY GROUP	P(D/G)	P(G/D)	2ND HIGHEST GROUP	P(G/D)	DISCRIMINANT SCORES...
1			1	**	2	0.6563	0.5033	1	0.4967	-0.0055
2			1		1	0.8748	0.6381	2	0.3619	-0.6370
3			1	**	2	0.8174	0.6535	1	0.3465	0.6705
4			1	**	2	0.5554	0.7240	1	0.2760	1.0292
5			1		1	0.3094	0.7952	2	0.2048	-1.4960
6			1		1	0.2307	0.8211	2	0.1789	-1.6782
7			1		1	0.2185	0.8254	2	0.1746	-1.7099
8			1	**	2	0.6850	0.5124	1	0.4876	0.0339
9			1	**	2	0.1326	0.8587	1	0.1413	1.9435
10			1		1	0.1793	0.8398	2	0.1602	-1.8224
11			1		1	0.2612	0.8108	2	0.1892	-1.6030
12			2	**	1	0.9983	0.6045	2	0.3955	-0.4816
13			2	**	1	0.6760	0.5095	2	0.4905	-0.0615
14			2		2	0.7025	0.6843	1	0.3157	0.8216
15			2		2	0.7613	0.6685	1	0.3315	0.7434
16			2		2	0.3796	0.7738	1	0.2262	1.3181
17			2		2	0.3211	0.7916	1	0.2084	1.4318
18			2		2	0.9970	0.6049	1	0.3951	0.4433
19			2		2	0.9801	0.6095	1	0.3905	0.4645
20			2		2	0.7272	0.5254	1	0.4746	0.0907
21			2		2	0.8371	0.6482	1	0.3518	0.6451
22			2	**	1	0.9184	0.5813	2	0.4187	-0.3770
23			2		2	0.8392	0.5587	1	0.4413	0.2366

Table A9.6:

ALL-GROUPS STACKED HISTOGRAM

CANONICAL DISCRIMINANT FUNCTION 1

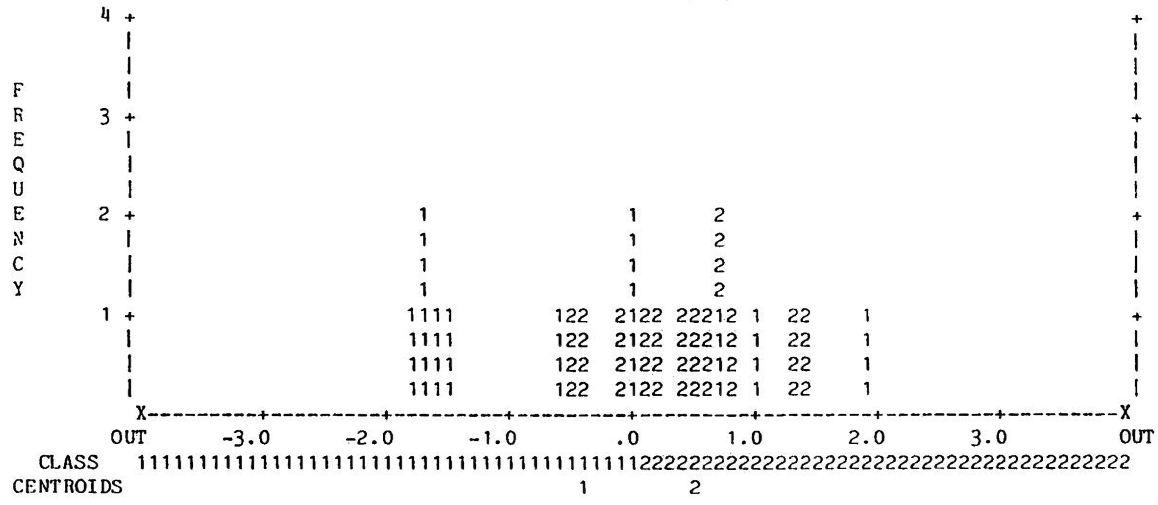

CLASSIFICATION RESULTS -

ACTUAL GROUP	NO. OF CASES	PREDICTED GROUP MEMBERSHIP 1	2
GROUP 1	11	6 54.5%	5 45.5%
GROUP 2	12	3 25.0%	9 75.0%

PERCENT OF "GROUPED" CASES CORRECTLY CLASSIFIED: 65.22%

STATISTICAL DISCRIMINATION ANALYSIS

Table A9.7:

ON IMPLANT_EXPLANT VALVE TISSUE
USING THE LOGARITHMETIC VALUES OF THE PARAMETERS a,b.

UNSTANDARDIZED CANONICAL DISCRIMINANT FUNCTION COEFFICIENTS

	FUNC 1
A	7.713937
B	0.9424659
(CONSTANT)	-19.30206

CASE SEQNUM	MIS VAL	SEL	ACTUAL GROUP		HIGHEST PROBABILITY GROUP	P(D/G)	P(G/D)	2ND HIGHEST GROUP	P(G/D)	DISCRIMINANT SCORES...
1			1		1	0.8700	0.8416	2	0.1584	-0.9993
2			1		1	0.1219	0.9817	2	0.0183	-2.3827
3			1		1	0.5315	0.5868	2	0.4132	-0.2100
4			1	**	2	0.4072	0.5029	1	0.4971	0.0069
5			1	**	2	0.5310	0.5865	1	0.4135	0.2091
6			1		1	0.9244	0.8257	2	0.1743	-0.9305
7			1		1	0.4793	0.9295	2	0.0705	-1.5431
8			2		2	0.1428	0.9791	1	0.0209	2.3010
9			2		2	0.6399	0.8983	1	0.1017	1.3036
10			2		2	0.7001	0.6798	1	0.3202	0.4505
11			2		2	0.5820	0.6170	1	0.3830	0.2852
12			2	**	1	0.8842	0.8375	2	0.1625	-0.9813
13			2		2	0.3845	0.9453	1	0.0547	1.7052
14			2		2	0.9599	0.7879	1	0.2121	0.7853

Table A9.8:

ALL-GROUPS STACKED HISTOGRAM

CANONICAL DISCRIMINANT FUNCTION 1

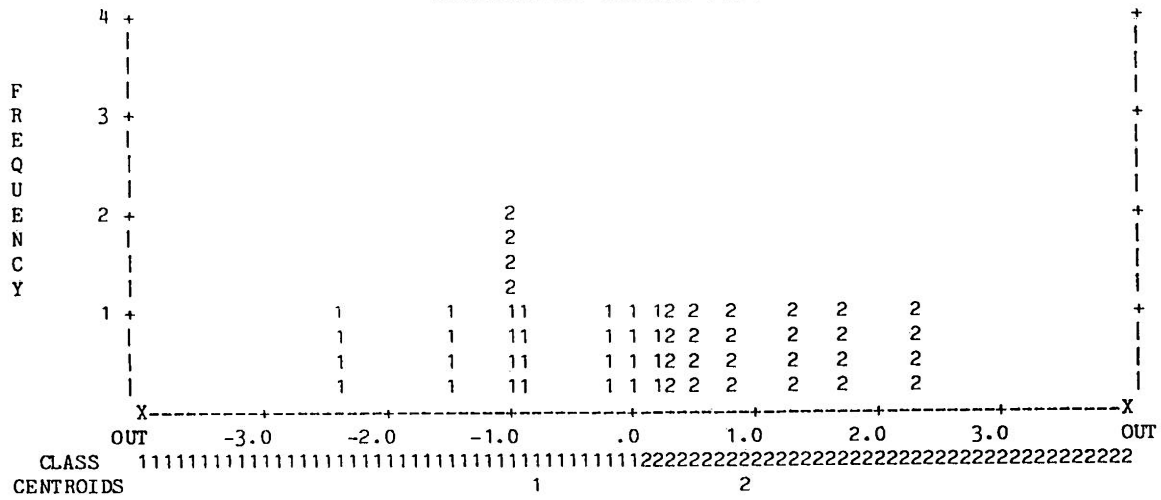

CLASSIFICATION RESULTS -

ACTUAL GROUP	NO. OF CASES	PREDICTED GROUP MEMBERSHIP 1	2
GROUP 1	7	5 71.4%	2 28.6%
GROUP 2	7	1 14.3%	6 85.7%

PERCENT OF "GROUPED" CASES CORRECTLY CLASSIFIED: 78.57%

APPENDIX Ch:10.

The computer program which applied the model of chapter10 in the case of uniform biaxial stretch and as it applies for the strong fibre-reinforced direction. Six different versions were created for applications along the two normal directions and for three different deformation modes.

```
C  PROGRAM TO CALCULATE STRESSES IN UNIFORM BIAXIAL STRETCH
C  PROGRAM YCIRC (it calculates AND stores data)
C  THE PROGRAM works along the strong circumferential direction of
C  coefficient A


DIMENSION OE(370),OL(370),OM(370)
DIMENSION ANS(100),STRESS(100),STRETCH(100)
DOUBLE PRECISION LAMBDA1,LAMBDA2,LAMBDATH,K2,K1,TH,THN,TERM
DOUBLE PRECISION MU,X,SD,FRST,ODD,EVEN,NMAX,LO
DOUBLE PRECISION DISTR,ANG
LOGICAL*1 IFILE(14),APANT
COMMON MU,SD,LAMBDATH
EXTERNAL F
INTRINSIC DEXP,DCOS,DSIN

PI=3.14159264

WRITE (5,10)
10FORMAT(//,' FILENAME? (MAX. OF 9 CHARACTERS)')
READ(5,15)(IFILE(I),I=1,9)
15FORMAT(9A1)
IFILE(10)='.'
IFILE(11)='D'
IFILE(12)='A'
IFILE(13)='T'
IFILE(14)=0

OPEN(UNIT=1,TYPE='NEW',NAME=IFILE,CARRIAGECONTROL='LIST',ERR=8000)

CWRITE(1,20)IFILE
C20FORMAT(1X,14A1)

WRITE(6,*)('ENTER MAX STRETCH RATIO (last stretch ratio of loop): ')
READ(5,*)LMAX
TYPE *,'MU fibre mean (peak point of fibre distribution)'
READ(5,*)MU
TYPE *,'SD st.deviation (of fibre distribution)'
READ(5,*)SD
TYPE *,'ELASTIN MODULUS K1'
READ(5,*)K1
TYPE *,'COLLAGEN MODULUS K2'
READ(5,*)K2
TYPE *,'NO. of iterations? less than 90'
READ(5,*)N

C''''''''''''''''''''''''''''''''''''''''''definition of constants''''''''''
A=0.535
B=0.101
LAMBDA1=1.0
LAMBDA2=1.0
NMAX=2*N

C
L=1.0

C''''''''''''''''''''''''''''''''''''''''''STRESS AT AN INCREASED STRETCH''''

50TH=1.57079                              !values defined only for
THN=(-TH)                                 !biaxial stretch and pure shear
      DTH=(TH-THN)/2/N                          !discretising the angle range

CFRST=DSQRT((1-LAMBDA1**2)/(LAMBDA2**2-1))
CTH=1.57079-DATAN(FRST)                   !new limits for integration
CTHN=(-TH)

C''''''''''''''''''''''''''''''''''''''''''''''''''''''''''''''''''''''''''''

DO 100 I=0,NMAX                           !calculation OE(I),OL(I)
ANG=(THN/2)+I*DTH                         !incrementing the angle/ANG

LAMBDATH=DSQRT(((LAMBDA1*DCOS(ANG))**2)+((LAMBDA2*DSIN(ANG))**2))
```

```
C'''''''''''''''''''''''''''''''''''''''''''''''''''''''''''ELASTIN CALCULATION''''''
OE(I)=K1*(LAMBDATH-1)

C''''''''''''''''''''''''''''''''''''''''''''''''''''''''''COLLAGEN CALCULATION'''''
  NLIMIT=0
IFAIL=0
C
TERM=D01AHF(1.0,LAMBDATH,0.0001,NPTS,RELERR,F,NLIMIT,IFAIL)
OL(I)=K2*TERM/(SD*SQRT(2*PI))                !calculated integral
C
DISTR=A*((DCOS(ANG))**2)+B*((DSIN(ANG))**2)
OM(I)=(OE(I)+OL(I))*((DCOS(ANG))**2)*DISTR/LAMBDATH
100CONTINUE

ODD=0.0                                      !numerical summation
DO 200 I=1,N
J=2*I-1
ODD=OM(J)+ODD
200CONTINUE

EVEN=0.0
DO 300 I=1,N
K=2*I-2
EVEN=OM(K)+EVEN
300 CONTINUE

ANS(L)=(DTH/3)*(OM(0)+OM(NMAX)+(4*ODD)+(2*EVEN))     !Simpson's rule
STRESS(L)=LAMBDA1*ANS(L)
STRETCH(L)=LAMBDA1
TYPE *,L
TYPE *,STRETCH(L),STRESS(L)

C'''''''''''''''''''''''''''''''''''''''''''incrementing the stretch ratio:LAMBDA''''''
LAMBDA1=LAMBDA1+0.05                     !for the next loop
LAMBDA2=LAMBDA1                          !for uniform biaxial stretch
L=L+1                                    !incrementing the counter
IF (LAMBDA1.LT.LMAX) GOTO 50             !repeating for a larger lambda

LO=L-1                                  !for use in storing data


C'''''''''''''''''''''''''''''''''''''calculation of the lateral contraction ratio'''
CLAMBDA2=1.795-(0.795*LAMBDA1)             !uniaxial stretch conditions
C''''''''''''''''''''''''''''''''''''''''''''''''''''''''''''''''''''''''''''''''''''''

C************************************************************STORING DATA***
DO 500 L=1,LO
WRITE(1,400)STRETCH(L),STRESS(L)
400FORMAT(F10.5,1X,F10.5)
500CONTINUE
CLOSE(UNIT=1)
GOTO 8200

C'''''''''''''''''''''''''''''''''''''''''''''''''''''''''''''''''''ERROR MESSAGES
8000WRITE(5,8100)
8100FORMAT('ERROR IN OPENING FILE')
GOTO 8200
8200STOP

END

C*******************************************************************
FUNCTION F(X)
DOUBLE PRECISION X,MU,SD,LAMBDATH
INTRINSIC DEXP
COMMON MU,SD,LAMBDATH
F=DEXP(-(X-MU)**2/(2*SD**2))*(LAMBDATH-X)/X
END
```

Thesis Dissemination Outputs

Research Papers in peer review journals:

- Zioupos P., Barbenel JC, Fisher J, 'Mechanical and Optical anisotropy of bovine pericardium.' *Med. Biol. Eng. Comp*., 30: 76 82, 1992.
- Zioupos P, Barbenel JC, 'Mechanics of native bovine pericardium-I. The multiangular behaviour of strength and stiffness of the tissue.' *Biomaterials*, 15: 366 373, 1994.
- Zioupos P, Barbenel JC, 'Mechanics of native bovine pericardium-II. A structure based model for the anisotropic mechanical behaviour of the tissue.' *Biomaterials*, 15: 374 382, 1994.
- Zioupos P, Barbenel JC, Fisher J, 'Anisotropic elasticity and strength of glutaraldehyde fixed bovine pericardium for use in pericardial bioprosthetic valves.' *J. Biomedical Materials Research*, 28, 49 57, 1994.
- Zioupos P., Barbenel JC, Fisher J, Wheatley DJ, 'Changes in the mechanical properties of bioprosthetic valve leaflets made of bovine pericardium, as a result of long-term mechanical conditioning in vitro and implantation in vivo.' *J. Mat. Sci. Mat. Med*., 4: 531 537, 1993.

Books, chapters and monographs:

- 'The mechanical properties of bovine pericardium', Barbenel,J.C., Zioupos,P., Fisher,J., (1986) in: *HEART VALVE ENGINEERING*, Mech.Eng.Publ. I.M.E., London, UK, 1986.
- 'The mechanical properties of bovine pericardium', Barbenel,J.C., Zioupos,P., Fisher,J., (1987) in: *BIOMATERIALS AND CLINICAL APPLICATIONS*, Elsevier Sci. Publ., UK, 1987.
- 'Directional variations in the extensibility of bovine pericardium', Barbenel,J.C., Zioupos,P., Fisher,J., (1987) in: *THE INFLUENCE OF NEW TECHNOLOGY ON MEDICAL PRACTICE*, McMillan Press, UK, 1988.
- 'The anisotropy of bovine pericardium', Barbenel,J.C., Zioupos,P., Fisher,J., (1989) in: *BLOOD FLOW IN ARTIFICIAL ORGANS AND CARDIOVASCULAR PROSTHESES*, Clarendon Press, Oxford, UK, 1989.
- 'Changes in the material properties and function of pericardial Bioprosthetic valves in-vivo', Fisher,J., Zioupos,P., Barbenel,J.C., Wheatley,D.J., (1989) in: *INTERFACES IN MEDICINE AND MECHANICS*, (Eds: Williams,K.R., Lesser,T.H.J.), Biomaterials Research Group, University of Wales Coll. of Medicine, Swansea, UK, 1989.

Reviewed Conference Proceedings:

- 'Anisotropy on Bovine pericardium.' Zioupos,P., Barbenel,J.C., Fisher,J., '2nd Hellenic Conf. Med. Physics & Biomed. Engng' 21-22nd Nov.1986, 'Agios Savvas' Hospital, Athens, Greece.
- 'Mechanical properties and structure of bovine pericardium.' Barbenel,J.C., Zioupos,P., USA-ITALY Joint Workshop on 'Polymers for Biomedical Applications' 11-16th June 1989, Capri, Italy.
- 'A Structure Inspired Model for the anisotropic mechanical behaviour of bovine pericardium.' Zioupos,P., Barbenel,J.C., '2nd World Cong.Biomech.' 10-15th July 1994, Amsterdam, Netherlands.